

Georgia State University

ScholarWorks @ Georgia State University

Physics and Astronomy Dissertations

Department of Physics and Astronomy

8-7-2007

Inspection and Characterization of Exoplanet Using the CHARA Array

Ellyn K. Baines

Follow this and additional works at: https://scholarworks.gsu.edu/phy_astr_diss



Part of the [Astrophysics and Astronomy Commons](#), and the [Physics Commons](#)

Recommended Citation

Baines, Ellyn K., "Inspection and Characterization of Exoplanet Using the CHARA Array." Dissertation, Georgia State University, 2007.

doi: <https://doi.org/10.57709/1059822>

This Dissertation is brought to you for free and open access by the Department of Physics and Astronomy at ScholarWorks @ Georgia State University. It has been accepted for inclusion in Physics and Astronomy Dissertations by an authorized administrator of ScholarWorks @ Georgia State University. For more information, please contact scholarworks@gsu.edu.

Inspection and Characterization of Exoplanet Systems Using the CHARA Array

by

Ellyn Baines

Under the Direction of Harold A. McAlister

Abstract

Until the last decade or so, our entire knowledge of planets around Sun-like stars consisted of those in our own Solar System. This is no longer the case. Over 200 planets have been discovered through radial velocity surveys and photometric studies, both of which depend on observing the planet's effects on its host star. Much of our knowledge of the planets orbiting these stars is uncertain, based on assumptions about the stars' masses and the planets' orbital inclinations.

This dissertation is comprised of two main sections. The first involves measuring the angular diameters for a sample of exoplanet host stars using Georgia State University's CHARA Array in order to learn more about the nature of these stars. These direct angular measurements are not dependent on the exoplanet systems' inclinations or the masses of the stars. Improved angular diameters lead to linear diameters when combined with *HIPPARCOS* parallax measurements, which in turn tell us of

the stars' ages and masses. Of the 82 exoplanet systems observable with the CHARA Array, 31 host stars were observed and stellar angular diameters were measured for 26 systems.

In the special case of an exoplanet system with a transiting planet, this direct measurement of the star's angular diameter leads to a direct measurement of the planet's diameter, when the planet-to-star-radii ratio is known from photometric studies. This was done for HD 189733. The star's angular diameter is 0.377 ± 0.024 mas, which produces a stellar linear radius of $0.779 \pm 0.052 R_{\odot}$ and a planetary diameter of $1.19 \pm 0.08 R_{\text{Jupiter}}$.

The second part of this project involved the inspection of the exoplanet systems for stellar companions masquerading as planets. From radial velocity studies alone, it is impossible to distinguish between a planet in a high-inclination orbit and a low-mass stellar companion in a low-inclination orbit. Using the CHARA Array, it was possible to rule out certain secondary spectral types for each exoplanet system observed by studying the errors in the diameter fit and searching for separated fringe packets. While no definitive stellar companions were found, two exoplanet systems, ν Andromedae and ρ Coronae Borealis, exhibited behavior that were not consistent with the host star being a simple limb-darkened disk.

Index Words: Optical/infrared interferometry, exoplanet systems, stellar diameters, stellar companions

Inspection and Characterization of Exoplanet Systems Using the CHARA Array

by

Ellyn Baines

A Dissertation Presented in Partial Fulfillment of Requirements for the Degree of

Doctor of Philosophy

in the College of Arts and Sciences

Georgia State University

2007

Copyright by
Ellyn Baines
2007

Inspection and Characterization of Exoplanet Systems Using the CHARA Array

by

Ellyn Baines

| | |
|------------------|------------------------|
| Major Professor: | Harold A. McAlister |
| Committee: | Theo A. ten Brummelaar |
| | Douglas R. Gies |
| | Todd J. Henry |
| | Nikolaus Dietz |

Electronic Version Approved:

Office of Graduate Studies
College of Arts & Sciences
Georgia State University
August 2007

Dedication

To Elsie Osman, my Auntie Sib

You'll have to let me know if I'm right -

Acknowledgments

My heartfelt thanks to my Mom and sister, who have been a fantastic support and comic relief while I've been working on this dissertation. Mom, I'll bet you never thought that when you taught us to like school that I'd still be at it at this point! Lorey, I can't wait to read yours. My apologies to my friends for turning into a bundle of anti-social nerves for the past few months and for having only one topic of conversation, as if no one had ever written a dissertation before. I'll be happy to listen your rambling about it when it's your turn.

Many, many thanks to the folks on Mount Wilson who kept the CHARA Array running smoothly despite every attempt that the weather, instrument, fires, mice, computer problems, and my mistakes made to hinder its operation. P.J. Goldfinger showed endless patience in teaching me to run the Array (late-night 80's dance party!), and Nils Turner, Laszlo and Judit Sturmann, Bob Cadman, and Steve Golden worked their magic to make everything easy.

Special thanks to my committee, whose care and meticulous attention to detail made this dissertation better for having their scrutiny. Hal McAlister, my advisor, whose help and guidance made this project possible; Theo ten Brummelaar, who always seemed to leave the mountain as I got there but was a great support; Doug Gies, whose advice turned a loosely-bound collection of data and facts into something re-

sembling a dissertation; Todd Henry, whose high expectations made me work harder; and Nikolaus Dietz, who graciously gave his time and attention to this dissertation.

Several people here at GSU made the writing process worlds easier: Alvin Das, who wrote the general dissertation template; Kevin Marshall, whose table-making script came in extremely handy; and Rajesh Deo, who kept the computers and network running, no small undertaking.

This research has made use of the *SIMBAD* database, operated at CDS, Strasbourg, France and the *VizieR Service* (Ochsenbein et al. 2000). This research also made use of data products from the Two Micron All Sky Survey, which is a joint project of the University of Massachusetts and the Infrared Processing and Analysis Center/California Institute of Technology, funded by the National Aeronautics and Space Administration and the National Science Foundation.

Contents

| | |
|---|--------------|
| Acknowledgments | v |
| Tables | xv |
| Figures | xviii |
| Abbreviations and Acronyms | xl |
| 1 Introduction | 1 |
| 1.1 Exoplanets Background | 1 |
| 1.2 Unknown Inclinations | 3 |
| 1.3 Stars Mimicking Planets | 6 |
| 1.4 Case Study: 51 Pegasi | 8 |
| 2 Long-Baseline Interferometry and the CHARA Array | 9 |
| 2.1 Basic Interferometry | 9 |
| 2.2 Early Interferometry | 11 |
| 2.3 Young's Double Slit Experiment | 12 |
| 2.4 Fringe Visibility | 14 |
| 2.5 Past and Present Interferometers | 18 |
| 2.6 The CHARA Array | 21 |
| 3 Method | 26 |
| 3.1 Calibrator Stars | 26 |
| 3.2 Baselines Used | 29 |

| | | |
|----------|--|-----------|
| 3.3 | Data Reduction Pipeline | 31 |
| 3.3.1 | Visibility Calculation | 32 |
| 3.3.2 | Visibility Calibration | 34 |
| 4 | Observations | 36 |
| 4.1 | Stellar and Planetary Parameters | 36 |
| 4.2 | Observing Log | 43 |
| 4.3 | Individual Target Data Format | 45 |
| 5 | Exoplanet Host Star Angular Diameters | 49 |
| 5.1 | Angular Diameter Calculation | 49 |
| 5.2 | Effect of the Limb-Darkening Coefficient | 56 |
| 5.3 | Stellar Diameters: Intermediate vs. Long Baseline Measurements | 57 |
| 5.4 | Estimated vs. Measured Stellar Diameters | 59 |
| 6 | Transiting Planet: HD 189733 | 61 |
| 6.1 | Introduction | 61 |
| 6.2 | Observations and Data Reduction | 62 |
| 6.3 | Diameter Fit | 65 |
| 6.4 | Estimate of the Angular Size of HD 189733 | 66 |
| 6.5 | Discussion | 70 |
| 6.6 | Non-Detection of Duplicity of HD 189733 | 71 |
| 6.7 | Conclusion | 71 |
| 7 | Searching for Stellar Companions | 74 |
| 7.1 | Previous Speckle Observations | 74 |
| 7.2 | Visibility Curve Variations | 75 |
| 7.3 | Separated Fringe Packets | 91 |
| 7.4 | Stellar Misfits | 102 |

| | | |
|----------|---|------------|
| 7.4.1 | <i>v</i> Andromedae | 102 |
| 7.4.2 | ρ Coronae Borealis | 106 |
| 8 | Discussion | 113 |
| 8.1 | Comparing Stellar Radii | 113 |
| 8.2 | Exoplanet Host Star Age | 114 |
| 8.2.1 | Stellar Evolution Model | 115 |
| 8.2.2 | New Mass and Age Estimates | 121 |
| 8.3 | General Conclusions and Future Work | 132 |
| | References | 134 |
| | Appendices | 145 |
| | A Spectral Energy Distribution Fits - Exoplanet Host Stars | 146 |
| | B Spectral Energy Distribution Fits - Calibrator Stars | 162 |
| | C Notes on Individual Targets | 182 |
| C.1 | HD 3651 | 182 |
| C.1.1 | Calibrated Visibilities | 182 |
| C.1.2 | Nightly Data Plots | 183 |
| C.1.3 | Diameter Calculation | 185 |
| C.1.4 | SFP Search | 185 |
| C.2 | HD 9826 | 188 |
| C.2.1 | Calibrated Visibilities | 188 |
| C.2.2 | Nightly Data Plots | 190 |
| C.2.3 | Diameter Calculation | 195 |
| C.2.4 | SFP Search | 195 |
| C.3 | HD 10697 | 200 |
| C.3.1 | Calibrated Visibilities | 200 |
| C.3.2 | Nightly Data Plots | 200 |

| | | |
|-------|-----------------------------------|-----|
| C.3.3 | Diameter Calculation | 203 |
| C.3.4 | SFP Search | 204 |
| C.4 | HD 11964 | 206 |
| C.4.1 | Calibrated Visibilities | 206 |
| C.4.2 | Nightly Data Plots | 206 |
| C.4.3 | Diameter Calculation | 209 |
| C.4.4 | SFP Search | 209 |
| C.5 | HD 13189 | 212 |
| C.5.1 | Calibrated Visibilities | 212 |
| C.5.2 | Nightly Data Plots | 212 |
| C.5.3 | Diameter Calculation | 214 |
| C.5.4 | SFP Search | 214 |
| C.5.5 | Companion Check | 215 |
| C.6 | HD 16141 | 217 |
| C.6.1 | Calibrated Visibilities | 217 |
| C.6.2 | Nightly Data Plots | 218 |
| C.6.3 | Diameter Calculation | 221 |
| C.6.4 | SFP Search | 221 |
| C.7 | HD 19994 | 225 |
| C.7.1 | Calibrated Visibilities | 225 |
| C.7.2 | Nightly Data Plots | 226 |
| C.7.3 | Diameter Calculation | 228 |
| C.7.4 | SFP Search | 228 |
| C.8 | HD 20367 | 231 |
| C.8.1 | Calibrated Visibilities | 231 |
| C.8.2 | Nightly Data Plots | 231 |
| C.8.3 | Diameter Calculation | 234 |
| C.8.4 | SFP Search | 234 |
| C.9 | HD 34445 | 237 |

| | | |
|--------|-----------------------------------|-----|
| C.9.1 | Calibrated Visibilities | 237 |
| C.9.2 | Nightly Data Plots | 237 |
| C.9.3 | Diameter Calculation | 239 |
| C.9.4 | SFP Search | 240 |
| C.10 | HD 38529 | 242 |
| C.10.1 | Calibrated Visibilities | 242 |
| C.10.2 | Nightly Data Plots | 243 |
| C.10.3 | Diameter Calculation | 246 |
| C.10.4 | SFP Search | 246 |
| C.11 | HD 50554 | 250 |
| C.11.1 | Calibrated Visibilities | 250 |
| C.11.2 | Nightly Data Plots | 250 |
| C.11.3 | Diameter Calculation | 253 |
| C.11.4 | SFP Search | 253 |
| C.12 | HD 59686 | 256 |
| C.12.1 | Calibrated Visibilities | 256 |
| C.12.2 | Nightly Data Plots | 257 |
| C.12.3 | Diameter Calculation | 259 |
| C.12.4 | SFP Search | 259 |
| C.13 | HD 75732 | 262 |
| C.13.1 | Calibrated Visibilities | 262 |
| C.13.2 | Nightly Data Plots | 262 |
| C.13.3 | Diameter Calculation | 264 |
| C.13.4 | SFP Search | 265 |
| C.14 | HD 95128 | 267 |
| C.14.1 | Calibrated Visibilities | 267 |
| C.14.2 | Nightly Data Plots | 268 |
| C.14.3 | SFP Search | 268 |
| C.15 | HD 104985 | 270 |

| | | |
|--------|-----------------------------------|-----|
| C.15.1 | Calibrated Visibilities | 270 |
| C.15.2 | Nightly Data Plots | 271 |
| C.15.3 | Diameter Calculation | 272 |
| C.15.4 | SFP Search | 273 |
| C.16 | HD 117176 | 275 |
| C.16.1 | Calibrated Visibilities | 275 |
| C.16.2 | Nightly Data Plots | 276 |
| C.16.3 | Diameter Calculation | 279 |
| C.16.4 | SFP Search | 280 |
| C.17 | HD 120136 | 284 |
| C.17.1 | Calibrated Visibilities | 284 |
| C.17.2 | Nightly Data Plots | 285 |
| C.17.3 | Diameter Calculation | 289 |
| C.17.4 | SFP Search | 290 |
| C.18 | HD 128311 | 294 |
| C.18.1 | Calibrated Visibilities | 294 |
| C.18.2 | Nightly Data Plots | 294 |
| C.18.3 | Diameter Calculation | 296 |
| C.18.4 | SFP Search | 297 |
| C.19 | HD 143761 | 299 |
| C.19.1 | Calibrated Visibilities | 299 |
| C.19.2 | Nightly Data Plots | 300 |
| C.19.3 | Diameter Calculation | 306 |
| C.19.4 | SFP Search | 306 |
| C.20 | HD 145675 | 311 |
| C.20.1 | Calibrated Visibilities | 311 |
| C.20.2 | Nightly Data Plots | 312 |
| C.20.3 | Diameter Calculation | 316 |
| C.20.4 | SFP Search | 317 |

| | |
|--|-----|
| C.20.5 Notes | 321 |
| C.21 HD 168443 | 322 |
| C.21.1 Calibrated Visibilities | 322 |
| C.21.2 Nightly Data Plots | 322 |
| C.21.3 Diameter Calculation | 326 |
| C.21.4 SFP Search | 327 |
| C.21.5 Notes | 330 |
| C.22 HD 177830 | 331 |
| C.22.1 Calibrated Visibilities | 331 |
| C.22.2 Nightly Data Plots | 332 |
| C.22.3 Diameter Calculation | 336 |
| C.22.4 SFP Search | 336 |
| C.23 HD 186427 | 340 |
| C.23.1 Calibrated Visibilities | 340 |
| C.23.2 Nightly Data Plots | 341 |
| C.23.3 Diameter Calculation | 343 |
| C.23.4 SFP Search | 344 |
| C.24 HD 190228 | 346 |
| C.24.1 Calibrated Visibilities | 346 |
| C.24.2 Nightly Data Plots | 347 |
| C.24.3 Diameter Calculation | 349 |
| C.24.4 SFP Search | 349 |
| C.25 HD 190360 | 352 |
| C.25.1 Calibrated Visibilities | 352 |
| C.25.2 Nightly Data Plots | 353 |
| C.25.3 Diameter Calculation | 355 |
| C.25.4 SFP Search | 356 |
| C.26 HD 192263 | 358 |
| C.26.1 Calibrated Visibilities | 358 |

| | |
|--|-----|
| C.26.2 Nightly Data Plots | 358 |
| C.26.3 SFP Search | 359 |
| C.27 HD 195019 | 360 |
| C.27.1 Calibrated Visibilities | 360 |
| C.27.2 Nightly Data Plots | 361 |
| C.27.3 Diameter Calculation | 364 |
| C.27.4 SFP Search | 364 |
| C.28 HD 196885 | 366 |
| C.28.1 Calibrated Visibilities | 366 |
| C.28.2 Nightly Data Plots | 367 |
| C.28.3 Diameter Calculation | 369 |
| C.28.4 SFP Search | 370 |
| C.29 HD 217014 | 373 |
| C.29.1 Calibrated Visibilities | 373 |
| C.29.2 Nightly Data Plots | 374 |
| C.29.3 Diameter Calculation | 376 |
| C.29.4 SFP Search | 377 |
| C.30 HD 217107 | 379 |
| C.30.1 Calibrated Visibilities | 379 |
| C.30.2 Nightly Data Plots | 379 |
| C.30.3 Diameter Calculation | 381 |
| C.30.4 SFP Search | 382 |

Tables

| | | |
|-----|--|----|
| 2.1 | Past and Present Interferometers | 19 |
| 2.2 | CHARA Baselines | 25 |
| 3.1 | Unreliable Calibrators | 27 |
| 4.1 | Basic Parameters for Exoplanet Host Stars | 37 |
| 4.2 | Basic Parameters for Calibrator Stars | 39 |
| 4.3 | Planetary Orbital Parameters | 41 |
| 4.4 | Observing Log | 43 |
| 4.5 | Symbols Used in Visibility Plots | 46 |
| 5.1 | Exoplanet Host Star Diameter Measurements | 52 |
| 5.2 | Past and Present Radius Determinations | 54 |
| 5.3 | Long vs. Intermediate-Baseline Diameter Measurements | 57 |
| 6.1 | Interferometric Measurements of HD 189733 | 63 |
| 6.2 | SED Fits for HD 189733 Photometry | 69 |
| 7.1 | Exoplanet Host Star Duplicity: Results from Speckle Interferometry | 75 |
| 7.2 | Exoplanet Host Star Observed Parameters | 81 |
| 7.3 | Possible Secondary Type Parameters | 83 |
| 7.4 | Calculated Secondary Star Angular Diameters | 85 |
| 7.5 | Companion Check: Comparing Visibility Residuals | 88 |

| | | |
|------|--|-----|
| 7.6 | Non-Detection Threshold for SFPs Assuming $\Delta K = 3.0$ Limit for All Stars | 99 |
| 7.7 | Stars Exhibiting Asymmetries in the Weighted Mean Fringe Envelope | 101 |
| 8.1 | Age Determination | 118 |
| 8.2 | Stellar Age Comparison | 120 |
| 8.3 | Mass' Effect on Age Determinations | 122 |
| 8.4 | New Stellar Mass and Age | 130 |
| C.1 | HD 3651: Calibrated Visibilities | 182 |
| C.2 | HD 9826: Calibrated Visibilities | 188 |
| C.3 | HD 10697: Calibrated Visibilities | 200 |
| C.4 | HD 11964: Calibrated Visibilities | 206 |
| C.5 | HD 13189: Calibrated Visibilities | 212 |
| C.6 | HD 16141: Calibrated Visibilities | 217 |
| C.7 | HD 19994: Calibrated Visibilities | 225 |
| C.8 | HD 20367: Calibrated Visibilities | 231 |
| C.9 | HD 34445: Calibrated Visibilities | 237 |
| C.10 | HD 38529: Calibrated Visibilities | 242 |
| C.11 | HD 50554: Calibrated Visibilities | 250 |
| C.12 | HD 59686: Calibrated Visibilities | 256 |
| C.13 | HD 75732: Calibrated Visibilities | 262 |
| C.14 | HD 95128: Calibrated Visibilities | 267 |
| C.15 | HD 104985: Calibrated Visibilities | 270 |
| C.16 | HD 117176: Calibrated Visibilities | 275 |
| C.17 | HD 120136: Calibrated Visibilities | 284 |
| C.18 | HD 128311: Calibrated Visibilities | 294 |

| | |
|---|-----|
| C.19 HD 143761: Calibrated Visibilities (all but 2006/05/12) | 299 |
| C.20 HD 143761: Calibrated Visibilities (from 2006/05/12 using calibrator HD 143681) | 300 |
| C.21 HD 143761: Calibrated Visibilities (from 2006/05/12 using calibrator HD 146025) | 300 |
| C.22 HD 145675: Calibrated Visibilities | 311 |
| C.23 HD 168443: Calibrated Visibilities | 322 |
| C.24 HD 177830: Calibrated Visibilities | 331 |
| C.25 HD 186427: Calibrated Visibilities | 340 |
| C.26 HD 190228: Calibrated Visibilities | 346 |
| C.27 HD 190360: Calibrated Visibilities | 352 |
| C.28 HD 192263: Calibrated Visibilities | 358 |
| C.29 HD 195019: Calibrated Visibilities | 360 |
| C.30 HD 196885: Calibrated Visibilities | 366 |
| C.31 HD 217014: Calibrated Visibilities | 373 |
| C.32 HD 217107: Calibrated Visibilities | 379 |

Figures

| | | |
|-----|--|----|
| 1.1 | Cumulative probability vs. inclination | 6 |
| 2.1 | Schematic of a basic interferometer | 10 |
| 2.2 | Schematic of Michelson's interferometer | 12 |
| 2.3 | Young's double slit experiment setup | 13 |
| 2.4 | Building an interferometric fringe | 14 |
| 2.5 | The effect of various Δm on the visibility curve for a binary system . | 17 |
| 2.6 | The effect of various projected stellar separations on the visibility curve for a binary system | 17 |
| 2.7 | The effect of various stellar angular diameters on the visibility curve . | 18 |
| 2.8 | The CHARA Array and its surroundings | 22 |
| 2.9 | The CHARA Array's telescope configuration | 23 |
| 3.1 | Examples of a good and a bad calibrators' SEDs | 30 |
| 3.2 | Example baseline vs. baseline position angle plot | 31 |
| 3.3 | Example data scan | 32 |
| 3.4 | Normalizing fringes | 34 |
| 3.5 | Example of visibility calibration | 35 |
| 4.1 | Example of nightly visibility plots | 48 |
| 5.1 | Comparing linear radii: Ribas et al. (2003) vs. interferometric mea- surements | 55 |

| | | |
|------|--|----|
| 5.2 | Comparing linear radii: Ramírez & Meléndez (2005) vs. interferometric measurements | 55 |
| 5.3 | Comparing linear radii: Fischer & Valenti (2005) vs. interferometric measurements | 56 |
| 5.4 | HD 190360: Calibrated visibility vs. baseline using the diameter measured from W1-W2 observations. | 58 |
| 5.5 | HD 190360: Calibrated visibility vs. baseline using the diameter measured from S1-E1 observations. | 59 |
| 5.6 | Comparing estimated SED diameters and measured LD diameters . . | 60 |
| 6.1 | SED fit for calibrator HD 190993 | 64 |
| 6.2 | The χ^2 fit to HD 189733's visibilities | 66 |
| 6.3 | SED fits of HD 189733 | 73 |
| 7.1 | Example of systematics in a single-star's visibility residuals | 76 |
| 7.2 | Example of systematics in a binary system's visibility residuals | 76 |
| 7.3 | Example of tracking indicative of a single star | 77 |
| 7.4 | Example of tracking indicative of a binary system | 78 |
| 7.5 | Example of single star visibility curve vs. binary star visibility curve. | 87 |
| 7.6 | Companion check: Eliminating companion spectral types | 90 |
| 7.7 | Example SFP for a $\Delta K=0$ binary system | 91 |
| 7.8 | Example SFP for a $\Delta K=2$ binary system | 92 |
| 7.9 | Searching for SFPs: Example of a weighted mean fringe envelope for a single star | 93 |
| 7.10 | Searching for SFPs: Example of a weighted mean fringe envelope for a binary system | 94 |
| 7.11 | Simulated SFPs: $\Delta K = 0.0$ to 0.75 | 96 |
| 7.12 | Simulated SFPs: $\Delta K = 1.0$ to 1.75 | 97 |
| 7.13 | Simulated SFPs: $\Delta K = 2.0$ to 2.75 | 97 |

| | | |
|------|---|-----|
| 7.14 | Simulated SFPs: $\Delta K = 3.0$ to 3.75 | 98 |
| 7.15 | Example of additional peaks in the mean fringe envelope | 100 |
| 7.16 | Example of smooth mean fringe envelope | 100 |
| 7.17 | HD 9826: Plots for 2005/08/10 data | 103 |
| 7.18 | HD 9826: Visibility vs. epoch for 2005/08/04 data with NIRO align- ments marked | 104 |
| 7.19 | HD 9826: Visibility vs. epoch for 2005/08/08 data with NIRO align- ments marked | 104 |
| 7.20 | HD 9826: Visibility vs. epoch for 2005/08/10 data with NIRO align- ments marked | 105 |
| 7.21 | HD 9826: Visibility vs. epoch for 2005/08/14 data with NIRO align- ment marked | 105 |
| 7.22 | HD 9826: Visibility vs. epoch for 2005/08/18 data with NIRO align- ments marked | 105 |
| 7.23 | HD 143761: Plots for 2005/06/29 data (calibrator HD 143393) | 108 |
| 7.24 | HD 143761: Plots for 2005/07/03 data (calibrator HD 143393) | 109 |
| 7.25 | HD 143761: Plots for 2006/05/12 data (calibrator HD 143687) | 109 |
| 7.26 | HD 143761: Plots for 2006/05/12 data (calibrator HD 146025) | 110 |
| 7.27 | HD 143761: Plots for 2006/05/19 data (calibrator HD 136849) | 110 |
| 7.28 | HD 143761: Visibility vs. epoch for 2005/06/29 data with NIRO align- ments marked | 112 |
| 7.29 | HD 143761: Visibility vs. epoch for 2006/05/12 data with NIRO align- ments marked | 112 |
| 7.30 | HD 143761: Visibility vs. epoch for 2006/05/12 data with the NIRO alignment marked | 112 |
| 8.1 | Log R vs. color index: Past and present stellar diameters | 114 |
| 8.2 | HD 3651: Determining stellar mass and age | 123 |
| 8.3 | HD 9826: Determining stellar mass and age | 123 |

| | | |
|------|---|-----|
| 8.4 | HD 19994: Determining stellar mass and age | 124 |
| 8.5 | HD 38529: Determining stellar mass and age | 124 |
| 8.6 | HD 59686: Determining stellar mass and age | 125 |
| 8.7 | HD 75732: Determining stellar mass and age | 125 |
| 8.8 | HD 104985: Determining stellar mass and age | 126 |
| 8.9 | HD 117176: Determining stellar mass and age | 126 |
| 8.10 | HD 120136: Determining stellar mass and age | 127 |
| 8.11 | HD 143761: Determining stellar mass and age | 127 |
| 8.12 | HD 189733: Determining stellar mass and age | 128 |
| 8.13 | HD 190360: Determining stellar mass and age | 128 |
| 8.14 | HD 196885: Determining stellar mass and age | 129 |
| 8.15 | HD 217014: Determining stellar mass and age | 129 |
| 8.16 | New vs. old stellar masses | 131 |
| A.1 | HD 3651 SED fit | 146 |
| A.2 | HD 9826 SED fit | 147 |
| A.3 | HD 10697 SED fit | 147 |
| A.4 | HD 11964 SED fit | 148 |
| A.5 | HD 13189 SED fit | 148 |
| A.6 | HD 16141 SED fit | 149 |
| A.7 | HD 19994 SED fit | 149 |
| A.8 | HD 20367 SED fit | 150 |
| A.9 | HD 34445 SED fit | 150 |
| A.10 | HD 38529 SED fit | 151 |
| A.11 | HD 50554 SED fit | 151 |
| A.12 | HD 59686 SED fit | 152 |

| | |
|----------------------------------|-----|
| A.13 HD 75732 SED fit | 152 |
| A.14 HD 95128 SED fit | 153 |
| A.15 HD 104985 SED fit | 153 |
| A.16 HD 117176 SED fit | 154 |
| A.17 HD 120136 SED fit | 154 |
| A.18 HD 128311 SED fit | 155 |
| A.19 HD 143761 SED fit | 155 |
| A.20 HD 145675 SED fit | 156 |
| A.21 HD 168443 SED fit | 156 |
| A.22 HD 177830 SED fit | 157 |
| A.23 HD 186427 SED fit | 157 |
| A.24 HD 189733 SED fit | 158 |
| A.25 HD 190228 SED fit | 158 |
| A.26 HD 190360 SED fit | 159 |
| A.27 HD 192263 SED fit | 159 |
| A.28 HD 195019 SED fit | 160 |
| A.29 HD 196885 SED fit | 160 |
| A.30 HD 217014 SED fit | 161 |
| A.31 HD 217107 SED fit | 161 |
| B.1 HD 4568 SED fit | 162 |
| B.2 HD 6920 SED fit | 163 |
| B.3 HD 8671 SED fit | 163 |
| B.4 HD 10477 SED fit | 164 |
| B.5 HD 11007 SED fit | 164 |
| B.6 HD 13456 SED fit | 165 |

| | | |
|------|-----------------------------|-----|
| B.7 | HD 13555 SED fit | 165 |
| B.8 | HD 14690 SED fit | 166 |
| B.9 | HD 16824 SED fit | 166 |
| B.10 | HD 19411 SED fit | 167 |
| B.11 | HD 21864 SED fit | 167 |
| B.12 | HD 31423 SED fit | 168 |
| B.13 | HD 42398 SED fit | 168 |
| B.14 | HD 43318 SED fit | 169 |
| B.15 | HD 49736 SED fit | 169 |
| B.16 | HD 61630 SED fit | 170 |
| B.17 | HD 72779 SED fit | 170 |
| B.18 | HD 90840 SED fit | 171 |
| B.19 | HD 97619 SED fit | 171 |
| B.20 | HD 119350 SED fit | 172 |
| B.21 | HD 121107 SED fit | 172 |
| B.22 | HD 125194 SED fit | 173 |
| B.23 | HD 136849 SED fit | 173 |
| B.24 | HD 143393 SED fit | 174 |
| B.25 | HD 143687 SED fit | 174 |
| B.26 | HD 144015 SED fit | 175 |
| B.27 | HD 146025 SED fit | 175 |
| B.28 | HD 151044 SED fit | 176 |
| B.29 | HD 169370 SED fit | 176 |
| B.30 | HD 173093 SED fit | 177 |
| B.31 | HD 176377 SED fit | 177 |

| | |
|---|-----|
| B.32 HD 176939 SED fit | 178 |
| B.33 HD 184960 SED fit | 178 |
| B.34 HD 188350 SED fit | 179 |
| B.35 HD 189108 SED fit | 179 |
| B.36 HD 190470 SED fit | 180 |
| B.37 HD 194012 SED fit | 180 |
| B.38 HD 216953 SED fit | 181 |
| B.39 HD 218261 SED fit | 181 |
| C.1 HD 3651: Long baseline plots for 2005/10/22 data | 183 |
| C.2 HD 3651: Long baseline plots for 2005/10/24 data | 183 |
| C.3 HD 3651: Long baseline plots for 2005/12/14 data | 184 |
| C.4 HD 3651: All data - Baseline vs. baseline position angle | 184 |
| C.5 HD 3651: LD disk diameter fit | 185 |
| C.6 HD 3651: SFP inspection for 2005/10/22 data | 185 |
| C.7 HD 3651: SFP inspection for 2005/10/24 data | 186 |
| C.8 HD 3651: SFP inspection for 2005/12/14 data | 186 |
| C.9 HD 4568: SFP inspection for 2005/10/22 data | 186 |
| C.10 HD 4568: SFP inspection for 2005/10/24 data | 187 |
| C.11 HD 4568: SFP inspection for 2005/12/14 data | 187 |
| C.12 HD 9826: Intermediate baseline plots for 2005/08/04 data | 191 |
| C.13 HD 9826: Intermediate baseline plots for 2005/08/08 data | 191 |
| C.14 HD 9826: Intermediate baseline plots for 2005/08/10 data | 192 |
| C.15 HD 9826: Intermediate baseline plots for 2005/08/14 data | 192 |
| C.16 HD 9826: Intermediate baseline plots for 2005/08/18 data | 193 |
| C.17 HD 9826: Intermediate baseline plots for 2005/08/19 data | 193 |

| | |
|--|-----|
| C.18 HD 9826: All data - Baseline vs. baseline position angle (using calibrator HD 6920) | 194 |
| C.19 HD 9826: All data - Baseline vs. baseline position angle (using calibrator HD 8671) | 194 |
| C.20 HD 9826: LD disk diameter fit | 195 |
| C.21 HD 9826: SFP inspection for 2005/08/04 data | 195 |
| C.22 HD 9826: SFP inspection for 2005/08/08 data | 196 |
| C.23 HD 9826: SFP inspection for 2005/08/10 data | 196 |
| C.24 HD 9826: SFP inspection for 2005/08/14 data | 196 |
| C.25 HD 9826: SFP inspection for 2005/08/18 data | 197 |
| C.26 HD 9826: SFP inspection for 2005/08/19 data | 197 |
| C.27 HD 6920: SFP inspection for 2005/08/04 data | 197 |
| C.28 HD 6920: SFP inspection for 2005/08/08 data | 198 |
| C.29 HD 6920: SFP inspection for 2005/08/14 data | 198 |
| C.30 HD 8671: SFP inspection for 2005/08/10 data | 198 |
| C.31 HD 8671: SFP inspection for 2005/08/18 data | 199 |
| C.32 HD 8671: SFP inspection for 2005/08/19 data | 199 |
| C.33 HD 10697: Long baseline plots for 2005/10/23 data | 201 |
| C.34 HD 10697: Long baseline plots for 2006/08/12 data | 201 |
| C.35 HD 10697: All data - Baseline vs. baseline position angle (using calibrator HD 10477) | 202 |
| C.36 HD 10697: All data - Baseline vs. baseline position angle (using calibrator HD 13555) | 202 |
| C.37 HD 10697: LD disk diameter fit | 203 |
| C.38 HD 10697: SFP inspection for 2005/10/23 data | 204 |
| C.39 HD 10697: SFP inspection for 2006/08/12 data | 204 |
| C.40 HD 10477: SFP inspection for 2005/10/23 data | 204 |

| | |
|--|-----|
| C.41 HD 13555: SFP inspection for 2006/08/12 data | 205 |
| C.42 HD 11964: Intermediate baseline plots for 2005/12/13 data | 207 |
| C.43 HD 11964: Intermediate baseline plots for 2005/12/16 data | 207 |
| C.44 HD 11964: Intermediate baseline plots for 2006/10/20 data | 208 |
| C.45 HD 11964: All data - Baseline vs. baseline position angle | 208 |
| C.46 HD 11964: LD disk diameter fit | 209 |
| C.47 HD 11964: SFP inspection for 2005/12/13 data | 209 |
| C.48 HD 11964: SFP inspection for 2005/12/16 data | 210 |
| C.49 HD 11964: SFP inspection for 2006/10/20 data | 210 |
| C.50 HD 13456: SFP inspection for 2005/12/13 data | 210 |
| C.51 HD 13456: SFP inspection for 2005/12/16 data | 211 |
| C.52 HD 13456: SFP inspection for 2006/10/20 data | 211 |
| C.53 HD 13189: Long baseline plots for 2005/12/12 data | 212 |
| C.54 HD 13189: Long baseline plots for 2006/08/14 data | 213 |
| C.55 HD 13189: All data - Baseline vs. baseline position angle | 213 |
| C.56 HD 13189: LD disk diameter fit | 214 |
| C.57 HD 13189: SFP inspection for 2005/12/12 data | 214 |
| C.58 HD 13189: SFP inspection for 2006/08/14 data | 215 |
| C.59 HD 11007: SFP inspection for 2005/12/12 data | 215 |
| C.60 HD 11007: SFP inspection for 2006/08/14 data | 215 |
| C.61 HD 16141: Long baseline plots for 2005/12/12 data | 218 |
| C.62 HD 16141: Intermediate baseline plots for 2005/12/14 data | 218 |
| C.63 HD 16141: Long baseline plots for 2006/08/13 data | 219 |
| C.64 HD 16141: Long baseline plots for 2006/08/14 data | 219 |

| | |
|--|-----|
| C.65 HD 16141: All data - Baseline vs. baseline position angle (using calibrator HD 14690) | 220 |
| C.66 HD 16141: All data - Baseline vs. baseline position angle (using calibrator HD 16824) | 220 |
| C.67 HD 16141: LD disk diameter fit | 221 |
| C.68 HD 16141: SFP inspection for 2005/12/12 data | 221 |
| C.69 HD 16141: SFP inspection for 2005/12/14 data | 222 |
| C.70 HD 16141: SFP inspection for 2006/08/13 data | 222 |
| C.71 HD 16141: SFP inspection for 2006/08/14 data | 222 |
| C.72 HD 16824: SFP inspection for 2005/12/12 data | 223 |
| C.73 HD 16824: SFP inspection for 2005/12/14 data | 223 |
| C.74 HD 14690: SFP inspection for 2006/08/13 data | 223 |
| C.75 HD 14690: SFP inspection for 2006/08/14 data | 224 |
| C.76 HD 19994: Long baseline plots for 2005/10/21 data | 226 |
| C.77 HD 19994: Long baseline plots for 2005/10/27 data | 226 |
| C.78 HD 19994: Long baseline plots for 2005/12/10 data | 227 |
| C.79 HD 19994: All data - Baseline vs. baseline position angle | 227 |
| C.80 HD 19994: LD disk diameter fit | 228 |
| C.81 HD 19994: SFP inspection for 2005/10/21 data | 228 |
| C.82 HD 19994: SFP inspection for 2005/10/27 data | 229 |
| C.83 HD 19994: SFP inspection for 2005/12/10 data | 229 |
| C.84 HD 19411: SFP inspection for 2005/10/21 data | 229 |
| C.85 HD 19411: SFP inspection for 2005/10/27 data | 230 |
| C.86 HD 19411: SFP inspection for 2005/12/10 data | 230 |
| C.87 HD 20367: Long baseline plots for 2005/12/12 data | 232 |
| C.88 HD 20367: Long baseline plots for 2007/01/24 data | 232 |

| | |
|---|-----|
| C.89 HD 20367: Long baseline plots for 2007/02/05 data | 233 |
| C.90 HD 20367: All data - Baseline vs. baseline position angle | 233 |
| C.91 HD 20367: LD disk diameter fit | 234 |
| C.92 HD 20367: SFP inspection for 2005/12/12 data | 234 |
| C.93 HD 20367: SFP inspection for 2007/01/24 data | 235 |
| C.94 HD 20367: SFP inspection for 2007/02/05 data | 235 |
| C.95 HD 21864: SFP inspection for 2005/12/12 data | 235 |
| C.96 HD 21864: SFP inspection for 2007/01/24 data | 236 |
| C.97 HD 21864: SFP inspection for 2007/02/05 data | 236 |
| C.98 HD 34445: Long baseline plots for 2005/12/07 data | 238 |
| C.99 HD 34445: Long baseline plots for 2005/12/10 data | 238 |
| C.100 HD 34445: All data - Baseline vs. baseline position angle | 239 |
| C.101 HD 34445: LD disk diameter fit | 240 |
| C.102 HD 34445: SFP inspection for 2005/12/07 data | 240 |
| C.103 HD 34445: SFP inspection for 2005/12/10 data | 241 |
| C.104 HD 31423: SFP inspection for 2005/12/07 data | 241 |
| C.105 HD 31423: SFP inspection for 2005/12/10 data | 241 |
| C.106 HD 38529: Long baseline plots for 2005/10/22 data | 243 |
| C.107 HD 38529: Long baseline plots for 2005/10/24 data | 244 |
| C.108 HD 38529: Long baseline plots for 2005/12/06 data | 244 |
| C.109 HD 38529: Intermediate baseline plots for 2005/12/14 data | 245 |
| C.110 HD 38529: All data - Baseline vs. baseline position angle | 245 |
| C.111 HD 38529: LD disk diameter fit | 246 |
| C.112 HD 38529: SFP inspection for 2005/10/22 data | 246 |
| C.113 HD 38529: SFP inspection for 2005/10/24 data | 247 |

| | |
|--|-----|
| C.114 HD 38529: SFP inspection for 2005/12/06 data | 247 |
| C.115 HD 38529: SFP inspection for 2005/12/14 data | 247 |
| C.116 HD 43318: SFP inspection for 2005/10/22 data | 248 |
| C.117 HD 43318: SFP inspection for 2005/10/24 data | 248 |
| C.118 HD 43318: SFP inspection for 2005/12/06 data | 248 |
| C.119 HD 43318: SFP inspection for 2005/12/14 data | 249 |
| C.120 HD 50554: Long baseline plots for 2005/12/07 data | 251 |
| C.121 HD 50554: Long baseline plots for 2005/12/12 data | 251 |
| C.122 HD 50554: Long baseline plots for 2007/02/06 data | 252 |
| C.123 HD 50554: All data - Baseline vs. baseline position angle (using calibrator HD 49736) | 252 |
| C.124 HD 50554: LD disk diameter fit | 253 |
| C.125 HD 50554: SFP inspection for 2005/12/07 data | 253 |
| C.126 HD 50554: SFP inspection for 2005/12/12 data | 254 |
| C.127 HD 50554: SFP inspection for 2007/02/06 data | 254 |
| C.128 HD 49736: SFP inspection for 2005/12/07 data | 254 |
| C.129 HD 49736: SFP inspection for 2005/12/12 data | 255 |
| C.130 HD 42398: SFP inspection for 2007/02/06 data | 255 |
| C.131 HD 59686: Long baseline plots for 2005/12/06 data | 257 |
| C.132 HD 59686: Intermediate baseline plots for 2005/12/16 data | 257 |
| C.133 HD 59686: Long baseline plots for 2007/04/02 data | 258 |
| C.134 HD 59686: All data - Baseline vs. baseline position angle | 258 |
| C.135 HD 59686: LD disk diameter fit | 259 |
| C.136 HD 59686: SFP inspection for 2005/12/06 data | 259 |
| C.137 HD 59686: SFP inspection for 2005/12/16 data | 260 |

| | |
|--|-----|
| C.138 HD 59686: SFP inspection for 2007/04/02 data | 260 |
| C.139 HD 61630: SFP inspection for 2005/12/06 data | 260 |
| C.140 HD 61630: SFP inspection for 2005/12/16 data | 261 |
| C.141 HD 61630: SFP inspection for 2007/04/02 data | 261 |
| C.142 HD 75732: Long baseline plots for 2007/03/26 data | 263 |
| C.143 HD 75732: Long baseline plots for 2007/03/30 data | 263 |
| C.144 HD 75732: All data - Baseline vs. baseline position angle | 264 |
| C.145 HD 75732: LD disk diameter fit | 264 |
| C.146 HD 75732: SFP inspection for 2007/03/26 data | 265 |
| C.147 HD 75732: SFP inspection for 2007/03/30 data | 265 |
| C.148 HD 72779: SFP inspection for 2007/03/26 data | 265 |
| C.149 HD 72779: SFP inspection for 2007/03/30 data | 266 |
| C.150 HD 95128: Long baseline plots for 2006/05/19 data | 268 |
| C.151 HD 95128: SFP inspection for 2006/05/19 data | 268 |
| C.152 HD 90840: SFP inspection for 2006/05/19 data | 269 |
| C.153 HD 104985: Intermediate baseline plots for 2006/05/17 data | 271 |
| C.154 HD 104985: Intermediate baseline plots for 2007/04/26 data | 271 |
| C.155 HD 104985: All data - Baseline vs. baseline position angle | 272 |
| C.156 HD 104985: LD disk diameter fit | 272 |
| C.157 HD 104985: SFP inspection for 2006/05/17 data | 273 |
| C.158 HD 104985: SFP inspection for 2007/04/26 data | 273 |
| C.159 HD 97619: SFP inspection for 2006/05/17 data | 273 |
| C.160 HD 97619: SFP inspection for 2007/04/26 data | 274 |
| C.161 HD 117176: Intermediate baseline plots for 2005/05/14 data | 276 |
| C.162 HD 117176: Intermediate baseline plots for 2006/05/13 data | 277 |

| | |
|--|-----|
| C.163 HD 117176: Long baseline plots for 2006/05/20 data | 277 |
| C.164 HD 117176: Long baseline plots for 2007/04/02 data | 278 |
| C.165 HD 117176: All data - Baseline vs. baseline position angle (using calibrator HD 119350) | 278 |
| C.166 HD 117176: All data - Baseline vs. baseline position angle (using calibrator HD 121107) | 279 |
| C.167 HD 117176: LD disk diameter fit | 279 |
| C.168 HD 117176: SFP inspection for 2005/05/13 data | 280 |
| C.169 HD 117176: SFP inspection for 2005/05/14 data | 280 |
| C.170 HD 117176: SFP inspection for 2006/05/13 data | 280 |
| C.171 HD 117176: SFP inspection for 2006/05/20 data | 281 |
| C.172 HD 117176: SFP inspection for 2007/04/02 data | 281 |
| C.173 HD 119350: SFP inspection for 2005/05/13 data | 281 |
| C.174 HD 119350: SFP inspection for 2005/05/14 data | 282 |
| C.175 HD 121107: SFP inspection for 2006/05/13 data | 282 |
| C.176 HD 121107: SFP inspection for 2006/05/20 data | 282 |
| C.177 HD 121107: SFP inspection for 2007/04/02 data | 283 |
| C.178 HD 120136: Intermediate baseline plots for 2005/05/12 data | 286 |
| C.179 HD 120136: Intermediate baseline plots for 2006/05/14 data | 286 |
| C.180 HD 120136: Long baseline plots for 2007/02/05 data | 287 |
| C.181 HD 120136: Long baseline plots for 2007/03/25 data | 287 |
| C.182 HD 120136: Long baseline plots for 2007/03/26 data | 288 |
| C.183 HD 120136: Long baseline plots for 2007/03/30 data | 288 |
| C.184 HD 120136: All data - Baseline vs. baseline position angle | 289 |
| C.185 HD 120136: LD disk diameter fit | 289 |
| C.186 HD 120136: SFP inspection for 2005/05/12 data | 290 |

| | |
|--|-----|
| C.187 HD 120136: SFP inspection for 2006/05/14 data | 290 |
| C.188 HD 120136: SFP inspection for 2007/02/05 data | 290 |
| C.189 HD 120136: SFP inspection for 2007/03/25 data | 291 |
| C.190 HD 120136: SFP inspection for 2007/03/26 data | 291 |
| C.191 HD 120136: SFP inspection for 2007/03/30 data | 291 |
| C.192 HD 121107: SFP inspection for 2005/05/12 data | 292 |
| C.193 HD 121107: SFP inspection for 2006/05/14 data | 292 |
| C.194 HD 121107: SFP inspection for 2007/02/05 data | 292 |
| C.195 HD 121107: SFP inspection for 2007/03/25 data | 293 |
| C.196 HD 121107: SFP inspection for 2007/03/26 data | 293 |
| C.197 HD 121107: SFP inspection for 2007/03/30 data | 293 |
| C.198 HD 128311: Intermediate baseline plots for 2005/06/30 data | 294 |
| C.199 HD 128311: Intermediate baseline plots for 2006/05/16 data | 295 |
| C.200 HD 128311: All data - Baseline vs. baseline position angle | 295 |
| C.201 HD 128311: LD disk diameter fit | 296 |
| C.202 HD 128311: SFP inspection for 2005/06/30 data | 297 |
| C.203 HD 128311: SFP inspection for 2006/05/16 data | 297 |
| C.204 HD 125194: SFP inspection for 2005/06/30 data | 297 |
| C.205 HD 125194: SFP inspection for 2006/05/16 data | 298 |
| C.206 HD 143761: Intermediate baseline plots for 2005/06/29 data | 301 |
| C.207 HD 143761: Intermediate baseline plots for 2005/07/03 data | 301 |
| C.208 HD 143761: Intermediate baseline plots for 2006/05/12 data using calibrator HD 143687 | 302 |
| C.209 HD 143761: Intermediate baseline plots for 2006/05/12 data using calibrator HD 146025 | 302 |
| C.210 HD 143761: Long baseline plots for 2006/05/19 data | 303 |

| | |
|--|-----|
| C.211 HD 143761: Long baseline plots for 2006/06/09 data | 303 |
| C.212 HD 143761: All data - Baseline vs. baseline position angle (using calibrator HD 136849) | 304 |
| C.213 HD 143761: All data - Baseline vs. baseline position angle (using calibrator HD 143393) | 304 |
| C.214 HD 143761: All data - Baseline vs. baseline position angle (using calibrator HD 143687) | 305 |
| C.215 HD 143761: All data - Baseline vs. baseline position angle (using calibrator HD 146025) | 305 |
| C.216 HD 143761: LD disk diameter fit | 306 |
| C.217 HD 143761: SFP inspection for 2005/06/29 data | 306 |
| C.218 HD 143761: SFP inspection for 2005/07/03 data | 307 |
| C.219 HD 143761: SFP inspection for 2006/05/12 data | 307 |
| C.220 HD 143761: SFP inspection for 2006/05/19 data | 307 |
| C.221 HD 143761: SFP inspection for 2006/06/09 data | 308 |
| C.222 HD 136849: SFP inspection for 2006/05/19 data | 308 |
| C.223 HD 136849: SFP inspection for 2006/06/09 data | 308 |
| C.224 HD 143393: SFP inspection for 2005/06/29 data | 309 |
| C.225 HD 143393: SFP inspection for 2005/07/03 data | 309 |
| C.226 HD 143687: SFP inspection for 2006/05/12 data | 309 |
| C.227 HD 146025: SFP inspection for 2006/05/12 data | 310 |
| C.228 HD 145675: Intermediate baseline plots for 2005/05/14 data | 312 |
| C.229 HD 145675: Intermediate baseline plots for 2005/07/04 data | 313 |
| C.230 HD 145675: Intermediate baseline plots for 2006/05/13 data | 313 |
| C.231 HD 145675: Intermediate baseline plots for 2006/08/07 data | 314 |
| C.232 HD 145675: Long baseline plots for 2006/08/11 data | 314 |
| C.233 HD 145675: Long baseline plots for 2006/08/12 data | 315 |

| | |
|---|-----|
| C.234 HD 145675: All data - Baseline vs. baseline position angle (using calibrator HD 144015) | 315 |
| C.235 HD 145675: All data - Baseline vs. baseline position angle (using calibrator HD 151044) | 316 |
| C.236 HD 145675: LD disk diameter fit | 316 |
| C.237 HD 145675: SFP inspection for 2005/05/14 data | 317 |
| C.238 HD 145675: SFP inspection for 2005/07/04 data | 317 |
| C.239 HD 145675: SFP inspection for 2006/05/13 data | 317 |
| C.240 HD 145675: SFP inspection for 2006/08/07 data | 318 |
| C.241 HD 145675: SFP inspection for 2006/08/11 data | 318 |
| C.242 HD 145675: SFP inspection for 2006/08/12 data | 318 |
| C.243 HD 144015: SFP inspection for 2005/05/14 data | 319 |
| C.244 HD 144015: SFP inspection for 2005/07/04 data | 319 |
| C.245 HD 144015: SFP inspection for 2006/05/13 data | 319 |
| C.246 HD 151044: SFP inspection for 2006/08/07 data | 320 |
| C.247 HD 151044: SFP inspection for 2006/08/11 data | 320 |
| C.248 HD 151044: SFP inspection for 2006/08/12 data | 320 |
| C.249 HD 168443: Intermediate baseline plots for 2005/08/10 data | 323 |
| C.250 HD 168443: Intermediate baseline plots for 2005/08/14 data | 324 |
| C.251 HD 168443: Intermediate baseline plots for 2005/08/20 data | 324 |
| C.252 HD 168443: Intermediate baseline plots for 2006/05/14 data | 325 |
| C.253 HD 168443: All data - Baseline vs. baseline position angle (using calibrator HD 169370) | 325 |
| C.254 HD 168443: All data - Baseline vs. baseline position angle (using calibrator HD 173093) | 326 |
| C.255 HD 168443: LD disk diameter fit | 327 |
| C.256 HD 168443: SFP inspection for 2005/08/10 data | 327 |

| | |
|---|-----|
| C.257 HD 168443: SFP inspection for 2005/08/14 data | 328 |
| C.258 HD 168443: SFP inspection for 2005/08/20 data | 328 |
| C.259 HD 168443: SFP inspection for 2006/05/14 data | 328 |
| C.260 HD 169370: SFP inspection for 2005/08/10 data | 329 |
| C.261 HD 169370: SFP inspection for 2005/08/14 data | 329 |
| C.262 HD 169370: SFP inspection for 2005/08/20 data | 329 |
| C.263 HD 173093: SFP inspection for 2006/05/14 data | 330 |
| C.264 HD 177830: Intermediate baseline plots for 2005/06/29 data | 332 |
| C.265 HD 177830: Intermediate baseline plots for 2005/08/08 data | 333 |
| C.266 HD 177830: Long baseline plots for 2006/06/09 data | 333 |
| C.267 HD 177830: Intermediate baseline plots for 2006/08/08 data | 334 |
| C.268 HD 177830: Long baseline plots for 2006/08/13 data | 334 |
| C.269 HD 177830: All data - Baseline vs. baseline position angle (using calibrator HD 17939) | 335 |
| C.270 HD 177830: All data - Baseline vs. baseline position angle (using calibrator HD 17939176377) | 335 |
| C.271 HD 177830: LD disk diameter fit | 336 |
| C.272 HD 177830: SFP inspection for 2005/06/29 data | 336 |
| C.273 HD 177830: SFP inspection for 2005/08/08 data | 337 |
| C.274 HD 177830: SFP inspection for 2006/06/09 data | 337 |
| C.275 HD 177830: SFP inspection for 2006/08/08 data | 337 |
| C.276 HD 177830: SFP inspection for 2006/08/13 data | 338 |
| C.277 HD 176939: SFP inspection for 2005/06/29 data | 338 |
| C.278 HD 176939: SFP inspection for 2005/08/08 data | 338 |
| C.279 HD 176377: SFP inspection for 2006/06/09 data | 339 |
| C.280 HD 176377: SFP inspection for 2006/08/08 data | 339 |

| | |
|--|-----|
| C.281 HD 176377: SFP inspection for 2006/08/13 data | 339 |
| C.282 HD 186427: Intermediate baseline plots for 2005/06/30 data | 341 |
| C.283 HD 186427: Intermediate baseline plots for 2005/08/04 data | 342 |
| C.284 HD 186427: Long baseline plots for 2006/08/13 data | 342 |
| C.285 HD 186427: All data - Baseline vs. baseline position angle | 343 |
| C.286 HD 186427: LD disk diameter fit | 343 |
| C.287 HD 186427: SFP inspection for 2005/06/30 data | 344 |
| C.288 HD 186427: SFP inspection for 2005/08/04 data | 344 |
| C.289 HD 186427: SFP inspection for 2006/08/13 data | 344 |
| C.290 HD 184960: SFP inspection for 2005/06/30 data | 345 |
| C.291 HD 184960: SFP inspection for 2005/08/04 data | 345 |
| C.292 HD 184960: SFP inspection for 2006/08/13 data | 345 |
| C.293 HD 190228: Intermediate baseline plots for 2005/07/01 data | 347 |
| C.294 HD 190228: Intermediate baseline plots for 2005/08/19 data | 347 |
| C.295 HD 190228: Long baseline plots for 2006/08/14 data | 348 |
| C.296 HD 190228: All data - Baseline vs. baseline position angle | 348 |
| C.297 HD 190228: LD disk diameter fit | 349 |
| C.298 HD 190228: SFP inspection for 2005/07/01 data | 349 |
| C.299 HD 190228: SFP inspection for 2005/08/19 data | 350 |
| C.300 HD 190228: SFP inspection for 2006/08/14 data | 350 |
| C.301 HD 190470: SFP inspection for 2005/07/01 data | 350 |
| C.302 HD 190470: SFP inspection for 2005/08/19 data | 351 |
| C.303 HD 190470: SFP inspection for 2006/08/14 data | 351 |
| C.304 HD 190360: Intermediate baseline plots for 2005/08/11 data | 353 |
| C.305 HD 190360: Long baseline plots for 2006/06/09 data | 354 |

| | |
|--|-----|
| C.306 HD 190360: Long baseline plots for 2006/08/11 data | 354 |
| C.307 HD 190360: All data - Baseline vs. baseline position angle | 355 |
| C.308 HD 190360: LD disk diameter fit | 355 |
| C.309 HD 190360: SFP inspection for 2005/08/11 data | 356 |
| C.310 HD 190360: SFP inspection for 2006/06/09 data | 356 |
| C.311 HD 190360: SFP inspection for 2006/08/11 data | 356 |
| C.312 HD 189108: SFP inspection for 2005/08/11 data | 357 |
| C.313 HD 189108: SFP inspection for 2006/06/09 data | 357 |
| C.314 HD 189108: SFP inspection for 2006/08/11 data | 357 |
| C.315 HD 192263: Long baseline plots for 2006/05/20 data | 358 |
| C.316 HD 192263: SFP inspection for 2006/05/20 data | 359 |
| C.317 HD 188350: SFP inspection for 2006/05/20 data | 359 |
| C.318 HD 195019: Intermediate baseline plots for 2005/08/11 data | 361 |
| C.319 HD 195019: Intermediate baseline plots for 2005/08/12 data | 362 |
| C.320 HD 195019: Long baseline plots for 2005/10/23 data | 362 |
| C.321 HD 195019: Intermediate baseline plots for 2006/08/06 data | 363 |
| C.322 HD 195019: All data - Baseline vs. baseline position angle | 363 |
| C.323 HD 195019: LD disk diameter fit | 364 |
| C.324 HD 195019: SFP inspection for 2005/08/11 data | 364 |
| C.325 HD 195019: SFP inspection for 2005/08/12 data | 365 |
| C.326 HD 195019: SFP inspection for 2005/10/23 data | 365 |
| C.327 HD 195019: SFP inspection for 2006/08/06 data | 365 |
| C.328 HD 196885: Long baseline plots for 2005/10/27 data | 367 |
| C.329 HD 196885: Intermediate baseline plots for 2005/10/29 data | 367 |
| C.330 HD 196885: Intermediate baseline plots for 2006/08/07 data | 368 |

| | |
|--|-----|
| C.331 HD 196885: Long baseline plots for 2006/08/14 data | 368 |
| C.332 HD 196885: All data - Baseline vs. baseline position angle | 369 |
| C.333 HD 196885: LD disk diameter fit | 369 |
| C.334 HD 196885: SFP inspection for 2005/10/27 data | 370 |
| C.335 HD 196885: SFP inspection for 2005/10/29 data | 370 |
| C.336 HD 196885: SFP inspection for 2006/08/07 data | 370 |
| C.337 HD 196885: SFP inspection for 2006/08/14 data | 371 |
| C.338 HD 194012: SFP inspection for 2005/10/27 data | 371 |
| C.339 HD 194012: SFP inspection for 2005/10/29 data | 371 |
| C.340 HD 194012: SFP inspection for 2006/08/07 data | 372 |
| C.341 HD 194012: SFP inspection for 2006/08/14 data | 372 |
| C.342 HD 217014: Intermediate baseline plots for 2005/08/03 data | 374 |
| C.343 HD 217014: Intermediate baseline plots for 2005/08/12 data | 375 |
| C.344 HD 217014: Long baseline plots for 2006/08/12 data | 375 |
| C.345 HD 217014: All data - Baseline vs. baseline position angle | 376 |
| C.346 HD 217014: LD disk diameter fit | 376 |
| C.347 HD 217014: SFP inspection for 2005/08/03 data | 377 |
| C.348 HD 217014: SFP inspection for 2005/08/12 data | 377 |
| C.349 HD 217014: SFP inspection for 2006/08/12 data | 377 |
| C.350 HD 218261: SFP inspection for 2005/08/03 data | 378 |
| C.351 HD 218261: SFP inspection for 2005/08/12 data | 378 |
| C.352 HD 218261: SFP inspection for 2006/08/12 data | 378 |
| C.353 HD 217107: Intermediate baseline plots for 2005/12/13 data | 380 |
| C.354 HD 217107: Intermediate baseline plots for 2006/10/20 data | 380 |
| C.355 HD 217107: All data - Baseline vs. baseline position angle | 381 |

| | |
|---|-----|
| C.356 HD 217107: SFP inspection for 2005/12/13 data | 382 |
| C.357 HD 217107: SFP inspection for 2006/10/20 data | 382 |
| C.358 HD 216953: SFP inspection for 2005/12/13 data | 382 |
| C.359 HD 216953: SFP inspection for 2006/10/20 data | 383 |

Abbreviations and Acronyms

| | |
|--------------|--|
| B | baseline |
| BSF | Beam Synthesis Facility |
| CHARA | Center for High Angular Resolution Astronomy |
| Gyr | gigayear |
| IR | infrared |
| LD | limb darkened |
| mas | milliarcseconds |
| MJD | Modified Julian Date |
| NIRO | Near InfraRed Observer |
| OPLE | Optical Path Length Equalization |
| PA | position angle |
| PoP | Pipes of Pan |
| SED | spectral energy distribution |
| SFP | separated fringe packet |
| S/N | signal-to-noise ratio |
| UD | uniform disk |

Everything starts somewhere, though many physicists disagree.
— Terry Pratchett

– 1 –

Introduction

This dissertation describes the properties of exoplanet systems’ host stars based upon observations made using Georgia State University’s Center for High Angular Resolution Astronomy (CHARA) Array. Chapter 1 starts with a brief history of exoplanet discoveries, focusing on assumptions made regarding the systems’ inclinations and whether certain types of binary star systems could mimic planetary systems. Chapter 2 presents an overview of interferometry and the CHARA Array, and Chapter 3 describes how calibrator stars were chosen, what baselines were used to observe, and the data reduction procedure. Chapter 4 discusses the observations while Chapter 5 details how stellar angular diameters were determined and lists the final diameter measurements. Chapter 6 features HD 189733, an exoplanet host star with a transiting planet. Chapter 7 presents the results of the search for stellar companions, and Chapter 8 is the more general discussion of the exoplanet host stars as a sample.

1.1 Exoplanets Background

Discovering planets orbiting other stars has long been a goal of those looking to the heavens. We want to know of our neighbors, to find if there are other life-bearing solar systems besides our own, and to learn more about our own world and its place in the cosmos by learning of others like us. How do we compare to other solar systems?

How are other planets the same as ours? More interestingly, how are they different?

The search for planets begins by looking for their effects on their parent stars. The first exoplanet system discovered consisted of three planets orbiting the pulsar PSR 1257+12. These were uncovered via perturbations in the radio pulses' timing and revealed extremely low-mass companions: $0.015 M_{\oplus}$, $3.4 M_{\oplus}$, and $2.8 M_{\oplus}$ (Wolszczan 1994). This is not the most productive discovery technique, though, as only one other pulsar is known to harbor planets (PSR B1620-26; Backer et al. 1993).

Most of the exoplanets known to date were discovered by observing variations in the host star's radial velocity curves due to the orbiting companion. Of the 248 planets known as of 2007/08/01, 236 of them were discovered in this manner (*Extrasolar Planets Encyclopedia*¹). The first potential exoplanet discovered using this method was found orbiting the star HD 114762 b (Latham et al. 1989). Latham et al. state that it is unclear whether the companion is a brown dwarf or a planet, and further study has not clarified the status of the companion (e.g., Mazeh et al. 1996; Patience et al. 2002). Half a decade later, Mayor & Queloz (1995) announced evidence of a Jupiter-mass planet orbiting the star 51 Pegasi, the first definitive detection of a planet orbiting a solar-type star (Marcy & Butler 1996).

Many of the early planetary systems detected tended towards short-period, small-separation orbits, mainly a selection effect of the detection technique. Longer-period planets were revealed as enough time passes for the planet to complete multiple orbits and radial velocity curves showed the periodic motion that indicates a companion

¹<http://vo.obspm.fr/exoplanetes/encyclo/catalog.php>

(e.g., HD 11964; Butler et al. 2006) as well as multiple planet systems (e.g., ν Andromedae; Butler et al. 1999).

In addition to radial velocity surveys, a few planets have been discovered via microlensing (4 planets; e.g., Bond et al. 2004; Beaulieu et al. 2006) and by direct imaging (4 planets; e.g., Guenther et al. 2005; Chauvin et al. 2005). An additional 23 planets have been detected during photometric transit events. These planets are typically the size of Jupiter with very close orbits (0.03 to 0.05 AU) around solar-type stars (e.g., Brown et al. 2001; Bouchy et al. 2005a; Sato et al. 2005).²

The planetary systems discovered using radial velocity variations do not resemble our Solar System in almost all cases. Most planets range from 0.02 to $4.0 M_{\text{Jupiter}}$ in mass and have periods of a year or less in a close orbit to the parent star (≤ 1.5 AU). The eccentricities, when known, are a bit more even across the board, spanning 0 to approximately 0.5 according to the *Extrasolar Planets Encyclopedia*. Inclinations of transiting planet systems are well constrained, but for other systems, this important orbital parameter remains a mystery.

1.2 Unknown Inclinations

In studies of exoplanet systems, certain assumptions are made about the inclination of the systems discovered; i.e., it is assumed the orbit has an intermediate to high inclination ($i \sim 45 - 90^\circ$) and the odds of the orbit being nearly face-on ($i \sim 0^\circ$) are

²For an excellent summary and list of references for transiting planets, see <http://obswww.unige.ch/~pont/TRANSITS.htm>.

extremely low. This assumption leads to the calculated companion mass, known only as the quantity $m_p \sin^3 i$ where m_p is the mass of the planet and i is the inclination of the system, being planetary in nature instead of stellar. While this is probably a safe conclusion for the majority of the exoplanets discovered, the chance remains that in a large enough sample, a few of the candidate planetary systems may be face-on binary star systems instead.

On the California and Carnegie Planet Search website³, Geoffrey Marcy makes several arguments in favor of the planetary candidates being true planets in high-inclination orbits rather than low-mass stellar companions in nearly face-on orbits. He argues there is no bias towards extreme face-on orbits, as the target stars are distributed evenly all over the sky and should exhibit completely random inclinations, which lowers the odds of seeing many objects with face-on orbits. What is not accounted for is the fact that the search for planetary companions has until recently dismissed known spectroscopic binary systems, which may bias the remaining sample slightly by including more orbits closer to face-on than edge-on, as the edge-on binary systems were not candidates for planet searches. Additionally, Raghavan et al. (2006) found that at least 23% of exoplanet systems have stellar companions, so known spectroscopic binaries should not be ignored.

Marcy also performs some calculations to determine how many brown dwarfs would have to be orbiting these stars for all the exoplanet candidates to be binary systems with brown dwarf companions. As expected, the odds are extremely low

³<http://exoplanets.org>

that this would be the case, but I am not proposing that *all* the potential exoplanet systems have companions more massive than planets, but that just a few might. The same is true for his argument that all solar-type stars within 30 parsecs would have to be extremely face-on, assuming stellar equators align with planets' orbital planes. Again, I am not claiming that all the planetary systems have brown dwarf or low-mass stellar companions.

The probability of a system's inclination being in the range i to $i + \Delta i$ is proportional to the ratio of the surface element of a hemisphere defined by that range and integrated over the azimuth angle (ϕ) to the surface area of the entire hemisphere. The area element for a given range of i is:

$$dA = di \times \sin i \, d\phi, \quad (1.1)$$

and the probability of a system having a specific range of i is:

$$P_{i,i+\Delta i} = \frac{\int_0^{2\pi} \int_i^{i+\Delta i} \sin i \, di \, d\phi}{\int_0^{2\pi} \int_0^{\pi/2} \sin i \, di \, d\phi} = \frac{-2\pi \cos i \Big|_i^{i+\Delta i}}{-2\pi \cos i \Big|_0^{\pi/2}} = \cos i - \cos(i + \Delta i). \quad (1.2)$$

Therefore, the probability of a planetary system having an inclination between 0 and 5° would be 0.38% (see Figure 1.1). The odds of finding that a system's companion is a low-mass star in a face-on orbit instead of a planetary companion in a high-inclination orbit are not high, but it is not inconceivable.

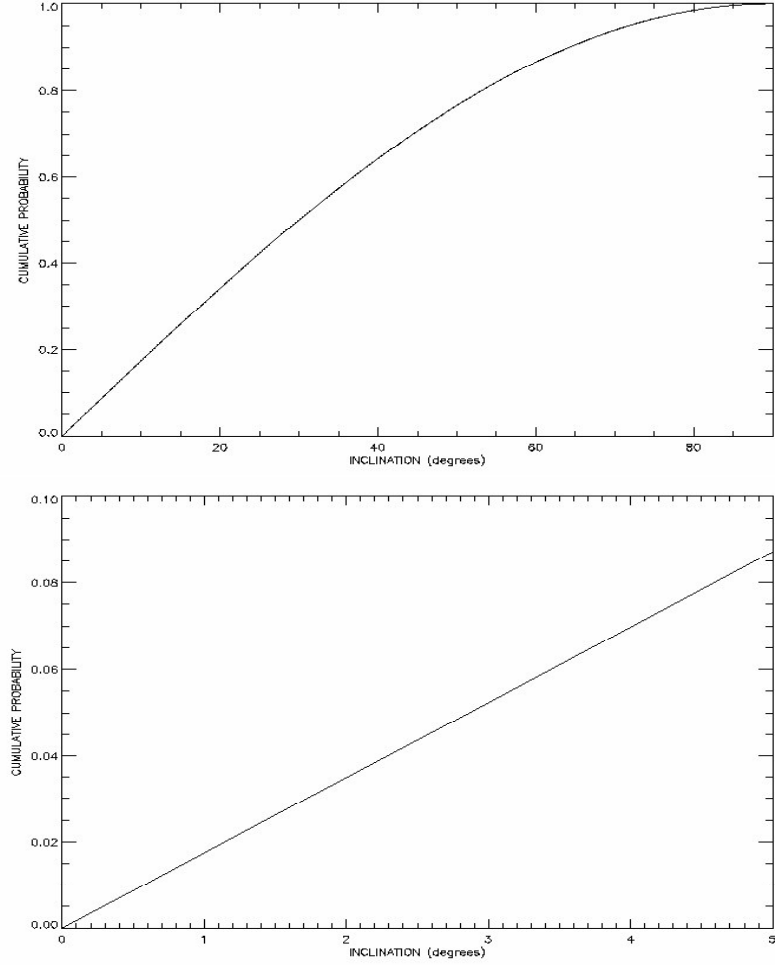


Figure. 1.1: Cumulative probability vs. inclination. The probability of a system having an inclination between i and $i + \Delta i$, where i ranges from 0 to 90° (top) and 0 to 5° (bottom).

1.3 Stars Mimicking Planets

Two studies have shown that radial velocity observations of exoplanet systems alone are insufficient to distinguish between high-inclination planetary systems and low-inclination binary star systems. Stepinski & Black (2001) estimated probability densities of orbital periods and eccentricities for a sample of exoplanet candidates and

a sample of spectroscopic binary star systems with solar-type primary stars in order to determine if there were any fundamental differences between the two types of systems. The samples were constrained by period and eccentricity so that the range of values was common to both, which left 217 spectroscopic binaries and 38 exoplanet candidates. They found the respective distributions of the two populations were statistically indistinguishable from each other in the context of orbital elements. This implies that there is no intrinsic orbital difference between exoplanet systems and binary star systems, and we cannot count on orbital elements to differentiate between them.

In an earlier study, Imbert & Prévot (1998) modeled nine known exoplanet systems as binary star systems to test if the radial velocity observations could be explained by low-mass stellar companions. They assumed the observed radial velocity amplitude was determined from blended lines of two stars with similar masses and predicted probabilities based on orbital inclination, mass ratio, and period constraints. Although the probability of binary star systems appearing as planetary systems was low, ranging from 10^{-4} to 4%, the model results described the observations satisfactorily and showed it is not impossible for a binary star system to mimic an exoplanet system.

1.4 Case Study: 51 Pegasi

This is not the first interferometric study of exoplanet systems. Boden et al. (1998) used the Palomar Testbed Interferometer (PTI) to study 51 Pegasi (HD 217014) to search for an unseen luminous companion. PTI operates in the K -band (2-2.4 μm) with a longest baseline of 110 meters and is located on Mount Palomar, California (Colavita et al. 1999). Boden et al. observed the star over 18 nights spanning 1997 July 19 through November 23 using two nearby calibrators (HD 215510 and HD 211006).

Their data were consistent with a single-star model and excluded any companions that would have a magnitude difference $\Delta K \leq 4.27$ for the 4.2-day orbital period indicated by spectroscopic measurements. That ΔK would lead to an absolute magnitude $M_K = 7.30$, implying a main-sequence stellar mass of less than $0.22 M_\odot$, which corresponds to a spectral type of M5 V or later.

While Boden et al. did not find evidence of a stellar companion, this study was a useful proof-of-concept that showed that this kind of work could be completed successfully.

It'll never work.
—*Theo ten Brummelaar, about the CHARA Array*

– 2 –

Long-Baseline Interferometry and the CHARA Array

This chapter aims to provide a basic understanding of long-baseline interferometry, reviews the definition of visibility, and gives an overview of the CHARA Array.

2.1 Basic Interferometry

To the human eye, the only star we can resolve without a telescope is our Sun, and gazing at this star with the naked eye is never a good idea. Besides the Sun, even the brightest and closest stars in our sky appear as point sources and we cannot see their physical disks. We therefore look to technology to learn more about these objects.

Interferometry depends on multiple light collectors, such as telescopes, to achieve resolutions greater than those produced by a single aperture. The criterion for the minimum resolvable detail on a single star is known as the Rayleigh criterion and is defined as $\theta = 1.22\lambda/B$ (for a circular aperture) where λ is the wavelength used to observe, B is the telescope aperture size, and θ is in units of radians. The advantage of using multiple apertures in interferometry is that the resolution is still at the Rayleigh limit, but B is now the distance between the telescopes instead of the diameter of their apertures, otherwise known as the “baseline”. The limiting resolution equation converts to $\theta = \lambda/2B$ in the case of resolving a binary system with an

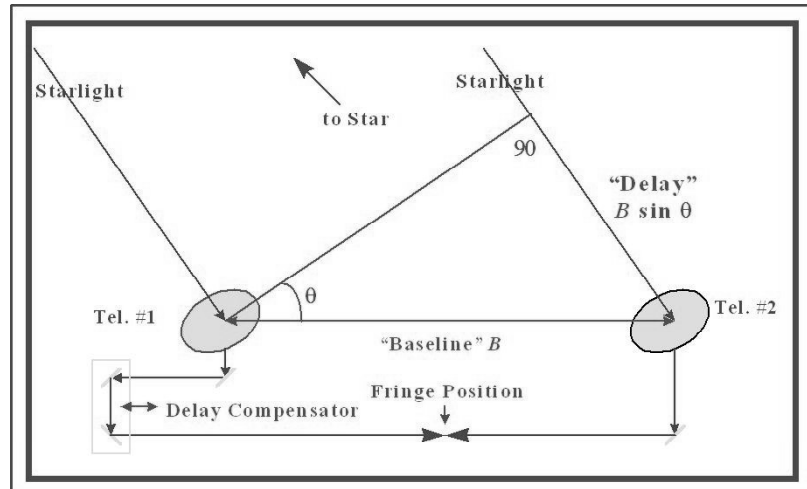


Figure. 2.1: Schematic of a basic interferometer (diagram by H. McAlister).

interferometer. This means long-baseline interferometry has a much higher resolution than single-aperture telescopes. Separating the telescopes to hundreds of meters results in resolutions of less than a milliarcsecond (mas) at visible wavelengths.

The light from a target is collected by multiple telescopes and interfered with itself to produce a fringe pattern at the point where the path lengths are equalized (see Figure 2.1). Interferometers measure the degree of complex coherence of an object, which leads to a powerful technique to measure stellar angular diameters, binary star separations, and/or the intensity distribution on the sky (Tango & Twiss 1980).

However, interferometry requires a complex infrastructure, multiple reflections reduce the amount of light available for data collection, and optics need delicate and precise alignment over large distances. In order to obtain a sufficient signal-to-noise ratio (S/N), integrations on the order of minutes are needed while maintaining path equalization, which is a non-negligible effort. The path length is constantly

changing due to the sidereal motion of the object, atmospheric effects, vibrations, and the gradual misalignment of optics over hours. Interferometers may boast very high resolution, but the prices are low sensitivity and operational complexity.

2.2 Early Interferometry

In 1868, Armand Fizeau was the first to note that the diameter of an extended disk could be measured interferometrically by measuring the baseline length where the fringe contrast dropped to zero (Fizeau 1868). The earliest interferometric measurement of a stellar diameter was performed by Michelson & Pease (1921) when they measured the diameter of Betelgeuse (α Orionis, HD 39801) using an interferometer installed on the 100-inch Hooker telescope on Mount Wilson. The instrument consisted of four flat mirrors arranged on a steel beam attached to the telescope's Cassegrain cage. The inner two mirrors remained fixed while the outer mirrors had a maximum separation of 20 feet (see Figure 2.2).

The first true long-baseline optical Michelson interferometer was used by Antoine Labeyrie, who obtained fringes from directly interfering light from two separate telescopes 12 meters apart (Labeyrie 1975). He observed Vega and while he was unable to glean any astrophysical information from the fringes, it was an important proof-of-concept experiment that paved the way for future instruments.

One of the earliest programs to measure stellar diameters interferometrically started in 1964 and was undertaken by Hanbury Brown et al. (1974a), who used

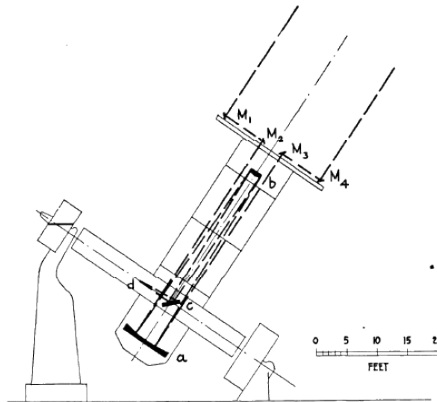


Figure. 2.2: Schematic of Michelson's interferometer (from Michelson & Pease (1921). Reproduced by permission of the AAS.).

the Narrabri Stellar Intensity Interferometer to measure the apparent angular diameters of 32 stars (see Table 2.1 for details on the instrument). The program stars included spectral types from O5f to F8, and data for nine multiple stars were also presented. Since that time, researchers using the Palomar Testbed Interferometer and the Navy Prototype Optical Interferometer have performed considerable work on stellar diameters, largely for giants and supergiants (e.g., van Belle et al. 1999; Lane et al. 2001; Nordgren et al. 1999; Armstrong et al. 2001).

2.3 Young's Double Slit Experiment

The basic concepts of interferometry are well demonstrated in Young's classic double slit experiment, which consists of passing light with a small bandwidth through two slits to be projected onto a screen. The light waves constructively and destructively interfere in order to produce a pattern of light and dark regions on the screen (see

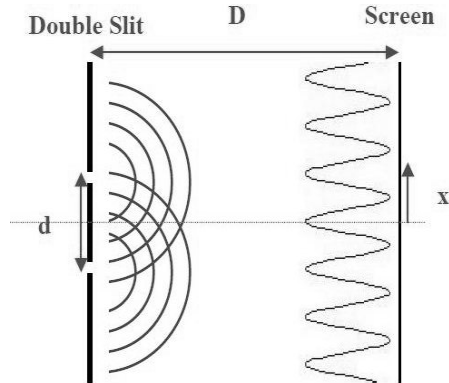


Figure. 2.3: Young's double slit experiment setup (diagram by H. McAlister). The light passing through the two pinholes constructively and destructively interfere, creating fringes of alternating dark and bright bands.

Figure 2.3). The resulting fringe intensity is given by

$$I(x) = 4A^2 \cos^2 \left[\frac{2\pi}{\lambda} \frac{xd}{D} \right], \quad (2.1)$$

where A is the amplitude of the two slits, λ is the wavelength of the incoming light, x is the distance from the center between the slits, d is the slit distance, D is the distance from the slits to the screen, and $D \gg d$. Bright fringes occur when $xd/D = 0, \lambda, 2\lambda, 3\lambda, \dots = m\lambda$, where the central fringe occurs at 0 and m is the “order of interference”.

The angular spacing of the fringe maxima is given by

$$\alpha = \frac{x}{D} = \frac{\lambda}{d}. \quad (2.2)$$

Figure 2.4 shows the effects of interfering light over a range of wavelengths and the resulting polychromatic fringe.

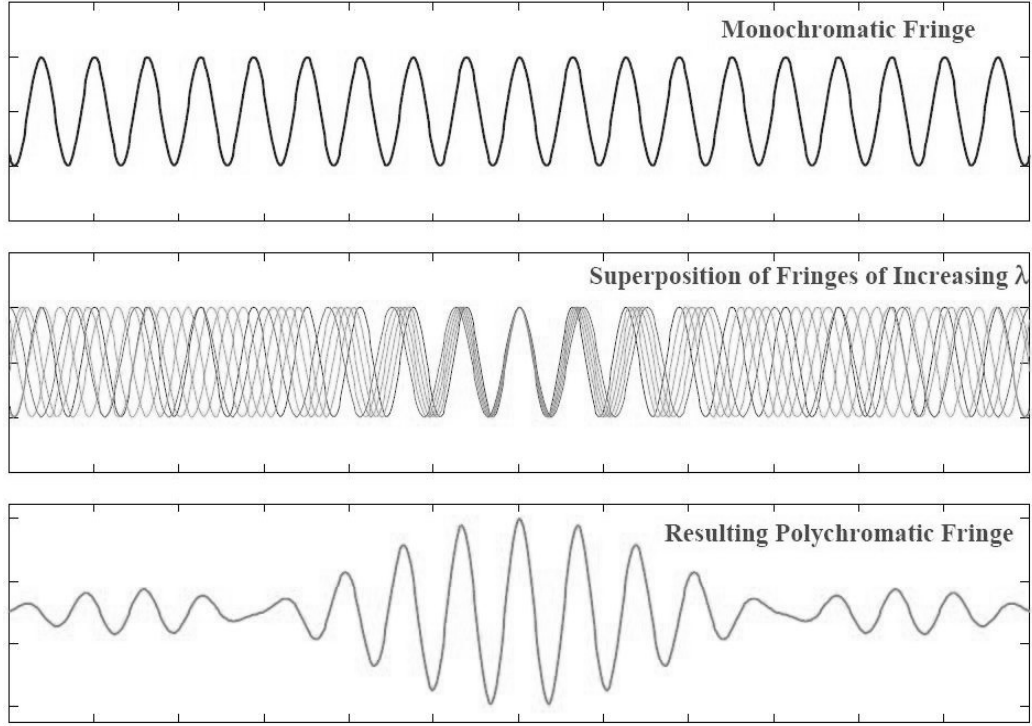


Figure. 2.4: Building an interferometric fringe (image by H. McAlister). Multiple wavelengths of light constructively and destructively interfere, creating the fringe pattern seen in the bottom panel.

2.4 Fringe Visibility

The van Cittert-Zernike theorem provides the basis of reconstructing information from interferometric measurements. It relates the complex degree of coherence, $\mu(\vec{B})$, with the intensity distribution on the sky for a given source, $I(\vec{\alpha})$, where \vec{B} is the baseline vector between the two telescopes and $\vec{\alpha}$ is the two-dimensional sky coordinate (Lawson 2000). The Fourier transform terms, $\mu(\vec{B})$ and $I(\vec{\alpha})$, are related as follows:

$$\mu(\vec{B}) = \frac{\int I(\vec{\alpha}) e^{-ik\vec{B} \cdot \vec{\alpha}} d\vec{\alpha}}{\int I(\vec{\alpha}) d\vec{\alpha}}, \quad (2.3)$$

where $k = 2\pi/\lambda$.

The power of this relation lies in the fact that when $I(\vec{\alpha})$ cannot be imaged for a given source, one can measure $\mu(\vec{B})$ and then infer $I(\vec{\alpha})$ in the ideal case. In real measurements, the phase component of $\mu(\vec{B})$ is degraded and lost through atmospheric turbulence (Tango & Twiss 1980) and all that remains is the amplitude of the term. This remaining information in the $\mu(\vec{B})$ term is what interferometers measure.

Observationally, the contrast of a fringe pattern is a measure of the visibility amplitude, more simply known as “visibility”. This is the basic observable of an interferometer, and was defined by Michelson (1920) as

$$V = \frac{I_{\max} - I_{\min}}{I_{\max} + I_{\min}}, \quad (2.4)$$

where I_{\max} is the maximum intensity of the fringe and I_{\min} is the minimum intensity. Visibility thus ranges from $V = 0$, where there is no contrast, fringes disappear, and the target is considered fully resolved, to $V = 1$, where there is maximum contrast, the fringes are well-defined, and the target is considered unresolved and is a point source.

In practice, the visibility equation is a bit more complex. Assuming a single star has a uniform brightness across its disk, the visibility equation is

$$V_{\text{UD}} = \frac{2J_1(\pi B\theta_{\text{UD}}/\lambda)}{\pi B\theta_{\text{UD}}/\lambda}, \quad (2.5)$$

where J_1 is the first order Bessel function, B is the baseline, θ_{UD} is the uniform disk (UD) diameter of the star in radians, and λ is the wavelength used to observe (Lawson 2000).

The visibility equation for a binary star is:

$$V^2(B) = (1 + \beta)^{-2} \left[\beta^2 V_1^2(B) + V_2^2(B) + 2\beta V_1(B)V_2(B) \cos \left(\frac{2\pi B \rho \cos \psi}{\lambda} \right) \right], \quad (2.6)$$

where B is the baseline, β is the brightness ratio between the two stars and $\beta \geq 1$, ρ is the angular separation of the binary, λ is the wavelength used to observe, ψ is the difference in position angle of the binary and the baseline as projected onto the sky, and $V_1^2(B)$ and $V_2^2(B)$ are the visibilities for each stellar component as seen in Equation 2.5 (Hanbury Brown et al. 1967).

The visibility curve (visibility vs. baseline) behaves differently depending on the star or star system observed. For a single star, the visibility curve appears as a smooth line with a gradual drop-off as the baseline increases (see the top line in Figure 2.5). Note the lack of modulation as a function of baseline. On the other hand, if the target observed is a binary star, the visibility curve displays sinusoidal modulations due to the additional flux from the companion star, even if the companion is unseen and unresolved. The bottom-most curve in Figure 2.5 shows the visibility curve for a binary system composed of two equally bright stars.

The separation between stars in a binary system will also affect the visibility curve, as can be seen in Figure 2.6. At larger separations, the visibility drops to zero and fringes disappear at shorter baselines, otherwise known as “first null”, and lower

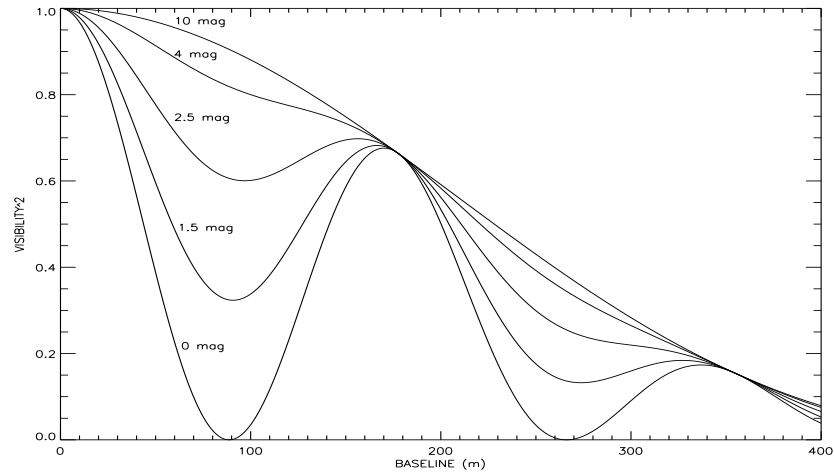


Figure. 2.5: The effect of various Δm on the visibility curve for a binary system in the K -band using a projected angular separation of 0° . Note how $\Delta m = 0$ creates the largest modulations in the visibility curve while $\Delta m = 10$ essentially represents a single star's visibility curve.

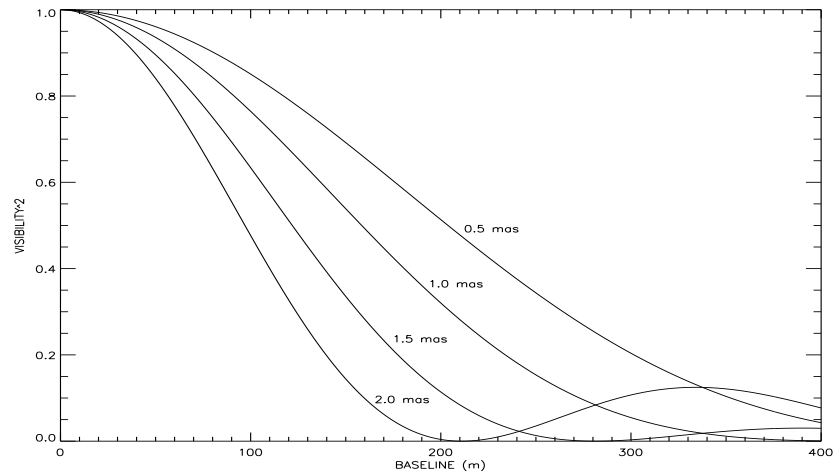


Figure. 2.6: The effect of various projected stellar separations on the visibility curve for a binary system in the K -band, assuming $\Delta m = 0$ and the position angle is 45° . As a binary system's angular separation increases, the visibility curve reaches first null towards shorter baselines.

visibilities are measured for more separated systems compared to the closer binaries at a given baseline. A similar pattern is seen as the angular diameter of a single star changes (see Figure 2.7).

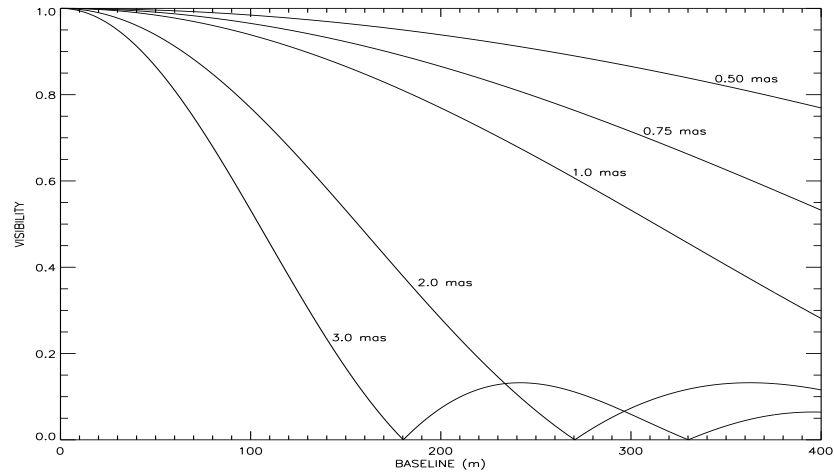


Figure. 2.7: The effect of various stellar angular diameters on the visibility curve. For reference, the Sun at 10 parsecs has a diameter of ~ 1 mas. The smaller a star's angular diameter, the less change is seen in the visibility curve as a function of baseline.

2.5 Past and Present Interferometers

As technology improves, interferometers have gotten significantly more complex and numerous. Table 2.1 lists past and present interferometers. The scientific output of modern interferometers is varied: measurements of stellar diameters (e.g., Ciardi et al. 2001; Berger et al. 2006), determining binary star orbits (e.g., Boden et al. 2006), observing rapidly rotating stars (e.g., McAlister et al. 2005; Aufdenberg et al. 2006), probing the circumstellar regions of Be and T Tauri stars (e.g., Tycner et al. 2005; Eisner et al. 2006), and even imaging stellar surfaces (e.g., Monnier et al. 2007).

Table. 2.1: Past and Present Interferometers

| Name | Site Location | No. of Collecting Elements | Element Aperture (cm) | Maximum Baseline (m) | Operating Wavelength (μ m) | Operating Status |
|----------|----------------------|----------------------------------|-----------------------------|----------------------------|---------------------------------------|---------------------|
| NSII | Narrabri, AUS | 2 | 670 | 188 | 0.44 & 0.46 | 1964-1972 |
| Mark I | Mt. Wilson, USA | 2 | 13 | 1.5 | 0.4-0.9 | 1979 |
| Mark II | Mt. Wilson, USA | 2 | 10 | 3.1 | 0.5-0.65 | 1982-1984 |
| Mark III | Mt. Wilson, USA | 3 | 7.5 | 20 | 0.4-0.8 | 1987-1992 |
| GI2T | Calern, FRA | 2 | 150 | 65 | 0.4-0.85 & >1.2 | 1985-2005 |
| ISI | Mt. Wilson, USA | 3 | 165 | ~80 | 11 | since 1990 |
| COAST | Cambridge, UK | 5 | 40 | 67 | 0.4-0.9 & 1.3-2.2 | since 1991 |
| SUSI | Narrabri, AUS | 11 | 14 | 640 | 0.4-0.90 | since 1991 |
| IOTA | Mt. Hopkins, USA | 3 | 45 | 38 | 0.5-2.2 | 1993-2006 |
| NPOI | Anderson Mesa, USA | 10 | 50 | 437 | 0.45-0.85 | since 1995 |
| PTI | Mt. Palomar, USA | 3 | 40 | 110 | 1.5-2.4 | since 1995 |
| MIRA-ST | Tokyo, JPN | 9 | 400 | 600 | 2.2 | since 1998 |
| CHARA | Mt. Wilson, USA | 6 | 100 | 331 | 1.65-2.13 | since 1999 |
| KI | Muana Kea, USA | 2(4) [†] | 1,000(180) [†] | 85 | 1.5-5 & 10 | since 2001 |
| VLTi | Cerro Paranal, CHL | 4(3) [‡] | 820(180) [‡] | 200 | 1-2.5 & 10-20 | since 2001 |
| LBT | Mt. Graham, USA | 2 | 840 | 14 | 0.4-400 | since 2005 |
| MROI | Magdalena Ridge, USA | 6 | 1,400 | 350 | 0.6-2.4 | expected 2009 |

Notes.

[†]Includes two permanent 1-m telescopes and four 180-cm outrigger telescopes.

[‡]Includes four “unit” 8.2-m telescopes and three auxilliary 1.8-m telescopes.

NSII: Narrabri Stellar Intensity Interferometer (Hanbury Brown et al. 1974a); Mark I (Shao & Staelin 1980); Mark II (Shao et al. 1987);

Mark III (Shao et al. 1988); GI2T: Grand Interféromètre à 2 Télescopes (Mourard et al. 1994); ISI: Infrared Spatial Interferometer (Hale

et al. 2000); COAST: Cambridge Optical Aperture Synthesis Telescope (Baldwin et al. 1998); SUSI: Sydney University Stellar Interferometer (Davis et al. 1999); IOTA: Infrared/Optical Telescope Array (Dyck et al. 1995); NPOI: Navy Prototype Optical Interferometer (Armstrong et al. 1998); PTI: Palomar Testbed Interferometer (Colavita et al. 1999); MIRA-ST: Mitaka Optical-Infrared Array (Yoshizawa et al. 2003); CHARA: Center for High Angular Resolution Astronomy Array (ten Brummelaar et al. 2005); KI: Keck Interferometer (Colavita et al. 2004); VLTI: Very Large Telescope Interferometer (Glindemann et al. 2003); LBT: Large Binocular Telescope (Hill et al. 2006); MROI: Magdalena Ridge Observatory Interferometer (Crech-Eakman et al. 2006)

2.6 The CHARA Array

Georgia State University's Center for High Angular Resolution Astronomy (CHARA) designed, constructed, and now operates the CHARA Array, an optical/near-infrared interferometric array on Mount Wilson, California. The CHARA Array is located on the grounds of the Mount Wilson Observatory, a site of fruitful past and present astronomical research, and was chosen based on its reputation for superb astronomical seeing (Buscher 1994). Figure 2.8 shows how well integrated the Array is with the other facilities on Mount Wilson. See ten Brummelaar et al. (2005) for a full description of the instrument.

The CHARA Array consists of six 1-meter alt-az telescopes that compress incoming starlight to a collimated 12.5-cm beam. The telescopes are arranged in a static Y configuration with two telescopes along each of the arms and are designated by their cardinal direction and the number 1 or 2. Number 1 denotes the telescope farther from the center of the CHARA Array; e.g., W1 is more distant than W2. Figure 2.9 shows the position of each telescope and its orientation.

The arrangement of the six telescopes leads to 15 non-redundant baselines ranging from 34 to 331 meters (see Table 2.2). The starlight is transported from the telescope to the Beam Synthesis Facility (BSF) via evacuated 20-cm diameter aluminum pipes. Keeping the pipes under vacuum reduces degradation of the light due to turbulent distortion in the air path that would otherwise be encountered. The BSF contains the Optical Path Length Equalization (OPLE) facility and the Beam Combining

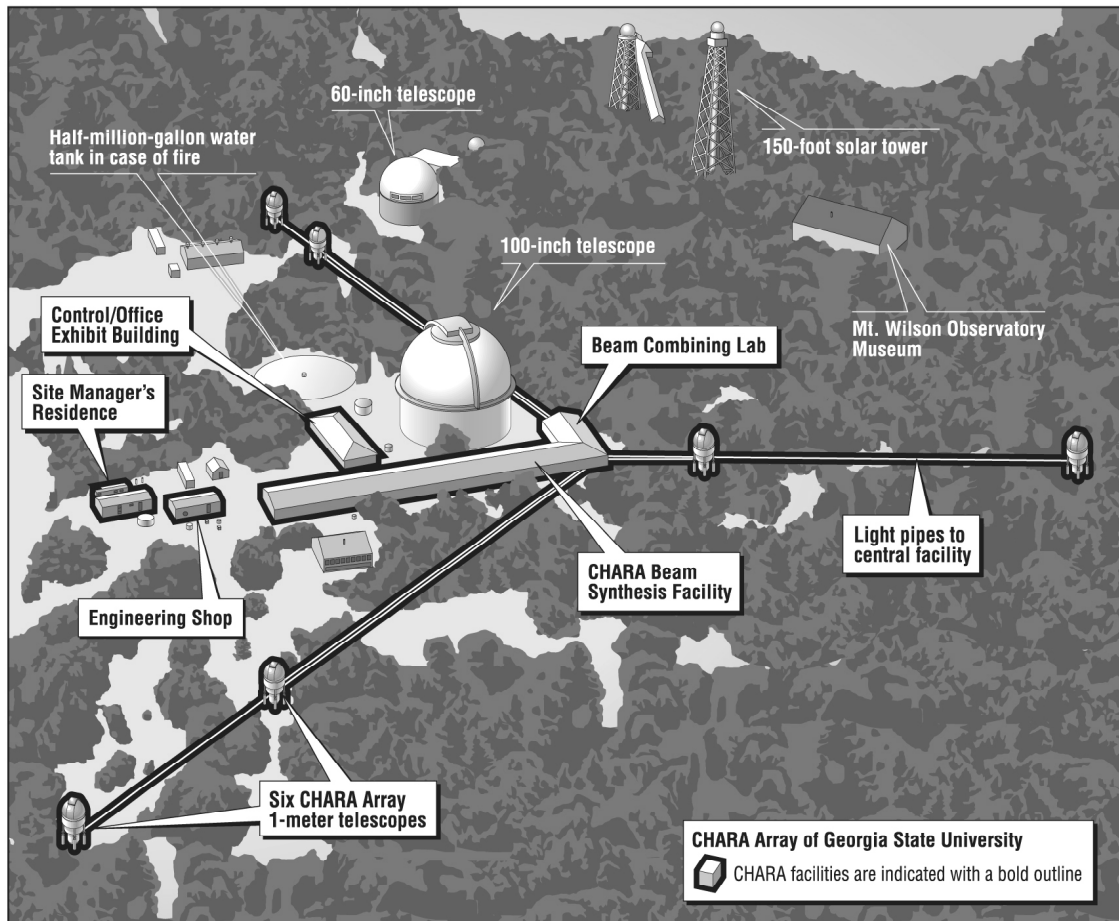


Figure. 2.8: The CHARA Array and its surroundings. North is to the lower right. (Diagram by the GSU Office of University Relations.)

Laboratory. The light's path length is equalized in two stages. The fixed delay lines, known as the "Pipes of Pan" (PoPs), introduce a predetermined amount of delay into the beam: 0, 36.6, 73.2, 109.7, or 143.1 m. This is accomplished by inserting a mirror into the vacuum tube in order to send the beam up to the continuous part of the delay system, which is the second stage of path length equalization.

The continuous delay is removed by the OPLE carts, which track the diurnal motion of the object as it moves across the sky. This sidereal motion of the target

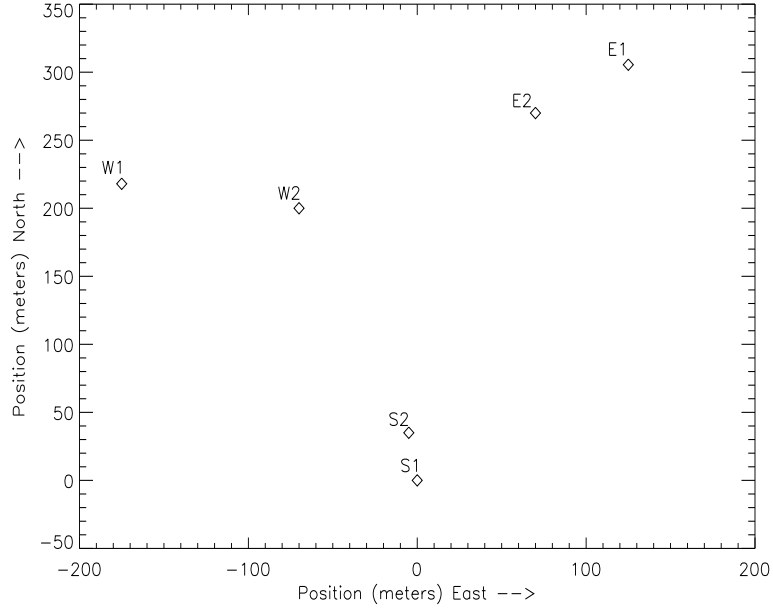


Figure. 2.9: The CHARA Array’s telescope configuration.

changes the projected baseline length over time. The OPLE carts’ positions are monitored to 2 nm using a laser metrology system operating at $1.3 \mu\text{m}$, which is controlled to 10 nm. The maximum delay compensation by the OPLE carts is ~ 90 m.

All observations for this project were obtained using the “CHARA Classic” infrared beam combiner, a pupil-plane beam combiner, where the beam is separately imaged onto two spots on the beam combining camera after passing through a dichroic beam splitter that separates the visible from infrared light at the $1 \mu\text{m}$ boundary. Fringes are then detected in a scanning mode created by dithering a mirror mounted to a piezoelectric translation stage.

The full resolution of the CHARA Array, formally defined in terms of reaching the first null of visibility, is 1.6 mas in the K' -band ($2.13 \mu\text{m}$) and 0.4 mas in V

(0.55 μm) using the S1-E1 baseline. In practice, higher resolutions can be achieved by accurately measuring visibilities higher up on the central lobe of the visibility curve. The CHARA Array also operates in the infrared H -band at 1.67 μm and work is being done towards observing in the J -band (1.22 μm). The limiting magnitudes for the Array are $K \leq +6.5$ and $V \leq +10$. If the star is fainter than $K=+6.5$, fringes disappear, and if it is fainter than $V=+10$, there are too few photons for the tip-tilt system to be able to lock onto the star. All observations except for those described in Chapter 6 were obtained using the K' -band filter.

For each baseline, the maximum field of view (FOV, in radians) was calculated for the K' -band:

$$\text{FOV} = \frac{\lambda/B}{\text{fringe dither size}} \times \text{total scan length}, \quad (2.7)$$

where λ is the wavelength of observation, B is the maximum baseline, *fringe dither size* is the number of dither steps necessary to sample from the fringe maximum to the fringe minimum, and *total scan length* is the number of dither steps of the entire scan. In reality, the FOV will be foreshortened from the maximum value due to the baseline position angle on the sky except for stars at the zenith at the time of observation.

Table. 2.2: CHARA Baselines

| Baseline | Length (m) | Maximum FOV (mas) |
|----------|---------------|----------------------|
| W2-S1 | 210.99 | 360 |
| W2-S2 | 177.46 | 420 |
| W2-E1 | 221.82 | 340 |
| W2-E2 | 156.28 | 480 |
| W2-W1 | 107.93 | 700 |
| W1-S1 | 278.51 | 270 |
| W1-S2 | 249.40 | 300 |
| W1-E1 | 313.54 | 240 |
| W1-E2 | 251.35 | 300 |
| E2-S1 | 278.79 | 270 |
| E2-S2 | 248.15 | 200 |
| E2-E1 | 65.87 | 1140 |
| E1-S1 | 330.67 | 230 |
| E1-S2 | 302.33 | 250 |
| S2-S1 | 34.08 | 2200 |

*The most exciting phrase to hear in science, the one that heralds new
discoveries, is not 'Eureka!' but 'That's funny...'*
— Isaac Asimov

– 3 –

Method

This chapter describes the selection of calibrator stars and data reduction tools used in this dissertation.

3.1 Calibrator Stars

Calibrator stars are a vital part of obtaining reliable data when measuring stellar diameters or searching for unseen stellar companions interferometrically. They function as the standard to which we compare the scientific objects. For example, changes in the visibility curve induced by a stellar companion can either be from the object star, assuming the calibrator is a single star, or from the calibrator itself if it is harboring an unseen companion. Ideally, calibrators would be single stars with low rotational velocities and no unusual features such as large starspots or circumstellar disks. There is no way to be completely sure a calibrator is a single, featureless star, but every effort was made to weed out bad calibrators.

If the visibility curve of an exoplanet system’s host star indicated a stellar companion, it was standard practice to find a new calibrator and reobserve the system to confirm it was not the calibrator that was a binary system. This occasionally led to the discovery of some binary calibrators, which was a bit disappointing in that it was an interesting calibrator, not an interesting object. Table 3.1 lists the problematic

calibrators found during this work. For more details on each one, see Appendix C.

Acceptable calibrators were chosen to have visibility amplitudes greater than 85% on the baselines used and most were within 5-8° of the target star. The high visibilities meant the calibrator was almost unresolved - a point source - and therefore uncertainties in the calibrator's diameter would not affect the object's diameter calculation as much as if the calibrator star had a significant angular size on the sky. The calibrator's diameter was considered a known value so that a visibility could be assigned to the calibrator based on its size.

Table. 3.1: Unreliable Calibrators

| HD | Reason | Calibrator for |
|--------|-----------------------------|----------------|
| 13555 | $V_{\text{calibrated}} > 1$ | HD 10697 |
| 16824 | $V_{\text{calibrated}} > 1$ | HD 16141 |
| 42398 | $V_{\text{calibrated}} > 1$ | HD 50554 |
| 119350 | Uneven visibility | HD 117176 |
| 144015 | Uneven visibility | HD 145675 |
| 169370 | $V_{\text{calibrated}} > 1$ | HD 168443 |
| 173093 | $V_{\text{calibrated}} > 1$ | HD 168443 |
| 176939 | $V_{\text{calibrated}} > 1$ | HD 177830 |

The smaller the calibrator, the better. For example, if a given calibrator has an angular diameter of 0.10 mas, its visibility is ~ 0.993 at the longest baseline in the *K*-band. When you change that diameter to 0.15 mas, a 50% increase, the visibility drops to 0.985, a difference of less than 1%. On the other hand, if a calibrator's angular diameter is 1.0 mas, its visibility is 0.453 and when you increase it by 50% to 1.5 mas, the visibility drops very significantly to 0.074 (see Figure 2.7). Therefore calibrators

should be as unresolved as possible. This was not always achievable due to the limited number of potential calibrators close to the target star with the appropriate magnitudes.

Another small source of potential systematic error in the object's diameter measurement comes from limb-darkening effects. If the object's visibilities are calibrated using the calibrator's uniform disk diameter, and if there is a large difference between the limb darkening between the calibrator and the object, some error will be introduced. However, the difference is only a few percent and is not as significant an effect in the K -band as it would be for measurements in visible wavelengths (Berger et al. 2006). For barely resolved calibrators, this effect is diminished even further.

In an effort to find reliable calibrators, spectral energy distribution (SED) fits based on published $UBVR IJHK$ photometric values¹ were produced for each calibrator to establish diameter estimates and to check if there was any excess emission that would indicate a low-mass stellar companion or circumstellar disk. Calibrator candidates with variable radial velocities reported in the literature or showing any other indication of a possible companion were discarded even if their SEDs displayed no characteristics of duplicity. See Figure 3.1 for examples of both good and bad potential calibrators. Limb-darkened angular diameter estimates for the calibrators were determined from Kurucz model atmospheres² fits to photometric values obtained from the literature. This was performed using IDL programs written by Douglas Gies.

¹All obtained using VizieR (<http://vizier.u-strasbg.fr/viz-bin/VizieR>).

²<http://kurucz.cfa.harvard.edu>

SED fits for all the calibrators and exoplanet host stars observed in this dissertation can be found in Appendices A (exoplanet host stars) and B (calibrator stars). The photometric sources are indicated for each star in the caption. Many calibrators in this dissertation were found using the *getCal* observing planning tool suite, a service provided by the Michelson Science Center³.

The observing pattern was calibrator-object-calibrator, etc., so every object observation was flanked by calibrator observations as close in time as possible. This is more commonly called a “bracketed observation”, so “10 bracketed observations” denotes 10 object observations and 11 calibrator observations.

3.2 Baselines Used

One of the advantages of the CHARA Array is its wide range of baseline lengths and orientations. Ideally, observations were obtained using two different baselines for each exoplanet system. I chose several intermediate-length baselines with generally east-west orientations (W1-W2, E2-W2, and W1-S1) and observed the exoplanet systems over the course of several hours as the system moved from east to transit or transit to west. As time passed and the object moved across the sky, the projected baseline changed as the hour angle changed, and there was significant baseline scanning, which allowed me to see if there were modulations in the visibility curve as a function of time as well as baseline that would indicate a stellar companion. See Figure 3.2 for

³<http://mscweb.ipac.caltech.edu/gcWeb/gcWeb.jsp>

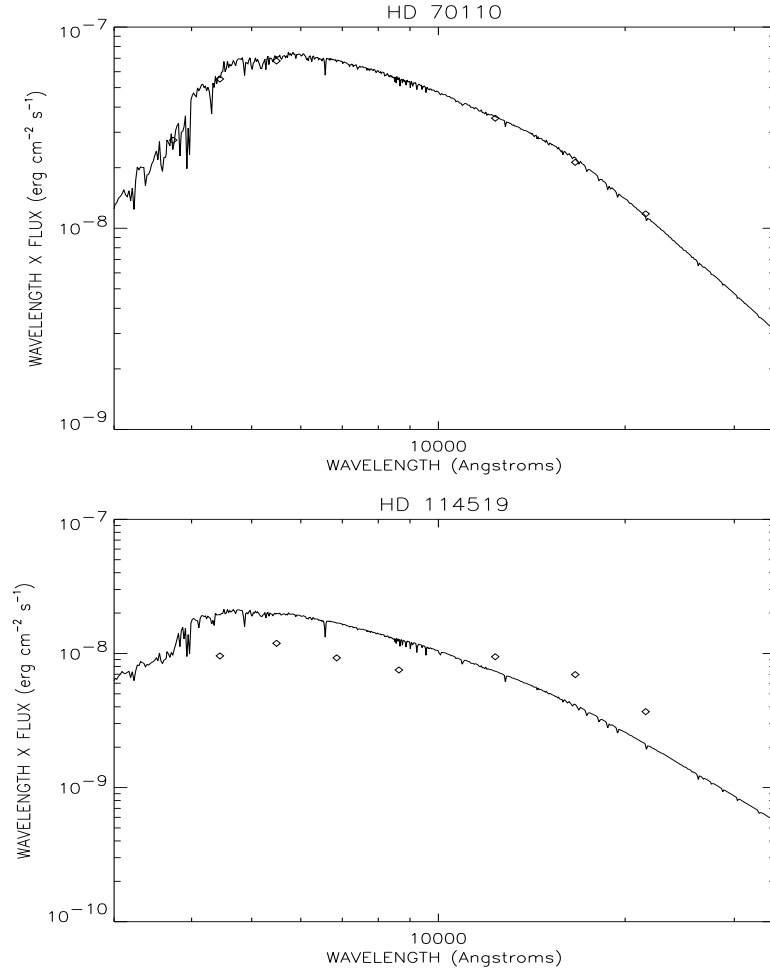


Figure. 3.1: Examples of a reliable (top) and an unreliable (bottom) calibrators' SEDs. The \diamond s are photometrically-derived fluxes and the solid line is the model SED for a star of a given T_{eff} and $\log g$. Note how well the datapoints overlay the model in the top plot while there appears to be excess flux at the longer wavelengths for the bottom plot. The bottom panel shows data for a known binary system and the excess flux is from the low-mass secondary star. Each tick on the x-axis represents 1,000 Angstroms.

an example of how the projected baseline orientation angle changes with respect to baseline as time passes.

I also observed using the longest baseline (S1-E1) to obtain the best possible stellar diameter measurement. The shorter baselines are not as sensitive to changes

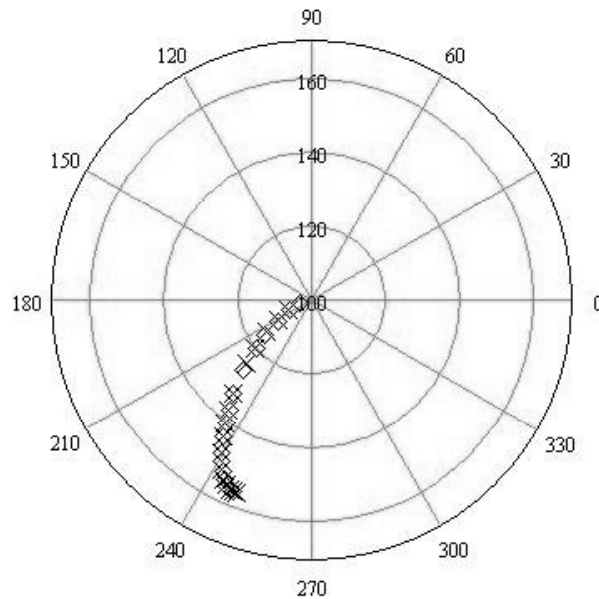


Figure. 3.2: Example baseline vs. baseline position orientation angle. \times = calibrator's projected baseline and \diamond = object's projected baseline at the time of observation. North is indicated by 0° , east is 90° , and so on. The values along the radial axis are in units of meters. As time passes, the baseline's projected position angle changes and significant baseline scanning is seen. (Data for τ Bootis, observed on 2005/05/12.)

in diameter, as can be seen in Figure 2.7. On the other hand, this longest baseline is oriented in a more north-south direction and is not as sensitive to stellar companions due to a lack of significant baseline scanning.

3.3 Data Reduction Pipeline

The main data reduction program used, *VisUVCalc*, is a Mathcad program developed by Harold McAlister and Anders Jerkstrand. It calculates visibility from the amplitude of the fringe packet as described by Benson et al. (1995).

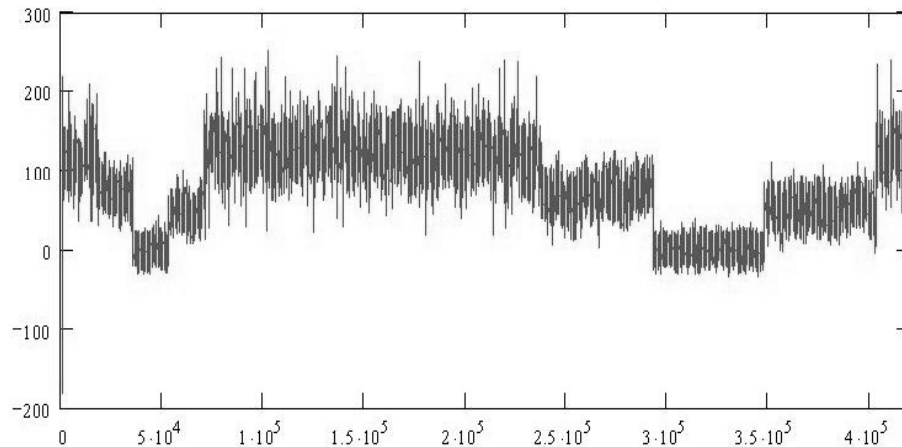


Figure. 3.3: Example data scan. The x-axis represents time and the y-axis represents signal strength. There are approximately 200 scans in between the shutter sequences (the stepped structures at the beginning and end of the dataset). Note the end shutter sequence is approximately three times longer than the beginning shutter sequence. This provides more dither scans to better characterize noise.

3.3.1 Visibility Calculation

During an observation, data are collected from both sides of the CHARA Classic beam splitter and the signals are denoted as IA and IB . Shutter sequences are performed at the beginning and end of the dataset to measure signal strengths, dark noise, and the degree of intensity balance in the two beams. Each shutter is closed one at a time (left and right wings of the stepped sequence) and both at once (lowest center part of sequence). See Figure 3.3 for an example of this.

The path length of the starlight is almost equalized using the delay lines and OPLE carts described in §2.6, but the exact location of the fringe is found by scanning a dither mirror through the zero path length region, which is the area most likely to harbor the fringes. Often the fringes are slightly offset from the estimated zero path

length region because the exact distance between the telescopes and PoP mirrors is not known to the accuracy needed to find fringes. Once the fringes are found, their offset is recorded and subsequent scans return to that position, so searching for fringes is not required for every observation. The offsets are generally stable or slowly drift in an easily predictable way. After the fringes are found, fringe tracking is started, which allows the instrument to keep the fringes centered in the data-acquisition window. Then data are recorded.

Approximately 200 individual scans comprise each dataset. Each scan is sent through a 15-Hz low-pass filter in order to characterize the low-frequency modulations in the fringe scan. These modulations are eliminated from the scan through normalization. IA is then subtracted from IB to give the signal for analysis following smoothing by a 50-Hz bandpass filter. See Figure 3.4 for an example of this process.

The fringe is fit after selecting initial values based on the nominal fringe frequency calculated from the dither mirror velocity and the wavenumber. The maximum in the fringe is found, and a model fringe is fit to the vicinity of that maximum. The fringes before and after the maximum fringe are also fit, and visibilities and the S/N are calculated for each of the three fits. Zero weight is assigned to outliers (when S/N exceeds a tolerance of 0.9) and where there are unrealistically large visibilities. These occur most often when no fringes were found for a given scan and the noise far exceeds the spurious measurements. The program's outputs include HD number, the

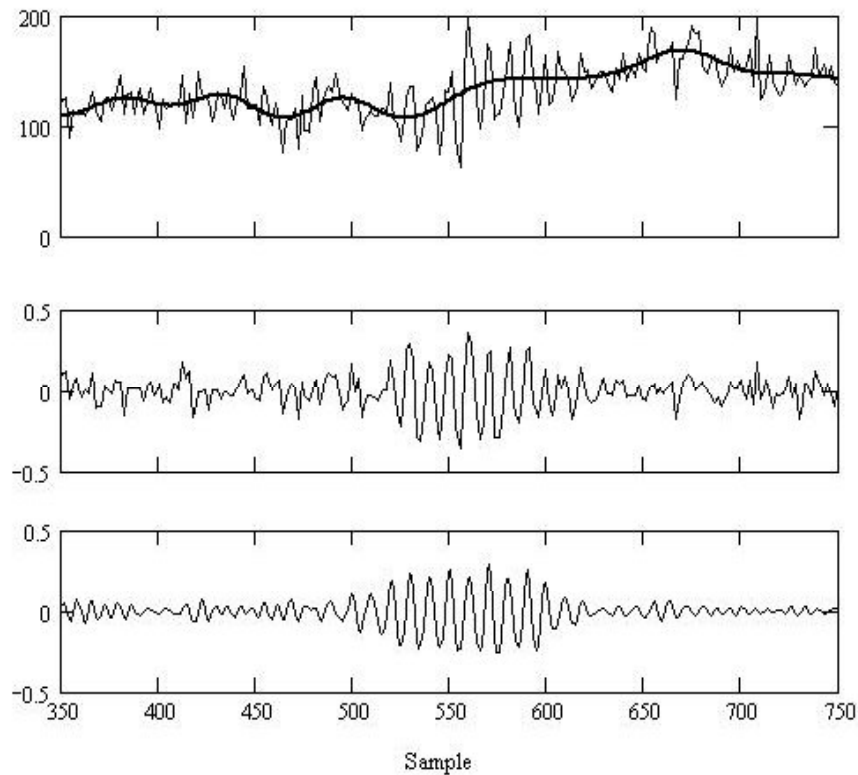


Figure. 3.4: The top panel shows an example fringe scan in its raw signal form and the solid line is the low-pass filter version of the data. The middle panel shows the same fringe after low-pass filter subtraction, which removes the low-frequency modulations seen in the top panel. The bottom panel is the fringe after processing with the bandpass filter.

altitude and azimuth of the star, the exact baseline at the time of observation, the raw and dark signals for the dataset, the frequency of the observation, the measured uncalibrated visibility, and the Julian Date.

3.3.2 Visibility Calibration

The output file is then read into the *Visibility Calibrator* Mathcad program, also written by Harold McAlister. The object's spectral type and *HIPPARCOS* parallax

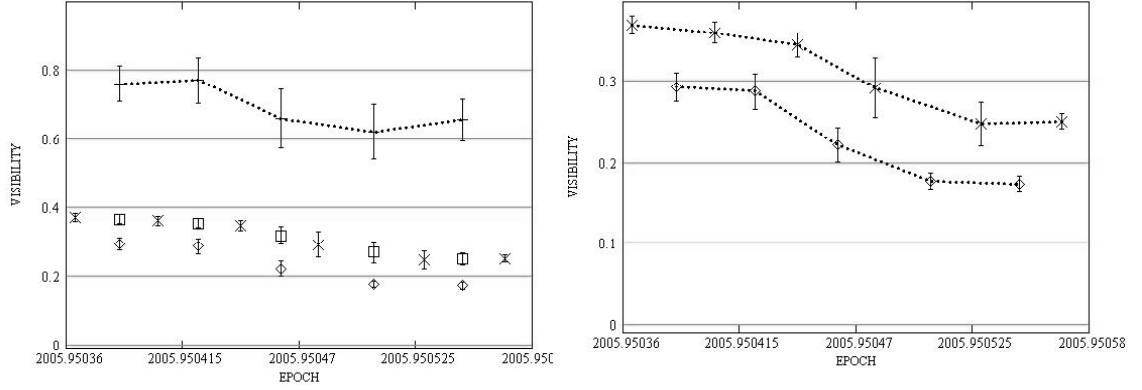


Figure. 3.5: Example of visibility calibration: Visibility vs. epoch. \times s = instrumental calibrator visibilities (V_{IC}); \diamond s = instrumental object visibilities (V_{IO}); \square s = calibrator visibilities interpolated to the time of object observations (V_{TC}); and $+$ s = calibrated visibilities (V_{TO}). The plot on the right is an expanded version of the plot seen on the bottom half of the left panel. (Data for HD 3651 from 2005/12/14.)

and the calibrator's diameter calculated from SED fits are entered. The object's visibility is calibrated using

$$\frac{V_{TO}}{V_{TC}} = \frac{V_{IO}}{V_{IC}}, \quad (3.1)$$

where V_{TO} and V_{TC} are the true visibilities of the object and calibrator, respectively, and V_{IO} and V_{IC} are the instrumental visibilities of the object and calibrator, respectively. V_{IO} and V_{IC} are measured, V_{TC} is calculated via a linear interpolation between calibrated visibility points to match the times of the object's visibility measurements, and V_{TO} represents the final calibrated visibilities of the observations (see Figure 3.5).

There are other worlds than these.

— *Stephen King*

Observations

This chapter starts with several tables listing the basic observables for the objects and calibrators observed in this dissertation, and an observing log. While the data and plots for the individual targets can be found in Appendix C, the presentation format is described here.

Of the 248 exoplanets in 225 systems known as of 2007/08/01 according to the *Extrasolar Planets Encyclopedia*, 82 are accessible to the CHARA Array. The main factors used to derive the observing list were declination (north of -10°) and limiting magnitudes ($K \sim +6.5$, $V \sim +10$). Ideally, I would have observed all 82 systems, but after the occasional inclement weather, time allocation constraints, and other time limitations, I was able to observe 31 of the 81 exoplanet systems.

4.1 Stellar and Planetary Parameters

Tables 4.1 and 4.2 list the basic observed parameters for the exoplanet host stars and calibrator stars. These parameters include the star’s coordinates, V - and K -band magnitudes, spectral classification, parallax, and projected rotational velocity ($v \sin i$) if known. Table 4.3 lists the orbital parameters for the exoplanets observed in this dissertation.

Table. 4.1: Basic Parameters for Exoplanet Host Stars

| HD | HR | HIP | Other Names | RA (hh mm ss.s) | Dec (dd mm ss.s) | V (mag) | K (mag) | Spectral Classification | Parallax (mas) | $v \sin i$ (km s ⁻¹) |
|--------|------|--------|----------------|--------------------|---------------------|--------------|--------------|----------------------------|-------------------|-------------------------------------|
| 3651 | 166 | 3093 | 54 Psc | 00 39 21.8 | +21 15 01.7 | 5.80 | 4.00 | K0 V | 90.03±0.72 | 1.1 |
| 9826 | 458 | 7513 | ν And | 01 36 47.8 | +41 24 19.7 | 4.09 | 2.86 | F8 V | 74.25±0.72 | 9.6 |
| 10697 | 508 | 8159 | 109 Psc | 01 44 55.8 | +20 04 59.3 | 6.29 | 4.60 | G5 IV | 30.71±0.81 | 2.5 |
| 11964 | - | 9094 | - | 01 57 09.6 | -10 14 32.7 | 6.42 | 4.49 | G5 | 29.43±0.91 | 2.7 |
| 13189 | - | 10085 | - | 02 09 40.2 | +32 18 59.2 | 7.57 | 4.00 | K2 II | 0.54±0.93 | N/A |
| 16141 | - | 12048 | 79 Cet | 02 35 19.9 | -03 33 38.2 | 6.78 | 5.27 | G5 IV | 27.85±1.39 | 1.9 |
| 19994 | 962 | 14954 | 94 Cet | 03 12 46.4 | -01 11 46.0 | 5.06 | 3.75 | F8 V | 44.69±0.75 | 8.6 |
| 20367 | - | 15323 | - | 03 17 40.0 | +31 07 37.4 | 6.41 | 5.04 | G0 V | 36.86±1.08 | N/A |
| 34445 | - | 24681 | - | 05 17 41.0 | +07 21 12.0 | 7.32 | 5.79 | G0 | 22.22±1.05 | 2.7 |
| 38529 | 1988 | 27253 | - | 05 46 34.9 | +01 10 05.5 | 5.94 | 4.21 | G4 IV | 23.57±0.92 | 3.9 |
| 50554 | - | 33212 | - | 06 54 42.8 | +24 14 44.0 | 6.86 | 5.47 | F8 | 32.23±1.01 | 3.9 |
| 59686 | 2877 | 36616 | - | 07 31 48.4 | +17 05 09.8 | 5.45 | 2.92 | K2 III | 10.81±0.75 | N/A |
| 75732 | 3522 | 43587 | 55 Cnc | 08 52 35.8 | +28 19 51.0 | 5.95 | 4.02 | G8 V | 79.80±0.84 | 2.5 |
| 95128 | 4277 | 53721 | 47 UMa | 10 59 28.0 | +40 25 48.9 | 5.10 | 3.75 | G0 V | 71.04±0.66 | 2.8 |
| 104985 | 4609 | 58952 | - | 12 05 15.1 | +76 54 20.6 | 5.80 | 3.27 | G9 III | 9.80±0.52 | N/A |
| 117176 | 5072 | 65721 | 70 Vir | 13 28 25.8 | +13 46 43.6 | 5.00 | 3.50 | G4 V | 55.22±0.73 | 2.7 |
| 120136 | 5185 | 67275 | τ Boo | 13 47 15.7 | +17 27 24.9 | 4.50 | 3.51 | F7 V | 64.12±0.70 | 15.0 |
| 128311 | - | 71395 | HN Boo | 14 36 00.6 | +09 44 47.5 | 7.51 | 5.14 | K0 V | 60.35±0.99 | 3.6 |
| 143761 | 5968 | 78459 | ρ CrB | 16 01 02.7 | +33 18 12.6 | 5.40 | 3.86 | G0 V | 57.38±0.71 | 1.6 |
| 145675 | - | 79248 | 14 Her | 16 10 24.3 | +43 49 03.5 | 6.67 | 4.71 | K0 V | 55.11±0.59 | 1.6 |
| 168443 | - | 89844 | - | 18 20 03.9 | -09 35 44.6 | 6.92 | 5.21 | G6 IV | 26.40±0.85 | 2.2 |
| 177830 | - | 93746 | - | 19 05 20.8 | +25 55 14.4 | 7.18 | 4.81 | K0 IV | 16.94±0.76 | 2.5 |
| 186427 | 7504 | 96901 | 16 Cyg B | 19 41 52.0 | +50 31 03.1 | 6.20 | 4.65 | G2.5 V | 46.70±0.52 | 2.2 |
| 189733 | - | 98505 | V452 Vul | 20 00 43.7 | +22 42 39.1 | 7.67 | 5.54 | K2 V | 51.94±0.87 | N/A |
| 190228 | - | 98714 | - | 20 03 00.8 | +28 18 24.7 | 7.31 | 5.35 | G5 IV | 16.10±0.81 | 1.9 |
| 190360 | 7670 | 98767 | - | 20 03 37.4 | +29 53 48.5 | 5.71 | 4.08 | G6 IV | 62.92±0.62 | 2.2 |
| 192263 | - | 99711 | V1703 Aql | 20 13 59.8 | -00 52 00.8 | 7.79 | 5.54 | K0 V | 50.27±1.13 | 2.6 |
| 195019 | - | 100970 | - | 20 28 18.6 | +18 46 10.2 | 6.91 | 5.26 | G3 IV-V | 26.77±0.89 | 2.5 |
| 196885 | 7907 | 101966 | - | 20 39 51.9 | +11 14 58.7 | 6.40 | 5.07 | F8 IV | 30.31±0.81 | 7.7 |

Continued on Next Page...

Table. 4.1 – Continued

| HD | HR | HIP | Other Names | RA (hh mm ss.s) | Dec (dd mm ss.s) | V (mag) | K (mag) | Spectral Classification | Parallax (mas) | $v \sin i$ (km s ⁻¹) |
|--------|------|--------|----------------|--------------------|---------------------|------------|------------|----------------------------|-------------------|-------------------------------------|
| 217014 | 8729 | 113357 | 51 Peg A | 22 57 28.0 | +20 46 07.8 | 5.49 | 3.91 | G2-3 V | 65.10±0.76 | 2.6 |
| 217107 | 8734 | 113421 | - | 22 58 15.5 | -02 23 43.4 | 6.18 | 4.54 | G7 V | 50.71±0.75 | 0.0 |

Note. All values were obtained using the *SIMBAD Astronomical Database* except for the *K* magnitudes, which were obtained from *The Two*

Micron All Sky Survey (Skrutskie et al. 2006), and the $v \sin i$ values, which are from Valenti & Fischer (2005).

Table. 4.2: Basic Parameters for Calibrator Stars

| HD | HR | HIP | Other Names | RA (hh mm ss.s) | Dec (dd mm ss.s) | V (mag) | K (mag) | Spectral Classification | Parallax (mas) | $v \sin i$ (km s ⁻¹) |
|--------|------|-------|----------------|--------------------|---------------------|------------|------------|----------------------------|-------------------|-------------------------------------|
| 4568 | 217 | 3730 | 61 Psc | 00 47 54.8 | +20 55 31.2 | 6.60 | 5.29 | F8 V | 17.41±0.87 | 10.5 |
| 6920 | 340 | 5493 | 44 And | 01 10 18.7 | +42 04 53.3 | 5.68 | 4.46 | F8 V | 18.98±0.71 | 15.0 |
| 8671 | 409 | 6711 | - | 01 26 18.7 | +43 27 27.9 | 5.99 | 4.72 | F7 V | 24.21±0.74 | 5.0 |
| 10477 | - | 7975 | - | 01 42 26.9 | +15 46 42.7 | 7.57 | 5.06 | K0 | 5.24±0.91 | N/A |
| 11007 | 523 | 8433 | - | 01 48 41.6 | +32 41 24.8 | 5.79 | 4.34 | F8 V | 36.65±0.73 | 5.0 |
| 13456 | 638 | 10215 | - | 02 11 22.2 | -10 03 07.8 | 6.01 | 4.98 | F5 V | 20.00±0.94 | 15.0 |
| 13555 | 646 | 10306 | η Ari | 02 12 48.1 | +21 12 39.6 | 5.24 | 4.12 | F5 V | 33.19±0.85 | 10.0 |
| 14690 | 691 | 11046 | 70 Cet | 02 22 12.4 | -00 53 05.5 | 5.43 | 4.58 | F0 V | 11.68±0.86 | 185.0 |
| 16824 | 795 | 12584 | - | 02 41 48.3 | -03 12 49.7 | 6.07 | 3.42 | G9 III | 4.49±0.98 | N/A |
| 19411 | - | 14494 | - | 03 07 12.8 | -01 48 09.9 | 6.96 | 4.77 | G5 | 1.73±0.92 | N/A |
| 21864 | - | 16507 | - | 03 32 32.1 | +31 38 52.7 | 7.75 | 5.09 | K0 | 3.36±1.09 | 3.3 |
| 31423 | - | 22938 | - | 04 56 09.0 | +07 54 16.9 | 6.43 | 5.41 | F5 | 17.02±1.10 | N/A |
| 42398 | 2185 | 29379 | 5 Gem | 06 11 32.3 | +24 25 12.9 | 5.84 | 3.32 | K0 III | 4.33±0.83 | 1.0 |
| 43318 | 2233 | 29716 | - | 06 15 34.3 | -00 30 43.9 | 5.65 | 4.32 | F6 V | 28.02±0.76 | N/A |
| 49736 | - | 32874 | - | 06 51 00.4 | +25 45 37.3 | 6.91 | 5.59 | F8 | 27.01±1.04 | N/A |
| 61630 | 2953 | 37404 | - | 07 40 47.2 | +13 46 16.5 | 6.22 | 3.12 | K0 | 3.15±0.79 | N/A |
| 72779 | 3387 | 42133 | 35 Cnc | 08 35 19.4 | +19 35 24.2 | 6.58 | 5.00 | G0 III | 5.57±0.91 | 85.0 |
| 90840 | 4113 | 51420 | 32 LMi | 10 30 06.4 | +38 55 30.5 | 5.79 | 5.48 | A4 V | 4.29±0.70 | 75.0 |
| 97619 | - | 55048 | - | 11 16 08.9 | +78 18 32.2 | 6.88 | 3.87 | K0 | 5.13±0.59 | N/A |
| 119350 | - | 66895 | - | 13 42 32.8 | +15 08 49.3 | 7.23 | 4.13 | K2 | 2.81±0.97 | N/A |
| 121107 | 5225 | 67787 | 7 Boo | 13 53 12.9 | +17 55 58.3 | 5.71 | 4.08 | G5 III | 4.77±0.79 | 15.8 |
| 125194 | - | 69841 | - | 14 17 36.9 | +11 20 06.9 | 7.60 | 4.47 | K0 | 2.79±0.92 | N/A |
| 136849 | 5718 | 75178 | 50 Boo | 15 21 48.6 | +32 56 01.3 | 5.38 | 5.49 | B9 V | 13.20±0.59 | 270.0 |
| 143393 | - | 78288 | - | 15 59 05.9 | +29 25 53.7 | 7.12 | 4.46 | K2 III | 6.85±0.75 | N/A |
| 143687 | - | 78429 | - | 16 00 42.5 | +31 34 05.7 | 6.62 | 4.06 | K0 | 8.65±0.69 | N/A |
| 144015 | - | 78537 | - | 16 02 02.1 | +40 01 22.3 | 6.85 | 3.82 | K0 | 4.16±0.63 | 3.2 |
| 146025 | - | 79452 | - | 16 12 51.0 | +32 35 57.2 | 7.49 | 4.97 | K2 | 6.29±0.78 | N/A |
| 151044 | - | 81800 | - | 16 42 27.8 | +49 56 11.2 | 6.47 | 5.15 | F8 V | 34.00±0.50 | 5.2 |
| 169370 | 6892 | 90238 | - | 18 24 42.1 | -07 04 33.4 | 6.30 | 3.55 | K0 | 11.62±0.95 | N/A |

Continued on Next Page...

Table. 4.2 – Continued

| HD | HR | HIP | Other Names | RA (hh mm ss.s) | Dec (dd mm ss.s) | V (mag) | K (mag) | Spectral Classification | Parallax (mas) | $v \sin i$ (km s ⁻¹) |
|--------|------|--------|----------------|--------------------|---------------------|------------|------------|----------------------------|-------------------|-------------------------------------|
| 173093 | 7034 | 91880 | - | 18 43 51.2 | -06 49 05.2 | 6.30 | 5.12 | F7 V | 14.36±0.87 | 25.0 |
| 176377 | - | 93185 | - | 18 58 51.0 | +30 10 50.3 | 6.78 | 5.30 | G0 | 42.68±0.64 | N/A |
| 176939 | 7206 | 93419 | - | 19 01 34.9 | +25 01 33.4 | 6.74 | 3.33 | K2 | 2.35±0.69 | N/A |
| 184960 | 7451 | 96258 | - | 19 34 19.8 | +51 14 11.8 | 5.70 | 4.49 | F7 V | 39.08±0.47 | 5.0 |
| 188350 | 7596 | 97980 | 58 Aql | 19 54 44.8 | +00 16 25.1 | 5.63 | 5.21 | A0 III | 9.45±1.15 | N/A |
| 189108 | - | 98209 | - | 19 57 23.7 | +28 41 38.0 | 6.78 | 4.64 | G8 III | 3.97±0.76 | N/A |
| 190470 | - | 98828 | - | 20 04 10.0 | +25 47 24.8 | 7.82 | 5.64 | K3 V | 46.28±0.91 | 4.8 |
| 190993 | 7688 | 99080 | 17 Vul | 20 06 53.4 | +23 36 51.9 | 5.06 | 5.57 | B3 V | 6.68±0.71 | 215.0 |
| 194012 | 7793 | 100511 | - | 20 22 52.4 | +14 33 04.0 | 6.17 | 4.90 | F8 V | 38.27±0.72 | 5.0 |
| 216953 | 8727 | 113345 | - | 22 57 17.2 | -04 48 36.3 | 6.32 | 4.16 | G9 III | 7.90±0.95 | N/A |
| 218261 | 8792 | 114096 | - | 23 06 31.9 | +19 54 39.1 | 6.30 | 5.14 | F7 V | 35.32±0.85 | 5.0 |

Note. All values were obtained using the *SIMBAD Astronomical Database* except for the *K* magnitudes, which were obtained from *The Two*

Micron All Sky Survey (Skrutskie et al. 2006), and the $v \sin i$ values, which are from Glebocki & Stawikowski (2000).

Table. 4.3: Planetary Orbital Parameters

| HD | M_{star} (M_{\odot}) | P (days) | T_p (JD-2,450,000) | e | ω (deg) | K_1 (m s^{-1}) | $M_p \sin i$ (M_{Jup}) | a (AU) | Ref |
|---------|--------------------------------------|---------------------|-------------------------|-------------------|-------------------|--------------------------------|--------------------------------------|-------------------|------|
| 3651b | 0.79 | 62.23 \pm 0.03 | 2501.7 \pm 1.2 | 0.63 \pm 0.04 | 235.7 \pm 6.6 | 15.9 \pm 1.7 | 0.20 | 0.284 | F03 |
| 9826b | 1.3 \pm 0.1 | 4.6170 \pm 0.0003 | 2.24 \pm 3.1 | 0.034 \pm 0.15 | 83.0 \pm 243 | 73.0 \pm 5 | 0.71 | 0.059 | B99 |
| 9826c | 1.3 \pm 0.1 | 241.2 \pm 1.1 | 154.9 \pm 20.8 | 0.18 \pm 0.11 | 243.6 \pm 33 | 58.0 \pm 7.9 | 2.11 | 0.83 | B99 |
| 9826d | 1.3 \pm 0.1 | 1266.6 \pm 30 | 1308.7 \pm 40.5 | 0.41 \pm 0.11 | 247.7 \pm 17.0 | 72.9 \pm 7.1 | 4.61 | 2.50 | B99 |
| 10697b | 1.10 | 1072.3 \pm 9.6 | 1482 \pm 39 | 0.12 \pm 0.02 | 113 \pm 14 | 119 \pm 3 | 6.35 | 2.12 | V00 |
| 11964b | 1.12 | 2110 \pm 270 | 2290 \pm 420 | 0.06 \pm 0.017 | 168 | 9.0 \pm 1.5 | 0.61 \pm 0.10 | 3.34 \pm 0.40 | B06 |
| 13189b | 2-7 | 471.6 \pm 6.0 | 2327.9 \pm 20.2 | 0.27 \pm 0.06 | 160.7 \pm 12.0 | 173.3 \pm 9.8 | 8-20 | - | H05 |
| 16141b | 1.01 | 75.82 \pm 0.4 | 1547.2 \pm 4.1 | 0.28 \pm 0.15 | 41 \pm 22 | 10.8 \pm 1.4 | 0.215 \pm 0.03 | 0.35 | M00 |
| 19994b | 1.34 | 535.7 \pm 3.1 | 1944 \pm 12 | 0.30 \pm 0.04 | 41 \pm 8 | 36.2 \pm 1.9 | 1.68 | 1.42 | M04 |
| 20367b | 1.17 | 469.5 \pm 9.3 | 1860 \pm 18 | 0.320 \pm 0.009 | 135 \pm 16 | 29.0 \pm 3.0 | 1.17 \pm 0.23 | 1.246 \pm 0.075 | B06 |
| 34445b | 1.11 | 126 | - | 0.4 | - | - | 0.58 | 0.51 | EE |
| 38529b | 1.4 | 14.32 \pm 0.8 | 1565.7 \pm 2.0 | 0.27 \pm 0.03 | 90.9 \pm 6.0 | 53.8 \pm 2.0 | 0.77 | 0.13 | F01 |
| 50554b | 1.11 | 1293 \pm 37 | 1832.4 \pm 15 | 0.501 \pm 0.030 | 355.7 \pm 4.4 | 104 \pm 5 | 5.16 | 2.41 | P03 |
| 59686b | - | 303 | - | - | - | 149.0 | 6.5 | - | M03 |
| 75732b | 0.95 | 14.653 \pm 0.0006 | 1479 | 0.020 \pm 0.02 | 99 \pm 35 | 72.2 \pm 1.0 | 0.84 \pm 0.07 | 0.115 \pm 0.003 | M02 |
| 75732c | 0.95 | 44.276 \pm 0.021 | 31.4 \pm 2.5 | 0.339 \pm 0.21 | 61 \pm 25 | 13.0 \pm 1.3 | 0.21 \pm 0.04 | 0.241 \pm 0.005 | M02 |
| 75732d | 0.95 | 5360 \pm 400 | 2785 \pm 250 | 0.16 \pm 0.06 | 201 \pm 22 | 49.3 \pm 2.5 | 4.05 \pm 0.04 | 5.9 \pm 0.9 | M02 |
| 95128b | 1.03 | 1089.0 \pm 2.9 | 356.0 \pm 33.6 | 0.061 \pm 0.014 | 171.8 \pm 15.2 | 49.3 \pm 1.2 | 2.54 | 2.09 | F02 |
| 95128c | 1.03 | 2594 \pm 90 | 1363.5 \pm 495.3 | 0.005 \pm 0.115 | 127.0 \pm 55.8 | 11.1 \pm 1.1 | 0.76 | 3.73 | F02 |
| 104985b | 1.6 | 198.2 \pm 0.3 | 1990 \pm 20 | 0.03 \pm 0.02 | 310 \pm 30 | 161 \pm 2 | 6.3 | 0.78 | S03a |
| 117176b | 0.92 | 116.67 \pm 0.01 | -1009.597 \pm 0.5 | 0.40 \pm 0.01 | 2.1 \pm 2 | 318 \pm 4 | 6.6 | 0.430 | MB96 |
| 120136b | 1.2 | 3.3128 \pm 0.0002 | 235.41 \pm 0.2 | 0.018 \pm 0.016 | 254 | 469 \pm 5 | 3.87 | 0.0462 | B97 |
| 128311b | 0.80 | 422 \pm 10 | 28 \pm 30 | 0.31 \pm 0.1 | 228 \pm 40 | 85 \pm 7 | 2.57 | 1.02 | B03 |
| 143761b | 1.0 | 39.645 \pm 0.088 | 657.88 \pm 0.54 | 0.028 \pm 0.040 | 30 \pm 74 | 67.4 \pm 2.2 | 1.1 | 0.23 | N97 |
| 145675b | 1.00 | 1724 \pm 50 | 1353 \pm 30 | 0.37 \pm 0.04 | 15 \pm 15 | 89 \pm 3 | 4.89 | 2.82 | B03 |
| 168443b | 1.01 | 58.10 \pm 0.006 | 47.58 \pm 0.2 | 0.53 \pm 0.003 | 172.9 \pm 0.4 | 472.7 \pm 1.8 | 7.73 | 0.295 | M01 |
| 168443c | 1.01 | 1770 \pm 25 | 250.6 \pm 18 | 0.20 \pm 0.01 | 62.9 \pm 3.2 | 289 \pm 3.8 | 17.15 | 2.87 | M01 |
| 177830b | 1.15 \pm 0.2 | 391.6 \pm 11 | 1333 \pm 14 | 0.41 \pm 0.13 | 5 \pm 35 | 34 \pm 14 | 1.22 | 1.10 | V00 |
| 186427b | 1.0 | 800.8 \pm 11.7 | -1064.7 \pm 12.0 | 0.634 \pm 0.082 | 83.2 \pm 12.7 | 43.9 \pm 6.9 | 1.5 | 1.6 | C97 |

Continued on Next Page...

Table. 4.3 – Continued

| HD | M_{star} (M_{\odot}) | P (days) | T_{P} (JD-2,450,000) | e | ω (deg) | K_1 (m s^{-1}) | $M_{\text{p}} \sin i$ (M_{Jup}) | a (AU) | Ref |
|---------|--------------------------------------|---------------|----------------------------------|---|---------------------------------------|--------------------------------|---|---------------|------|
| 189733b | 0.82 | 2.219±0.0005 | 3629.3890±0.0004 | 0 | - | 205±6 | 1.15±0.04 | 0.0313±0.0004 | B05 |
| 190228b | 0.83 | 1146±16 | 1236±25 | 0.499 ^{+0.047} _{-0.024} | 100.7 ^{+2.9} _{-3.2} | 91±5 | 3.58 | 2.02 | P03 |
| 190360b | 0.96 | 3902±1758 | 557±89 | 0.48±0.20 | 361±13 | 20.0±3.0 | 1.33±0.019 | 4.8 | N03 |
| 192263b | 0.75 | 24.348±0.005 | 1979.28±0.08 | 0.0 | 0.0 | 61±1 | 0.72 | 0.15 | S03b |
| 195019b | 0.98±0.6 | 18.27±0.14 | 1072.16±1.6 | 0.03±0.02 | 250±31 | 275.28±5.0 | 3.51±0.4 | 0.13 | F99 |
| 196885b | 1.27 | 386 | - | 0.3 | - | - | 1.84 | 1.12 | EE |
| 217014b | 1.0 | 4.2311±0.0005 | 203.947±0.03 | 0.012±0.01 | - | 55.9±0.8 | 0.45 | 0.051 | M97 |
| 217107b | 0.96±0.6 | 7.12±0.02 | 1067.42±0.30 | 0.14±0.05 | 19±14 | 139.5±4.1 | 1.27±0.4 | 0.07 | F99 |

B97: Butler et al. (1997); B99: Butler et al. (1999); B03: Butler et al. (2003); B05: Bouchy et al. (2005b); B06: Butler et al. (2006); C97: Cochran et al. (1997); EE: Extrasolar Planets Encyclopedia; F99: Fischer et al. (1999); F01: Fischer et al. (2001); F02: Fischer et al. (2002); F03: Fischer et al. (2003); H05: Hatzes et al. (2005); K05: Konacki (2005); M97: Marcy et al. (1997); M99: Marcy et al. (1999); M00: Marcy et al. (2000); M01: Marcy et al. (2001); M02: Marcy et al. (2002); M03: Mitchell et al. (2003); M04: Mayor et al. (2004); MB96: Marcy & Butler (1996); N03: Naef et al. (2003); N97: Noyes et al. (1997); P03: Pernier et al. (2003); S03a: Sato et al. (2003); S03b: Santos et al. (2003); V00: Vogt et al. (2000); V02: Vogt et al. (2002)

4.2 Observing Log

Data were obtained using the CHARA Array during multiple observing runs spanning 2005 May to 2007 May. Table 4.4 lists the observed objects, their calibrators, observation date, the number of bracketed observations, and the baseline used.

Table. 4.4: Observing Log

| Object HD | Calib. HD | UT Date | # Obs | Baseline |
|-----------|-----------|------------|-------|----------|
| 3651 | 4568 | 2005/10/22 | 2 | S1-E1 |
| | | 2005/10/24 | 6 | S1-E1 |
| | | 2005/12/14 | 5 | W1-S1 |
| 9826 | 6920 | 2005/08/04 | 11 | W1-W2 |
| | | 2005/08/08 | 14 | W1-W2 |
| | | 2005/08/14 | 10 | W1-W2 |
| | 8671 | 2005/08/10 | 16 | W1-W2 |
| | | 2005/08/18 | 25 | W1-W2 |
| | | 2005/08/19 | 19 | W1-W2 |
| 10697 | 10477 | 2005/10/23 | 7 | S1-E1 |
| | 13555 | 2006/08/12 | 7 | S1-E1 |
| 11964 | 13456 | 2005/12/13 | 1 | W1-S1 |
| | | 2005/12/16 | 5 | W1-S1 |
| | | 2006/10/20 | 7 | W1-W2 |
| 13189 | 11007 | 2005/12/12 | 4 | S1-E1 |
| | | 2006/08/14 | 4 | S1-E1 |
| 16141 | 16824 | 2005/12/12 | 8 | S1-E1 |
| | | 2005/12/14 | 7 | W1-S1 |
| | 14690 | 2006/08/13 | 4 | S1-E1 |
| | | 2006/08/14 | 4 | S1-E1 |
| 19994 | 19411 | 2005/10/21 | 4 | S1-E1 |
| | | 2005/10/27 | 6 | S1-E1 |
| | | 2005/12/10 | 6 | S1-E1 |
| 20367 | 21864 | 2005/12/12 | 5 | S1-E1 |
| | | 2007/01/24 | 2 | S1-E1 |
| | | 2007/02/05 | 2 | S1-E1 |
| 34445 | 31423 | 2005/12/07 | 8 | S1-E1 |
| | | 2005/12/10 | 4 | S1-E1 |
| 38529 | 43318 | 2005/10/22 | 2 | S1-E1 |
| | | 2005/10/24 | 2 | S1-E1 |
| | | 2005/12/06 | 8 | S1-E1 |
| | | 2005/12/14 | 5 | W1-S1 |
| 50554 | 49736 | 2005/12/07 | 3 | S1-E1 |
| | | 2005/12/12 | 5 | S1-E1 |

Continued on Next Page...

Table. 4.4 - Continued

| Object HD | Calib. HD | UT Date | # Obs | Baseline |
|-----------|-----------|------------|-------|----------|
| | 42398 | 2007/02/06 | 3 | S1-E1 |
| 59686 | 61630 | 2005/12/06 | 8 | S1-E1 |
| | | 2005/12/16 | 8 | W1-S1 |
| | | 2007/04/02 | 9 | S1-E1 |
| 75732 | 72779 | 2007/03/26 | 5 | S1-E1 |
| | | 2007/03/30 | 6 | S1-E1 |
| 95128 | 90840 | 2006/05/19 | 3 | S1-E1 |
| 104985 | 97619 | 2006/05/17 | 10 | W1-W2 |
| | | 2007/04/26 | 7 | E1-W1 |
| 117176 | 119350 | 2005/05/14 | 6 | E2-W2 |
| | 121107 | 2006/05/13 | 10 | W1-W2 |
| | | 2006/05/20 | 6 | S1-E1 |
| | | 2007/04/02 | 7 | S1-E1 |
| 120136 | 121107 | 2005/05/12 | 16 | E2-W2 |
| | | 2006/05/14 | 11 | W1-W2 |
| | | 2007/02/05 | 10 | S1-E1 |
| | | 2007/03/25 | 2 | S1-E1 |
| | | 2007/03/26 | 5 | S1-E1 |
| | | 2007/03/30 | 8 | S1-E1 |
| 128311 | 125194 | 2005/06/30 | 5 | E2-W2 |
| | | 2006/05/16 | 6 | W1-W2 |
| 143761 | 143393 | 2005/06/29 | 6 | E2-W2 |
| | | 2005/07/03 | 7 | E2-W2 |
| | 143687 | 2006/05/12 | 8 | W1-W2 |
| | 146025 | 2006/05/12 | 5 | W1-W2 |
| | 136849 | 2006/05/19 | 4 | S1-E1 |
| | | 2006/06/09 | 1 | S1-E1 |
| 145675 | 144015 | 2005/05/14 | 5 | E2-W2 |
| | | 2005/07/04 | 11 | E2-W2 |
| | | 2006/05/13 | 10 | W1-W2 |
| | 151044 | 2006/08/07 | 10 | W1-W2 |
| | | 2006/08/11 | 3 | S1-E1 |
| | | 2006/08/12 | 7 | S1-E1 |
| 168443 | 169370 | 2005/08/10 | 7 | W1-W2 |
| | | 2005/08/14 | 6 | W1-W2 |
| | | 2005/08/20 | 4 | W1-W2 |
| | 173093 | 2006/05/14 | 9 | W1-W2 |
| 177830 | 176939 | 2005/06/29 | 4 | E2-W2 |
| | | 2005/08/08 | 5 | W1-W2 |
| | 176377 | 2006/06/09 | 1 | S1-E1 |
| | | 2006/08/08 | 7 | W1-W2 |
| | | 2006/08/13 | 6 | S1-E1 |
| 186427 | 184960 | 2005/06/30 | 8 | E2-W2 |
| | | 2006/08/04 | 10 | W1-W2 |
| | | 2006/08/13 | 6 | S1-E1 |
| 189733 | 190993 | 2006/06/01 | 3 | S1-E1 |
| | | 2006/06/08 | 1 | S1-E1 |

Continued on Next Page...

Table. 4.4 - Continued

| Object HD | Calib. HD | UT Date | # Obs | Baseline |
|-----------|---------------|------------|-------|----------|
| | 192044 | 2006/06/08 | 4 | S1-E1 |
| | 190993+192044 | 2006/05/29 | 3 | S1-E1 |
| | | 2006/05/30 | 4 | S1-E1 |
| | | 2006/05/31 | 3 | S1-E1 |
| | | 2006/06/01 | 1 | S1-E1 |
| | Both+184385 | 2006/06/02 | 3 | S1-E1 |
| | | 190993 | 9 | S1-E1 |
| 190228 | 190470 | 2005/07/01 | 6 | E2-W2 |
| | | 2005/08/19 | 5 | W1-W2 |
| | | 2006/08/14 | 8 | S1-E1 |
| 190360 | 189108 | 2005/08/11 | 10 | W1-W2 |
| | | 2006/06/09 | 1 | S1-E1 |
| | | 2006/08/11 | 9 | S1-E1 |
| 192263 | 188350 | 2006/05/20 | 2 | S1-E1 |
| 195015 | 194012 | 2005/08/11 | 5 | W1-W2 |
| | | 2005/08/12 | 10 | W1-W2 |
| | | 2005/10/23 | 10 | S1-E1 |
| | | 2006/08/06 | 6 | W1-W2 |
| 196885 | 194012 | 2005/10/27 | 4 | S1-E1 |
| | | 2005/10/29 | 5 | E2-W2 |
| | | 2006/08/07 | 10 | W1-W2 |
| | | 2006/08/14 | 5 | S1-E1 |
| 217014 | 218261 | 2005/08/03 | 4 | W1-W2 |
| | | 2005/08/12 | 14 | W1-W2 |
| | | 2006/08/12 | 7 | S1-E1 |
| 217107 | 216953 | 2005/12/13 | 3 | W1-S1 |
| | | 2006/10/20 | 8 | W1-W2 |

4.3 Individual Target Data Format

Data and notes on the individual exoplanet host stars are presented in Appendix C and the format is the same for each star: §C.x.1 lists the calibrated visibilities from CHARA Array observations, including the Modified Julian Date (MJD) and the exact baseline (B) of the observations, the position angle (PA), the calibrated visibility (V_c), and the error in V_c ($\sigma(V_c)$).

Table. 4.5: Symbols Used in Visibility Plots

| Symbol | Represents |
|-------------|---|
| \times | Instrumental calibrator visibility (V_{IC}) |
| \diamond | Instrumental object visibility (V_{IO}) |
| \square | Calibrator visibility interpolated to time of object observation (V_{TC}) |
| $+$ | Calibrated visibility (V_{TO}) |
| \circ | Residuals to diameter fit |
| Solid line | Theoretical visibility curve for star with measured diameter |
| Dashed line | Error in the theoretical visibility curve |

Section C.x.2 includes plots of the uncalibrated and calibrated visibilities for each night's observations. There is one dataset per night of observation, and each dataset is made of three plots: the two upper panels show uncalibrated visibility vs. epoch while the bottom panel displays calibrated visibility vs. baseline. See Figure 4.1 for an example. Table 4.5 lists the symbols used in these plots. After these, a plot of the baseline vs. baseline position orientation angle is shown (see Figure 3.2 for an example).

It should be noted that for each night's visibility vs. baseline plot, the visibility curve shown represents the best UD diameter fit for that night's dataset alone and is not the visibility curve derived from the final LD diameter fit. The final LD diameter listed in Table 5.1 is derived from all the long-baseline data available for the star, which includes multiple nights of data for some stars. For each LD diameter fit plot, the visibility curve corresponds to the final diameter measurement.

If any datapoints were taken out of the diameter fit, it is explained why they were removed in this section. The two most common reasons for giving datapoints zero weight were: (1) instrumental or weather problems led to a large gap in time between calibrator and object observations. This was undesirable because the calibration process is most reliable when there is little time between the object's and calibrator's observations so that seeing variations and instrumental drifts with time are minimized; or (2) a few of the datapoints were affected by bad seeing and have much higher errors than the rest of the data. If this was the case, it affected both calibrator and object observations similarly and was most commonly seen early in the night before the atmosphere had settled after sunset.

The next section (§C.x.3) describes which of the data were used in the diameter calculation, and a visibility vs. baseline plot is shown for the limb-darkened disk diameter fit. Section C.x.4 shows the results of the search for separated fringe packets (SFPs; see §7.2). For each night's observations, two datasets were inspected for SFPs, usually the first and last observation of the night. This way there was the maximum available change in the projected position angle between the two observations. The search for SFPs was performed for both the object and the calibrator. For each dataset, a plot shows the weighted mean fringe envelope.

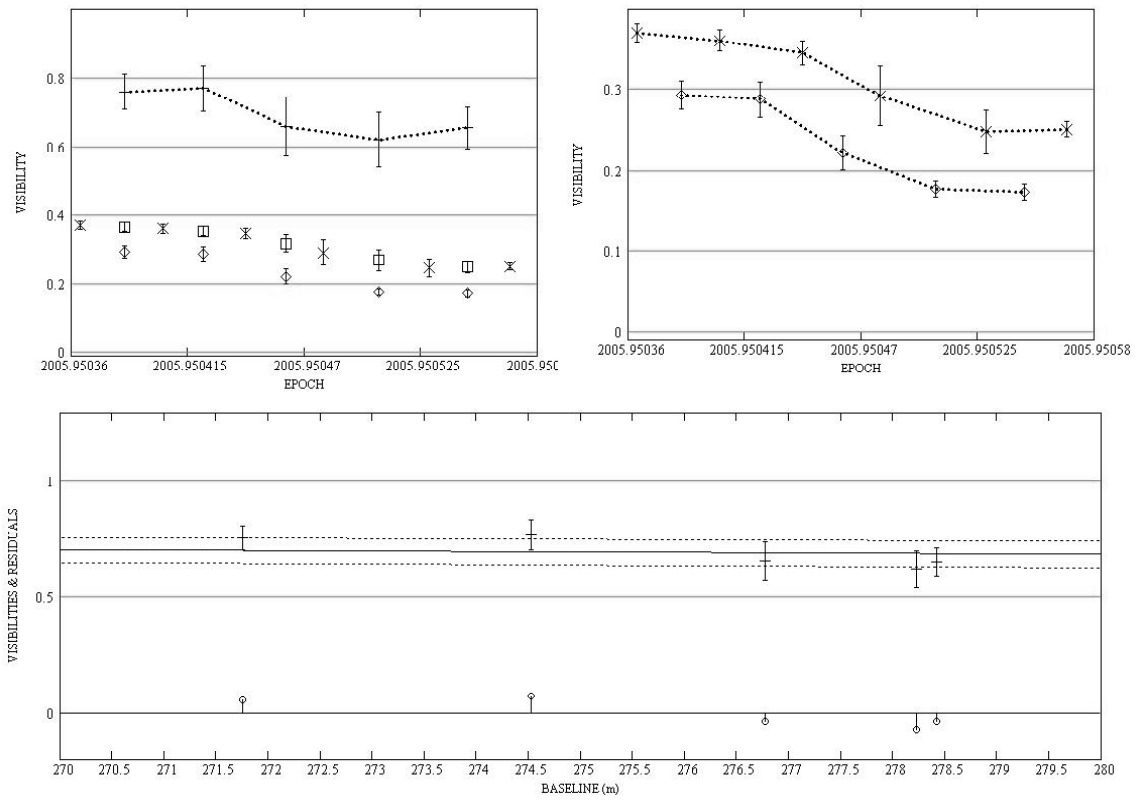


Figure. 4.1: Example of nightly plots. *Top panels:* Visibility vs. epoch (*left:* calibrated visibility; *right:* instrumental visibilities for both the object and calibrator stars). *Bottom panel:* Calibrated visibility vs. baseline. Residuals to the diameter fit are shown along the $V = 0$ line. (Data for HD 3651 from 2005/12/14.)

*Science may set limits to knowledge, but should not set limits to
imagination.*

— *Bertrand Russell*

– 5 –

Exoplanet Host Star Angular Diameters

This chapter outlines the method and equations used to calculate the exoplanet host stars’ angular diameters.

5.1 Angular Diameter Calculation

After the visibilities are calibrated as described in §3.3.2, the output file is read into the *Diameter Fitter* Mathcad program, written by Harold McAlister. A range of potential diameters are fit to the calibrated visibilities and residuals are calculated for each fit. The minimum χ^2 is found and the corresponding diameter is the program’s output.

Diameter fits to the visibilities are based upon the uniform disk (UD) approximation given by

$$V^2 = \left[\frac{2J_1(x)}{x} \right]^2, \quad (5.1)$$

where J_1 is the first-order Bessel function and

$$x = \pi B \theta_{\text{UD}} \lambda^{-1}, \quad (5.2)$$

where B is the projected baseline at the star’s position, θ_{UD} is the apparent UD angular diameter of the star, and λ is the wavelength of the observation. The limb-

darkened (LD) relationship incorporating the linear limb darkening coefficient μ_λ (Hanbury Brown et al. 1974b) is given by:

$$V^2 = \left(\frac{1 - \mu_\lambda}{2} + \frac{\mu_\lambda}{3} \right)^{-2} \times \left[(1 - \mu_\lambda) \frac{J_1(x)}{x} + \mu_\lambda \left(\frac{\pi}{2} \right)^{1/2} \frac{J_{3/2}(x)}{x^{3/2}} \right]^2. \quad (5.3)$$

The μ_λ value was obtained from Claret et al. (1995) after adopting the $\log g$ and T_{eff} values needed for each star observed. The average difference between the UD and LD diameters are on the order of a few percent. There are many published LD relationships but they are essentially indistinguishable from each other with respect to interferometric data, so this one was chosen as representative.

For each LD diameter fit, the errors were derived via the χ^2 minimization method: the diameter fit with the lowest χ^2 was found and the corresponding diameter was the final LD diameter for the star. The errors were calculated by finding the diameter at $\chi^2 + 1$ on either side of the minimum χ^2 .

Table 5.1 lists the parameters required for converting the UD diameter to an LD diameter: T_{eff} and $\log g$ from spectroscopic studies define the limb-darkening coefficient. The UD diameter (θ_{UD}) is converted to an LD diameter (θ_{LD}) using μ_λ , and the LD diameter combined with the exoplanet host star's *HIPPARCOS* parallax (Perryman et al. 1997) leads to a linear radius for the star. Table 5.1 also includes LD diameters estimated from SED fits (θ_{SED}) as a comparison to the measured diameters. Of the 31 exoplanet host stars observed, 26 have diameters listed in Table 5.1. The diameter measurements for the remaining five boasted errors at least as large as the diameter and were therefore not reliable. See Appendix C for details on each star

and which data were used in the diameter calculation.

Table 5.2 compares the newly measured stellar linear radii with previous radii determinations from several sources: Ribas et al. (2003) and Ramírez & Meléndez (2005), who both used photometric methods to derive stellar radii, and Fischer & Valenti (2005), who used spectroscopic methods. HD 13189 was not included in Table 5.2 due to its large linear radius error derived from the large error in the parallax for that star.

Table 5.1: Exoplanet Host Star Diameter Measurements

| HD | T_{eff} (K) | $\log g$ | μ_{λ} | π (mas) | θ_{SED} (mas) | θ_{UD} (mas) | θ_{LD} (mas) | σ_{LD} % | R_{linear} (R_{\odot}) |
|--------|-------------------------|-------------------|-----------------|----------------|--------------------------------|-------------------------------|-------------------------------|---------------------------|--|
| 3651 | 5173 | 4.37 | 0.28 | 90.03±0.72 | 0.767±0.078 | 0.771±0.026 | 0.788±0.027 | 4 | 0.941±0.033 |
| 9826 | 6212 | 4.26 | 0.24 | 74.25±0.72 | 1.095±0.032 | 1.500±0.059 | 1.526±0.061 | 4 | 2.209±0.091 |
| 10697 | 5641 | 4.05 | 0.28 | 30.71±0.81 | 0.496±0.015 | 0.346±0.103 | 0.353±0.106 | 30 | 1.24±0.37 |
| 11964 | 5248 [†] | 3.82 [†] | 0.30 | 29.43±0.91 | 0.553±0.013 | 0.622±0.068 | 0.637±0.070 | 11 | 2.33±0.27 |
| 13189 | 4050* | 1.74* | 0.37 | 0.54±0.93 | 0.783±0.043 | 0.806±0.028 | 0.831±0.029 | 3 | 165.4±284.9 |
| 16141 | 5801 | 4.22 | 0.27 | 27.85±1.39 | 0.369±0.006 | 0.209±0.154 | 0.301±0.154 | 51 | 1.16±0.60 |
| 19994 | 6217 | 4.29 | 0.24 | 44.69±0.75 | 0.693±0.025 | 0.771±0.026 | 0.785±0.026 | 3 | 1.888±0.070 |
| 20367 | 6138 | 4.53 | 0.25 | 36.86±1.08 | 0.386±0.014 | 0.392±0.110 | 0.399±0.112 | 28 | 1.16±0.33 |
| 34445 | 5888 [†] | 4.21 [†] | 0.26 | 22.22±1.05 | 0.283±0.012 | 0.252±0.183 | 0.257±0.186 | 72 | 1.24±0.90 |
| 38529 | 5674 | 3.94 | 0.28 | 23.57±0.92 | 0.570±0.028 | 0.559±0.048 | 0.571±0.049 | 9 | 2.60±0.25 |
| 50554 | 6026 | 4.41 | 0.26 | 32.23±1.01 | 0.326±0.009 | 0.343±0.099 | 0.341±0.101 | 30 | 1.14±0.34 |
| 59686 | 4571 [†] | 2.40 [†] | 0.34 | 10.81±0.75 | 1.287±0.064 | 1.049±0.011 | 1.080±0.012 | 1 | 10.74±0.75 |
| 75732 | 5279 | 4.37 | 0.30 | 79.80±0.84 | 0.666±0.029 | 0.832±0.024 | 0.853±0.024 | 3 | 1.149±0.035 |
| 104985 | 4877* | 2.85* | 0.31 | 9.80±0.52 | 0.955±0.085 | 0.993±0.023 | 1.018±0.024 | 2 | 11.16±0.65 |
| 117176 | 5560 | 4.07 | 0.28 | 55.22±0.73 | 0.951±0.068 | 0.972±0.023 | 0.995±0.024 | 2 | 1.937±0.053 |
| 120136 | 6339 | 4.19 | 0.24 | 64.12±0.70 | 0.853±0.037 | 0.762±0.015 | 0.776±0.016 | 2 | 1.301±0.030 |
| 143761 | 5853 | 4.41 | 0.26 | 57.38±0.71 | 0.700±0.049 | 0.673±0.043 | 0.686±0.044 | 6 | 1.285±0.084 |
| 145675 | 5311 | 4.42 | 0.30 | 55.11±0.59 | 0.498±0.008 | 0.334±0.049 | 0.342±0.050 | 15 | 0.667±0.096 |
| 177830 | 4804 | 3.57 | 0.33 | 16.94±0.76 | 0.515±0.023 | 0.452±0.057 | 0.464±0.059 | 13 | 2.94±0.40 |
| 186427 | 5772 | 4.40 | 0.27 | 46.70±0.52 | 0.494±0.019 | 0.285±0.122 | 0.291±0.124 | 43 | 0.67±0.29 |
| 189733 | 5051 [†] | 4.53 [†] | 0.36 | 51.94±0.87 | 0.363±0.011 | 0.366±0.024 | 0.377±0.024 | 6 | 0.779±0.052 |
| 190228 | 5312 | 3.87 | 0.30 | 16.10±0.81 | 0.375±0.032 | 0.439±0.045 | 0.449±0.047 | 10 | 3.00±0.35 |
| 190360 | 5584 | 4.37 | 0.28 | 62.92±0.62 | 0.658±0.031 | 0.674±0.019 | 0.689±0.020 | 3 | 1.177±0.036 |

Continued on Next Page...

Table. 5.1 – Continued

| HD | T_{eff} (K) | $\log g$ | μ_{λ} | π (mas) | θ_{SED} (mas) | θ_{UD} (mas) | θ_{LD} (mas) | σ_{LD} % | R_{linear} (R_{\odot}) |
|--------|-------------------------|------------------|-----------------|------------------|--------------------------------|-------------------------------|-------------------------------|---------------------------|--|
| 195019 | 5859 | 4.32 | 0.26 | 26.77 ± 0.89 | 0.353 ± 0.018 | 0.311 ± 0.085 | 0.317 ± 0.086 | 27 | 1.27 ± 0.35 |
| 196885 | 6310^{\dagger} | 4.32^{\dagger} | 0.24 | 30.31 ± 0.81 | 0.365 ± 0.016 | 0.478 ± 0.046 | 0.487 ± 0.047 | 10 | 1.73 ± 0.17 |
| 217014 | 5804 | 4.42 | 0.27 | 65.10 ± 0.76 | 0.665 ± 0.047 | 0.731 ± 0.026 | 0.746 ± 0.027 | 4 | 1.232 ± 0.047 |

Notes.

All T_{eff} and $\log g$ from Santos et al. (2004) unless otherwise noted.

μ_{λ} values calculated using Claret et al. (1995) and π values are from Perryman et al. (1997).

† Allende Prieto & Lambert (1999); * Cox (2000); * Takeda et al. (2005); ‡ Sousa et al. (2006)

Table. 5.2: Past and Present Radius Determinations

| HD | R03 (R_{\odot}) | RM05 (R_{\odot}) | FV05 (R_{\odot}) | This study (R_{\odot}) |
|-----------|-------------------------------|--------------------------------|--------------------------------|--------------------------------------|
| 3651 | 0.829±0.020 | 0.861±0.023 | 0.88 | 0.941±0.033 |
| 9826 | - | - | 1.57 | 2.209±0.091 |
| 10697 | 1.796±0.051 | 1.837±0.066 | 1.73 | 1.24±0.37 |
| 11964 | - | - | - | 2.33±0.27 |
| 16141 | 1.428±0.047 | 1.459±0.082 | 1.40 | 1.16±0.60 |
| 19994 | - | 1.801±0.053 | - | 1.888±0.070 |
| 20367 | 1.182±0.029 | 1.198±0.048 | 1.21 | 1.16±0.33 |
| 34445 | - | - | 1.39 | 1.24±0.90 |
| 38529 | 2.784±0.108 | 2.809±0.129 | 2.58 | 2.60±0.25 |
| 50554 | 1.117±0.035 | 1.140±0.047 | 1.15 | 1.14±0.34 |
| 59686 | - | - | - | 10.74±0.75 |
| 75732 | 0.925±0.023 | 0.933±0.027 | 0.95 | 1.149±0.035 |
| 104985 | - | 10.484±0.641 | - | 11.16±0.65 |
| 117176 | - | 1.654±0.043 | 1.86 | 1.937±0.053 |
| 120136 | - | 1.317±0.033 | 1.42 | 1.301±0.030 |
| 143761 | 1.327±0.027 | - | 1.32 | 1.285±0.084 |
| 145675 | 0.978±0.013 | 1.022±0.031 | 0.94 | 0.677±0.096 |
| 177830 | 3.268±0.091 | 3.299±0.169 | 2.99 | 2.94±0.40 |
| 186427 | 1.154±0.019 | - | 1.15 | 0.67±0.29 |
| 189733 | - | - | - | 0.779±0.052 |
| 190228 | 2.555±0.065 | 2.617±0.145 | 2.40 | 3.00±0.35 |
| 190360 | 1.113±0.023 | - | 1.14 | 1.177±0.036 |
| 195019 | 1.538±0.041 | 1.582±0.066 | 1.38 | 1.27±0.35 |
| 196885 | - | - | 1.35 | 1.73±0.17 |
| 217014 | 1.133±0.022 | 1.162±0.031 | 1.14 | 1.232±0.047 |

R03: Ribas et al. (2003); RM05: Ramírez & Meléndez (2005); FV05: Fischer & Valenti (2005)

Figures 5.1, 5.2, and 5.3 plot the photometrically and spectroscopically-derived radii from the three studies listed in Table 5.2 versus the linear radii measured interferometrically. Overall, the measurements match the photometric and spectroscopic estimates fairly well with a slight tendency for the sizes of smaller stars to be overestimated using photometric and spectroscopic methods, though the errors on some of the interferometric measurements are large.

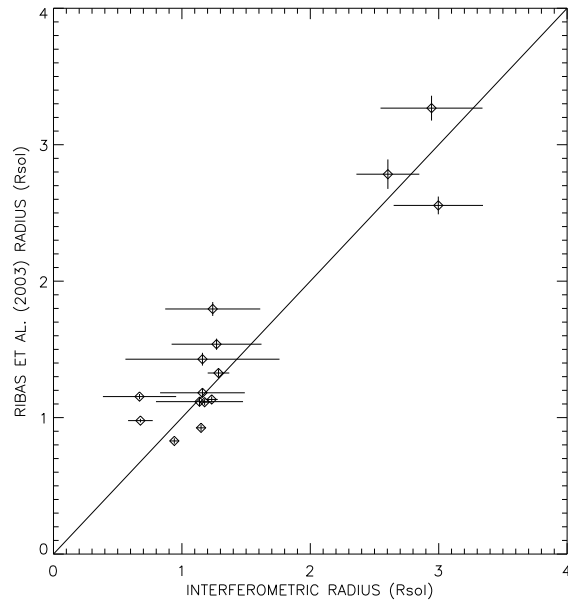


Figure. 5.1: Comparing linear radii: Ribas et al. (2003) vs. interferometric measurements. The solid line indicates a 1:1 ratio for the radii.

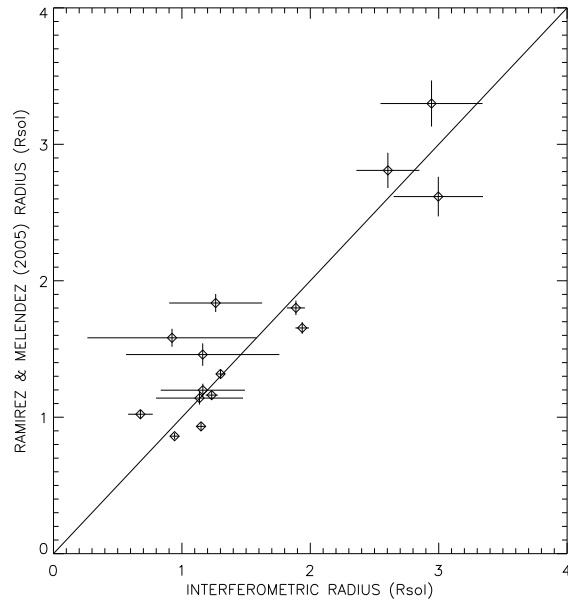


Figure. 5.2: Comparing linear radii: Ramírez & Meléndez (2005) vs. interferometric measurements. The solid line indicates a 1:1 ratio for the radii.

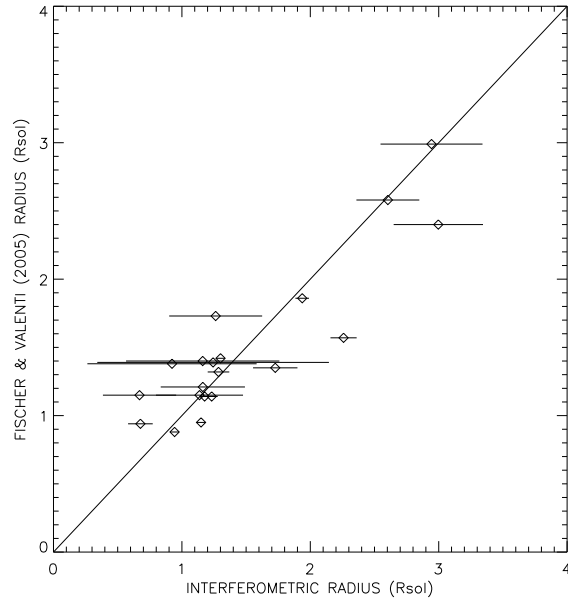


Figure. 5.3: Comparing linear radii: Fischer & Valenti (2005) vs. interferometric measurements. The solid line indicates a 1:1 ratio for the radii.

5.2 Effect of the Limb-Darkening Coefficient

In an effort to determine how μ_λ affected the final LD diameter, I selected five stars and varied their μ_λ by 20%. I recalculated the LD diameter and found that even with a 20% change in μ_λ , the resulting diameters never varied by more than 0.6%. This indicates a low dependence on μ_λ , which in turn indicates that even if the T_{eff} and $\log g$ are not well constrained and therefore μ_λ is not precisely known, the effect on the LD diameter will not be significant.

5.3 Stellar Diameters: Intermediate vs. Long Baseline Measurements

In order to confirm that long-baseline observations are more reliable than intermediate-baseline observations when measuring stellar diameters, five exoplanet host stars with low θ_{LD} errors that had both long- and intermediate-baseline observations were chosen. The angular diameter was calculated for each night's data in order to check how the baseline affected the diameter measurement. Table 5.3 shows the results of this process. The average error for the intermediate-baseline diameters average 16% while the errors in the long-baseline diameters average 4%.

Table. 5.3: Long vs. Intermediate-Baseline Diameter Measurements

| HD | Date | Baseline (m) | θ_{LD} (mas) | σ_{LD} | % Error |
|--------|------------|-----------------|------------------------|---------------|---------|
| 3651 | 2005/10/22 | S1-E1 | 0.836 | 0.062 | 7 |
| | 2005/10/24 | S1-E1 | 0.778 | 0.030 | 4 |
| | 2005/12/14 | W1-S1 | 0.843 | 0.047 | 6 |
| 59686 | 2005/12/06 | S1-E1 | 1.105 | 0.020 | 2 |
| | 2005/12/16 | W1-S1 | 1.144 | 0.031 | 3 |
| | 2007/04/02 | S1-E1 | 1.068 | 0.015 | 1 |
| 117176 | 2005/05/14 | E2-W2 | 0.955 | 0.401 | 42 |
| | 2006/05/13 | W1-W2 | 1.279 | 0.142 | 11 |
| | 2006/05/20 | S1-E1 | 0.961 | 0.038 | 4 |
| | 2007/04/02 | S1-E1 | 1.006 | 0.029 | 3 |
| 120136 | 2005/05/12 | E2-W2 | 0.949 | 0.095 | 10 |
| | 2006/05/14 | W1-W2 | 0.989 | 0.196 | 20 |
| | 2007/02/05 | S1-E1 | 0.779 | 0.021 | 3 |
| | 2007/03/25 | S1-E1 | 0.786 | 0.071 | 9 |
| | 2007/03/26 | S1-E1 | 0.762 | 0.035 | 5 |
| | 2007/03/30 | S1-E1 | 0.783 | 0.037 | 5 |
| 190360 | 2005/08/11 | W1-W2 | 1.050 | 0.212 | 20 |
| | 2006/08/11 | S1-E1 | 0.689 | 0.020 | 3 |

In all cases but one, the diameters derived from each night's observations for a given star match within the error bars, with the long-baseline measurements boasting smaller errors. The exception is for HD 190360, where the two nights of data produce diameters significantly different from each other. Figures 5.4 and 5.5 show visibility vs. baseline for all of HD 190360's data. Figure 5.4 shows the visibility curve resulting from the intermediate-baseline diameter measurement ($\theta_{LD} = 1.050 \pm 0.212$ mas), and the long-baseline points lie well outside the projected errors. On the other hand, Figure 5.5 shows the visibility curve based on the long-baseline diameter ($\theta_{LD} = 0.689 \pm 0.020$ mas). The fit to the intermediate-baseline observations does not change significantly from the fit seen in Figure 5.4, and the general fit to all the points is far better in Figure 5.5 than Figure 5.4. This illustrates the value of using long-baseline observations for these stars when measuring diameters.

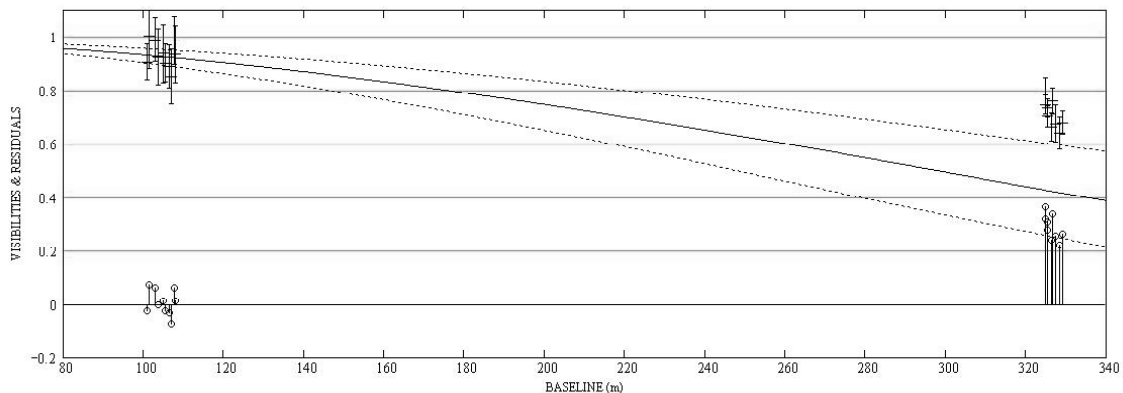


Figure. 5.4: HD 190360: Calibrated visibility vs. baseline. The visibility curve was forced to fit the diameter measured using intermediate-baseline observations. Note how badly the long-baseline datapoints are fit when using this diameter.

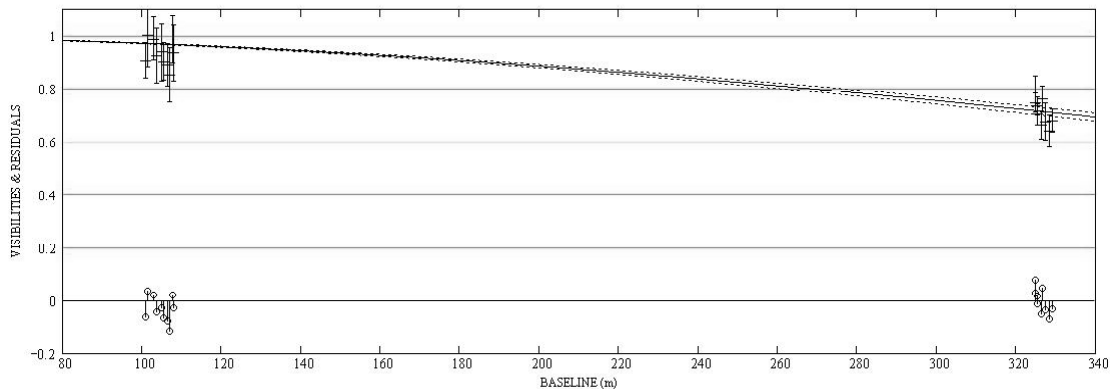


Figure. 5.5: HD 190360: Calibrated visibility vs. baseline. The visibility curve was forced to fit the diameter measured using the long-baseline observations. Note how well all the datapoints are fit when using this diameter.

5.4 Estimated vs. Measured Stellar Diameters

To check the correspondence between the estimated and measured diameters, Figure 5.6 plots the measured LD diameters versus the diameters estimated from SED fits. At diameters $\gtrsim 0.6$ mas, the error bars for the LD diameters become smaller than those for the SED diameters. This is to be expected, as the smaller diameters are nearing the resolution limit of the CHARA Array, and the uncertainties will be larger for these measurements.

The main outliers are HD 59686 (to the lower right of the solid line) and HD 9826 (to the upper left of the solid line), both of which have apparently precise diameter measurements. HD 59686 is a K2 giant star with otherwise normal interferometric observations, and HD 9826 is an F8 V star whose visibilities exhibit considerable peculiarities as described in §7.4.1.

In order to characterize the scatter in the diameters, the departure from the 1:1

line was calculated for each star after removing the two outliers. The mean was calculated, and standard deviation of the mean was 0.091, which indicates a fairly good correspondence between the estimated and measured diameters.

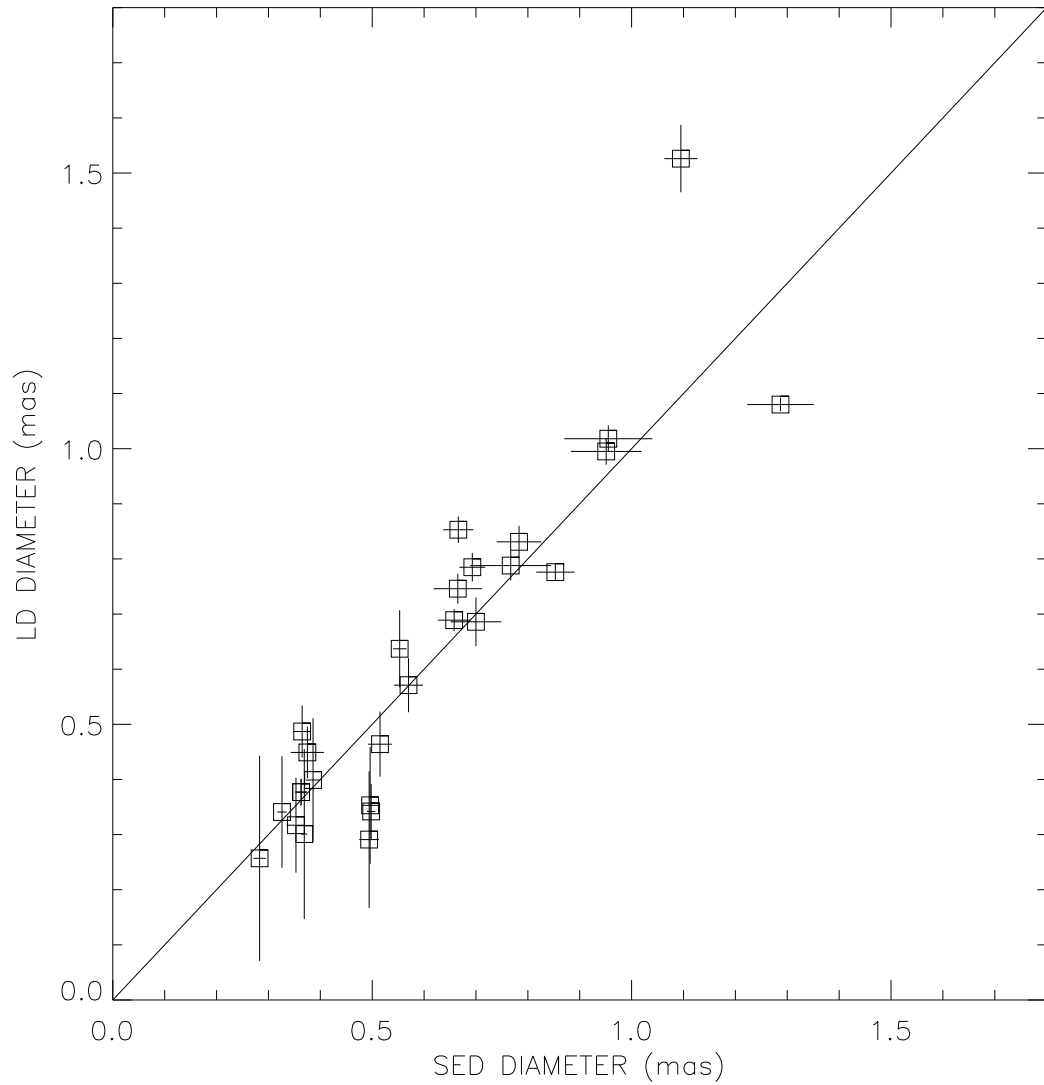


Figure. 5.6: Comparing estimated SED diameters and measured LD diameters. The solid line indicates a 1:1 ratio for the diameters. Note that at $\theta \sim 0.6$ mas, the errors for the measured LD diameters become equal to or smaller than the errors from the SED diameter estimates.

*The sun, with all those planets revolving around it and dependent on it,
can still ripen a bunch of grapes as if it had nothing else
in the universe to do.*

— Galileo

– 6 –

Transiting Planet: HD 189733

This chapter focuses on the star HD 189733, an exoplanet system whose planet transits the star. The work described in this chapter was suggested by Mark Swain and was completed with Gerard van Belle, Theo ten Brummelaar, and Harold McAlister with the support of Nils Turner, Laszlo Sturmann, and Judit Sturmann and was published by Baines et al. (2007). This chapter is an excerpt of that paper.

6.1 Introduction

A handful of extrasolar planets transit their host stars, causing a reduction in stellar flux as the planet blocks part of the star’s disk. The planet orbiting HD 189733 is one of the 23 known transiting planets as of 2007/08/01 (*Extrasolar Planets Encyclopedia*). Using radial velocity and photometric measurements made at the Haute-Provence Observatory, Bouchy et al. (2005b) discovered a hot Jupiter-like planet with an orbital period of 2.219 days and estimated the star’s radius to be $0.76 \pm 0.01 R_{\odot}$. This value, along with a planet-to-star radius ratio of 0.172 ± 0.003 , led to a planetary radius of $1.26 \pm 0.03 R_{\text{Jupiter}}$. More recently, Bakos et al. (2006a) refined the orbital parameters using *BVRI* multi-band photometry and found the planet’s radius to be $1.154 \pm 0.032 R_{\text{Jupiter}}$.

We observed HD 189733 using the CHARA Array in order to directly determine

the host star’s radius and thereby calculate, in a strictly geometric manner, the radius and density of the planet.

Planetary densities were previously estimated from photometric observations of the transiting planets and range from 0.38 g cm^{-3} for HD 209458b (Charbonneau et al. 2000) to 1.17 g cm^{-3} for HD 149026b (Sato et al. 2005). These density calculations are highly dependent on estimated stellar diameters based on SED fits using published photometric values, which are fundamentally indirect in nature, relying upon *a priori* assumptions regarding the host stars’ stellar atmospheres. For the four “bright” ($V < 12$) transit host stars, these angular sizes are in the range of 0.05 to 0.40 mas. The longest baselines of the CHARA Array are capable of resolving the largest and brightest of these objects.

6.2 Observations and Data Reduction

Observations of HD 189733 were obtained using both the K - and H -band filters, though due to the small angular diameter for the star, only the H -band observations obtained using S1-E1 are used in our final diameter analysis.

HD 189733 was observed on several nights during the summer of 2006 along with the calibrator star HD 190993, a B3 V star offset by 1.7° , selected on the basis of its small estimated angular diameter and its apparent lack of any close companion. The latter criterion was verified by a thorough literature search while a SED fit to HD 190993 led to an estimated angular diameter of 0.167 ± 0.035 mas with no residuals

suggestive of a companion (see Figure 6.1). This results in a predicted visibility (V) for the calibrator of $V_{\text{cal}} = 0.961^{+0.019}_{-0.008}$ at the longest baseline, resulting in a contribution of $\sigma_V \simeq 0.01$ to 0.02 to the calibrated visibility errors seen in Table 6.1.

Table. 6.1: Interferometric Measurements of HD 189733

| MJD (53886.0 +)) | B (m) | V | σV |
|-----------------------------------|------------------------|----------|------------------------------|
| 0.905 | 330.5 | 0.851 | 0.071 |
| 1.936 | 327.9 | 0.843 | 0.056 |
| 1.958 | 324.9 | 0.857 | 0.054 |
| 8.865 | 330.5 | 0.869 | 0.034 |
| 76.742 | 326.5 | 0.909 | 0.069 |
| 76.761 | 323.8 | 0.863 | 0.049 |
| 76.778 | 321.3 | 0.877 | 0.045 |
| 76.793 | 319.0 | 0.839 | 0.045 |
| 76.824 | 315.5 | 0.829 | 0.061 |

The small angular size and high visibility of the calibrator mean that HD 190993 is essentially unresolved using the CHARA Array, and the uncertainty in visibility due to calibrator diameter error is small compared to the measurement error. Therefore uncertainties in the calibrator diameter will not affect the HD 189733 diameter measurement significantly (van Belle & van Belle 2005). Even HD 190993's considerable $v \sin i$ does not contribute an error to our diameter fits due to its small angular size.

We note that the M-dwarf companion to HD 189733 reported by Bakos et al. (2006b) on the basis of common space motion at an angular separation of $11.2''$ is well outside the interferometric field of view, and its presence has no effect on our

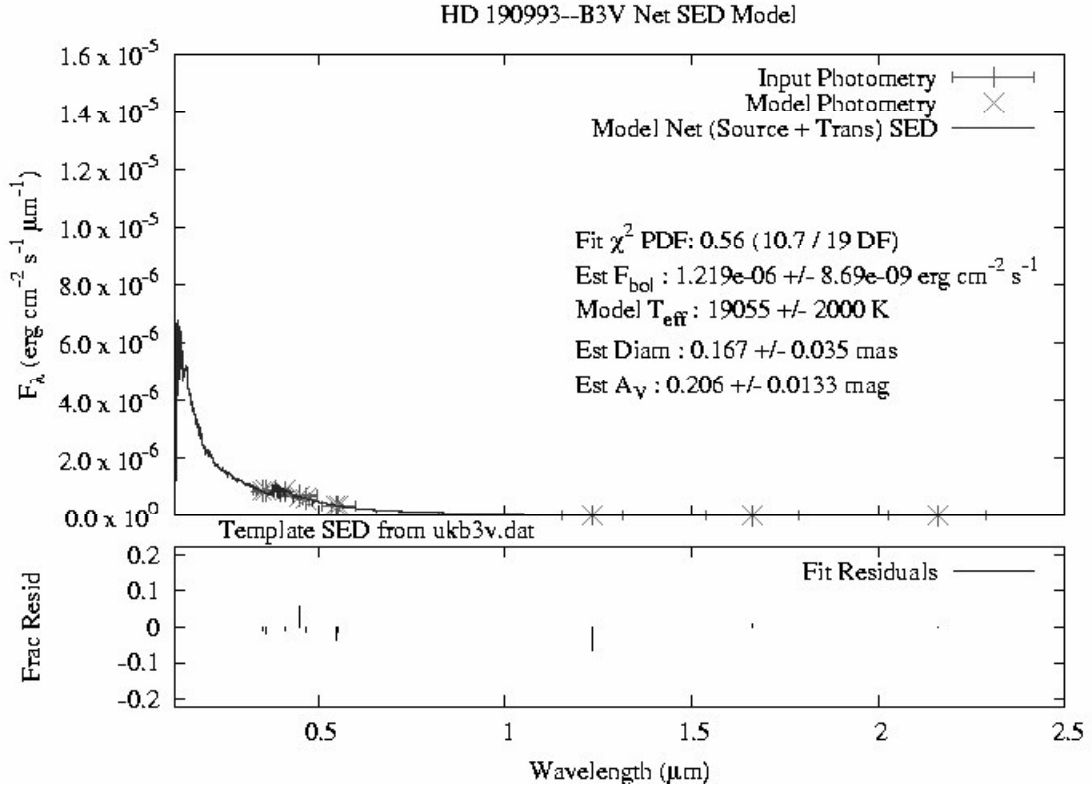


Figure. 6.1: SED fit for the calibrator HD 190993. In the top panel, vertical bars represent the errors for the data points they overlay and the horizontal bars represent the bandpass of the data point. In the bottom panel, the fractional residuals (difference between data point and fit point, normalized by that data point) are shown for each data point.

results. Although the effect on visibility would be small in the first lobe of the $V(B)$ curve, we have confirmed that our observed epochs do not occur within the predicted times of planetary transit or eclipse using the period and reference time of central transit of Bakos et al. (2006a).

All our observations were obtained with the CHARA Classic beam combiner, and we employed the standard practice of observing the object and calibrator sequentially to provide a series of time-bracketed observations from which the instrumental

visibilities could be reduced to calibrated values for the target star. The observing practice and reduction process employed here are identical to those described by ten Brummelaar et al. (2005). The results of this process are summarized in Table 6.1.

6.3 Diameter Fit

Diameter fits to the visibilities and baselines from Table 6.1 were performed using the UD and LD approximations described in §5.1, which resulted in $\theta_{\text{UD}} = 0.366 \pm 0.024$ mas and $\theta_{\text{LD}} = 0.377 \pm 0.024$ mas, the latter incorporating $\mu_{\lambda} = 0.36$ taken from Claret et al. (1995) after adopting $\log g = 4.5$ and $T_{\text{eff}} = 5000$ K for HD 189733 (see Figure 6.2). The reduced χ^2 minimization in both cases yielded a value of 1.593, and the errors quoted are for an increase of the χ^2 value of 1.0, that is, the 68% confidence interval. Dividing this χ^2 by the number of degrees of freedom, which in our case is 8, yields 0.199, which is much less than 1.0, showing that the fit is quite good and that our error estimates for the visibility points are conservative. If we rescale these error bars to force χ^2 to be equal to the number of degrees of freedom, which assumes that there are no systematics in the measurements, they are approximately half the size that they are shown in Figure 6.2 and would also reduce our final error estimates by a factor of 2. However, we will remain conservative and continue to use the error estimate based on the raw χ^2 value.

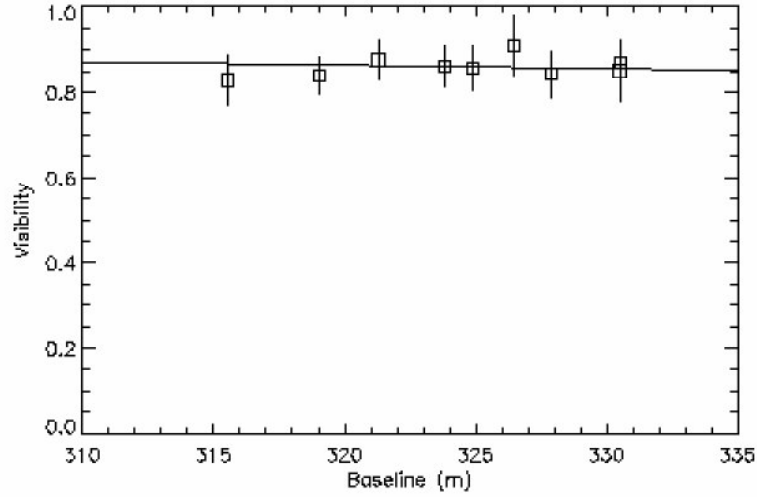


Figure. 6.2: The χ^2 fit to HD 189733’s visibilities. The solid line represents a theoretical visibility curve for a star with a limb-darkened diameter of 0.377 mas, the boxes are the measured visibilities, and the vertical lines are the measured errors.

6.4 Estimate of the Angular Size of HD 189733

An *a priori* estimate of the angular size of HD 189733 is a parameter of considerable interest, because the size of HD 189733b is determined only relative to the size of its parent star from the photometric transit timing data. Bakos et al. (2006a) consider no fewer than four separate methods in their investigation of the system: $V - K$ color angular radius prediction (Kervella et al. 2004), temperature radius, isochrone radii from Girardi et al. (2002) and Baraffe et al. (1998), and the Johnson V -2MASS T_{eff} calibration of Masana et al. (2006).

None of these approaches are completely reliable, as the only primary data we have been able to find in the literature were Tycho B_T , V_T (Bessell 2000), Strömgren $ubvy$ (Olsen 1993), and 2MASS JHK photometry (Cutri et al. 2003). Neither spec-

troscopy nor measures of $\log g$ nor direct measures of Johnson photometry appear to be available in the literature. The values of V used in Kervella et al. (2004) and Masana et al. (2006) appear to have been extrapolated from V_T . Furthermore, sustained long-term observations of HD 189733 by the *MOST* asteroseismology satellite have found the star to be photometrically variable (J. Rowe 2007, private communication), casting significant doubt on any radius derived from a photometric relationship. Based on this information, we consider the size errors for HD 189733 quoted in Bouchy et al. (2005b) and Bakos et al. (2006a), derived from the methods cited above, to be underestimates.

To explore what is a more appropriate error for an inferred angular size, we executed a SED fit of the available spectrophotometry for HD 189733 cited above. Given the known variability of HD 189733, the quoted millimagnitude error estimates of the Tycho and Strömgren photometric data points were increased by a factor of 10. These photometric data points were fit to the solar-abundance K0 V and K2 V templates available from Pickles (1998), with the resulting fit values for reddening, bolometric flux, and angular diameter seen in Table 6.2, along with the appropriate χ^2 per degree of freedom (χ^2 PDF) values. Unfortunately, a K1 V template is not available in that library, although an estimate of one from interpolating between the two bracketing spectral types was synthesized by us for testing this spectral type. These fits are seen in Figure 6.3.

The appropriate model spectrum from Munari et al. (2005) for a 5000 K star was

fit with a χ^2 PDF of 2.80, but this model (and the others available in the literature) unfortunately only covered the visible portion of the spectrum. The 115 - 2500 nm range of Pickles (1998) was necessary to fully characterize the available photometry, and thus we constrained our analysis to this particular set of stellar templates.

Our finding is that, even with this highly detailed analysis of the stellar SED, the most appropriate modeling of that SED reveals a predicted angular size of only $\theta = 0.363 \pm 0.011$ mas - a 3% error bar - which corresponds to a stellar linear radius of $0.752 \pm 0.026 R_{\odot}$.

Table. 6.2: SED Fits for HD 189733 Photometry

| Model Parameters ^a | | Fitted Parameters ^b | | | |
|-------------------------------|-------------------------|--------------------------------|-------------------|---|-------------------|
| Spectral Type | T_{eff} (K) | χ^2 PDF | A_V (mag) | F_{bol} ($10^{-8} \text{ erg cm}^{-2} \text{ s}^{-1} \mu\text{m}^{-1}$) | θ (mas) |
| K0 V | 5188 ± 50 | 2.62 | 0.308 ± 0.031 | 3.207 ± 0.061 | 0.365 ± 0.008 |
| K1 V ^c | 5040 ± 70 | 1.94 | 0.105 ± 0.031 | 2.828 ± 0.049 | 0.363 ± 0.011 |
| K2 V | 4887 ± 50 | 2.39 | 0.00 ± 0.030 | 2.613 ± 0.043 | 0.371 ± 0.008 |

^aModels from Pickles (1998); T_{eff} is the effective temperature.

^b A_V is the reddening, F_{bol} is the bolometric flux, and θ is the angular diameter.

^cK1 V model interpolated from the K0 V and K2 V models.

6.5 Discussion

Our new direct determination for the angular diameter of HD 189733 of $\theta_{\text{LD}} = 0.377 \pm 0.024$ mas can be combined with the *HIPPARCOS* parallax for the star of 51.9 ± 0.9 mas (Perryman et al. 1997) to give a physical radius for the star of $R_{\text{star}} = 0.779 \pm 0.052 R_{\odot}$, which is about 3% larger than that adopted by Bakos et al. (2006b).

By the nature of the light-curve analysis, the relative increase in the radius of the host star will directly translate into the same relative increase in the radius of the planet HD 189733b. Thus, revising the radius of Bakos et al. (2006a) of $1.154 R_{\text{Jupiter}}$, our new estimate for this value is $R_{\text{planet}} = 1.19 \pm 0.08 R_{\text{Jupiter}}$. Furthermore, adopting the value of Bouchy et al. (2005b) for the mass of the planet of $1.15 M_{\text{Jupiter}}$, we derive a new estimate for the density of HD 189733b of $\rho = 0.91 \pm 0.18 \text{ g cm}^{-3}$. These values are in good agreement with Winn et al. (2007), who used transit photometry to constrain the stellar and planetary radii. The values of M_{planet} , R_{planet} , and ρ_{planet} are all consistent with the modest collection of these parameters presently available for transiting exoplanet systems, and they support the conclusion that HD 189733b is not among the few hot Jupiters that present extraordinarily large radii for their masses.

6.6 Non-Detection of Duplicity of HD 189733

Given the higher resolution of interferometric arrays, a possible close-separation tertiary companion may affect our measures of HD 189733’s visibility and thereby complicate our interpretation. As such, it was prudent for us to also observe HD 189733 with the Palomar Testbed Interferometer (PTI, Colavita et al. 1999), an instrument with intermediate baselines on a variety of sky projections, suitable for exploration of possible unseen nearby luminous (stellar) companions. PTI has been demonstrated to be sensitive to nearby companions with $\Delta K < 4.0$ (Boden et al. 1998), which for a K2-3 V primary star rules out any M-dwarf companions (Bessell & Brett 1988).

PTI observed HD 189733 in the *K*-band on the nights of 2006 June 10-12, 2006 June 24, and 2006 July 8-10. Four of those nights used PTI’s 85-m northwest baseline configuration, two used the 110-m north-south baseline, and one night used the 85-m southwest baseline. For all of these nights, HD 189733’s normalized visibility data points were indistinguishable from unit visibility, which corresponds to a completely unresolved point source, as would be expected for a single ~ 0.37 mas star being observed by PTI at $2.2\ \mu\text{m}$.

6.7 Conclusion

Our results for the radii of the host star and planet in the HD 189733 exoplanet system are formally in good agreement with existing measurements of these parameters as well as with the estimate for the density of the planet, and they have the

additional and significant merit that they represent direct measurements of stellar and planetary diameters that do not rely on inferences about stellar atmospheres. While the diameter measurements are currently at a 6% level of accuracy, we expect to improve this considerably as we implement fringe detection at shorter wavelengths at the CHARA Array.

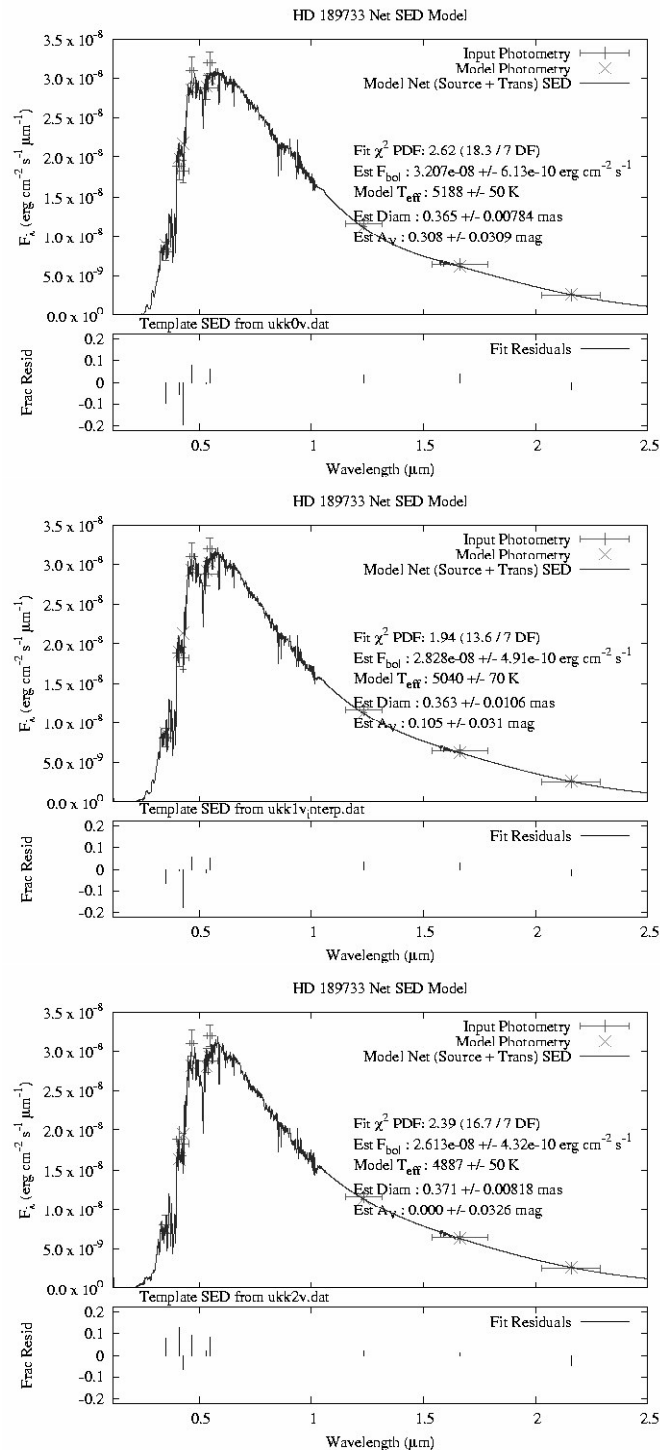


Figure. 6.3: SED fits of HD 189733. The top panel shows the photometric fit for a K0 V, the middle panel shows the K1 V fit, and the bottom panel shows the K2 V fit. All three fits allowed the reddening factor to vary.

*I know nothing with any certainty, but the sight of the stars
makes me dream.*

— Vincent van Gogh

– 7 –

Searching for Stellar Companions

This chapter describes the search for stellar companions in low-inclination orbits using two methods: looking for variations in the visibility curve and checking for separated fringe packets. Two stars of the 31 observed have shown characteristics of possible stellar duplicity - ν Andromedae and ρ Coronae Borealis - and their results are discussed in detail in §7.4.

7.1 Previous Speckle Observations

Approximately a third of the exoplanet host stars described here were also previously observed using speckle interferometry. This technique involves taking what are essentially multiple snapshots of a star and then studying the power spectrum for the star after it is deconvolved with the power spectrum of a nearby calibrator star. If the target star is single, no fringes are seen in the deconvolved power spectrum, which is relatively flat. If the target star has a companion, a fringe pattern will be seen in the power spectrum where fringe spacing and orientation are dependent on the separation and position angle of the two stars (Horch et al. 2002). Table 7.1 lists the results of speckle studies for stars included in the sample here.

Table. 7.1: Exoplanet Host Star Duplicity: Results from Speckle

Interferometry

| HD | Reference | Results |
|--------|-----------------------------|---|
| 9826 | McAlister (1978) | Unresolved binary |
| | Hartkopf & McAlister (1984) | Unresolved spectroscopic binary |
| | Isobe (1991) | Spectroscopic binary – no fringes found |
| 16141 | Horch et al. (2002) | No evidence of duplicity |
| 38529 | Mason et al. (1999) | Unresolved <i>HIPPARCOS</i> problem star |
| 95128 | McAlister et al. (1989) | Inspected for duplicity (no result shown) |
| 143761 | McAlister et al. (1987) | Negative result for duplicity |
| 177830 | Lu et al. (1987) | Negative result for duplicity |
| 190360 | McAlister et al. (1987) | Negative result for duplicity |
| 195019 | Lu et al. (1987) | Negative result for duplicity |
| 217014 | McAlister et al. (1987) | Negative result for duplicity |
| 217107 | McAlister et al. (1987) | Negative result for duplicity |

7.2 Visibility Curve Variations

The first method in searching for stellar companions involves studying the systematics in the residuals, which are the error in the fit to each visibility data point. For a single star, the residuals show a Gaussian distribution about 0 (see Figure 7.1). On the other hand, Figure 7.2 shows the more unusual behavior in the residual systematics for a known binary star system. On the short-baseline side of the observations (all taken on one night), the residuals are below the line marked at $V = 0$ while on the long-baseline side of the observations the residuals are above the $V = 0$ line. The standard deviation for the (observed - calculated) residuals (σ_{res}) for Figure 7.1 is 0.056 while $\sigma_{\text{res}} = 0.106$ for Figure 7.2.

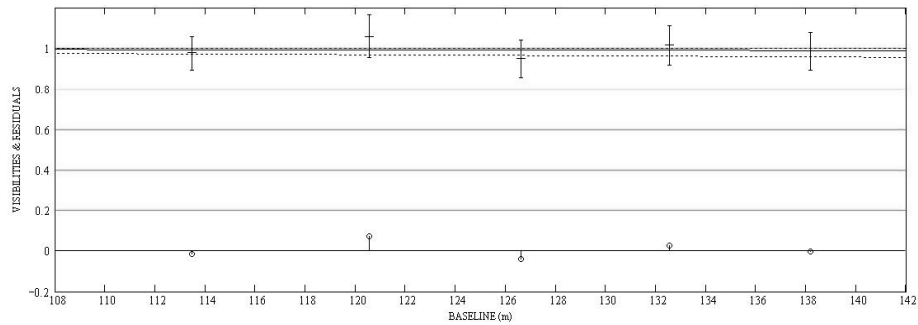


Figure. 7.1: Example of visibility residual systematics indicative of a single star (HD 128311). Note how the residuals fall evenly both above and below the line at $V = 0$ and show no trends.

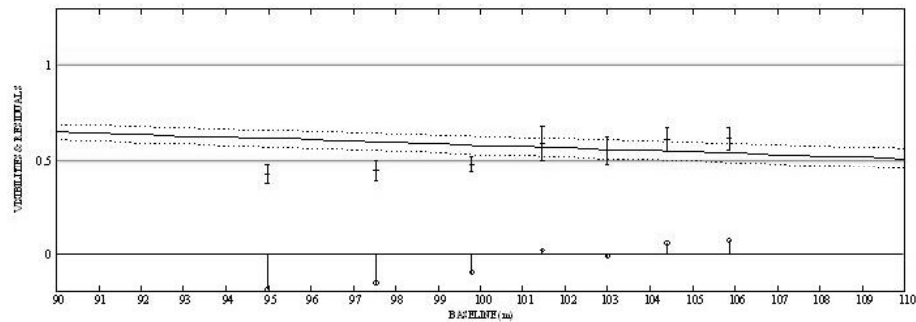


Figure. 7.2: Example of visibility residual systematics indicative of a binary star (β Aurigae). Note how the residuals are systematically low for the shorter-baseline observations and systematically high for the longer-baseline observation.

The typical σ_{res} for a single star is well under 0.100 (see Table 7.5) while σ_{res} for a binary with a low ΔK is usually over 0.100. For example, the binary system HD 146361 was observed by Deepak Raghavan for three nights in 2007 May along with the calibrator star HD 152598. The binary is composed of a G0 V and an F6 V (Sanz-Forcada et al. 2003) and therefore has a $\Delta K \sim 0.5$. The measured σ_{res} for the three nights observations are 0.180, 0.229, and 0.118 indicating a departure from the single-star model for this system.

A related way to distinguish between a single star and a binary system is to inspect the tracking between the object and the calibrator over the course of the entire dataset. “Tracking” refers to the behavior of the object and calibrator raw visibilities over time and how they relate to each other. For a single star, the object’s and calibrator’s visibilities will “track together”, or stay the same distance apart over the entire dataset. In some cases the visibilities for both calibrator and object will be nearly equal, and they overlay each other as can be seen in Figure 7.3. In other cases, the visibilities will be offset due to the resolved nature of the object but will show the same patterns and keep the same relative distance between them (see right panel in Figure 3.5).

Figure 7.4 shows the tracking of a known binary star. The relative distance between the object’s and calibrator’s visibilities changes over the course of the dataset and indicates that either the calibrator or object is changing over time.

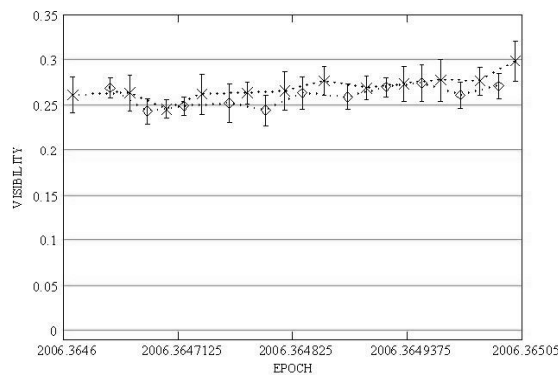


Figure. 7.3: Example of tracking indicative of a single star (τ Bootis, observed 2006/05/14). Note how the visibilities for both the calibrator and object remain constant and the same relative distance apart.

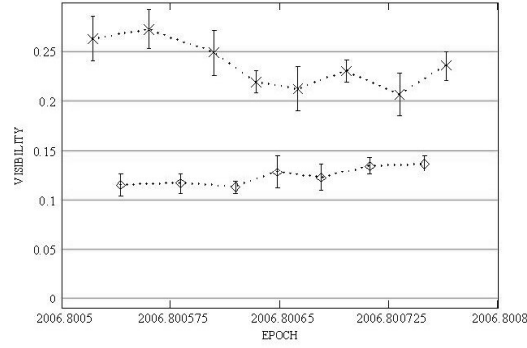


Figure. 7.4: Example of tracking indicative of binary system (β Aurigae, observed 2006/10/20). Note how the relative distance between the calibrator's and object's visibilities change over time, indicating one of the stars is changing. Assuming the calibrator is a single star, the object is not single.

For each exoplanet system, a variety of low-mass stellar companions were considered in order to calculate whether an unseen companion would be detectable in the visibility curve: G5 V, K0 V, K5 V, M0 V, and M5 V. Most of the stars in the sample are solar-type stars, so more massive main sequence spectral types need not be considered. The magnitude difference (ΔM_K , listed as ΔK in the tables) and angular separation (α) of a face-on orbit between the host star and companion were calculated for each possible pairing:

$$\Delta M_K = M_s + (M_h - M_h) - M_h, \quad (7.1)$$

where M_s is the absolute magnitude of the potential secondary star, M_h is the absolute magnitude of the host star, m_h is the apparent magnitude of the host star, and

$$(m_h - M_h) = 5 \log \left(\frac{100}{\pi} \right), \quad (7.2)$$

where π is the host star's parallax in mas. The angular separation was calculated using

$$\alpha = \left[(M_h + M_s) \times \left(\frac{P}{365.25} \right)^2 \right]^{\frac{1}{3}} \times \pi, \quad (7.3)$$

where M_h is the mass of the exoplanet's host star, M_s is the mass of the potential secondary star, and P is the companion's orbital period.

The inclination required for the system to have a secondary companion of a given type was calculated:

$$i_o = \arcsin \left\{ \left[(M_h + M_s)^2 f(M) \right]^{\frac{1}{3}} M_h^{-1} \right\}, \quad (7.4)$$

where

$$f(M) = 1.036 \times 10^{-7} k_1^3 P (1 - e^2)^{\frac{3}{2}}, \quad (7.5)$$

where e is the system's eccentricity and k_1 is the semi-amplitude of the radial velocity for the host star in km s^{-1} .

The angular size of the possible companion was estimated using the calibration of radius as a function of spectral classifications from *Allen's Astrophysical Quantities* (Cox 2000) and the parallax of the host star. Tables 7.2, 7.3, and 7.4 present the results of these calculations. For each exoplanet host star studied, the observed values required for the calculations described above are listed in Table 7.2 (multiple lines for some of the targets indicate multiple planets), while Table 7.3 shows the calculated i , ΔK , and α for each type of possible secondary star. Table 7.4 lists the calculated angular diameters of the potential secondary companions for each system. It should

be noted that if the companion star is a pre-main-sequence star, the resulting ΔK becomes smaller due to the star's increased brightness prior to hydrogen fusion and therefore has a higher probability of being detected.

Table. 7.2: Exoplanet Host Star Observed Parameters

| Observed Parameters | | | | | | | | | | | Calculated Values | | Inferred Values | |
|---------------------|----------------|-----------|-----------------------------------|-------------|---------|------|-----------------------------|-------------------------------|--------------------------------------|-------------------|-----------------------------------|--|-----------------|--|
| HD | Spectral Class | K (mag) | M_{star} (M_{\odot}) | π (mas) | P (d) | e | K_1 (m s^{-1}) | $a_{\text{star}} \sin i$ (AU) | $f(M_{\text{star}})$ (M_{\odot}) | $a_p \sin i$ (AU) | $M_p \sin i$ (M_{Jup}) | | | |
| 3651 | K0 V | 4.0 | 0.79 | 90.0 | 0.2 | 0.63 | 15.9 | 7.06E-05 | 1.213E-11 | 0.28 | 0.20 | | | |
| 9826b | F8 V | 2.7 | 1.3 | 74.3 | 0.6 | 0.03 | 73.0 | 3.10E-05 | 1.858E-10 | 0.06 | 0.71 | | | |
| 9826c | - | - | - | - | - | 0.18 | 58.0 | 1.27E-03 | 4.641E-09 | 0.83 | 2.11 | | | |
| 9826d | - | - | - | - | - | 0.41 | 72.9 | 7.74E-03 | 3.857E-08 | 2.50 | 4.61 | | | |
| 10697 | G5 IV | 4.7 | 1.10 | 30.7 | 2.6 | 0.12 | 119.0 | 1.16E-02 | 1.832E-07 | 2.12 | 6.35 | | | |
| 11964 | G5 | 4.5 | 1.12 | 29.4 | 2.7 | 0.06 | 9.0 | 1.74E-03 | 1.585E-10 | 3.34 | 0.61 | | | |
| 13189 | K2 II | 4.0 | 2.0 | 0.5 | 11.3 | 0.27 | 173.3 | 7.23E-03 | 2.270E-07 | - | 8-20 | | | |
| 16141 | G5 IV | 5.2 | 1.01 | 27.9 | 2.8 | 0.28 | 10.8 | 7.23E-05 | 8.754E-12 | 0.35 | 0.22 | | | |
| 19994 | F8 V | 3.7 | 1.34 | 44.7 | 1.7 | 0.30 | 36.2 | 1.70E-03 | 2.285E-09 | 1.42 | 1.68 | | | |
| 20367 | G0 V | 5.0 | 1.17 | 36.9 | 2.2 | 0.32 | 29.0 | 1.19E-03 | 1.009E-09 | 1.25 | 1.17 | | | |
| 34445 | G0 | 5.8 | 1.11 | 22.2 | 3.3 | 0.40 | 10.0 [†] | 1.06E-04 | 1.005E-11 | 0.51 | 0.58 | | | |
| 38529 | G4 IV | 4.4 | 1.4 | 23.6 | 3.1 | 0.27 | 53.8 | 6.86E-05 | 2.074E-10 | 0.13 | 0.70 | | | |
| 50554 | F8 | 5.5 | 1.11 | 32.2 | 2.5 | 0.50 | 104.0 | 1.07E-02 | 9.787E-08 | 2.41 | 5.16 | | | |
| 59686 | K2 III | 2.9 | 1.15 [†] | 10.8 | 4.8 | 0.00 | 149.0 | 4.15E-03 | 1.038E-07 | - | 6.50 | | | |
| 75732b | G8 V | 4.2 | 0.95 | 79.8 | 0.5 | 0.02 | 72.2 | 9.73E-05 | 5.713E-10 | 0.12 | 0.84 | | | |
| 75732c | - | - | - | - | - | 0.34 | 13.0 | 4.98E-05 | 8.382E-12 | 0.24 | 0.21 | | | |
| 75732d | - | - | - | - | - | 0.16 | 49.3 | 2.40E-02 | 6.400E-08 | 5.90 | 4.05 | | | |
| 95128b | G0 V | 3.7 | 1.03 | 71.0 | 0.7 | 0.61 | 49.3 | 3.91E-03 | 6.726E-09 | 2.09 | 2.54 | | | |
| 95128c | - | - | - | - | - | 0.01 | 11.1 | 2.65E-03 | 3.675E-10 | 3.73 | 0.76 | | | |
| 104985 | G9 III | 3.3 | 1.6 | 9.8 | 5.0 | 0.03 | 161.0 | 2.93E-03 | 8.558E-08 | 0.78 | 6.30 | | | |
| 117176 | G4 V | 3.5 | 0.92 | 55.2 | 1.3 | 0.40 | 318.0 | 3.13E-03 | 2.993E-07 | 0.43 | 6.60 | | | |
| 120136 | F7 V | 3.3 | 1.2 | 64.1 | 1.0 | 0.02 | 469.0 | 1.43E-04 | 3.539E-08 | 0.05 | 3.87 | | | |
| 128311 | K0 V | 5.1 | 0.80 | 60.4 | 1.1 | 0.31 | 85.0 | 3.13E-03 | 2.307E-08 | 1.02 | 2.57 | | | |
| 143761 | G0 V | 4.0 | 1.0 | 57.4 | 1.2 | 0.03 | 67.4 | 2.46E-04 | 1.256E-09 | 0.23 | 1.10 | | | |
| 145675 | K0 V | 4.7 | 1.00 | 55.1 | 1.3 | 0.37 | 89.0 | 1.31E-02 | 1.010E-07 | 2.82 | 4.89 | | | |
| 168443b | G6 IV | 5.3 | 1.01 | 26.4 | 2.9 | 0.53 | 472.7 | 2.14E-03 | 3.877E-07 | 0.30 | 7.73 | | | |
| 168443c | - | - | - | - | - | 0.20 | 289.0 | 4.61E-02 | 4.163E-06 | 2.87 | 17.15 | | | |

Continued on Next Page...

Table. 7.2 – Continued

| Observed Parameters | | | | | | | | | | | | Calculated Values | | Inferred Values | |
|---------------------|----------------|--------------|--------------------------------------|----------------|-------|----------|------|-------------------------|----------------------------------|---|----------------------|--------------------------------------|--|-----------------|--|
| HD | Spectral Class | K (mag) | M_{star} (M_{\odot}) | π (mas) | (m-M) | P (d) | e | K_1 (m s $^{-1}$) | $a_{\text{star}} \sin i$ (AU) | $f(M_{\text{star}})$ (M_{\odot}) | $a_p \sin i$ (AU) | $M_p \sin i$ (M_{Jup}) | | | |
| 177830 | K0 IV | 5.2 | 1.15 | 16.9 | 3.9 | 391.6 | 0.41 | 34.0 | 1.12E-03 | 1.210E-09 | 1.10 | 1.22 | | | |
| 186427 | G2.5 V | 4.7 | 1.0 | 46.7 | 1.7 | 800.8 | 0.63 | 43.9 | 2.51E-03 | 3.287E-09 | 1.60 | 1.50 | | | |
| 189733 | K1 V | 5.5 | 0.82 | 51.9 | 1.4 | 2.2 | 0.00 | 205.0 | 4.15E-05 | 1.964E-09 | 0.03 | 1.15 | | | |
| 190228 | G5 IV | 5.7 | 0.83 | 16.1 | 4.0 | 1146.0 | 0.50 | 91.0 | 8.30E-03 | 5.811E-08 | 2.02 | 3.58 | | | |
| 190360 | G6 IV | 4.1 | 0.96 | 62.9 | 1.0 | 3902.0 | 0.48 | 20.0 | 6.29E-03 | 2.183E-09 | 4.80 | 1.33 | | | |
| 192263 | K0 V | 6.1 | 0.75 | 50.3 | 1.5 | 24.3 | 0.00 | 61.0 | 1.36E-04 | 5.714E-10 | 0.15 | 0.72 | | | |
| 195019 | G3 IV-V | 5.4 | 0.98 | 26.8 | 2.9 | 18.3 | 0.03 | 275.3 | 4.62E-04 | 3.944E-08 | 0.13 | 3.51 | | | |
| 196885 | F8 IV | 5.1 | 1.27 | 30.3 | 2.6 | 386.0 | 0.30 | 10.0 † | 3.38E-04 | 3.471E-11 | 1.12 | 1.84 | | | |
| 217014 | G2-3 V | 4.0 | 1.0 | 65.1 | 0.9 | 4.2 | 0.01 | 55.9 | 2.17E-05 | 7.652E-11 | 0.05 | 0.45 | | | |
| 217107 | G7 V | 4.5 | 0.96 | 50.7 | 1.5 | 7.1 | 0.14 | 139.5 | 9.05E-05 | 1.947E-09 | 0.07 | 1.27 | | | |

Notes.

All spectral types were obtained from the paper announcing the planetary candidate's discovery (listed in Table 4.3) except the following:

HD 11964 and HD 34445 from VizieR; HD 20367 from Skiff (2004).

[†]HD 34445 and HD 196885 had no K_1 given in the literature, so a K_1 of 10.0 m s⁻¹ was assigned for the calculations.

[‡]HD 59686's mass was obtained from Cox (2000).

Table. 7.3: Possible Secondary Type Parameters

| Host | Possible Secondary Type | | | | | | | | | | | | | | |
|---------|-------------------------|---------------------|-------------------|--------------|---------------------|-------------------|--------------|---------------------|-------------------|--------------|---------------------|-------------------|--------------|---------------------|-------------------|
| | G5 V | | | | | K0 V | | | | | K5 V | | | | |
| | i (deg) | ΔK (mag) | α (mas) | i (deg) | ΔK (mag) | α (mas) | i (deg) | ΔK (mag) | α (mas) | i (deg) | ΔK (mag) | α (mas) | i (deg) | ΔK (mag) | α (mas) |
| HD | | | | | | | | | | | | | | | |
| 3651 | 0.02 | -0.3 | 33 | 0.02 | 0.1 | 32 | 0.03 | 0.7 | 31 | 0.03 | 1.4 | 30 | 0.06 | 2.4 | 29 |
| 9826b | 0.06 | 1.2 | 5 | 0.07 | 1.6 | 5 | 0.08 | 2.2 | 5 | 0.10 | 2.9 | 5 | 0.20 | 3.9 | 5 |
| 9826c | 0.18 | 1.2 | 73 | 0.20 | 1.6 | 72 | 0.22 | 2.2 | 71 | 0.28 | 2.9 | 69 | 0.60 | 3.9 | 67 |
| 9826d | 0.36 | 1.2 | 222 | 0.40 | 1.6 | 217 | 0.45 | 2.2 | 213 | 0.56 | 2.9 | 207 | 1.21 | 3.9 | 203 |
| 10697 | 0.57 | 1.5 | 80 | 0.63 | 1.9 | 78 | 0.71 | 2.5 | 76 | 0.88 | 3.1 | 74 | 1.86 | 4.1 | 72 |
| 11964 | 0.05 | 1.7 | 120 | 0.06 | 2.1 | 117 | 0.07 | 2.7 | 115 | 0.08 | 3.3 | 111 | 0.18 | 4.3 | 109 |
| 13189 | 0.53 | 10.8 | 1 | 0.59 | 11.2 | 1 | 0.66 | 11.8 | 1 | 0.80 | 12.5 | 1 | 1.62 | 13.5 | 1 |
| 16141 | 0.02 | 1.0 | 12 | 0.02 | 1.4 | 12 | 0.02 | 2.0 | 12 | 0.03 | 2.6 | 11 | 0.06 | 3.6 | 11 |
| 19994 | 0.14 | 1.4 | 76 | 0.16 | 1.8 | 74 | 0.18 | 2.4 | 73 | 0.22 | 3.1 | 71 | 0.48 | 4.1 | 69 |
| 20367 | 0.10 | 0.6 | 56 | 0.11 | 1.0 | 55 | 0.13 | 1.6 | 53 | 0.16 | 2.3 | 52 | 0.34 | 3.3 | 51 |
| 34445 | 0.02 | 1.0 | 14 | 0.02 | 1.4 | 14 | 0.03 | 2.0 | 13 | 0.03 | 2.6 | 13 | 0.07 | 3.6 | 13 |
| 38529 | 0.06 | 2.4 | 4 | 0.07 | 2.8 | 4 | 0.08 | 3.4 | 3 | 0.10 | 4.1 | 3 | 0.22 | 5.1 | 3 |
| 50554 | 0.46 | 0.5 | 95 | 0.51 | 0.9 | 93 | 0.58 | 1.5 | 91 | 0.71 | 2.1 | 88 | 1.51 | 3.1 | 86 |
| 59686 | 0.48 | 5.4 | 12 | 0.53 | 5.8 | 12 | 0.60 | 6.4 | 12 | 0.74 | 7.1 | 11 | 1.57 | 8.0 | 11 |
| 75732b | 0.08 | 0.0 | 12 | 0.09 | 0.4 | 11 | 0.10 | 1.0 | 11 | 0.12 | 1.6 | 11 | 0.25 | 2.6 | 10 |
| 75732c | 0.02 | 0.0 | 24 | 0.02 | 0.4 | 24 | 0.02 | 1.0 | 23 | 0.03 | 1.6 | 22 | 0.06 | 2.6 | 22 |
| 75732d | 0.38 | -3.5 | 589 | 0.42 | 0.0 | 575 | 0.47 | 0.4 | 562 | 0.58 | 1.0 | 543 | 1.20 | 1.6 | 529 |
| 95128b | 0.18 | 0.4 | 184 | 0.20 | 0.8 | 180 | 0.23 | 1.4 | 176 | 0.28 | 2.1 | 170 | 0.59 | 3.1 | 166 |
| 95128c | 0.07 | 0.4 | 328 | 0.08 | 0.8 | 320 | 0.09 | 1.4 | 313 | 0.11 | 2.1 | 303 | 0.23 | 3.1 | 296 |
| 104985 | 0.51 | 5.3 | 9 | 0.57 | 5.7 | 9 | 0.65 | 6.3 | 9 | 0.81 | 6.9 | 8 | 1.79 | 7.9 | 8 |
| 117176 | 0.63 | 1.3 | 32 | 0.69 | 1.7 | 31 | 0.78 | 2.3 | 30 | 0.95 | 2.9 | 29 | 1.98 | 3.9 | 28 |
| 120136 | 0.34 | 1.0 | 4 | 0.38 | 1.4 | 4 | 0.43 | 2.0 | 3 | 0.53 | 2.6 | 3 | 1.13 | 3.6 | 3 |
| 128311 | 0.25 | -0.5 | 80 | 0.28 | -0.1 | 78 | 0.31 | 0.5 | 76 | 0.38 | 1.1 | 73 | 0.78 | 2.1 | 71 |
| 143761 | 0.10 | 0.8 | 16 | 0.12 | 1.2 | 16 | 0.13 | 1.8 | 15 | 0.16 | 2.5 | 15 | 0.33 | 3.4 | 15 |
| 145675 | 0.45 | 0.1 | 193 | 0.50 | 0.5 | 188 | 0.56 | 1.1 | 184 | 0.69 | 1.7 | 178 | 1.44 | 2.7 | 173 |
| 168443b | 0.70 | 1.2 | 10 | 0.78 | 1.6 | 9 | 0.88 | 2.2 | 9 | 1.08 | 2.8 | 9 | 2.27 | 3.8 | 9 |

Continued on Next Page...

Table. 7.3 – Continued

| Host | Possible Secondary Type | | | | | | | | | | | |
|---------|-------------------------|---------------------|-------------------|--------------|---------------------|-------------------|--------------|---------------------|-------------------|--------------|---------------------|-------------------|
| | G5 V | | | K0 V | | | K5 V | | | M0 V | | |
| HD | i (deg) | ΔK (mag) | α (mas) | i (deg) | ΔK (mag) | α (mas) | i (deg) | ΔK (mag) | α (mas) | i (deg) | ΔK (mag) | α (mas) |
| 168443c | 1.55 | 1.2 | 94 | 1.73 | 1.6 | 92 | 1.94 | 2.2 | 90 | 2.39 | 2.8 | 87 |
| 177830 | 0.11 | 2.6 | 23 | 0.12 | 3.0 | 22 | 0.14 | 3.6 | 22 | 0.17 | 4.2 | 21 |
| 186427 | 0.14 | 0.5 | 98 | 0.16 | 0.9 | 96 | 0.18 | 1.5 | 94 | 0.22 | 2.1 | 90 |
| 189733 | 0.11 | -0.6 | 2 | 0.12 | -0.2 | 2 | 0.14 | 0.4 | 2 | 0.17 | 1.0 | 2 |
| 190228 | 0.35 | 2.1 | 42 | 0.39 | 2.5 | 41 | 0.43 | 3.1 | 39 | 0.53 | 3.7 | 38 |
| 190360 | 0.12 | 0.4 | 377 | 0.14 | 0.8 | 368 | 0.15 | 1.4 | 359 | 0.19 | 2.1 | 347 |
| 192263 | 0.07 | -0.5 | 10 | 0.08 | -0.1 | 10 | 0.09 | 0.5 | 9 | 0.11 | 1.1 | 9 |
| 195019 | 0.33 | 1.1 | 5 | 0.36 | 1.5 | 4 | 0.41 | 2.1 | 4 | 0.50 | 2.7 | 4 |
| 196885 | 0.03 | 1.0 | 41 | 0.04 | 1.4 | 40 | 0.04 | 2.0 | 39 | 0.05 | 2.7 | 38 |
| 217014 | 0.04 | 0.5 | 4 | 0.05 | 0.9 | 4 | 0.05 | 1.5 | 4 | 0.06 | 2.2 | 4 |
| 217107 | 0.12 | 0.4 | 5 | 0.13 | 0.8 | 4 | 0.15 | 1.4 | 4 | 0.18 | 2.1 | 4 |

Note. Values for M_K were obtained from Cox (2000): $M_{K(G5V)} = 3.5$, $M_{K(K0V)} = 3.9$, $M_{K(K5V)} = 4.5$, $M_{K(M0V)} = 5.2$, and $M_{K(M5V)} = 6.1$.

Table. 7.4: Calculated Secondary Star Angular Diameters

| Host Star HD | Angular Diameter (mas) | | | | |
|-----------------|------------------------|------|------|------|------|
| | G5 V | K0 V | K5 V | M0 V | M5 V |
| 3651 | 0.77 | 0.71 | 0.60 | 0.50 | 0.23 |
| 9826 | 0.64 | 0.59 | 0.50 | 0.41 | 0.19 |
| 10697 | 0.26 | 0.24 | 0.21 | 0.17 | 0.08 |
| 11964 | 0.25 | 0.23 | 0.20 | 0.16 | 0.07 |
| 13189 | 0.00 | 0.00 | 0.00 | 0.00 | 0.00 |
| 16141 | 0.24 | 0.22 | 0.19 | 0.16 | 0.07 |
| 19994 | 0.38 | 0.35 | 0.30 | 0.25 | 0.11 |
| 20367 | 0.32 | 0.29 | 0.25 | 0.21 | 0.09 |
| 34445 | 0.19 | 0.18 | 0.15 | 0.12 | 0.06 |
| 38529 | 0.20 | 0.19 | 0.16 | 0.13 | 0.06 |
| 50554 | 0.28 | 0.25 | 0.22 | 0.18 | 0.08 |
| 59686 | 0.09 | 0.09 | 0.07 | 0.06 | 0.03 |
| 75732 | 0.68 | 0.63 | 0.53 | 0.45 | 0.20 |
| 95128 | 0.61 | 0.56 | 0.48 | 0.40 | 0.18 |
| 104985 | 0.08 | 0.08 | 0.07 | 0.05 | 0.02 |
| 117176 | 0.47 | 0.44 | 0.37 | 0.31 | 0.14 |
| 120136 | 0.55 | 0.51 | 0.43 | 0.36 | 0.16 |
| 128311 | 0.52 | 0.48 | 0.40 | 0.34 | 0.15 |
| 143761 | 0.49 | 0.45 | 0.38 | 0.32 | 0.14 |
| 145675 | 0.47 | 0.44 | 0.37 | 0.31 | 0.14 |
| 168443 | 0.23 | 0.21 | 0.18 | 0.15 | 0.07 |
| 177830 | 0.15 | 0.13 | 0.11 | 0.09 | 0.04 |
| 186427 | 0.40 | 0.37 | 0.31 | 0.26 | 0.12 |
| 190228 | 0.14 | 0.13 | 0.11 | 0.09 | 0.04 |
| 190360 | 0.54 | 0.50 | 0.42 | 0.35 | 0.16 |
| 192263 | 0.43 | 0.40 | 0.34 | 0.28 | 0.13 |
| 195019 | 0.23 | 0.21 | 0.18 | 0.15 | 0.07 |
| 196885 | 0.26 | 0.24 | 0.20 | 0.17 | 0.08 |
| 217014 | 0.56 | 0.51 | 0.44 | 0.36 | 0.16 |
| 217107 | 0.43 | 0.40 | 0.34 | 0.28 | 0.13 |

Note. The radii used in these calculations: G5 V = $0.92 R_{\odot}$; K0 V = $0.85 R_{\odot}$; K5 V = $0.72 R_{\odot}$;

M0 V = $0.60 R_{\odot}$; M5 V = $0.27 R_{\odot}$. These were obtained from Cox (2000).

The resulting values for θ , ΔK , and α were then entered into the *Visibility Estimator* Mathcad program written by Harold McAlister to plot the visibility curves

for both a single star with the host star’s diameter and for a binary system with the calculated parameters. A projected position angle of 0° was adopted to explore the effects of the maximum separation exhibited by the secondary, as the actual projected position angle is not known. When the position angle decreases, modulations caused by the binary are less extreme and the binary’s visibility curve resembles a single star’s visibility curve.

To estimate the detection sensitivity, the difference between the visibility curve for the single star (dotted line in Figure 7.5) and the visibility curve for a binary system with the parameters listed in Table 7.3 (solid line in Figure 7.5) was calculated. This quantity was ΔK , and ΔK_{\max} then represented the maximum deviation of the binary visibility curve from the single-star curve.

The lower limit to rule out stellar companions was chosen to be $2\sigma_{\text{res}}$, where σ_{res} is the standard deviation of the residuals to the diameter fit; i.e., if $\Delta K_{\max} \geq 2\sigma_{\text{res}}$ for a given secondary type, that particular spectral type can be eliminated as a possible stellar companion. If $\Delta K_{\max} \leq 2\sigma_{\text{res}}$, the effects of the companion would not be clearly seen in the visibility curve, and that spectral type cannot be ruled out. For each object, Table 7.5 lists σ_{res} and the ΔK_{\max} for each secondary type considered and the final column indicates the cutoff point for the non-detection of a stellar companion. For example, if “K5 V” is listed in the last column, the spectral types more massive than a K5 V could be eliminated from consideration but the K5 V, M0 V, and M5 V stars are still possible companions. A dash in this column indicates

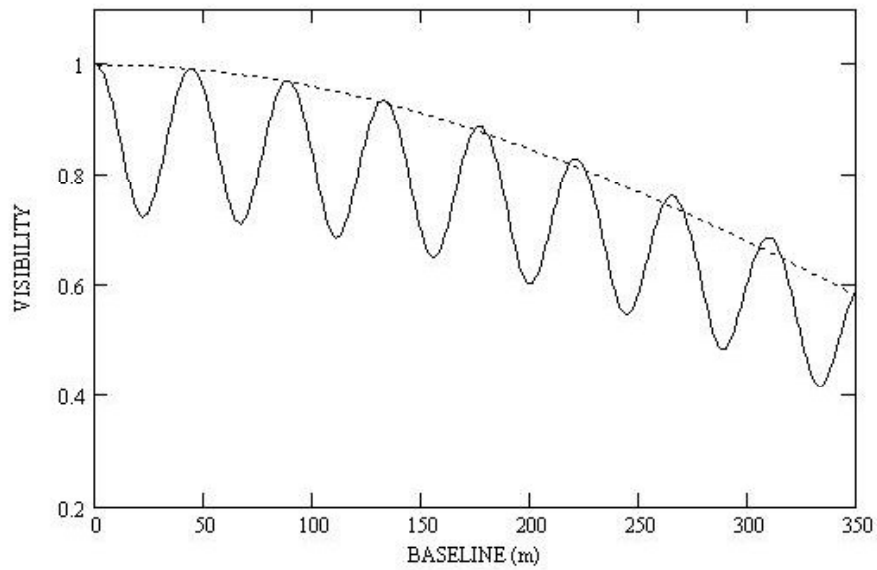


Figure. 7.5: Example of single star visibility curve vs. binary star visibility curve. The dotted line represents a single star with a given diameter and the solid line represents the visibility curve of a binary system. The parameters used in this example are: $\theta_{\text{primary}} = 0.5$ mas, $\theta_{\text{secondary}} = 0.25$ mas, $\alpha = 10$ mas, and $\Delta m = 2.0$.

all companion spectral types tested can be ruled out.

If a dataset had three or fewer bracketed observations, it was not used in the companion check process because it would not represent a large enough sample of datapoints to calculate a reliable σ_{res} . This was true for four of the exoplanet host stars observed.

Table. 7.5: Companion Check: Comparing Visibility Residuals

| HD | Date of Obs | σ_{res} | ΔK_{max} of Secondary Type | | | | | Non-Detection Threshold |
|--------|----------------|-----------------------|---|-------|-------|-------|-------|----------------------------|
| | | | G5 V | K0 V | K5 V | M0 V | M5 V | |
| 3651 | 2005/10/24 | 0.044 | 0.609 | 0.695 | 0.467 | 0.277 | 0.119 | - |
| | 2005/12/14 | 0.056 | 0.608 | 0.694 | 0.467 | 0.277 | 0.119 | - |
| 9826 | 2005/08/04 | 0.114 | 0.301 | 0.209 | 0.202 | 0.210 | 0.212 | M5 V |
| | 2005/08/08 | 0.069 | 0.301 | 0.209 | 0.202 | 0.210 | 0.212 | - |
| | 2005/08/10 | 0.072 | 0.301 | 0.209 | 0.202 | 0.210 | 0.212 | - |
| | 2005/08/14 | 0.064 | 0.301 | 0.209 | 0.202 | 0.210 | 0.212 | - |
| | 2005/08/18 | 0.047 | 0.301 | 0.209 | 0.202 | 0.210 | 0.212 | - |
| | 2005/08/19 | 0.056 | 0.301 | 0.209 | 0.202 | 0.210 | 0.212 | - |
| 10697 | 2005/10/23 | 0.082 | 0.226 | 0.163 | 0.098 | 0.059 | 0.024 | K5 V |
| | 2006/08/12 | 0.121 | 0.226 | 0.163 | 0.098 | 0.059 | 0.024 | G5 V |
| 11964 | 2005/12/16 | 0.037 | 0.206 | 0.148 | 0.088 | 0.053 | 0.021 | M0 V |
| | 2006/10/20 | 0.064 | 0.206 | 0.148 | 0.088 | 0.053 | 0.021 | K5 V |
| 16141 | 2005/12/12 | 0.249 | 0.323 | 0.239 | 0.147 | 0.090 | 0.037 | G5 V |
| | 2005/12/14 | 0.428 | 0.323 | 0.239 | 0.147 | 0.090 | 0.037 | G5 V |
| | 2006/08/13 | 0.044 | 0.323 | 0.239 | 0.147 | 0.090 | 0.037 | M5 V |
| | 2006/08/14 | 0.025 | 0.323 | 0.239 | 0.147 | 0.090 | 0.037 | M5 V |
| 19994 | 2005/10/21 | 0.063 | 0.272 | 0.197 | 0.120 | 0.064 | 0.026 | K5 V |
| | 2005/10/27 | 0.034 | 0.272 | 0.197 | 0.120 | 0.064 | 0.026 | M0 V |
| | 2005/12/10 | 0.037 | 0.272 | 0.197 | 0.120 | 0.064 | 0.026 | M0 V |
| 20367 | 2005/12/12 | 0.042 | 0.446 | 0.334 | 0.210 | 0.117 | 0.049 | M5 V |
| 34445 | 2005/12/07 | 0.081 | 0.320 | 0.236 | 0.145 | 0.087 | 0.036 | K5 V |
| | 2005/12/10 | 0.064 | 0.320 | 0.236 | 0.145 | 0.087 | 0.036 | M0 V |
| 38529 | 2005/12/06 | 0.055 | 0.112 | 0.079 | 0.048 | 0.025 | 0.010 | K0 V |
| | 2005/12/14 | 0.159 | 0.112 | 0.079 | 0.048 | 0.025 | 0.010 | G5 V |
| 50554 | 2005/12/12 | 0.043 | 0.471 | 0.354 | 0.223 | 0.137 | 0.058 | M5 V |
| 59686 | 2005/12/06 | 0.007 | 0.008 | 0.006 | 0.003 | 0.002 | 0.001 | G5 V |
| | 2005/12/16 | 0.039 | 0.008 | 0.006 | 0.003 | 0.002 | 0.001 | G5 V |
| | 2007/04/02 | 0.012 | 0.008 | 0.006 | 0.003 | 0.002 | 0.001 | G5 V |
| 75732 | 2007/03/30 | 0.053 | 0.720 | 0.586 | 0.383 | 0.240 | 0.101 | M5 V |
| 104985 | 2006/05/17 | 0.027 | 0.009 | 0.006 | 0.004 | 0.002 | 0.001 | G5 V |
| | 2007/04/26 | 0.029 | 0.009 | 0.006 | 0.004 | 0.002 | 0.001 | G5 V |
| 117176 | 2005/05/14 | 0.054 | 0.313 | 0.227 | 0.136 | 0.081 | 0.033 | M0 V |
| | 2006/05/13 | 0.052 | 0.313 | 0.227 | 0.136 | 0.081 | 0.033 | M0 V |
| | 2006/05/20 | 0.019 | 0.313 | 0.227 | 0.136 | 0.081 | 0.033 | M5 V |
| | 2007/04/02 | 0.095 | 0.313 | 0.227 | 0.136 | 0.081 | 0.033 | K5 V |
| 120136 | 2005/05/12 | 0.071 | 0.371 | 0.274 | 0.169 | 0.101 | 0.041 | M0 V |
| | 2006/05/14 | 0.027 | 0.371 | 0.274 | 0.169 | 0.101 | 0.041 | M5 V |
| | 2007/02/05 | 0.021 | 0.371 | 0.274 | 0.169 | 0.101 | 0.041 | M5 V |
| | 2007/03/26 | 0.072 | 0.371 | 0.274 | 0.169 | 0.101 | 0.041 | M0 V |
| | 2007/03/30 | 0.035 | 0.371 | 0.274 | 0.169 | 0.101 | 0.041 | M5 V |
| 128311 | 2005/06/30 | 0.051 | 0.500 | 0.584 | 0.446 | 0.297 | 0.134 | - |
| | 2006/05/16 | 0.061 | 0.500 | 0.584 | 0.446 | 0.297 | 0.134 | - |
| 143761 | 2005/06/29 | 0.048 | 0.422 | 0.314 | 0.195 | 0.108 | 0.048 | M5 V |

Continued on Next Page...

Table. 7.5 – Continued

| HD | Date of Obs | σ_{res} | ΔK_{max} of Secondary Type | | | | | Non-Detection Threshold |
|--------|-------------------------|-----------------------|---|-------|-------|-------|-------|----------------------------|
| | | | G5 V | K0 V | K5 V | M0 V | M5 V | |
| | 2005/07/03 | 0.080 | 0.422 | 0.314 | 0.195 | 0.108 | 0.048 | M0 V |
| | 2005/05/12 [†] | 0.035 | 0.422 | 0.314 | 0.195 | 0.108 | 0.048 | M5 V |
| | 2005/05/12 [‡] | 0.028 | 0.422 | 0.314 | 0.195 | 0.108 | 0.048 | M5 V |
| | 2006/05/19 | 0.075 | 0.422 | 0.314 | 0.195 | 0.108 | 0.048 | M0 V |
| 145675 | 2006/08/07 | 0.067 | 0.600 | 0.463 | 0.304 | 0.190 | 0.082 | M5 V |
| | 2006/08/12 | 0.052 | 0.600 | 0.463 | 0.304 | 0.190 | 0.082 | M5 V |
| 168443 | 2005/08/10 | 0.140 | 0.288 | 0.211 | 0.129 | 0.077 | 0.032 | K0 V |
| | 2005/08/14 | 0.093 | 0.288 | 0.211 | 0.129 | 0.077 | 0.032 | K5 V |
| 177830 | 2005/06/29 | 0.053 | 0.092 | 0.065 | 0.038 | 0.022 | 0.001 | G5 V |
| | 2005/08/08 | 0.104 | 0.092 | 0.065 | 0.038 | 0.022 | 0.001 | G5 V |
| | 2006/08/08 | 0.053 | 0.092 | 0.065 | 0.038 | 0.022 | 0.001 | G5 V |
| | 2006/08/13 | 0.109 | 0.092 | 0.065 | 0.038 | 0.022 | 0.001 | G5 V |
| 186427 | 2005/06/30 | 0.071 | 0.458 | 0.347 | 0.221 | 0.136 | 0.057 | M0 V |
| | 2005/08/04 | 0.038 | 0.458 | 0.347 | 0.221 | 0.136 | 0.057 | M5 V |
| | 2006/08/13 | 0.074 | 0.458 | 0.347 | 0.221 | 0.136 | 0.057 | M0 V |
| 190228 | 2005/07/01 | 0.078 | 0.141 | 0.101 | 0.059 | 0.035 | 0.014 | G5 V |
| | 2005/08/19 | 0.044 | 0.141 | 0.101 | 0.059 | 0.035 | 0.014 | K5 V |
| | 2006/08/14 | 0.042 | 0.141 | 0.101 | 0.059 | 0.035 | 0.014 | K5 V |
| 190360 | 2005/08/11 | 0.047 | 0.557 | 0.422 | 0.266 | 0.151 | 0.063 | M5 V |
| | 2006/08/11 | 0.044 | 0.557 | 0.422 | 0.266 | 0.151 | 0.063 | M5 V |
| 195019 | 2005/08/11 | 0.048 | 0.352 | 0.256 | 0.155 | 0.092 | 0.038 | M0 V |
| | 2005/08/12 | 0.075 | 0.352 | 0.256 | 0.155 | 0.092 | 0.038 | M0 V |
| | 2005/10/23 | 0.086 | 0.352 | 0.256 | 0.155 | 0.092 | 0.038 | K5 V |
| | 2006/08/06 | 0.070 | 0.352 | 0.256 | 0.155 | 0.092 | 0.038 | M0 V |
| 196885 | 2005/10/27 | 0.064 | 0.342 | 0.251 | 0.155 | 0.085 | 0.035 | M0 V |
| | 2005/10/29 | 0.050 | 0.342 | 0.251 | 0.155 | 0.085 | 0.035 | M0 V |
| | 2006/08/07 | 0.038 | 0.342 | 0.251 | 0.155 | 0.085 | 0.035 | M5 V |
| | 2006/08/14 | 0.055 | 0.342 | 0.251 | 0.155 | 0.085 | 0.035 | M0 V |
| 217104 | 2005/08/12 | 0.071 | 0.524 | 0.395 | 0.250 | 0.140 | 0.058 | M0 V |
| | 2006/08/12 | 0.034 | 0.524 | 0.395 | 0.250 | 0.140 | 0.058 | M5 V |
| 217107 | 2006/10/20 | 0.079 | 0.520 | 0.398 | 0.254 | 0.144 | 0.060 | M0 V |

[†]Using HD 143687 as the calibrator; [‡]Using HD 146025 as the calibrator.

Using the data from Table 7.5, Figure 7.6 was created to demonstrate the sensitivity of the interferometric observations to stellar companions. For each exoplanet host star observed, the absolute V -band magnitude was found from *The Hipparcos and Tycho Catalogues* (Perryman & ESA 1997). Then the night with the lowest σK_{obs} was chosen to be the best case scenario when determining which secondary stars could be

eliminated from consideration. Figure 7.6 shows that the general cutoff for low-mass stellar companions lies between the K5 V and M0 V range for most of the stars.

The difficulty of ruling out the more massive companion types for the intrinsically brighter stars makes sense, as the ΔK will already be large even for the brighter companions. Host stars that are less massive are fainter, and the ΔK lies more within the sensitivity limit of the CHARA Array.

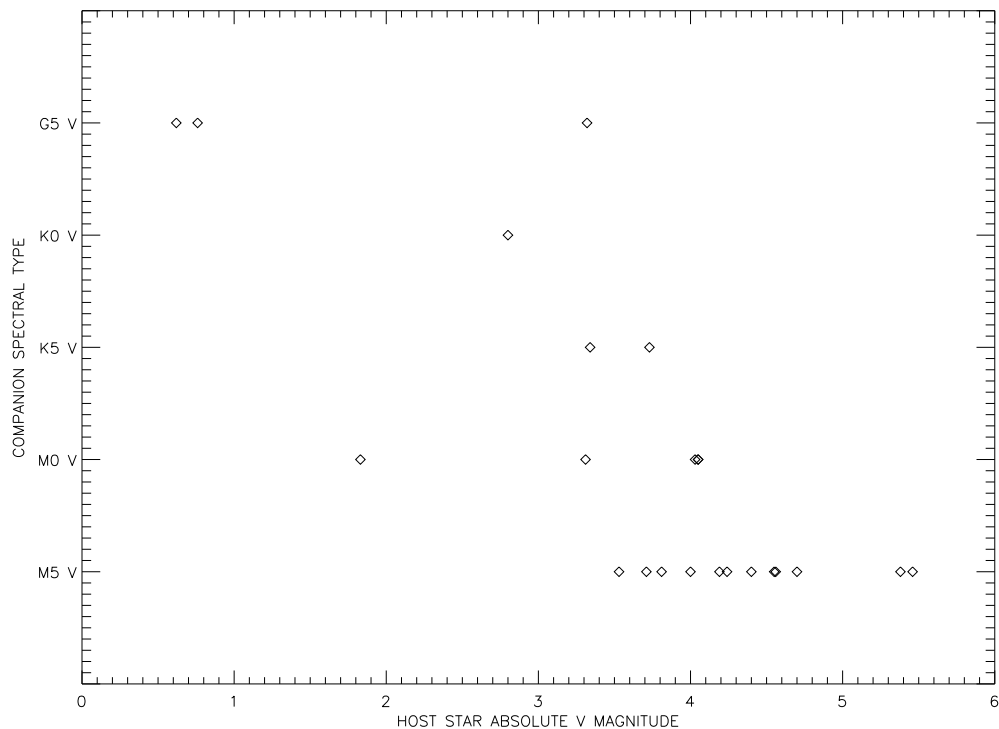


Figure. 7.6: Companion check: Eliminating companion spectral types. The x-axis represents the absolute magnitude for the observed exoplanet host stars and the y-axis represents the lowest-mass secondary that is still a possibility for each observed star. The three stars for which all the possible secondary types were ruled out are not plotted.

7.3 Separated Fringe Packets

The second method to check for unseen low-mass stellar companions is by searching for separated fringe packets (SFPs). When a star has a wide companion (~ 10 to 100 mas), two fringe packets - one from each star - may be observed if the baseline orientation is favorable; i.e., if the projected baseline angle is approximately parallel to the position angle of the binary and both fringe packets are within the scan window. However, if the two stars have a small angular separation or the position angle is perpendicular to the projected baseline angle, the two fringe packets will overlay each other and appear as one fringe packet.

For example, if a binary system with a $\Delta K=0$ has a separation of more than ~ 10 mas and is in the optimal orientation as described above, SFPs may be visible, as can be seen in Figure 7.7. If the same system has a $\Delta K \sim 2$ or is not in the optimal orientation, no secondary fringe would be observed, as is shown in Figure 7.8.

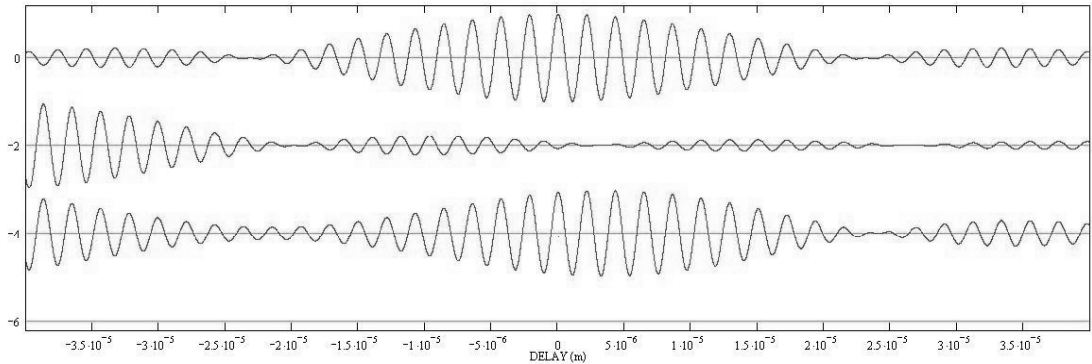


Figure. 7.7: Example SFP for a $\Delta K=0$ binary system. The top panel shows the primary star's fringe, the middle panel shows the secondary star's fringe, and the bottom panel shows the combination of the two.

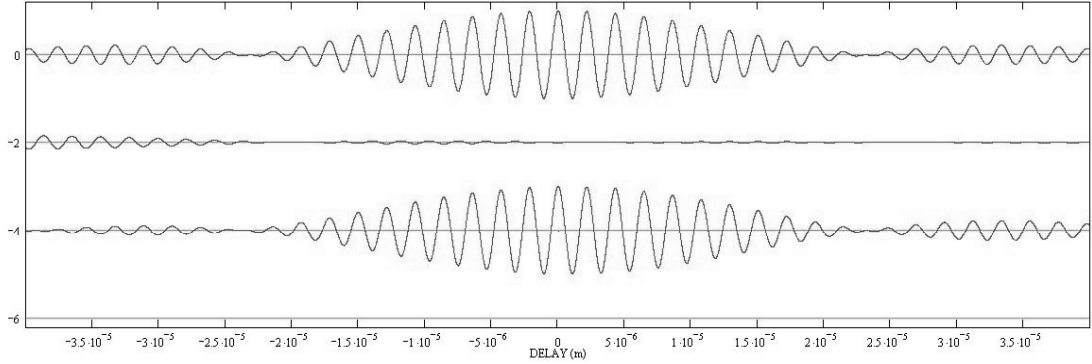


Figure. 7.8: Example SFP for a $\Delta K=2$ binary system. The top panel shows the primary star's fringe, the middle panel shows the secondary star's fringe, and the bottom panel shows the combination of the two.

The detection of SFPs depends partly on whether both fringe packets lie within the scan window. The width of the scan window depends on the baseline, wavelength used, and the frequency of the observations. For an average observation in the K -band at 100 Hz using a 100-m baseline, the scan window will cover ~ 300 mas while at a 300-m baseline, the scan window width is ~ 100 mas. If the SFP is wider than the scan window width, the second fringe will not be detected.

For completeness, all the stars observed in this dissertation were checked for SFPs, whether or not the calculated separation of the secondary star would indicate the possibility of separated fringes. This was done using the *VisUVCalc-SFPB* program written in Mathcad by Harold McAlister. For each of the individual ~ 200 scans in each dataset, the strongest fringe was located and a fringe envelope was fit to the fringe. The fringe envelope was created by taking the Fourier transform of the fringe, setting the negative frequencies to zero, and taking the modulus of the inverse Fourier transform. This is known as the “Hilbert transform”.

Then the peak of the primary fringe packet envelope for each of the data scans was located and shifted so that the fringe envelopes for all the scans overlaid each other and the fringe amplitudes were added together. This “shift and add” approach made it possible to view multiple fringe envelopes at once to see if there was any indication of a SFP. The result was a plot of the weighted mean fringe envelope (see Figures 7.9 and 7.10 for examples of this).

If there were three or fewer bracketed observations in the dataset, only one observation from each of the calibrator and object stars was inspected for SFPs. Otherwise the first and last observations in a night’s dataset were inspected from SFPs for both the object and the calibrator in order to maximize changes in the stars’ position angle with respect to the baseline over time.

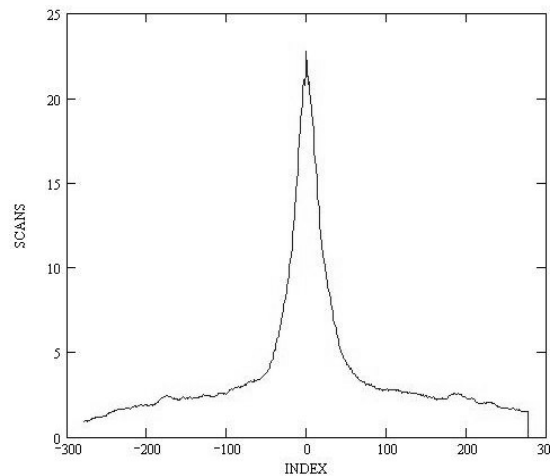


Figure. 7.9: Searching for SFPs: Example of a weighted mean fringe envelope for a single star (τ Boo, observed 2007/03/25). The solid line shows the sum of all the scans in the dataset. The x-axis represents the distance of the fringe envelope from the peak and the y-axis represents the cumulative fringe strength.

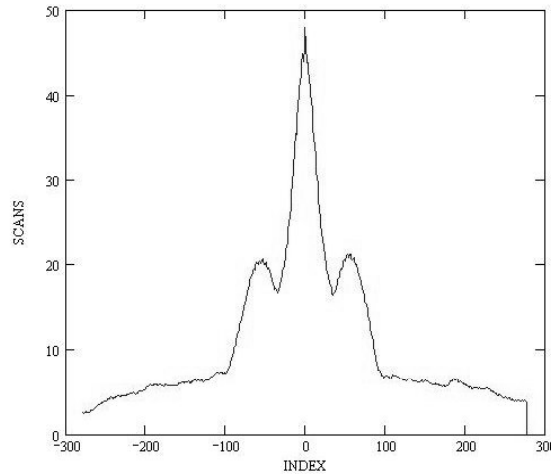


Figure. 7.10: Searching for SFPs: Example of a weighted mean fringe envelope for a known binary system (HD 79096). The solid line shows the sum of all the scans in the dataset. The x-axis represents the distance of the fringe envelope from the peak and the y-axis represents the cumulative fringe strength. The image shows three peaks instead of two due to the nature of the data reduction software, which chooses the bigger fringe to center for each scan. In this case, the two fringes are nearly identical in size, which creates a 180° ambiguity when centering the larger fringe. Image courtesy of Deepak Raghavan.

The weighted mean fringe envelope plots were then compared to the simulated SFP plots shown in Figures 7.11 through 7.14. These plots were generated using a Mathcad program *Fringe Envelope Inspector - SFP Simulator* written by Harold McAlister. First, a good dataset with large, clean, steady fringes was selected as a model. The input file consisted of 211 scans of 1024 lines each, which measured the fringe envelope for the 211 scans.

A second dataset was then created from the model dataset where the fringe envelope was offset by a certain value X and then was added to the model dataset to simulate an SFP. The parameter X was created using a random number generator

with a normal distribution around a central value of 150, i.e., the secondary fringe was offset from the primary fringe by an average of 150 steps but the exact value was different for each of the 211 scans. This was a simple simulation of piston error arising from the finite length of time for each scan and atmospheric effects.

Converting the number of steps in X to the angular separation of the two stars on the sky depends on the baseline used. For a 100-m baseline, the separation represented by $X = 150$ would be ~ 70 mas while the separation would be ~ 20 mas using a 300-m baseline. If the angular separation of the binary increased, the fringes would separate until the two packets were too wide to fit onto the scan window for a given baseline. If a binary's angular separation decreases, the fringe packets get closer together until they overlay each other and are seen as a single fringe packet.

This process was then repeated after scaling the second dataset by a factor R , which is related to ΔM_K , listed as ΔK , by:

$$R = (10^{0.4\Delta K})^{-1}. \quad (7.6)$$

Plots were generated using steps of 0.25 in ΔK and resulted in Figures 7.11 through 7.14. As can be seen from the plots, a secondary star with a ΔK up to ~ 3.0 would be detected if the system was in the optimal orientation. The vertical line in each plot separates the primary from the secondary fringe.

Given the limiting sensitivity of $\Delta K \sim 3.0$, certain companion types can be ruled out using the values calculated in Table 7.3. Table 7.6 lists the non-detection thresh-

old applying the criteria that companions with a $\Delta K \leq 3.0$ would be detected if conditions are ideal. For example, if “M0 V” is listed in the second column, stars more massive than that type can be ruled out while the M0 and M5 dwarfs are still possibilities. If no spectral type is listed, all stellar companion types tested could be ruled out.

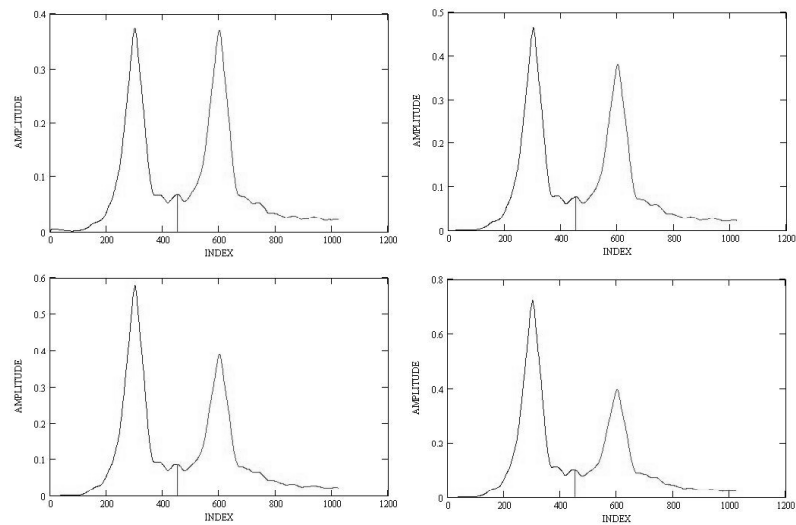


Figure. 7.11: Simulated SFPs: $\Delta K = 0.0$ to 0.75 . *Upper left*: $\Delta K = 0.0$; *upper right*: $\Delta K = 0.25$; *lower left*: $\Delta K = 0.5$; *lower right*: $\Delta K = 0.75$. The x-axis represents the width of the scan window and the y-axis represents the strength of the fringe envelope.

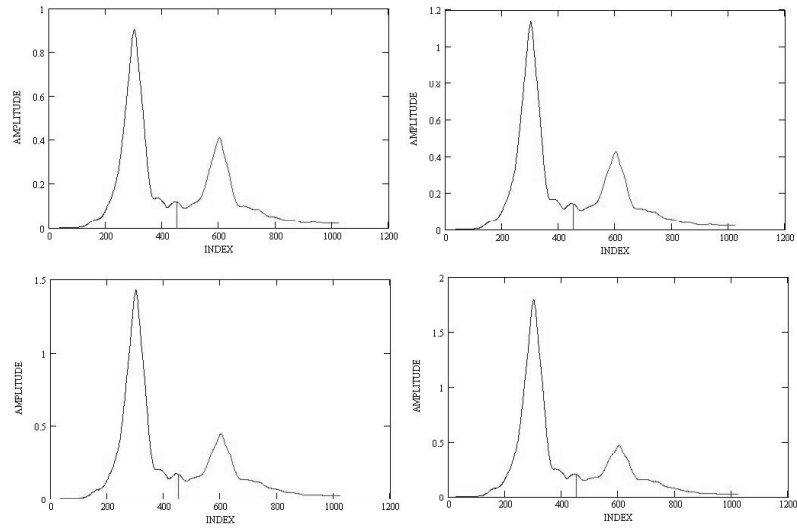


Figure. 7.12: Simulated SFPs: $\Delta K = 1.0$ to 1.75 . *Upper left*: $\Delta K = 1.0$; *upper right*: $\Delta K = 1.25$; *lower left*: $\Delta K = 1.5$; *lower right*: $\Delta K = 1.75$. The x-axis represents the width of the scan window and the y-axis represents the strength of the fringe envelope.

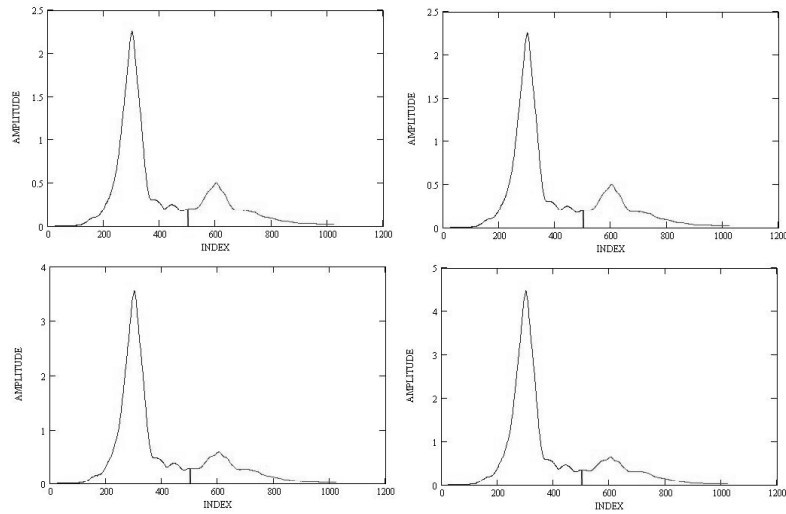


Figure. 7.13: Simulated SFPs: $\Delta K = 2.0$ to 2.75 . *Upper left*: $\Delta K = 2.0$; *upper right*: $\Delta K = 2.25$; *lower left*: $\Delta K = 2.5$; *lower right*: $\Delta K = 2.75$. The x-axis represents the width of the scan window and the y-axis represents the strength of the fringe envelope.

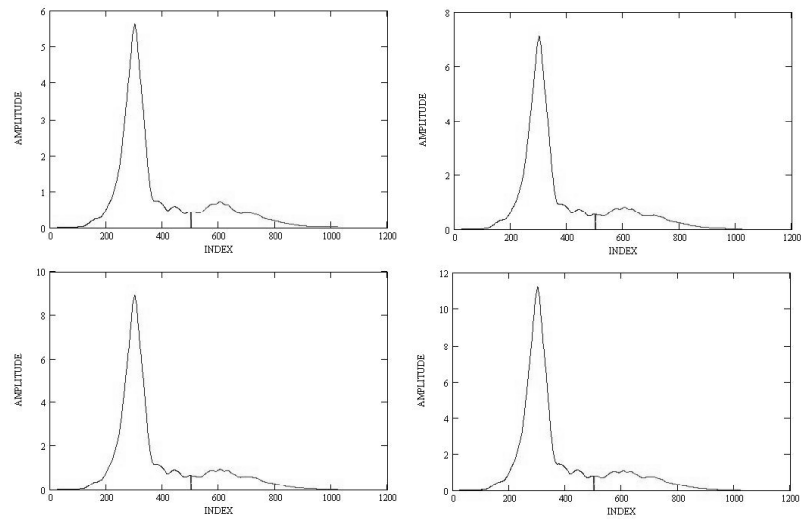


Figure. 7.14: Simulated SFPs: $\Delta K = 3.0$ to 3.75 . *Upper left:* $\Delta K = 3.0$; *upper right:* $\Delta K = 3.25$; *lower left:* $\Delta K = 3.5$; *lower right:* $\Delta K = 3.75$. The x-axis represents the width of the scan window and the y-axis represents the strength of the fringe envelope.

Table. 7.6: Non-Detection Threshold for SFPs Assuming $\Delta K = 3.0$

Limit for All Stars

| HD | Non-Detection Threshold |
|-----------|------------------------------------|
| 3651 | - |
| 9826 | M0 V |
| 10697 | M0 V |
| 11964 | K5 V |
| 13189 | G5 V |
| 16141 | M0 V |
| 19994 | M0 V |
| 20367 | M5 V |
| 34445 | M5 V |
| 38529 | K5 V |
| 50554 | M5 V |
| 59686 | G5 V |
| 75732 | - |
| 95128 | M5 V |
| 104985 | G5 V |
| 117176 | M5 V |
| 120136 | M5 V |
| 128311 | - |
| 143761 | M5 V |
| 145675 | - |
| 168443 | M5 V |
| 177830 | K5 V |
| 186427 | M5 V |
| 189733 | - |
| 190228 | K5 V |
| 190360 | M5 V |
| 192263 | - |
| 195019 | M5 V |
| 196885 | M5 V |
| 217014 | M5 V |
| 217107 | M5 V |

Several of the stars exhibit small wing-like structures on either side of the main fringe envelope after the shift and add process for one night's set of observations (see Figure 7.15 for an example of this) and not for another night's (see Figure 7.16). Both

figures show data for the same star taken on different nights using the same baseline. What is noteworthy about this is that nearly all the triple-peaked or asymmetrical patterns seen are for data obtained in 2005. In most cases, this is true for both the object and the calibrator, leading to the conclusion that the triple peaks are due to an unknown instrumental cause and are not true SFPs. See Table 7.7 for a list of which stars show this structure on which nights.

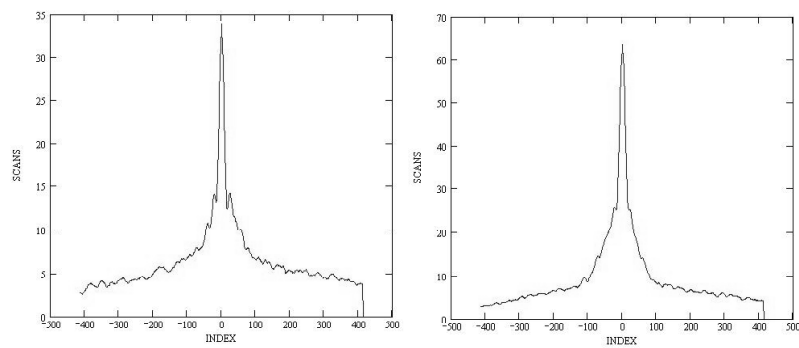


Figure. 7.15: Example of additional peaks in the mean fringe envelope. Data from 2005/12/12 for HD 16141.

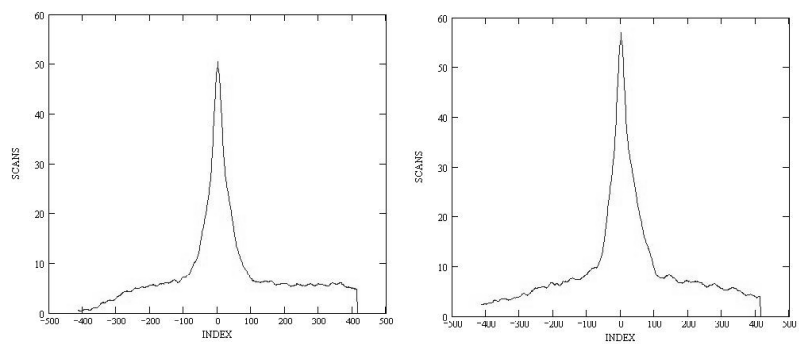


Figure. 7.16: Example of smooth mean fringe envelope. Data from 2006/08/13 for HD 16141.

Table. 7.7: Stars Exhibiting Asymmetries in the Weighted Mean
Fringe Envelope

| HD | Type | Date |
|--------|------------|------------------------------------|
| 10697 | Object | 2005/10/23 |
| 10477 | Calibrator | 2005/10/23 |
| 11964 | Object | 2005/12/16 |
| 13456 | Calibrator | 2005/12/16 |
| 13189 | Object | 2005/12/12 |
| 11007 | Calibrator | 2005/12/12 |
| 16141 | Object | 2005/12/12, 2005/12/14 |
| 16824 | Calibrator | 2005/12/12, 2005/12/14 |
| 19994 | Object | 2005/12/10 |
| 19411 | Calibrator | 2005/10/21 |
| 20367 | Object | 2005/12/12 |
| 21864 | Calibrator | 2005/12/12 |
| 34445 | Object | 2005/12/07, 2005/12/10 |
| 31425 | Calibrator | 2005/12/07, 2005/12/10 |
| 38529 | Object | 2005/12/06, 2006/12/14 |
| 43318 | Calibrator | 2005/12/06, 2006/12/14 |
| 50554 | Object | 2005/12/07, 2005/12/12 |
| 49736 | Calibrator | 2005/12/07, 2005/12/12 |
| 59686 | Object | 2005/12/06, 2005/12/16 |
| 61630 | Calibrator | 2005/12/06, 2005/12/16 |
| 117176 | Object | 2005/05/20 |
| 121107 | Calibrator | 2005/05/20 |
| 120136 | Object | 2005/05/12 |
| 121107 | Calibrator | 2005/05/12 |
| 128311 | Object | 2005/06/30 |
| 125194 | Calibrator | 2005/06/30 |
| 143761 | Object | 2005/06/29, 2006/05/12 |
| 143393 | Calibrator | 2005/06/29 |
| 146025 | Calibrator | 2006/05/12 |
| 143687 | Calibrator | 2006/05/12 |
| 145675 | Object | 2005/07/04, 2006/05/13 |
| 144015 | Calibrator | 2005/05/14, 2005/07/04, 2006/05/13 |
| 168443 | Object | 2006/05/14 |
| 173093 | Calibrator | 2006/05/14 |
| 177830 | Object | 2006/08/08 |
| 176377 | Calibrator | 2006/08/08 |
| 217107 | Object | 2005/12/13 |
| 216953 | Calibrator | 2005/12/13 |

7.4 Stellar Misfits

7.4.1 *v* Andromedae

The first planetary candidate for HD 9826 (*v* Andromedae) was announced in 1997 (Butler et al. 1997) and two more planets were discovered two years later (Butler et al. 1999). An M4.5 V stellar companion was then discovered accompanying HD 9826 at a distance of ~ 750 AU from the central star (Lowrance et al. 2002). This star would not have affected our search for more close-in stellar companions, as the angular distance from the host star is $55''$ and is well out of the field of view of the CHARA Array.

HD 9826 was part of an intensive observing campaign in 2005 August using the CHARA Array and the data cannot be fit with a simple LD disk. The tracking for every night except 2005/08/18 shows the relative distance between the object's and calibrator's visibilities changing over time, on both long and short timescales (see plots in §C.2.2). This remained true when observing with two different calibrators.

Despite the problematic tracking, most of the nights' data fit the single-star visibility curves reasonably well with no systematics in the residuals. The exception to this is the data for 2005/08/10 (see Figure 7.17), for which the data fit the single-star visibility curve well until the final five datapoints, when the calibrated visibilities drop and the residuals to the diameter fit are systematically low. The tracking of the object's and calibrator's visibilities also separate over the course of the observation.

In order to check that the oddities in the tracking were not due to a mid-observation

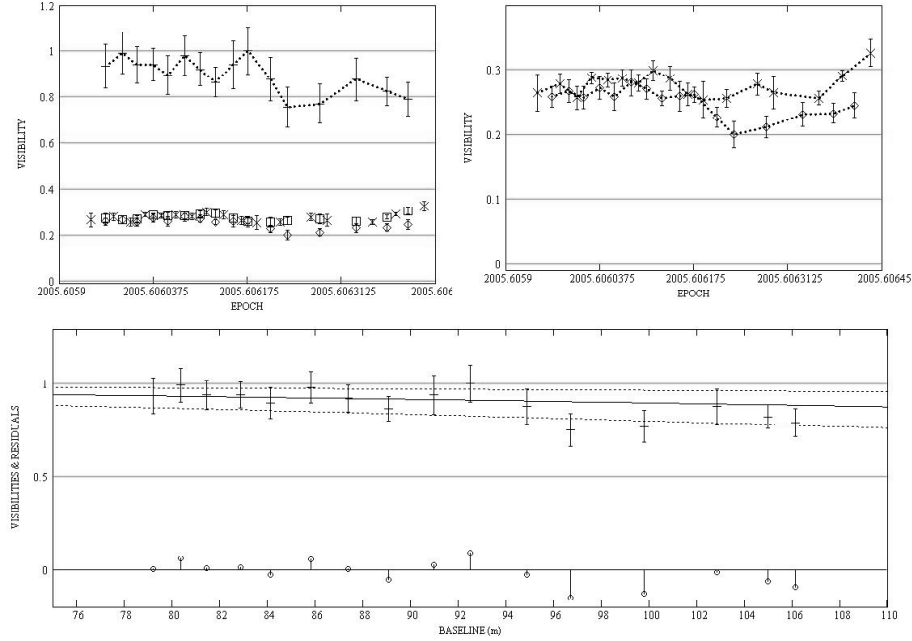


Figure. 7.17: HD 9826: Plots for 2005/08/10 data. *Upper panels:* Visibility vs. epoch; *lower panel:* visibility vs. baseline. Note how the last five observations have a systematically lower visibility than the preceding points.

alignment of the Near InfraRed Observer (NIRO) camera, the times of NIRO alignment were plotted with the data (see Figures 7.18 through 7.22; the times of NIRO alignment were not available for the 2005/08/19 data). Because the alignment was performed in between a calibrator and an object observation, the system changed slightly between the two observations and those points can no longer be considered strictly calibrated.

This led to modifying the data to remove any effects of the alignment: given the frequency of the NIRO alignments in the early part of the 2005/08/08 dataset, the first six object and calibrator datapoints were given zero weight; and due to the rapid dips in the calibrator's visibilities in the last half of the 2005/08/18 dataset, all

datapoints after the second alignment were given zero weight. If the NIRO alignment was performed in between an object and a calibrator observations, the last object's datapoint before the alignment was given zero weight. Similarly, if the alignment took place in between a calibrator and an object's observations, the first object's datapoint after the alignment was given zero weight. This essentially broke the datasets into separately calibrated sections.

After these modifications were made, the LD diameter was re-calculated as well as the σ_{res} for each night. These are the values listed in Tables 5.1 and 7.5. The modifications to the data had little effect on either the diameter calculation or the σ_{res} , only changing the diameter by 3% and the σ_{res} by an average of a few percent.

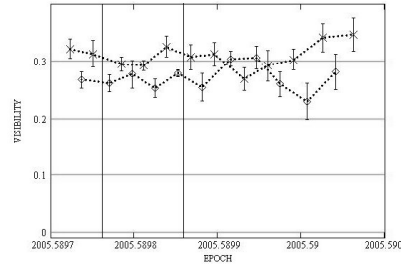


Figure. 7.18: HD 9826: Visibility vs. epoch for 2005/08/04 data with NIRO alignments marked. The vertical lines indicate the time of the alignments.

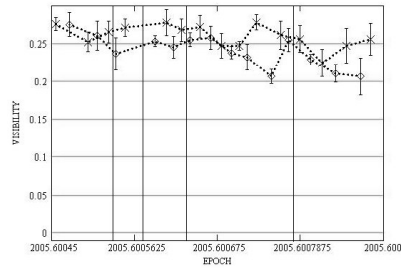


Figure. 7.19: HD 9826: Visibility vs. epoch for 2005/08/08 data with NIRO alignments marked. The vertical lines indicate the time of the alignments.

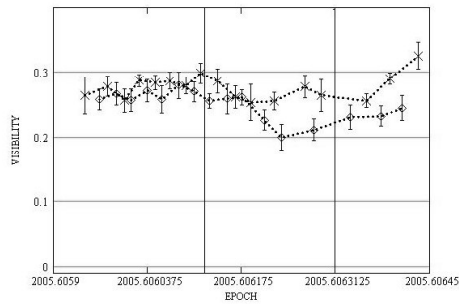


Figure. 7.20: HD 9826: Visibility vs. epoch for 2005/08/10 data with NIRO alignments marked. The vertical lines indicate the time of the alignments.

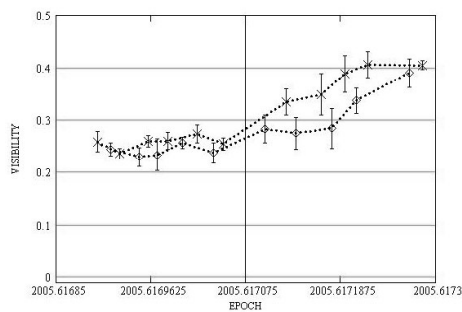


Figure. 7.21: HD 9826: Visibility vs. epoch for 2005/08/14 data with the NIRO alignment marked. The vertical line indicates the time of the alignment.

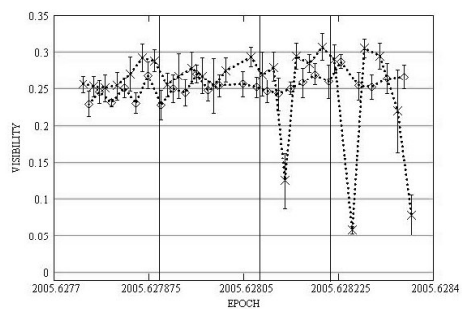


Figure. 7.22: HD 9826: Visibility vs. epoch for 2005/08/18 data with NIRO alignments marked. The vertical lines indicate the time of the alignments.

Interestingly, Harrington et al. (2006) claim to see variations in the light curve that they believe is caused by heating effects on the innermost planet itself. They observed HD 9826 using the Multiband Imaging Photometer for Spitzer (Werner et al. 2004) for almost an entire orbital period and found the photometric variations corresponded to the known 4.617-day period of the planet. However, it is unlikely that the behavior of the visibility curve described above is caused by this phenomenon, as they see variations of 0.3% at 24 μm and the fractional contribution of light from the planet diminishes at smaller wavelengths. Therefore, at the K -band, the variations would be at the 10^{-4} level (B. Hansen 2007, private communication), which is far beyond the sensitivity of the CHARA Array.

While no stellar companions to HD 9826 are proven, the data cannot be fit by a simple stellar model for one night of observations. While diameter fits to individual nights of data all result in diameters within 1σ of each other, the measured angular diameter is $\sim 30\%$ larger than that predicted using SED fits. This star requires further scrutiny using multiple baselines and calibrators before any definitive conclusions can be drawn.

7.4.2 ρ Coronae Borealis

In 1997, a planetary companion to HD 143761 (ρ Coronae Borealis) was announced with an orbital period of ~ 40 days and a minimum mass of $1.1 M_{\text{Jupiter}}$ after studying radial velocity variations (Noyes et al. 1997). The star was then part of the study by Imbert & Prévot (1998) (described in §1.3) where they found the data could fit a

low-inclination binary star model, albeit with a very low probability of 10^{-4} at most.

A later study by Gatewood et al. (2001) used *HIPPARCOS* and the Multichannel Astrometric Photometer to derive a face-on orbit and a companion mass much larger than the M_{Jupiter} announced by Noyes et al. (1997). In fact, they calculated the secondary's mass to be $0.14 \pm 0.05 M_{\odot}$, which put the companion into the realm of M dwarfs.

This claim was then refuted by Bender et al. (2005), who used high dispersion infrared spectroscopy to determine if they could detect any flux from an M dwarf companion, as it would lie within the sensitivity limits of the technique. They detected no such excess flux and concluded the companion was planetary in nature.

All in all, the controversy surrounding this system made it an interesting target to observe using the CHARA Array. HD 143761 was observed five times spanning 2005/06/29 to 2006/06/09 using three baselines and four calibrators. The results proved to be as contradictory as the studies described above.

Figure 7.23 shows the data taken on 2005/06/29. The relative distance between the calibrator's and object's visibilities changes over the course of the observations, and the residuals in the diameter fit are systematically high for the first half of the dataset and low for the second half. Similar behavior can be seen in the data from 2005/07/03 (Figure 7.24). In the event that the departure from a single star model proved to be due to the calibrator, several more calibrators were chosen. The data from 2006/05/19, which were taken using a different calibrator than earlier

observations, showed the same characteristics in the visibility measurements as the earlier data (Figure 7.27).

On the other hand, data obtained on 2006/05/12 using two different calibrators (Figures 7.25 and 7.26) show no indications of stellar companions. The calibrator and object track well together and there are no systematics in the residuals to a single star visibility curve fit.

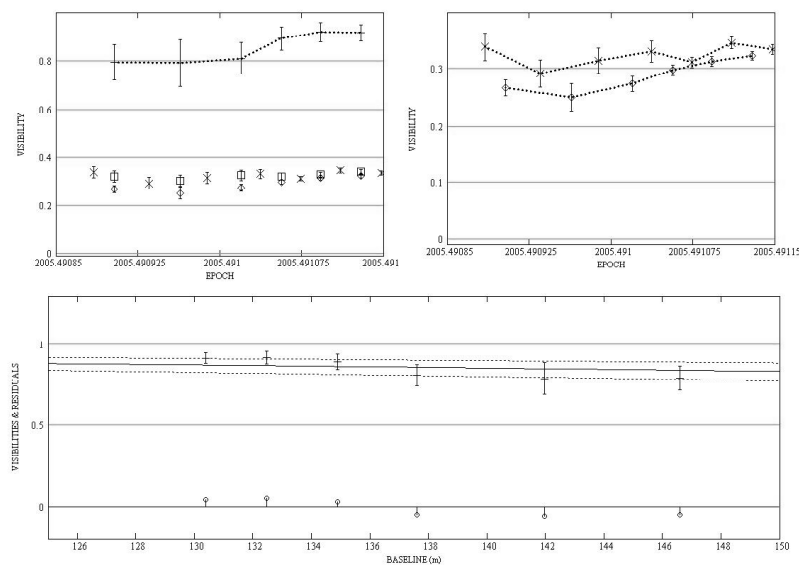


Figure. 7.23: HD 143761: Plots for 2005/06/29 data (calibrator HD 143393). Note how the residuals are systematically high towards the shorter-baseline datapoints and systematically low towards the longer-baseline datapoints.

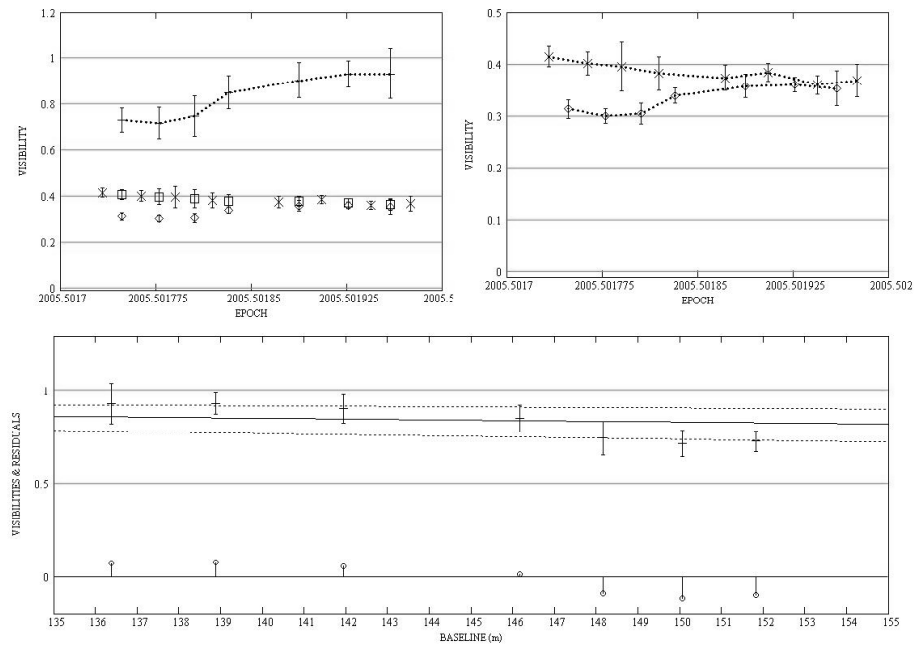


Figure. 7.24: HD 143761: Intermediate baseline plots for 2005/07/03 data (calibrator HD 143393). Note how the residuals are systematically high towards the shorter-baseline datapoints and systematically low towards the longer-baseline datapoints.

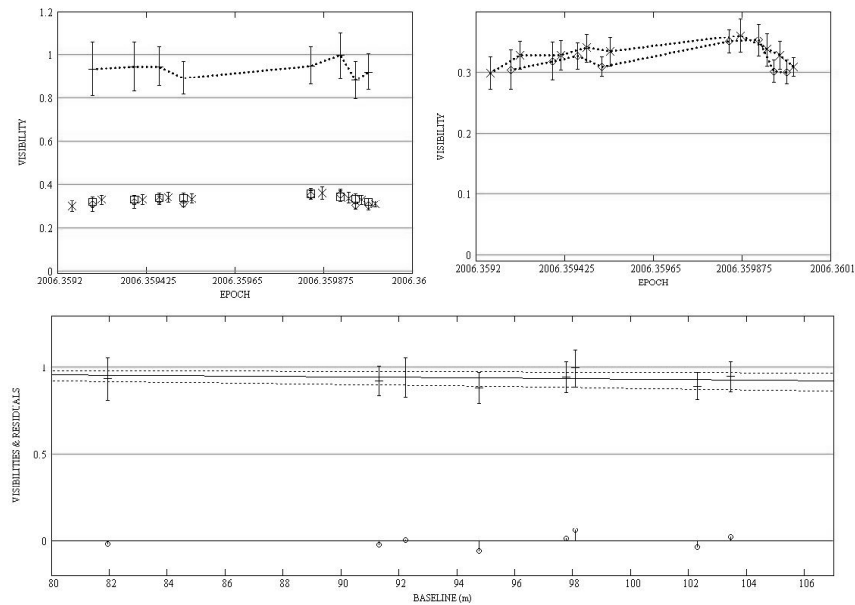


Figure. 7.25: HD 143761: Plots for 2006/05/12 data (calibrator HD 143687). Note the lack of any systematics in the visibility residuals.

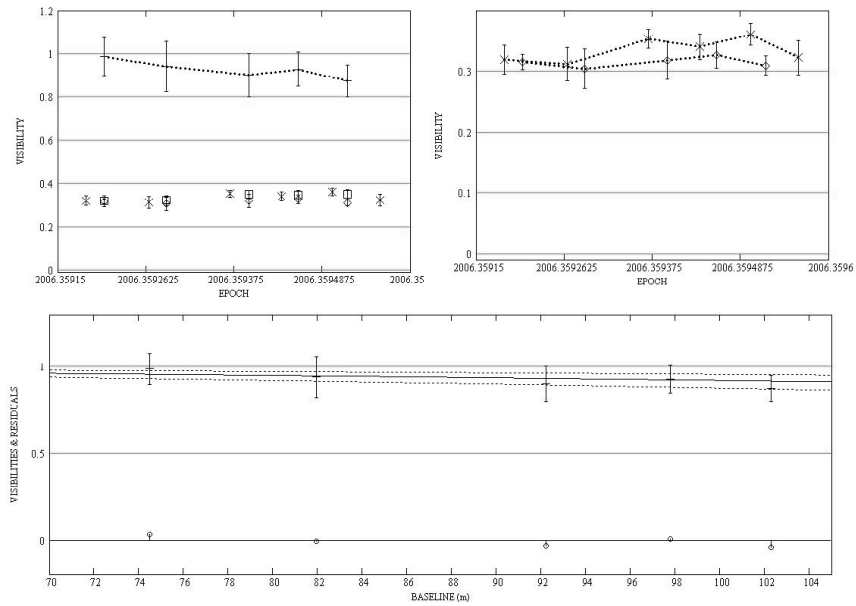


Figure. 7.26: HD 143761: Plots for 2006/05/12 data (calibrator HD 146025). Note the lack of any systematics in the visibility residuals.

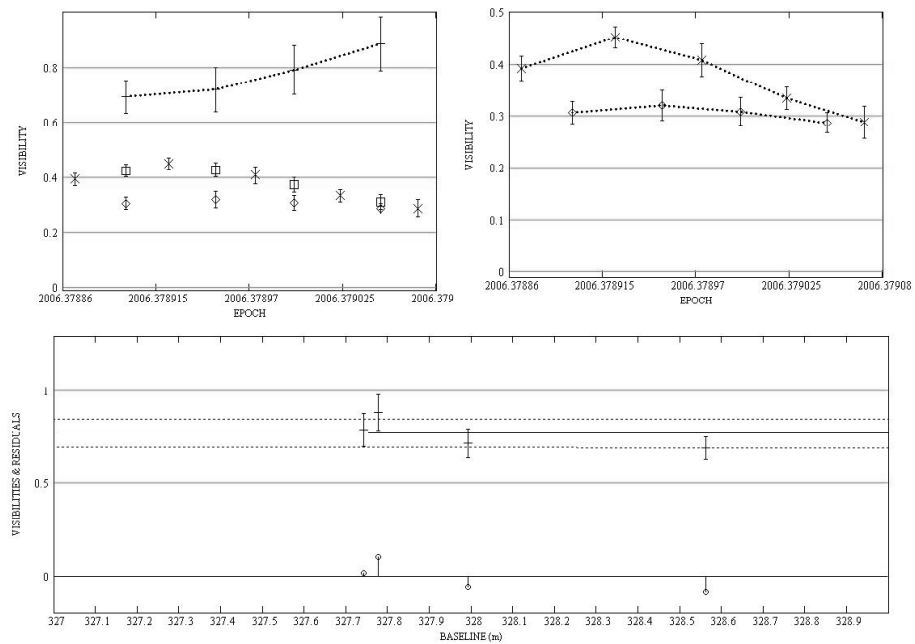


Figure. 7.27: HD 143761: Plots for 2006/05/19 data (calibrator HD 136849). Note the lack of any systematics in the visibility residuals.

The timings of the NIRO alignments were investigated to check if they were a possible source of error in the data (see Figures 7.28 through 7.30). If no plot is shown for a given night indicating the NIRO alignment, it is because there were no alignments performed during the dataset.

This check resulted in modifying some of the data: the first two object's and calibrator's visibility measurements were given zero weight in the 2005/06/29 data; the 2006/05/12 data (using the calibrator HD 143687) were unaffected by the alignments because the object's visibility just before the second alignment was already given zero weight due to the large gap in time between observations; and the second to last object's visibility in the 2006/05/12 data (using the calibrator HD 146025) was given zero weight, which split the dataset into two bracketed sections.

These changes had only minor effects on the LD diameter and σ_{res} , and the recalculated values are listed in Tables 5.1 and 7.5. All in all, the NIRO alignments do not explain the unusual trends in the tracking, or the systematics in the residuals.

HD 143761 shows even more unusual behavior than HD 9826 and the data cannot be fitted using a simple single-star model. The data are of good quality and were largely unaffected by NIRO alignments and indicate something more complex than a single star with planets. However, as with HD 9826, more observations are required before the situation becomes clear.

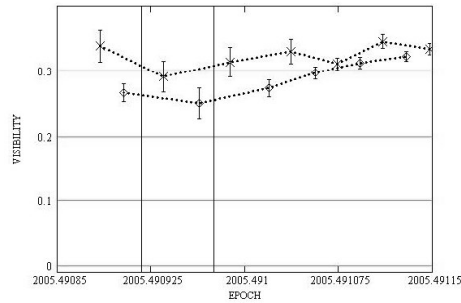


Figure. 7.28: HD 143761: Visibility vs. epoch for 2005/06/29 data with NIRO alignments marked. The vertical lines indicate the time of the alignments.

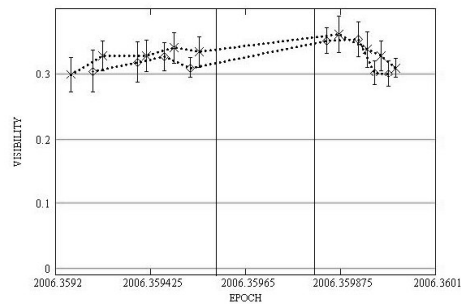


Figure. 7.29: HD 143761: Visibility vs. epoch for 2006/05/12 data with NIRO alignments marked (using the calibrator HD 143867). The vertical lines indicate the time of the alignments (using the calibrator HD 143867).

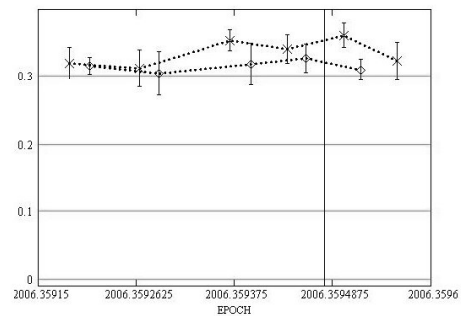


Figure. 7.30: HD 143761: Visibility vs. epoch for 2006/05/12 data with the NIRO alignment marked (using the calibrator HD 146025). The vertical line indicates the time of the alignment (using the calibrator HD 146025).

*They both savoured the strange warm glow of being much more ignorant
than ordinary people, who were only ignorant of ordinary things.*

— Terry Pratchett

– 8 –

Discussion

8.1 Comparing Stellar Radii

It was of particular interest to compare interferometrically-measured stellar radii with radii determined using other means. Some of the most precise stellar radii come from measuring detached, double-lined eclipsing binary systems, as described in Andersen (1991). His sample encompasses all spectral types from O8 V to M1 V and includes one system of two evolved stars. The errors in the radii measurements are $\leq 2\%$ and the values are presumed to be valid for single stars.

Figure 8.1 shows the stellar diameters measured from eclipsing binaries and the exoplanet host stars’ diameters measured here with errors $\leq 10\%$. The Andersen sample has few G and K-dwarfs and this work was able to better populate the low-mass range by more than doubling the number of stellar radii in the $0.5 \leq (B - V) \leq 1.0$ portion of the plot. Though 14 stars measured here had linear radii errors $\leq 10\%$, only 12 are shown in Figure 8.1. The remaining objects are HD 59686, a K2 III star, and HD 104985, a G9 III star.

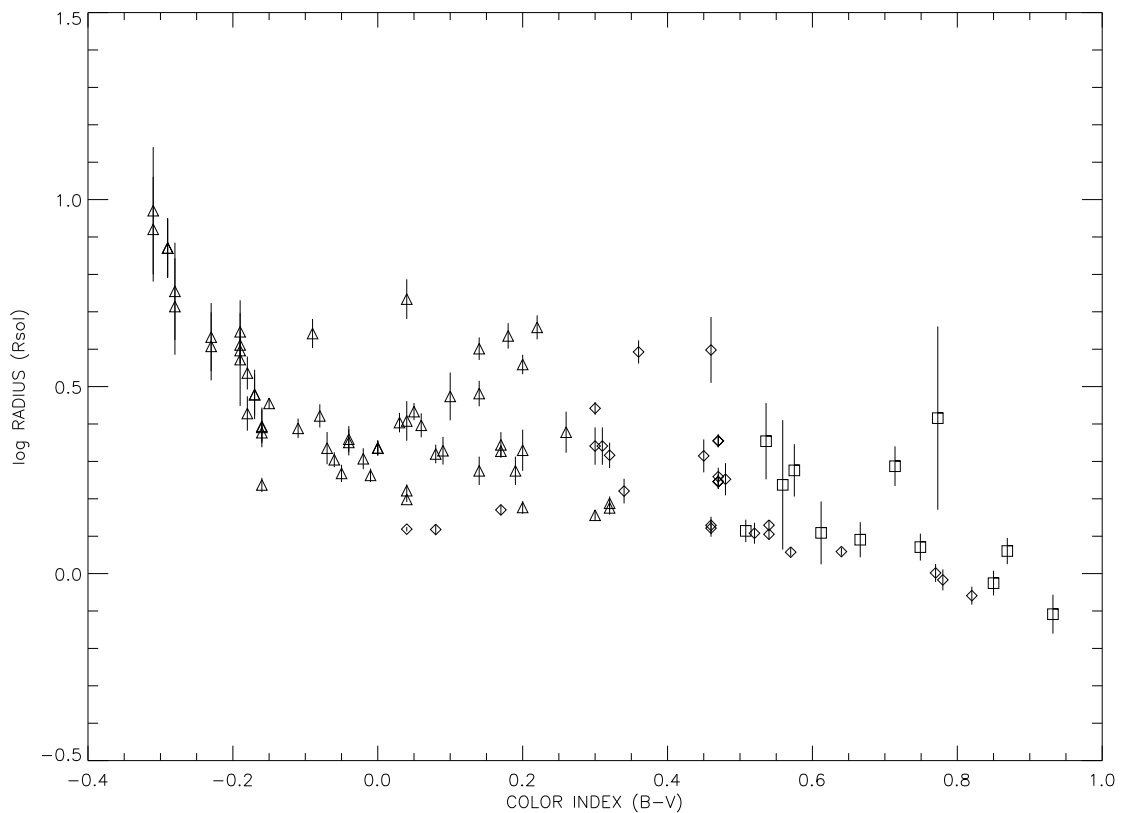


Figure. 8.1: Log R vs. color index: Past and present stellar diameters. \triangle = O, B, and A-dwarf stars from the Andersen sample (Andersen 1991); \diamond = F, G, and K-dwarf stars from the Andersen sample; and \square = exoplanet host stars' diameters measured here with errors $\leq 10\%$.

8.2 Exoplanet Host Star Age

Determining stellar ages turns out to be a tricky process. Most of the exoplanet host stars described in this dissertation were observed by Nordström et al. (2004), who studied a sample of 16,682 nearby F and G dwarf stars in an effort to catalog their ages, metallicities, and kinematic properties. They derived stellar ages using the isochrone method, which involves plotting the stars on a theoretical Hertzsprung-Russell (H-R) diagram and comparing the observations to theoretically-computed

isochrones. Their results are listed in Table 8.2.

Approximately half of the exoplanet host stars observed here were also observed by Saffe et al. (2005), who studied the Ca II *H* and *K* lines to determine a star's age. These lines measure stellar chromospheric emission, which in turn tells of the chromospheric activity. As a star of a given spectral type ages, its rotation slows and the amount of chromospheric activity decreases. Therefore knowing the level of chromospheric activity can put constraints on the star's age. The ages were determined using calculations developed by Donahue (1993), who studied the differential rotation of cool dwarf stars. It should be noted, however, that the typical uncertainty in ages derived via this method are approximately 30 to 50%, which makes it something of a mystery why they present stellar ages to two decimal places in most cases (see Table 8.2).

8.2.1 Stellar Evolution Model

There is often a wide range in ages produced by the methods of Nordström et al. (2004) and Saffe et al. (2005), so it was of interest to compare their ages to those derived from the interferometric radii measured here. The stellar model used in this study was the *Dartmouth Stellar Evolution Web Server*¹, an online Java applet that allows the user to calculate models for stellar evolution based on a range of input values: mass, helium and heavy element compositions, and the age at which to end the run. The outputs include age, $\log(L/L_\odot)$, $\log(R/R_\odot)$, $\log g$, T_{eff} , etc. (Chaboyer

¹<http://stellar.dartmouth.edu/~evolve/>

et al. 2001; Guenther et al. 1992).

The relative metallicity of the exoplanet host stars, $[\text{Fe}/\text{H}]_{\text{star}}$, was converted to a true metallicity, $(\text{Fe}/\text{H})_{\text{star}}$, using the following:

$$[\text{Fe}/\text{H}]_{\text{star}} = \log_{10} \left(\frac{(\text{Fe}/\text{H})_{\text{star}}}{(\text{Fe}/\text{H})_{\odot}} \right), \quad (8.1)$$

where $[\text{Fe}/\text{H}]_{\text{star}}$ is given in the literature and $(\text{Fe}/\text{H})_{\odot} = 0.019$ (Cox 2000).

For each exoplanet host star studied, a stellar evolution model was produced using the stellar mass quoted in the planet discovery papers and the metallicity derived from spectroscopic studies. The star's $\log(R/R_{\odot})$ was calculated from interferometric measurements of LD angular diameters and the *HIPPARCOS* parallax with the standard errors of these values propagated into $\sigma \log(R/R_{\odot})$. Comparison of these linear radii with the models then yielded the age of the host star and a resulting uncertainty in that age. The corresponding age is shown in the sixth column of Table 8.1. Table 8.2 compares the ages listed in the *Extrasolar Planets Encyclopedia*, those from Nordström et al. (2004) and Saffe et al. (2005), and ages produced using the *Dartmouth Stellar Evolution Web Server*.

Stellar radii are helpful in determining age because as a star ages, its radius increases even when it is stably burning hydrogen to helium on the main-sequence (M-S). For example, the Sun will increase in radius by over 50% over the course of its time on the M-S (Sackmann et al. 1993), so knowing its radius helps constrain its age.

In some cases, the age determined using this method turns out to be older than

the universe, which is obviously not physical, at least in the realm of this dissertation. Also, most of the ages produced using the *Dartmouth Stellar Evolution Web Server* do not match the ages listed in the *Extrasolar Planets Encyclopedia*. These discrepancies and the stars with large ages led me to inspect the effect of the star's mass on the final age determination.

Table. 8.1: Age Determination

| HD | $\log(R/R_{\odot})$ | M (M_{\odot}) | [Fe/H] | (Fe/H) | Age (Gyr) |
|---------------------|----------------------------|------------------------|--------|--------|---------------------------|
| 3651 | $-0.027^{+0.015}_{-0.016}$ | 0.79 | 0.12 | 0.025 | $24.0^{+1.0}_{-1.4}$ |
| 9826 | 0.344 ± 0.018 | 1.3 | 0.13 | 0.025 | $4.78^{+0.05}_{-0.04}$ |
| 10697 | $0.092^{+0.114}_{-0.156}$ | 1.10 | 0.14 | 0.026 | $5.9^{+3.0}_{-1.3}$ |
| 11964 | $0.367^{+0.047}_{-0.053}$ | 1.12 | 0.14 | 0.026 | $8.6^{+0.2}_{-0.1}$ |
| 13189 [†] | 2.218 | 2.0 | -0.39 | 0.008 | N/A |
| 16141 | $0.065^{+0.180}_{-0.313}$ | 1.01 | 0.15 | 0.027 | $9.8^{+2.7}_{-N/A}$ |
| 19994 | 0.276 ± 0.016 | 1.34 | 0.25 | 0.033 | $4.8^{+0.1}_{-0.3}$ |
| 20367 | $0.066^{+0.108}_{-0.144}$ | 1.17 | 0.17 | 0.028 | $2.4^{+4.1}_{-N/A}$ |
| 34445 [†] | $0.136^{+0.027}_{-0.028}$ | 1.11 | 0.24 | 0.033 | $8.6^{+0.7}_{-1.2}$ |
| 38529 | $0.416^{+0.039}_{-0.043}$ | 1.4 | 0.40 | 0.047 | $5.19^{+0.03}_{-0.05}$ |
| 50554 | $0.056^{+0.113}_{-0.154}$ | 1.11 | 0.01 | 0.019 | $2.8^{+3.9}_{-N/A}$ |
| 59686 | $1.031^{+0.029}_{-0.032}$ | 1.15 | - | 0.020 | $7.387^{+0.005}_{-0.006}$ |
| 75732 | 0.060 ± 0.013 | 0.95 | 0.33 | 0.020 | $10.6^{+0.4}_{-0.5}$ |
| 95128 [†] | 0.065 ± 0.017 | 1.03 | 0.06 | 0.020 | $6.5^{+0.6}_{-0.8}$ |
| 104985 | $1.048^{+0.025}_{-0.026}$ | 1.6 | -0.15 | 0.013 | $1.984^{+0.005}_{-0.003}$ |
| 117176 | 0.287 ± 0.012 | 0.92 | -0.06 | 0.016 | 13.77 ± 0.04 |
| 120136 | 0.114 ± 0.010 | 1.2 | 0.23 | 0.032 | 4.0 ± 0.4 |
| 128311 [†] | $-0.093^{+0.060}_{-0.070}$ | 0.80 | 0.03 | 0.020 | $12.3^{+7.0}_{-N/A}$ |
| 143761 | $0.109^{+0.027}_{-0.029}$ | 1.0 | -0.21 | 0.012 | $7.3^{+0.6}_{-0.9}$ |
| 145675 | $-0.176^{+0.059}_{-0.069}$ | 1.00 | 0.43 | 0.051 | N/A |
| 168443 [†] | $0.188^{+0.022}_{-0.024}$ | 1.01 | 0.06 | 0.022 | $10.8^{+0.2}_{-0.4}$ |

Continued on Next Page...

Table. 8.1 – Continued

| HD | $\log(R/R_{\odot})$ | M (M_{\odot}) | [Fe/H] | (Fe/H) | Age (Gyr) |
|---------------------|----------------------------|------------------------|--------|--------|----------------------|
| 177830 | $0.469^{+0.055}_{-0.063}$ | 1.15 | 0.33 | 0.040 | 10.0 ± 0.1 |
| 186427 | $-0.174^{+0.154}_{-0.241}$ | 1.0 | 0.08 | 0.023 | N/A |
| 189733 | $-0.108^{+0.028}_{-0.030}$ | 0.82 | -0.03 | 0.018 | $6.7^{+4.4}_{-6.0}$ |
| 190228 | $0.477^{+0.048}_{-0.054}$ | 0.83 | -0.25 | 0.011 | 17.3 ± 0.1 |
| 190360 | $0.071^{+0.013}_{-0.014}$ | 0.96 | 0.24 | 0.033 | $14.1^{+0.5}_{-0.7}$ |
| 192263 [†] | -0.124 ± 0.014 | 0.75 | -0.02 | 0.018 | $13.5^{+2.7}_{-2.9}$ |
| 195019 | $0.105^{+0.105}_{-0.139}$ | 0.98 | 0.09 | 0.023 | $11.1^{+1.6}_{-7.5}$ |
| 196885 | $0.237^{+0.041}_{-0.046}$ | 1.27 | 0.29 | 0.037 | $6.2^{+0.1}_{-1.2}$ |
| 217014 | $0.090^{+0.016}_{-0.017}$ | 1.0 | 0.20 | 0.030 | 11.3 ± 0.5 |
| 217107 [†] | 0.043 ± 0.014 | 0.96 | 0.37 | 0.044 | $15.3^{+0.7}_{-0.9}$ |

Notes.

[†]Indicates $\log(R/R_{\odot})$ was derived from SED diameter estimates due to large errors in the interferometric measurements.

“N/A” in the Age column indicates no match to the $\log(R/R_{\odot})$ could be found in the model results.

HD 13189: Due to the extremely large uncertainty in this star’s parallax, no $\log(R/R_{\odot})$ errors was determined for this star.

HD 59686: The mass was obtained from Cox (2000) for a K2 III.

All [Fe/H] values were obtained from Santos et al. (2004) except the following: HD 11964, HD 13189,

HD 34445, HD 189733, and HD 196885 from Sousa et al. (2006); HD 104985 from Takeda et al.

(2005); HD 59686: No [Fe/H] value found in the literature, so I used solar $[\text{Fe}/\text{H}] = 0.020$.

Table. 8.2: Stellar Age Comparison

| HD | EE (Gyr) | N04 (Gyr) | S05 (Gyr) | Here (Gyr) |
|--------|-----------------|------------------------|----------------------|----------------------------|
| 3651 | 5.13 | 17.0 $^{+N/A}_{-14.4}$ | 5.13 | 24.0 $^{+1.0}_{-1.4}$ |
| 9826 | 3.8 \pm 0.1 | 3.3 $^{+1.7}_{-0.5}$ | N/A | 4.78 $^{+0.05}_{-0.04}$ |
| 10697 | 6.9 \pm 0.6 | 7.1 $^{+0.8}_{-0.7}$ | 8.48 | 6.7 $^{+1.8}_{-N/A}$ |
| 11964 | 9.56 | N/A | 9.56 | 8.6 $^{+0.2}_{-0.1}$ |
| 13189 | N/A | N/A | N/A | N/A |
| 16141 | 7.76 | 11.2 $^{+1.7}_{-1.5}$ | 7.76 | 9.8 $^{+2.7}_{-N/A}$ |
| 19994 | 8.91 | 4.7 $^{+0.5}_{-1.6}$ | 4.7 $^{+0.5}_{-1.6}$ | 4.8 $^{+0.1}_{-0.3}$ |
| 20367 | 0.87 | 6.4 $^{+2.5}_{-2.8}$ | 0.87 | 2.4 $^{+4.1}_{-N/A}$ |
| 34445 | 9.5 \pm 1.6 | 9.5 $^{+1.6}_{-1.5}$ | N/A | 8.6 $^{+0.7}_{-1.2}$ |
| 38529 | 5.09 | N/A | 5.09 | 5.19 $^{+0.03}_{-0.05}$ |
| 50554 | 4.58 | 7.0 $^{+2.9}_{-3.7}$ | 4.58 | 2.8 $^{+3.9}_{-N/A}$ |
| 59686 | N/A | N/A | N/A | 7.387 $^{+0.005}_{-0.006}$ |
| 75732 | 5.5 | N/A | 5.5 | 10.6 $^{+0.4}_{-0.5}$ |
| 95128 | 7.4 \pm 1.9 | 8.7 $^{+3.2}_{-3.4}$ | 6.03 | 6.5 $^{+0.6}_{-0.8}$ |
| 104985 | 2.95 \pm 0.65 | 3.1 $^{+0.5}_{-0.8}$ | 3.1 $^{+0.5}_{-0.8}$ | 1.984 $^{+0.005}_{-0.003}$ |
| 117176 | 7.09 | 7.4 $^{+0.5}_{-0.7}$ | 7.09 | 13.77 \pm 0.04 |
| 120136 | 2.52 | 2.4 $^{+0.7}_{-1.1}$ | 2.4 | 4.0 \pm 0.4 |
| 128311 | 0.39 | N/A | N/A | 12.3 $^{+7.0}_{-N/A}$ |
| 143761 | 9 \pm 1.7 | 12.1 $^{+1.8}_{-2.0}$ | N/A | 7.3 $^{+0.6}_{-0.9}$ |
| 145675 | 0.7062 | N/A | N/A | N/A |
| 168443 | 9.8 \pm 1 | 10.6 $^{+1.2}_{-1.1}$ | 5.90 | 10.8 $^{+0.2}_{-0.4}$ |
| 177830 | 4.03 | N/A | N/A | 10.0 \pm 0.1 |

Continued on Next Page...

Table. 8.2 – Continued

| HD | EE (Gyr) | N04 (Gyr) | S05 (Gyr) | Here (Gyr) |
|-----------|---------------------|----------------------|----------------------|-----------------------|
| 186427 | 8 ± 1.8 | $9.9^{+3.3}_{-4.3}$ | 7.59 | N/A |
| 189733 | >0.6 | N/A | N/A | $6.7^{+4.4}_{-6.0}$ |
| 190228 | 10.16 | $5.1^{+1.5}_{-1.0}$ | N/A | 17.3 ± 0.1 |
| 190360 | 12.11 | N/A | N/A | $14.1^{+0.5}_{-0.7}$ |
| 192263 | 0.57 | N/A | N/A | $13.5^{+2.7}_{-2.9}$ |
| 195019 | 5.33 | 10.6 ± 1.2 | N/A | $11.1^{+1.6}_{-7.5}$ |
| 196885 | 8.4 ± 1.3 | $8.4^{+1.3}_{-1.2}$ | N/A | $6.2^{+0.1}_{-1.2}$ |
| 217014 | 4 ± 2.5 | $9.2^{+2.8}_{-4.4}$ | 6.6 | 11.3 ± 0.5 |
| 217107 | 7.32 | N/A | N/A | $15.3^{+0.7}_{-0.9}$ |

EE: *Extrasolar Planets Encyclopedia*; N04: Nordström et al. (2004); S05: Saffe et al. (2005)

8.2.2 New Mass and Age Estimates

By far the largest limiting factor when determining stellar ages is the uncertainty in the mass of the star. To explore the extent of the effect of mass when calculating age, I selected five stars, varied their masses by 20%, and recalculated their ages using the method described in the previous section. As Table 8.3 shows, even a 20% error in the mass leads to an enormous difference in the ages of the stars, up to a factor of 10.

Table. 8.3: Mass' Effect on Age Determinations

| HD | Varying mass: | | | Age corresponding to: | | |
|--------|-----------------------------------|------------------------|-----------------------------------|-------------------------|--------------|-------------------------|
| | $0.8 \times M$ (M_{\odot}) | M (M_{\odot}) | $1.2 \times M$ (M_{\odot}) | $0.8 \times M$ (Gyr) | M (Gyr) | $1.2 \times M$ (Gyr) |
| 3651 | 0.63 | 0.79 | 0.95 | 60.0 | 24.0 | 6.6 |
| 19994 | 1.07 | 1.34 | 1.61 | 11.3 | 4.8 | 1.1 |
| 177830 | 0.92 | 1.15 | 1.38 | 22.5 | 10.0 | 5.1 |
| 190228 | 0.66 | 0.83 | 1.00 | 39.1 | 17.3 | 8.8 |
| 190360 | 0.77 | 0.96 | 1.15 | 35.8 | 14.1 | 3.9 |

Given the small errors in the exoplanet host stars' T_{eff} and the new stellar radii measured here, it was possible to run a range of stellar models using the *Dartmouth Stellar Evolution Web Server* for a given star. The metallicity listed in Santos et al. (2004) remained the same while a variety of masses for each star was considered. The mass listed in the planet discovery paper was the starting point, and then a range of different masses were tested until the datapoint was fit. This procedure was performed for stars whose error in the linear radius was $\leq 10\%$, which amounted to 15 stars. The results are shown in Figures 8.2 through 8.15. All T_{eff} are from (Santos et al. 2004) unless otherwise noted in Table 8.4.

The errors for these masses were estimated by moving the observed datapoint by 1σ towards an evolutionary track other than the best fit track. The new datapoint was then compared to the distance between the two evolutionary tracks and converted to a mass difference. For example, say two evolutionary tracks were for two masses of $1.0 M_{\odot}$ and a $1.1 M_{\odot}$ with the $1.0 M_{\odot}$ track being the best fit for the observed datapoint. If when the datapoint was moved one-sigma towards the $1.1 M_{\odot}$ evolutionary track,

it covered half the distance between the tracks, then the error in the mass would be $0.05 M_{\odot}$.

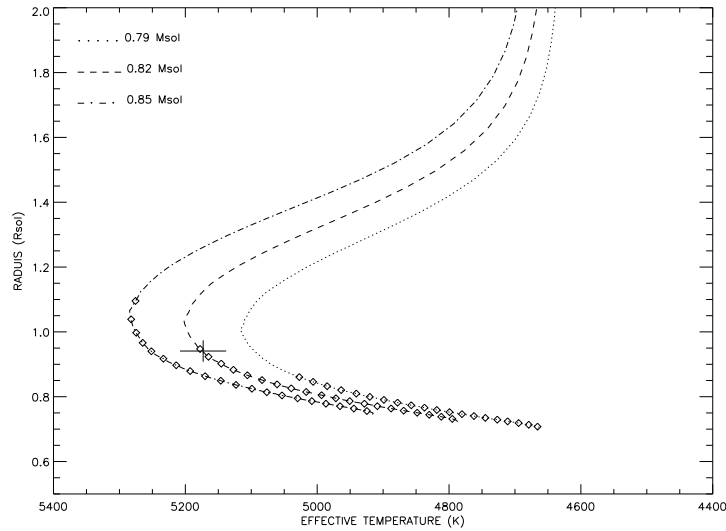


Figure. 8.2: HD 3651: Determining stellar mass and age. The three lines represent evolutionary tracks for stars of the masses listed on the plot; \diamond s represent 1-Gyr intervals; and $+$ represents the measured T_{eff} and R with error bars.

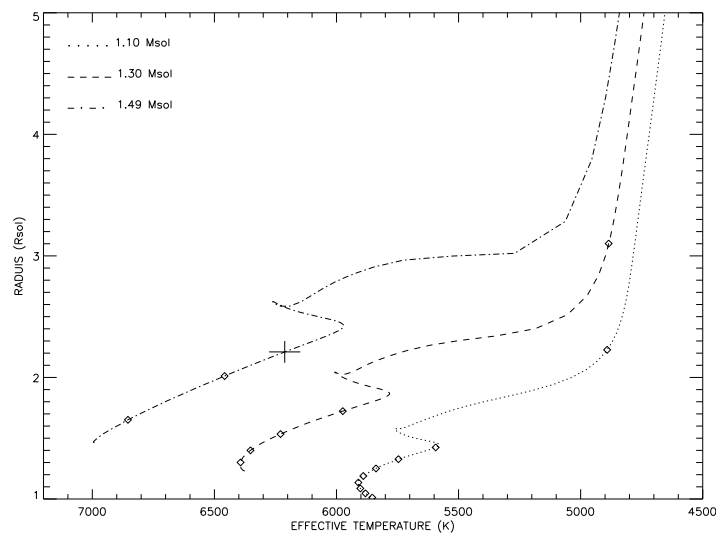


Figure. 8.3: HD 9826: Determining stellar mass and age. The three lines represent evolutionary tracks for stars of the masses listed on the plot; \diamond s represent 1-Gyr intervals; and $+$ represents the measured T_{eff} and R with error bars.

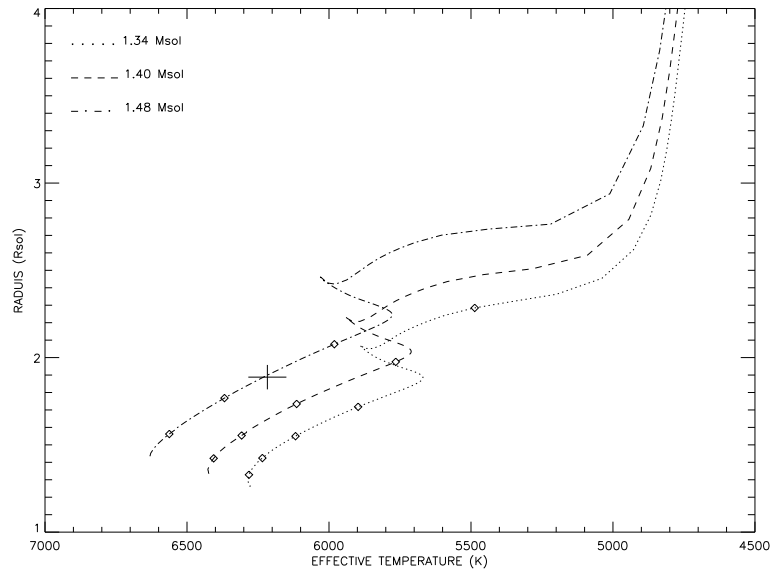


Figure. 8.4: HD 19994: Determining stellar mass and age. The three lines represent evolutionary tracks for stars of the masses listed on the plot; \diamond s represent 1-Gyr intervals; and + represents the measured T_{eff} and R with error bars.

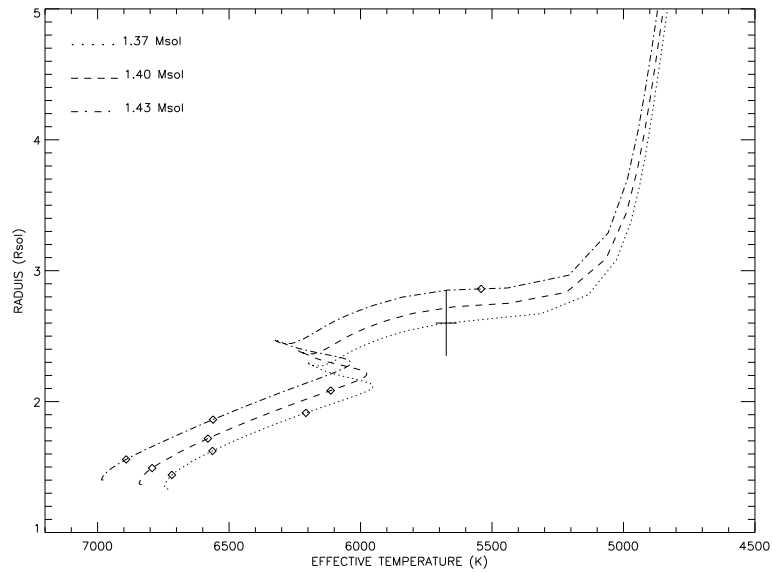


Figure. 8.5: HD 38529: Determining stellar mass and age. The three lines represent evolutionary tracks for stars of the masses listed on the plot; \diamond s represent 1-Gyr intervals; and + represents the measured T_{eff} and R with error bars.

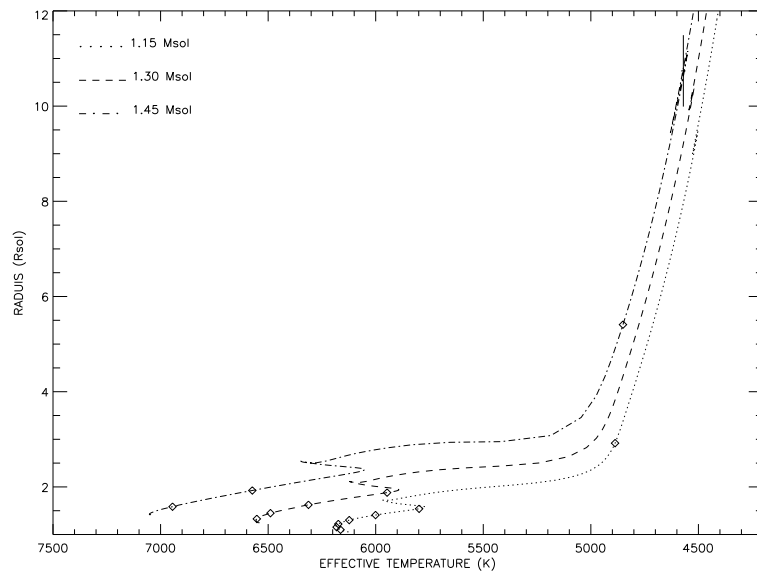


Figure. 8.6: HD 59686: Determining stellar mass and age. The three lines represent evolutionary tracks for stars of the masses listed on the plot; \diamond s represent 1-Gyr intervals; and + represents the measured T_{eff} and R with error bars. Allende Prieto & Lambert (1999) claim a 1 K error on their T_{eff} but the error bar printed here is 10 K so it is visible.

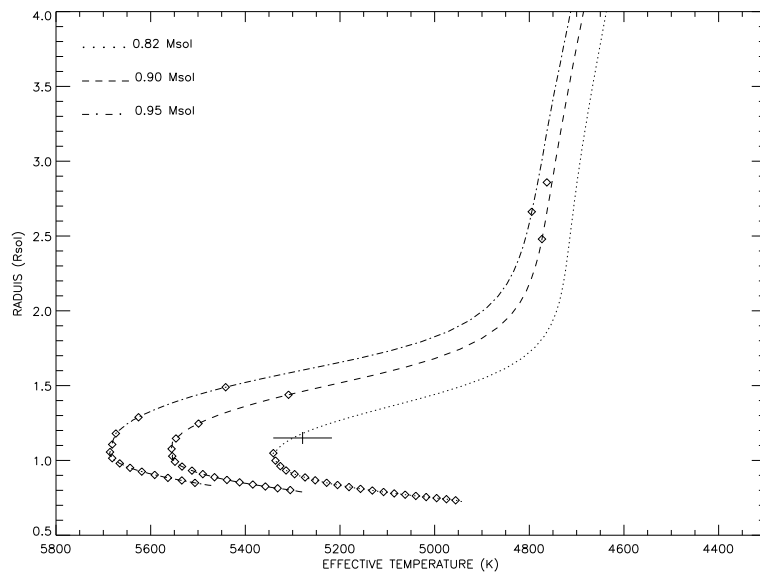


Figure. 8.7: HD 75732: Determining stellar mass and age. The three lines represent evolutionary tracks for stars of the masses listed on the plot; \diamond s represent 1-Gyr intervals; and + represents the measured T_{eff} and R with error bars.

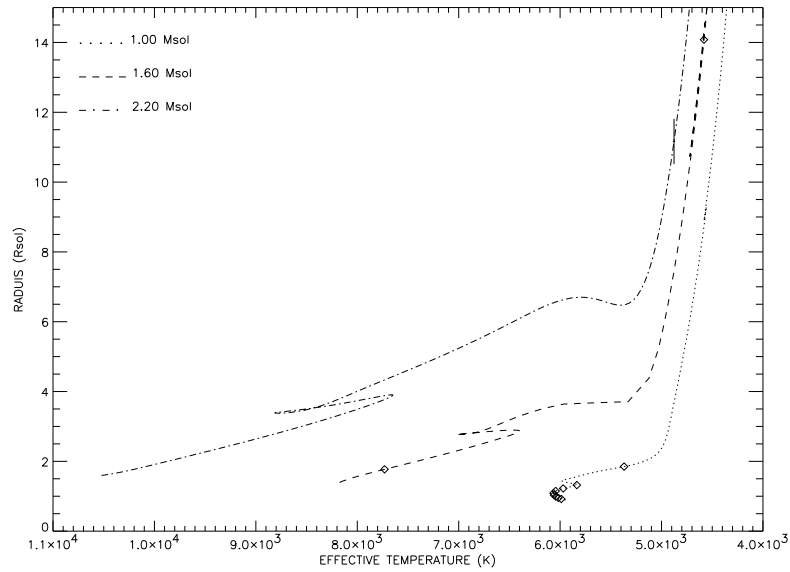


Figure. 8.8: HD 104985: Determining stellar mass and age. The three lines represent evolutionary tracks for stars of the masses listed on the plot; \diamond s represent 1-Gyr intervals; and + represents the measured T_{eff} and R with error bars. T_{eff} is from (Takeda et al. 2005), who quotes no error bars, so a 10-K error bar was assigned.

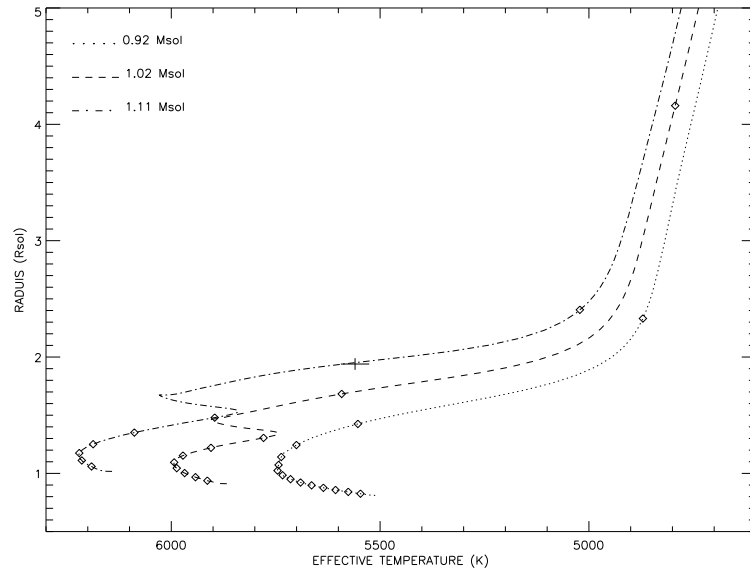


Figure. 8.9: HD 117176: Determining stellar mass and age. The three lines represent evolutionary tracks for stars of the masses listed on the plot; \diamond s represent 1-Gyr intervals; and + represents the measured T_{eff} and R with error bars.

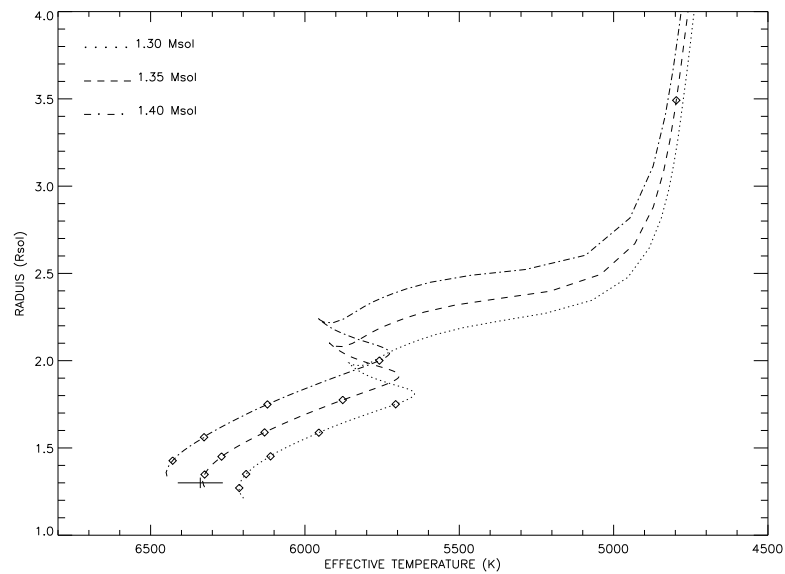


Figure. 8.10: HD 120136: Determining stellar mass and age. The three lines represent evolutionary tracks for stars of the masses listed on the plot; \diamond s represent 1-Gyr intervals; and + represents the measured T_{eff} and R with error bars.

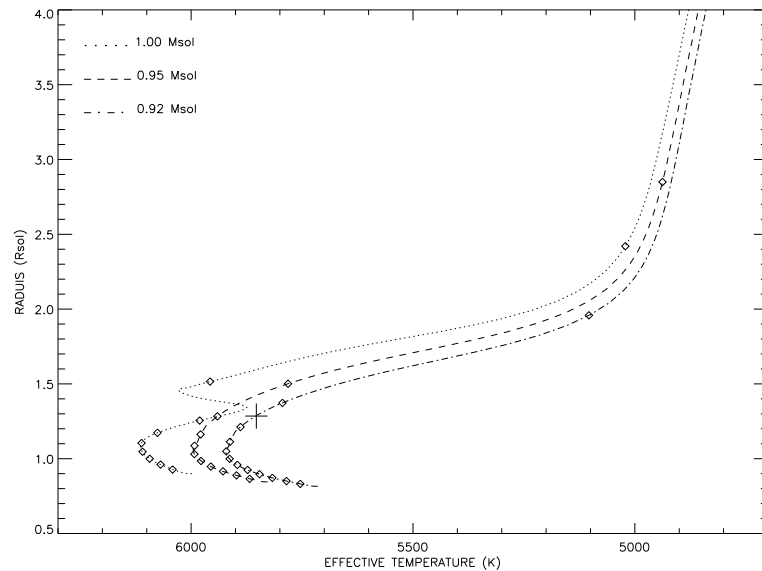


Figure. 8.11: HD 143761: Determining stellar mass and age. The three lines represent evolutionary tracks for stars of the masses listed on the plot; \diamond s represent 1-Gyr intervals; and + represents the measured T_{eff} and R with error bars.

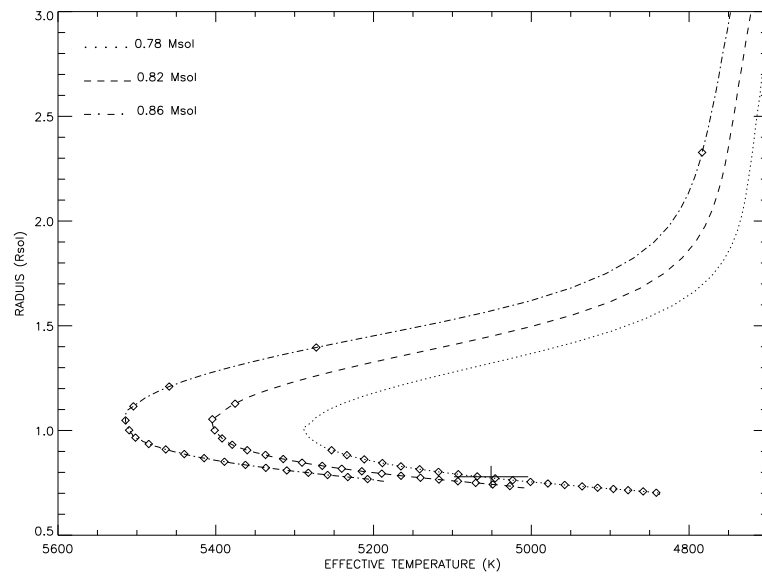


Figure. 8.12: HD 189733: Determining stellar mass and age. The three lines represent evolutionary tracks for stars of the masses listed on the plot; \diamond s represent 1-Gyr intervals; and + represents the measured T_{eff} and R with error bars.

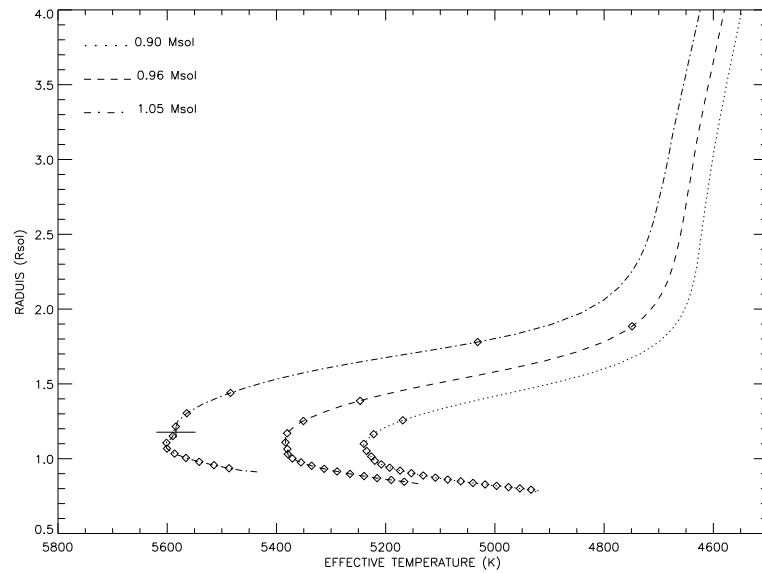


Figure. 8.13: HD 190360: Determining stellar mass and age. The three lines represent evolutionary tracks for stars of the masses listed on the plot; \diamond s represent 1-Gyr intervals; and + represents the measured T_{eff} and R with error bars.

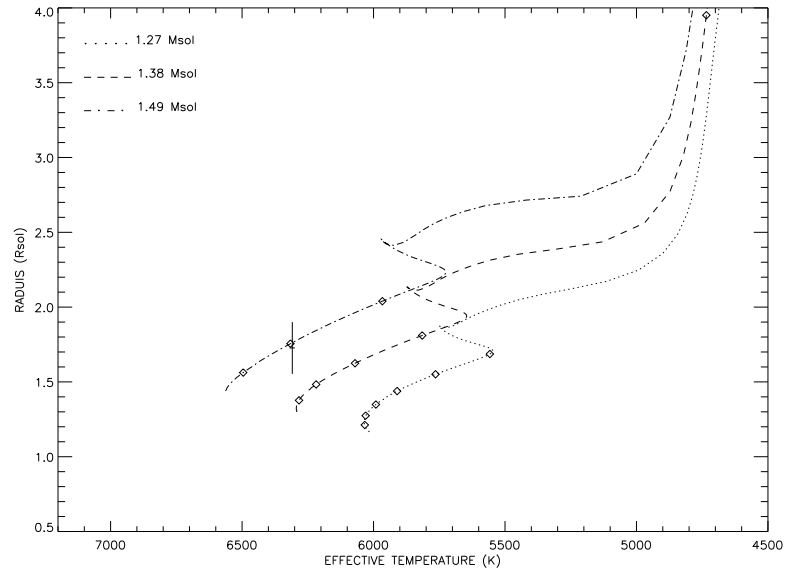


Figure. 8.14: HD 196885: Determining stellar mass and age. The three lines represent evolutionary tracks for stars of the masses listed on the plot; ◇s represent 1-Gyr intervals; and + represents the measured T_{eff} and R with error bars. Allende Prieto & Lambert (1999) claim a 10 K error on their T_{eff} but the error bar printed here is 10 K so it is visible.

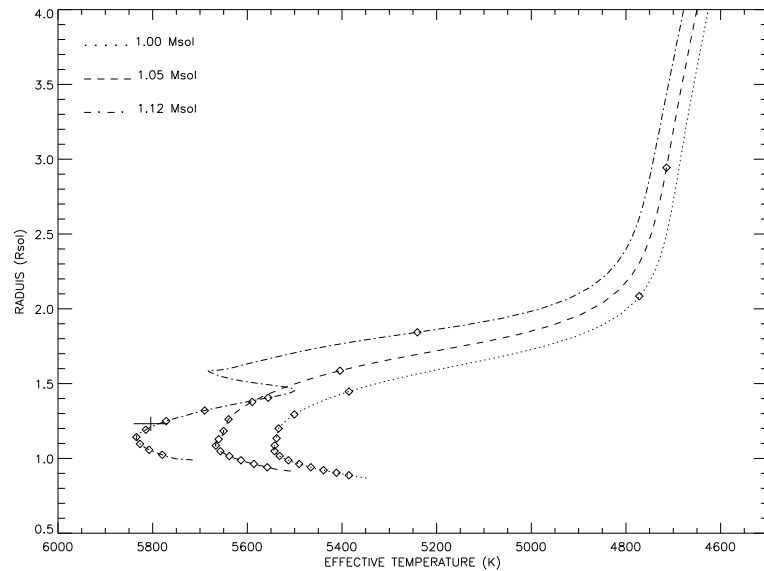


Figure. 8.15: HD 217014: Determining stellar mass and age. The three lines represent evolutionary tracks for stars of the masses listed on the plot; ◇s represent 1-Gyr intervals; and + represents the measured T_{eff} and R with error bars.

Table. 8.4: New Stellar Mass and Age

| HD | T_{eff} (K) | R (R_{\odot}) | M_{original} (M_{\odot}) | M_{new} (M_{\odot}) | Age _{original} (Gyr) | Age _{new} (Gyr) | EE Age (Gyr) |
|--------|-------------------------|------------------------|--|-------------------------------------|----------------------------------|-----------------------------|-----------------|
| 3651 | 5173±35 | 0.94±0.03 | 0.79 | 0.82±0.01 | 24.0 | ~20 | 5.1 |
| 9826 | 6212±64 | 2.21±0.09 | 1.3 | 1.49±0.05 | 4.8 | 2-3 | 3.8 |
| 19994 | 6217±67 | 1.89±0.07 | 1.34 | 1.48±0.04 | 4.8 | 2-3 | 8.9 |
| 38529 | 5674±40 | 2.60±0.25 | 1.4 | 1.37±0.06 | 5.2 | 3-4 | 5.1 |
| 59686 | 4571±1 | 10.74±0.75 | 1.15 | 1.45±0.15 | 7.4 | 2-3 | - |
| 75732 | 5279±62 | 1.15±0.04 | 0.95 | 0.82±0.02 | 10.6 | 20-21 | 5.5 |
| 104985 | 4877 | 11.16±0.65 | 1.6 | 2.20±0.30 | 2.0 | 0-1 | 3.0 |
| 117176 | 5560±34 | 1.94±0.05 | 0.92 | 1.11±0.03 | 13.8 | 6-7 | 7.1 |
| 120136 | 6339±73 | 1.30±0.03 | 1.2 | 1.35±0.03 | 4.0 | 0-1 | 2.5 |
| 143761 | 5853±25 | 1.29±0.08 | 1.0 | 0.92±0.01 | 7.3 | 10-11 | 9 |
| 189733 | 5051±47 | 0.78±0.05 | 0.82 | 0.78±0.04 | 6.7 | ~11 | >0.6 |
| 190360 | 5584±36 | 1.18±0.04 | 0.96 | 1.05±0.02 | 14.1 | 8-9 | 12.1 |
| 196885 | 6310 | 1.73±0.17 | 1.27 | 1.49±0.06 | 6.2 | ~2 | 8.4 |
| 217014 | 5804±36 | 1.23±0.05 | 1.0 | 1.12±0.02 | 11.3 | 5-6 | 4 |

Note. All T_{eff} from Santos et al. (2004) except the following: HD 34445, HD 59686, and HD 196885 are from Allende Prieto & Lambert (1999), HD 104985 is from Takeda et al. (2005), and HD 189733 is from Sousa et al. (2006).

Figure 8.16 plots the new mass versus the original mass from the planet discovery papers, and in almost all cases, the new mass is larger than the original one, which also increases the mass of the companion. The mean $M_{\text{new}}/M_{\text{original}}$ is 1.09, and the standard deviation of that mean is 0.14, indicating a significant departure from the original mass estimate. These systematic effects may be an effect of the stellar model used.

The errors for the original masses were estimated using the following method: for each star, the mass corresponding to the subtypes surrounding the given spectral

classification was determined using Cox (2000). For example, if the star's spectral classification was listed as a K2 V in the planet discovery paper, the masses for the K1 V and K3 V types were determined. Then the difference between the given mass and the mass for each surrounding subtype was calculated for each star and then averaged for the 15 stars seen in Figures 8.2 through 8.15. The average was $\sim 6\%$, so the original masses show 6% error bars in Figure 8.16. This is a rough estimate, as few planet discovery papers list error estimates for the stellar masses.

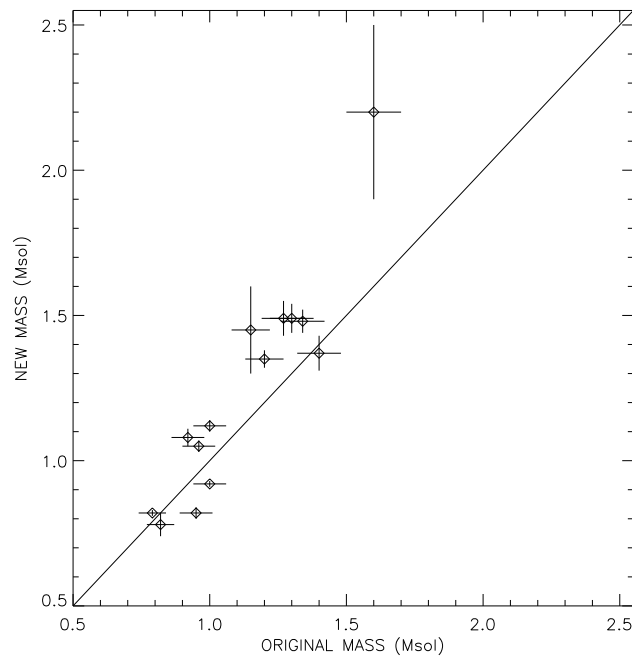


Figure. 8.16: New vs. old stellar masses. The solid line represents the 1:1 ratio for the masses. Note how almost all the new mass estimates are larger than the previous estimates. The largest outlier is for HD 104985.

8.3 General Conclusions and Future Work

I observed 31 exoplanet systems in order to measure the host star’s diameter and to check for stellar companions. I obtained 16 limb-darkened angular diameters with errors $\leq 10\%$ and 8 with errors between 11 and 50%. When the LD diameters were converted to linear radii when combined with *HIPPARCOS* parallax, 14 dwarf stars boasted errors $\leq 10\%$ and were plotted with the sample from Andersen (1991). These new radii more than doubled the number of stars in the $0.5 \leq (B - V) \leq 1.0$ range.

The data were inspected in two ways for evidence of stellar companions: systematics in the residuals from the diameter fit and searching for separated fringe packets. While no stellar companions were discovered, companion spectral types down to early- to mid-M dwarfs were ruled out for most of the systems observed.

Two stars, ν Andromedae and ρ Coronae Borealis, showed unusual behavior in their visibility curves that could not be fit with simple LD disk diameters. The diameter fit to ν Andromedae was almost 30% larger than that predicted by the star’s spectral type and SED fit. More observations are needed on both of these targets before any final conclusions can be drawn.

The new interferometric diameter measurements were used to determine the ages of the exoplanet host stars. The ages turned out to be so dependent on mass, which is not well known, that a variety of masses was tested for those stars with low linear radii measurements and reliable T_{eff} from spectroscopic studies. The new masses were larger than those listed in the planet discovery papers for most of the stars analyzed.

As new exoplanet systems are discovered on a regular basis, the observing list for this project constantly grows. I plan to continue this work in an effort to observe the exoplanet systems not covered in this dissertation and to observe all possible exoplanet host stars, particularly those systems with transiting planets that are bright enough to observe with the CHARA Array. This will hopefully prove a valuable body of work, not only in characterizing the exoplanet host stars, but also as a source of stellar diameters for Sun-like stars, more refined masses for the host stars, and better estimates of the ages for these suns.

References

- Allende Prieto, C., & Lambert, D. L. 1999, *A&A*, 352, 555
- Andersen, J. 1991, *A&A Rev.*, 3, 91
- Armstrong, J. T. et al. 1998, *ApJ*, 496, 550
- Armstrong, J. T., Nordgren, T. E., Germain, M. E., Hajian, A. R., Hindsley, R. B., Hummel, C. A., Mozurkewich, D., & Thessin, R. N. 2001, *AJ*, 121, 476
- Aufdenberg, J. P. et al. 2006, *ApJ*, 645, 664
- Backer, D. C., Foster, R. S., & Sallmen, S. 1993, *Nature*, 365, 817
- Baines, E. K., van Belle, G. T., ten Brummelaar, T. A., McAlister, H. A., Swain, M., Turner, N. H., Sturmann, L., & Sturmann, J. 2007, *ApJ*, 661, L195
- Bakos, G. Á. et al. 2006a, *ApJ*, 650, 1160
- Bakos, G. Á., Pál, A., Latham, D. W., Noyes, R. W., & Stefanik, R. P. 2006b, *ApJ*, 641, L57
- Baldwin, J. E. et al. 1998, in *Astronomical Interferometry, Proceedings of the SPIE*, ed. R. D. Reasenberg, Vol. 3350, 736
- Baraffe, I., Chabrier, G., Allard, F., & Hauschildt, P. H. 1998, *A&A*, 337, 403
- Beaulieu, J.-P. et al. 2006, *Nature*, 439, 437
- Bender, C., Simon, M., Prato, L., Mazeh, T., & Zucker, S. 2005, *AJ*, 129, 402
- Benson, J. A., Dyck, H. M., & Howell, R. R. 1995, *Appl. Opt.*, 34, 51

- Berger, D. H. et al. 2006, *ApJ*, 644, 475
- Bessell, M. S. 2000, *PASP*, 112, 961
- Bessell, M. S., & Brett, J. M. 1988, *PASP*, 100, 1134
- Boden, A. F., Torres, G., & Latham, D. W. 2006, *ApJ*, 644, 1193
- Boden, A. F. et al. 1998, *ApJ*, 504, L39
- Bond, I. A. et al. 2004, *ApJ*, 606, L155
- Bouchy, F., Pont, F., Melo, C., Santos, N. C., Mayor, M., Queloz, D., & Udry, S. 2005a, *A&A*, 431, 1105
- Bouchy, F. et al. 2005b, *A&A*, 444, L15
- Brown, T. M., Charbonneau, D., Gilliland, R. L., Noyes, R. W., & Burrows, A. 2001, *ApJ*, 552, 699
- Buscher, D. F. 1994, in *Amplitude and Intensity Spatial Interferometry II*, Proceedings of the SPIE, ed. J. B. Breckinridge, Vol. 2200, 260
- Butler, R. P., Marcy, G. W., Fischer, D. A., Brown, T. M., Contos, A. R., Korzennik, S. G., Nisenson, P., & Noyes, R. W. 1999, *ApJ*, 526, 916
- Butler, R. P., Marcy, G. W., Vogt, S. S., Fischer, D. A., Henry, G. W., Laughlin, G., & Wright, J. T. 2003, *ApJ*, 582, 455
- Butler, R. P., Marcy, G. W., Williams, E., Hauser, H., & Shirts, P. 1997, *ApJ*, 474, L115
- Butler, R. P. et al. 2006, *ApJ*, 646, 505
- Chaboyer, B., Fenton, W. H., Nelan, J. E., Patnaude, D. J., & Simon, F. E. 2001,

- ApJ, 562, 521
- Charbonneau, D., Brown, T. M., Latham, D. W., & Mayor, M. 2000, ApJ, 529, L45
- Chauvin, G., Lagrange, A.-M., Dumas, C., Zuckerman, B., Mouillet, D., Song, I., Beuzit, J.-L., & Lowrance, P. 2005, A&A, 438, L25
- Ciardi, D. R., van Belle, G. T., Akeson, R. L., Thompson, R. R., Lada, E. A., & Howell, S. B. 2001, ApJ, 559, 1147
- Claret, A., Diaz-Cordoves, J., & Gimenez, A. 1995, A&AS, 114, 247
- Clem, J. L., VandenBerg, D. A., Grundahl, F., & Bell, R. A. 2004, AJ, 127, 1227
- Cochran, W. D., Hatzes, A. P., Butler, R. P., & Marcy, G. W. 1997, ApJ, 483, 457
- Colavita, M. M. et al. 1999, ApJ, 510, 505
- Colavita, M. M., Wizinowich, P. L., & Akeson, R. L. 2004, in *New Frontiers in Stellar Interferometry*, Proceedings of the SPIE, ed. W. A. Traub, Vol. 5491, 454
- Cox, A. N. 2000, *Allen's astrophysical quantities*, 4th ed., Edited by A. N. Cox (New York: AIP Press; Springer)
- Creech-Eakman, M. J. et al. 2006, in *Advances in Stellar Interferometry*, Proceedings of the SPIE, eds. J. D. Monnier, M. Schöller, & W.C. Danchi, Vol. 6268, 60
- Cutri, R. M. et al. 2003, 2MASS All Sky Catalog of point sources. (The IRSA 2MASS All-Sky Point Source Catalog, NASA/IPAC Infrared Science Archive. <http://irsa.ipac.caltech.edu/applications/Gator/>)
- Davis, J., Tango, W. J., Booth, A. J., ten Brummelaar, T. A., Minard, R. A., & Owens, S. M. 1999, MNRAS, 303, 773

- Donahue, R. A. 1993, PhD thesis, AA(New Mexico State Univ., University Park.)
- Droege, T. F., Richmond, M. W., Sallman, M. P., & Creager, R. P. 2006, PASP, 118, 1666
- Dyck, H. M. et al. 1995, AJ, 109, 378
- Eisner, J. A., Chiang, E. I., & Hillenbrand, L. A. 2006, ApJ, 637, L133
- Fischer, D. A., Butler, R. P., Marcy, G. W., Vogt, S. S., & Henry, G. W. 2003, ApJ, 590, 1081
- Fischer, D. A., Marcy, G. W., Butler, R. P., Laughlin, G., & Vogt, S. S. 2002, ApJ, 564, 1028
- Fischer, D. A., Marcy, G. W., Butler, R. P., Vogt, S. S., & Apps, K. 1999, PASP, 111, 50
- Fischer, D. A., Marcy, G. W., Butler, R. P., Vogt, S. S., Frink, S., & Apps, K. 2001, ApJ, 551, 1107
- Fischer, D. A., & Valenti, J. 2005, ApJ, 622, 1102
- Fizeau, A. H. 1868, C. R. Acad. Sci., 66, 934
- Gatewood, G., Han, I., & Black, D. C. 2001, ApJ, 548, L61
- Girardi, L., Bertelli, G., Bressan, A., Chiosi, C., Groenewegen, M. A. T., Marigo, P., Salasnich, B., & Weiss, A. 2002, A&A, 391, 195
- Glebocki, R., & Stawikowski, A. 2000, Acta Astronomica, 50, 509
- Glindemann, A. et al. 2003, in Interferometry for Optical Astronomy II, Proceedings of the SPIE, ed. W. A. Traub, Vol. 4838, 89

- Gray, R. O., Corbally, C. J., Garrison, R. F., McFadden, M. T., & Robinson, P. E. 2003, *AJ*, 126, 2048
- Guarinos, J. 1995, *VizieR Online Data Catalog*, 5086, 0
- Guenther, D. B., Demarque, P., Kim, Y.-C., & Pinsonneault, M. H. 1992, *ApJ*, 387, 372
- Guenther, E. W., Neuhäuser, R., Wuchterl, G., Mugrauer, M., Bedalov, A., & Hauschildt, P. H. 2005, *Astronomische Nachrichten*, 326, 958
- Hale, D. D. S. et al. 2000, *ApJ*, 537, 998
- Hanbury Brown, R., Davis, J., & Allen, L. R. 1974a, *MNRAS*, 167, 121
- Hanbury Brown, R., Davis, J., Lake, R. J. W., & Thompson, R. J. 1974b, *MNRAS*, 167, 475
- Hanbury Brown, R. H., Davis, J., Allen, L. R., & Rome, J. M. 1967, *MNRAS*, 137, 393
- Harrington, J., Hansen, B. M., Luszcz, S. H., Seager, S., Deming, D., Menou, K., Cho, J. Y.-K., & Richardson, L. J. 2006, *Science*, 314, 623
- Hartkopf, W. I., & McAlister, H. A. 1984, *PASP*, 96, 105
- Hatzes, A. P., Guenther, E. W., Endl, M., Cochran, W. D., Döllinger, M. P., & Bedalov, A. 2005, *A&A*, 437, 743
- Hill, J. M., Green, R. F., & Slagle, J. H. 2006, in *Ground-based and Airborne Telescopes*, Proceedings of the SPIE, ed. L. M. Stepp, Vol. 6267, 31
- Horch, E. P., Robinson, S. E., Ninkov, Z., van Altena, W. F., Meyer, R. D., Urban,

- S. E., & Mason, B. D. 2002, *AJ*, 124, 2245
- Imbert, M., & Prévot, L. 1998, *A&A*, 334, L37
- Isobe, S. 1991, *Proceedings of the Astronomical Society of Australia*, 9, 270
- Johnson, H. L., Iriarte, B., Mitchell, R. I., & Wisniewskj, W. Z. 1966, *Communications of the Lunar and Planetary Laboratory*, 4, 99
- Kervella, P., Thévenin, F., Di Folco, E., & Ségransan, D. 2004, *A&A*, 426, 297
- Kislyuk, V., Yatsenko, A., Ivanov, G., Pakulyak, L., & Sergeeva, T. 2000, in *Journées 1999 - systèmes de référence spatio-temporels and IX. Lohrmann-Kolloquium. Motion of celestial bodies, astrometry and astronomical reference frames*, Dresden, ed. M. Soffel & N. Capitaine, 61
- Konacki, M. 2005, *Nature*, 436, 230
- Labeyrie, A. 1975, *ApJ*, 196, L71
- Lambert, D. L., & Reddy, B. E. 2004, *MNRAS*, 349, 757
- Lane, B. F., Boden, A. F., & Kulkarni, S. R. 2001, *ApJ*, 551, L81
- Latham, D. W., Stefanik, R. P., Mazeh, T., Mayor, M., & Burki, G. 1989, *Nature*, 339, 38
- Lawson, P. R., ed. 2000, *Principles of Long Baseline Stellar Interferometry*
- Lowrance, P. J., Kirkpatrick, J. D., & Beichman, C. A. 2002, *ApJ*, 572, L79
- Lu, P. K., Demarque, P., van Altena, W., McAlister, H., & Hartkopf, W. 1987, *AJ*, 94, 1318
- Marcy, G. W., & Butler, R. P. 1996, *ApJ*, 464, L147

- Marcy, G. W., Butler, R. P., Fischer, D. A., Laughlin, G., Vogt, S. S., Henry, G. W.,
& Pourbaix, D. 2002, *ApJ*, 581, 1375
- Marcy, G. W., Butler, R. P., & Vogt, S. S. 2000, *ApJ*, 536, L43
- Marcy, G. W., Butler, R. P., Vogt, S. S., Fischer, D., & Liu, M. C. 1999, *ApJ*, 520,
239
- Marcy, G. W. et al. 2001, *ApJ*, 555, 418
- Marcy, G. W., Butler, R. P., Williams, E., Bildsten, L., Graham, J. R., Ghez, A. M.,
& Jernigan, J. G. 1997, *ApJ*, 481, 926
- Masana, E., Jordi, C., & Ribas, I. 2006, *A&A*, 450, 735
- Mason, B. D. et al. 1999, *AJ*, 117, 1890
- Mayor, M., & Queloz, D. 1995, *Nature*, 378, 355
- Mayor, M., Udry, S., Naef, D., Pepe, F., Queloz, D., Santos, N. C., & Burnet, M.
2004, *A&A*, 415, 391
- Mazeh, T., Latham, D. W., & Stefanik, R. P. 1996, *ApJ*, 466, 415
- McAlister, H. A. 1978, *PASP*, 90, 288
- McAlister, H. A., Hartkopf, W. I., Hutter, D. J., Shara, M. M., & Franz, O. G. 1987,
AJ, 93, 183
- McAlister, H. A., Hartkopf, W. I., Sowell, J. R., Dombrowski, E. G., & Franz, O. G.
1989, *AJ*, 97, 510
- McAlister, H. A. et al. 2005, *ApJ*, 628, 439
- Mermilliod, J. C. 1997, *VizieR Online Data Catalog*, 2168, 0

- Michelson, A. A. 1920, ApJ, 51, 257
- Michelson, A. A., & Pease, F. G. 1921, ApJ, 53, 249
- Mitchell, D. S., Frink, S., Quirrenbach, A., Fischer, D. A., Marcy, G. W., & Butler, R. P. 2003, in Bulletin of the American Astronomical Society, Vol. 35, 1234
- Monet, D. G. et al. 2003, AJ, 125, 984
- Monnier, J. D. et al. 2007, ArXiv e-prints, 706
- Morel, M., & Magnenat, P. 1978, A&AS, 34, 477
- Mourard, D., Tallon-Bosc, I., Blazit, A., Bonneau, D., Merlin, G., Morand, F., Vakili, F., & Labeyrie, A. 1994, A&A, 283, 705
- Munari, U., Sordo, R., Castelli, F., & Zwitter, T. 2005, A&A, 442, 1127
- Myers, J. R., Sande, C. B., Miller, A. C., Warren, Jr., W. H., & Tracewell, D. A. 2001, VizieR Online Data Catalog, 5109, 0
- Naef, D. et al. 2003, A&A, 410, 1051
- Nordgren, T. E. et al. 1999, AJ, 118, 3032
- Nordström, B. et al. 2004, A&A, 418, 989
- Noyes, R. W., Jha, S., Korzennik, S. G., Krockenberger, M., Nisenson, P., Brown, T. M., Kennelly, E. J., & Horner, S. D. 1997, ApJ, 483, L111
- Ochsenbein, F., Bauer, P., & Marcout, J. 2000, A&AS, 143, 23
- Oja, T. 1991, A&AS, 89, 415
- Olsen, E. H. 1993, A&AS, 102, 89
- Patience, J. et al. 2002, ApJ, 581, 654

- Perrier, C., Sivan, J.-P., Naef, D., Beuzit, J. L., Mayor, M., Queloz, D., & Udry, S. 2003, *A&A*, 410, 1039
- Perryman, M. A. C., & ESA. 1997, *The HIPPARCOS and TYCHO catalogues* (Noordwijk, Netherlands: ESA Publications Division, Series: ESA SP Series vol no: 1200)
- Perryman, M. A. C. et al. 1997, *A&A*, 323, L49
- Pickles, A. J. 1998, *PASP*, 110, 863
- Raghavan, D., Henry, T. J., Mason, B. D., Subasavage, J. P., Jao, W.-C., Beaulieu, T. D., & Hambly, N. C. 2006, *ApJ*, 646, 523
- Ramírez, I., & Meléndez, J. 2005, *ApJ*, 626, 446
- Ribas, I., Solano, E., Masana, E., & Giménez, A. 2003, *A&A*, 411, L501
- Sackmann, I.-J., Boothroyd, A. I., & Kraemer, K. E. 1993, *ApJ*, 418, 457
- Saffe, C., Gómez, M., & Chavero, C. 2005, *A&A*, 443, 609
- Santos, N. C., Israelian, G., & Mayor, M. 2004, *A&A*, 415, 1153
- Santos, N. C. et al. 2003, *A&A*, 406, 373
- Sanz-Forcada, J., Brickhouse, N. S., & Dupree, A. K. 2003, *ApJS*, 145, 147
- Sato, B. et al. 2003, *ApJ*, 597, L157
- . 2005, *ApJ*, 633, 465
- Sato, K., & Kuji, S. 1990, *A&AS*, 85, 1069
- Shao, M., Colavita, M., Staelin, D. H., Johnston, K. J., Simon, R. S., Hughes, J. A., & Hershey, J. L. 1987, *AJ*, 93, 1280

- Shao, M., Colavita, M. M., Hines, B. E., Staelin, D. H., & Hutter, D. J. 1988, *A&A*, 193, 357
- Shao, M., & Staelin, D. H. 1980, *Appl. Opt.*, 19, 1519
- Skiff, A. B. 2004, *VizieR Online Data Catalog*, 3233, 0
- Skrutskie, M. F. et al. 2006, *AJ*, 131, 1163
- Sousa, S. G., Santos, N. C., Israelian, G., Mayor, M., & Monteiro, M. J. P. F. G. 2006, *A&A*, 458, 873
- Stepinski, T. F., & Black, D. C. 2001, *A&A*, 371, 250
- Takeda, Y., Sato, B., Kambe, E., Izumiura, H., Masuda, S., & Ando, H. 2005, *PASJ*, 57, 109
- Tango, W. J., & Twiss, R. Q. 1980, in *Progress in optics*. Volume 17. (Amsterdam, North-Holland Publishing Co.), 239
- ten Brummelaar, T. A. et al. 2005, *ApJ*, 628, 453
- Tycner, C. et al. 2005, *ApJ*, 624, 359
- Valenti, J. A., & Fischer, D. A. 2005, *ApJS*, 159, 141
- van Belle, G. T. et al. 1999, *AJ*, 117, 521
- van Belle, G. T., & van Belle, G. 2005, *PASP*, 117, 1263
- Vogt, S. S., Butler, R. P., Marcy, G. W., Fischer, D. A., Pourbaix, D., Apps, K., & Laughlin, G. 2002, *ApJ*, 568, 352
- Vogt, S. S., Marcy, G. W., Butler, R. P., & Apps, K. 2000, *ApJ*, 536, 902
- Werner, M. W. et al. 2004, *ApJS*, 154, 1

Winn, J. N. et al. 2007, *AJ*, 133, 1828

Wolszczan, A. 1994, *Science*, 264, 538

Yoshizawa, M., Sato, K., Nishikawa, J., Ohishi, N., & Kotani, T. 2003, in *Interferometry for Optical Astronomy II*, Proceedings of the SPIE, ed. W. A. Traub, Vol. 4838, 1282

Appendices

– A –

Spectral Energy Distribution Fits - Exoplanet Host Stars

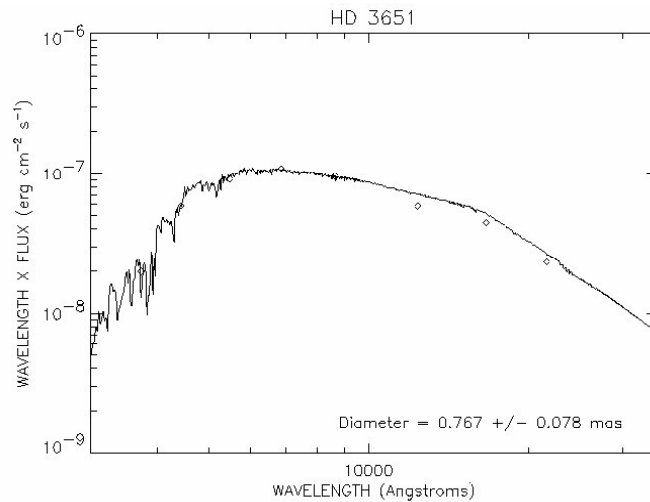


Figure. A.1: HD 3651: SED fit. The \diamond s are fluxes derived from *UBVRIJHK* photometry (left to right) and the solid line is the stellar model of a star using $T_{\text{eff}} = 5173$ K and $\log g = 4.37$ from Santos et al. (2004). There were no quoted errors for the *UBVRI* measurements, $\sigma_J \sim \sigma_H \sim 5\%$, and $\sigma_K \sim 1\%$. *UBVRI* photometry is from Morel & Magnenat (1978) and *JHK* photometry is from the *2MASS All-Sky Point Source Catalog* (Skrutskie et al. 2006). The diameter shown is an estimated LD diameter.

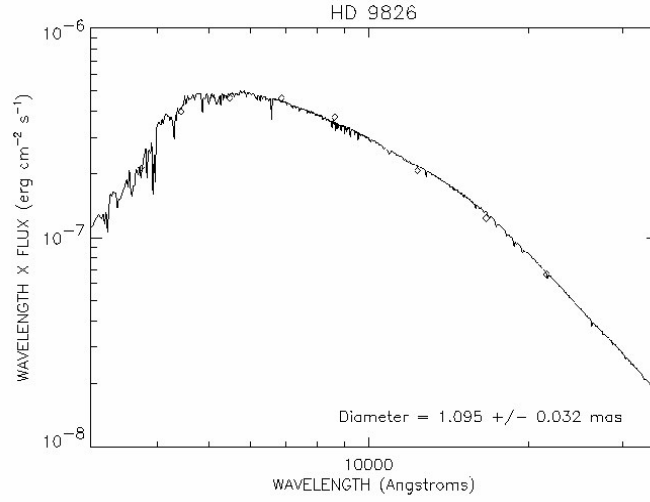


Figure. A.2: HD 9826: SED fit. The \diamond s are fluxes derived from *UBVRIJHK* photometry (left to right) and the solid line is the stellar model of a star using $T_{\text{eff}} = 6212$ K and $\log g = 4.26$ from Santos et al. (2004). There were no quoted errors for the *UBVRI* measurements, $\sigma_J \sim \sigma_H \sim 6\%$, and $\sigma_K \sim 10\%$. *UBVRI* photometry is from Morel & Magnenat (1978) and *JHK* photometry is from the *2MASS All-Sky Point Source Catalog* (Skrutskie et al. 2006). The diameter shown is an estimated LD diameter.

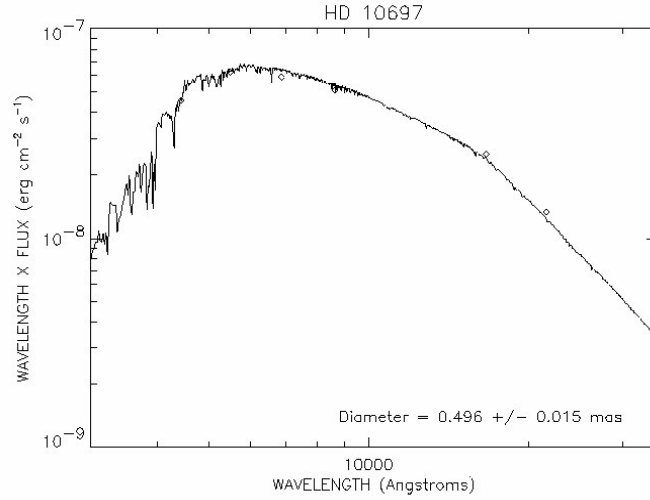


Figure. A.3: HD 10697: SED fit. The \diamond s are fluxes derived from *BVRIJHK* photometry (left to right) and the solid line is the stellar model of a star using $T_{\text{eff}} = 5641$ K and $\log g = 4.05$ from Santos et al. (2004). There were no quoted errors for the *BVRI* measurements, $\sigma_J \sim 5\%$, and $\sigma_H \sim \sigma_K \sim 1\%$. *BV* photometry is from Perryman & ESA (1997), *RI* photometry is from Monet et al. (2003), and *JHK* photometry is from the *2MASS All-Sky Point Source Catalog* (Skrutskie et al. 2006). The diameter shown is an estimated LD diameter.

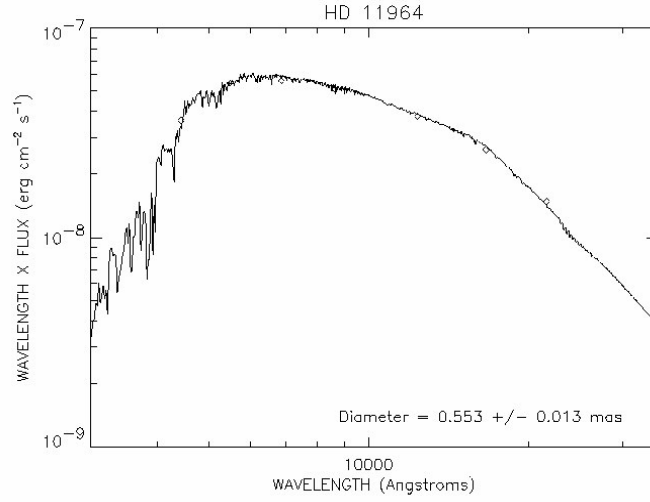


Figure. A.4: HD 11964: SED fit. The \diamond s are fluxes derived from *BVRIJHK* photometry (left to right) and the solid line is the stellar model of a star using $T_{\text{eff}} = 5248$ K and $\log g = 3.82$ from Allende Prieto & Lambert (1999). There were no quoted errors for the *BVRI* measurements and $\sigma_J \sim \sigma_H \sim \sigma_K \sim 0.5\%$. *BV* photometry is from Perryman & ESA (1997), *RI* photometry is from Monet et al. (2003), and *JHK* photometry is from the *2MASS All-Sky Point Source Catalog* (Skrutskie et al. 2006). The diameter shown is an estimated LD diameter.

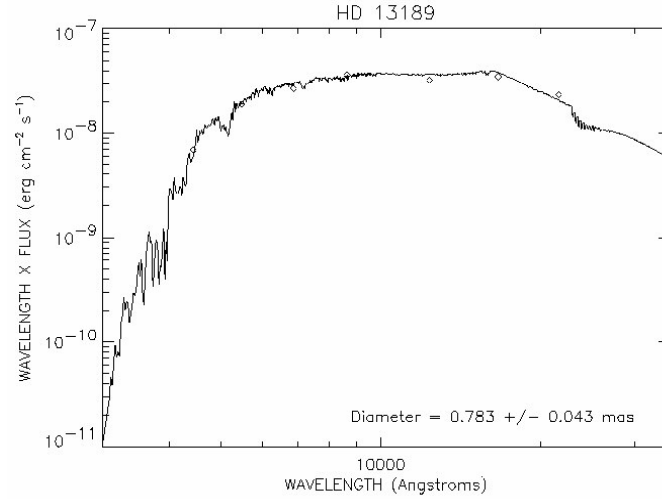


Figure. A.5: HD 13189: SED fit. The \diamond s are fluxes derived from *BVRIJHK* photometry (left to right) and the solid line is the stellar model of a star using $T_{\text{eff}} = 4050$ K and $\log g = 1.74$ from Cox (2000) (appropriate values for a K2 III star, which best fit the photometry). There were no quoted errors for the *BVRI* measurements, $\sigma_J \sim \sigma_H \sim 6\%$, and $\sigma_K \sim 0.6\%$. *BV* photometry is from Perryman & ESA (1997), *RI* photometry is from Monet et al. (2003), and *JHK* photometry is from the *2MASS All-Sky Point Source Catalog* (Skrutskie et al. 2006). The diameter shown is an estimated LD diameter.

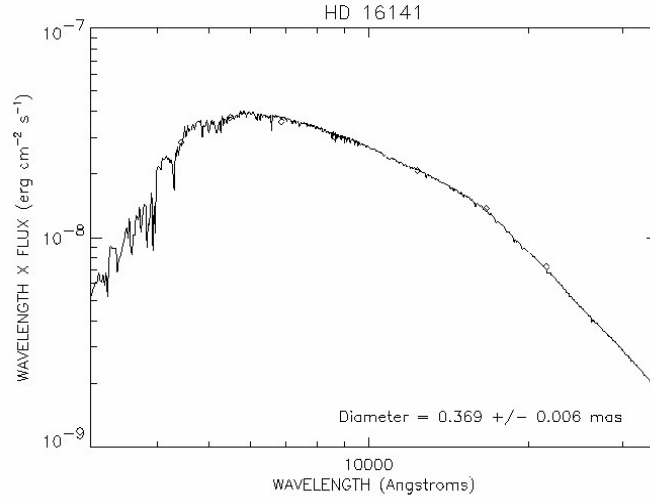


Figure. A.6: HD 16141: SED fit. The \diamond s are fluxes derived from *BVRIJHK* photometry (left to right) and the solid line is the stellar model of a star using $T_{\text{eff}} = 5720$ K and $\log g = 4.00$ from Santos et al. (2004). There were no quoted errors for the *BVRI* measurements and $\sigma_J \sim \sigma_H \sim \sigma_K \sim 0.5\%$. *BV* photometry is from Perryman & ESA (1997), *RI* photometry is from Monet et al. (2003), and *JHK* photometry is from the *2MASS All-Sky Point Source Catalog* (Skrutskie et al. 2006). The diameter shown is an estimated LD diameter.

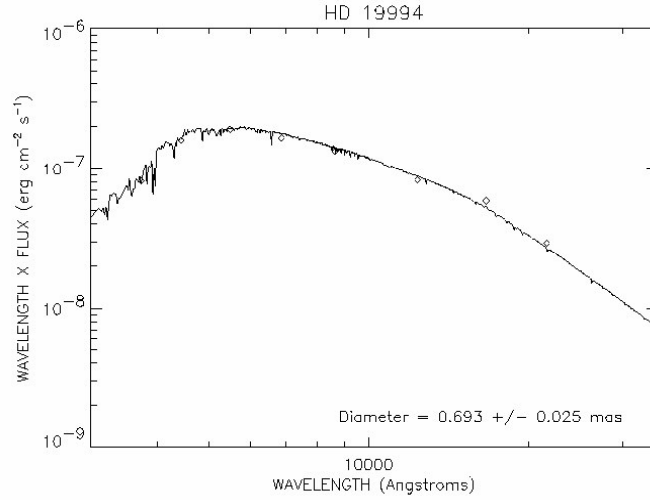


Figure. A.7: HD 19994: SED fit. The \diamond s are fluxes derived from *UBVRJHK* photometry (left to right) and the solid line is the stellar model of a star using $T_{\text{eff}} = 6217$ K and $\log g = 4.29$ from Santos et al. (2004). There were no quoted errors for the *UBVRI* measurements and $\sigma_J \sim \sigma_H \sim \sigma_K \sim 6\%$. *UBV* photometry is from Johnson et al. (1966), *RI* photometry is from Monet et al. (2003), and *JHK* photometry is from the *2MASS All-Sky Point Source Catalog* (Skrutskie et al. 2006). The diameter shown is an estimated LD diameter.

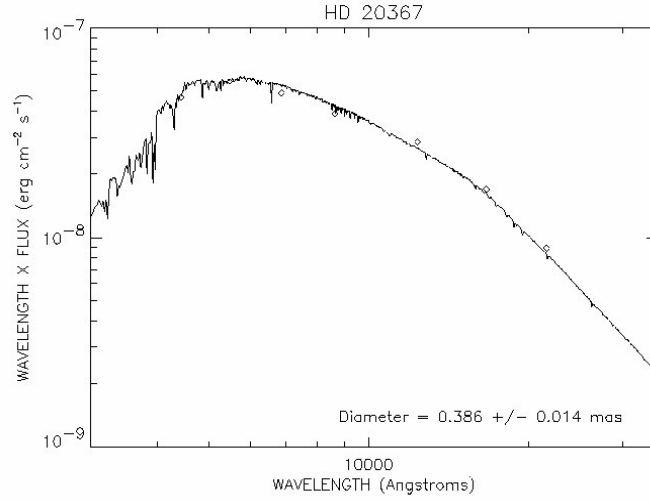


Figure. A.8: HD 20367: SED fit. The \diamond s are fluxes derived from *BVRIJHK* photometry (left to right) and the solid line is the stellar model of a star using $T_{\text{eff}} = 6138$ K and $\log g = 4.53$ from Santos et al. (2004). There were no quoted errors for the *BVRI* measurements and $\sigma_J \sim \sigma_H \sim \sigma_K \sim 0.5\%$. *BV* photometry is from Perryman & ESA (1997), *RI* photometry is from Monet et al. (2003), and *JHK* photometry is from the *2MASS All-Sky Point Source Catalog* (Skrutskie et al. 2006). The diameter shown is an estimated LD diameter.

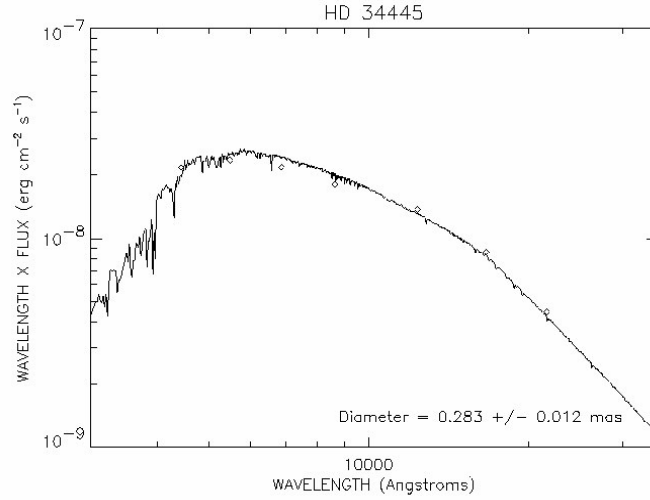


Figure. A.9: HD 34445: SED fit. The \diamond s are fluxes derived from *BVRIJHK* photometry (left to right) and the solid line is the stellar model of a star using $T_{\text{eff}} = 5888$ K and $\log g = 4.21$ from Allende Prieto & Lambert (1999). There were no quoted errors for the *BVRI* measurements and $\sigma_J \sim \sigma_H \sim \sigma_K \sim 0.4\%$. *BV* photometry is from Perryman & ESA (1997), *RI* photometry is from Monet et al. (2003), and *JHK* photometry is from the *2MASS All-Sky Point Source Catalog* (Skrutskie et al. 2006). The diameter shown is an estimated LD diameter.

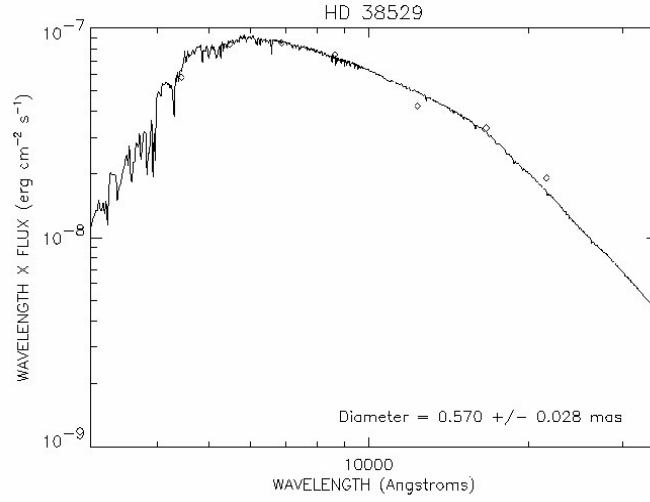


Figure. A.10: HD 38529: SED fit. The \diamond s are fluxes derived from *BVRIJHK* photometry (left to right) and the solid line is the stellar model of a star using $T_{\text{eff}} = 5674$ K and $\log g = 3.94$ from Santos et al. (2004). There were no quoted errors for the *BVRI* measurements, $\sigma_J \sim 5\%$, and $\sigma_H \sim \sigma_K \sim 2\%$. *BV* photometry is from Perryman & ESA (1997), *RI* photometry is from Monet et al. (2003), and *JHK* photometry is from the *2MASS All-Sky Point Source Catalog* (Skrutskie et al. 2006). The diameter shown is an estimated LD diameter.

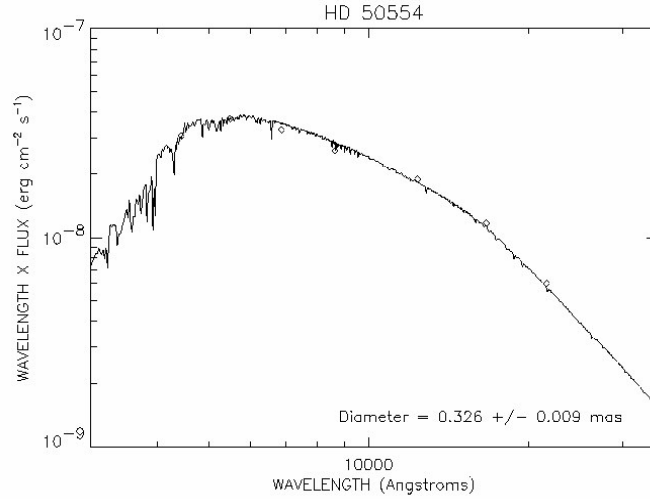


Figure. A.11: HD 50554: SED fit. The \diamond s are fluxes derived from *BVRIJHK* photometry (left to right) and the solid line is the stellar model of a star using $T_{\text{eff}} = 6024$ K and $\log g = 4.41$ from Santos et al. (2004). There were no quoted errors for the *BVRI* measurements and $\sigma_J \sim \sigma_H \sim \sigma_K \sim 0.4\%$. *BV* photometry is from Perryman & ESA (1997), *RI* photometry is from Monet et al. (2003), and *JHK* photometry is from the *2MASS All-Sky Point Source Catalog* (Skrutskie et al. 2006). The diameter shown is an estimated LD diameter.

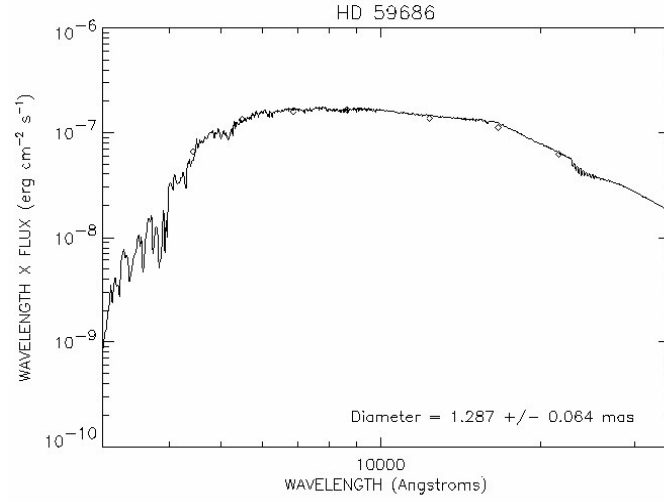


Figure. A.12: HD 59686: SED fit. The \diamond s are fluxes derived from *BVRIJHK* photometry (left to right) and the solid line is the stellar model of a star using $T_{\text{eff}} = 4570$ K and $\log g = 4.2$ from Allende Prieto & Lambert (1999). There were no quoted errors for the *BVRI* measurements, $\sigma_J \sim \sigma_H \sim 7\%$, and $\sigma_K \sim 10\%$. *BV* photometry is from Perryman & ESA (1997), *RI* photometry is from Monet et al. (2003), and *JHK* photometry is from the *2MASS All-Sky Point Source Catalog* (Skrutskie et al. 2006). The diameter shown is an estimated LD diameter.

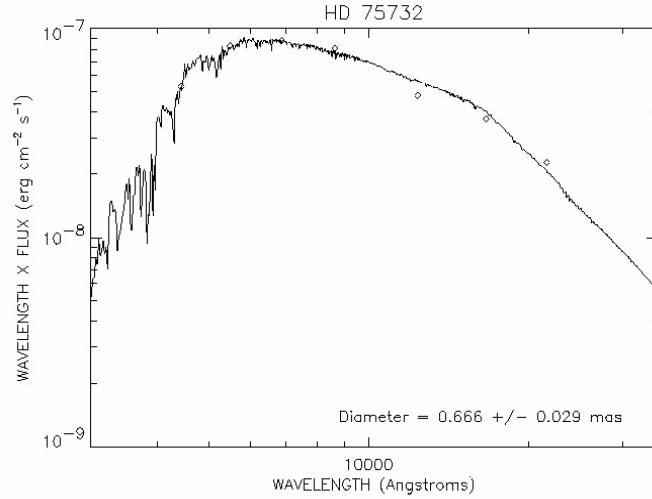


Figure. A.13: HD 75732: SED fit. The \diamond s are fluxes derived from *BVRIJHK* photometry (left to right) and the solid line is the stellar model of a star using $T_{\text{eff}} = 5279$ K and $\log g = 4.37$ from Santos et al. (2004). There were no quoted errors for the *BVRI* measurements, $\sigma_J \sim \sigma_H \sim 5\%$, and $\sigma_K \sim 0.9\%$. *BV* photometry is from Perryman & ESA (1997), *RI* photometry is from Monet et al. (2003), and *JHK* photometry is from the *2MASS All-Sky Point Source Catalog* (Skrutskie et al. 2006). The diameter shown is an estimated LD diameter.

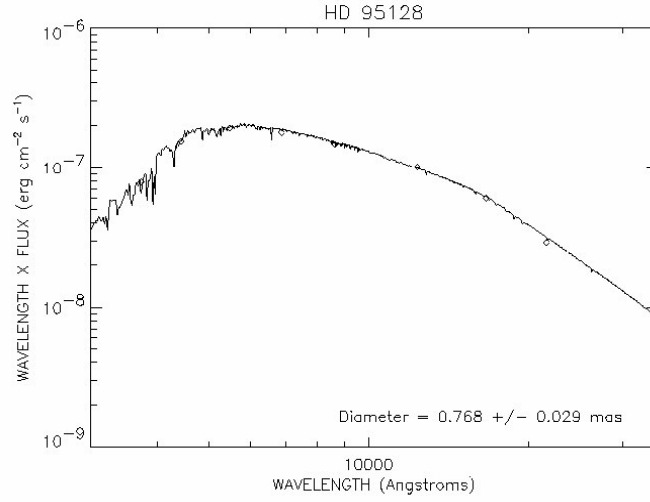


Figure. A.14: HD 95128: SED fit. The \diamond s are fluxes derived from *UBVRIJHK* photometry (left to right) and the solid line is the stellar model of a star using $T_{\text{eff}} = 5954$ K and $\log g = 4.44$ from Santos et al. (2004). There were no quoted errors for the *UBVRI* measurements and $\sigma_J \sim \sigma_H \sim \sigma_K \sim 8\%$. *UBV* photometry is from Johnson et al. (1966), *RI* photometry is from Monet et al. (2003), and *JHK* photometry is from the *2MASS All-Sky Point Source Catalog* (Skrutskie et al. 2006). The diameter shown is an estimated LD diameter.

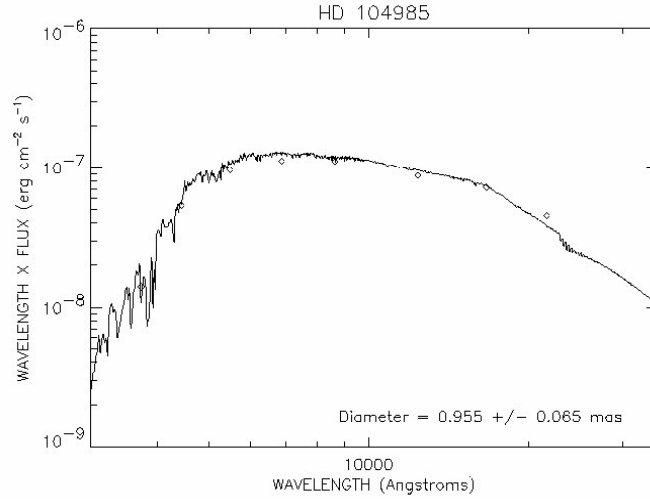


Figure. A.15: HD 104985: SED fit. The \diamond s are fluxes derived from *UBVRIJHK* photometry (left to right) and the solid line is the stellar model of a star using $T_{\text{eff}} = 4877$ K and $\log g = 2.85$ from Takeda et al. (2005). There were no quoted errors for the *UBVRI* measurements, $\sigma_J \sim \sigma_H \sim 5\%$, and $\sigma_K \sim 10\%$. *UBV* photometry is from Johnson et al. (1966), *RI* photometry is from Monet et al. (2003), and *JHK* photometry is from the *2MASS All-Sky Point Source Catalog* (Skrutskie et al. 2006). The diameter shown is an estimated LD diameter.

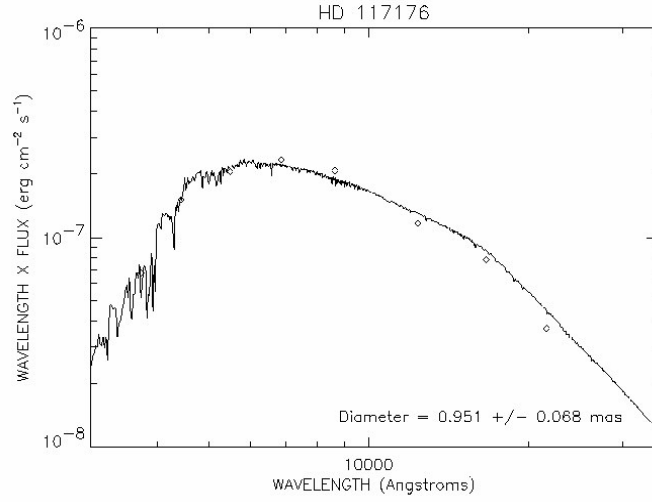


Figure. A.16: HD 117176: SED fit. The \diamond s are fluxes derived from *UBVRIJHK* photometry (left to right) and the solid line is the stellar model of a star using $T_{\text{eff}} = 5560$ K and $\log g = 4.07$ from Santos et al. (2004). There were no quoted errors for the *UBVRI* measurements and $\sigma_J \sim \sigma_H \sim \sigma_K \sim 7\%$. *UBVRI* photometry is from Morel & Magnenat (1978) and *JHK* photometry is from the *2MASS All-Sky Point Source Catalog* (Skrutskie et al. 2006). The diameter shown is an estimated LD diameter.

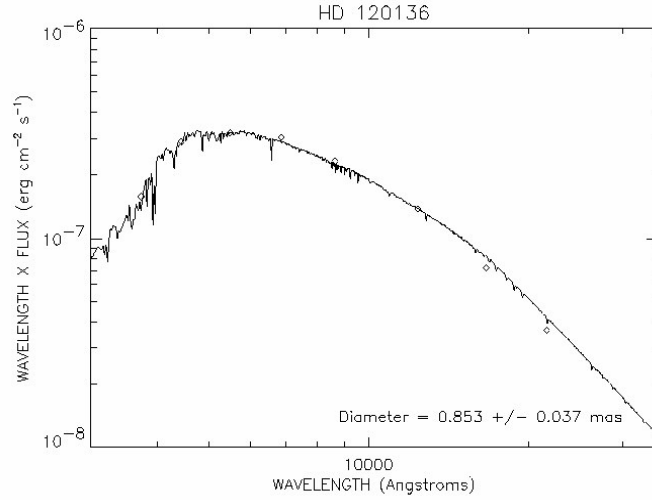


Figure. A.17: HD 120136: SED fit. The \diamond s are fluxes derived from *UBVRIJHK* photometry (left to right) and the solid line is the stellar model of a star using $T_{\text{eff}} = 6339$ K and $\log g = 4.19$ from Santos et al. (2004). There were no quoted errors for the *UBVRI* measurements and $\sigma_J \sim \sigma_H \sim \sigma_K \sim 10\%$. *UBVRI* photometry is from Morel & Magnenat (1978) and *JHK* photometry is from the *2MASS All-Sky Point Source Catalog* (Skrutskie et al. 2006). The diameter shown is an estimated LD diameter.

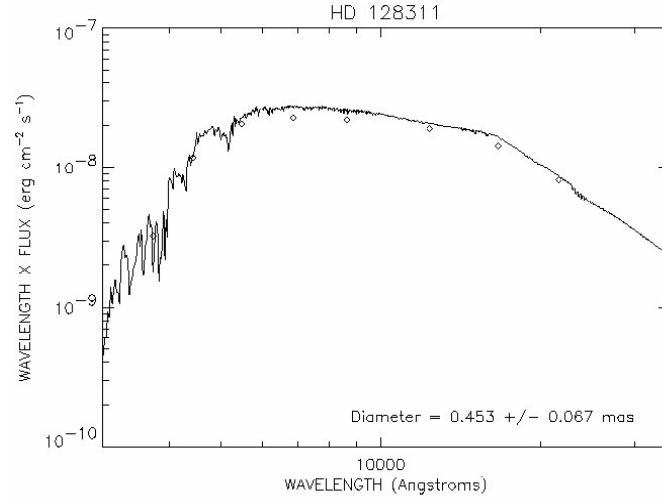


Figure. A.18: HD 128311: SED fit. The \diamond s are fluxes derived from *UBVRIJHK* photometry (left to right) and the solid line is the stellar model of a star using $T_{\text{eff}} = 4835$ K and $\log g = 4.44$ from Santos et al. (2004). There were no quoted errors for the *UBVRI* measurements and $\sigma_J \sim \sigma_H \sim \sigma_K \sim 0.5\%$. *UBV* photometry is from Myers et al. (2001), *RI* photometry is from Monet et al. (2003), and *JHK* photometry is from the *2MASS All-Sky Point Source Catalog* (Skrutskie et al. 2006). The diameter shown is an estimated LD diameter.

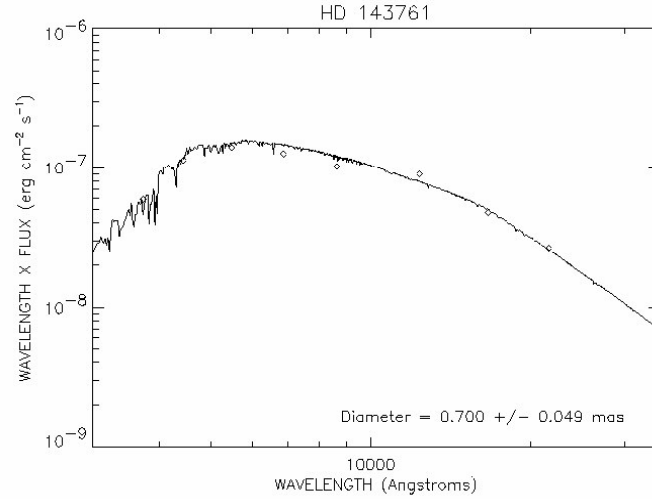


Figure. A.19: HD 143761: SED fit. The \diamond s are fluxes derived from *UBVRIJHK* photometry (left to right) and the solid line is the stellar model of a star using $T_{\text{eff}} = 5853$ K and $\log g = 4.41$ from Santos et al. (2004). There were no quoted errors for the *UBVRI* measurements and $\sigma_J \sim 6\%$, and $\sigma_H \sim \sigma_K \sim 0.9\%$. *UBV* photometry is from Johnson et al. (1966), *RI* photometry is from Monet et al. (2003), and *JHK* photometry is from the *2MASS All-Sky Point Source Catalog* (Skrutskie et al. 2006). The diameter shown is an estimated LD diameter.

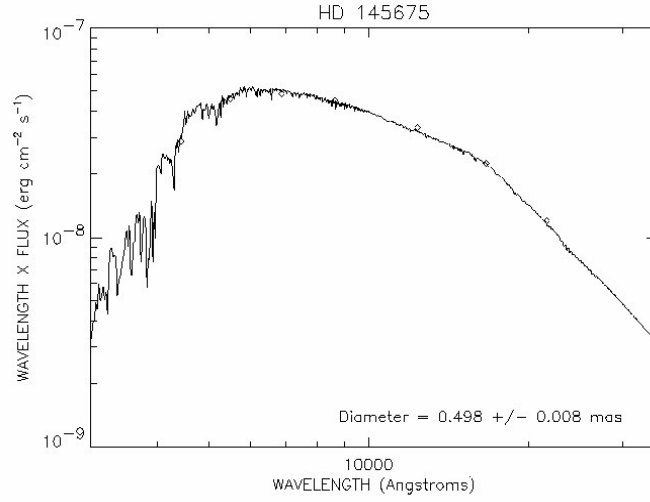


Figure. A.20: HD 145675: SED fit. The \diamond s are fluxes derived from *BVRIJHK* photometry (left to right) and the solid line is the stellar model of a star using $T_{\text{eff}} = 5311$ K and $\log g = 4.42$ from Santos et al. (2004). There were no quoted errors for the *BVRI* measurements and $\sigma_J \sim \sigma_H \sim \sigma_K \sim 0.4\%$. *BV* photometry is from Perryman & ESA (1997), *RI* photometry is from Monet et al. (2003), and *JHK* photometry is from the *2MASS All-Sky Point Source Catalog* (Skrutskie et al. 2006). The diameter shown is an estimated LD diameter.

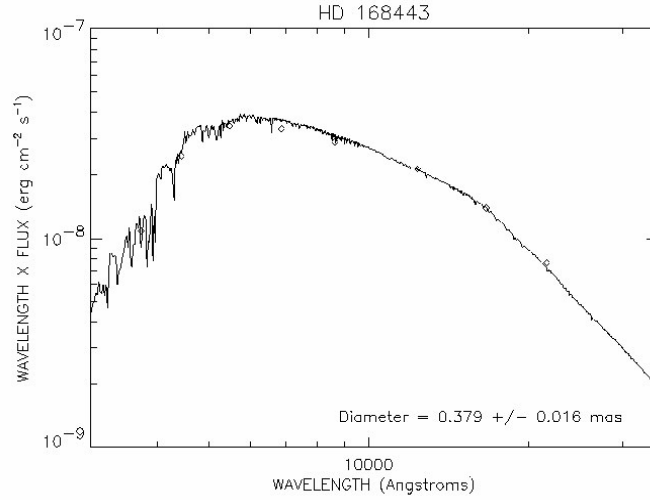


Figure. A.21: HD 168443: SED fit. The \diamond s are fluxes derived from *UBVRIJHK* photometry (left to right) and the solid line is the stellar model of a star using $T_{\text{eff}} = 5617$ K and $\log g = 4.22$ from Santos et al. (2004). There were no quoted errors for the *UBVRI* measurements and $\sigma_J \sim \sigma_H \sim \sigma_K \sim 0.3\%$. *UBV* photometry is from Myers et al. (2001), *RI* photometry is from Monet et al. (2003), and *JHK* photometry is from the *2MASS All-Sky Point Source Catalog* (Skrutskie et al. 2006). The diameter shown is an estimated LD diameter.

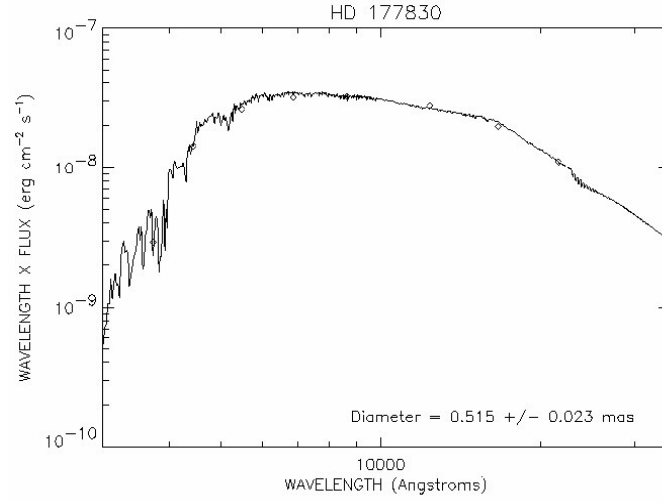


Figure. A.22: HD 177830: SED fit. The \diamond s are fluxes derived from *UBVRIJHK* photometry (left to right) and the solid line is the stellar model of a star using $T_{\text{eff}} = 4804$ K and $\log g = 3.57$ from Santos et al. (2004). There were no quoted errors for the *UBVRI* measurements and $\sigma_J \sim \sigma_H \sim \sigma_K \sim 0.6\%$. *UBV* photometry is from Mermilliod (1997), *RI* photometry is from Monet et al. (2003), and *JHK* photometry is from the *2MASS All-Sky Point Source Catalog* (Skrutskie et al. 2006). The diameter shown is an estimated LD diameter.

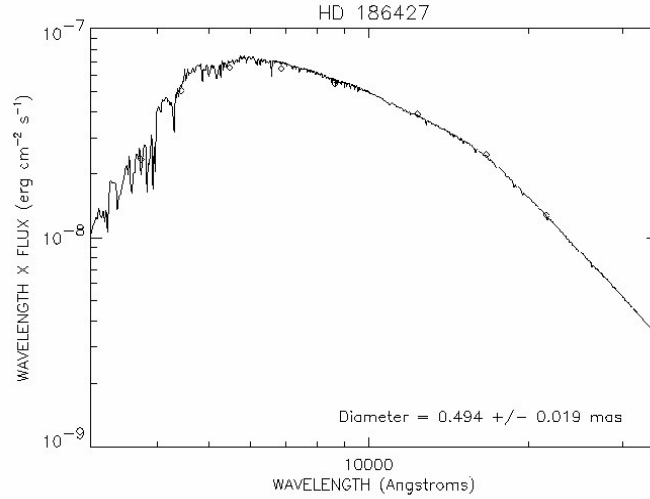


Figure. A.23: HD 186427: SED fit. The \diamond s are fluxes derived from *UBVRIJHK* photometry (left to right) and the solid line is the stellar model of a star using $T_{\text{eff}} = 5772$ K and $\log g = 4.40$ from Santos et al. (2004). There were no quoted errors for the *UBVRI* measurements and $\sigma_J \sim \sigma_H \sim \sigma_K \sim 0.7\%$. *UBV* photometry is from Johnson et al. (1966), *RI* photometry is from Monet et al. (2003), and *JHK* photometry is from the *2MASS All-Sky Point Source Catalog* (Skrutskie et al. 2006). The diameter shown is an estimated LD diameter.

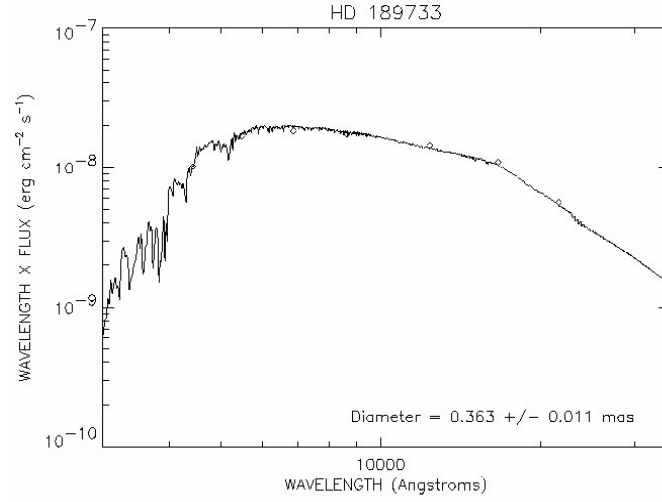


Figure. A.24: HD 189733: SED fit. The \diamond s are fluxes derived from *BVRIJHK* photometry (left to right) and the solid line is the stellar model of a star using $T_{\text{eff}} = 5051$ K and $\log g = 4.53$ from Sousa et al. (2006). There were no quoted errors for the *BVRI* measurements and $\sigma_J \sim \sigma_H \sim \sigma_K \sim 0.5\%$. *BV* photometry is from Perryman & ESA (1997), *RI* photometry is from Monet et al. (2003), and *JHK* photometry is from the *2MASS All-Sky Point Source Catalog* (Skrutskie et al. 2006). The diameter shown is an estimated LD diameter.

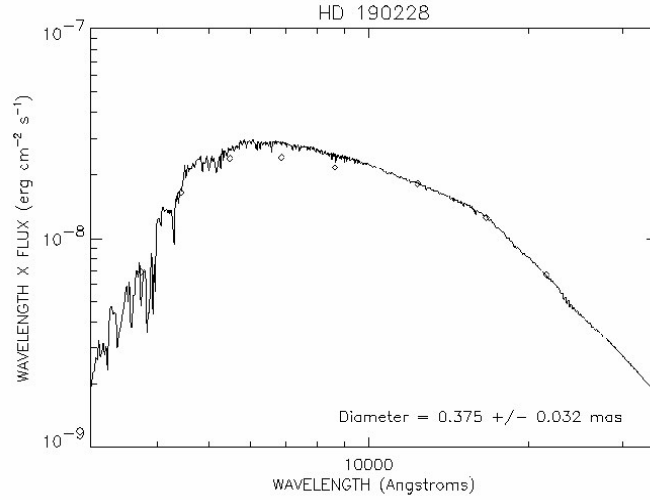


Figure. A.25: HD 190228: SED fit. The \diamond s are fluxes derived from *UBVRIJHK* photometry (left to right) and the solid line is the stellar model of a star using $T_{\text{eff}} = 5312$ K and $\log g = 3.87$ from Santos et al. (2004). There were no quoted errors for the *UBVRI* measurements and $\sigma_J \sim \sigma_H \sim \sigma_K \sim 0.3\%$. *UBV* photometry is from Myers et al. (2001), *RI* photometry is from Monet et al. (2003), and *JHK* photometry is from the *2MASS All-Sky Point Source Catalog* (Skrutskie et al. 2006). The diameter shown is an estimated LD diameter.

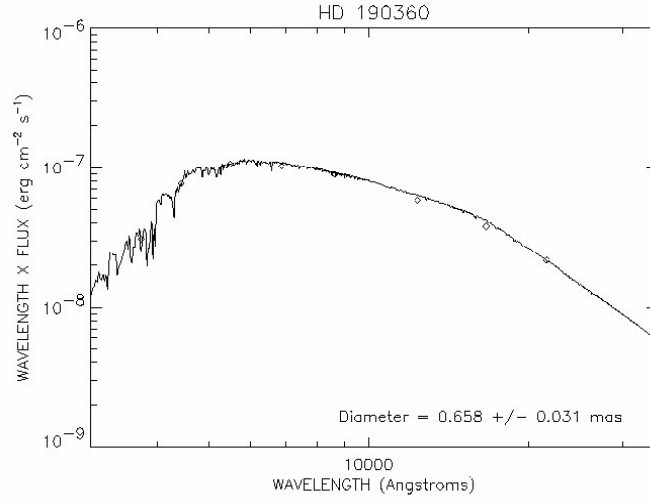


Figure. A.26: HD 190360: SED fit. The \diamond s are fluxes derived from *UBVRIJHK* photometry (left to right) and the solid line is the stellar model of a star using $T_{\text{eff}} = 5584$ K and $\log g = 4.37$ from Santos et al. (2004). There were no quoted errors for the *UBVRI* measurements, $\sigma_J \sim \sigma_H \sim 5\%$, and $\sigma_K \sim 0.7\%$. *UBV* photometry is from Johnson et al. (1966), *RI* photometry is from Monet et al. (2003), and *JHK* photometry is from the *2MASS All-Sky Point Source Catalog* (Skrutskie et al. 2006). The diameter shown is an estimated LD diameter.

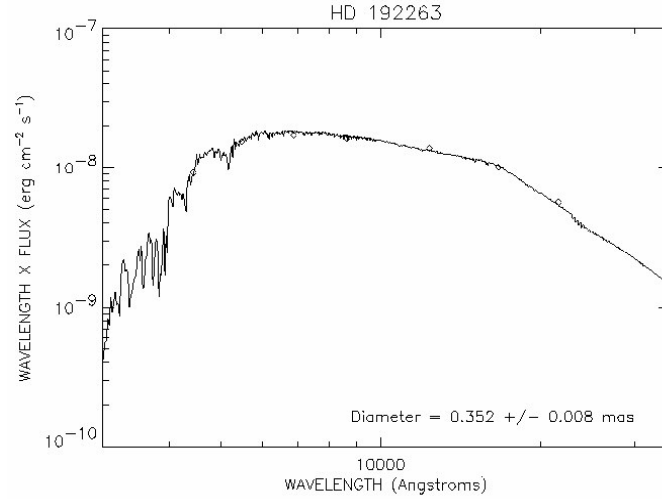


Figure. A.27: HD 192263: SED fit. The \diamond s are fluxes derived from *BVRIJHK* photometry (left to right) and the solid line is the stellar model of a star using $T_{\text{eff}} = 4947$ K and $\log g = 4.51$ from Santos et al. (2004). There were no quoted errors for the *BVRI* measurements, $\sigma_J \sim \sigma_H \sim 5\%$, and $\sigma_K \sim 0.4\%$. *BV* photometry is from Perryman & ESA (1997), *RI* photometry is from Monet et al. (2003), and *JHK* photometry is from the *2MASS All-Sky Point Source Catalog* (Skrutskie et al. 2006). The diameter shown is an estimated LD diameter.

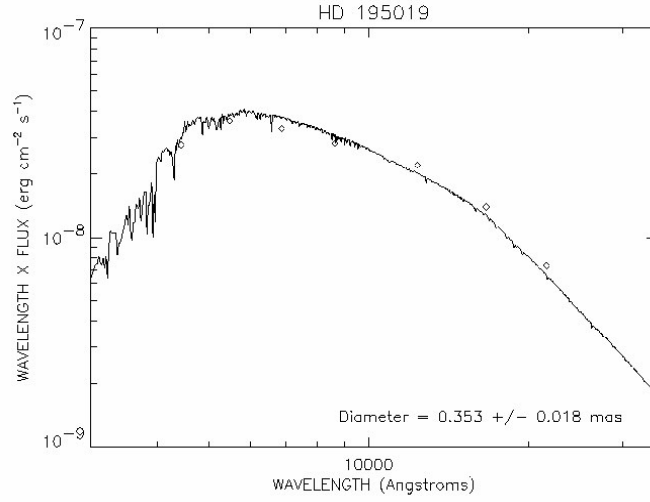


Figure. A.28: HD 195019: SED fit. The \diamond s are fluxes derived from *BVRIJHK* photometry (left to right) and the solid line is the stellar model of a star using $T_{\text{eff}} = 5859$ K and $\log g = 4.32$ from Santos et al. (2004). There were no quoted errors for the *BVRI* measurements and $\sigma_J \sim \sigma_H \sim \sigma_K \sim 0.3\%$. *BV* photometry is from Perryman & ESA (1997), *RI* photometry is from Monet et al. (2003), and *JHK* photometry is from the *2MASS All-Sky Point Source Catalog* (Skrutskie et al. 2006). The diameter shown is an estimated LD diameter.

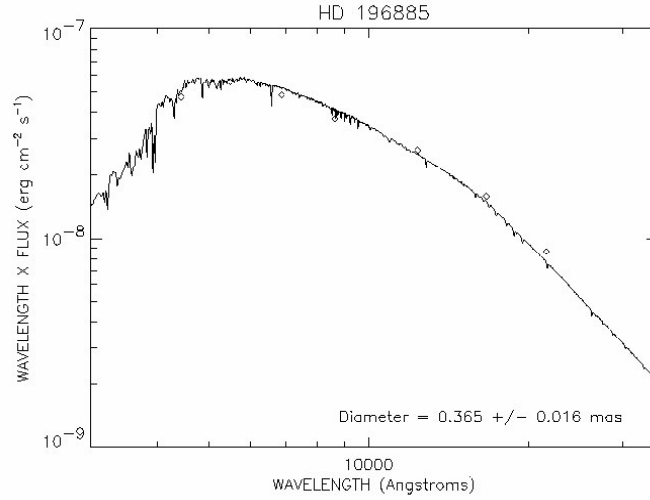


Figure. A.29: HD 196885: SED fit. The \diamond s are fluxes derived from *BVRIJHK* photometry (left to right) and the solid line is the stellar model of a star using $T_{\text{eff}} = 6309$ K and $\log g = 4.32$ from Allende Prieto & Lambert (1999). There were no quoted errors for the *BVRI* measurements and $\sigma_J \sim \sigma_H \sim \sigma_K \sim 0.4\%$. *BV* photometry is from Perryman & ESA (1997), *RI* photometry is from Monet et al. (2003), and *JHK* photometry is from the *2MASS All-Sky Point Source Catalog* (Skrutskie et al. 2006). The diameter shown is an estimated LD diameter.

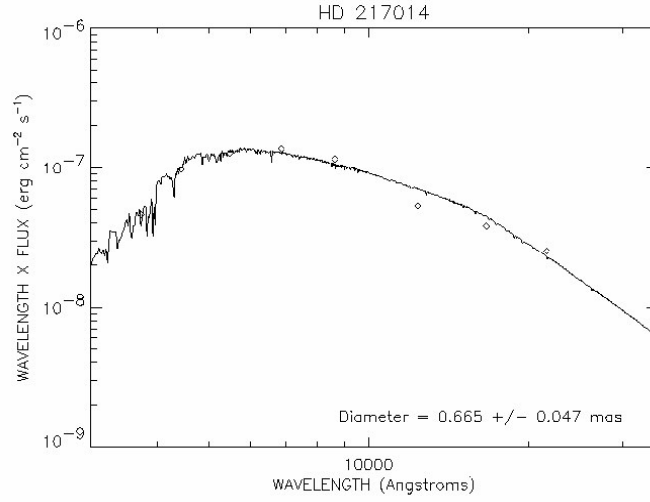


Figure. A.30: HD 217014: SED fit. The ◇s are fluxes derived from *UBVRIJHK* photometry (left to right) and the solid line is the stellar model of a star using $T_{\text{eff}} = 5804$ K and $\log g = 4.42$ from Santos et al. (2004). There were no quoted errors for the *UBVRI* measurements, $\sigma_J \sim \sigma_H \sim 6\%$, and $\sigma_K \sim 0.5\%$. *UBVR* photometry is from (?), *I* photometry is from Monet et al. (2003), and *JHK* photometry is from the *2MASS All-Sky Point Source Catalog* (Skrutskie et al. 2006). The diameter shown is an estimated LD diameter.

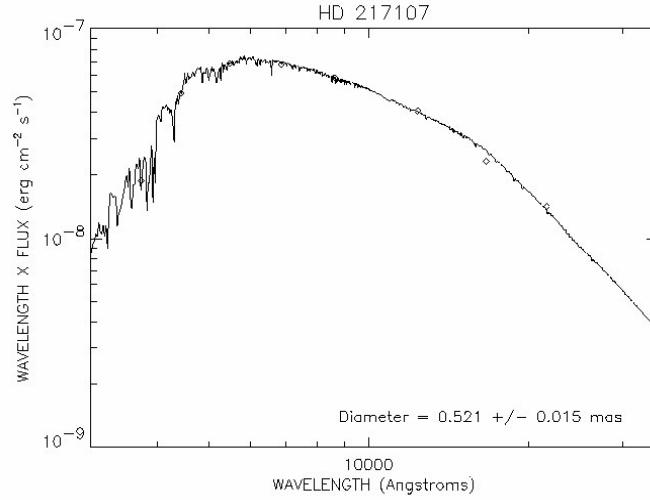


Figure. A.31: HD 217107: SED fit. The ◇s are fluxes derived from *UBVRIJHK* photometry (left to right) and the solid line is the stellar model of a star using $T_{\text{eff}} = 5623$ K and $\log g = 4.33$ from Allende Prieto & Lambert (1999). There were no quoted errors for the *UBVRI* measurements and $\sigma_J \sim \sigma_H \sim \sigma_K \sim 1\%$. *UBV* photometry is from Johnson et al. (1966), *RI* photometry is from Monet et al. (2003), and *JHK* photometry is from the *2MASS All-Sky Point Source Catalog* (Skrutskie et al. 2006). The diameter shown is an estimated LD diameter.

– B –

Spectral Energy Distribution Fits - Calibrator Stars

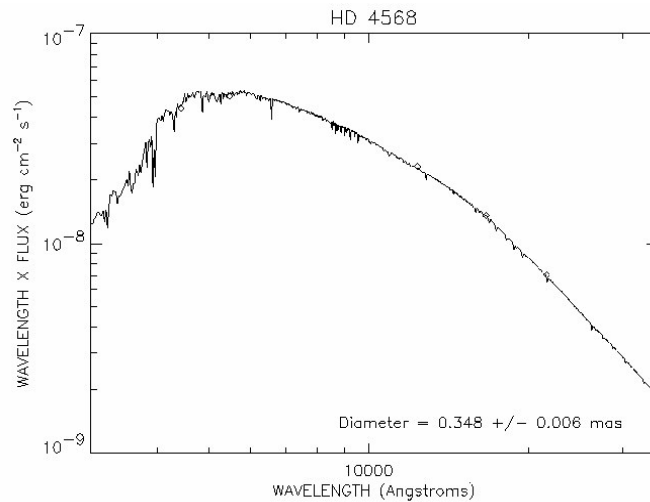


Figure. B.1: HD 4568: SED fit. The \diamond s are fluxes derived from *BVJHK* photometry (left to right) and the solid line is the stellar model of a star using $T_{\text{eff}} = 6300$ K and $\log g = 3.95$ from Allende Prieto & Lambert (1999). There were no quoted errors for the *BV* measurements and $\sigma_J \sim \sigma_H \sim \sigma_K \sim 0.4\%$. *BV* photometry is from Perryman & ESA (1997) and *JHK* photometry is from the *2MASS All-Sky Point Source Catalog* (Skrutskie et al. 2006). The diameter shown is an estimated UD disk diameter.

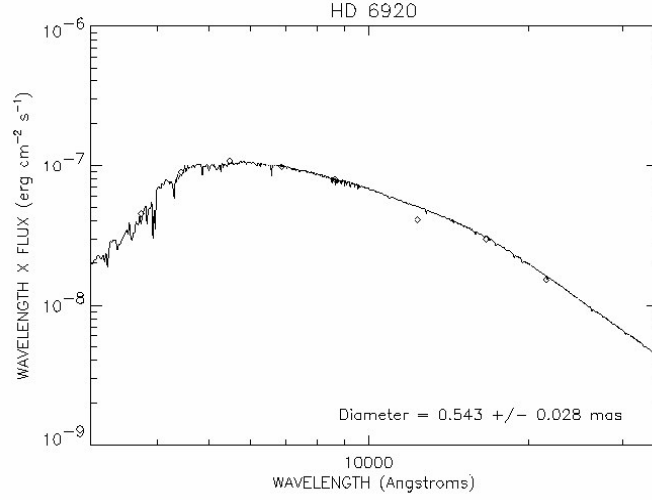


Figure. B.2: HD 6920: SED fit. The \diamond s are fluxes derived from *UBVRJHK* photometry (left to right) and the solid line is the stellar model of a star using $T_{\text{eff}} = 6026$ K and $\log g = 3.67$ from Allende Prieto & Lambert (1999). There were no quoted errors for the *UBV* measurements and $\sigma_J \sim \sigma_H \sim \sigma_K \sim 7\%$. *UBV* photometry is from Sato & Kuji (1990), *RI* photometry is from Monet et al. (2003), and *JHK* photometry is from the *2MASS All-Sky Point Source Catalog* (Skrutskie et al. 2006). The diameter shown is an estimated UD disk diameter.

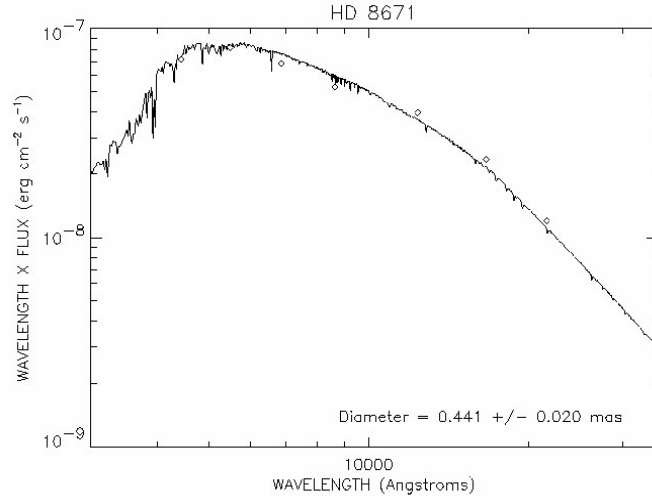


Figure. B.3: HD 8671: SED fit. The \diamond s are fluxes derived from *BVRJHK* photometry (left to right) and the solid line is the stellar model of a star using $T_{\text{eff}} = 6310$ K and $\log g = 4.00$ from Allende Prieto & Lambert (1999). There were no quoted errors for the *BV* measurements and $\sigma_J \sim \sigma_H \sim \sigma_K \sim 0.6\%$. *BV* photometry is from Perryman & ESA (1997), *RI* photometry is from Monet et al. (2003), and *JHK* photometry is from the *2MASS All-Sky Point Source Catalog* (Skrutskie et al. 2006). The diameter shown is an estimated UD disk diameter.

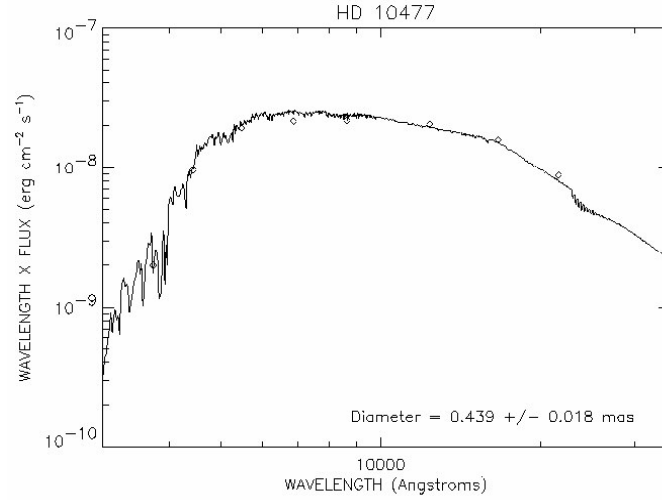


Figure. B.4: HD 10477: SED fit. The ◇s are fluxes derived from *UBVRIJHK* photometry (left to right) and the solid line is the stellar model of a star using $T_{\text{eff}} = 4800$ K and $\log g = 2.24$ from Cox (2000) (appropriate values for a G9 III star). There were no quoted errors for the *UBVRI* measurements and $\sigma_J \sim \sigma_H \sim \sigma_K \sim 0.3\%$. *UBV* photometry is from Mermilliod (1997), *RI* photometry is from Monet et al. (2003), and *JHK* photometry is from the *2MASS All-Sky Point Source Catalog* (Skrutskie et al. 2006). The diameter shown is an estimated LD diameter.

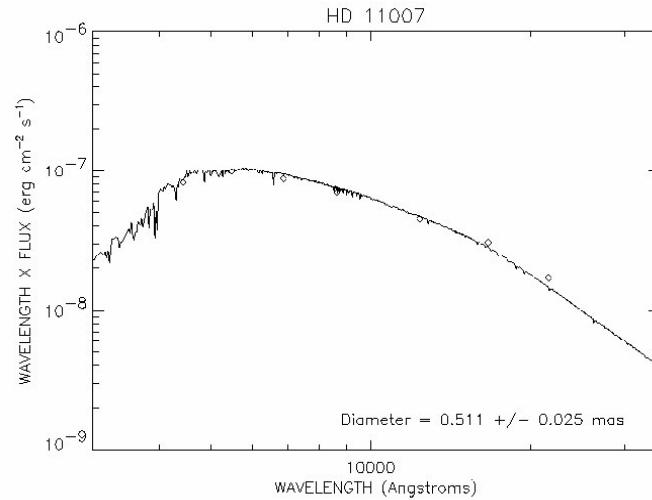


Figure. B.5: HD 11007: SED fit. The ◇s are fluxes derived from *BVRIJHK* photometry (left to right) and the solid line is the stellar model of a star using $T_{\text{eff}} = 6165$ K and $\log g = 4.20$ from Allende Prieto & Lambert (1999). There were no quoted errors for the *BVRI* measurements, $\sigma_J \sim \sigma_H \sim 4\%$, and $\sigma_K \sim 0.5\%$. *BV* photometry is from Perryman & ESA (1997), *RI* photometry is from Monet et al. (2003), and *JHK* photometry is from the *2MASS All-Sky Point Source Catalog* (Skrutskie et al. 2006). The diameter shown is an estimated LD diameter.

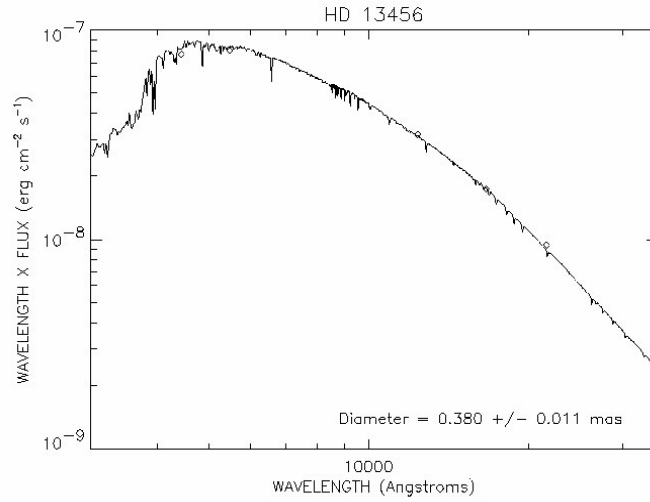


Figure. B.6: HD 13456: SED fit. The \diamond s are fluxes derived from *BVRIJHK* photometry (left to right) and the solid line is the stellar model of a star using $T_{\text{eff}} = 6760$ K and $\log g = 4.00$ from Allende Prieto & Lambert (1999). There were no quoted errors for the *BVRI* measurements, $\sigma_J \sim 6\%$, and $\sigma_H \sim \sigma_K \sim 0.5\%$. *BV* photometry is from Perryman & ESA (1997), *RI* photometry is from Monet et al. (2003), and *JHK* photometry is from the *2MASS All-Sky Point Source Catalog* (Skrutskie et al. 2006). The diameter shown is an estimated LD diameter.

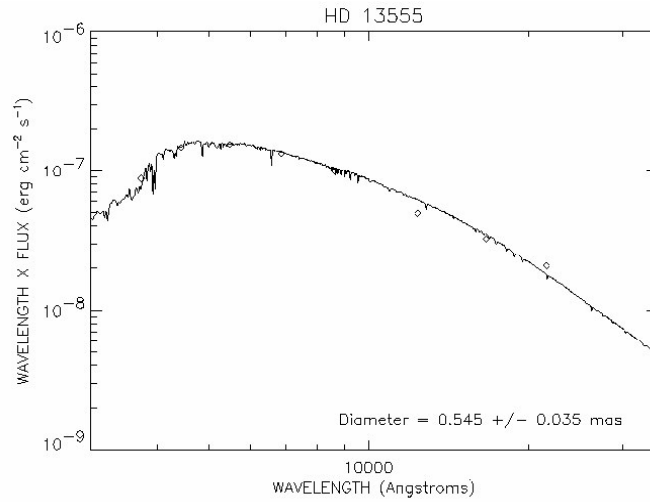


Figure. B.7: HD 13555: SED fit. The \diamond s are fluxes derived from *UBVRJHK* photometry (left to right) and the solid line is the stellar model of a star using $T_{\text{eff}} = 6606$ K and $\log g = 4.08$ from Allende Prieto & Lambert (1999). There were no quoted errors for the *UBVRI* measurements, $\sigma_J \sim \sigma_H \sim 7\%$, and $\sigma_K \sim 1\%$. *UBV* photometry is from Mermilliod (1997), *RI* photometry is from Monet et al. (2003), and *JHK* photometry is from the *2MASS All-Sky Point Source Catalog* (Skrutskie et al. 2006). The diameter shown is an estimated LD diameter.

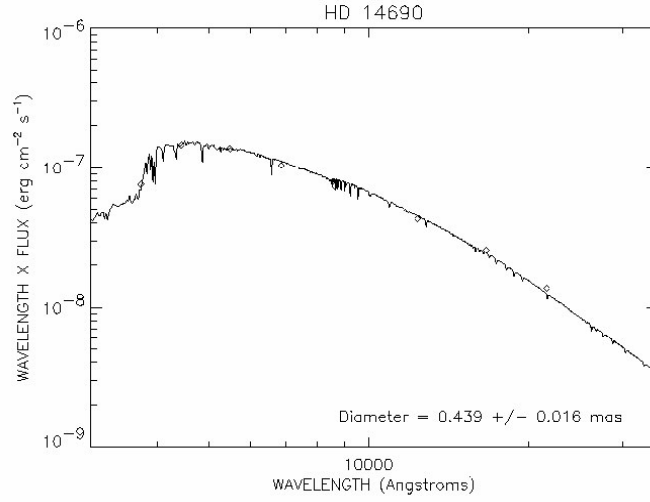


Figure. B.8: HD 14690: SED fit. The \diamond s are fluxes derived from *UBVR IJHK* photometry (left to right) and the solid line is the stellar model of a star using $T_{\text{eff}} = 7079$ K and $\log g = 3.57$ from Allende Prieto & Lambert (1999). There were no quoted errors for the *UBVR I* measurements and $\sigma_J \sim \sigma_H \sim \sigma_K \sim 0.5\%$. *UBV* photometry is from Johnson et al. (1966), *RI* photometry is from Monet et al. (2003), and *JHK* photometry is from the *2MASS All-Sky Point Source Catalog* (Skrutskie et al. 2006). The diameter shown is an estimated LD diameter.

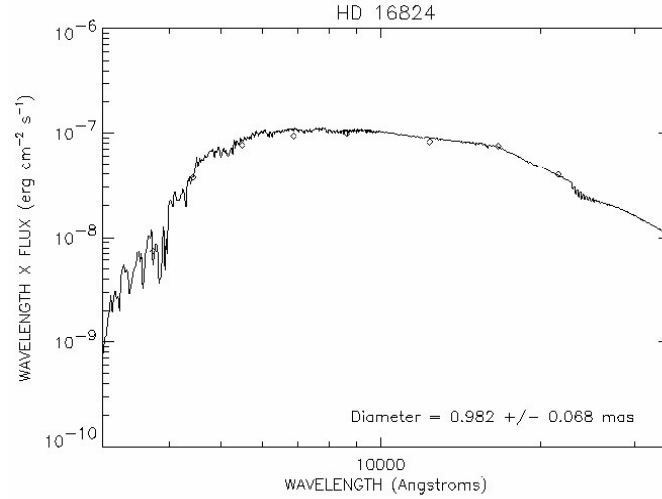


Figure. B.9: HD 16824: SED fit. The \diamond s are fluxes derived from *UBVR IJHK* photometry (left to right) and the solid line is the stellar model of a star using $T_{\text{eff}} = 4660$ K and $\log g = 2.14$ from Cox (2000) (values appropriate for a K0 III). There were no quoted errors for the *UBVR I* measurements and $\sigma_J \sim \sigma_H \sim \sigma_K \sim 7\%$. *UBV* photometry is from Johnson et al. (1966), *RI* photometry is from Monet et al. (2003), and *JHK* photometry is from the *2MASS All-Sky Point Source Catalog* (Skrutskie et al. 2006). The diameter shown is an estimated LD diameter.

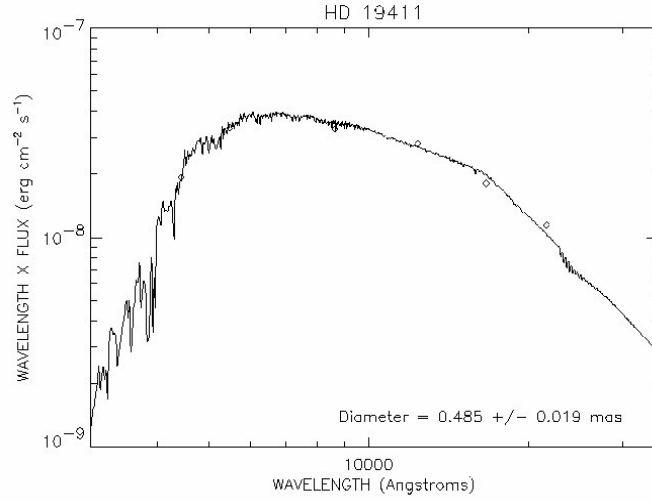


Figure. B.10: HD 19411: SED fit. The \diamond s are fluxes derived from *BVRIJHK* photometry (left to right) and the solid line is the stellar model of a star using $T_{\text{eff}} = 5050$ K and $\log g = 2.54$ from Cox (2000) (appropriate values for a G5 III star). There were no quoted errors for the *BVR* measurements, $\sigma_I \sim 2\%$, and $\sigma_J \sim \sigma_H \sim \sigma_K \sim 0.4\%$. *BV* photometry is from Perryman & ESA (1997), *R* photometry is from Kislyuk et al. (2000), *I* photometry is from Droege et al. (2006), and *JHK* photometry is from the *2MASS All-Sky Point Source Catalog* (Skrutskie et al. 2006). The diameter shown is an estimated UD disk diameter.

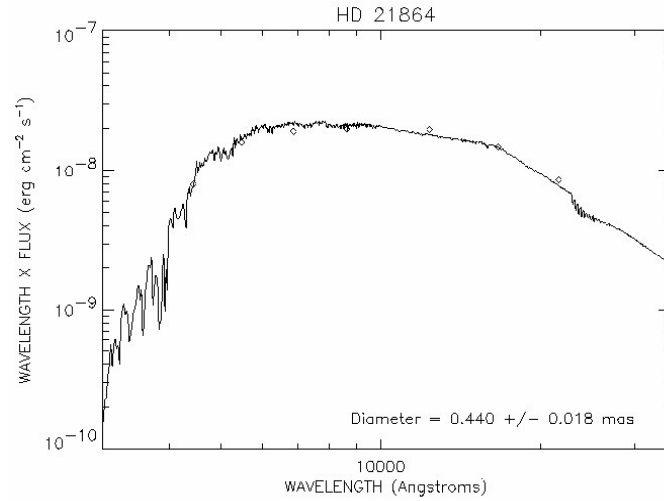


Figure. B.11: HD 21864: SED fit. The \diamond s are fluxes derived from *BVRIJHK* photometry (left to right) and the solid line is the stellar model of a star using $T_{\text{eff}} = 4660$ K and $\log g = 2.14$ from Cox (2000) (appropriate values for a K0 III star). There were no quoted errors for the *BVRI* measurements and $\sigma_I \sim \sigma_J \sim \sigma_H \sim \sigma_K \sim 0.4\%$. *BV* photometry is from Perryman & ESA (1997), *RI* photometry is from Monet et al. (2003), and *JHK* photometry is from the *2MASS All-Sky Point Source Catalog* (Skrutskie et al. 2006). The diameter shown is an estimated UD disk diameter.

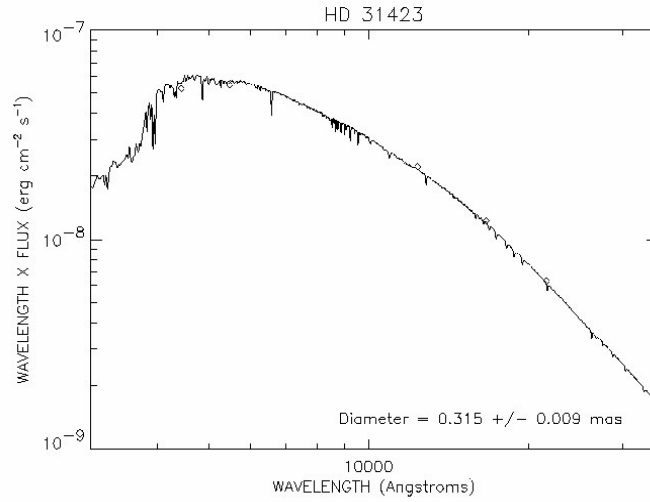


Figure. B.12: HD 31423: SED fit. The \diamond s are fluxes derived from *BVJHK* photometry (left to right) and the solid line is the stellar model of a star using $T_{\text{eff}} = 6760$ K and $\log g = 4.11$ from Allende Prieto & Lambert (1999). There were no quoted errors for the *BV* measurements, $\sigma_J \sim \sigma_H \sim 0.3\%$, and $\sigma_K \sim 0.8\%$. *BV* photometry is from Perryman & ESA (1997) and *JHK* photometry is from the *2MASS All-Sky Point Source Catalog* (Skrutskie et al. 2006). The diameter shown is an estimated LD diameter.

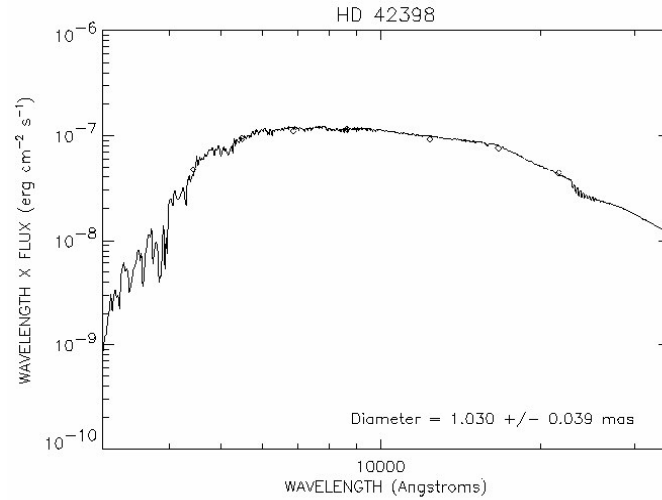


Figure. B.13: HD 42398: SED fit. The \diamond s are fluxes derived from *BVRJHK* photometry (left to right) and the solid line is the stellar model of a star using $T_{\text{eff}} = 4660$ K and $\log g = 2.14$ from Cox (2000) (values appropriate to a K0 III). There were no quoted errors for the *BVRI* measurements, $\sigma_J \sim \sigma_H \sim \sigma_K \sim 7\%$. *BV* photometry is from Perryman & ESA (1997), *RI* photometry is from Monet et al. (2003), and *JHK* photometry is from the *2MASS All-Sky Point Source Catalog* (Skrutskie et al. 2006). The diameter shown is an estimated LD diameter.

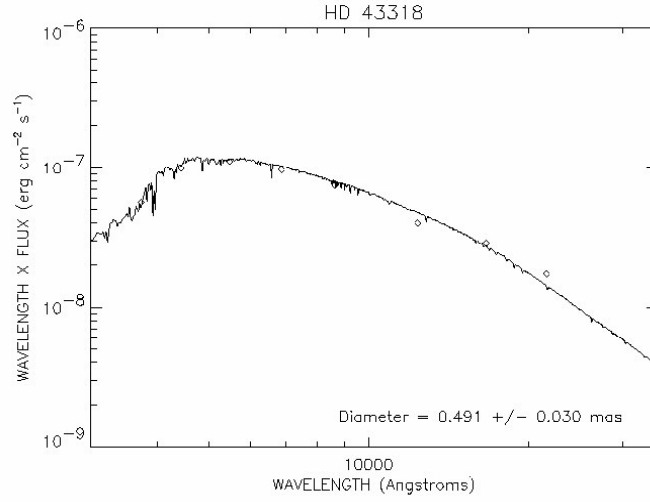


Figure. B.14: HD 43318: SED fit. The \diamond s are fluxes derived from *UBVRIJHK* photometry (left to right) and the solid line is the stellar model of a star using $T_{\text{eff}} = 6454$ K and $\log g = 4.01$ from Allende Prieto & Lambert (1999). There were no quoted errors for the *UBVRI* measurements, $\sigma_J \sim \sigma_H \sim 5\%$, and $\sigma_K \sim 8\%$. *UBV* photometry is from Johnson et al. (1966), *RI* photometry is from Monet et al. (2003), and *JHK* photometry is from the *2MASS All-Sky Point Source Catalog* (Skrutskie et al. 2006). The diameter shown is an estimated LD diameter.

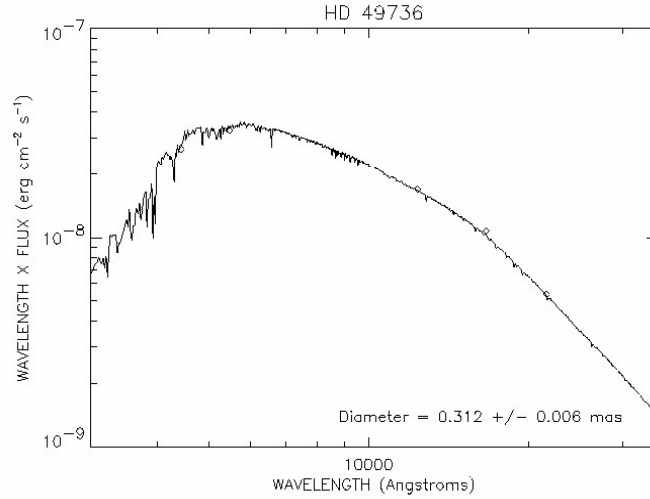


Figure. B.15: HD 49736: SED fit. The \diamond s are fluxes derived from *BVRJIHK* photometry (left to right) and the solid line is the stellar model of a star using $T_{\text{eff}} = 6026$ K and $\log g = 4.25$ from Allende Prieto & Lambert (1999). There were no quoted errors for the *BVRI* measurements and $\sigma_J \sim \sigma_H \sim \sigma_K \sim 0.3\%$. *BV* photometry is from Perryman & ESA (1997), *RI* photometry is from Monet et al. (2003), and *JHK* photometry is from the *2MASS All-Sky Point Source Catalog* (Skrutskie et al. 2006). The diameter shown is an estimated LD diameter.

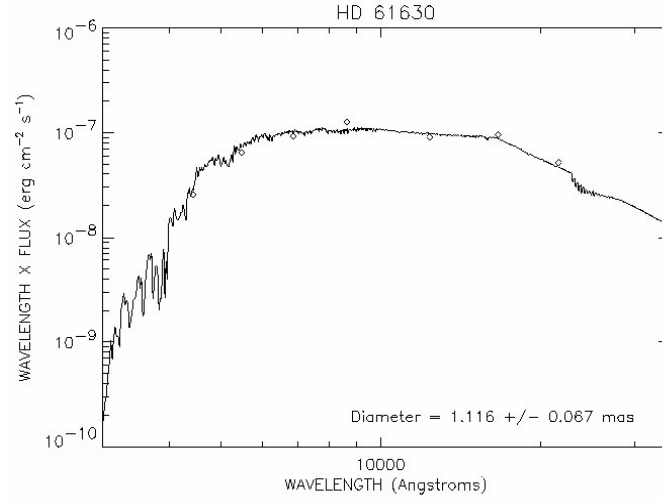


Figure. B.16: HD 61630: SED fit. The \diamond s are fluxes derived from *BVJHK* photometry (left to right) and the solid line is the stellar model of a star using $T_{\text{eff}} = 4400$ K and $\log g = 1.94$ from Cox (2000) (appropriate values for a K2 III star.). There were no quoted errors for the *BVRI* measurements, $\sigma_J \sim \sigma_H \sim 7\%$, and $\sigma_K \sim 8\%$. *BV* photometry is from Perryman & ESA (1997), *RI* photometry is from Monet et al. (2003), and *JHK* photometry is from the *2MASS All-Sky Point Source Catalog* (Skrutskie et al. 2006). The diameter shown is an estimated LD diameter.

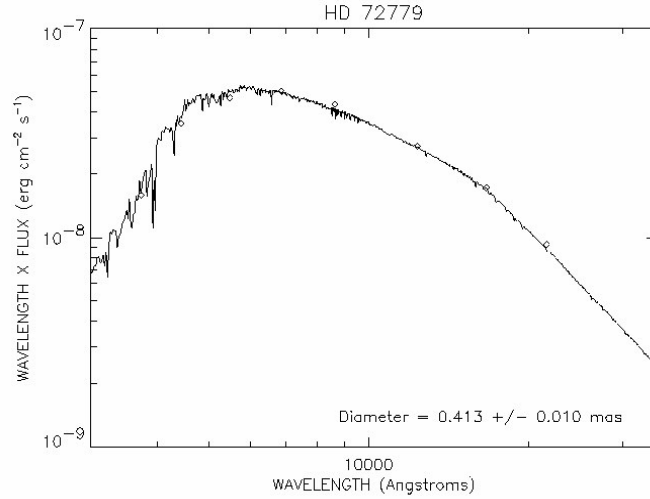


Figure. B.17: HD 72779: SED fit. The \diamond s are fluxes derived from *BVRIJHK* photometry (left to right) and the solid line is the stellar model of a star using $T_{\text{eff}} = 6703$ K and $\log g = 3.87$ from Lambert & Reddy (2004). There were no quoted errors for the *BVRI* measurements and $\sigma_J \sim \sigma_H \sim \sigma_K \sim 0.5\%$. *BV* photometry is from Perryman & ESA (1997), *RI* photometry is from Monet et al. (2003), and *JHK* photometry is from the *2MASS All-Sky Point Source Catalog* (Skrutskie et al. 2006). The diameter shown is an estimated LD diameter.

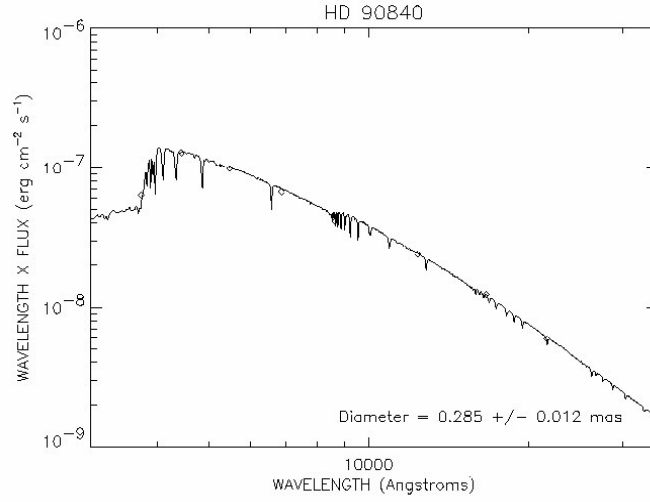


Figure. B.18: HD 90840: SED fit. The \diamond s are fluxes derived from *UBVR_IJHK* photometry (left to right) and the solid line is the stellar model of a star using $T_{\text{eff}} = 8180$ K and $\log g = 4.29$ from Cox (2000) (values appropriate for an A5 V star). There were no quoted errors for the *UBVR_I* measurements and $\sigma_J \sim \sigma_H \sim \sigma_K \sim 0.4\%$. *UBV* photometry is from Guarinos (1995), *RI* photometry is from Monet et al. (2003), and *JHK* photometry is from the *2MASS All-Sky Point Source Catalog* (Skrutskie et al. 2006). The diameter shown is an estimated LD diameter.

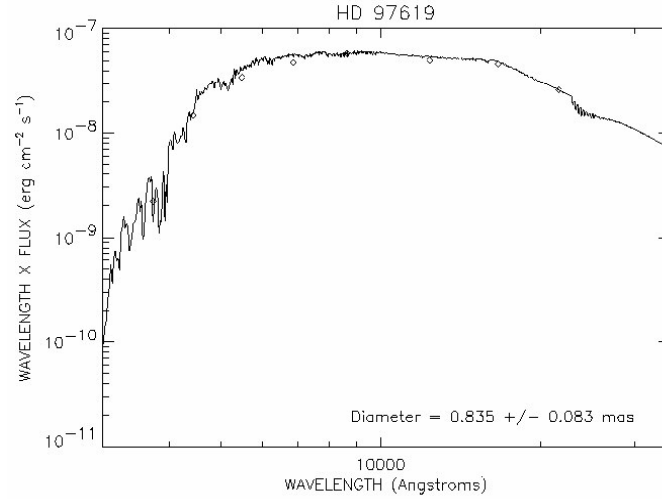


Figure. B.19: HD 97619: SED fit. The \diamond s are fluxes derived from *UBVJHK* photometry (left to right) and the solid line is the stellar model of a star using $T_{\text{eff}} = 4390$ K and $\log g = 1.94$ from Cox (2000) (appropriate values for a K2 III star.). There were no quoted errors for the *UBVR_I* measurements and $\sigma_J \sim \sigma_H \sim \sigma_K \sim 6\%$. *UBV* photometry is from Myers et al. (2001), *RI* photometry is from Monet et al. (2003), and *JHK* photometry is from the *2MASS All-Sky Point Source Catalog* (Skrutskie et al. 2006). The diameter shown is an estimated LD diameter.

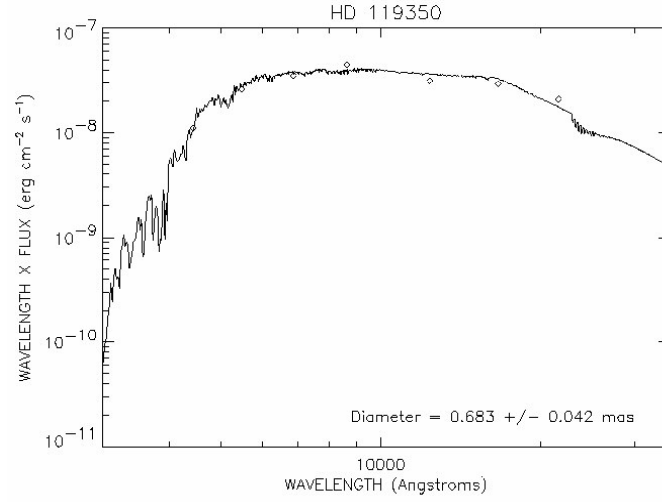


Figure. B.20: HD 119350: SED fit. The \diamond s are fluxes derived from *BVRIJHK* photometry (left to right) and the solid line is the stellar model of a star using $T_{\text{eff}} = 4390$ K and $\log g = 1.92$ from Cox (2000) (appropriate values for a K2 III star.). There were no quoted errors for the *BVRI* measurements, $\sigma_J \sim \sigma_H \sim 5\%$, and $\sigma_K \sim 0.6\%$. *BV* photometry is from Perryman & ESA (1997), *RI* photometry is from Monet et al. (2003), and *JHK* photometry is from the *2MASS All-Sky Point Source Catalog* (Skrutskie et al. 2006). The diameter shown is an estimated LD diameter.

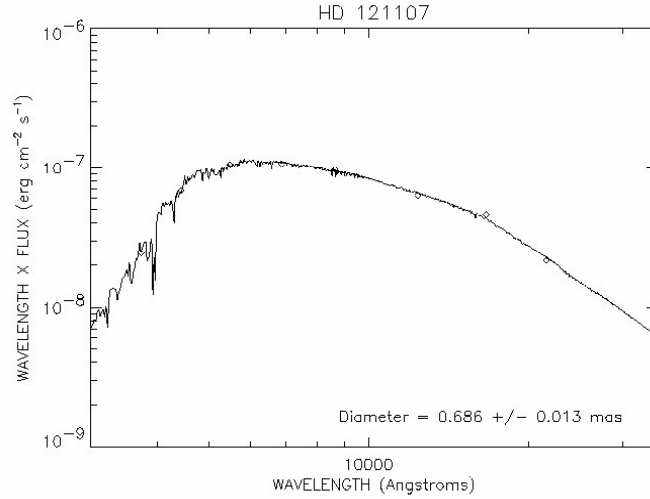


Figure. B.21: HD 121107: SED fit. The \diamond s are fluxes derived from *UBVRIJHK* photometry (left to right) and the solid line is the stellar model of a star using $T_{\text{eff}} = 5450$ K and $\log g = 1.74$ from Cox (2000) (appropriate values for a G3 III star.). There were no quoted errors for the *UBVRI* measurements and $\sigma_J \sim \sigma_H \sim \sigma_K \sim 7\%$. *UBV* photometry is from Guarinos (1995), *RI* photometry is from Monet et al. (2003), and *JHK* photometry is from the *2MASS All-Sky Point Source Catalog* (Skrutskie et al. 2006). The diameter shown is an estimated LD diameter.

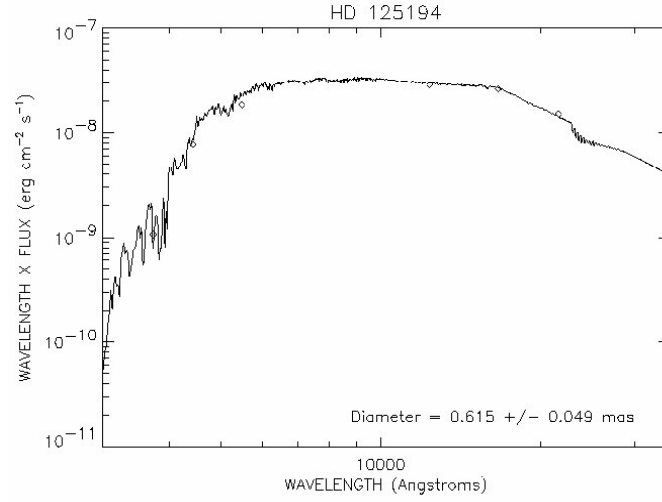


Figure. B.22: HD 125194: SED fit. The \diamond s are fluxes derived from *UBVJHK* photometry (left to right) and the solid line is the stellar model of a star using $T_{\text{eff}} = 4400$ K and $\log g = 1.94$ from Cox (2000) (values appropriate for a K2 III). There were no quoted errors for the *UBV* measurements and $\sigma_J \sim \sigma_H \sim \sigma_K \sim 1\%$. *UBV* photometry is from Myers et al. (2001) and *JHK* photometry is from the *2MASS All-Sky Point Source Catalog* (Skrutskie et al. 2006). The diameter shown is an estimated LD diameter.

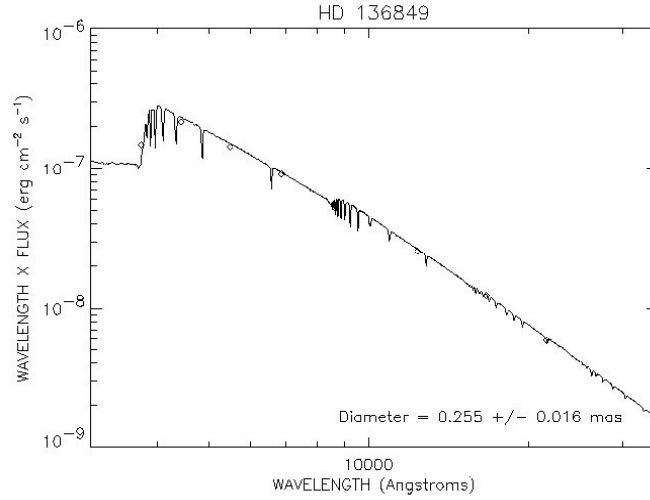


Figure. B.23: HD 136849: SED fit. The \diamond s are fluxes derived from *UBVRJHK* photometry (left to right) and the solid line is the stellar model of a star using $T_{\text{eff}} = 10471$ K and $\log g = 4.24$ from ?). There were no quoted errors for the *UBVRJ* measurements and $\sigma_J \sim \sigma_H \sim \sigma_K \sim 0.5\%$. *UBV* photometry is from Johnson et al. (1966), *RI* photometry is from Monet et al. (2003), and *JHK* photometry is from the *2MASS All-Sky Point Source Catalog* (Skrutskie et al. 2006). The diameter shown is an estimated LD diameter.

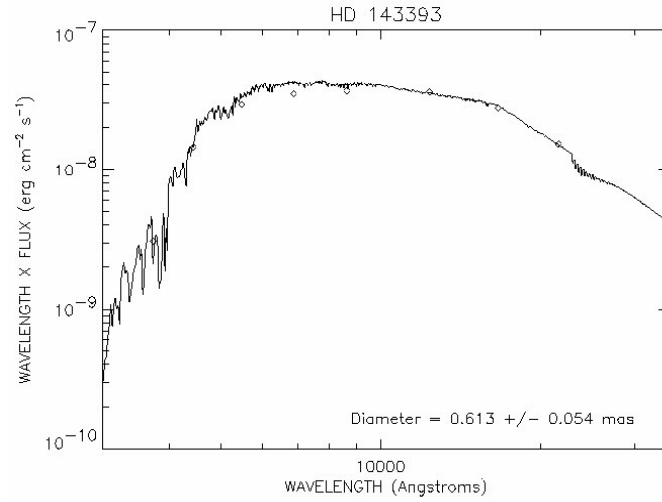


Figure. B.24: HD 143393: SED fit. The \diamond s are fluxes derived from *UBVRIJHK* photometry (left to right) and the solid line is the stellar model of a star using $T_{\text{eff}} = 4660$ K and $\log g = 2.14$ from Cox (2000) (values appropriate for a K0 III). There were no quoted errors for the *UBVRI* measurements, $\sigma_J \sim 5\%$, and $\sigma_H \sim \sigma_K \sim 0.7\%$. *UBV* photometry is from Myers et al. (2001), *RI* photometry is from Monet et al. (2003), and *JHK* photometry is from the *2MASS All-Sky Point Source Catalog* (Skrutskie et al. 2006). The diameter shown is an estimated LD diameter.

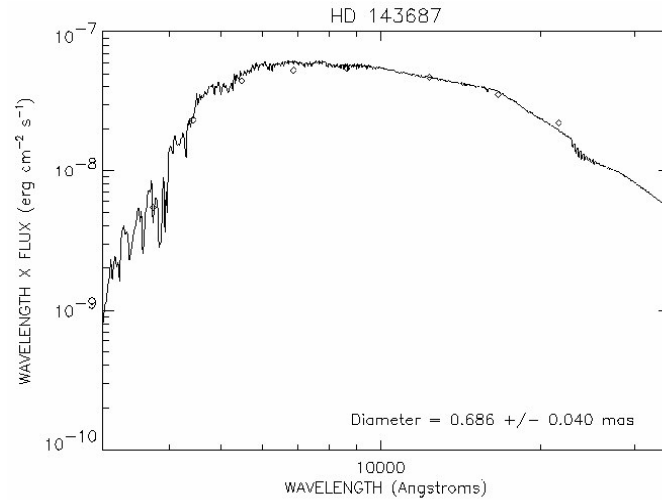


Figure. B.25: HD 143687: SED fit. The \diamond s are fluxes derived from *UBVRIJHK* photometry (left to right) and the solid line is the stellar model of a star using $T_{\text{eff}} = 4800$ K and $\log g = 2.3$ from Cox (2000) (values appropriate for a G8 III). There were no quoted errors for the *UBVRI* measurements, $\sigma_J \sim 5\%$, and $\sigma_H \sim \sigma_K \sim 0.7\%$. *UBV* photometry is from Sato & Kuji (1990), *RI* photometry is from Monet et al. (2003), and *JHK* photometry is from the *2MASS All-Sky Point Source Catalog* (Skrutskie et al. 2006). The diameter shown is an estimated LD diameter.

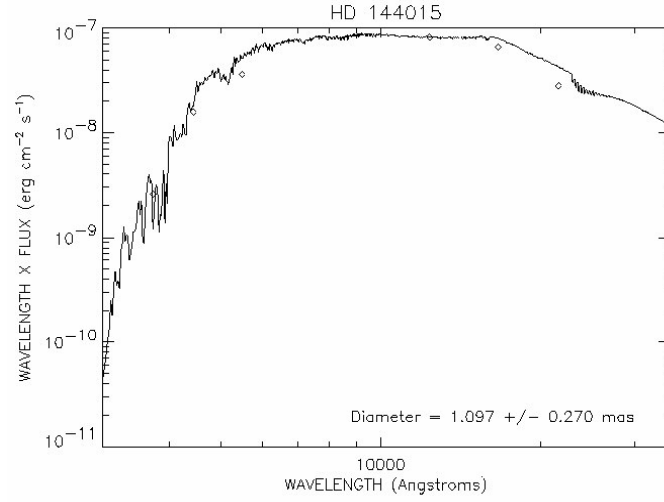


Figure. B.26: HD 144015: SED fit. The \diamond s are fluxes derived from *BVR**I**JHK* photometry (left to right) and the solid line is the stellar model of a star using $T_{\text{eff}} = 4220$ K and $\log g = 1.94$ from Cox (2000) (values appropriate for a K2 III). There were no quoted errors for the *UBVR* measurements, $\sigma_J \sim \sigma_H \sim 5\%$, and $\sigma_K \sim 0.4\%$. *UBV* photometry is from Sato & Kuji (1990) and *JHK* photometry is from the *2MASS All-Sky Point Source Catalog* (Skrutskie et al. 2006). The diameter shown is an estimated LD diameter.

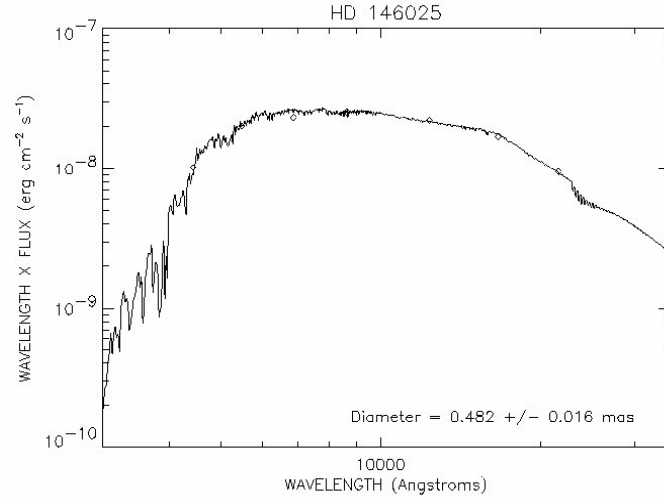


Figure. B.27: HD 146025: SED fit. The \diamond s are fluxes derived from *BVR**I**JHK* photometry (left to right) and the solid line is the stellar model of a star using $T_{\text{eff}} = 4660$ K and $\log g = 2.14$ from Cox (2000) (values appropriate for a K0 III). There were no quoted errors for the *BVR* measurements, $\sigma_J \sim \sigma_H \sim \sigma_K \sim 0.5\%$. *BV* photometry is from Perryman & ESA (1997), *RI* photometry is from Monet et al. (2003), and *JHK* photometry is from the *2MASS All-Sky Point Source Catalog* (Skrutskie et al. 2006). The diameter shown is an estimated LD diameter.

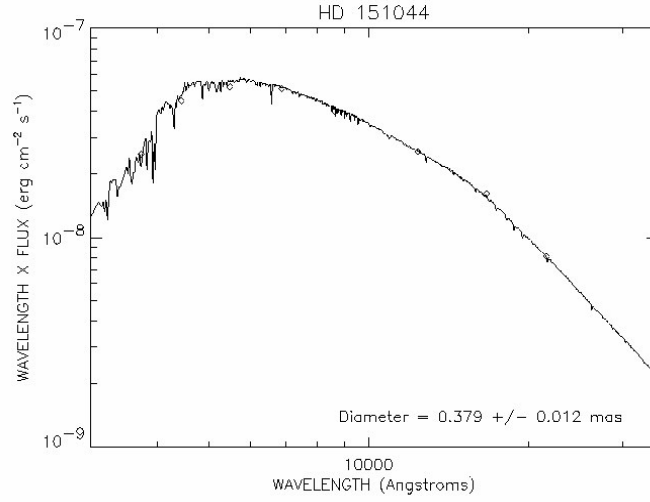


Figure. B.28: HD 151044: SED fit. The ◇s are fluxes derived from *UBVR**JHK* photometry (left to right) and the solid line is the stellar model of a star using $T_{\text{eff}} = 6166$ K and $\log g = 4.38$ from Allende Prieto & Lambert (1999). There were no quoted errors for the *UBVR* measurements and $\sigma_J \sim \sigma_H \sim \sigma_K \sim 0.5\%$. *UBVR* photometry is from Morel & Magnenat (1978) and *JHK* photometry is from the *2MASS All-Sky Point Source Catalog* (Skrutskie et al. 2006). The diameter shown is an estimated LD diameter.

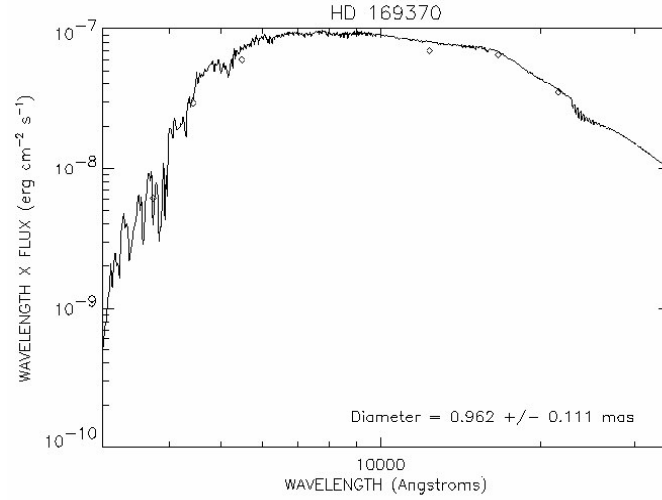


Figure. B.29: HD 169370: SED fit. The ◇s are fluxes derived from *UBVR**JHK* photometry (left to right) and the solid line is the stellar model of a star using $T_{\text{eff}} = 4570$ K and $\log g = 2.76$ from Allende Prieto & Lambert (1999). There were no quoted errors for the *UBVR* measurements and $\sigma_J \sim \sigma_H \sim \sigma_K \sim 8\%$. *UBV* photometry is from Johnson et al. (1966), *RI* photometry is from Monet et al. (2003), and *JHK* photometry is from the *2MASS All-Sky Point Source Catalog* (Skrutskie et al. 2006). The diameter shown is an estimated LD diameter.

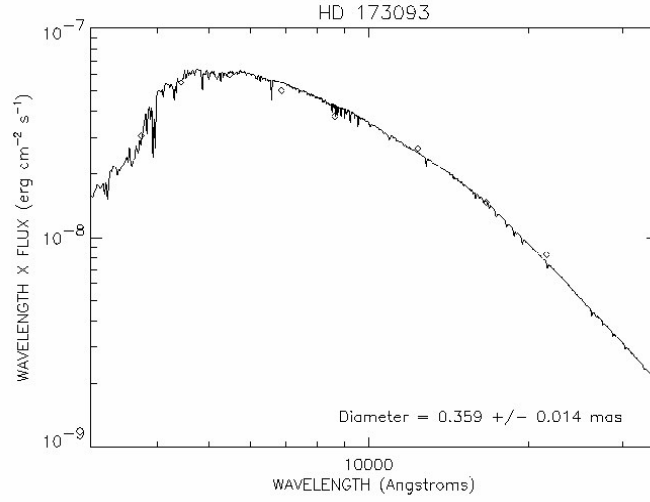


Figure. B.30: HD 173093: SED fit. The \diamond s are fluxes derived from *UBVRIJHK* photometry (left to right) and the solid line is the stellar model of a star using $T_{\text{eff}} = 6456$ K and $\log g = 3.77$ from Allende Prieto & Lambert (1999). There were no quoted errors for the *UBVRI* measurements and $\sigma_J \sim \sigma_H \sim \sigma_K \sim 0.7\%$. *UBV* photometry is from Johnson et al. (1966), *RI* photometry is from Monet et al. (2003), and *JHK* photometry is from the *2MASS All-Sky Point Source Catalog* (Skrutskie et al. 2006). The diameter shown is an estimated LD diameter.

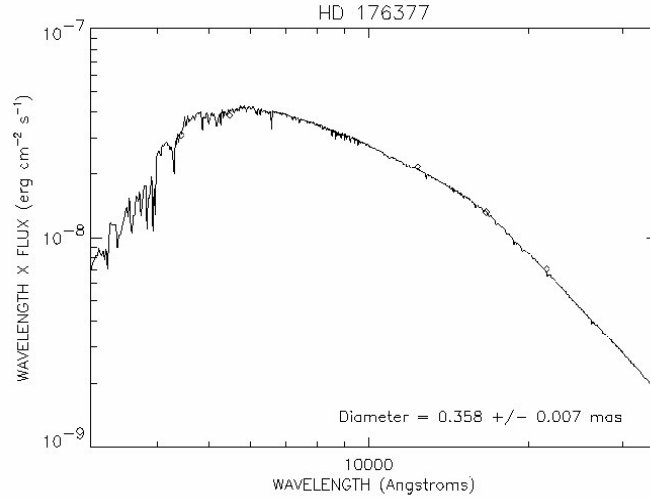


Figure. B.31: HD 176377: SED fit. The \diamond s are fluxes derived from *BVRIJHK* photometry (left to right) and the solid line is the stellar model of a star using $T_{\text{eff}} = 5888$ K and $\log g = 4.47$ from Allende Prieto & Lambert (1999). There were no quoted errors for the *UBVRI* measurements, $\sigma_J \sim \sigma_H \sim 0.3\%$, and $\sigma_K \sim 190\%$. *BV* photometry is from Perryman & ESA (1997), *RI* photometry is from Monet et al. (2003), and *JHK* photometry is from the *2MASS All-Sky Point Source Catalog* (Skrutskie et al. 2006). The diameter shown is an estimated LD diameter.

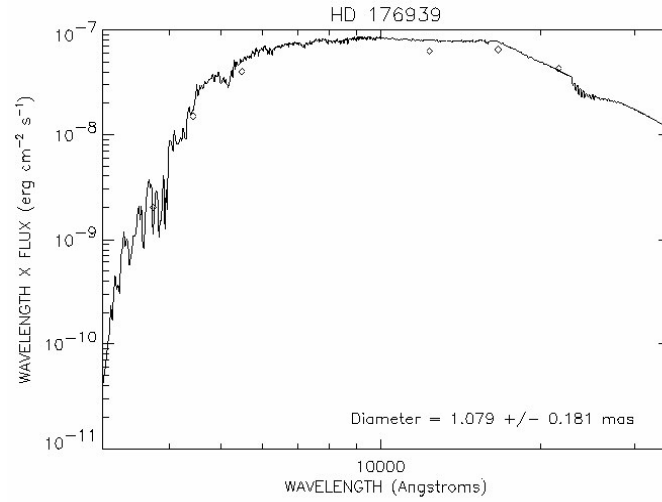


Figure. B.32: HD 176939: SED fit. The \diamond s are fluxes derived from *UBVRIJHK* photometry (left to right) and the solid line is the stellar model of a star using $T_{\text{eff}} = 4220$ K and $\log g = 1.84$ from Cox (2000) (values appropriate for a K3 III). There were no quoted errors for the *UBVRI* measurements and $\sigma_J \sim \sigma_H \sim \sigma_K \sim 8\%$. *UBV* photometry is from Oja (1991), *RI* photometry is from Monet et al. (2003), and *JHK* photometry is from the *2MASS All-Sky Point Source Catalog* (Skrutskie et al. 2006). The diameter shown is an estimated LD diameter.

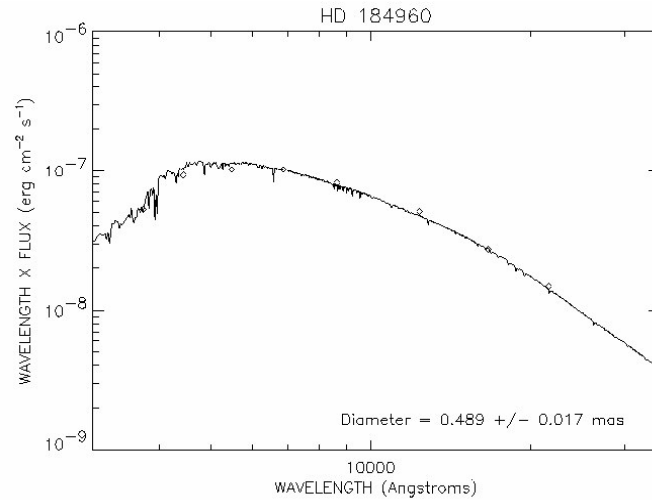


Figure. B.33: HD 184960: SED fit. The \diamond s are fluxes derived from *UBVRIJHK* photometry (left to right) and the solid line is the stellar model of a star using $T_{\text{eff}} = 6456$ K and $\log g = 4.33$ from Allende Prieto & Lambert (1999). There were no quoted errors for the *UBVRI* measurements and $\sigma_J \sim \sigma_H \sim \sigma_K \sim 0.8\%$. *UBVRI* photometry is from Morel & Magnenat (1978) and *JHK* photometry is from the *2MASS All-Sky Point Source Catalog* (Skrutskie et al. 2006). The diameter shown is an estimated LD diameter.

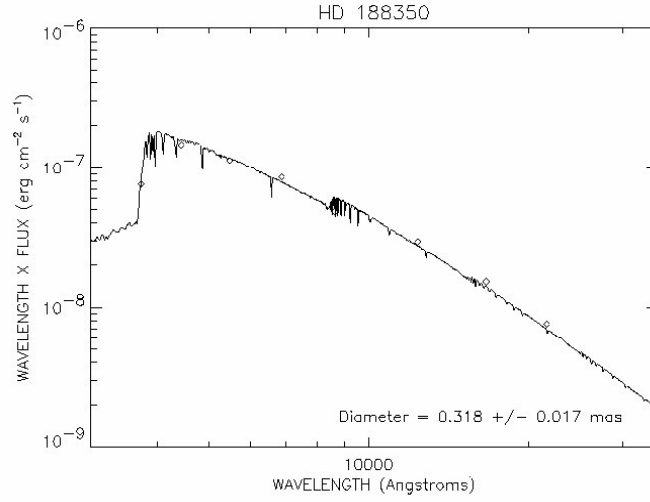


Figure. B.34: HD 188350: SED fit. The \diamond s are fluxes derived from *UBVRIJHK* photometry (left to right) and the solid line is the stellar model of a star using $T_{\text{eff}} = 7946$ K and $\log g = 2.00$ from Clem et al. (2004). There were no quoted errors for the *UBVRI* measurements and $\sigma_J \sim \sigma_H \sim \sigma_K \sim 0.4\%$. *UBV* photometry is from Morel & Magnenat (1978), *RI* photometry is from Monet et al. (2003), and *JHK* photometry is from the *2MASS All-Sky Point Source Catalog* (Skrutskie et al. 2006). The diameter shown is an estimated LD diameter.

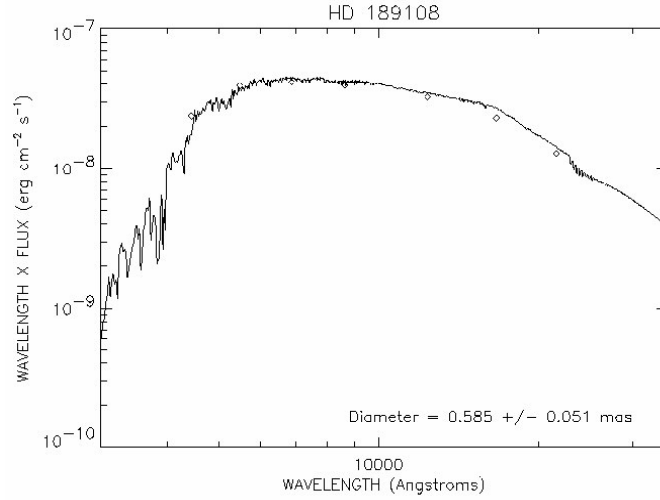


Figure. B.35: HD 189108: SED fit. The \diamond s are fluxes derived from *BVRIJHK* photometry (left to right) and the solid line is the stellar model of a star using $T_{\text{eff}} = 4800$ K and $\log g = 2.34$ from Cox (2000) (values appropriate for a G8 III). There were no quoted errors for the *BVRI* measurements and $\sigma_J \sim \sigma_H \sim \sigma_K \sim 0.6\%$. *BV* photometry is from Perryman & ESA (1997), *RI* photometry is from Monet et al. (2003), and *JHK* photometry is from the *2MASS All-Sky Point Source Catalog* (Skrutskie et al. 2006). The diameter shown is an estimated LD diameter.

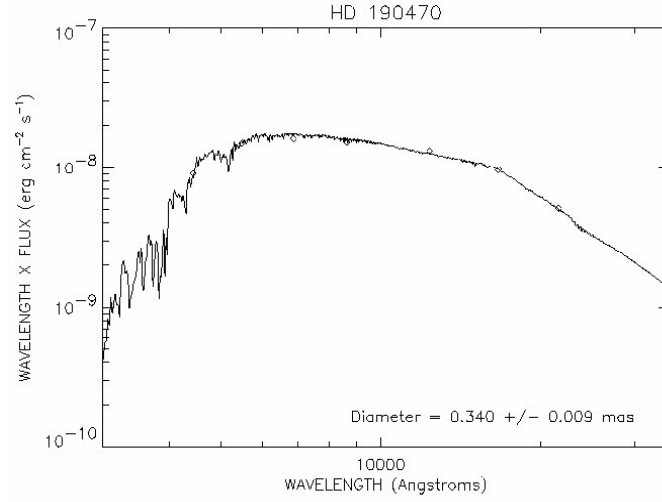


Figure. B.36: HD 190470: SED fit. The \diamond s are fluxes derived from *BVRIJHK* photometry (left to right) and the solid line is the stellar model of a star using $T_{\text{eff}} = 4968$ K and $\log g = 4.5$ from Gray et al. (2003). There were no quoted errors for the *BVRI* measurements and $\sigma_J \sim \sigma_H \sim \sigma_K \sim 0.4\%$. *BV* photometry is from Perryman & ESA (1997), *RI* photometry is from Monet et al. (2003), and *JHK* photometry is from the *2MASS All-Sky Point Source Catalog* (Skrutskie et al. 2006). The diameter shown is an estimated LD diameter.

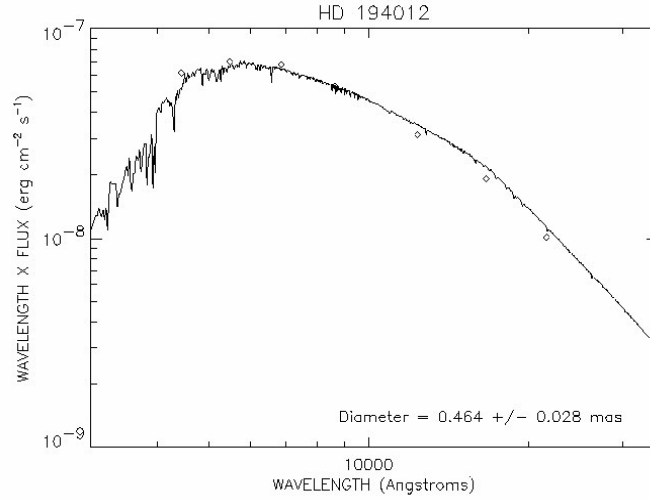


Figure. B.37: HD 194012: SED fit. The \diamond s are fluxes derived from *BVRIJHK* photometry (left to right) and the solid line is the stellar model of a star using $T_{\text{eff}} = 5859$ K and $\log g = 4.32$ from Santos et al. (2004). There were no quoted errors for the *BVRI* measurements and $\sigma_J \sim \sigma_H \sim \sigma_K \sim 0.3\%$. *BVRI* photometry is from Morel & Magnenat (1978) and *JHK* photometry is from the *2MASS All-Sky Point Source Catalog* (Skrutskie et al. 2006). The diameter shown is an estimated LD diameter.

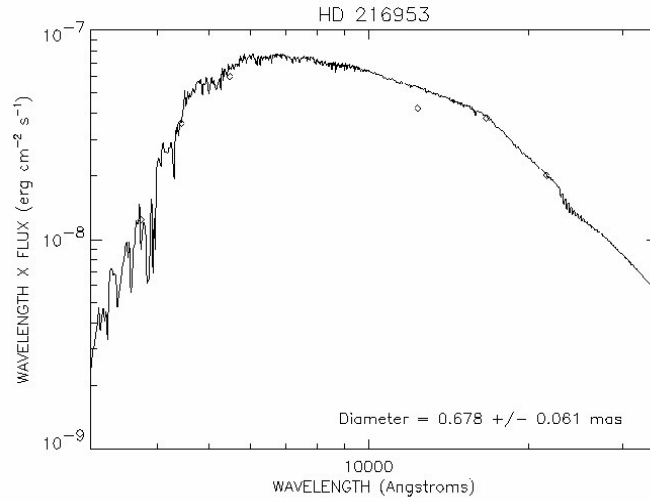


Figure. B.38: HD 216953: SED fit. The \diamond s are fluxes derived from *UBVRIJHK* photometry (left to right) and the solid line is the stellar model of a star using $T_{\text{eff}} = 5050$ K and $\log g = 2.54$ from Cox (2000) (values appropriate for a G5 III). There were no quoted errors for the *UBVRI* measurements, $\sigma_J \sim \sigma_H \sim 5\%$, and $\sigma_K \sim 0.9\%$. *UBV* photometry is from Johnson et al. (1966), *RI* photometry is from Monet et al. (2003), and *JHK* photometry is from the *2MASS All-Sky Point Source Catalog* (Skrutskie et al. 2006). The diameter shown is an estimated LD diameter.

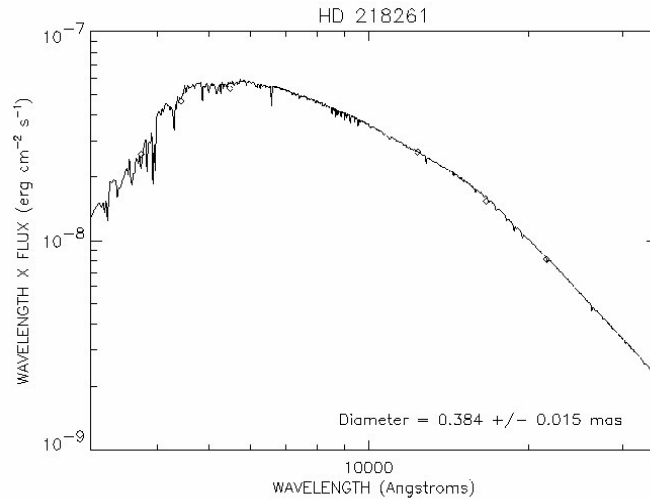


Figure. B.39: HD 218261: SED fit. The \diamond s are fluxes derived from *UBVJHK* photometry (left to right) and the solid line is the stellar model of a star using $T_{\text{eff}} = 6165$ K and $\log g = 4.40$ from Allende Prieto & Lambert (1999). There were no quoted errors for the *UBV* measurements and $\sigma_J \sim \sigma_H \sim \sigma_K \sim 0.3\%$. *UBV* photometry is from Morel & Magnenat (1978) and *JHK* photometry is from the *2MASS All-Sky Point Source Catalog* (Skrutskie et al. 2006). The diameter shown is an estimated LD diameter.

– C –

Notes on Individual Targets

C.1 HD 3651

C.1.1 Calibrated Visibilities

Table. C.1: HD 3651: Calibrated Visibilities

| MJD | B (m) | PA (deg) | V_c | $\sigma(V_c)$ |
|-----------|----------|-------------|-------|---------------|
| 53665.387 | 311.95 | 174.5 | 0.622 | 0.072 |
| 53665.400 | 312.97 | 171.3 | 0.647 | 0.059 |
| 53667.328 | 312.67 | 187.9 | 0.704 | 0.041 |
| 53667.347 | 311.52 | 183.3 | 0.724 | 0.059 |
| 53667.364 | 311.29 | 179.0 | 0.677 | 0.046 |
| 53667.377 | 311.69 | 175.7 | 0.714 | 0.072 |
| 53667.390 | 312.53 | 172.5 | 0.654 | 0.053 |
| 53667.402 | 313.79 | 169.4 | 0.591 | 0.064 |
| 53718.121 | 271.75 | 140.3 | 0.759 | 0.052 |
| 53718.134 | 274.52 | 137.9 | 0.769 | 0.066 |
| 53718.149 | 276.77 | 135.5 | 0.658 | 0.084 |
| 53718.165 | 278.22 | 133.1 | 0.620 | 0.080 |
| 53718.180 | 278.41 | 131.1 | 0.654 | 0.061 |

C.1.2 Nightly Data Plots

Because there are only two data points in the 2005/10/22 dataset, it was not used in the companion check.

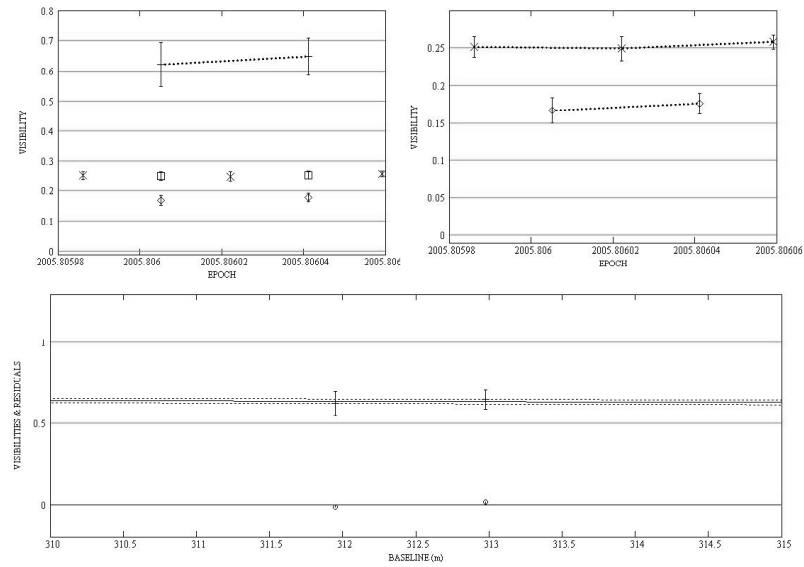


Figure. C.1: HD 3651: Long baseline plots for 2005/10/22 data.

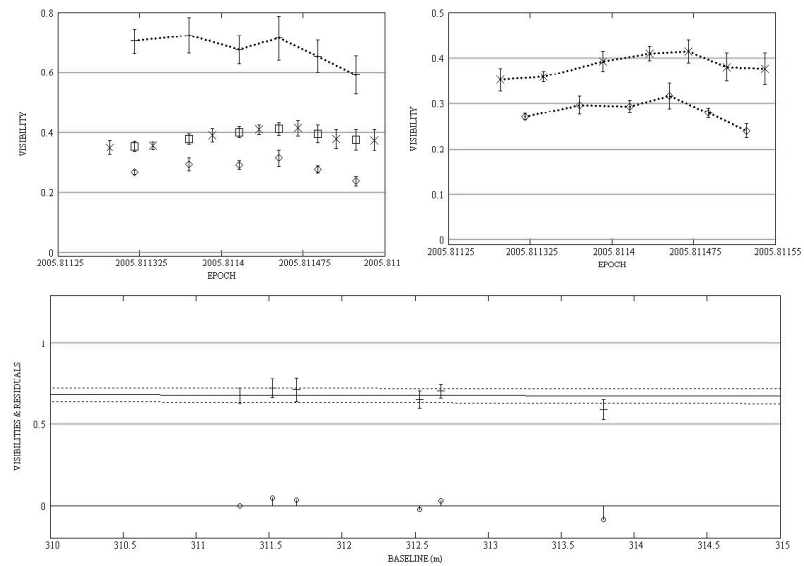


Figure. C.2: HD 3651: Long baseline plots for 2005/10/24 data.

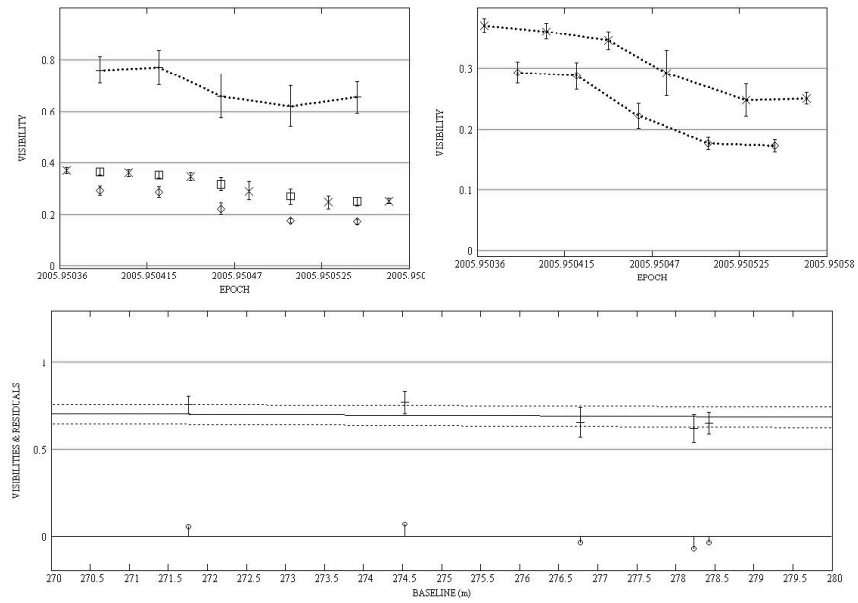


Figure. C.3: HD 3651: Long baseline plots for 2005/12/14 data.

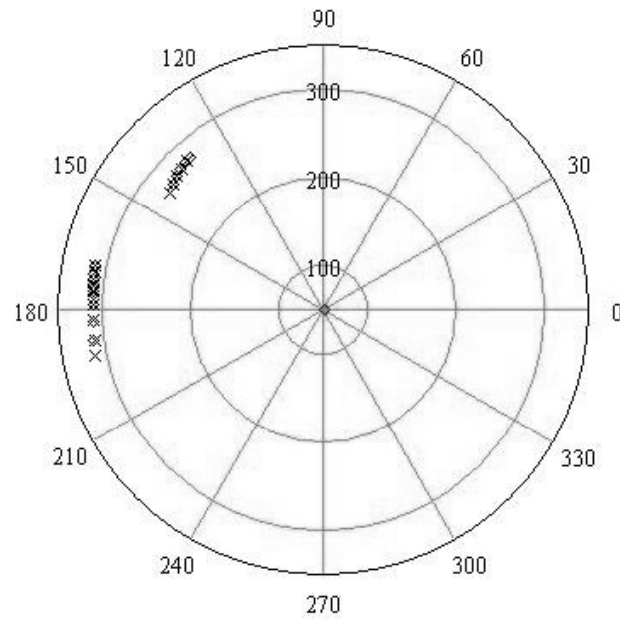


Figure. C.4: HD 3651: All data - Baseline vs. baseline position angle.

C.1.3 Diameter Calculation

I used all the S1-E1 data for the diameter calculation.

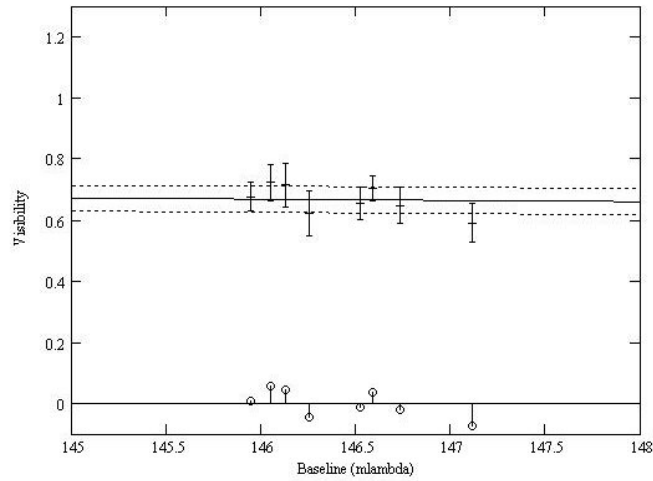


Figure. C.5: HD 3651: LD disk diameter fit: Visibility vs. baseline.

C.1.4 SFP Search

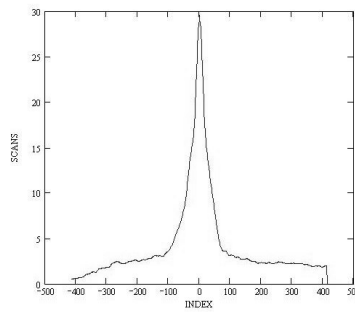


Figure. C.6: HD 3651: SFP inspection for 2005/10/22 data.

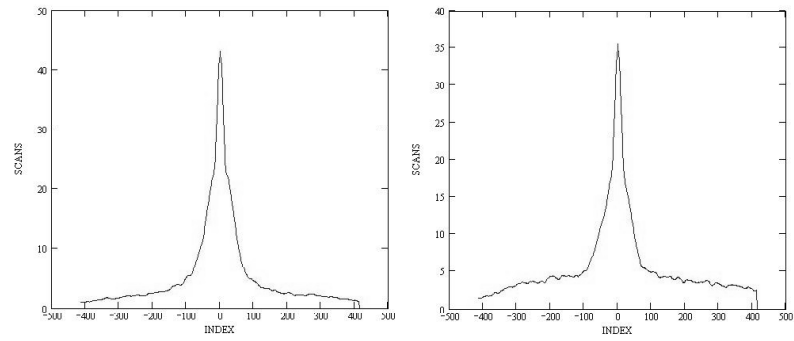


Figure. C.7: HD 3651: SFP inspection for 2005/10/24 data.

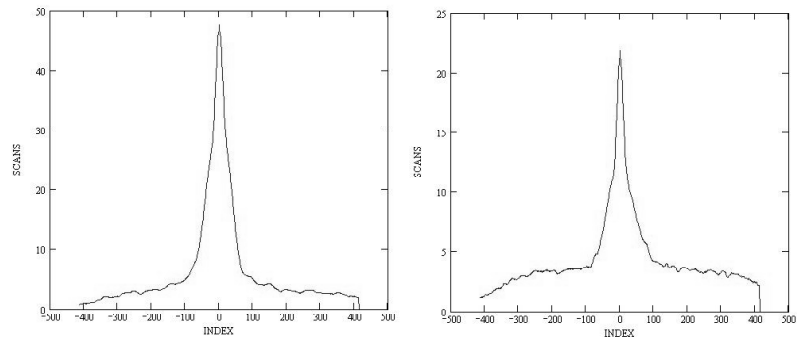


Figure. C.8: HD 3651: SFP inspection for 2005/12/14 data.

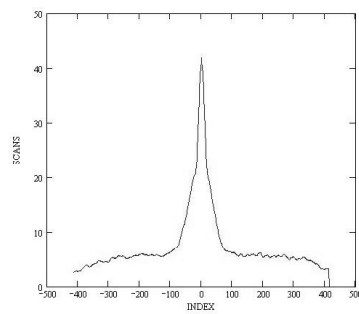


Figure. C.9: HD 4568: SFP inspection for 2005/10/22 data.

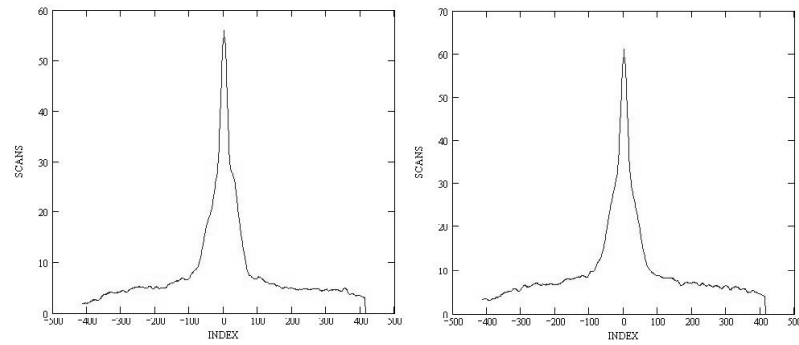


Figure. C.10: HD 4568: SFP inspection for 2005/10/24 data.

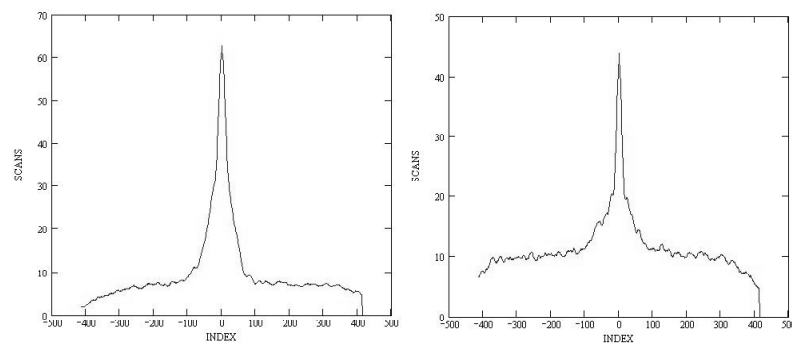


Figure. C.11: HD 4568: SFP inspection for 2005/12/14 data.

C.2 HD 9826

C.2.1 Calibrated Visibilities

Table. C.2: HD 9826: Calibrated Visibilities

| MJD | B (m) | PA (deg) | V_c | $\sigma(V_c)$ |
|-----------|----------|-------------|-------|---------------|
| 53586.397 | 88.42 | 137.2 | 0.829 | 0.069 |
| 53586.409 | 90.88 | 132.7 | 0.850 | 0.069 |
| 53586.419 | 92.87 | 129.2 | 0.927 | 0.088 |
| 53586.429 | 94.88 | 125.9 | 0.806 | 0.063 |
| 53586.439 | 96.87 | 122.6 | 0.863 | 0.058 |
| 53586.449 | 98.80 | 119.5 | 0.806 | 0.095 |
| 53586.462 | 100.93 | 115.8 | 1.034 | 0.085 |
| 53586.473 | 102.63 | 112.8 | 1.065 | 0.113 |
| 53586.483 | 104.05 | 110.0 | 0.855 | 0.098 |
| 53586.495 | 105.41 | 106.9 | 0.700 | 0.108 |
| 53586.508 | 106.59 | 103.7 | 0.801 | 0.109 |
| 53590.319 | 78.08 | 166.7 | 1.023 | 0.071 |
| 53590.332 | 79.40 | 160.3 | 0.998 | 0.090 |
| 53590.341 | 80.62 | 155.8 | 0.873 | 0.088 |
| 53590.361 | 83.69 | 147.2 | 0.905 | 0.054 |
| 53590.370 | 85.32 | 143.5 | 0.887 | 0.072 |
| 53590.378 | 86.84 | 140.3 | 0.932 | 0.060 |
| 53590.388 | 88.85 | 136.4 | 0.974 | 0.081 |
| 53590.398 | 90.91 | 132.6 | 0.947 | 0.052 |
| 53590.406 | 92.52 | 129.8 | 0.872 | 0.069 |
| 53590.418 | 94.95 | 125.8 | 0.761 | 0.053 |
| 53590.427 | 96.59 | 123.1 | 0.965 | 0.088 |
| 53590.438 | 98.60 | 119.8 | 0.935 | 0.075 |
| 53590.450 | 100.75 | 116.1 | 0.871 | 0.091 |
| 53590.463 | 102.65 | 112.7 | 0.803 | 0.118 |
| 53592.325 | 79.20 | 161.1 | 0.936 | 0.095 |
| 53592.334 | 80.34 | 156.8 | 0.992 | 0.091 |
| 53592.342 | 81.43 | 153.3 | 0.940 | 0.080 |
| 53592.350 | 82.84 | 149.4 | 0.942 | 0.069 |
| 53592.358 | 84.11 | 146.2 | 0.897 | 0.084 |
| 53592.367 | 85.79 | 142.4 | 0.980 | 0.085 |
| 53592.375 | 87.35 | 139.3 | 0.922 | 0.071 |
| 53592.384 | 89.04 | 136.0 | 0.865 | 0.064 |
| 53592.393 | 90.95 | 132.6 | 0.940 | 0.104 |
| 53592.401 | 92.47 | 129.9 | 1.001 | 0.101 |
| 53592.413 | 94.86 | 125.9 | 0.877 | 0.094 |
| 53592.422 | 96.69 | 122.9 | 0.754 | 0.088 |
| 53592.439 | 99.76 | 117.8 | 0.771 | 0.085 |

Continued on Next Page...

Table. C.2 – Continued

| MJD | B (m) | PA (deg) | V_c | $\sigma(V_c)$ |
|------------|------------------|---------------------|-------------------------|---------------------------------|
| 53592.458 | 102.83 | 112.4 | 0.877 | 0.093 |
| 53592.475 | 104.98 | 108.0 | 0.823 | 0.063 |
| 53592.486 | 106.11 | 105.1 | 0.790 | 0.074 |
| 53596.323 | 80.33 | 156.8 | 0.981 | 0.077 |
| 53596.335 | 82.17 | 151.2 | 0.899 | 0.082 |
| 53596.344 | 83.53 | 147.6 | 0.888 | 0.123 |
| 53596.354 | 85.47 | 143.1 | 0.946 | 0.071 |
| 53596.367 | 87.99 | 138.0 | 0.892 | 0.087 |
| 53596.390 | 92.49 | 129.9 | 0.904 | 0.100 |
| 53596.403 | 95.17 | 125.4 | 0.795 | 0.116 |
| 53596.419 | 98.15 | 120.5 | 0.758 | 0.128 |
| 53596.430 | 100.04 | 117.4 | 0.830 | 0.086 |
| 53596.453 | 103.56 | 111.0 | 0.942 | 0.077 |
| 53600.285 | 77.66 | 169.6 | 0.894 | 0.079 |
| 53600.293 | 78.22 | 165.8 | 0.965 | 0.087 |
| 53600.301 | 78.97 | 162.1 | 0.905 | 0.072 |
| 53600.310 | 80.00 | 157.9 | 0.948 | 0.094 |
| 53600.318 | 81.12 | 154.2 | 0.812 | 0.078 |
| 53600.326 | 82.37 | 150.6 | 0.916 | 0.082 |
| 53600.335 | 83.87 | 146.8 | 0.833 | 0.087 |
| 53600.343 | 85.33 | 143.5 | 0.949 | 0.112 |
| 53600.351 | 86.90 | 140.1 | 0.888 | 0.109 |
| 53600.358 | 88.37 | 137.3 | 0.981 | 0.096 |
| 53600.366 | 89.94 | 134.4 | 0.940 | 0.125 |
| 53600.374 | 91.49 | 131.6 | 0.950 | 0.114 |
| 53600.389 | 94.61 | 126.3 | 0.881 | 0.076 |
| 53600.399 | 96.39 | 123.4 | 0.884 | 0.084 |
| 53600.406 | 97.82 | 121.1 | 0.885 | 0.099 |
| 53600.414 | 99.19 | 118.8 | 1.164 | 0.200 |
| 53600.422 | 100.57 | 116.5 | 1.176 | 0.160 |
| 53600.430 | 101.85 | 114.2 | 0.878 | 0.082 |
| 53600.438 | 103.06 | 112.0 | 0.904 | 0.068 |
| 53600.447 | 104.28 | 109.5 | 0.857 | 0.094 |
| 53600.456 | 105.24 | 107.3 | 1.393 | 0.106 |
| 53600.467 | 106.36 | 104.4 | 1.337 | 0.119 |
| 53600.476 | 107.03 | 102.1 | 0.826 | 0.069 |
| 53600.487 | 107.57 | 99.6 | 0.985 | 0.160 |
| 53600.498 | 107.88 | 96.8 | 1.697 | 0.486 |
| 53601.274 | 77.22 | 173.8 | 0.901 | 0.099 |
| 53601.282 | 77.61 | 169.9 | 0.872 | 0.090 |
| 53601.290 | 78.16 | 166.2 | 0.928 | 0.112 |
| 53601.298 | 78.93 | 162.3 | 0.480 | 0.291 |
| 53601.307 | 80.02 | 157.9 | 0.797 | 0.097 |
| 53601.316 | 81.24 | 153.9 | 0.873 | 0.089 |
| 53601.325 | 82.62 | 149.9 | 0.914 | 0.121 |
| 53601.332 | 83.88 | 146.8 | 0.833 | 0.072 |

Continued on Next Page...

Table. C.2 – Continued

| MJD | B (m) | PA (deg) | V_c | $\sigma(V_c)$ |
|------------|------------------|---------------------|-------------------------|---------------------------------|
| 53601.340 | 85.29 | 143.5 | 0.897 | 0.091 |
| 53601.347 | 86.68 | 140.6 | 0.923 | 0.080 |
| 53601.355 | 88.25 | 137.5 | 0.895 | 0.083 |
| 53601.364 | 90.06 | 134.1 | 0.853 | 0.106 |
| 53601.372 | 91.75 | 131.2 | 0.835 | 0.091 |
| 53601.381 | 93.39 | 128.4 | 1.029 | 0.131 |
| 53601.388 | 94.95 | 125.8 | 0.795 | 0.116 |
| 53601.404 | 97.99 | 120.8 | 0.823 | 0.137 |
| 53601.412 | 99.36 | 118.5 | 0.818 | 0.106 |
| 53601.432 | 102.57 | 112.9 | 0.807 | 0.090 |
| 53601.440 | 103.68 | 110.7 | 0.787 | 0.060 |

C.2.2 Nightly Data Plots

The data for 2005/08/18 show some extreme dips in the calibrator’s visibilities in the second half of the dataset. This is probably not due to seeing conditions, as the surrounding object and calibrator visibilities remain steady, so were most likely due to some instrumental difficulties. These data points, and the object’s data points immediately before and after, were given zero weight in the diameter calculation and the companion check.

Something similar occurred in the 2005/08/19 dataset, though only once. This object’s data point was given zero weight and not taken into account for the diameter measurement or companion check.

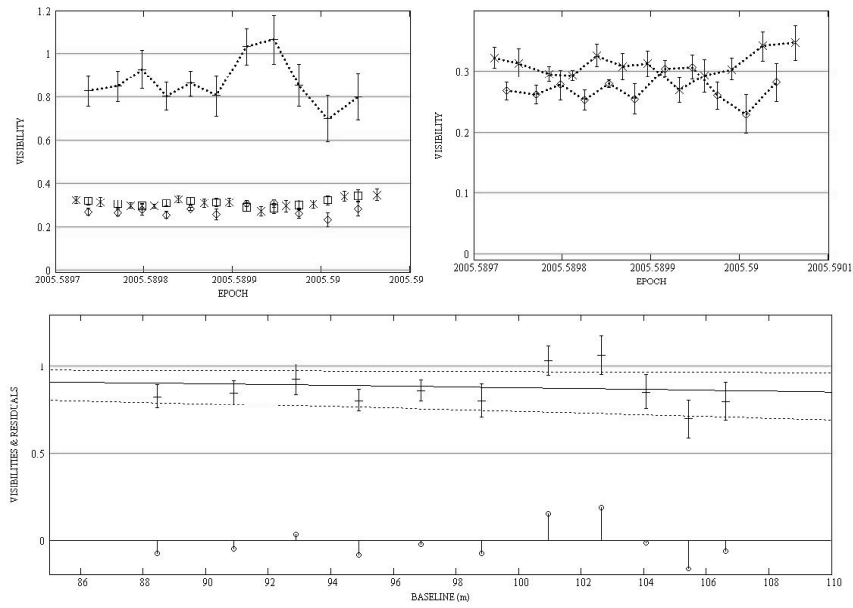


Figure. C.12: HD 9826: Intermediate baseline plots for 2005/08/04 data.

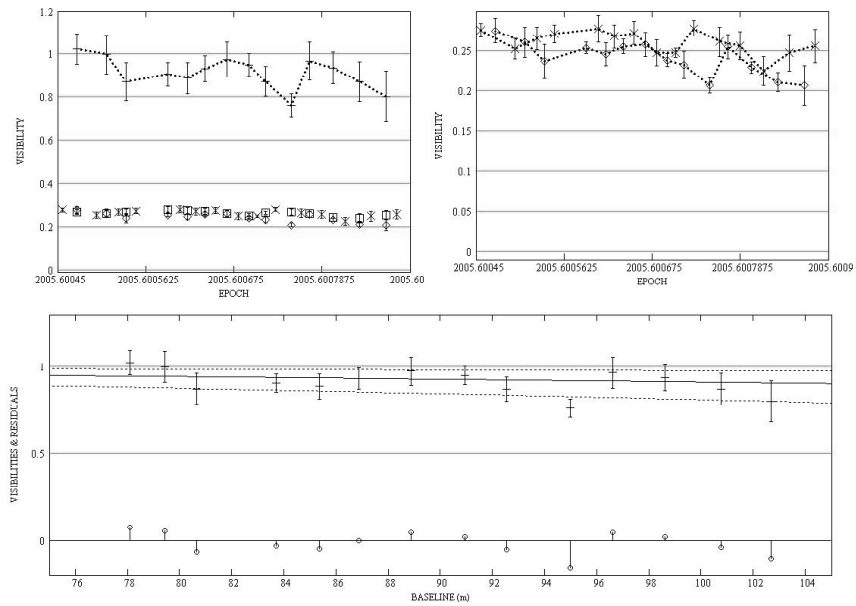


Figure. C.13: HD 9826: Intermediate baseline plots for 2005/08/08 data.

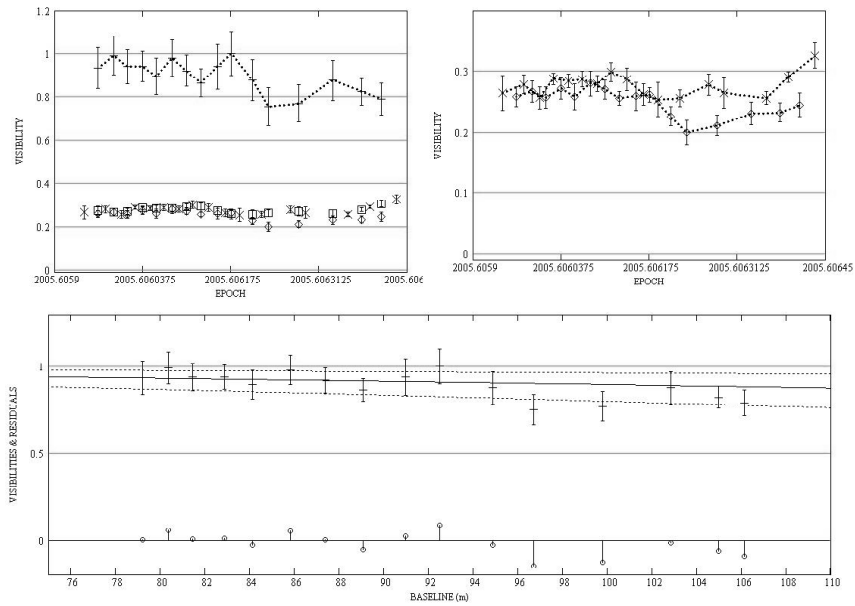


Figure. C.14: HD 9826: Intermediate baseline plots for 2005/08/10 data.

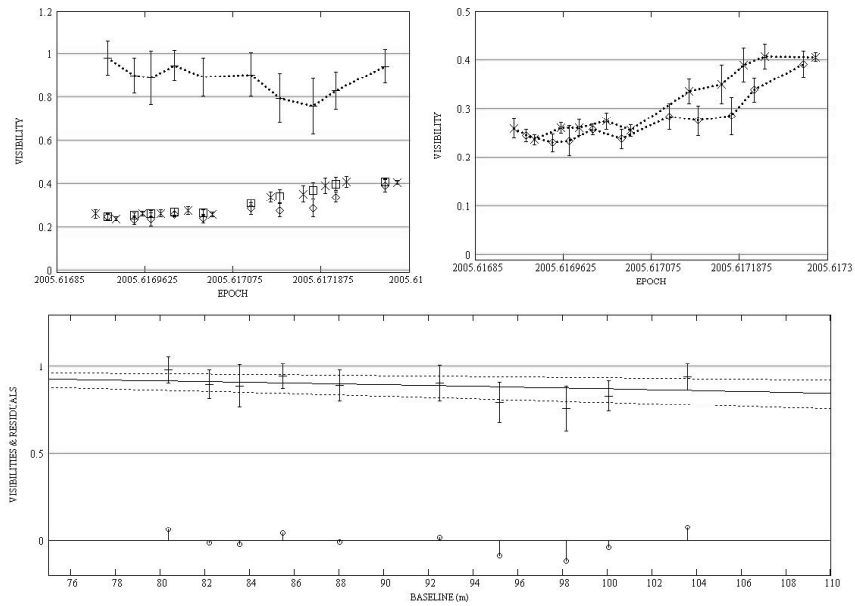


Figure. C.15: HD 9826: Intermediate baseline plots for 2005/08/14 data.

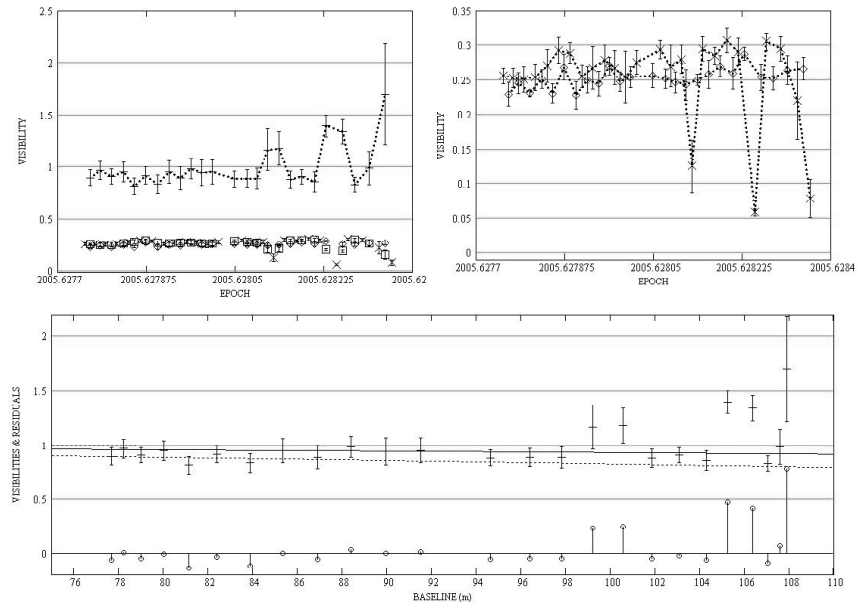


Figure. C.16: HD 9826: Intermediate baseline plots for 2005/08/18 data.

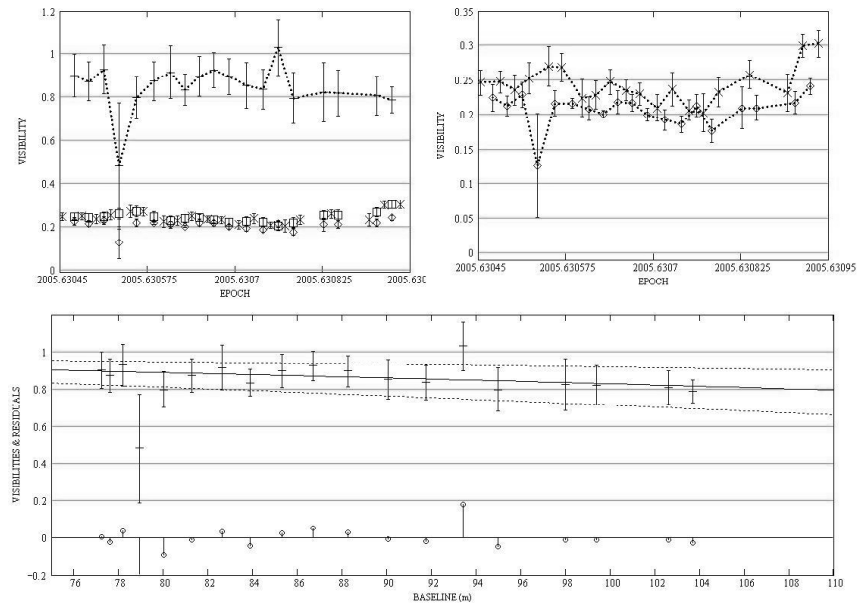


Figure. C.17: HD 9826: Intermediate baseline plots for 2005/08/19 data.

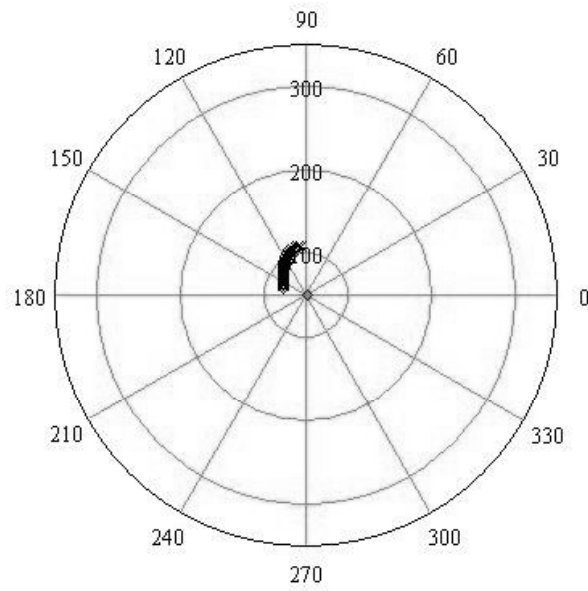


Figure. C.18: HD 9826: All data - Baseline vs. baseline position angle (using calibrator HD 6920).

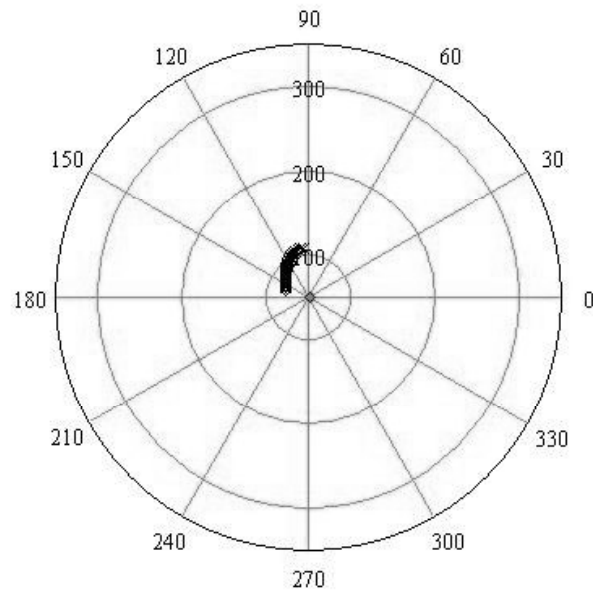


Figure. C.19: HD 9826: All data - Baseline vs. baseline position angle (using calibrator HD 8671).

C.2.3 Diameter Calculation

Due to the lack of long-baseline observations, I used all the intermediate-baseline data in the diameter calculation.

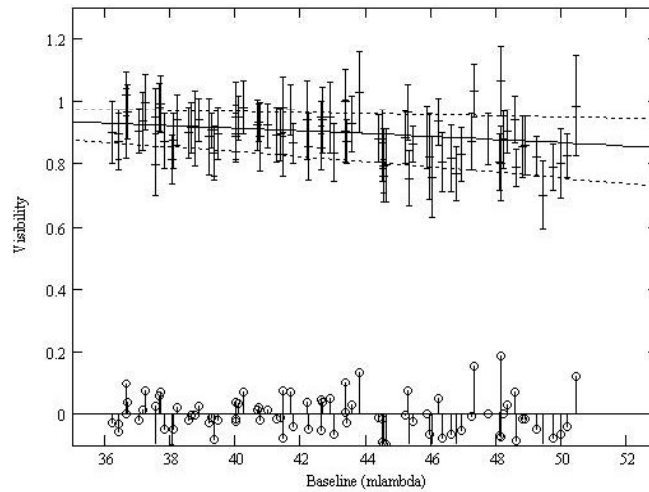


Figure. C.20: HD 9826: LD disk diameter fits: Visibility vs. baseline.

C.2.4 SFP Search

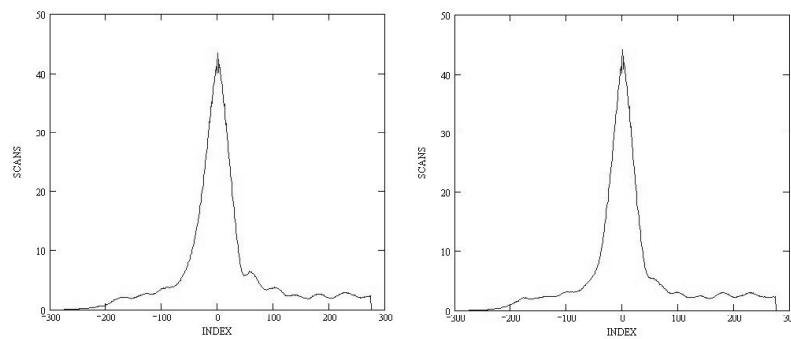


Figure. C.21: HD 9826: SFP inspection for 2005/08/04 data.

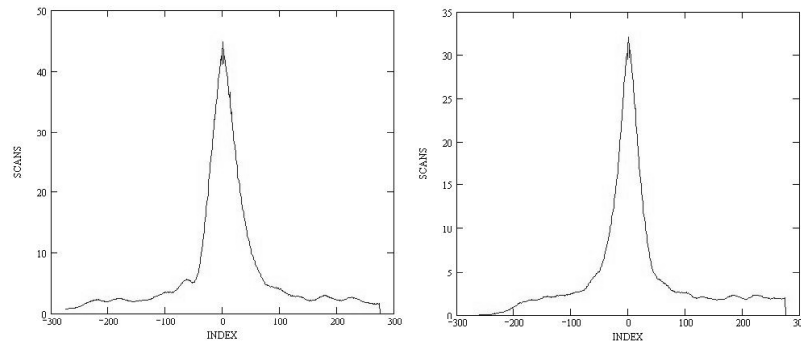


Figure. C.22: HD 9826: SFP inspection for 2005/08/08 data.

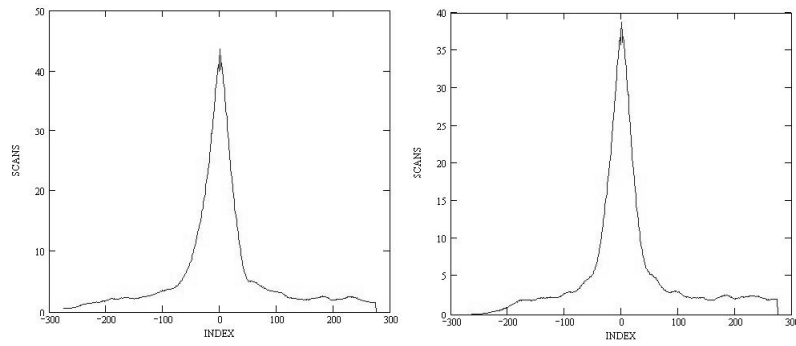


Figure. C.23: HD 9826: SFP inspection for 2005/08/10 data.

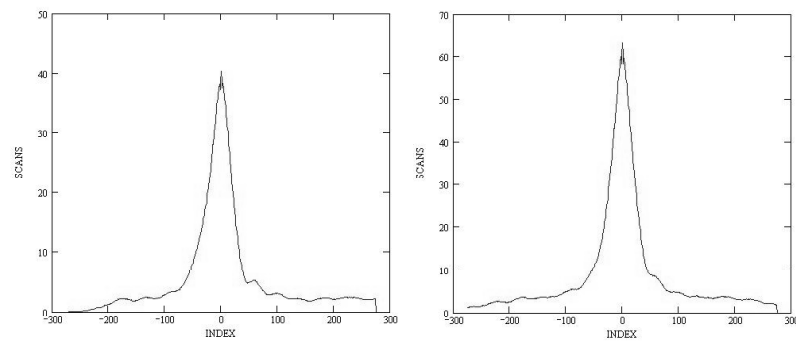


Figure. C.24: HD 9826: SFP inspection for 2005/08/14 data.

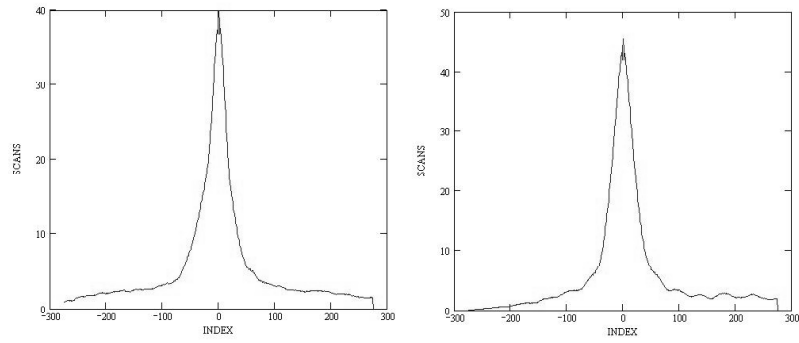


Figure. C.25: HD 9826: SFP inspection for 2005/08/18 data.

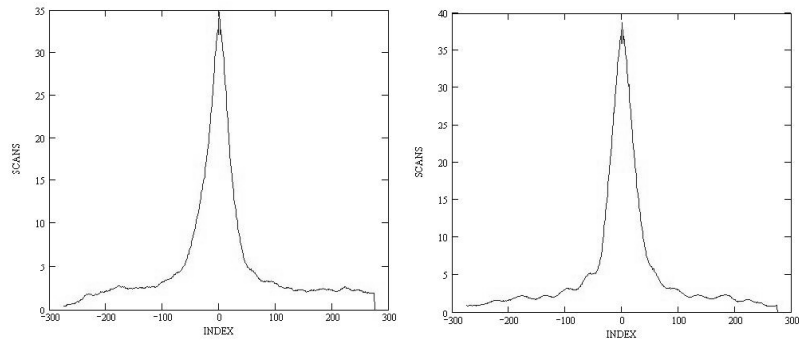


Figure. C.26: HD 9826: SFP inspection for 2005/08/19 data.

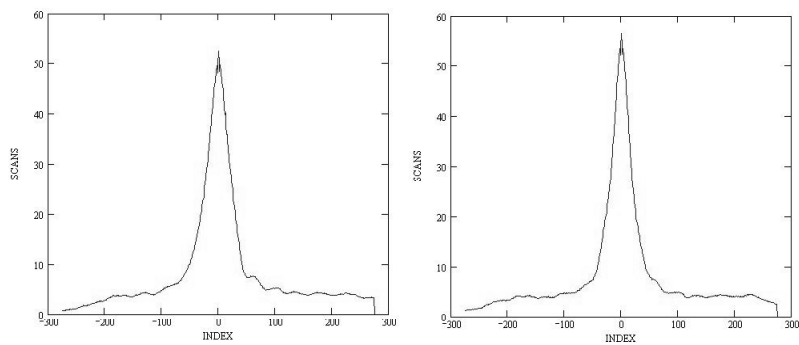


Figure. C.27: HD 6920: SFP inspection for 2005/08/04 data.

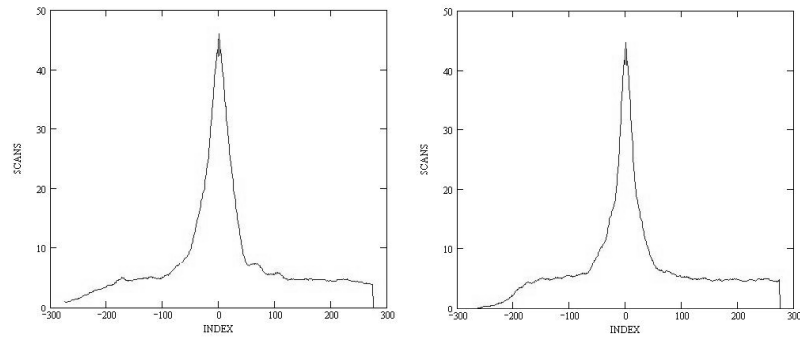


Figure. C.28: HD 6920: SFP inspection for 2005/08/08 data.

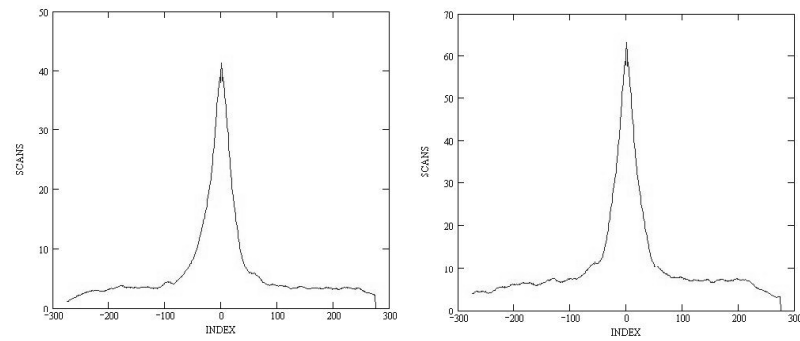


Figure. C.29: HD 6920: SFP inspection for 2005/08/14 data.

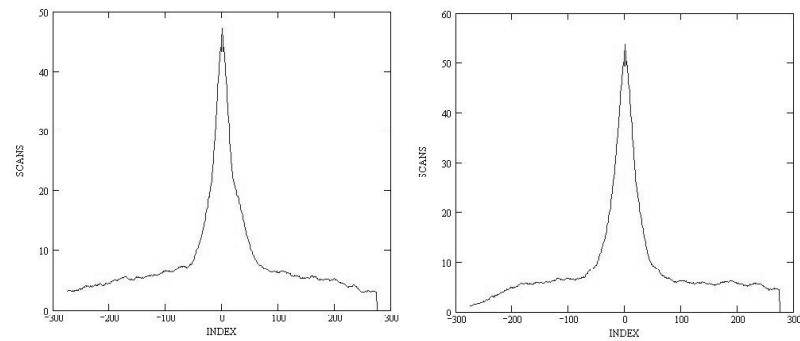


Figure. C.30: HD 8671: SFP inspection for 2005/08/10 data.

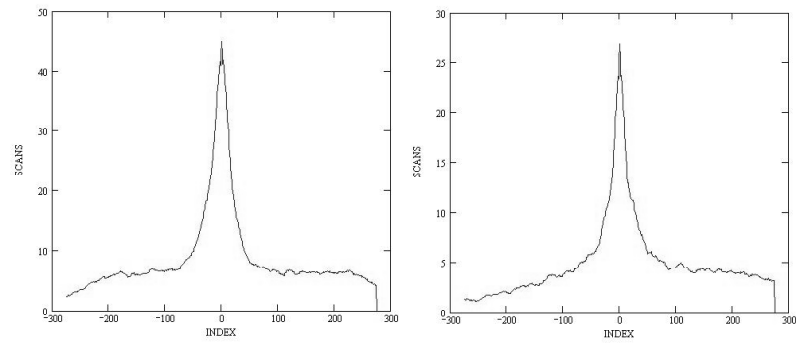


Figure. C.31: HD 8671: SFP inspection for 2005/08/18 data.

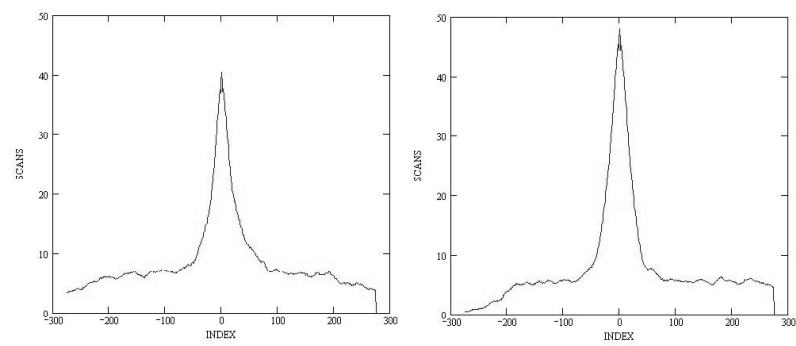


Figure. C.32: HD 8671: SFP inspection for 2005/08/19 data.

C.3 HD 10697

C.3.1 Calibrated Visibilities

Table. C.3: HD 10697: Calibrated Visibilities

| MJD | B (m) | PA (deg) | V_c | $\sigma(V_c)$ |
|-----------|----------|-------------|-------|---------------|
| 53666.348 | 313.95 | 194.6 | 0.807 | 0.089 |
| 53666.375 | 310.54 | 188.2 | 0.829 | 0.072 |
| 53666.389 | 309.46 | 184.7 | 0.831 | 0.078 |
| 53666.427 | 309.50 | 175.2 | 1.032 | 0.089 |
| 53666.443 | 310.79 | 171.2 | 0.919 | 0.068 |
| 53666.456 | 312.37 | 167.9 | 0.993 | 0.103 |
| 53666.470 | 314.46 | 164.6 | 0.823 | 0.075 |
| 53959.407 | 330.02 | 218.5 | 1.049 | 0.068 |
| 53959.422 | 330.65 | 216.8 | 1.192 | 0.121 |
| 53959.440 | 330.23 | 214.6 | 1.103 | 0.141 |
| 53959.455 | 328.99 | 212.3 | 1.102 | 0.105 |
| 53959.471 | 327.01 | 209.8 | 1.040 | 0.096 |
| 53959.486 | 324.57 | 207.1 | 0.896 | 0.068 |
| 53959.501 | 321.84 | 204.2 | 0.848 | 0.066 |

C.3.2 Nightly Data Plots

The first three calibrator and object measurements were removed from the 2005/10/23 dataset due to long spacing between observations. Figure C.33 shows all the observations, but only the final four bracketed observations were used in the diameter measurement and companion check. With the trend of the visibilities rising, which was probably due to changing seeing, the gaps in time became important as it was not at all certain that the sky conditions were the same between observations.

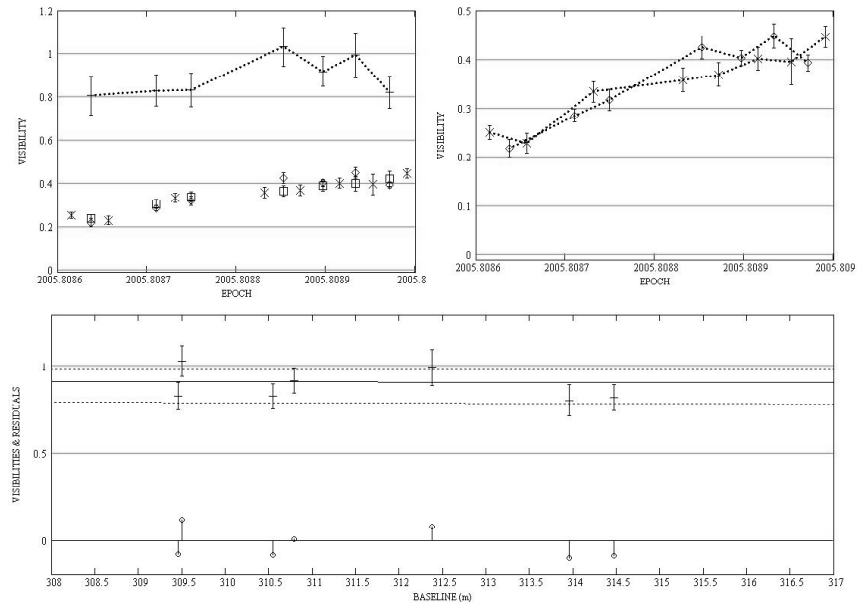


Figure. C.33: HD 10697: Long baseline plots for 2005/10/23 data.

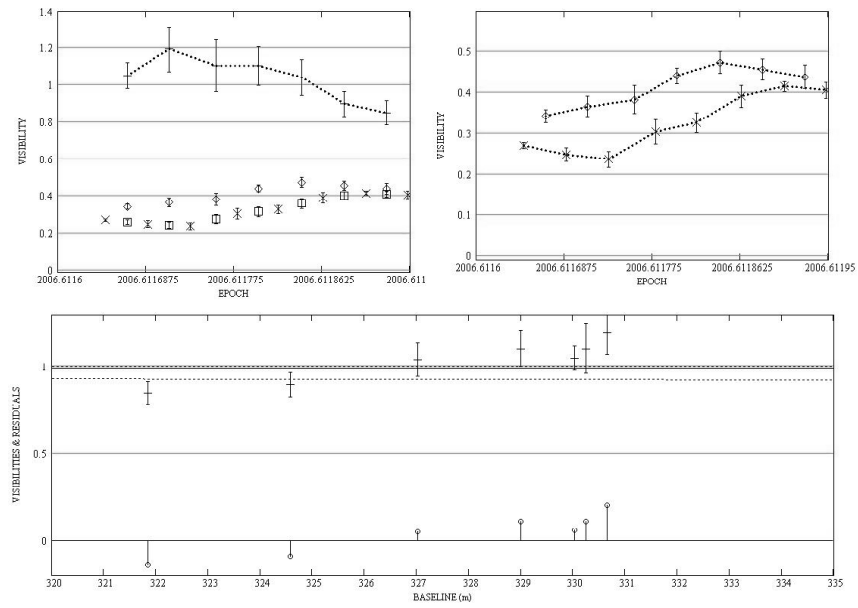


Figure. C.34: HD 10697: Long baseline plots for 2006/08/12 data.

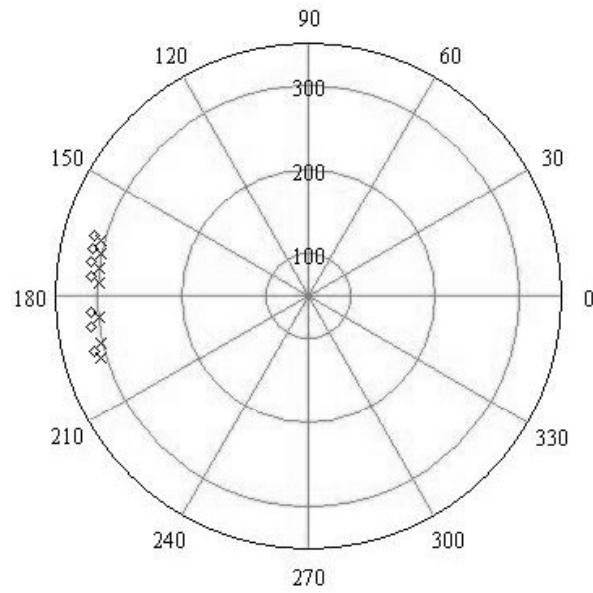


Figure. C.35: HD 10697: All data - Baseline vs. baseline position angle (using calibrator HD 10477).

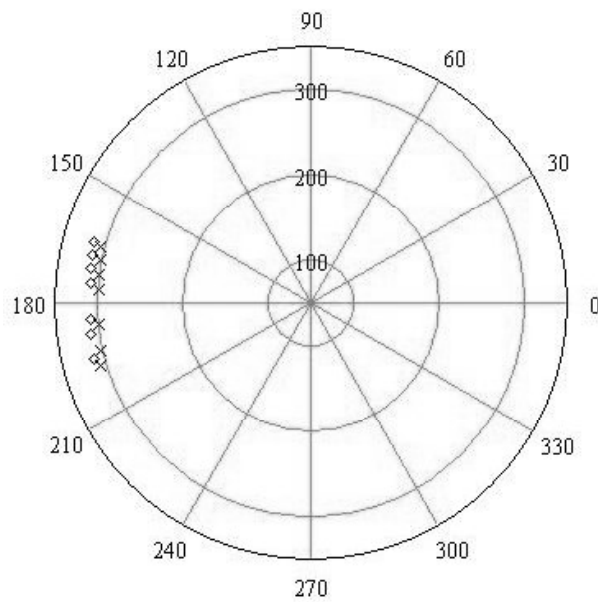


Figure. C.36: HD 10697: All data - Baseline vs. baseline position angle (using calibrator HD 13555).

C.3.3 Diameter Calculation

For the diameter measurement, I used the dataset from 2005/10/23 alone due to the fact that the diameter produced by the 2006/08/12 dataset boasted an error approximately twice that of the diameter itself ($\theta_{\text{UD}} = 0.128 \pm 0.203$ mas). Even the diameter obtained from the 2005/10/23 data has a $\sim 70\%$ error, which is far from ideal, but is an improvement over the other dataset.

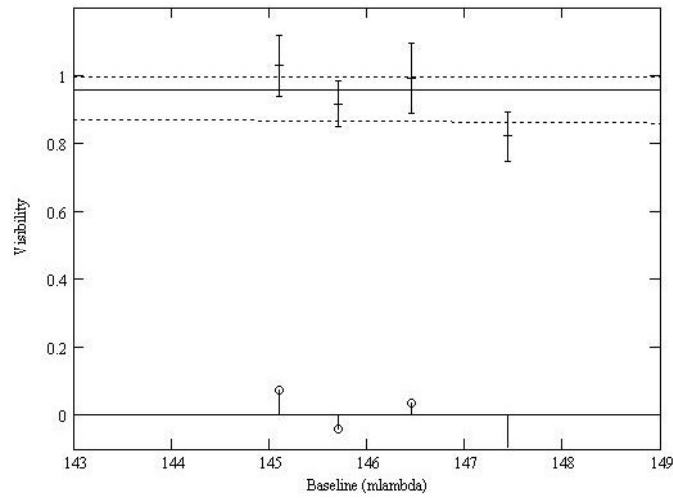


Figure. C.37: HD 10697: LD disk diameter fits: Visibility vs. baseline.

C.3.4 SFP Search

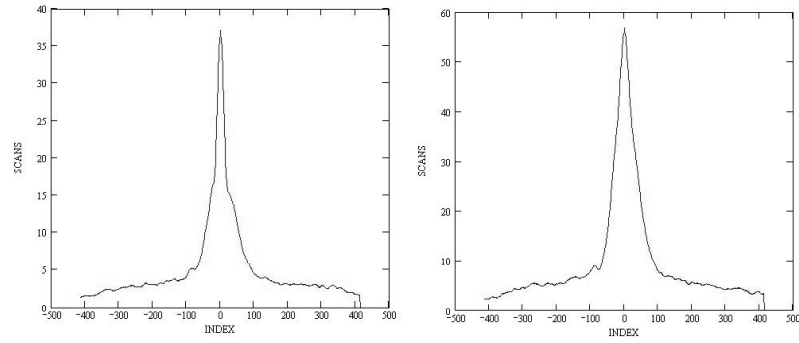


Figure. C.38: HD 10697: SFP inspection for 2005/10/23 data.

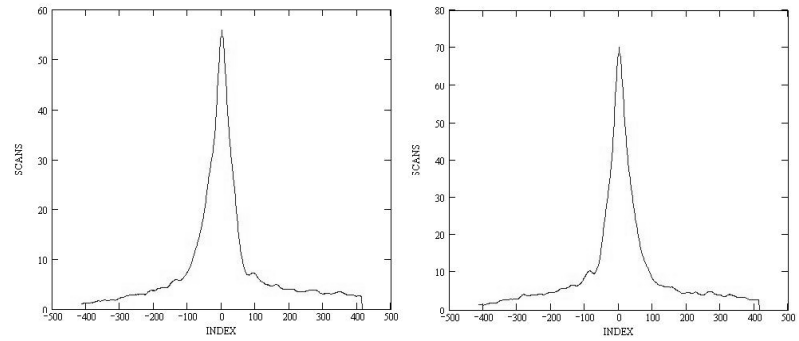


Figure. C.39: HD 10697: SFP inspection for 2006/08/12 data.

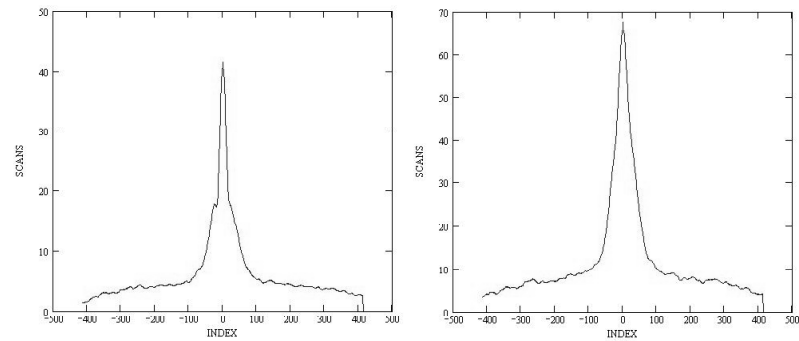


Figure. C.40: HD 10477: SFP inspection for 2005/10/23 data.

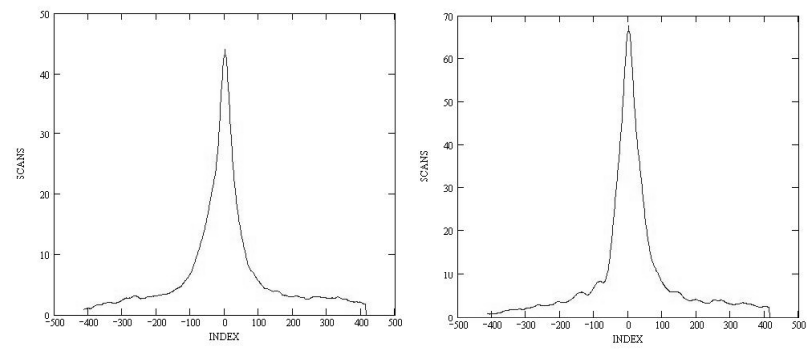


Figure. C.41: HD 13555: SFP inspection for 2006/08/12 data.

C.4 HD 11964

C.4.1 Calibrated Visibilities

Table. C.4: HD 11964: Calibrated Visibilities

| MJD | B (m) | PA (deg) | V_c | $\sigma(V_c)$ |
|-----------|----------|-------------|-------|---------------|
| 53717.251 | 269.51 | 127.3 | 0.831 | 0.103 |
| 53720.235 | 266.70 | 127.3 | 0.847 | 0.062 |
| 53720.249 | 271.65 | 127.3 | 0.822 | 0.064 |
| 53720.262 | 274.99 | 127.6 | 0.774 | 0.092 |
| 53720.276 | 277.41 | 128.1 | 0.832 | 0.147 |
| 53720.293 | 278.47 | 128.9 | 0.885 | 0.132 |
| 54028.265 | 90.42 | 268.5 | 0.915 | 0.097 |
| 54028.276 | 94.30 | 269.3 | 0.875 | 0.087 |
| 54028.289 | 98.01 | 90.0 | 0.951 | 0.097 |
| 54028.312 | 103.60 | 91.4 | 0.802 | 0.112 |
| 54028.323 | 105.45 | 92.1 | 0.960 | 0.108 |
| 54028.335 | 106.82 | 92.8 | 0.999 | 0.100 |
| 54028.349 | 107.75 | 93.6 | 0.935 | 0.107 |

C.4.2 Nightly Data Plots

The 2005/12/13 dataset only has one bracketed data point, and while that is useful for calculating diameter (when combined with the 2005/12/16 data), it was not considered in the companion search.

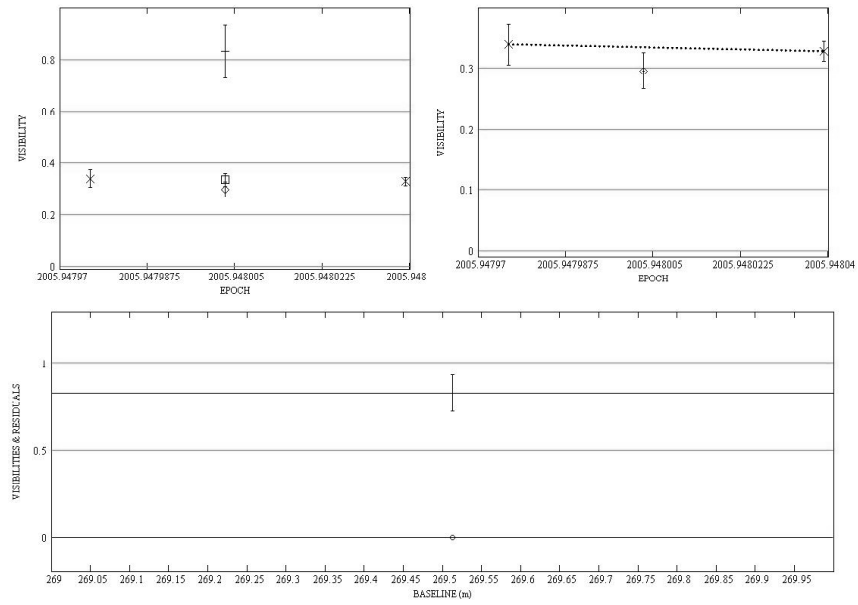


Figure. C.42: HD 11964: Intermediate baseline plots for 2005/12/13 data.

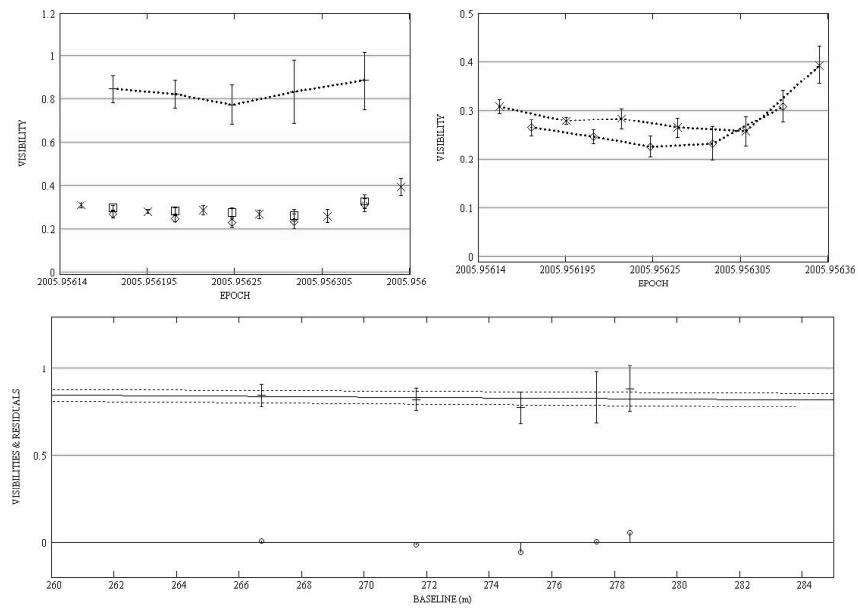


Figure. C.43: HD 11964: Intermediate baseline plots for 2005/12/16 data.

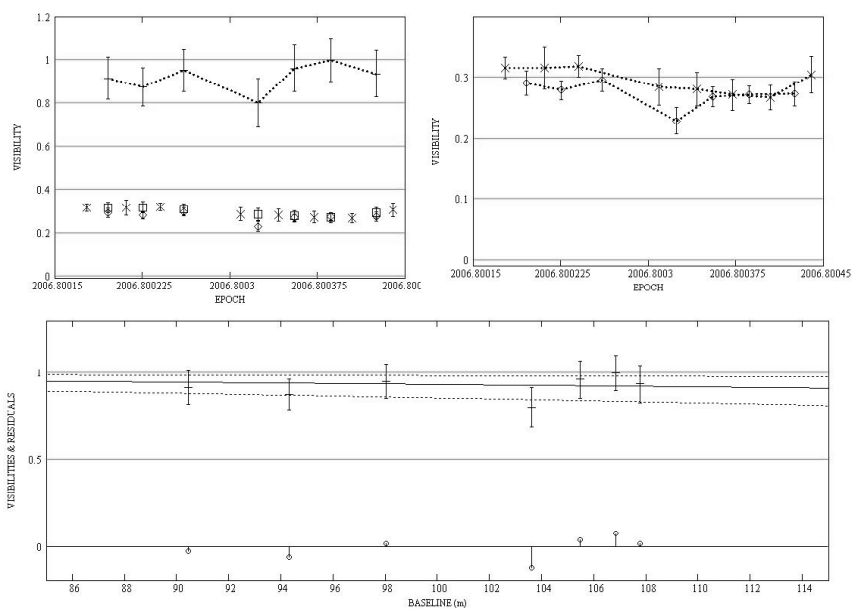


Figure. C.44: HD 11964: Intermediate baseline plots for 2006/10/20 data.

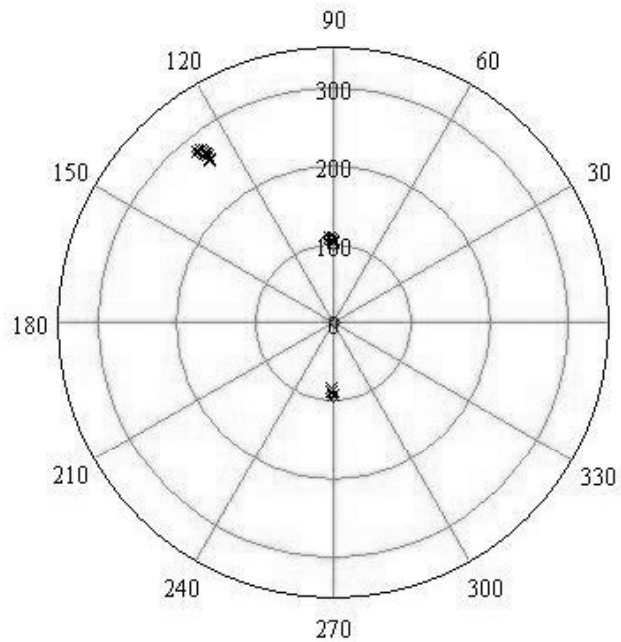


Figure. C.45: HD 11964: All data - Baseline vs. baseline position angle.

C.4.3 Diameter Calculation

Because no data were obtained with the longest baseline, I used the W1-S1 data to calculate the angular diameter, as it is significantly longer than the W1-W2 baseline (279 m as opposed to 108 m) and is the next best substitute to S1-E1 baseline observations.

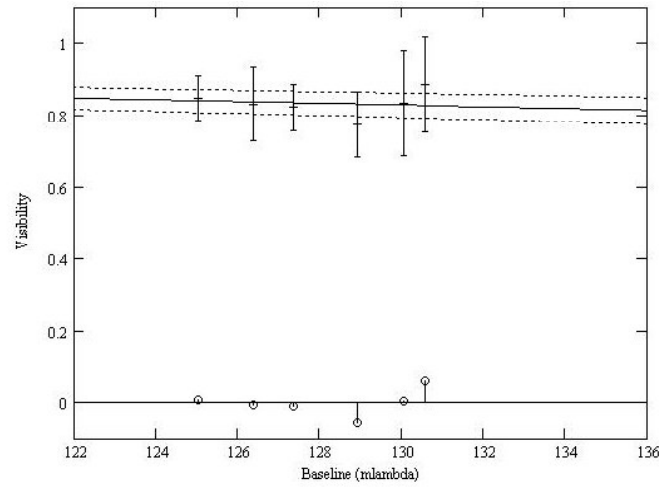


Figure. C.46: HD 11964: LD disk diameter fit: Visibility vs. baseline.

C.4.4 SFP Search

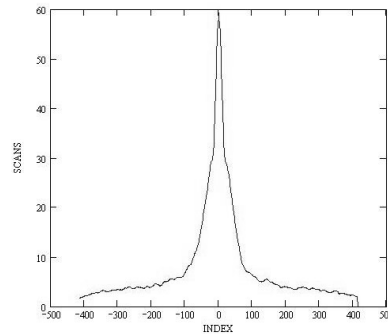


Figure. C.47: HD 11964: SFP inspection for 2005/12/13 data.

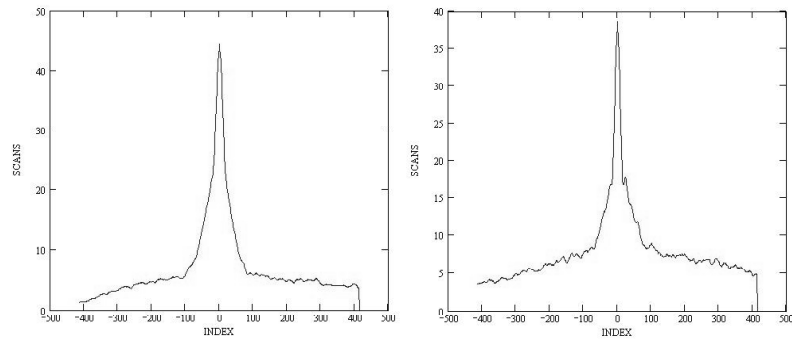


Figure. C.48: HD 11964: SFP inspection for 2005/12/16 data.

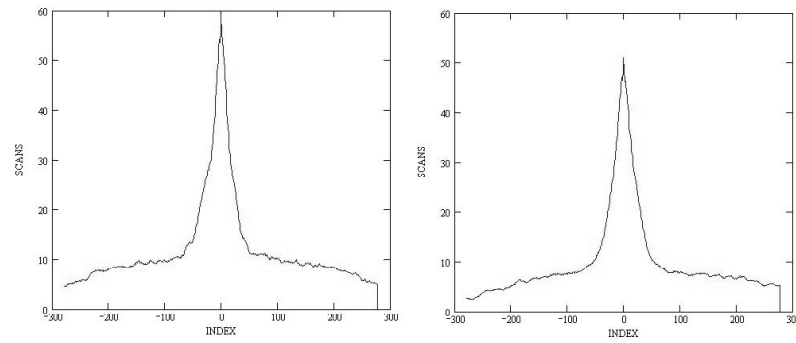


Figure. C.49: HD 11964: SFP inspection for 2006/10/20 data.

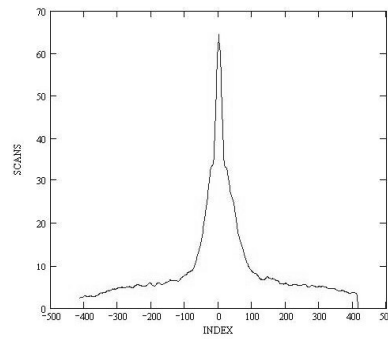


Figure. C.50: HD 13456: SFP inspection for 2005/12/13 data.

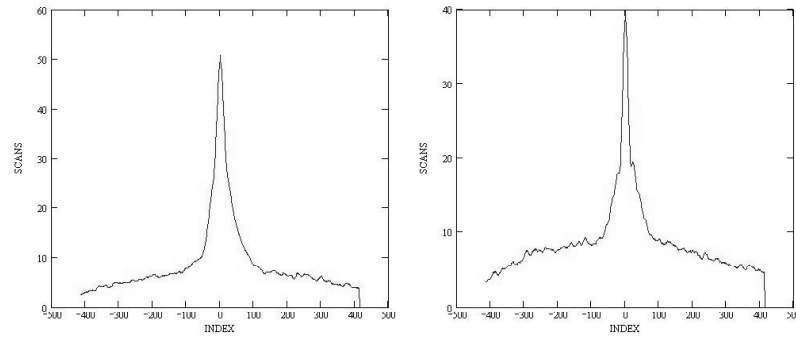


Figure. C.51: HD 13456: SFP inspection for 2005/12/16 data.

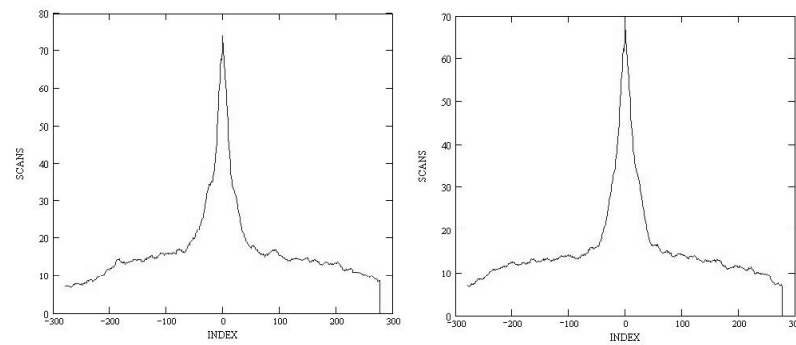


Figure. C.52: HD 13456: SFP inspection for 2006/10/20 data.

C.5 HD 13189

C.5.1 Calibrated Visibilities

Table. C.5: HD 13189: Calibrated Visibilities

| MJD | B (m) | PA (deg) | V_c | $\sigma(V_c)$ |
|-----------|----------|-------------|-------|---------------|
| 53716.270 | 327.09 | 184.4 | 0.610 | 0.056 |
| 53716.285 | 326.91 | 180.9 | 0.533 | 0.082 |
| 53716.298 | 326.96 | 177.7 | 0.591 | 0.096 |
| 53716.312 | 327.21 | 174.3 | 0.578 | 0.131 |
| 53961.441 | 326.60 | 216.4 | 0.625 | 0.052 |
| 53961.454 | 328.41 | 214.4 | 0.651 | 0.063 |
| 53961.467 | 329.65 | 212.2 | 0.646 | 0.073 |
| 53961.481 | 330.38 | 209.8 | 0.610 | 0.040 |

C.5.2 Nightly Data Plots

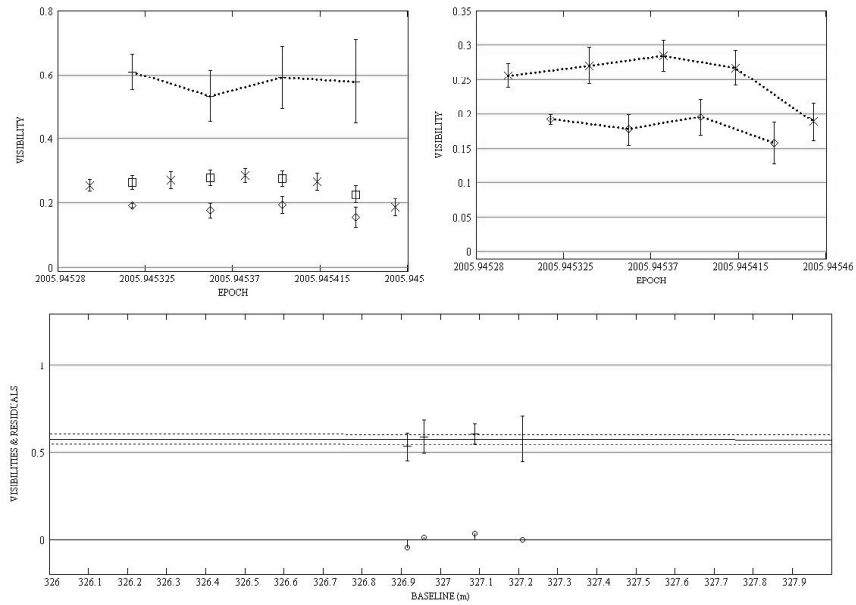


Figure. C.53: HD 13189: Long baseline plots for 2005/12/12 data.

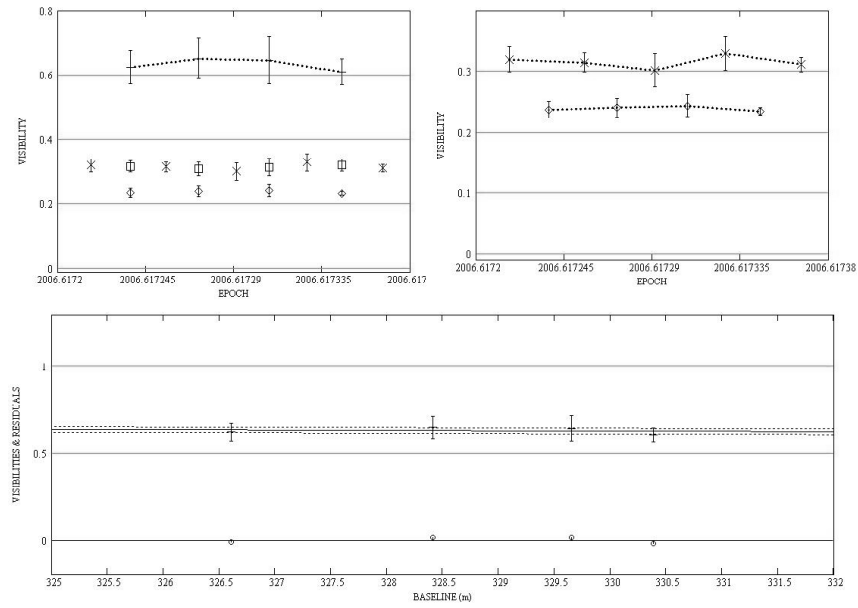


Figure. C.54: HD 13189: Long baseline plots for 2006/08/14 data.

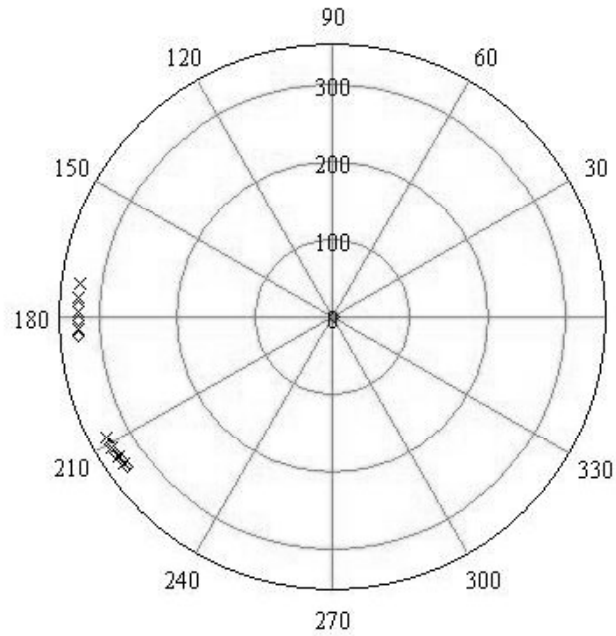


Figure. C.55: HD 13189: All data - Baseline vs. baseline position angle.

C.5.3 Diameter Calculation

All the data were used in the diameter calculation.

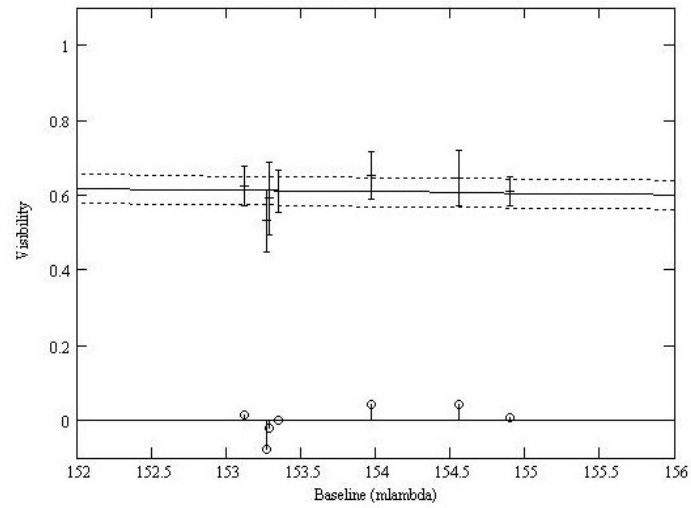


Figure. C.56: HD 13189: LD disk diameter fit: Visibility vs. baseline.

C.5.4 SFP Search

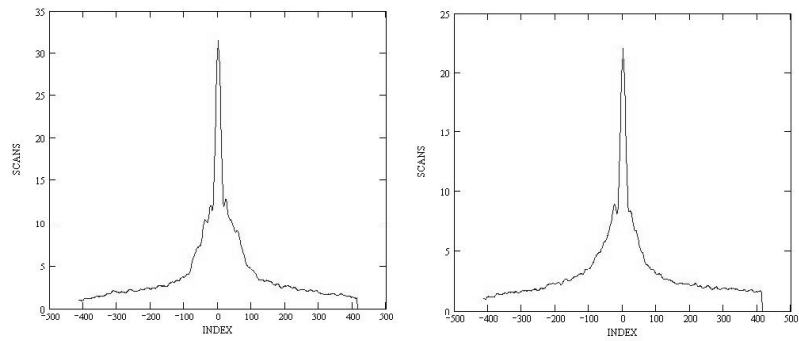


Figure. C.57: HD 13189: SFP inspection for 2005/12/12 data.

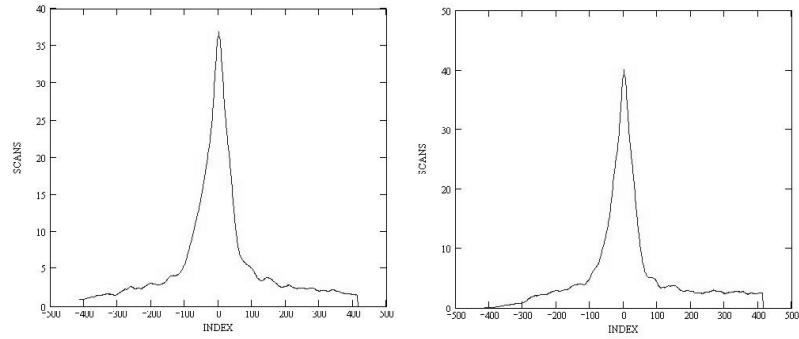


Figure. C.58: HD 13189: SFP inspection for 2006/08/14 data.

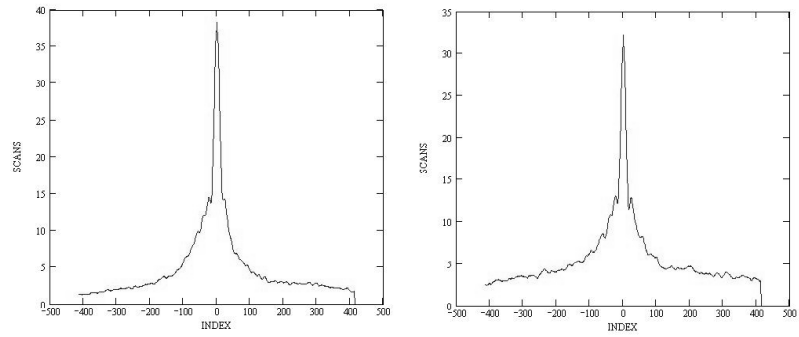


Figure. C.59: HD 11007: SFP inspection for 2005/12/12 data.

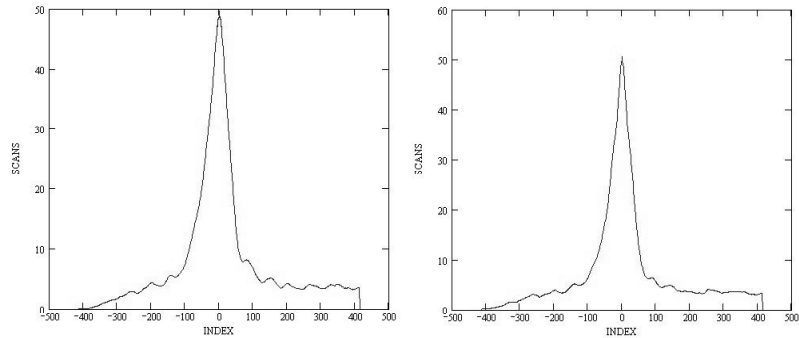


Figure. C.60: HD 11007: SFP inspection for 2006/08/14 data.

C.5.5 Companion Check

Due to the very small parallax of HD 13189 (0.54 mas), the calculation for secondary stars' angular sizes produced diameters < 0.005 mas for all cases. Given that the host

star is a K2 III and the ΔK between HD 13189 and the brightest possible companion, a G5 V, would have been 10.8 magnitudes, I did not even make the attempt to find stellar companions in the data. All binary visibility curves would have been essentially identical to the single star visibility curves.

C.6 HD 16141

C.6.1 Calibrated Visibilities

Table. C.6: HD 16141: Calibrated Visibilities

| MJD | B (m) | PA (deg) | V_c | $\sigma(V_c)$ |
|-----------|----------|-------------|-------|---------------|
| 53716.107 | 321.23 | 219.9 | 1.293 | 0.346 |
| 53716.127 | 314.31 | 218.6 | 1.027 | 0.218 |
| 53716.140 | 308.47 | 217.5 | 0.952 | 0.173 |
| 53716.154 | 301.68 | 216.0 | 0.942 | 0.145 |
| 53716.170 | 293.80 | 214.1 | 1.102 | 0.137 |
| 53716.187 | 284.05 | 211.3 | 0.494 | 0.120 |
| 53716.204 | 275.11 | 208.4 | 1.138 | 0.103 |
| 53716.231 | 260.54 | 202.2 | 0.657 | 0.195 |
| 53718.238 | 261.28 | 130.3 | 1.152 | 0.084 |
| 53718.251 | 266.84 | 129.4 | 1.102 | 0.102 |
| 53718.264 | 271.37 | 128.9 | 1.268 | 0.131 |
| 53718.278 | 274.95 | 128.5 | 1.121 | 0.133 |
| 53718.292 | 277.41 | 128.3 | 1.032 | 0.142 |
| 53718.307 | 278.45 | 128.3 | 1.295 | 0.156 |
| 53718.323 | 277.92 | 128.7 | 2.036 | 0.235 |
| 53960.413 | 327.64 | 220.8 | 1.011 | 0.134 |
| 53960.426 | 324.76 | 220.4 | 1.019 | 0.123 |
| 53960.439 | 320.99 | 219.8 | 0.986 | 0.072 |
| 53960.454 | 315.74 | 218.9 | 0.910 | 0.091 |
| 53961.373 | 330.61 | 220.8 | 0.985 | 0.098 |
| 53961.386 | 330.43 | 221.0 | 0.930 | 0.082 |
| 53961.400 | 329.24 | 221.0 | 0.993 | 0.094 |
| 53961.413 | 327.07 | 220.7 | 0.978 | 0.097 |

C.6.2 Nightly Data Plots

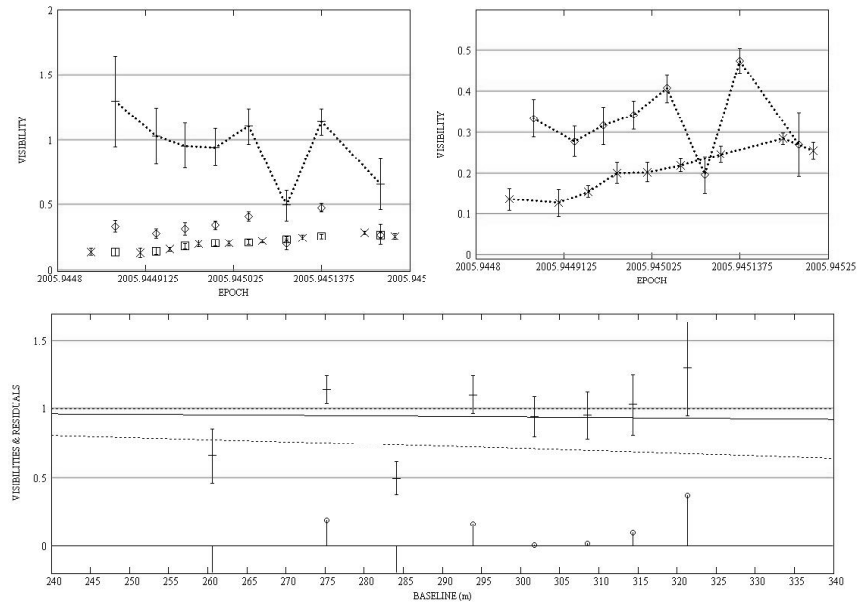


Figure. C.61: HD 16141: Long baseline plots for 2005/12/12 data.

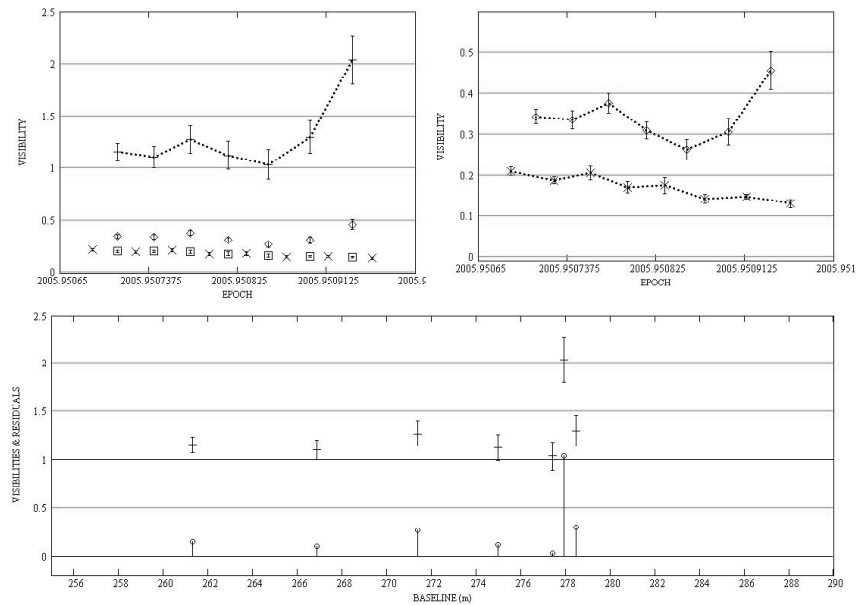


Figure. C.62: HD 16141: Intermediate baseline plots for 2005/12/14 data.

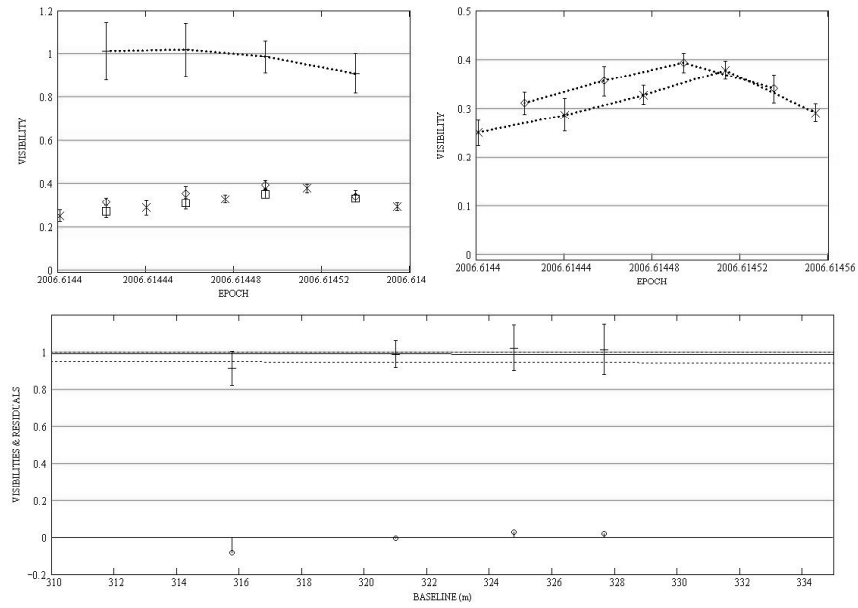


Figure. C.63: HD 16141: Long baseline plots for 2006/08/13 data.

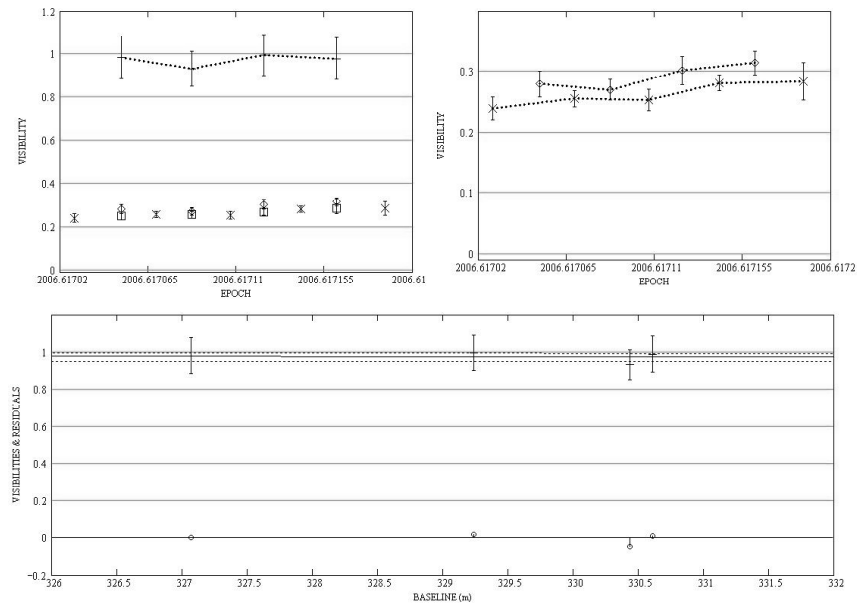


Figure. C.64: HD 16141: Long baseline plots for 2006/08/14 data.

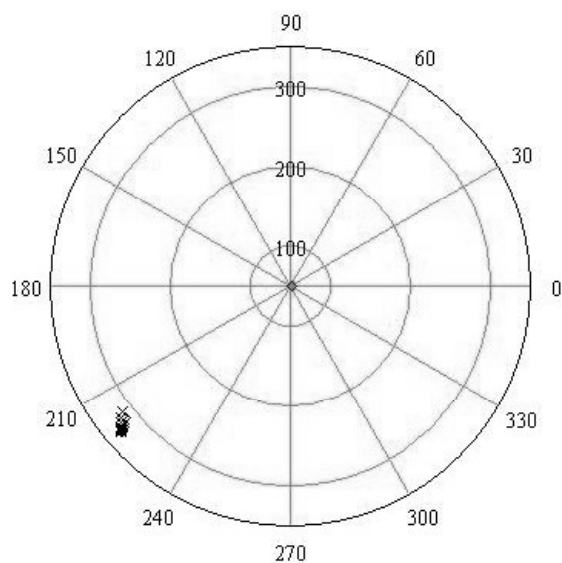


Figure. C.65: HD 16141: All data - Baseline vs. baseline position angle (using calibrator HD 14690).

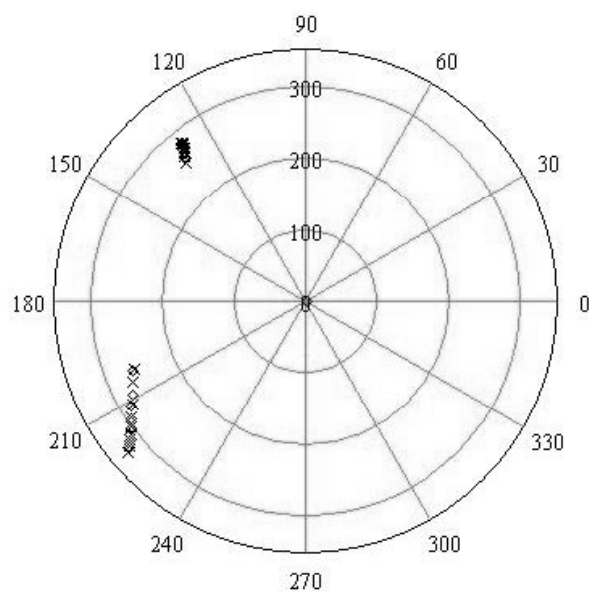


Figure. C.66: HD 16141: All data - Baseline vs. baseline position angle (using calibrator HD 16824).

C.6.3 Diameter Calculation

Only the data obtained using HD 14690 as a calibrator were used in the diameter calculation, as the one night of S1-E1 data using the calibrator HD 16824 produced a UD diameter measurement of 0.332 ± 0.420 mas. The final diameter has a 50% error bar, due to the fact that the exoplanet host star is almost unresolved.

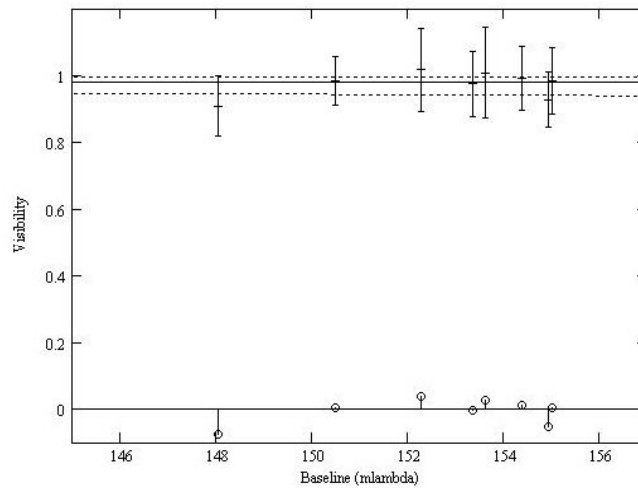


Figure. C.67: HD 16141: LD disk diameter fit: Visibility vs. baseline.

C.6.4 SFP Search

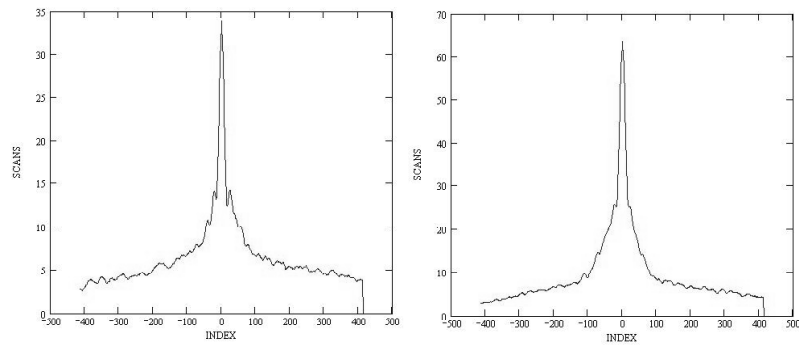


Figure. C.68: HD 16141: SFP inspection for 2005/12/12 data.

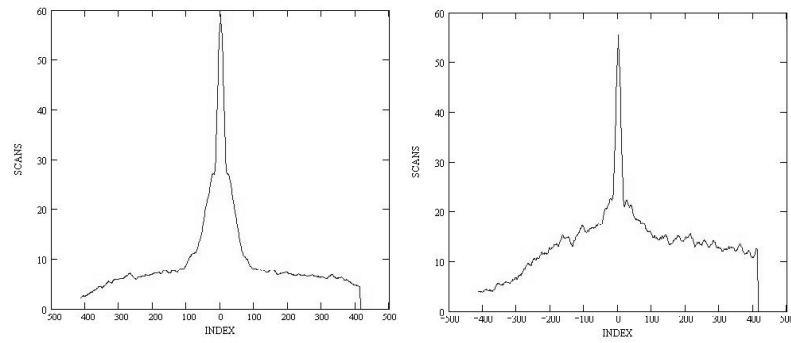


Figure. C.69: HD 16141: SFP inspection for 2005/12/14 data.

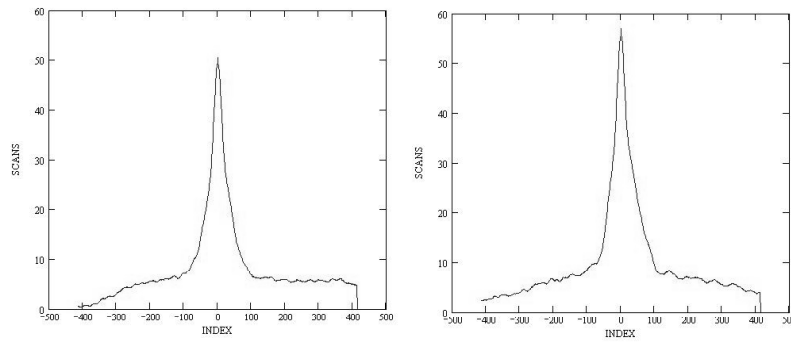


Figure. C.70: HD 16141: SFP inspection for 2006/08/13 data.

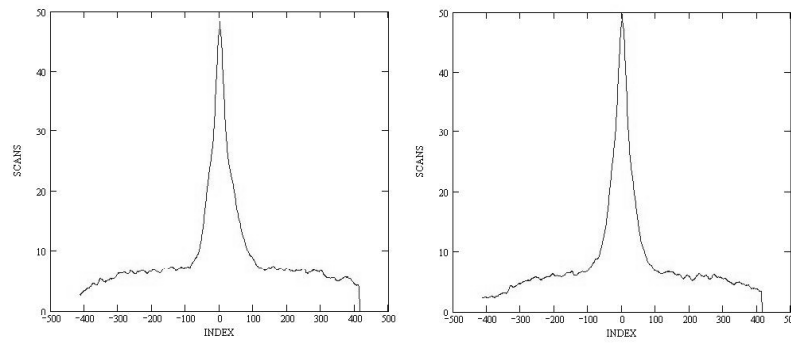


Figure. C.71: HD 16141: SFP inspection for 2006/08/14 data.

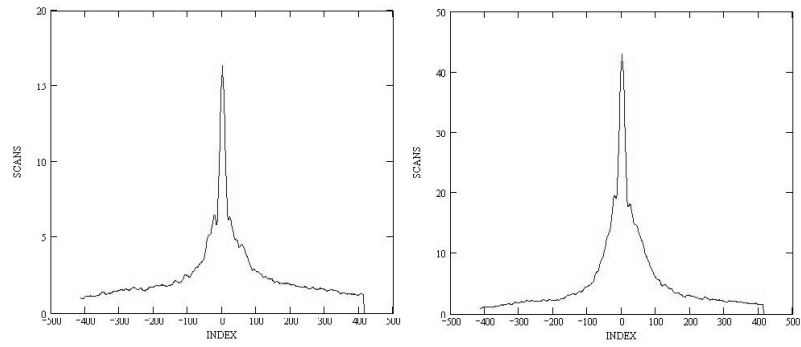


Figure. C.72: HD 16824: SFP inspection for 2005/12/12 data.

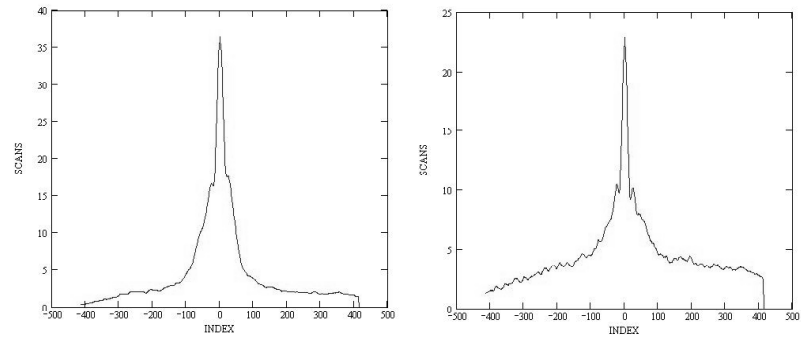


Figure. C.73: HD 16824: SFP inspection for 2005/12/14 data.

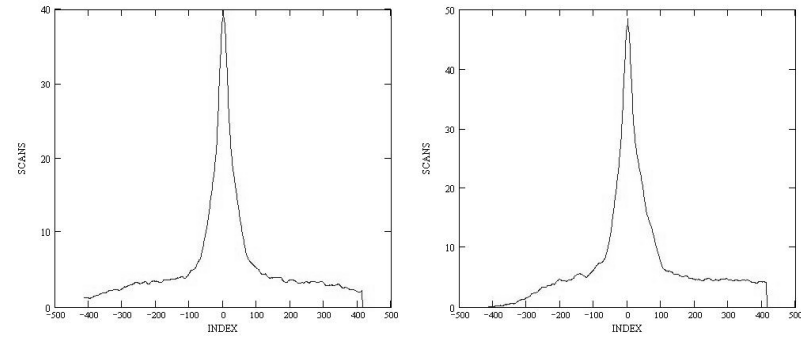


Figure. C.74: HD 14690: SFP inspection for 2006/08/13 data.

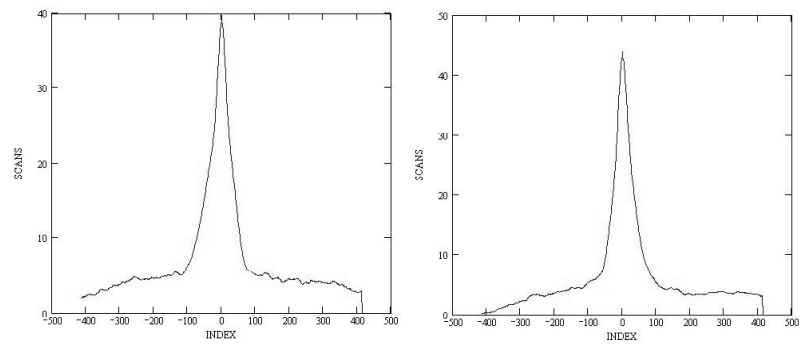


Figure. C.75: HD 14690: SFP inspection for 2006/08/14 data.

C.7 HD 19994

C.7.1 Calibrated Visibilities

Table. C.7: HD 19994: Calibrated Visibilities

| MJD | B (m) | PA (deg) | V_c | $\sigma(V_c)$ |
|-----------|----------|-------------|-------|---------------|
| 53664.336 | 298.13 | 213.8 | 0.589 | 0.068 |
| 53664.352 | 289.93 | 211.4 | 0.736 | 0.073 |
| 53664.365 | 282.82 | 209.0 | 0.669 | 0.056 |
| 53664.379 | 275.99 | 206.4 | 0.597 | 0.062 |
| 53670.286 | 313.43 | 217.6 | 0.752 | 0.080 |
| 53670.301 | 306.97 | 216.1 | 0.728 | 0.084 |
| 53670.316 | 299.70 | 214.3 | 0.692 | 0.056 |
| 53670.333 | 291.04 | 211.8 | 0.764 | 0.076 |
| 53670.350 | 282.40 | 208.9 | 0.706 | 0.050 |
| 53670.367 | 273.57 | 205.4 | 0.791 | 0.048 |
| 53714.182 | 306.59 | 216.0 | 0.714 | 0.083 |
| 53714.208 | 293.70 | 212.6 | 0.796 | 0.107 |
| 53714.220 | 287.27 | 210.6 | 0.787 | 0.078 |
| 53714.239 | 277.71 | 207.1 | 0.713 | 0.069 |
| 53714.254 | 270.20 | 203.9 | 0.774 | 0.067 |
| 53714.266 | 264.26 | 200.9 | 0.831 | 0.096 |

C.7.2 Nightly Data Plots

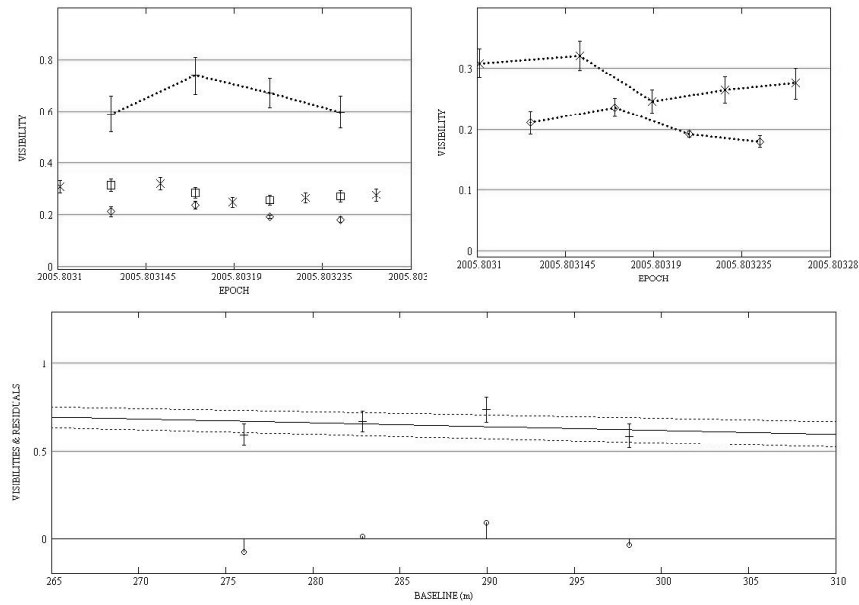


Figure. C.76: HD 19994: Long baseline plots for 2005/10/21 data.

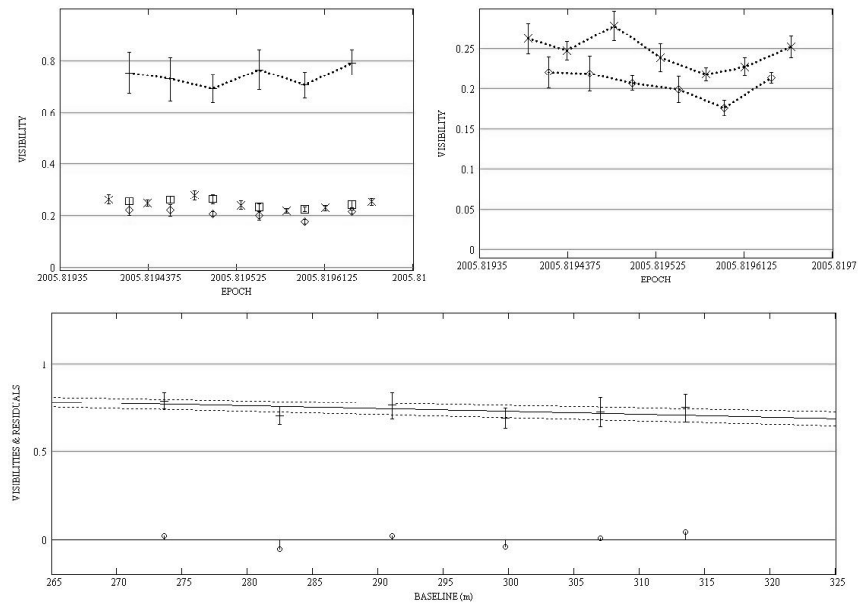


Figure. C.77: HD 19994: Long baseline plots for 2005/10/27 data.

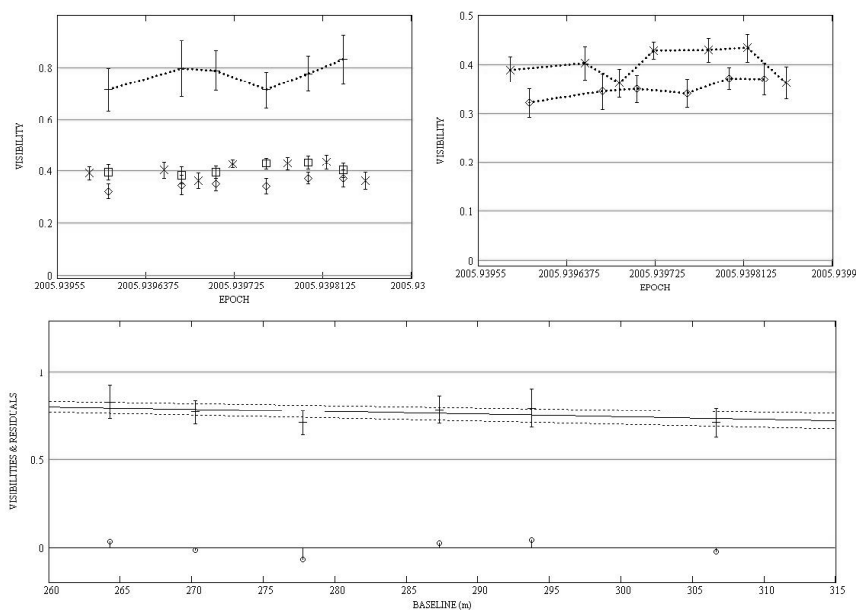


Figure. C.78: HD 19994: Long baseline plots for 2005/12/10 data.

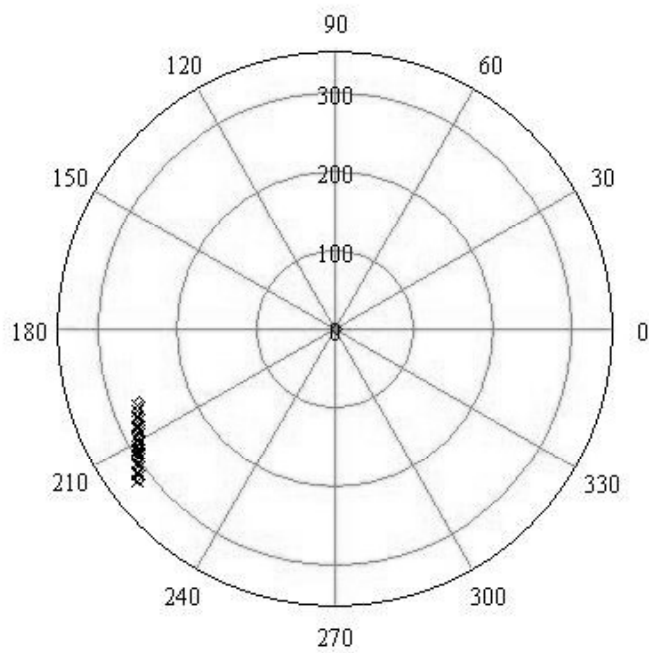


Figure. C.79: HD 19994: All data - Baseline vs. baseline position angle.

C.7.3 Diameter Calculation

All the data were used in the diameter calculation.

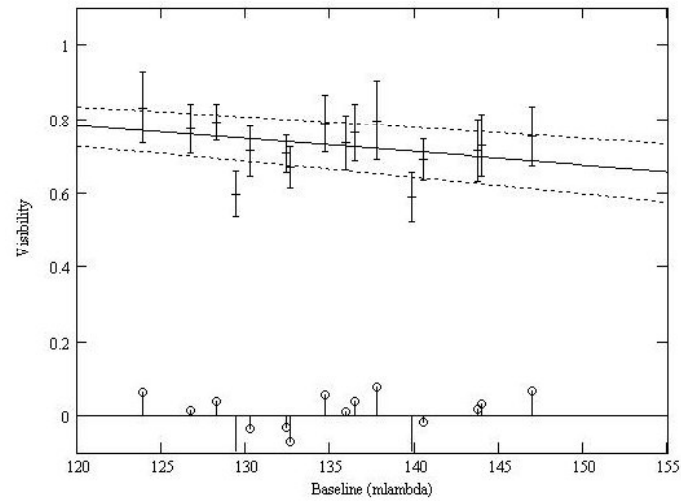


Figure. C.80: HD 19994: LD disk diameter fit: Visibility vs. baseline.

C.7.4 SFP Search

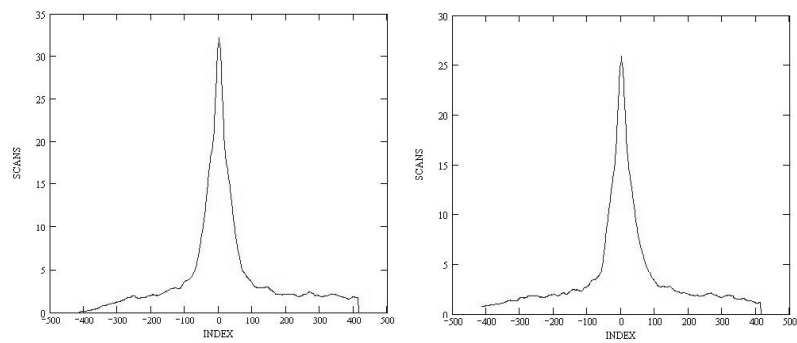


Figure. C.81: HD 19994: SFP inspection for 2005/10/21 data.

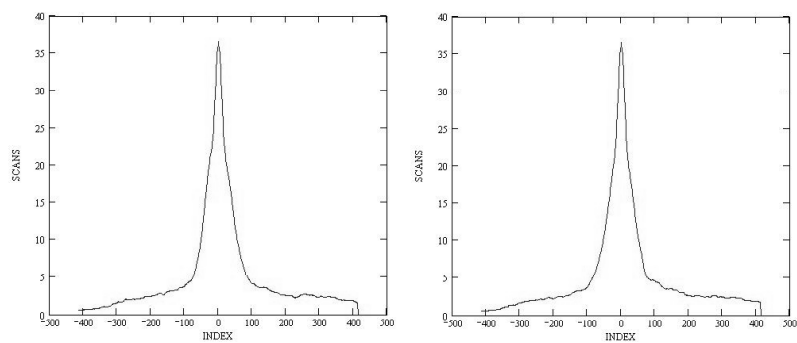


Figure. C.82: HD 19994: SFP inspection for 2005/10/27 data.

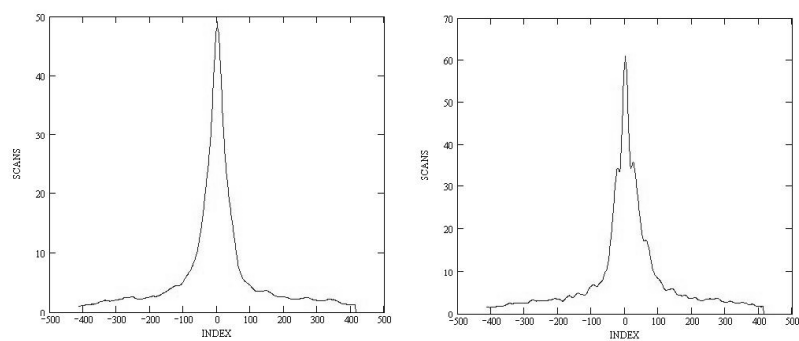


Figure. C.83: HD 19994: SFP inspection for 2005/12/10 data.

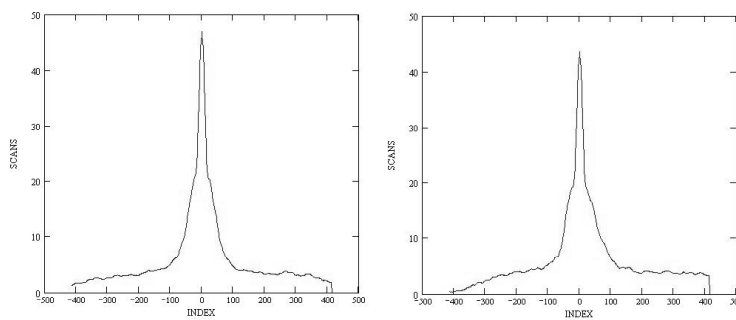


Figure. C.84: HD 19411: SFP inspection for 2005/10/21 data.

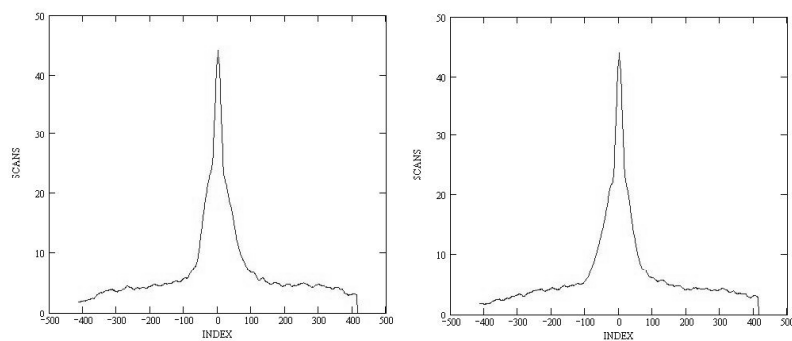


Figure. C.85: HD 19411: SFP inspection for 2005/10/27 data.

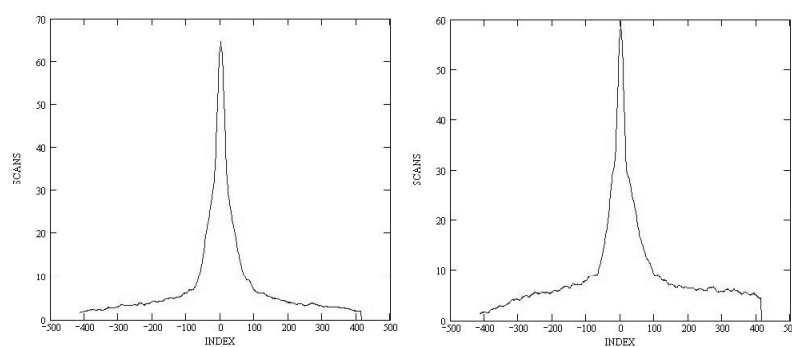


Figure. C.86: HD 19411: SFP inspection for 2005/12/10 data.

C.8 HD 20367

C.8.1 Calibrated Visibilities

Table. C.8: HD 20367: Calibrated Visibilities

| MJD | B (m) | PA (deg) | V_c | $\sigma(V_c)$ |
|-----------|----------|-------------|-------|---------------|
| 53716.339 | 325.81 | 179.2 | 0.859 | 0.148 |
| 53716.353 | 326.00 | 175.8 | 0.938 | 0.163 |
| 53716.367 | 326.40 | 172.6 | 0.883 | 0.119 |
| 53716.380 | 326.96 | 169.5 | 0.929 | 0.125 |
| 53716.393 | 327.66 | 166.4 | 0.826 | 0.175 |
| 54124.220 | 325.80 | 270.0 | 0.910 | 0.139 |
| 54124.232 | 325.91 | 176.9 | 0.924 | 0.132 |
| 54136.247 | 327.81 | 165.9 | 0.985 | 0.097 |
| 54136.259 | 328.54 | 163.0 | 1.053 | 0.095 |

C.8.2 Nightly Data Plots

The first calibrator and object data points were removed from the 2007/01/24 data due to the large gap in time between them.

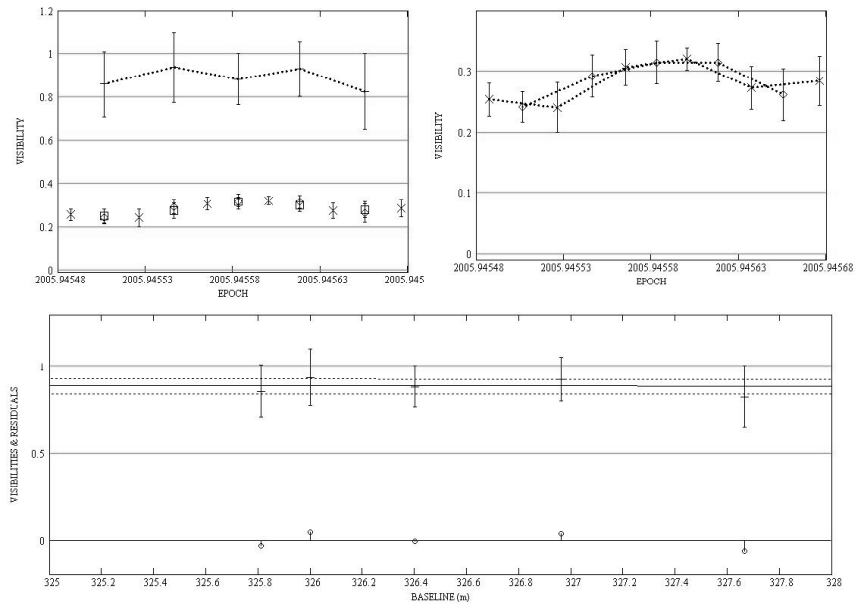


Figure. C.87: HD 20367: Long baseline plots for 2005/12/12 data.

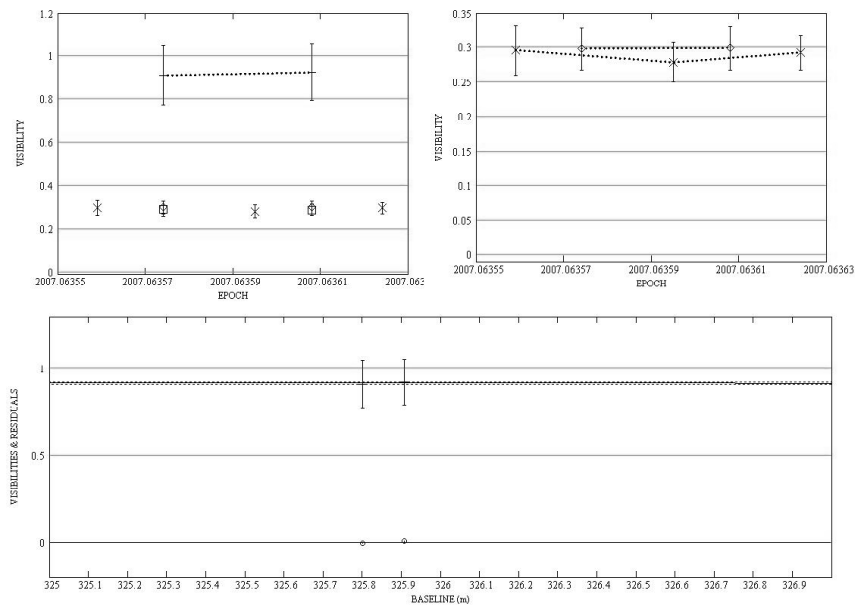


Figure. C.88: HD 20367: Long baseline plots for 2007/01/24 data.

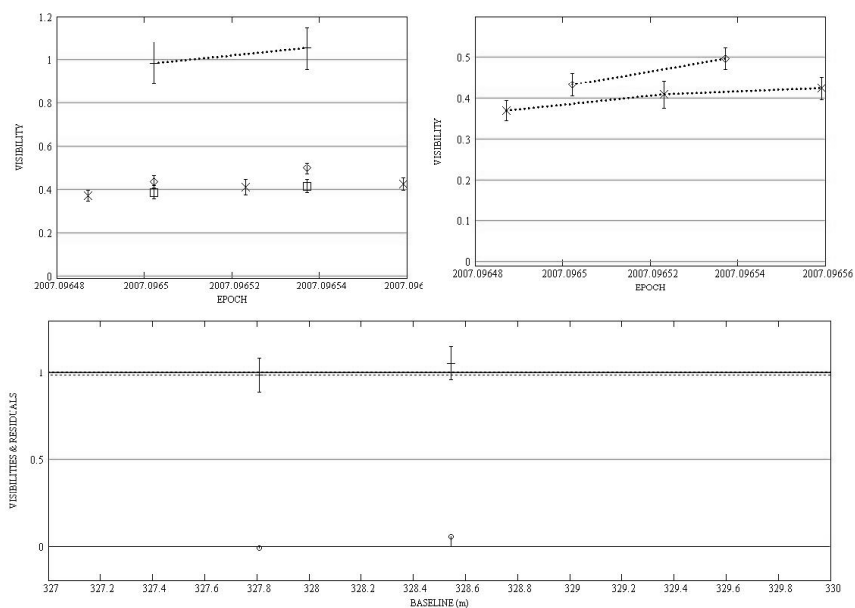


Figure. C.89: HD 20367: Long baseline plots for 2007/02/05 data.

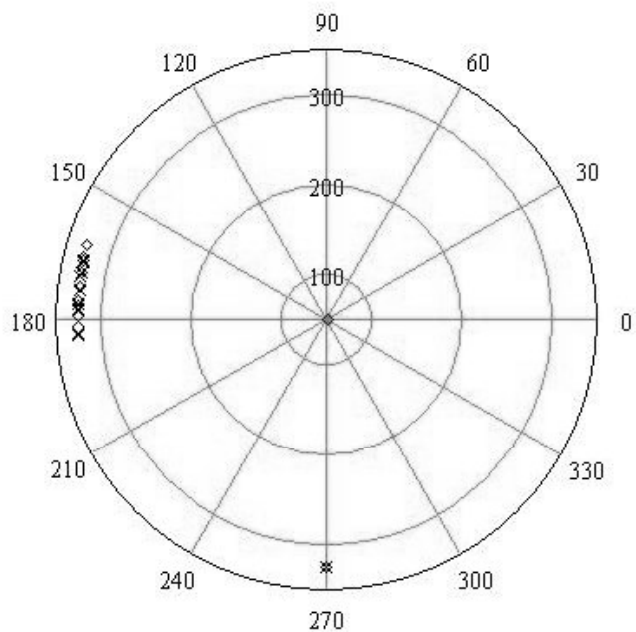


Figure. C.90: HD 20367: All data - Baseline vs. baseline position angle.

C.8.3 Diameter Calculation

I used the long-baseline data from 2005/12/12 and 2007/01/24 in the diameter fit.

The diameter produced using the 2007/02/05 data was $\theta = 0.065 \pm 0.073$ mas, so those data were not used.

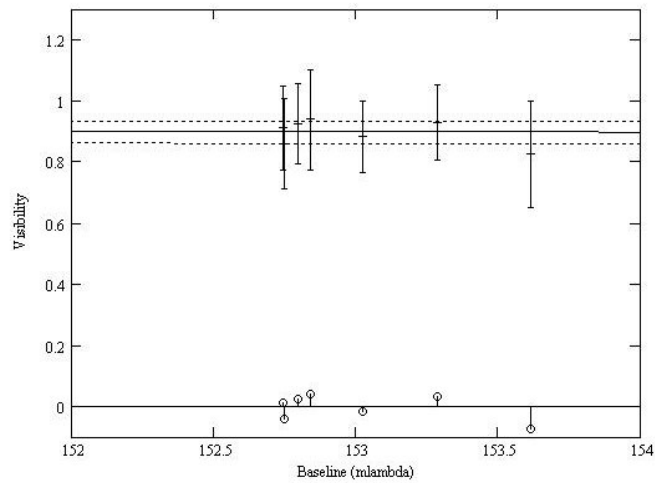


Figure. C.91: HD 20367: LD disk diameter fit: Visibility vs. baseline.

C.8.4 SFP Search

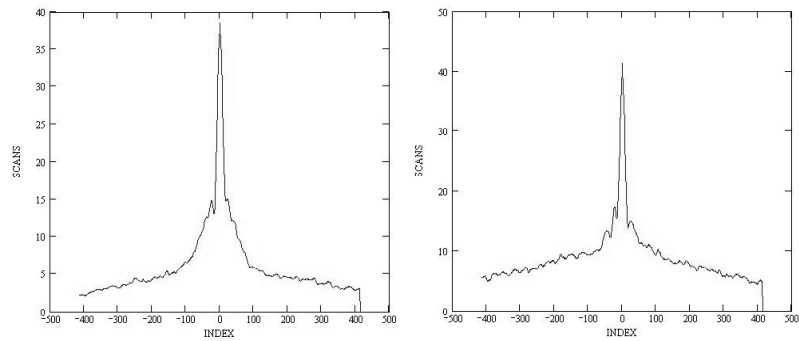


Figure. C.92: HD 20367: SFP inspection for 2005/12/12 data.

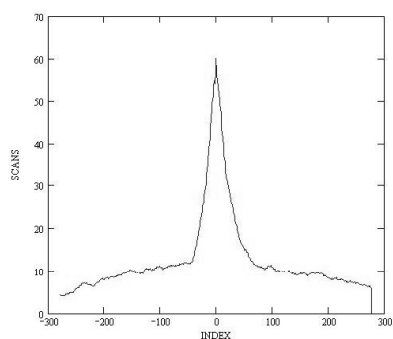


Figure. C.93: HD 20367: SFP inspection for 2007/01/24 data.

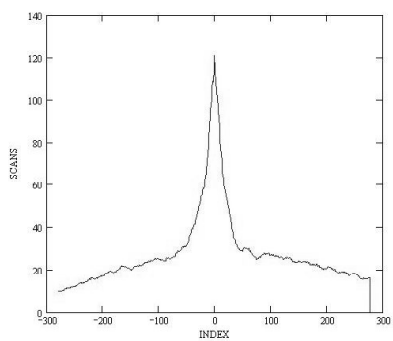


Figure. C.94: HD 20367: SFP inspection for 2007/02/05 data.

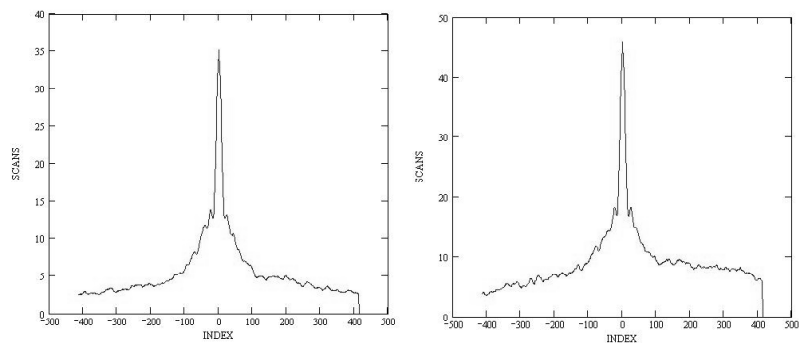


Figure. C.95: HD 21864: SFP inspection for 2005/12/12 data.

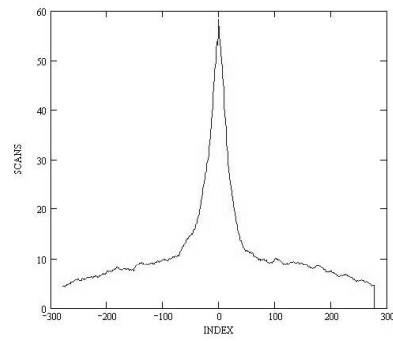


Figure. C.96: HD 21864: SFP inspection for 2007/01/24 data.

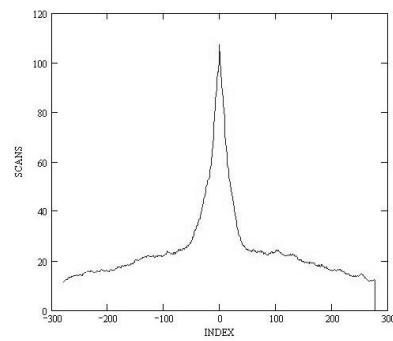


Figure. C.97: HD 21864: SFP inspection for 2007/02/05 data.

C.9 HD 34445

C.9.1 Calibrated Visibilities

Table. C.9: HD 34445: Calibrated Visibilities

| MJD | B (m) | PA (deg) | V_c | $\sigma(V_c)$ |
|-----------|----------|-------------|-------|---------------|
| 53711.355 | 290.43 | 200.4 | 1.077 | 0.128 |
| 53711.368 | 286.11 | 197.3 | 1.089 | 0.133 |
| 53711.383 | 282.04 | 193.7 | 1.008 | 0.143 |
| 53711.397 | 278.89 | 190.0 | 0.862 | 0.152 |
| 53711.416 | 276.09 | 184.6 | 0.944 | 0.156 |
| 53711.430 | 275.38 | 180.7 | 0.896 | 0.130 |
| 53711.446 | 275.88 | 176.1 | 0.958 | 0.146 |
| 53711.461 | 277.65 | 171.9 | 0.846 | 0.122 |
| 53714.316 | 301.97 | 207.0 | 0.905 | 0.091 |
| 53714.330 | 296.62 | 204.2 | 0.894 | 0.097 |
| 53714.344 | 291.30 | 201.0 | 1.000 | 0.094 |
| 53714.360 | 286.28 | 197.5 | 1.043 | 0.112 |

C.9.2 Nightly Data Plots

The last object and calibrator’s visibilities in the 2005/12/07 dataset were given zero weight due to the large jump in visibility by the final calibrator data point. All the data are shown in Figure C.98, though the diameter calculation and companion check do not include these data points.

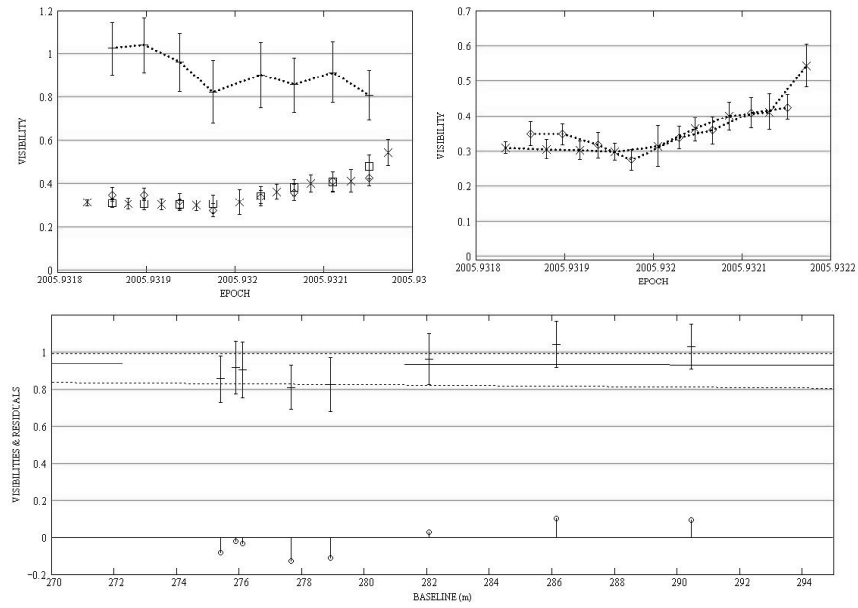


Figure. C.98: HD 34445: Long baseline plots for 2005/12/07 data.

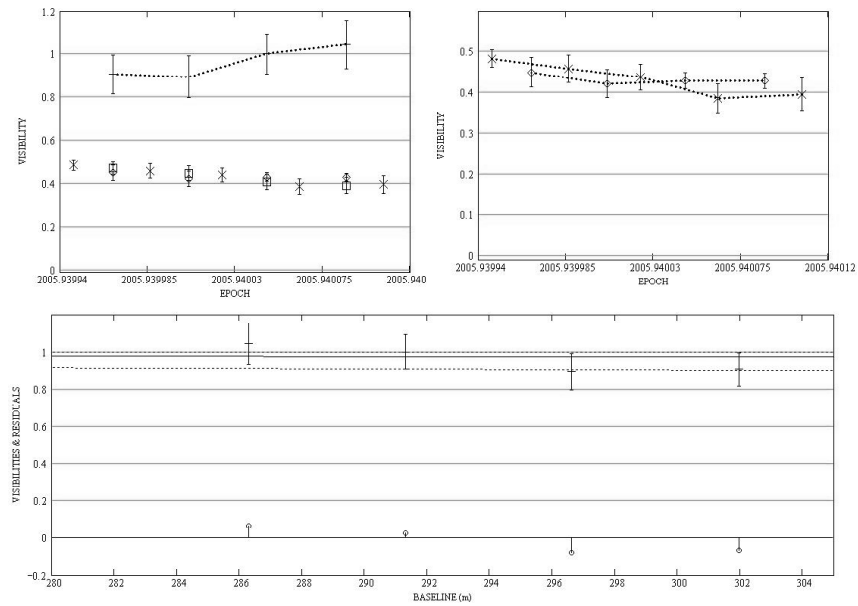


Figure. C.99: HD 34445: Long baseline plots for 2005/12/10 data.

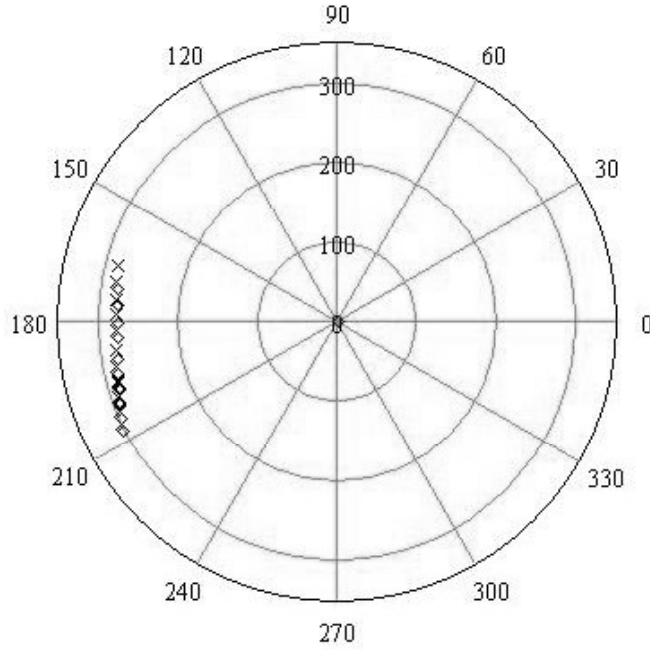


Figure. C.100: HD 34445: All data - Baseline vs. baseline position angle.

C.9.3 Diameter Calculation

The resulting LD diameter was 0.257 ± 0.186 mas ($1.243 \pm 0.902 R_{\odot}$). Given the 72% error bar and the unresolved nature of this star, I would not label this diameter particularly trustworthy, though it matches the one other previous diameter determination by Fischer & Valenti (2005) of $1.39 R_{\odot}$.

Given that the diameter has an error of 72%, I used the diameter estimated from HD 34445's SED fit of 0.280 mas to calculate the ΔK_{\max} for the secondary types under consideration.

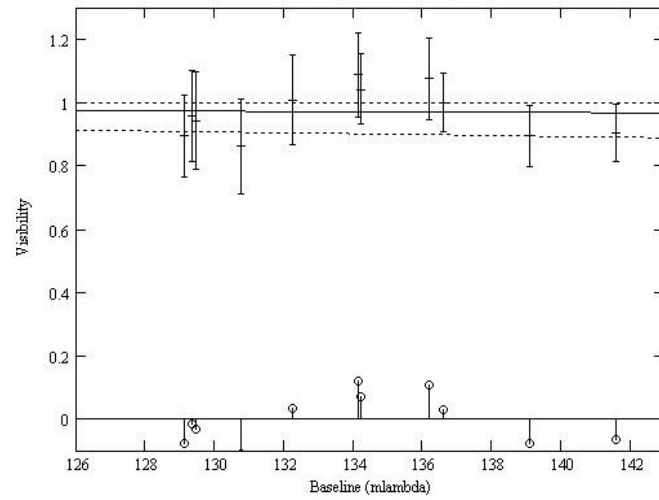


Figure. C.101: HD 34445: LD disk diameter fit: Visibility vs. baseline.

C.9.4 SFP Search

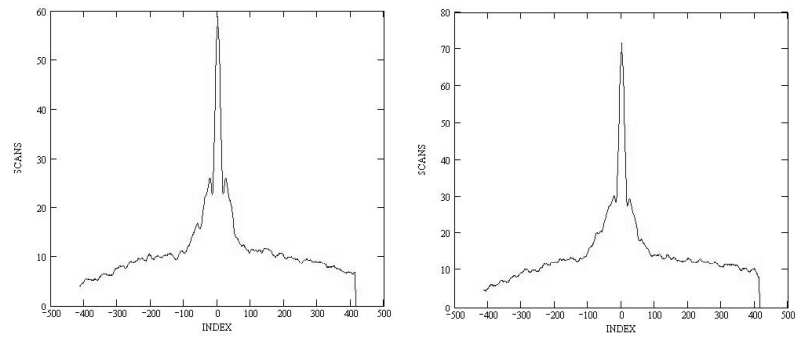


Figure. C.102: HD 34445: SFP inspection for 2005/12/07 data.

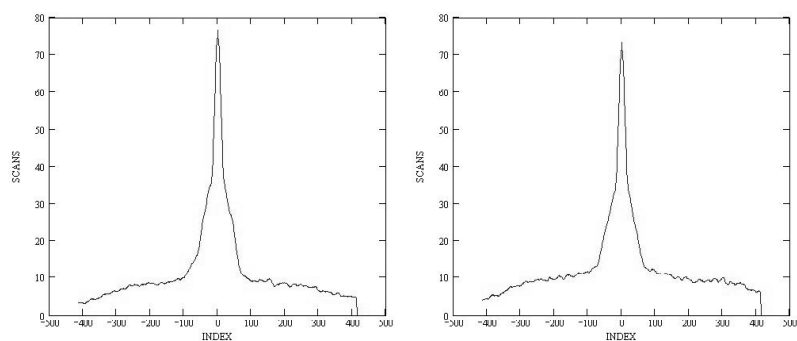


Figure. C.103: HD 34445: SFP inspection for 2005/12/10 data.

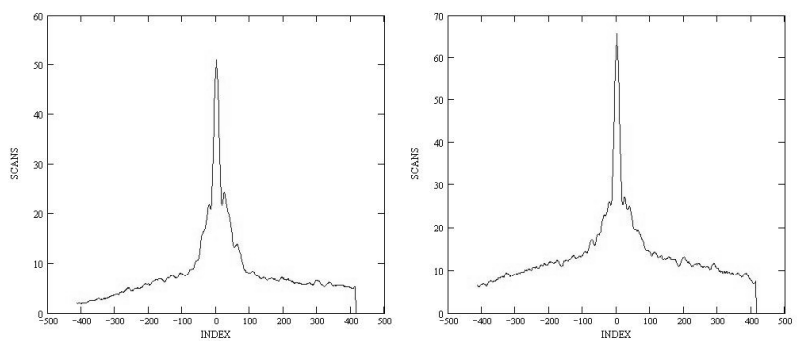


Figure. C.104: HD 31423: SFP inspection for 2005/12/07 data.

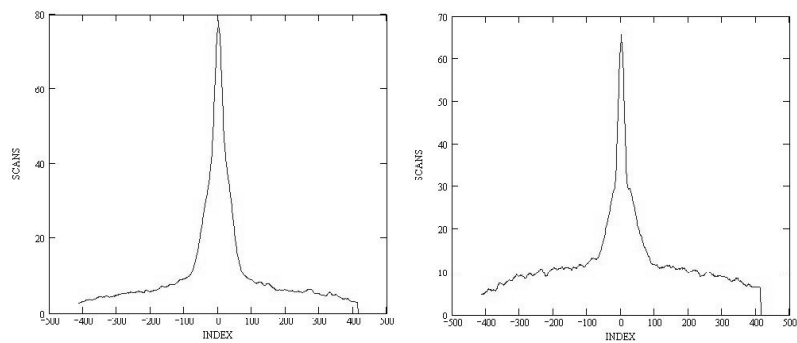


Figure. C.105: HD 31423: SFP inspection for 2005/12/10 data.

C.10 HD 38529

C.10.1 Calibrated Visibilities

Table. C.10: HD 38529: Calibrated Visibilities

| MJD | B (m) | PA (deg) | V_c | $\sigma(V_c)$ |
|-----------|----------|-------------|-------|---------------|
| 53665.444 | 300.02 | 212.7 | 0.810 | 0.073 |
| 53665.457 | 293.84 | 210.6 | 0.867 | 0.101 |
| 53667.451 | 294.23 | 210.8 | 0.880 | 0.239 |
| 53667.464 | 287.76 | 208.4 | 0.802 | 0.085 |
| 53710.300 | 309.45 | 215.5 | 0.891 | 0.086 |
| 53710.314 | 303.49 | 213.7 | 0.824 | 0.104 |
| 53710.330 | 295.82 | 211.3 | 0.806 | 0.089 |
| 53710.344 | 289.06 | 208.9 | 0.727 | 0.105 |
| 53710.357 | 282.69 | 206.4 | 0.809 | 0.081 |
| 53710.370 | 276.47 | 203.6 | 0.888 | 0.065 |
| 53710.384 | 270.24 | 200.2 | 0.895 | 0.087 |
| 53710.397 | 265.25 | 196.9 | 0.902 | 0.083 |
| 53718.390 | 271.76 | 129.8 | 0.733 | 0.066 |
| 53718.404 | 275.39 | 129.1 | 0.598 | 0.069 |
| 53718.421 | 277.89 | 128.5 | 0.779 | 0.115 |
| 53718.438 | 278.43 | 128.3 | 0.655 | 0.102 |
| 53718.455 | 277.00 | 128.4 | 1.045 | 0.138 |

C.10.2 Nightly Data Plots

Due to the fact that there were only two bracketed observations each in the 2005/10/22 and 2005/10/24 datasets, they were not considered when searching for the effects of stellar companions.

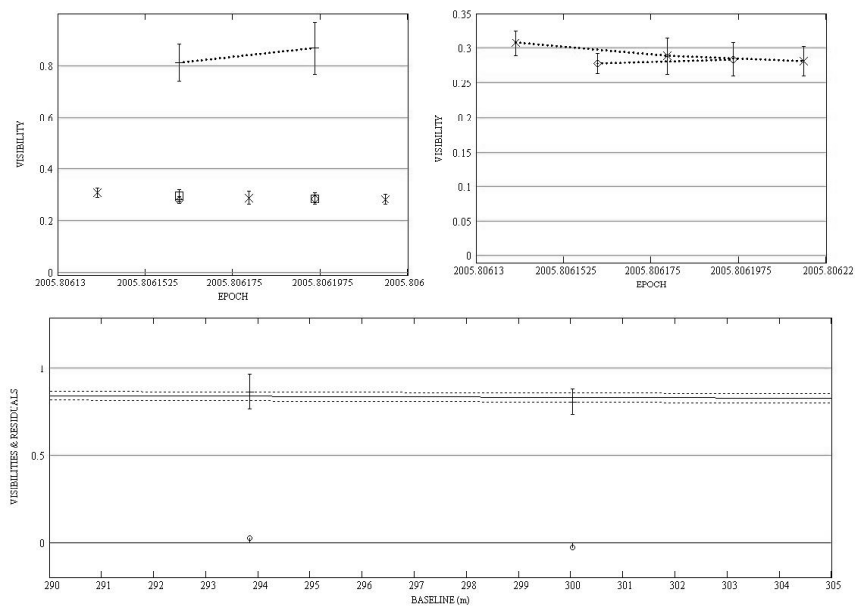


Figure. C.106: HD 38529: Long baseline plots for 2005/10/22 data.

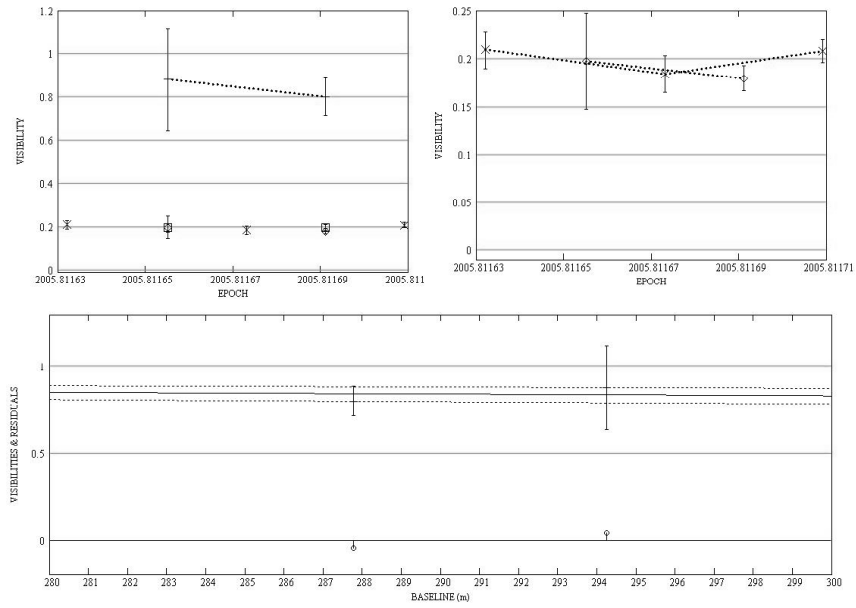


Figure. C.107: HD 38529: Long baseline plots for 2005/10/24 data.

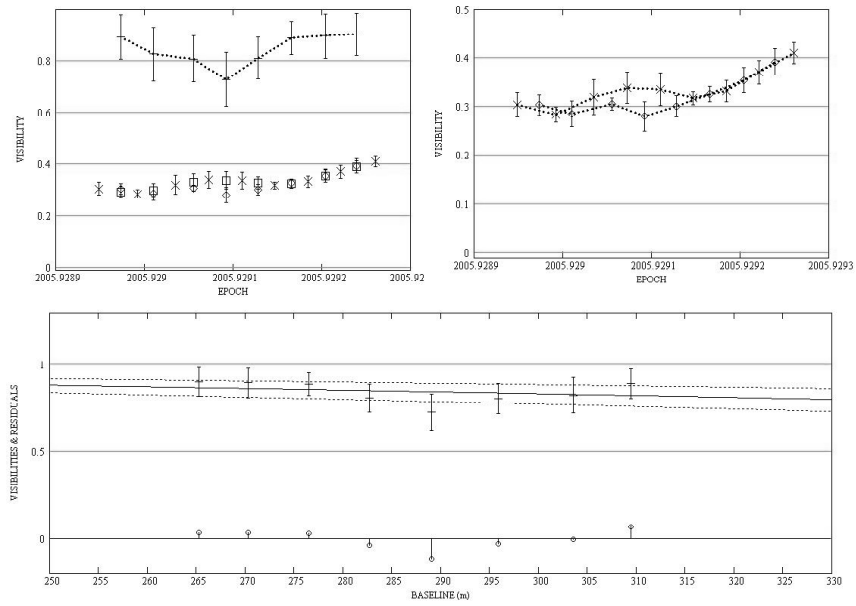


Figure. C.108: HD 38529: Long baseline plots for 2005/12/06 data.

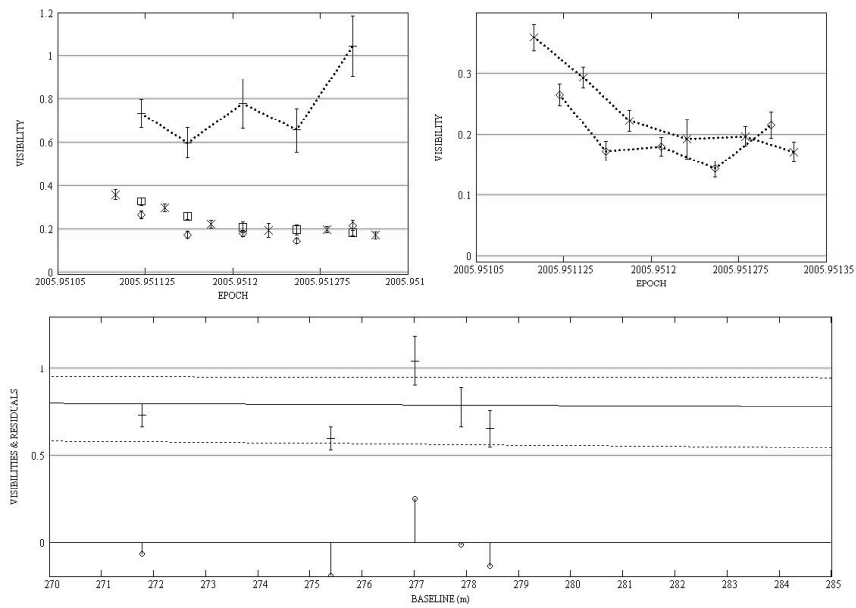


Figure. C.109: HD 38529: Intermediate baseline plots for 2005/12/14 data.

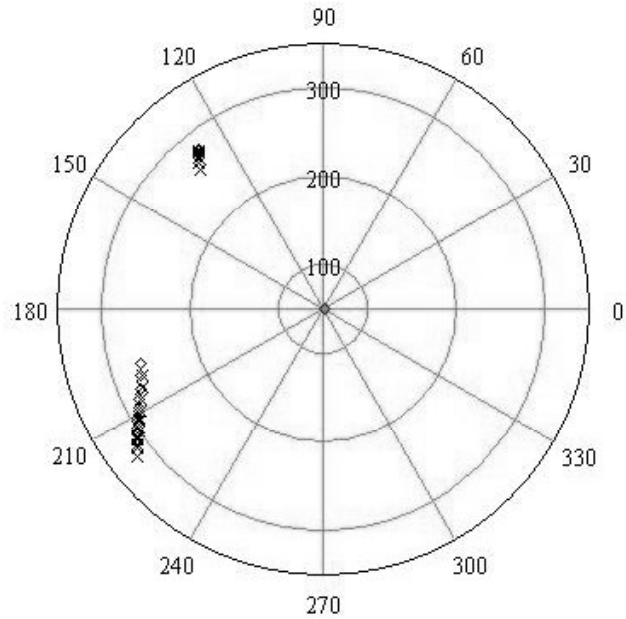


Figure. C.110: HD 38529: All data - Baseline vs. baseline position angle.

C.10.3 Diameter Calculation

In the diameter calculation, I used all three nights of S1-E1 data.

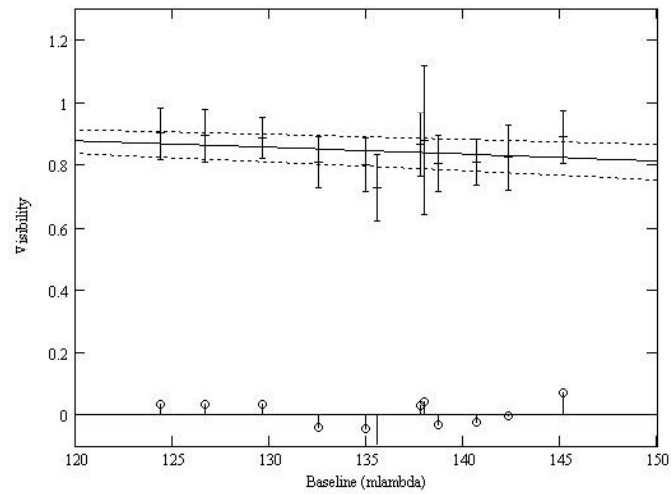


Figure. C.111: HD 38529: LD disk diameter fit: Visibility vs. baseline.

C.10.4 SFP Search

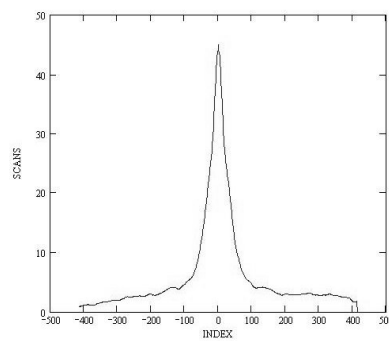


Figure. C.112: HD 38529: SFP inspection for 2005/10/22 data.

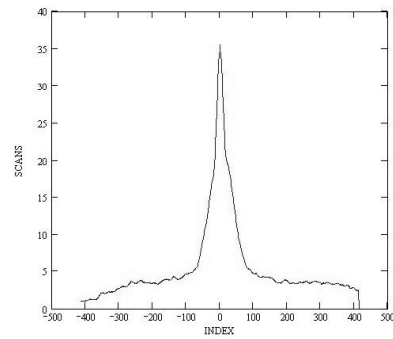


Figure. C.113: HD 38529: SFP inspection for 2005/10/24 data.

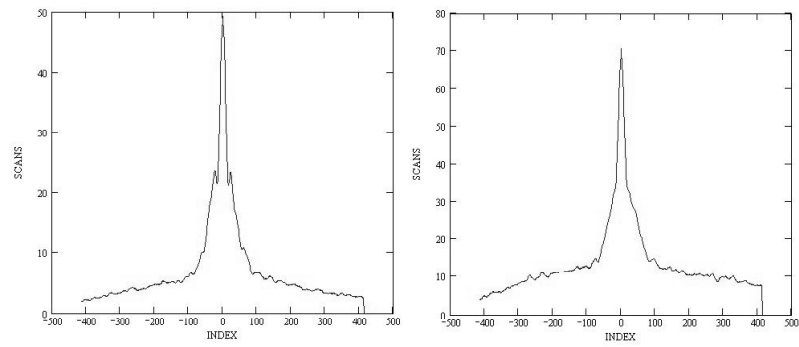


Figure. C.114: HD 38529: SFP inspection for 2005/12/06 data.

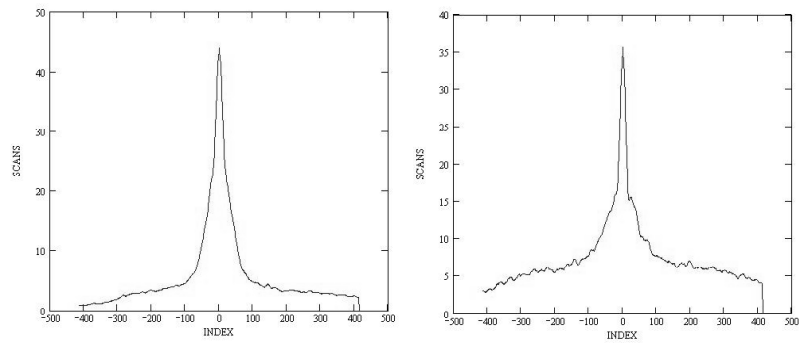


Figure. C.115: HD 38529: SFP inspection for 2005/12/14 data.

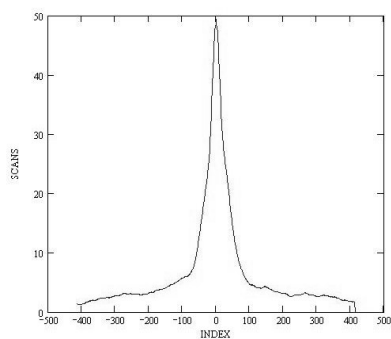


Figure. C.116: HD 43318: SFP inspection for 2005/10/22 data.

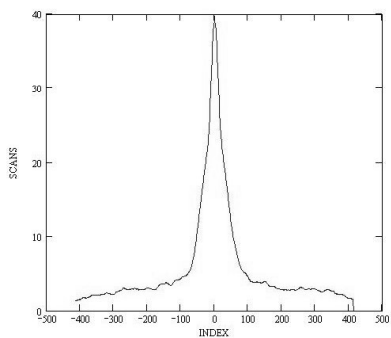


Figure. C.117: HD 43318: SFP inspection for 2005/10/24 data.

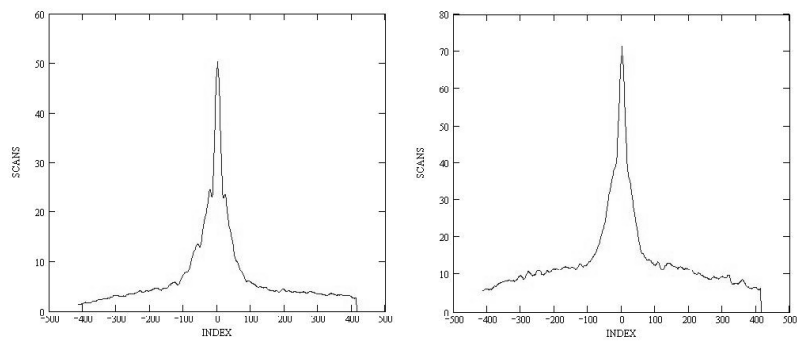


Figure. C.118: HD 43318: SFP inspection for 2005/12/06 data.

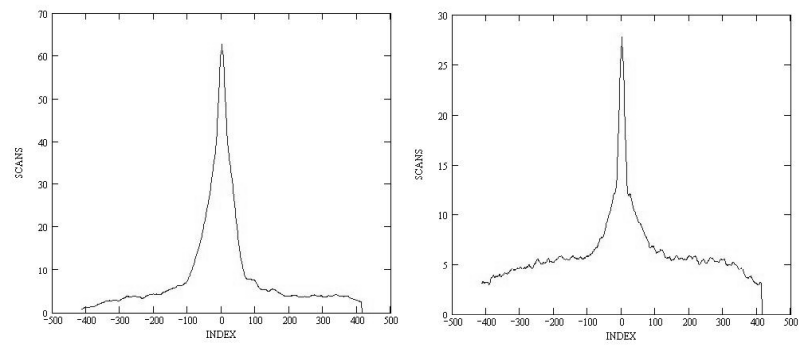


Figure. C.119: HD 43318: SFP inspection for 2005/12/14 data.

C.11 HD 50554

C.11.1 Calibrated Visibilities

Table. C.11: HD 50554: Calibrated Visibilities

| MJD | B (m) | PA (deg) | V_c | $\sigma(V_c)$ |
|-----------|----------|-------------|-------|---------------|
| 53711.497 | 316.69 | 180.6 | 0.812 | 0.115 |
| 53711.523 | 317.33 | 174.2 | 0.875 | 0.127 |
| 53711.537 | 318.32 | 170.7 | 0.784 | 0.090 |
| 53716.422 | 321.04 | 195.4 | 1.007 | 0.139 |
| 53716.435 | 319.48 | 192.2 | 0.906 | 0.091 |
| 53716.449 | 318.20 | 189.0 | 0.985 | 0.083 |
| 53716.463 | 317.30 | 185.7 | 1.029 | 0.096 |
| 53716.479 | 316.73 | 181.7 | 0.958 | 0.150 |
| 54137.174 | 330.66 | 213.7 | 1.249 | 0.099 |
| 54137.191 | 330.05 | 211.0 | 1.309 | 0.164 |
| 54137.215 | 327.91 | 206.7 | 1.422 | 0.199 |

C.11.2 Nightly Data Plots

The first calibrator and object data points in the 2005/12/07 dataset were given zero weight, as there was a gap in time between the first object's and the second calibrator's observations. All data points are shown in Figure C.120 but the first data points were not taken into consideration for the diameter calculation. Because there were only two bracketed observations in the 2005/12/07 dataset, it was not used in the companion check.

The data obtained using HD 42938 as the calibrator (2007/02/06) were not used in the diameter calculation or the companion check as the $V_{\text{calibrated}} > 1$.

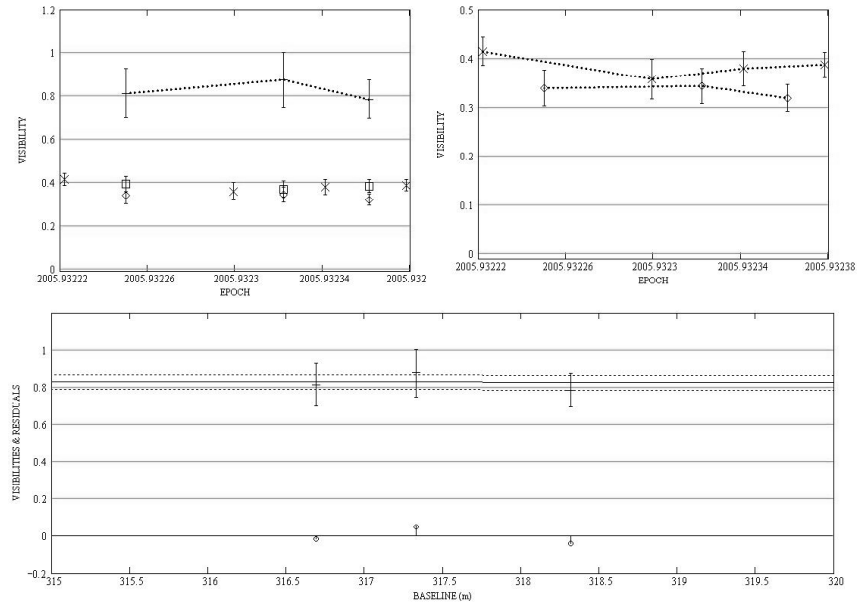


Figure. C.120: HD 50554: Long baseline plots for 2005/12/07 data.

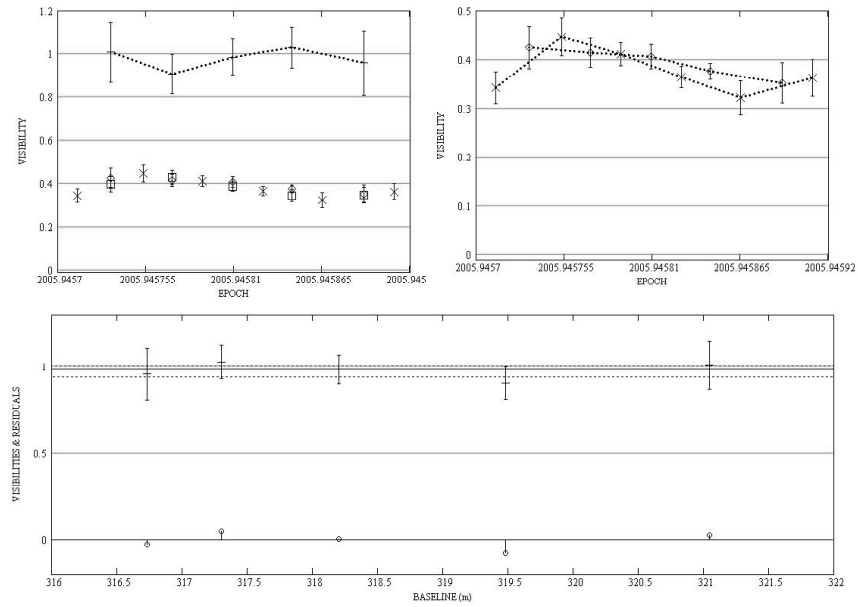


Figure. C.121: HD 50554: Long baseline plots for 2005/12/12 data.

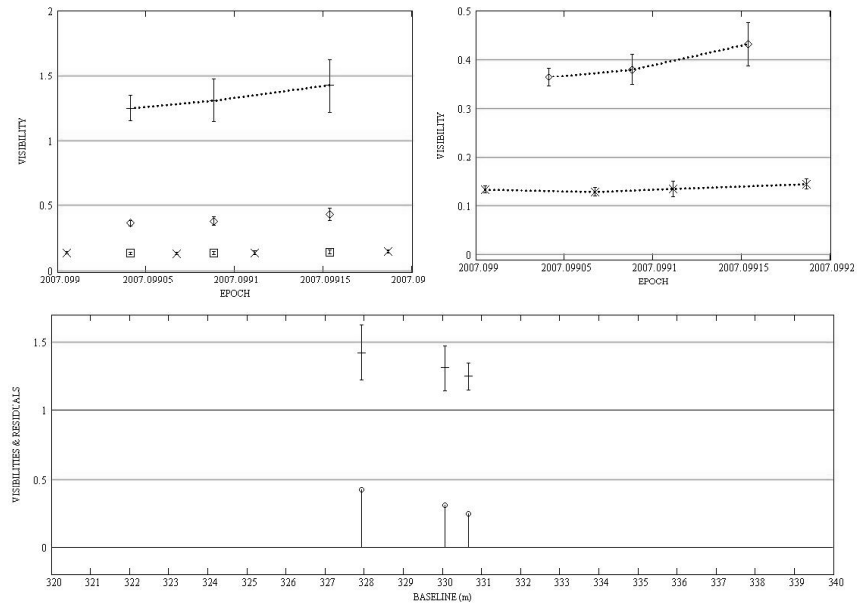


Figure. C.122: HD 50554: Long baseline plots for 2007/02/06 data.

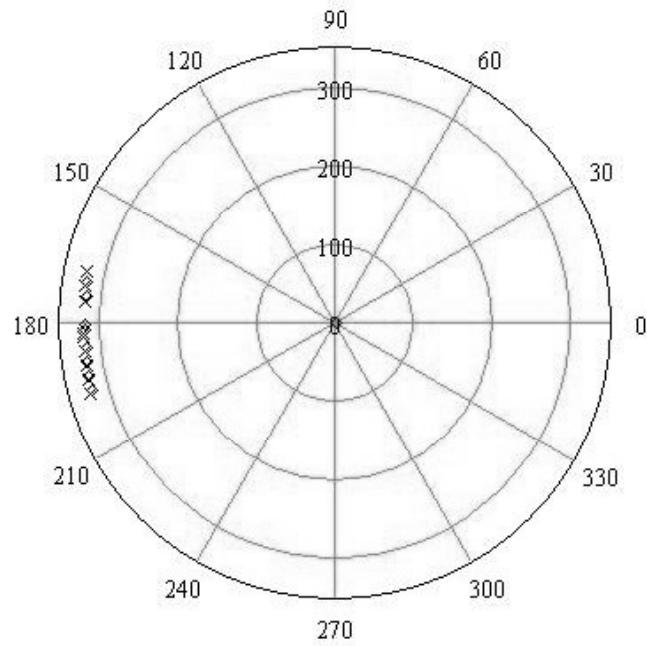


Figure. C.123: HD 50554: All data - Baseline vs. baseline position angle (using calibrator HD 49736).

C.11.3 Diameter Calculation

All the S1-E1 data were used in the diameter calculation.

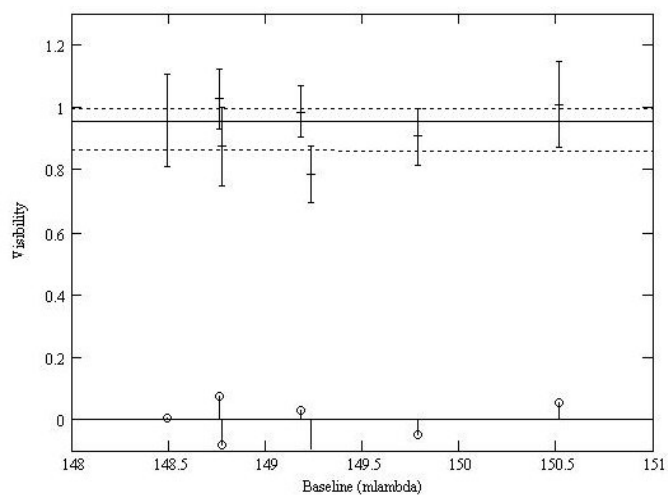


Figure. C.124: HD 50554: LD disk diameter fit: Visibility vs. baseline.

C.11.4 SFP Search

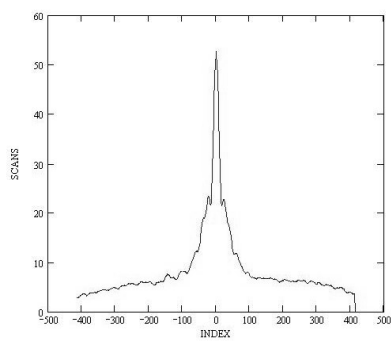


Figure. C.125: HD 50554: SFP inspection for 2005/12/07 data.

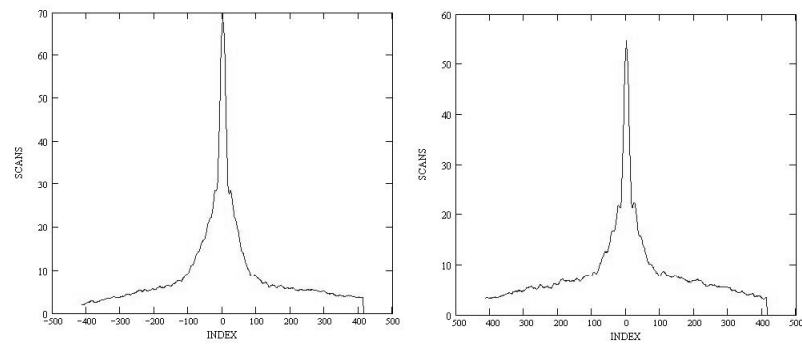


Figure. C.126: HD 50554: SFP inspection for 2005/12/12 data.

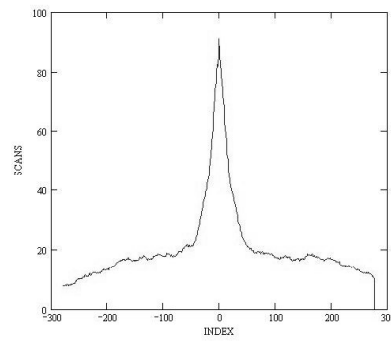


Figure. C.127: HD 50554: SFP inspection for 2007/02/06 data.

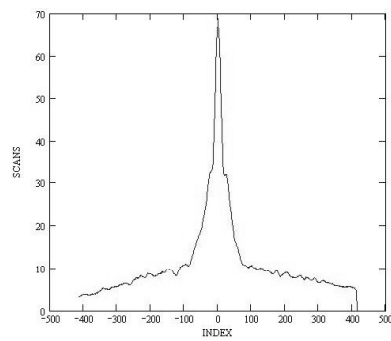


Figure. C.128: HD 49736: SFP inspection for 2005/12/07 data.

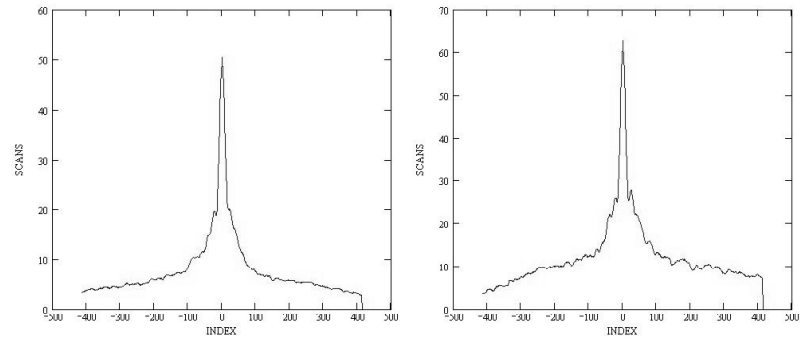


Figure. C.129: HD 49736: SFP inspection for 2005/12/12 data.

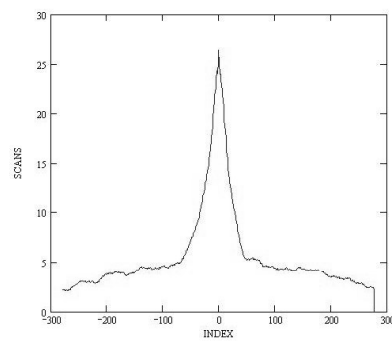


Figure. C.130: HD 42398: SFP inspection for 2007/02/06 data.

C.12 HD 59686

C.12.1 Calibrated Visibilities

Table. C.12: HD 59686: Calibrated Visibilities

| MJD | B (m) | PA (deg) | V_c | $\sigma(V_c)$ |
|-----------|----------|-------------|-------|---------------|
| 53710.430 | 316.56 | 203.4 | 0.427 | 0.040 |
| 53710.445 | 313.18 | 200.3 | 0.431 | 0.048 |
| 53710.460 | 309.92 | 196.8 | 0.429 | 0.057 |
| 53710.474 | 307.34 | 193.6 | 0.439 | 0.064 |
| 53710.487 | 305.25 | 190.4 | 0.459 | 0.047 |
| 53710.501 | 303.69 | 187.0 | 0.454 | 0.033 |
| 53710.514 | 302.71 | 183.6 | 0.473 | 0.046 |
| 53710.527 | 302.35 | 90.2 | 0.465 | 0.039 |
| 53720.381 | 261.34 | 143.6 | 0.557 | 0.056 |
| 53720.394 | 265.74 | 140.9 | 0.573 | 0.082 |
| 53720.408 | 269.99 | 138.4 | 0.578 | 0.062 |
| 53720.425 | 274.01 | 135.7 | 0.579 | 0.067 |
| 53720.440 | 276.71 | 133.5 | 0.493 | 0.065 |
| 53720.458 | 278.33 | 131.3 | 0.434 | 0.047 |
| 53720.474 | 278.28 | 129.6 | 0.500 | 0.045 |
| 53720.489 | 276.84 | 128.3 | 0.504 | 0.080 |
| 54192.202 | 302.46 | 182.1 | 0.477 | 0.040 |
| 54192.223 | 302.65 | 176.6 | 0.510 | 0.041 |
| 54192.235 | 303.49 | 173.5 | 0.467 | 0.037 |
| 54192.246 | 304.67 | 170.7 | 0.485 | 0.053 |
| 54192.257 | 306.19 | 168.1 | 0.471 | 0.044 |
| 54192.268 | 307.97 | 165.5 | 0.482 | 0.033 |
| 54192.279 | 310.10 | 163.0 | 0.467 | 0.031 |
| 54192.290 | 312.37 | 160.5 | 0.459 | 0.028 |
| 54192.300 | 314.78 | 158.2 | 0.466 | 0.023 |

C.12.2 Nightly Data Plots

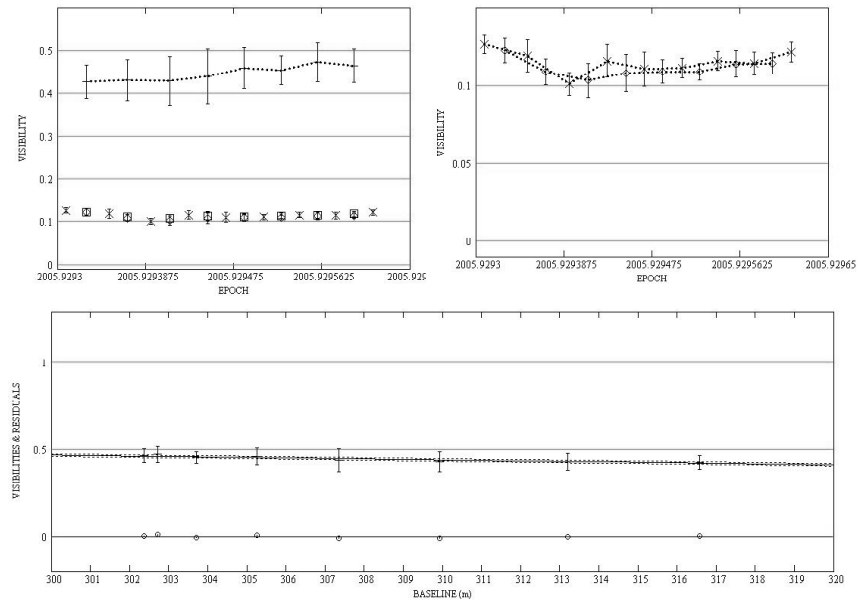


Figure. C.131: HD 59686: Long baseline plots for 2005/12/06 data.

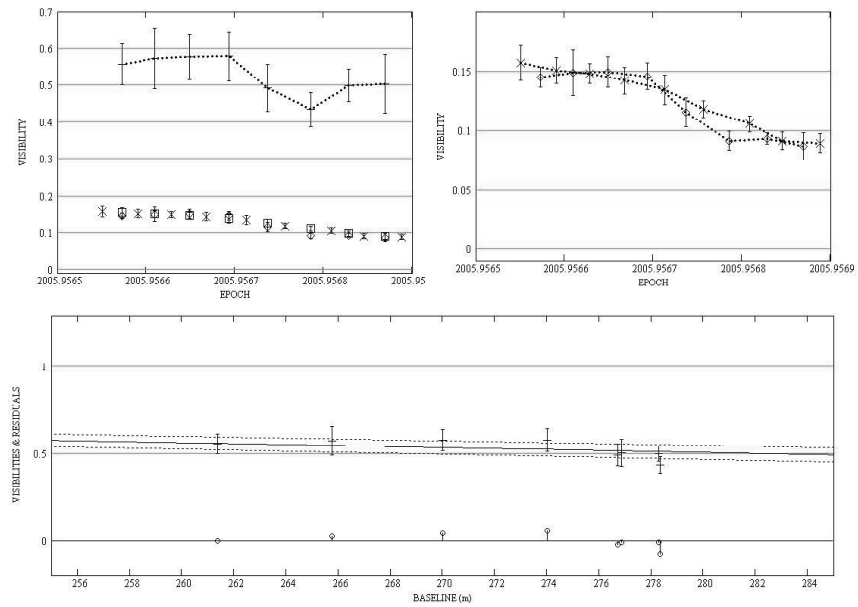


Figure. C.132: HD 59686: Intermediate baseline plots for 2005/12/16 data.

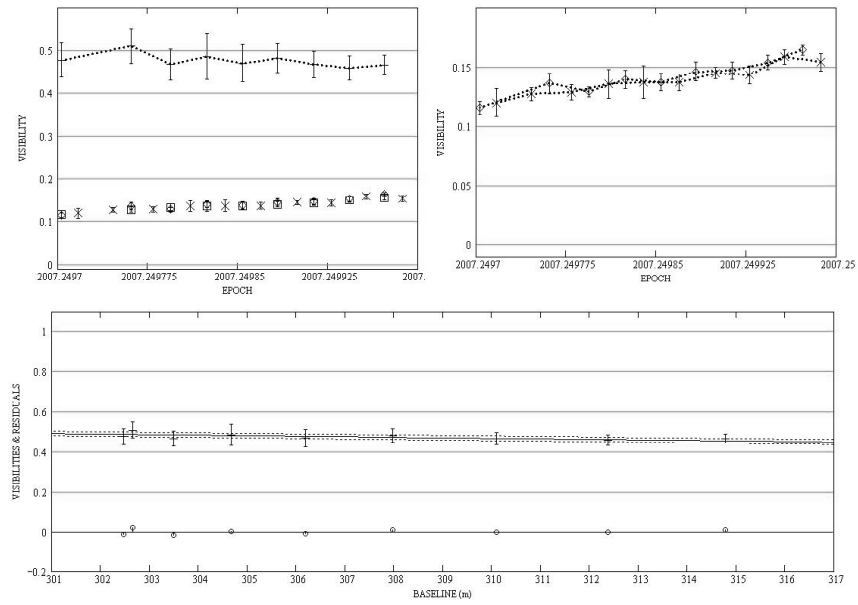


Figure. C.133: HD 59686: Long baseline plots for 2007/04/02 data.

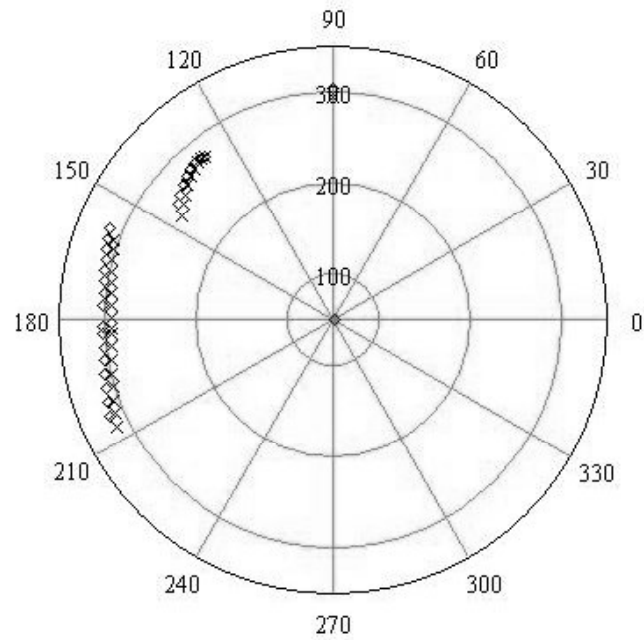


Figure. C.134: HD 59686: All data - Baseline vs. baseline position angle.

C.12.3 Diameter Calculation

I used both nights of S1-E1 data in the diameter measurement.

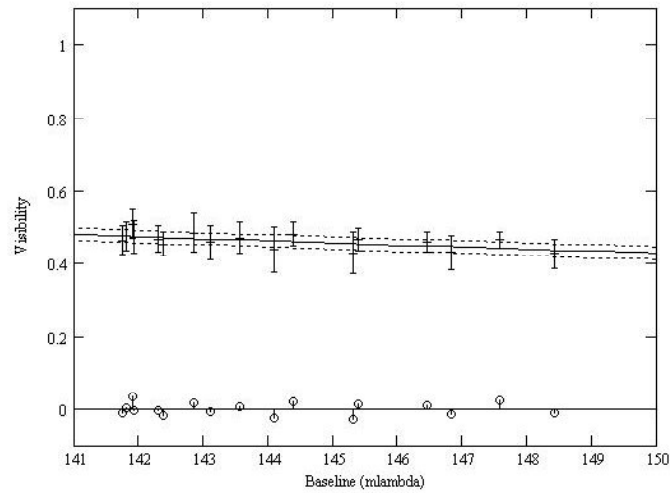


Figure. C.135: HD 59686: LD disk diameter fit: Visibility vs. baseline.

C.12.4 SFP Search

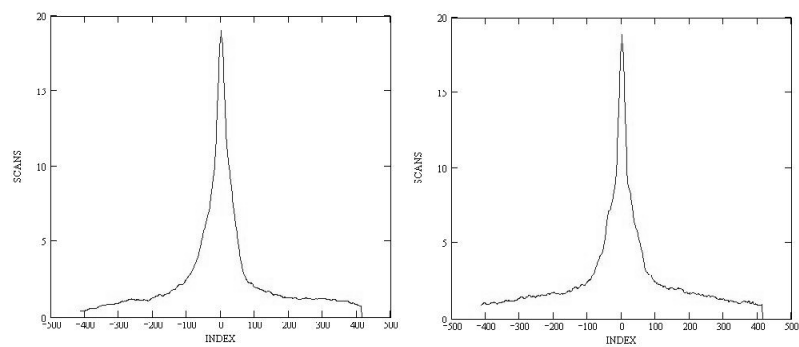


Figure. C.136: HD 59686: SFP inspection for 2005/12/06 data.

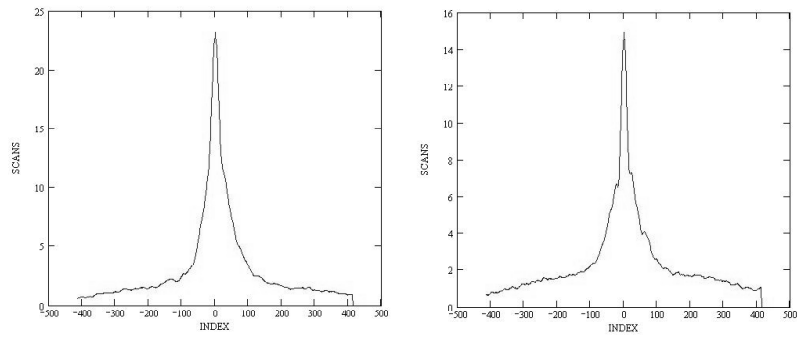


Figure. C.137: HD 59686: SFP inspection for 2005/12/16 data.

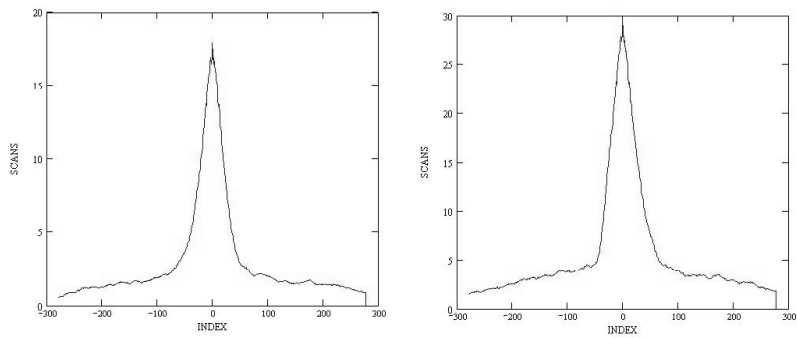


Figure. C.138: HD 59686: SFP inspection for 2007/04/02 data.

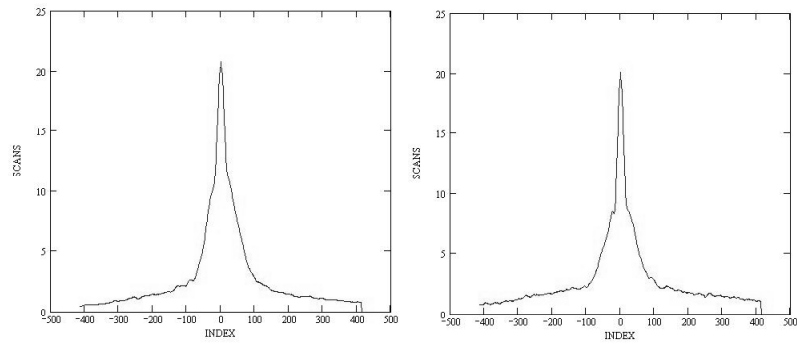


Figure. C.139: HD 61630: SFP inspection for 2005/12/06 data.

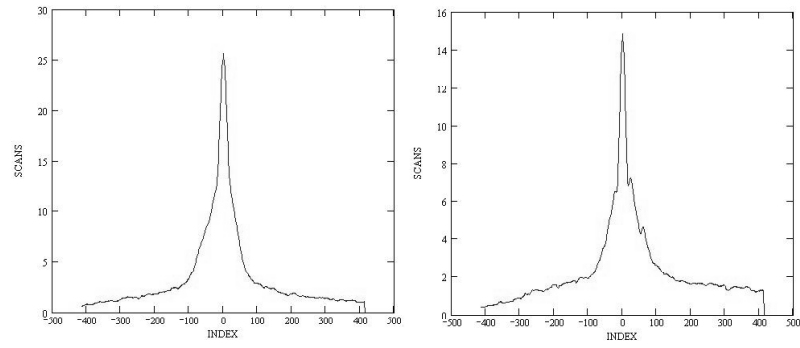


Figure. C.140: HD 61630: SFP inspection for 2005/12/16 data.

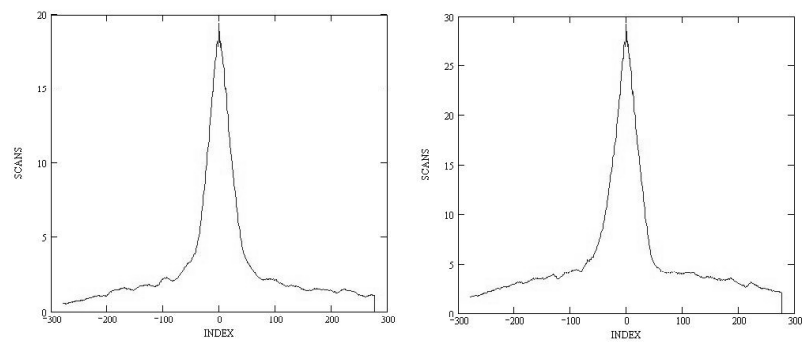


Figure. C.141: HD 61630: SFP inspection for 2007/04/02 data.

C.13 HD 75732

C.13.1 Calibrated Visibilities

Table. C.13: HD 75732: Calibrated Visibilities

| MJD | B (m) | PA (deg) | V_c | $\sigma(V_c)$ |
|-----------|----------|-------------|-------|---------------|
| 54185.221 | 325.59 | 195.2 | 0.562 | 0.061 |
| 54185.234 | 324.51 | 192.1 | 0.579 | 0.065 |
| 54185.304 | 322.77 | 175.4 | 0.568 | 0.054 |
| 54185.317 | 323.32 | 172.3 | 0.576 | 0.058 |
| 54185.330 | 324.09 | 169.2 | 0.527 | 0.038 |
| 54189.207 | 325.83 | 195.9 | 0.730 | 0.079 |
| 54189.221 | 324.70 | 192.7 | 0.651 | 0.090 |
| 54189.235 | 323.75 | 189.5 | 0.743 | 0.078 |
| 54189.249 | 323.02 | 186.2 | 0.660 | 0.078 |
| 54189.264 | 322.56 | 182.6 | 0.765 | 0.080 |
| 54189.278 | 322.47 | 179.1 | 0.625 | 0.079 |

C.13.2 Nightly Data Plots

Due to the long gap in time between the second object and the third calibrator data points in the 2007/03/26 dataset, the second object data point was given zero weight in the diameter calculation. As this left only four bracketed observations in the 2007/03/26 dataset, the companion check relied on the 2007/03/30 data.

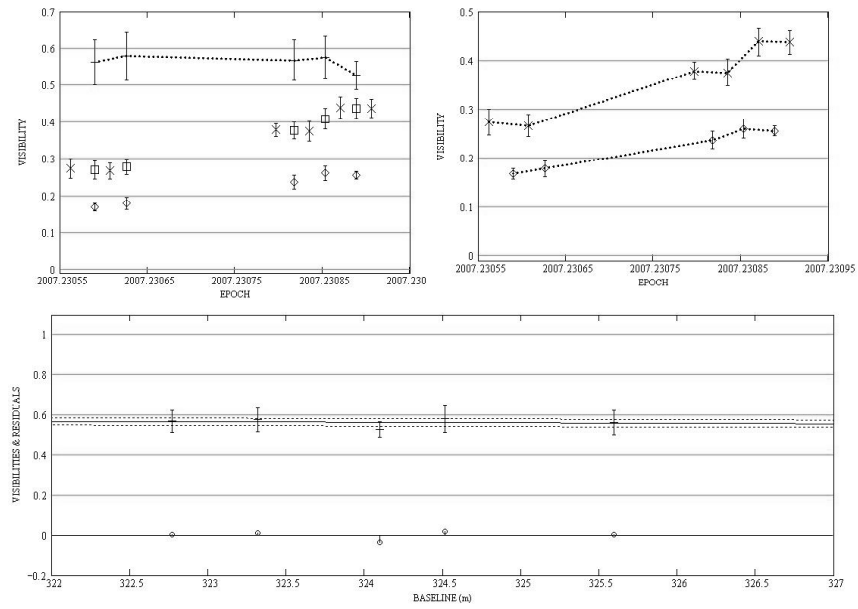


Figure. C.142: HD 75732: Long baseline plots for 2007/03/26 data.

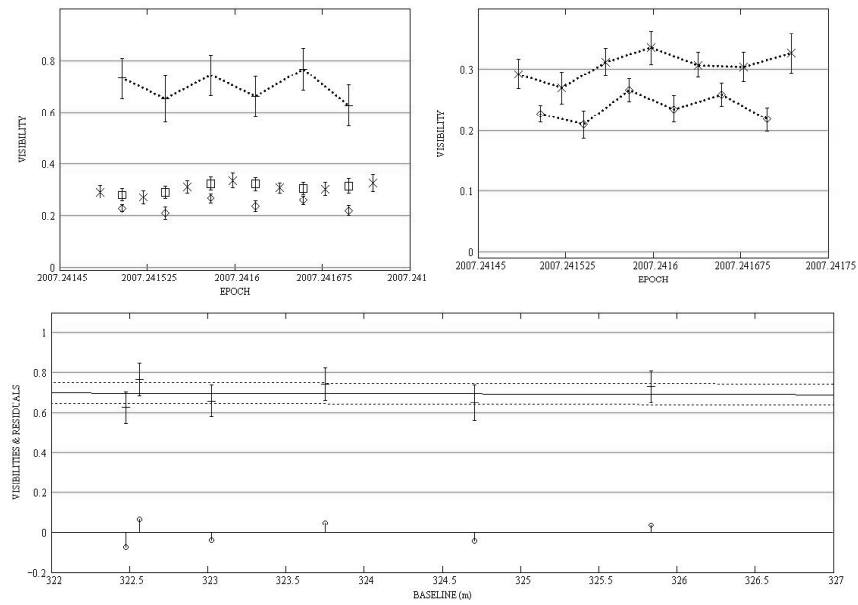


Figure. C.143: HD 75732: Long baseline plots for 2007/03/30 data.

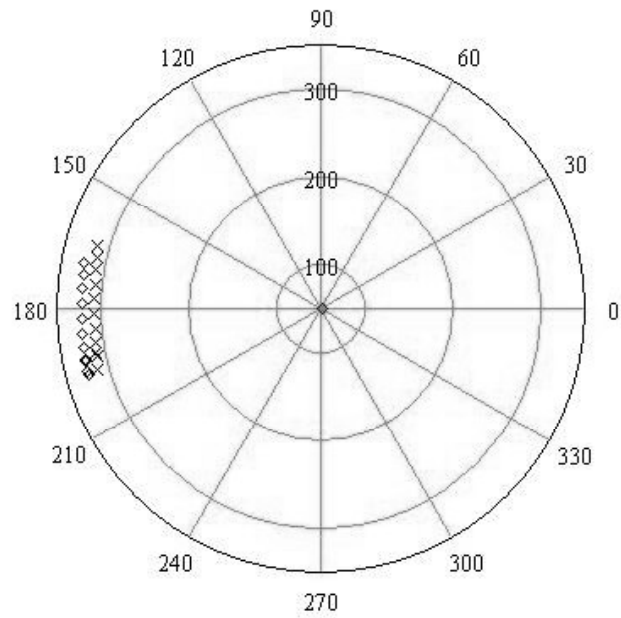


Figure. C.144: HD 75732: All data - Baseline vs. baseline position angle.

C.13.3 Diameter Calculation

All S1-E1 data were used in the diameter measurement.

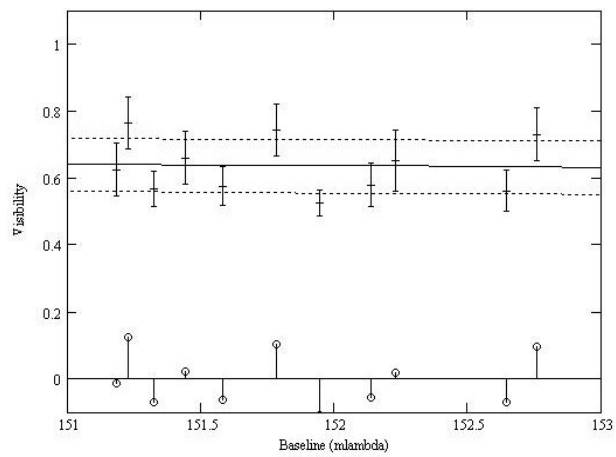


Figure. C.145: HD 75732: LD disk diameter fit: Visibility vs. baseline.

C.13.4 SFP Search

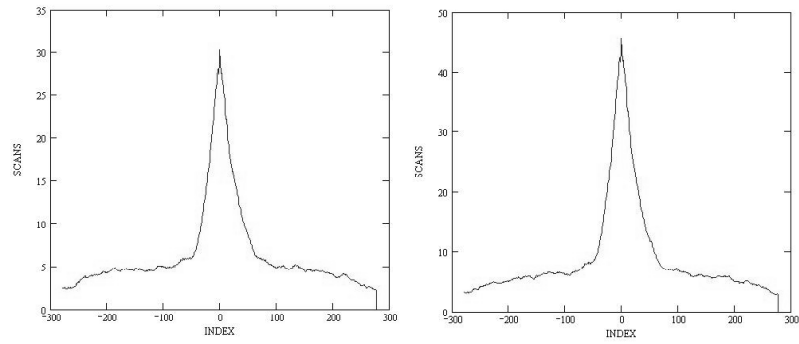


Figure. C.146: HD 75732: SFP inspection for 2007/03/26 data.

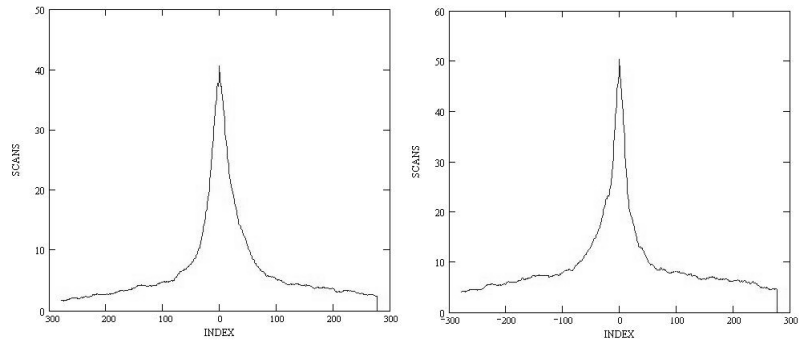


Figure. C.147: HD 75732: SFP inspection for 2007/03/30 data.

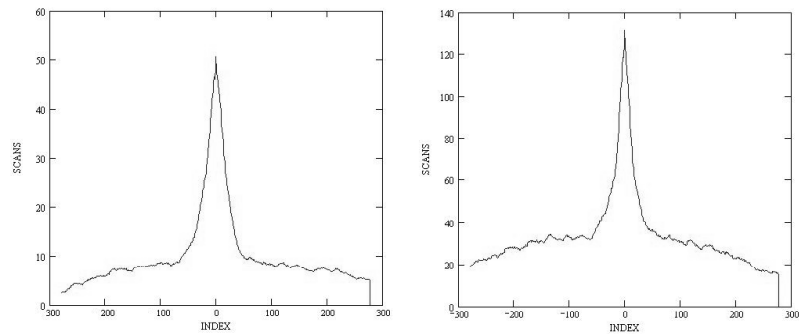


Figure. C.148: HD 72779: SFP inspection for 2007/03/26 data.

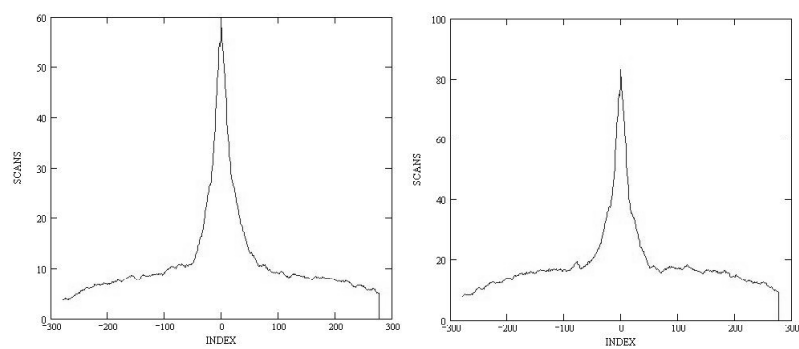


Figure. C.149: HD 72779: SFP inspection for 2007/03/30 data.

C.14 HD 95128

C.14.1 Calibrated Visibilities

There were only three bracketed observations in the 2006/05/19 dataset, and there was a gap in time between the first object and second calibrator observations. Normally I would remove the first calibrator and object data points and proceed with the diameter calculation and companion check, but in this case they were left intact. I am not willing to publish stellar diameters or perform the companion check with only two bracketed observations.

Table. C.14: HD 95128: Calibrated Visibilities

| MJD | B (m) | PA (deg) | V_c | $\sigma(V_c)$ |
|------------|------------------|---------------------|-------------------------|---------------------------------|
| 53874.246 | 330.67 | 174.7 | 0.665 | 0.060 |
| 53874.282 | 330.54 | 166.5 | 0.719 | 0.089 |
| 53874.230 | 330.25 | 162.4 | 0.558 | 0.049 |

C.14.2 Nightly Data Plots

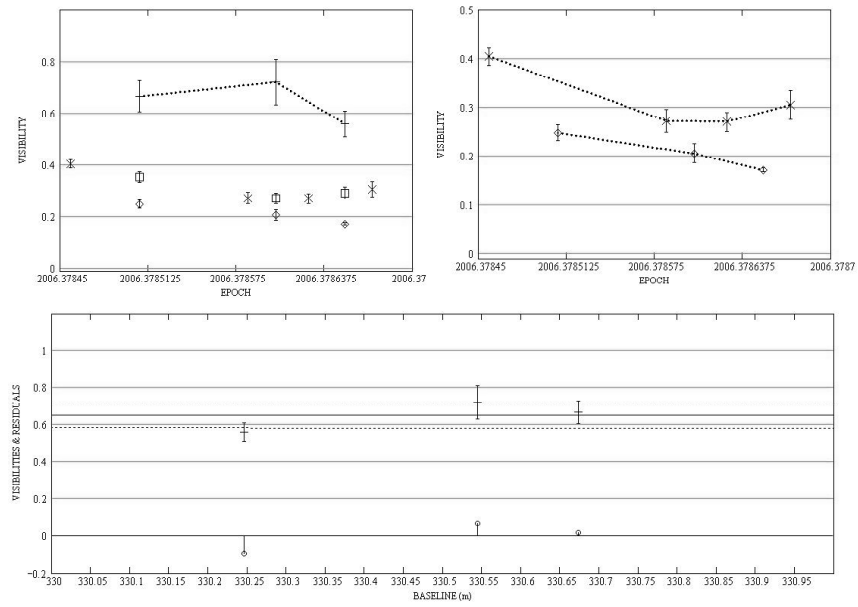


Figure. C.150: HD 95128: Long baseline plots for 2006/05/19 data.

C.14.3 SFP Search

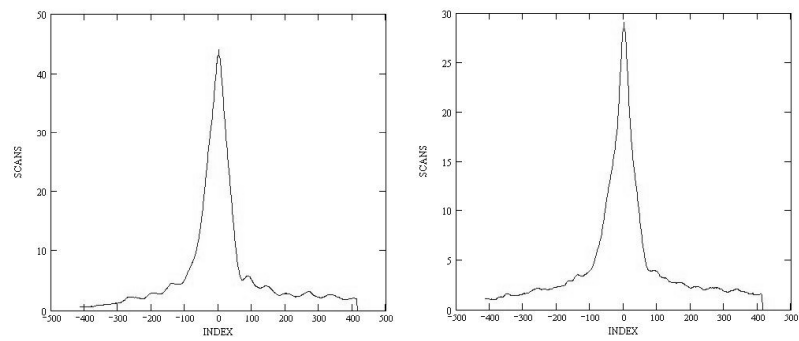


Figure. C.151: HD 95128: SFP inspection for 2006/05/19 data.

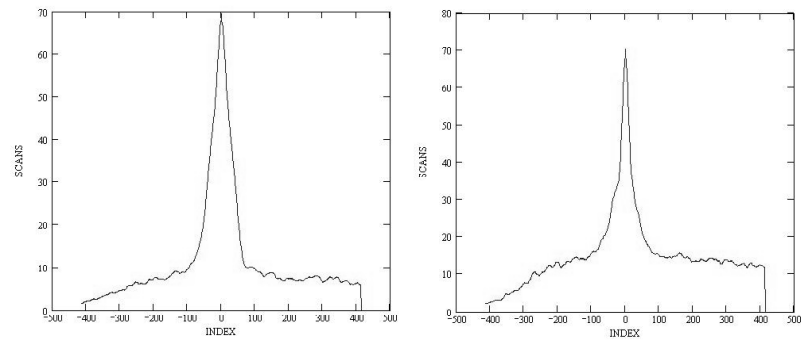


Figure. C.152: HD 90840: SFP inspection for 2006/05/19 data.

C.15 HD 104985

C.15.1 Calibrated Visibilities

Table. C.15: HD 104985: Calibrated Visibilities

| MJD | B (m) | PA (deg) | V_c | $\sigma(V_c)$ |
|-----------|----------|-------------|-------|---------------|
| 53872.276 | 106.41 | 245.9 | 0.950 | 0.079 |
| 53872.289 | 106.10 | 241.4 | 0.886 | 0.076 |
| 53872.301 | 105.79 | 236.9 | 0.905 | 0.095 |
| 53872.314 | 105.46 | 232.3 | 0.896 | 0.074 |
| 53872.327 | 105.12 | 227.4 | 0.889 | 0.099 |
| 53872.340 | 104.80 | 222.8 | 0.872 | 0.094 |
| 53872.352 | 104.49 | 218.1 | 0.887 | 0.095 |
| 53872.365 | 104.19 | 213.4 | 0.921 | 0.096 |
| 53872.378 | 103.93 | 208.8 | 0.926 | 0.066 |
| 53872.392 | 103.66 | 203.4 | 0.959 | 0.068 |
| 54216.214 | 304.67 | 266.0 | 0.466 | 0.046 |
| 54216.249 | 307.95 | 253.8 | 0.536 | 0.047 |
| 54216.281 | 310.19 | 242.6 | 0.551 | 0.054 |
| 54216.299 | 311.13 | 236.3 | 0.496 | 0.052 |
| 54216.315 | 311.80 | 230.7 | 0.487 | 0.057 |
| 54216.326 | 312.13 | 227.2 | 0.500 | 0.040 |
| 54216.336 | 312.43 | 223.6 | 0.508 | 0.046 |

C.15.2 Nightly Data Plots

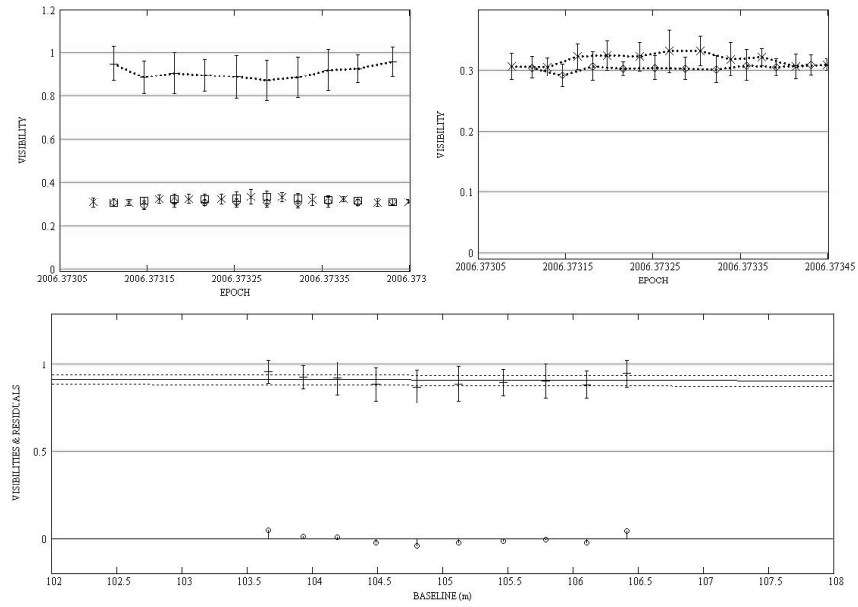


Figure. C.153: HD 104985: Intermediate baseline plots for 2006/05/17 data.

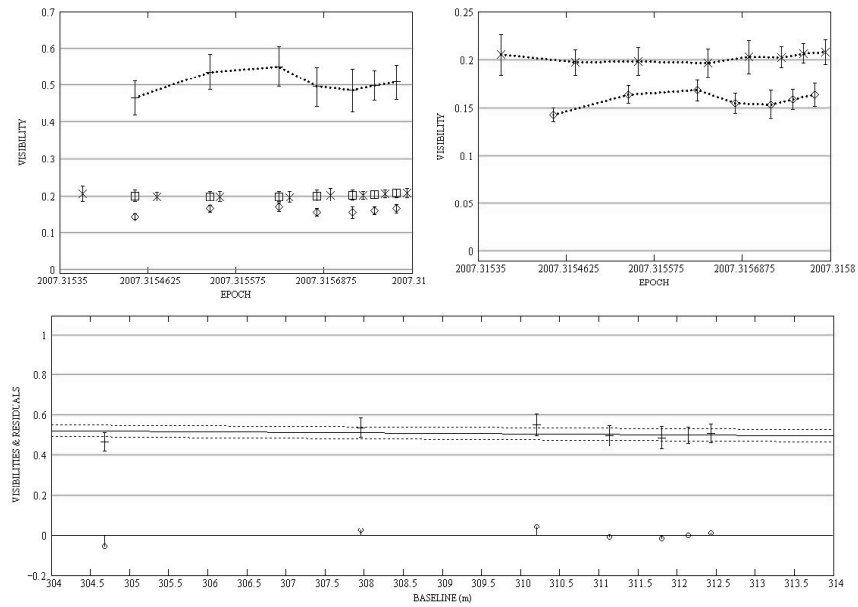


Figure. C.154: HD 104985: Intermediate baseline plots for 2007/04/26 data.

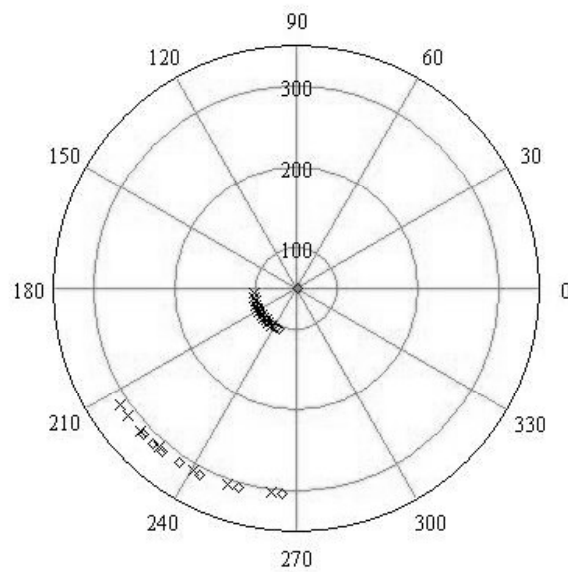


Figure. C.155: HD 104985: All data - Baseline vs. baseline position angle.

C.15.3 Diameter Calculation

The 2007/04/26 data were used in the diameter calculation, as the E1-W1 baseline is much longer than the W1-W2 baseline (314 m vs. 108 m).

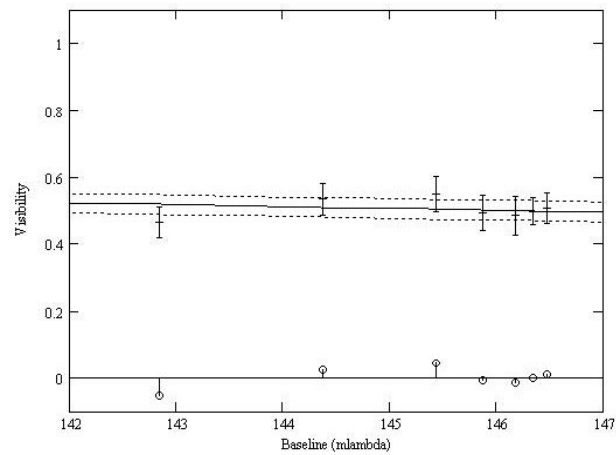


Figure. C.156: HD 104985: LD disk diameter fit: Visibility vs. baseline.

C.15.4 SFP Search

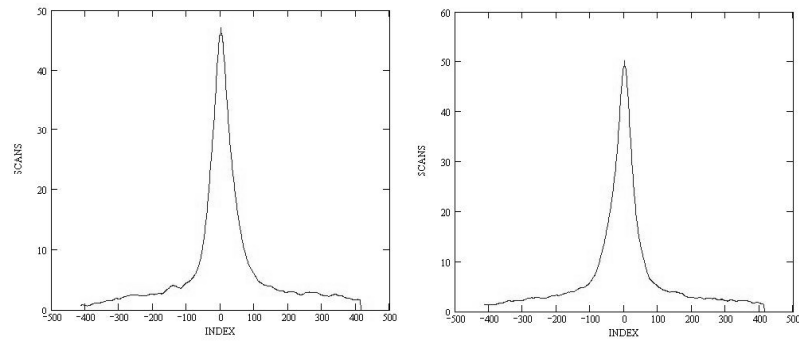


Figure. C.157: HD 104985: SFP inspection for 2006/05/17 data.

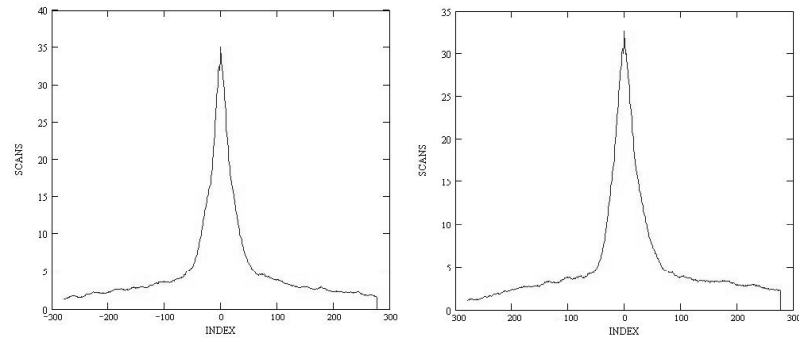


Figure. C.158: HD 104985: SFP inspection for 2007/04/26 data.

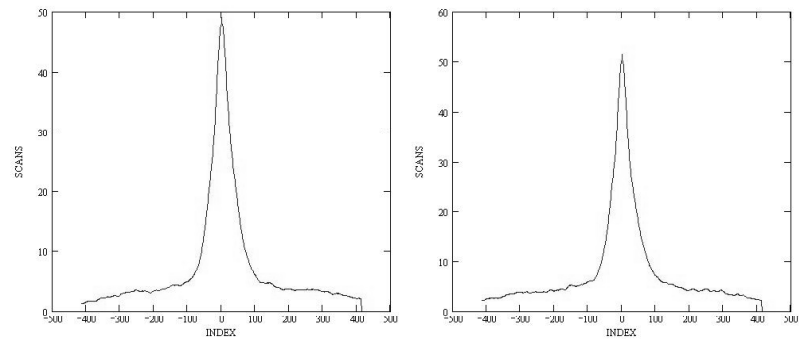


Figure. C.159: HD 97619: SFP inspection for 2006/05/17 data.

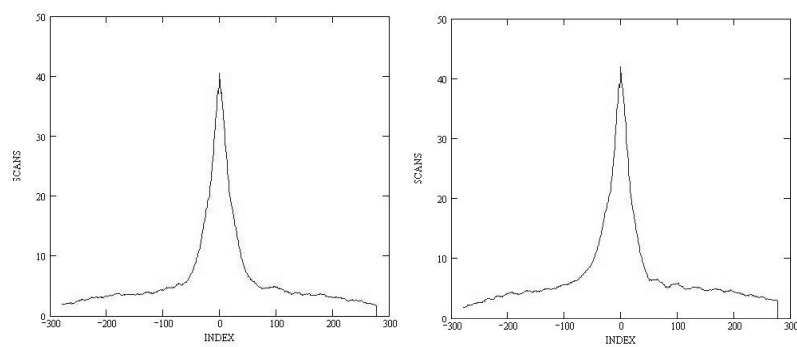


Figure. C.160: HD 97619: SFP inspection for 2007/04/26 data.

C.16 HD 117176

C.16.1 Calibrated Visibilities

Table. C.16: HD 117176: Calibrated Visibilities

| MJD | B (m) | PA (deg) | V_c | σV_c |
|-----------|----------|-------------|-------|--------------|
| 53504.300 | 138.35 | 236.7 | 0.749 | 0.056 |
| 53504.313 | 133.66 | 234.3 | 0.846 | 0.096 |
| 53504.324 | 128.99 | 231.8 | 0.980 | 0.143 |
| 53504.335 | 124.01 | 229.0 | 0.983 | 0.156 |
| 53504.347 | 119.00 | 225.8 | 0.932 | 0.097 |
| 53504.361 | 112.46 | 221.2 | 0.814 | 0.087 |
| 53868.190 | 95.31 | 102.3 | 0.906 | 0.087 |
| 53868.205 | 99.28 | 100.6 | 0.849 | 0.074 |
| 53868.219 | 102.50 | 99.1 | 0.814 | 0.072 |
| 53868.235 | 105.36 | 97.4 | 0.963 | 0.062 |
| 53868.250 | 107.03 | 96.1 | 0.810 | 0.066 |
| 53868.265 | 107.84 | 94.7 | 0.907 | 0.065 |
| 53868.280 | 107.74 | 93.4 | 0.928 | 0.073 |
| 53868.295 | 106.74 | 92.2 | 0.874 | 0.075 |
| 53868.310 | 104.89 | 90.9 | 0.951 | 0.065 |
| 53868.324 | 102.38 | 269.8 | 0.918 | 0.082 |
| 53875.270 | 300.08 | 194.0 | 0.552 | 0.062 |
| 53875.292 | 296.28 | 188.4 | 0.543 | 0.079 |
| 53875.316 | 294.27 | 182.2 | 0.605 | 0.074 |
| 53875.335 | 294.34 | 177.3 | 0.573 | 0.059 |
| 53875.352 | 295.80 | 172.6 | 0.576 | 0.056 |
| 53875.389 | 302.55 | 163.3 | 0.654 | 0.086 |
| 54192.359 | 311.20 | 203.9 | 0.656 | 0.236 |
| 54192.370 | 308.00 | 201.5 | 0.608 | 0.162 |
| 54192.383 | 304.58 | 198.6 | 0.507 | 0.144 |
| 54192.394 | 301.98 | 196.1 | 0.543 | 0.207 |
| 54192.429 | 295.83 | 187.5 | 0.623 | 0.188 |
| 54192.440 | 294.74 | 184.6 | 0.688 | 0.159 |
| 54192.450 | 294.20 | 181.7 | 0.562 | 0.098 |

C.16.2 Nightly Data Plots

There was only one bracketed data point in the 2005/05/13 data, so it was not used in the companion check or in the diameter calculation. There was a gap in time between the first calibrator and first object data points in the 2005/05/14 data, so those two data points were given zero weight and the rest of the data were used in the companion check.

Due to the gap in time between the sixth calibrator and sixth object data points in the 2006/05/20 dataset, the last object and calibrator data points were given zero weight in the diameter calculation and companion check. Similarly, there is a large gap in time between in the fourth object and fifth calibrator data points in the 2007/04/02 dataset, the fourth object observation was given a zero weight, which essentially broke the dataset into two bracketed sections.

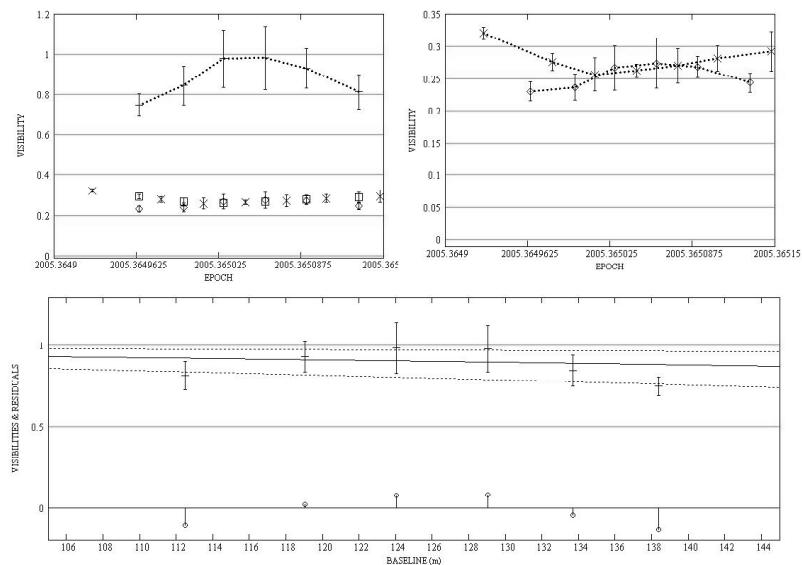


Figure. C.161: HD 117176: Intermediate baseline plots for 2005/05/14 data.

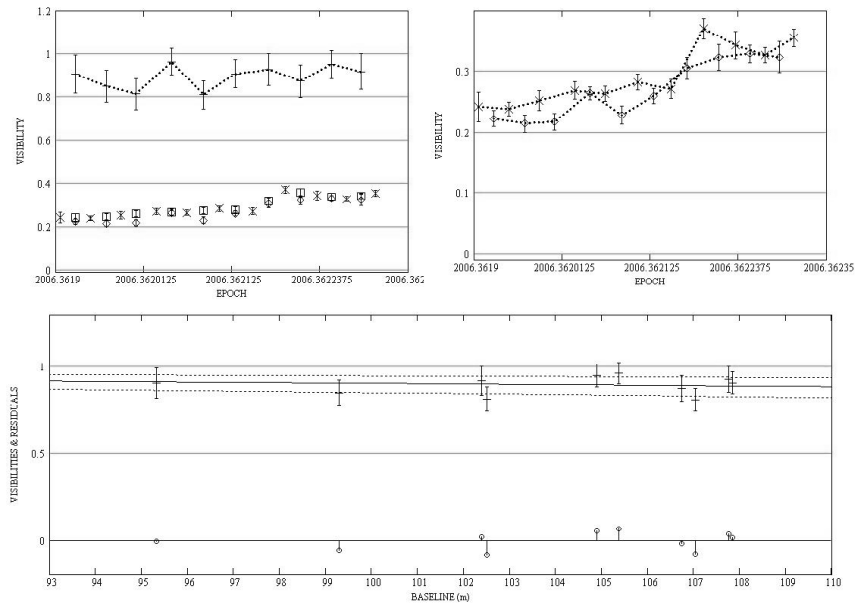


Figure. C.162: HD 117176: Intermediate baseline plots for 2006/05/13 data.

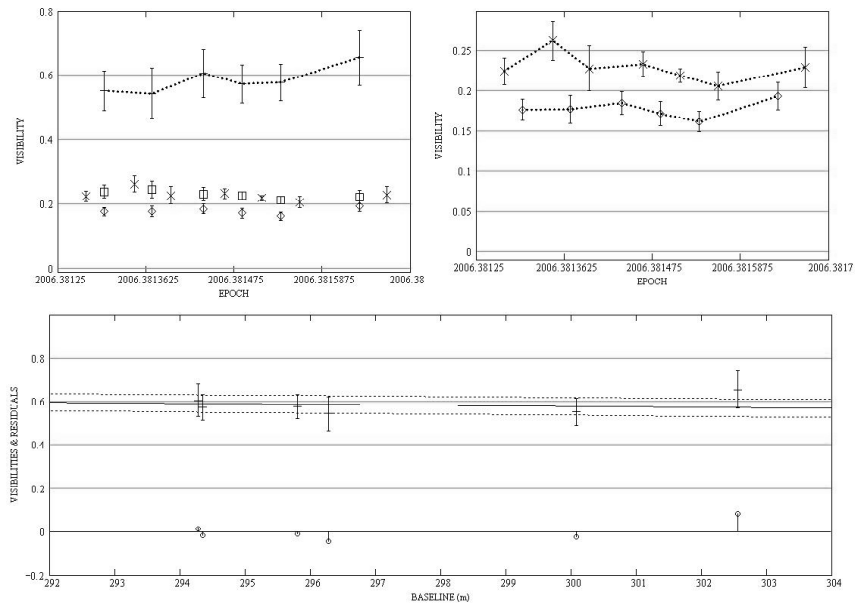


Figure. C.163: HD 117176: Long baseline plots for 2006/05/20 data.

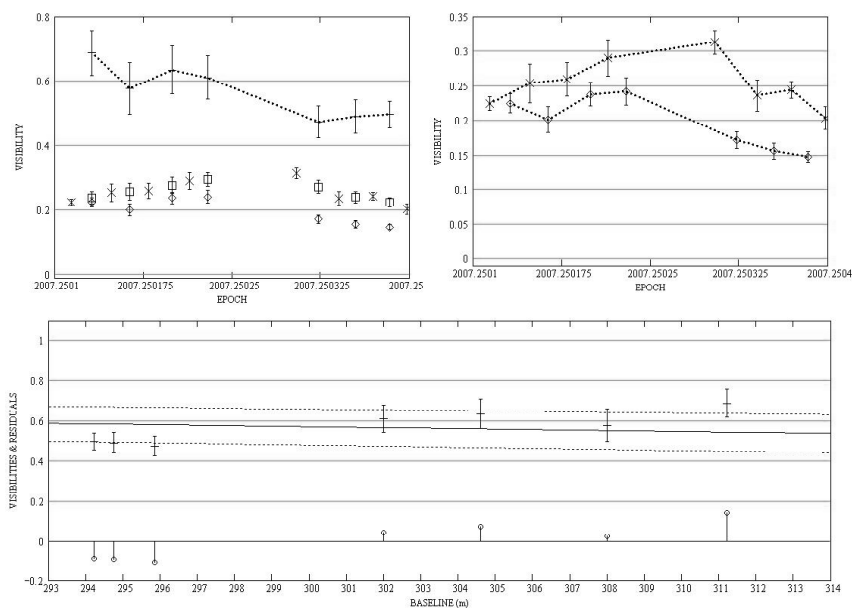


Figure. C.164: HD 117176: Long baseline plots for 2007/04/02 data.

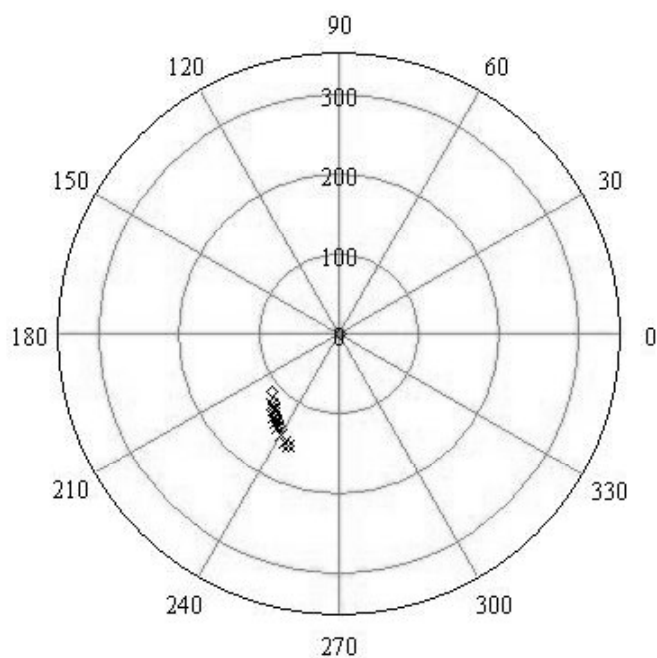


Figure. C.165: HD 117176: All data - Baseline vs. baseline position angle (using calibrator HD 119350).

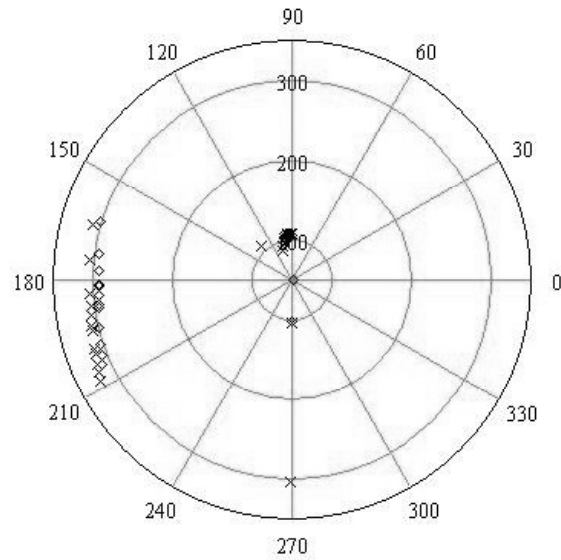


Figure. C.166: HD 117176: All data - Baseline vs. baseline position angle (using calibrator HD 121107).

C.16.3 Diameter Calculation

All the S1-E1 data were used in the diameter calculation.

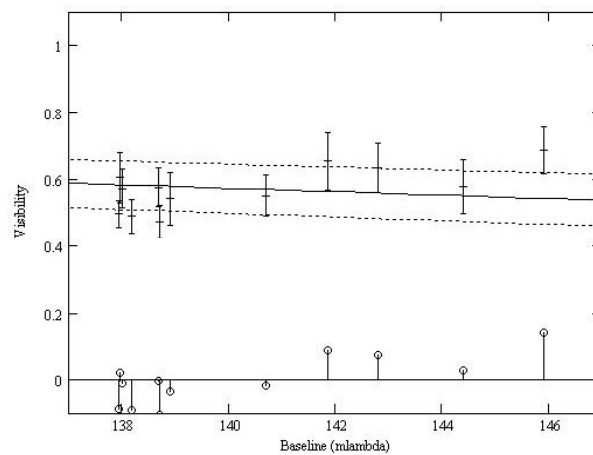


Figure. C.167: HD 117176: LD disk diameter fit: Visibility vs. baseline.

C.16.4 SFP Search

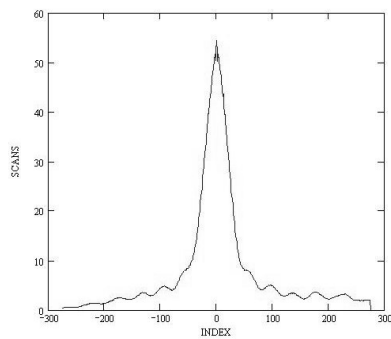


Figure. C.168: HD 117176: SFP inspection for 2005/05/13 data.

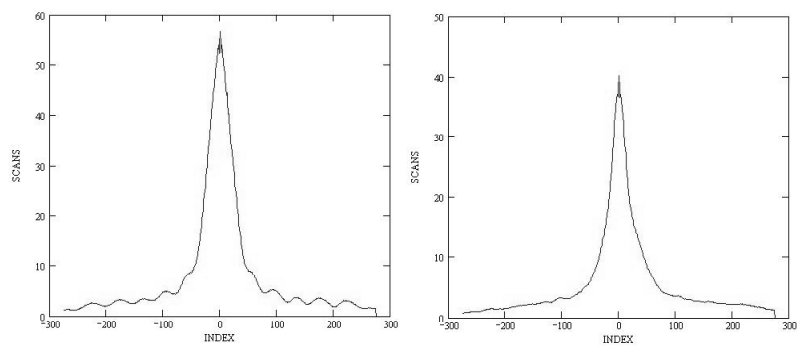


Figure. C.169: HD 117176: SFP inspection for 2005/05/14 data.

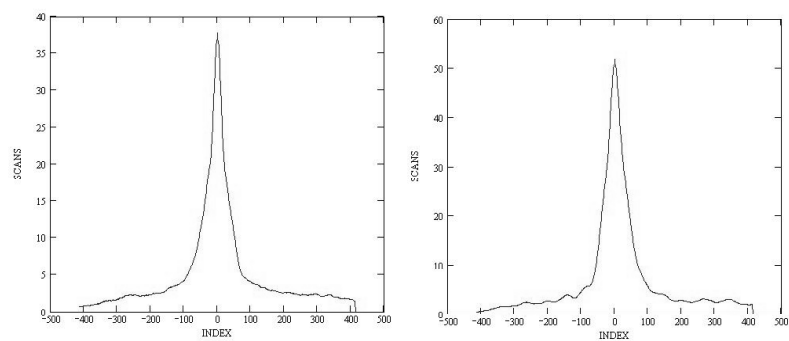


Figure. C.170: HD 117176: SFP inspection for 2006/05/13 data.

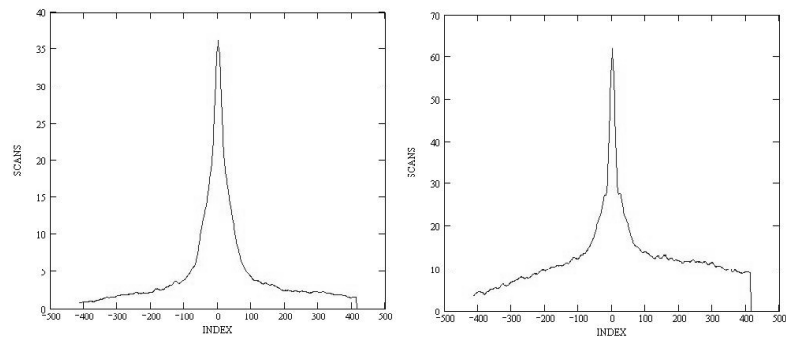


Figure. C.171: HD 117176: SFP inspection for 2006/05/20 data.

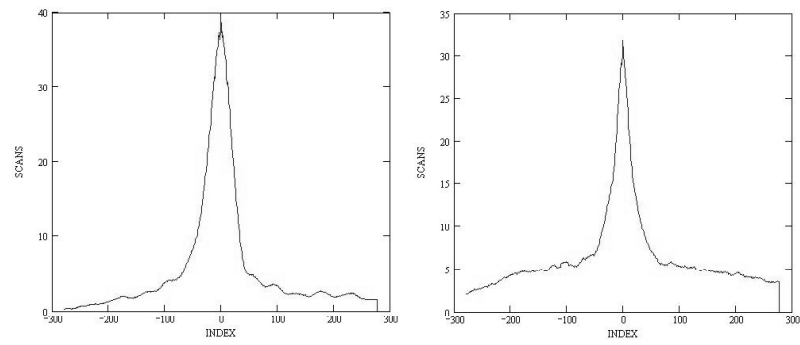


Figure. C.172: HD 117176: SFP inspection for 2007/04/02 data.

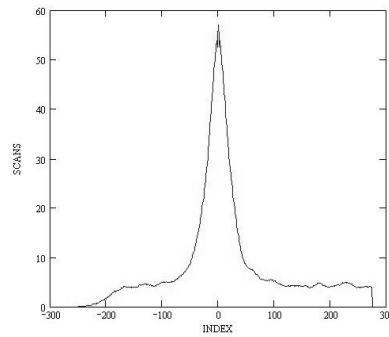


Figure. C.173: HD 119350: SFP inspection for 2005/05/13 data.

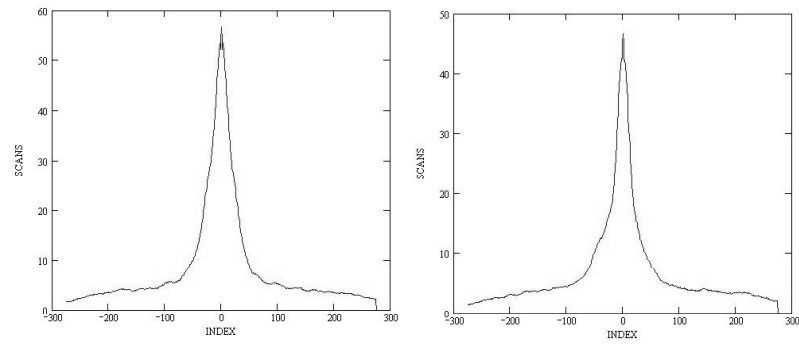


Figure. C.174: HD 119350: SFP inspection for 2005/05/14 data.

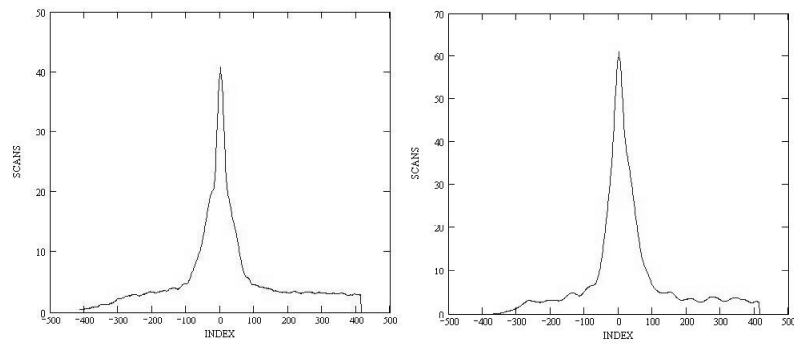


Figure. C.175: HD 121107: SFP inspection for 2006/05/13 data.

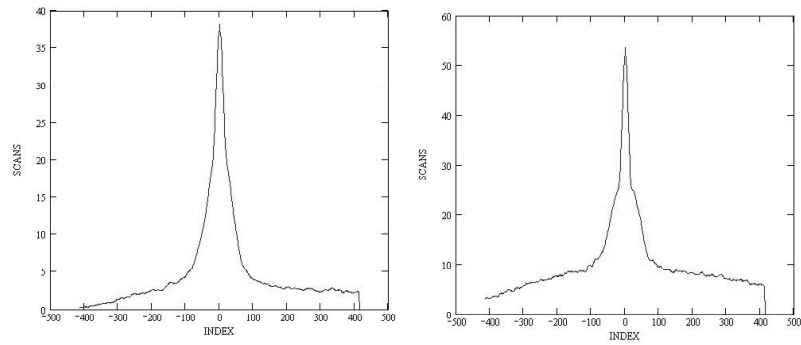


Figure. C.176: HD 121107: SFP inspection for 2006/05/20 data.

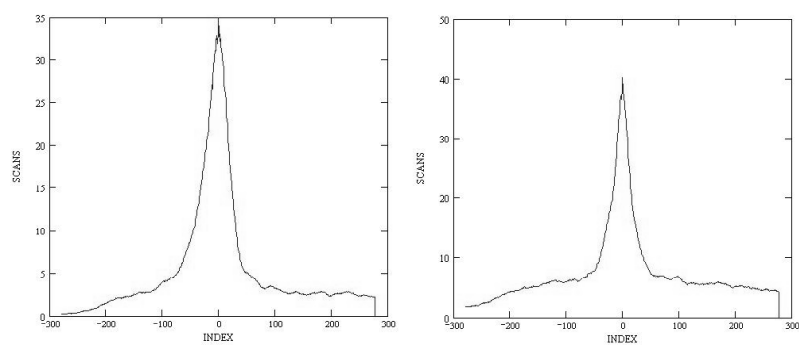


Figure. C.177: HD 121107: SFP inspection for 2007/04/02 data.

C.17 HD 120136

C.17.1 Calibrated Visibilities

Table. C.17: HD 120136: Calibrated Visibilities

| MJD | B (m) | PA (deg) | V_c | $\sigma(V_c)$ |
|-----------|----------|-------------|-------|---------------|
| 53502.235 | 156.27 | 247.7 | 0.891 | 0.079 |
| 53502.245 | 156.02 | 246.6 | 1.021 | 0.057 |
| 53502.254 | 155.37 | 245.5 | 0.927 | 0.082 |
| 53502.265 | 154.08 | 244.1 | 0.853 | 0.060 |
| 53502.275 | 152.38 | 242.7 | 0.817 | 0.093 |
| 53502.294 | 148.27 | 239.8 | 0.825 | 0.074 |
| 53502.309 | 144.15 | 237.2 | 0.968 | 0.098 |
| 53502.319 | 140.89 | 235.2 | 0.909 | 0.108 |
| 53502.329 | 137.20 | 233.0 | 0.901 | 0.124 |
| 53502.340 | 133.15 | 230.4 | 0.808 | 0.066 |
| 53502.357 | 126.52 | 226.0 | 1.018 | 0.119 |
| 53502.373 | 120.20 | 221.1 | 0.718 | 0.080 |
| 53502.384 | 116.02 | 217.5 | 0.800 | 0.078 |
| 53502.397 | 111.10 | 212.5 | 0.965 | 0.074 |
| 53502.410 | 106.81 | 207.2 | 1.032 | 0.125 |
| 53502.422 | 103.46 | 202.0 | 0.787 | 0.104 |
| 53869.184 | 90.83 | 106.9 | 1.000 | 0.085 |
| 53869.197 | 95.08 | 104.7 | 0.932 | 0.074 |
| 53869.210 | 98.68 | 102.8 | 0.954 | 0.070 |
| 53869.226 | 102.37 | 100.6 | 0.931 | 0.097 |
| 53869.240 | 104.75 | 98.9 | 0.894 | 0.084 |
| 53869.253 | 106.46 | 97.4 | 0.940 | 0.089 |
| 53869.269 | 107.66 | 95.5 | 0.921 | 0.068 |
| 53869.283 | 107.90 | 94.1 | 0.961 | 0.068 |
| 53869.296 | 107.46 | 92.7 | 0.964 | 0.103 |
| 53869.309 | 106.28 | 91.2 | 0.912 | 0.081 |
| 53869.323 | 104.44 | 269.7 | 0.913 | 0.077 |
| 54136.370 | 321.01 | 222.5 | 0.635 | 0.056 |
| 54136.381 | 324.27 | 221.9 | 0.668 | 0.058 |
| 54136.391 | 326.49 | 221.3 | 0.658 | 0.063 |
| 54136.400 | 328.20 | 220.6 | 0.641 | 0.052 |
| 54136.411 | 329.58 | 219.8 | 0.688 | 0.047 |
| 54136.423 | 330.44 | 218.7 | 0.657 | 0.060 |
| 54136.434 | 330.67 | 217.6 | 0.656 | 0.044 |
| 54136.445 | 330.34 | 216.3 | 0.612 | 0.046 |
| 54136.456 | 329.54 | 214.9 | 0.637 | 0.045 |
| 54136.466 | 328.37 | 213.5 | 0.638 | 0.052 |
| 54184.452 | 305.95 | 190.2 | 0.702 | 0.077 |

Continued on Next Page...

Table. C.17 – Continued

| MJD | B (m) | PA (deg) | V_c | $\sigma(V_c)$ |
|------------|------------------|---------------------|-------------------------|---------------------------------|
| 54184.470 | 304.03 | 185.5 | 0.674 | 0.065 |
| 54185.359 | 323.92 | 209.3 | 0.753 | 0.079 |
| 54185.370 | 321.72 | 207.4 | 0.726 | 0.050 |
| 54185.382 | 319.17 | 205.2 | 0.743 | 0.067 |
| 54185.393 | 316.66 | 202.9 | 0.635 | 0.049 |
| 54185.403 | 314.46 | 200.9 | 0.586 | 0.057 |
| 54189.375 | 318.31 | 204.4 | 0.663 | 0.088 |
| 54189.391 | 314.63 | 201.0 | 0.690 | 0.089 |
| 54189.403 | 312.13 | 198.5 | 0.689 | 0.055 |
| 54189.413 | 310.24 | 196.4 | 0.743 | 0.075 |
| 54189.422 | 308.31 | 193.9 | 0.686 | 0.084 |
| 54189.435 | 306.50 | 191.1 | 0.667 | 0.080 |
| 54189.444 | 305.25 | 188.8 | 0.657 | 0.069 |
| 54189.455 | 304.17 | 186.0 | 0.630 | 0.074 |

C.17.2 Nightly Data Plots

A little more than halfway through the 2005/05/12 dataset, the visibility changes abruptly with a signature characteristic of a rapid change in seeing conditions. The calibrator and visibilities track well up until that point and then rise over a very short period of time, separate, then come together. Given the nature of the tracking on the other night of intermediate-baseline data, I suspect quickly changing seeing effects created this unusual pattern instead of a stellar companion. Therefore I removed these points when calculating the visibility residuals when performing the companion check.

The 2007/03/25 dataset was not considered in the companion check as there were only two bracketed data points in the observation. The rest of the nights' data were used.

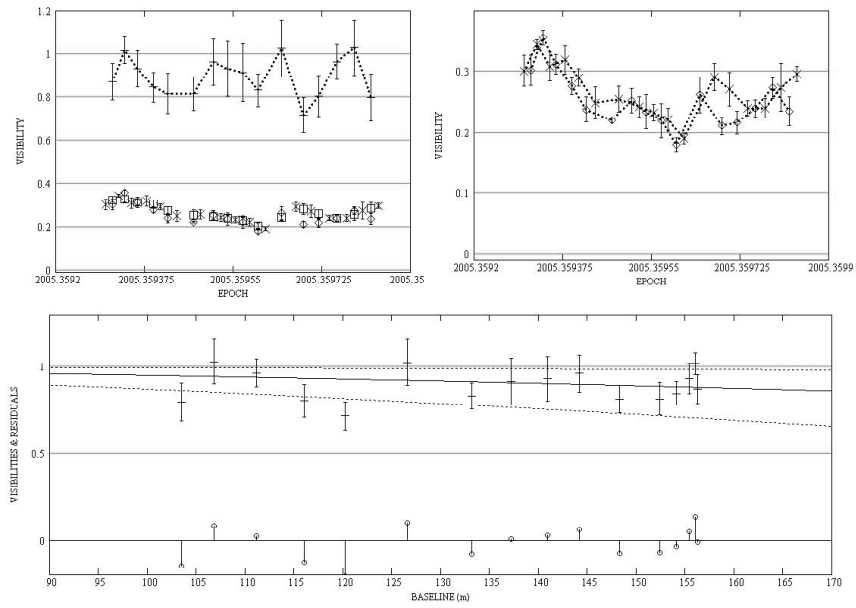


Figure. C.178: HD 120136: Intermediate baseline plots for 2005/05/12 data.

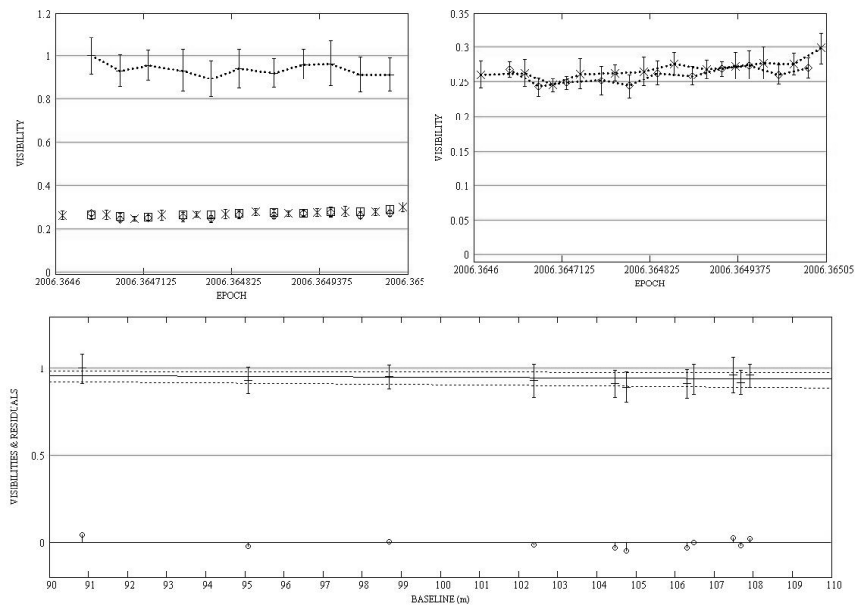


Figure. C.179: HD 120136: Intermediate baseline plots for 2006/05/14 data.

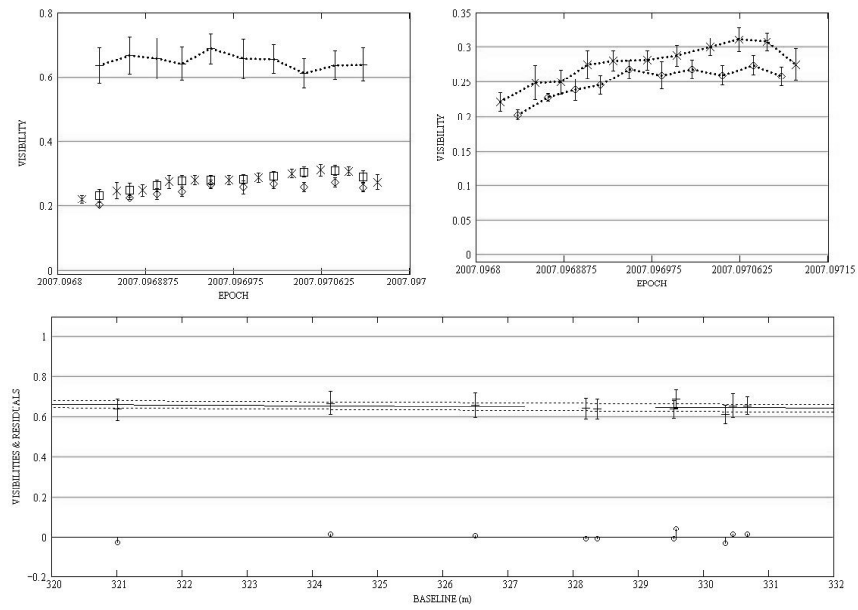


Figure. C.180: HD 120136: Long baseline plots for 2007/02/05 data.

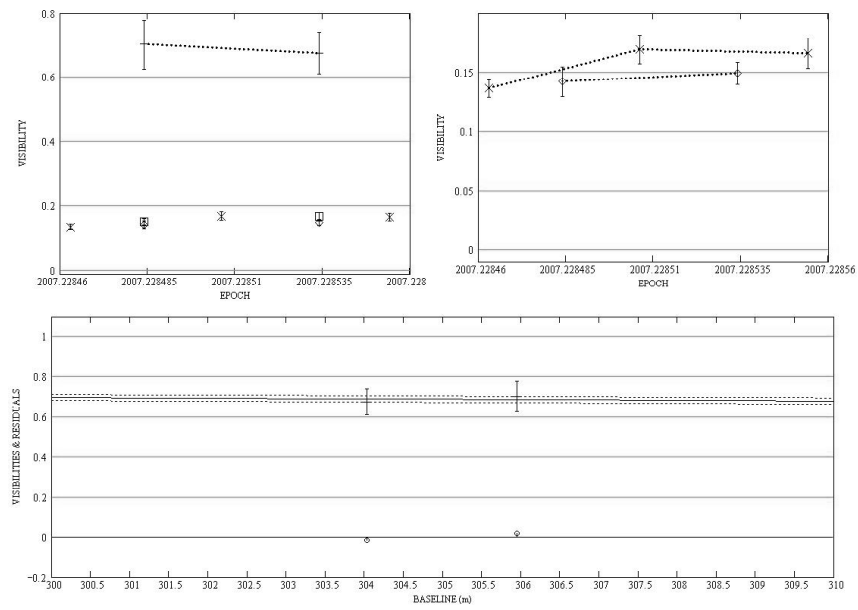


Figure. C.181: HD 120136: Long baseline plots for 2007/03/25 data.

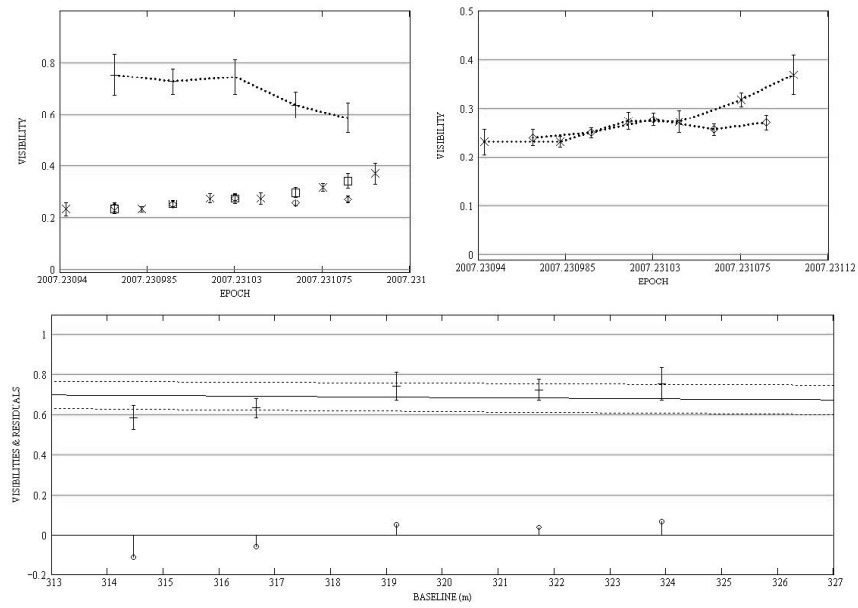


Figure. C.182: HD 120136: Long baseline plots for 2007/03/26 data.

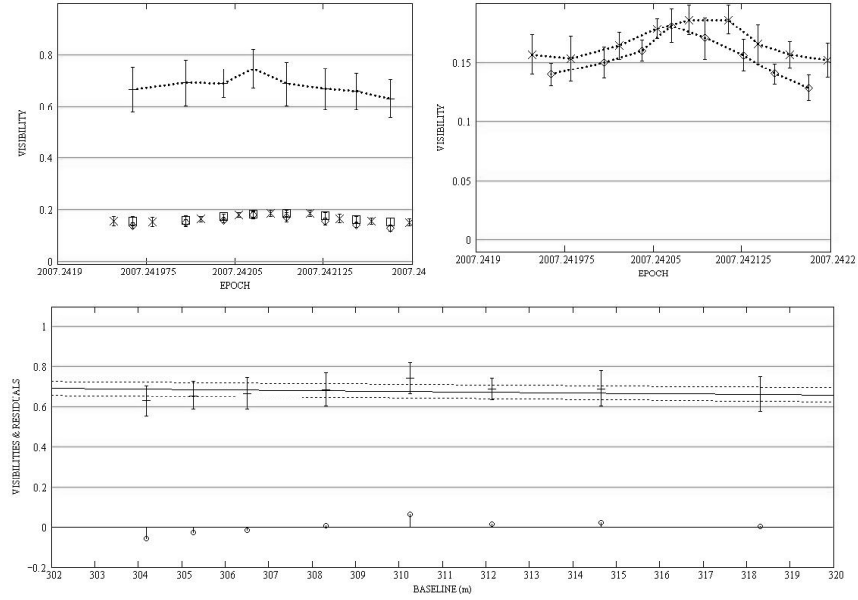


Figure. C.183: HD 120136: Long baseline plots for 2007/03/30 data.

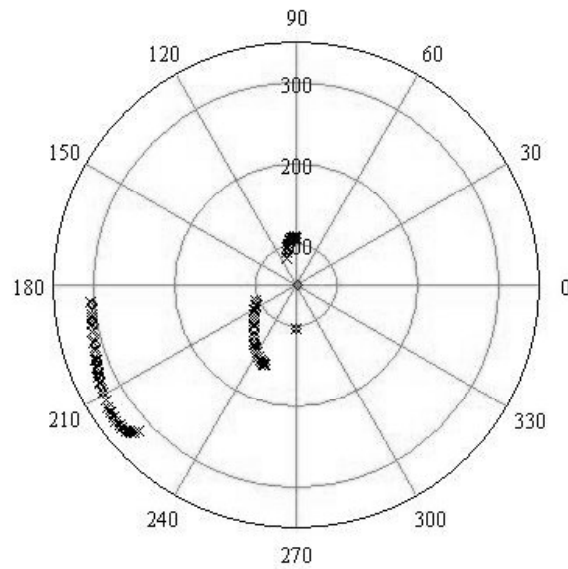


Figure. C.184: HD 120136: All data - Baseline vs. baseline position angle.

C.17.3 Diameter Calculation

I used all the S1-E1 data in the diameter calculation.

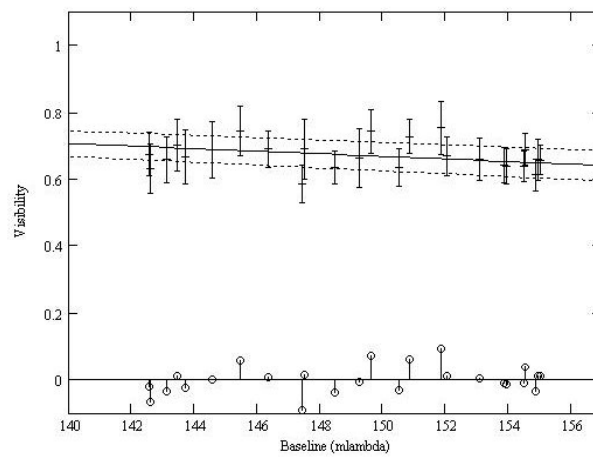


Figure. C.185: HD 120136: LD disk diameter fit: Visibility vs. baseline.

C.17.4 SFP Search

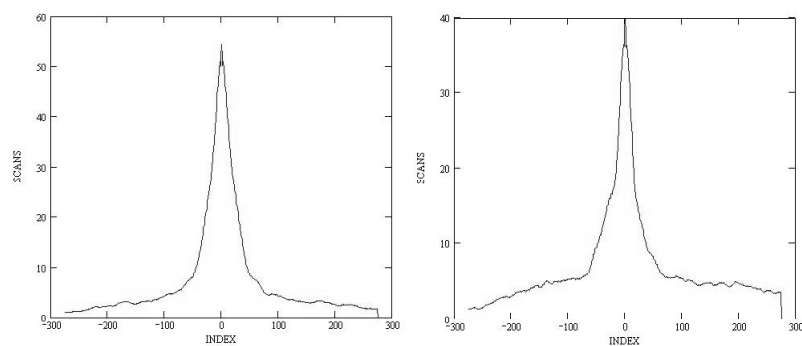


Figure. C.186: HD 120136: SFP inspection for 2005/05/12 data.

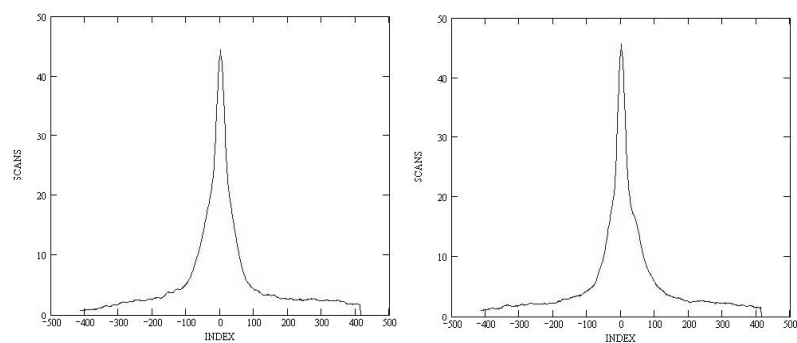


Figure. C.187: HD 120136: SFP inspection for 2006/05/14 data.

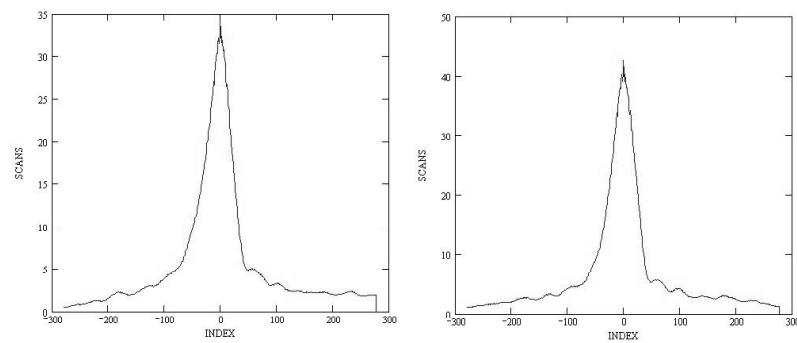


Figure. C.188: HD 120136: SFP inspection for 2007/02/05 data.

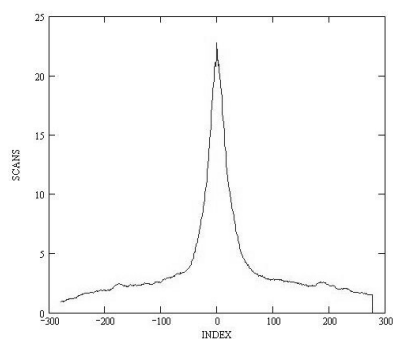


Figure. C.189: HD 120136: SFP inspection for 2007/03/25 data.

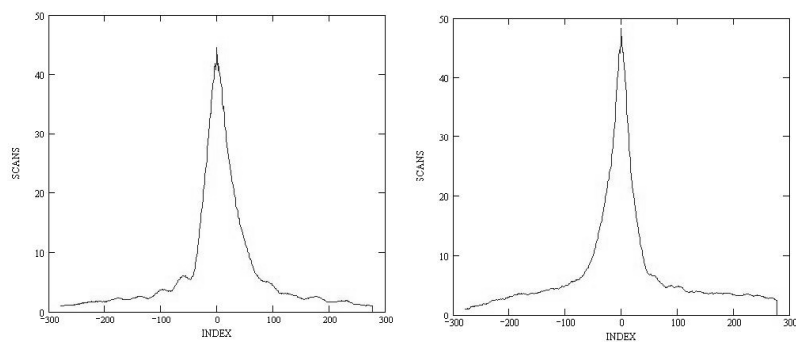


Figure. C.190: HD 120136: SFP inspection for 2007/03/26 data.

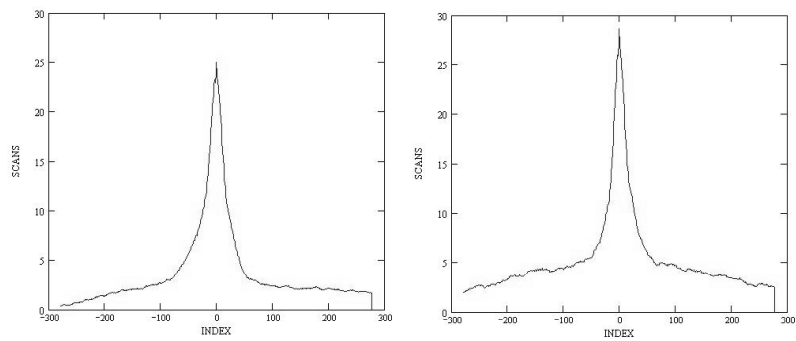


Figure. C.191: HD 120136: SFP inspection for 2007/03/30 data.

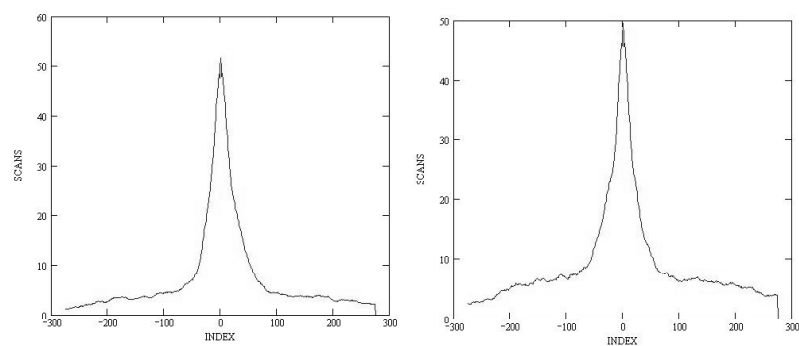


Figure. C.192: HD 121107: SFP inspection for 2005/05/12 data.

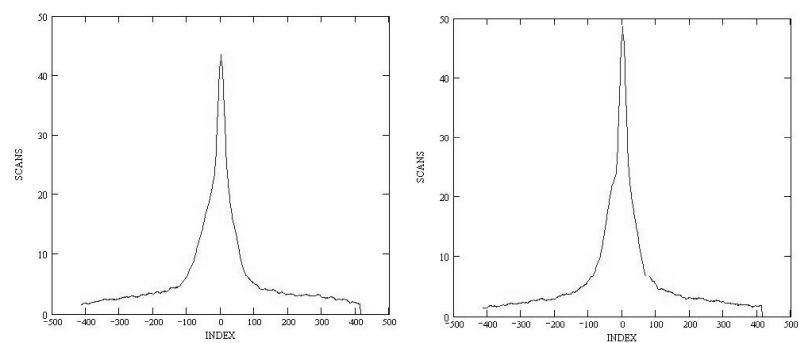


Figure. C.193: HD 121107: SFP inspection for 2006/05/14 data.

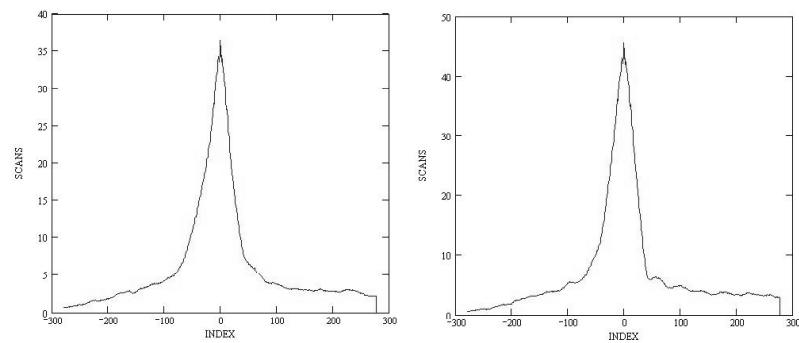


Figure. C.194: HD 121107: SFP inspection for 2007/02/05 data.

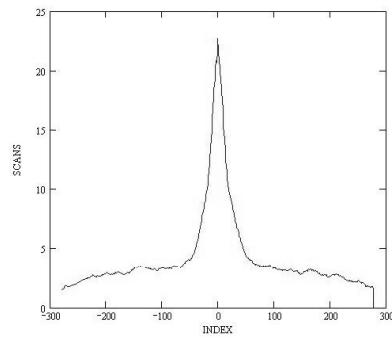


Figure. C.195: HD 121107: SFP inspection for 2007/03/25 data.

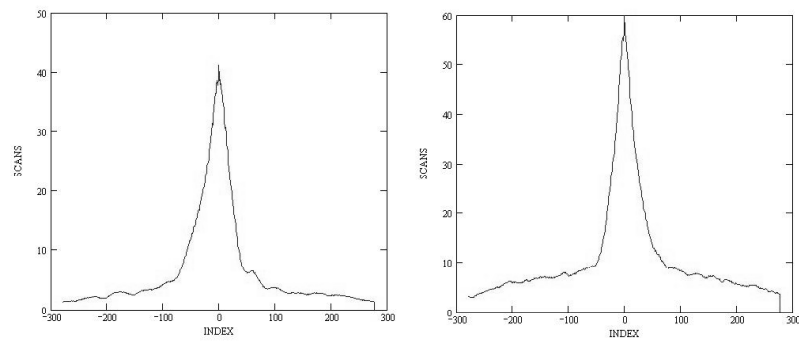


Figure. C.196: HD 121107: SFP inspection for 2007/03/26 data.

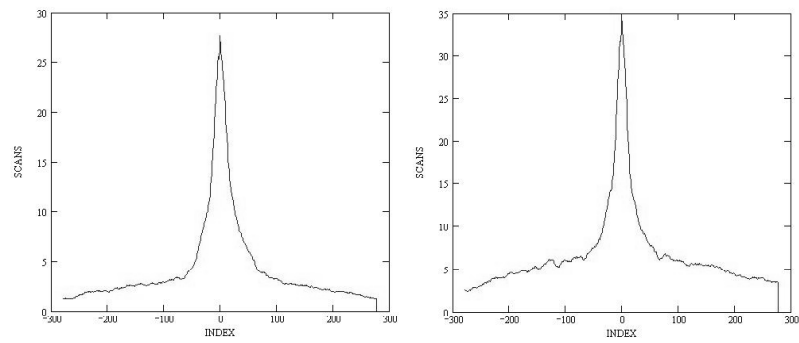


Figure. C.197: HD 121107: SFP inspection for 2007/03/30 data.

C.18 HD 128311

C.18.1 Calibrated Visibilities

Table. C.18: HD 128311: Calibrated Visibilities

| MJD | B (m) | PA (deg) | V_c | $\sigma(V_c)$ |
|-----------|----------|-------------|-------|---------------|
| 53551.211 | 138.16 | 239.7 | 1.000 | 0.090 |
| 53551.225 | 132.54 | 237.4 | 1.038 | 0.101 |
| 53551.238 | 126.60 | 234.8 | 0.965 | 0.092 |
| 53551.251 | 120.55 | 232.0 | 1.095 | 0.114 |
| 53551.265 | 113.45 | 228.2 | 0.977 | 0.084 |
| 53871.244 | 99.11 | 98.8 | 1.093 | 0.114 |
| 53871.263 | 103.25 | 97.4 | 1.016 | 0.116 |
| 53871.277 | 105.58 | 96.3 | 1.071 | 0.116 |
| 53871.293 | 107.32 | 95.2 | 1.090 | 0.089 |
| 53871.313 | 107.90 | 94.0 | 1.015 | 0.108 |
| 53871.327 | 107.37 | 93.2 | 1.007 | 0.092 |

C.18.2 Nightly Data Plots

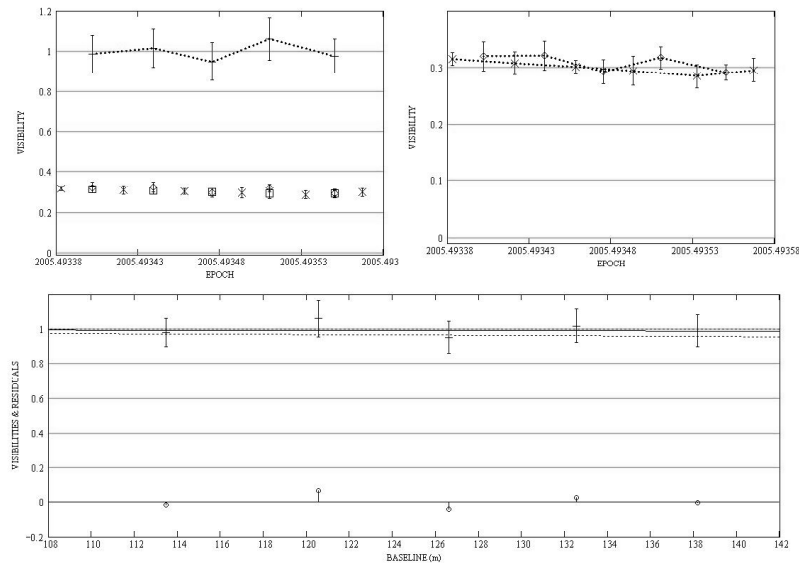


Figure. C.198: HD 128311: Intermediate baseline plots for 2005/06/30 data.

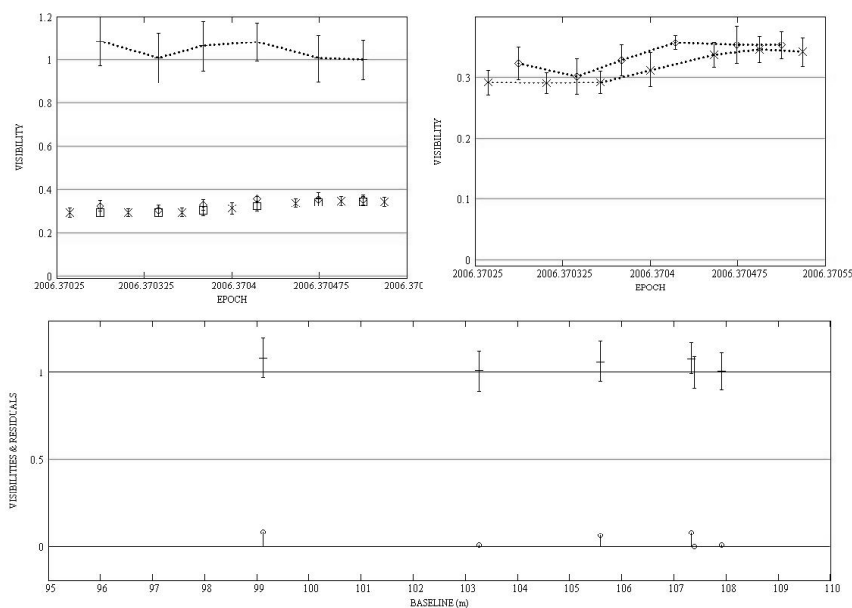


Figure. C.199: HD 128311: Intermediate baseline plots for 2006/05/16 data.

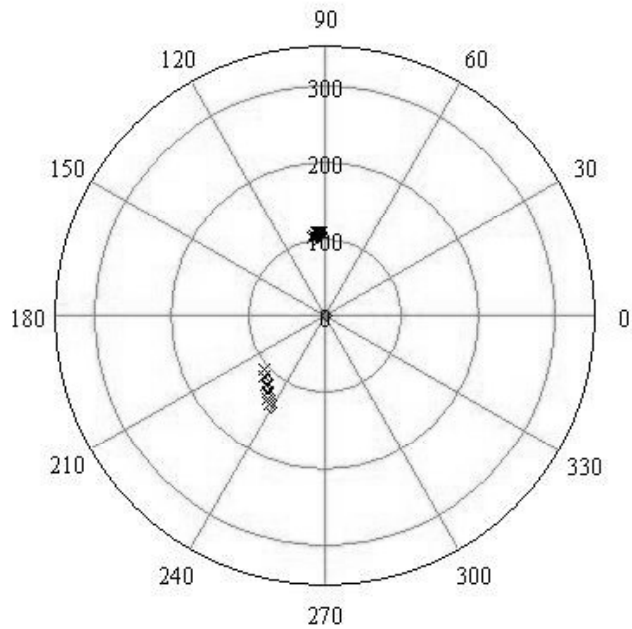


Figure. C.200: HD 128311: All data - Baseline vs. baseline position angle.

C.18.3 Diameter Calculation

The diameter calculation for 2006/05/16 failed, producing a diameter of 0.001 mas, indicating the star is unresolved. The 2005/06/30 data confirms this with a LD diameter measurement of 0.244 ± 0.261 mas.

Considering the error to the diameter fit for HD 128311 is 107% the diameter itself, the diameter estimated from the SED (0.438 mas) was used for the companion check.

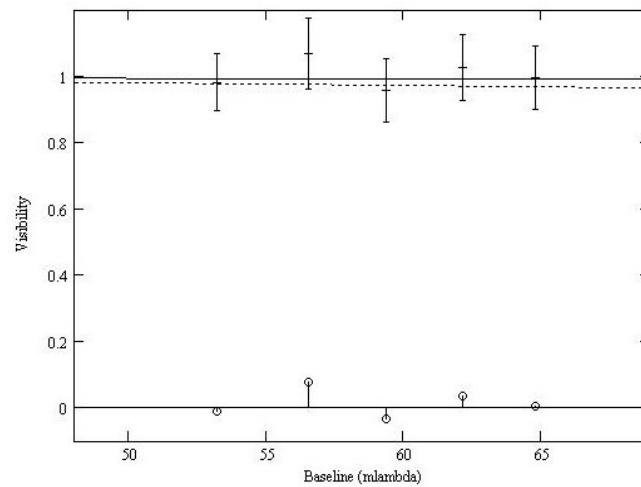


Figure. C.201: HD 128311: LD disk diameter fit: Visibility vs. baseline.

C.18.4 SFP Search

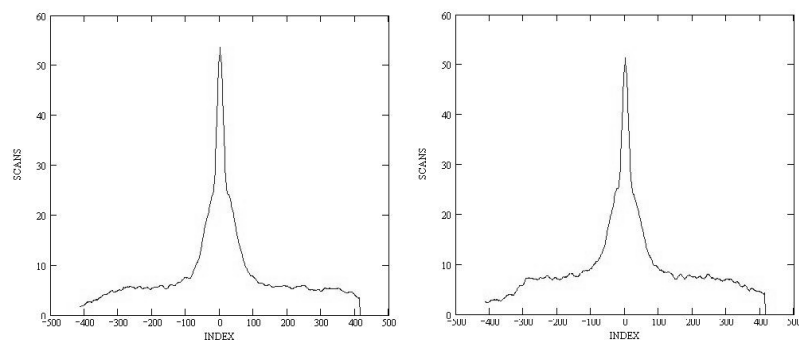


Figure. C.202: HD 128311: SFP inspection for 2005/06/30 data.

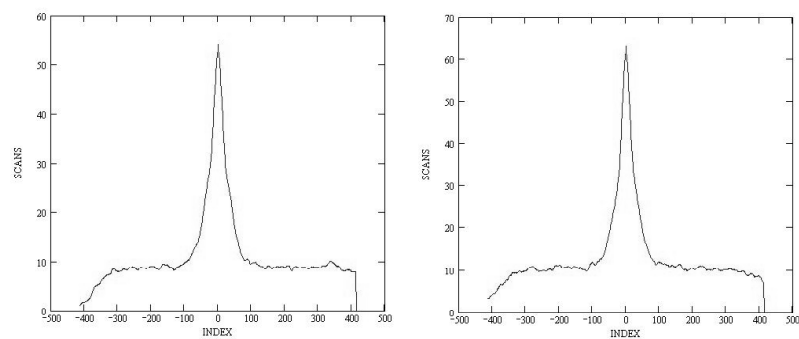


Figure. C.203: HD 128311: SFP inspection for 2006/05/16 data.

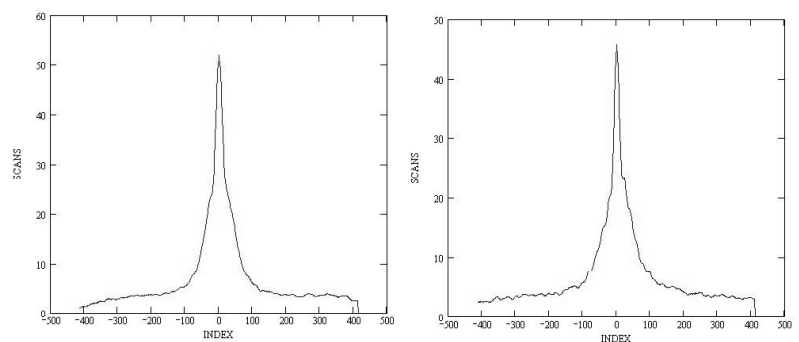


Figure. C.204: HD 125194: SFP inspection for 2005/06/30 data.

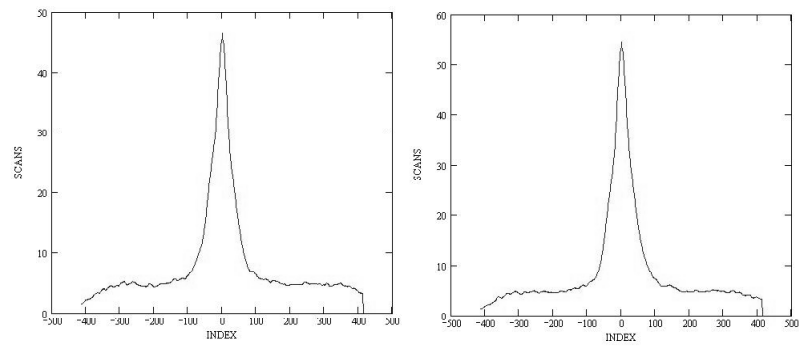


Figure. C.205: HD 125194: SFP inspection for 2006/05/16 data.

C.19 HD 143761

C.19.1 Calibrated Visibilities

HD 143761 was observed with four different calibrators, usually one calibrator per night. The exception to this was the 2006/05/12 data, when HD 143761 was observed using two calibrators. This is the reason there are three tables with calibrated visibilities (V_c) instead of the customary one table. Table C.19 lists V_c for all the data except that taken on 2006/05/12; Table C.20 lists V_c for 2006/05/12 data taken using HD 143687 as the calibrator; and Table C.21 lists V_c for 2006/05/12 data obtained using HD 146025 as the calibrator.

Table. C.19: HD 143761: Calibrated Visibilities (all but 2006/05/12)

| MJD | B (m) | PA (deg) | V_c | $\sigma(V_c)$ |
|-----------|----------|-------------|-------|---------------|
| 53550.299 | 146.56 | 225.3 | 0.792 | 0.073 |
| 53550.320 | 141.94 | 218.9 | 0.790 | 0.097 |
| 53550.341 | 137.58 | 212.4 | 0.808 | 0.066 |
| 53550.354 | 134.87 | 207.8 | 0.892 | 0.049 |
| 53550.367 | 132.46 | 203.0 | 0.918 | 0.039 |
| 53550.381 | 130.37 | 197.9 | 0.916 | 0.034 |
| 53554.259 | 151.82 | 232.8 | 0.729 | 0.055 |
| 53554.270 | 150.06 | 230.2 | 0.718 | 0.070 |
| 53554.280 | 148.15 | 227.5 | 0.747 | 0.089 |
| 53554.290 | 146.15 | 224.7 | 0.851 | 0.072 |
| 53554.310 | 141.92 | 218.9 | 0.904 | 0.076 |
| 53554.324 | 138.87 | 214.4 | 0.931 | 0.057 |
| 53554.336 | 136.37 | 210.4 | 0.932 | 0.107 |
| 53874.389 | 328.56 | 190.3 | 0.692 | 0.061 |
| 53874.409 | 327.99 | 185.8 | 0.718 | 0.079 |
| 53874.425 | 327.74 | 181.8 | 0.790 | 0.088 |
| 53874.444 | 327.78 | 177.3 | 0.884 | 0.096 |
| 53895.224 | 329.09 | 212.5 | 0.658 | 0.056 |

Table. C.20: HD 143761: Calibrated Visibilities (from 2006/05/12
using calibrator HD 143681)

| MJD | B (m) | PA (deg) | V_c | $\sigma(V_c)$ |
|------------|------------------|---------------------|-------------------------|---------------------------------|
| 53867.227 | 81.92 | 132.5 | 0.934 | 0.122 |
| 53867.265 | 92.20 | 120.0 | 0.945 | 0.113 |
| 53867.289 | 97.74 | 113.7 | 0.946 | 0.090 |
| 53867.312 | 102.29 | 108.1 | 0.893 | 0.077 |
| 53867.430 | 103.44 | 263.9 | 0.950 | 0.086 |
| 53867.457 | 98.07 | 258.0 | 0.997 | 0.107 |
| 53867.470 | 94.75 | 254.9 | 0.883 | 0.087 |
| 53867.483 | 91.30 | 251.7 | 0.922 | 0.082 |

Table. C.21: HD 143761: Calibrated Visibilities (from 2006/05/12
using calibrator HD 146025)

| MJD | B (m) | PA (deg) | V_c | $\sigma(V_c)$ |
|------------|------------------|---------------------|-------------------------|---------------------------------|
| 53867.198 | 74.45 | 144.4 | 0.987 | 0.088 |
| 53867.227 | 81.92 | 132.5 | 0.940 | 0.117 |
| 53867.265 | 92.20 | 120.0 | 0.901 | 0.100 |
| 53867.289 | 97.74 | 113.7 | 0.929 | 0.079 |
| 53867.312 | 102.29 | 108.1 | 0.874 | 0.074 |

C.19.2 Nightly Data Plots

As there is only one bracketed observation in the 2006/06/09 dataset, it was used in the diameter calculation but was not included in the companion check.

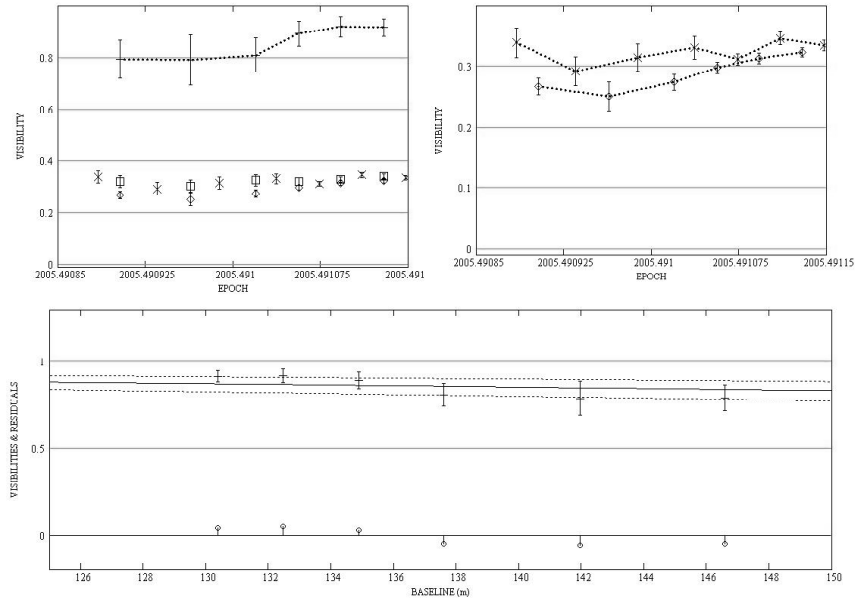


Figure. C.206: HD 143761: Intermediate baseline plots for 2005/06/29 data.

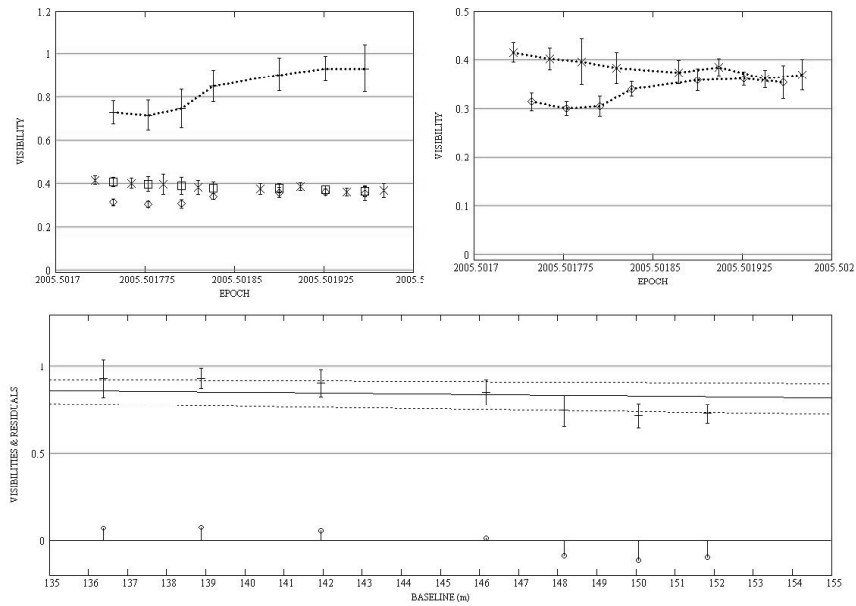


Figure. C.207: HD 143761: Intermediate baseline plots for 2005/07/03 data.

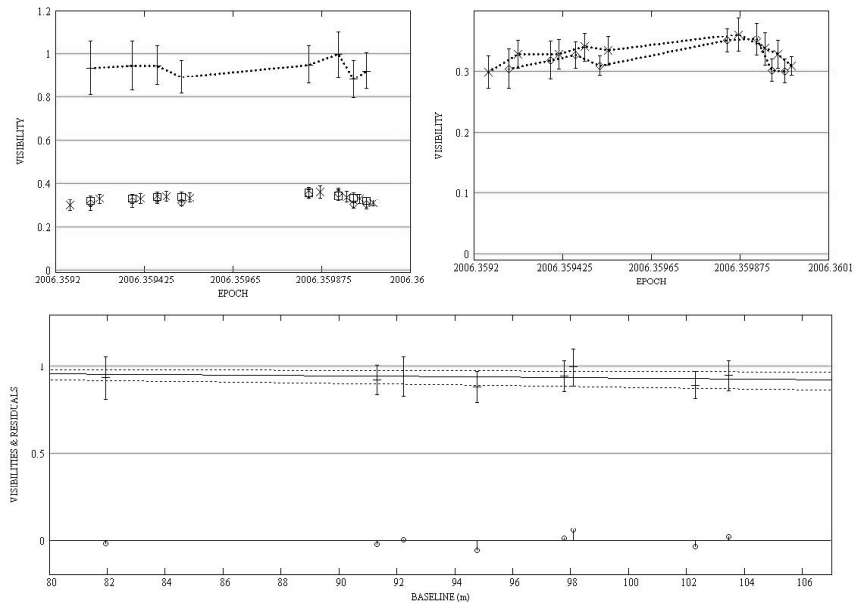


Figure. C.208: HD 143761: Intermediate baseline plots for 2006/05/12 data using calibrator HD 143687.

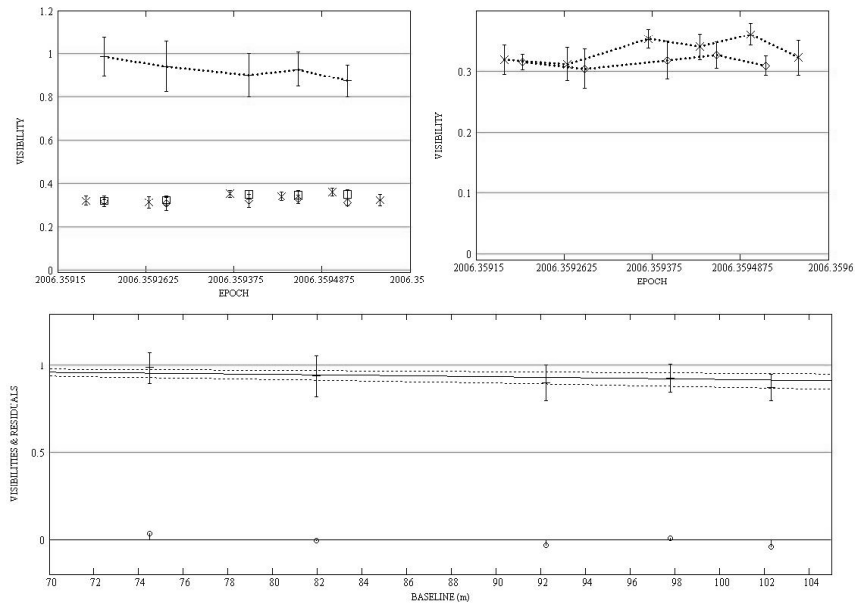


Figure. C.209: HD 143761: Intermediate baseline plots for 2006/05/12 data using calibrator HD 146025.

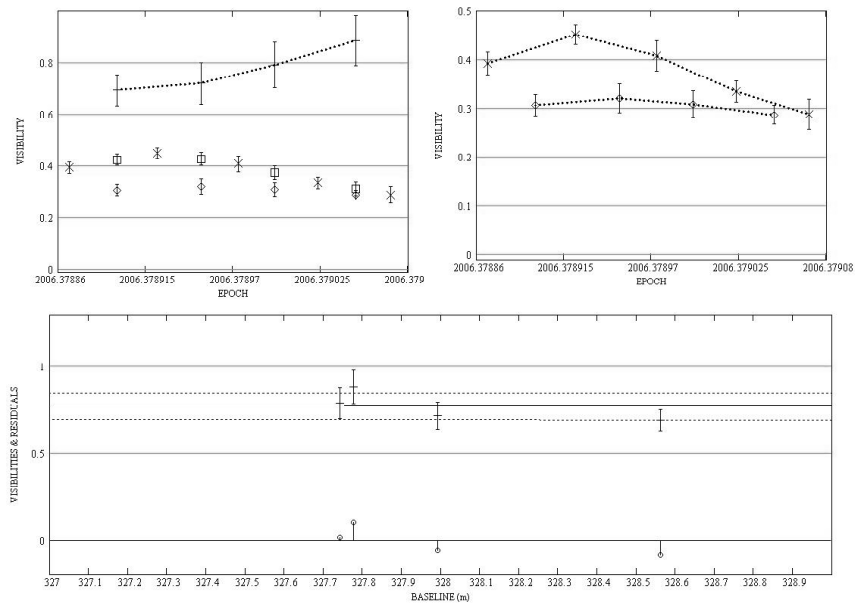


Figure. C.210: HD 143761: Long baseline plots for 2006/05/19 data.

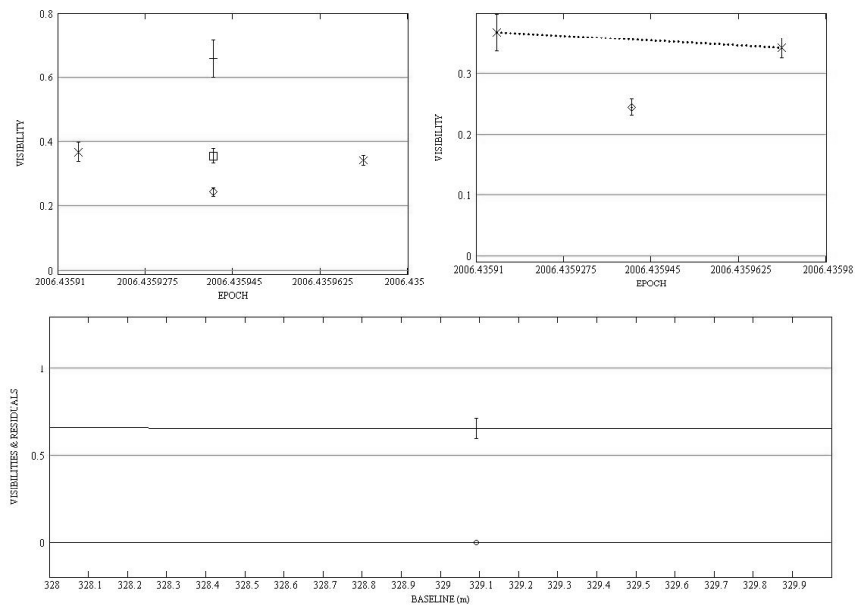


Figure. C.211: HD 143761: Long baseline plots for 2006/06/09 data.

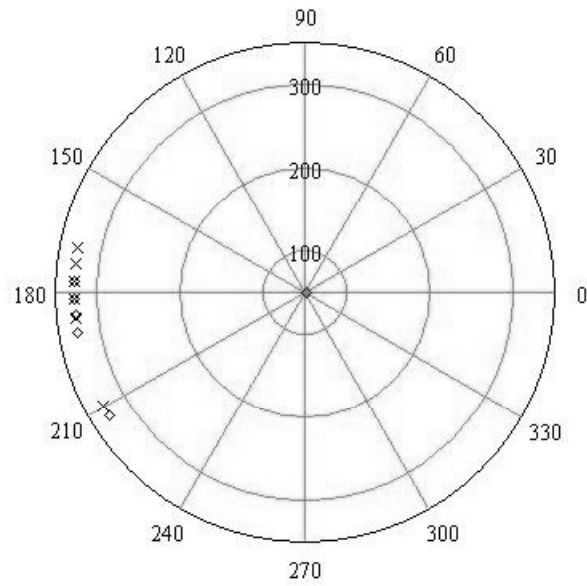


Figure. C.212: HD 143761: All data - Baseline vs. baseline position angle (using calibrator HD 136849).

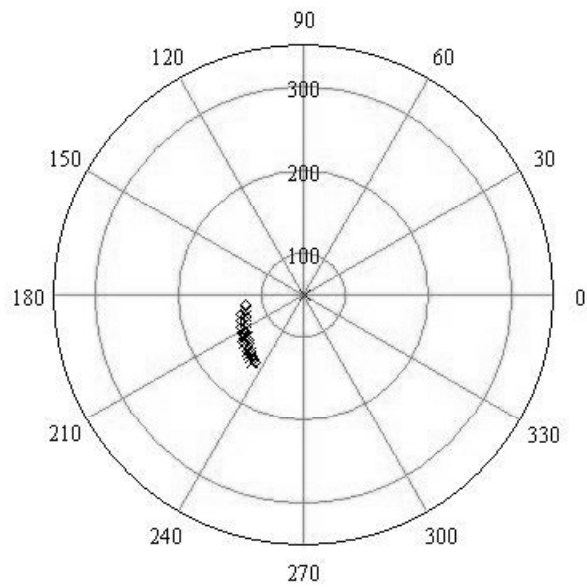


Figure. C.213: HD 143761: All data - Baseline vs. baseline position angle (using calibrator HD 143393).

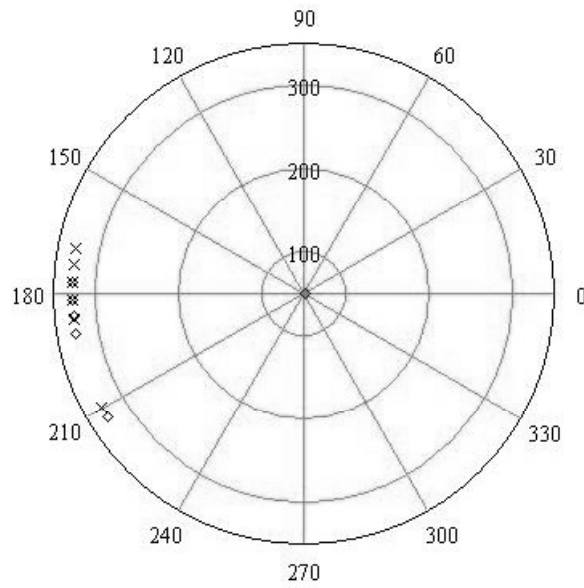


Figure. C.214: HD 143761: All data - Baseline vs. baseline position angle (using calibrator HD 143687).

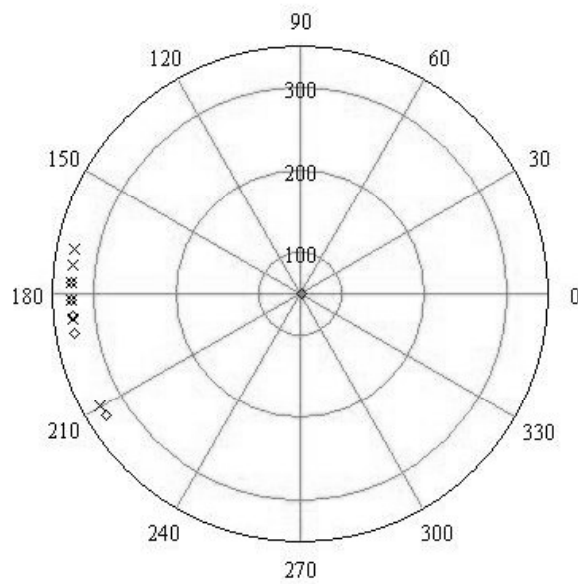


Figure. C.215: HD 143761: All data - Baseline vs. baseline position angle (using calibrator HD 146025).

C.19.3 Diameter Calculation

All S1-E1 data were used to calculate the stellar diameter.

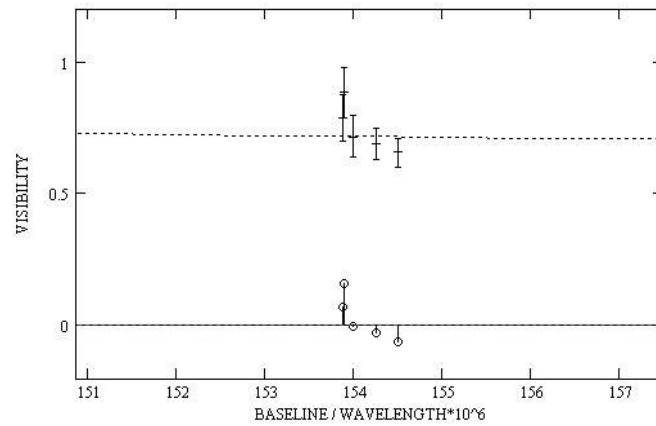


Figure. C.216: HD 143761: LD disk diameter fit: Visibility vs. baseline.

C.19.4 SFP Search

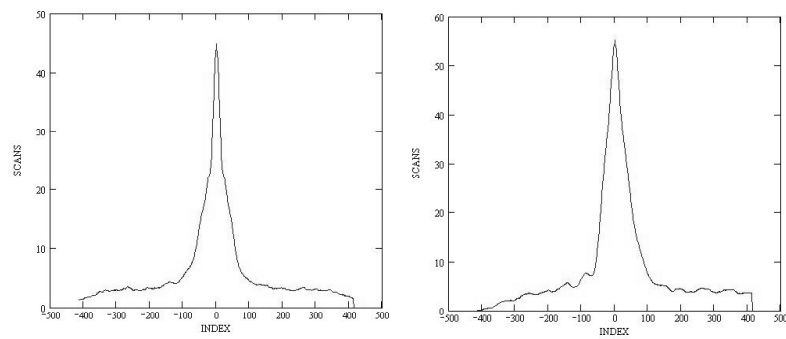


Figure. C.217: HD 143761: SFP inspection for 2005/06/29 data.

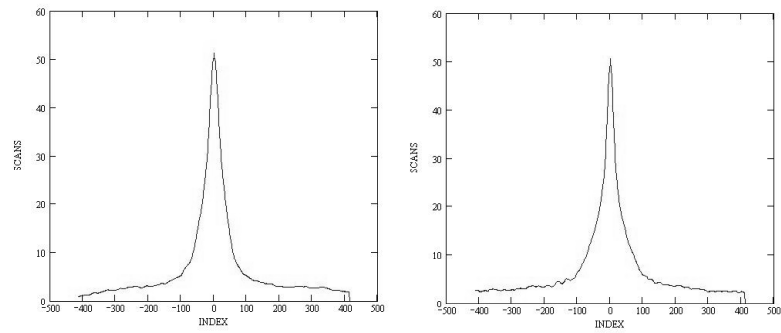


Figure. C.218: HD 143761: SFP inspection for 2005/07/03 data.

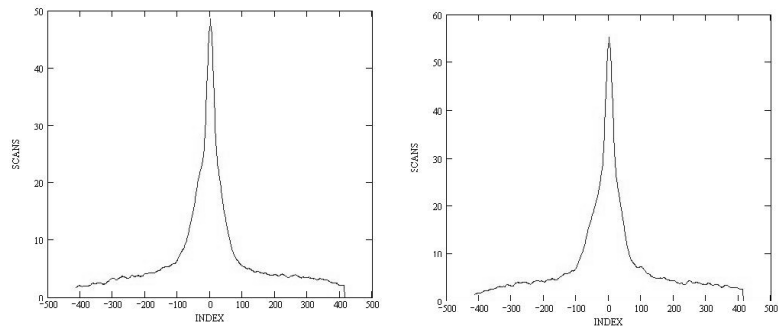


Figure. C.219: HD 143761: SFP inspection for 2006/05/12 data.

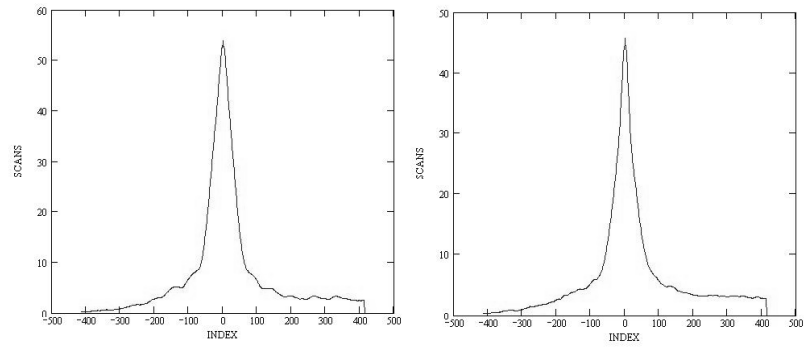


Figure. C.220: HD 143761: SFP inspection for 2006/05/19 data.

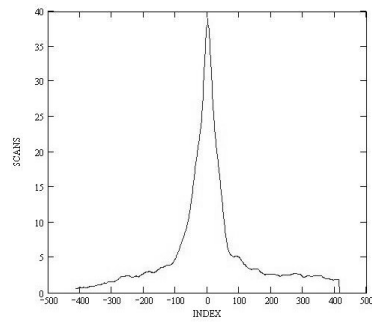


Figure. C.221: HD 143761: SFP inspection for 2006/06/09 data.

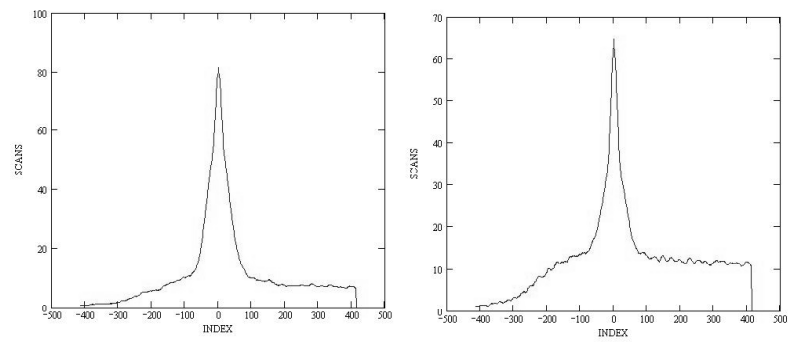


Figure. C.222: HD 136849: SFP inspection for 2006/05/19 data.

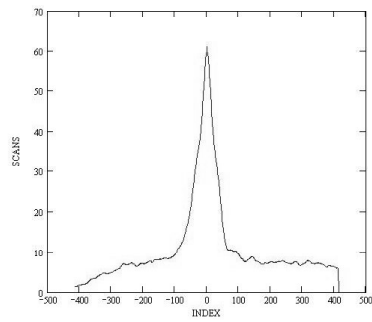


Figure. C.223: HD 136849: SFP inspection for 2005/06/09 data.

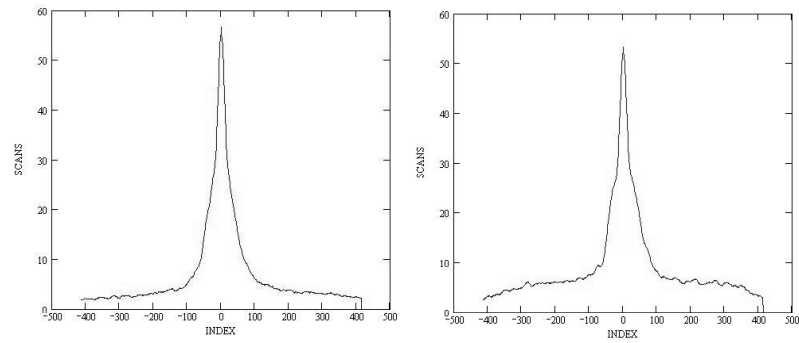


Figure. C.224: HD 143393: SFP inspection for 2005/06/29 data.

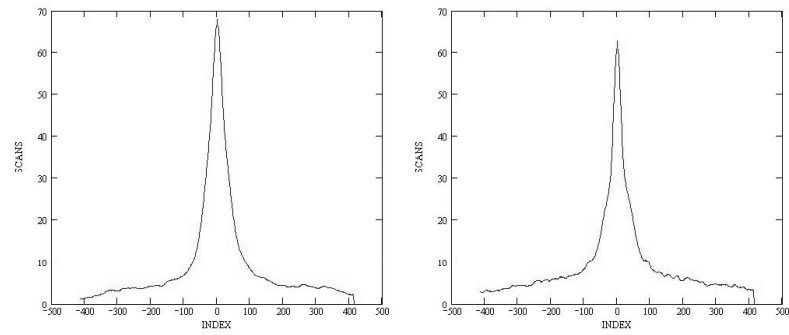


Figure. C.225: HD 143393: SFP inspection for 2005/07/03 data.

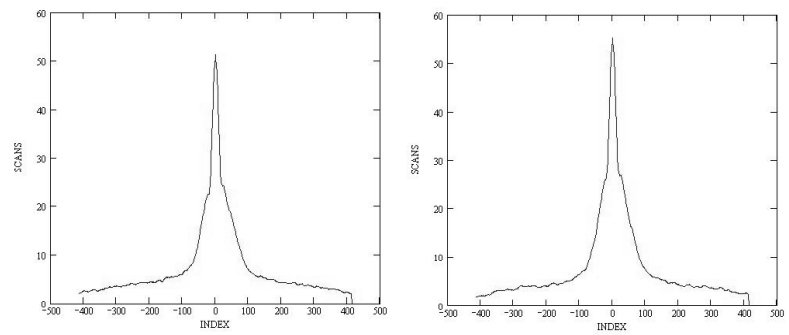


Figure. C.226: HD 143687: SFP inspection for 2006/05/12 data.

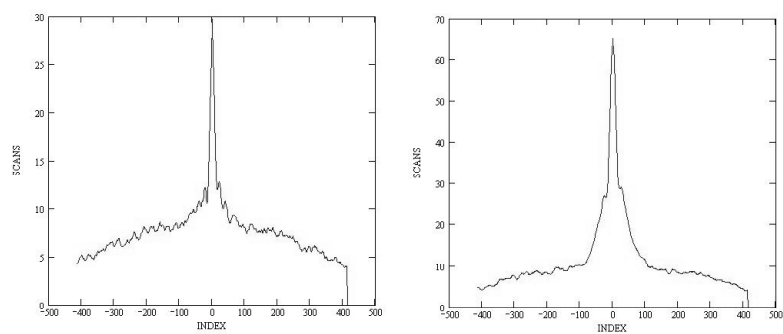


Figure. C.227: HD 146025: SFP inspection for 2006/05/12 data.

C.20 HD 145675

C.20.1 Calibrated Visibilities

Table. C.22: HD 145675: Calibrated Visibilities

| MJD | B (m) | PA (deg) | V_c | $\sigma(V_c)$ |
|-----------|----------|-------------|-------|---------------|
| 53504.431 | 152.50 | 223.3 | 0.728 | 0.051 |
| 53504.442 | 151.29 | 220.1 | 0.715 | 0.077 |
| 53504.453 | 149.96 | 216.6 | 0.878 | 0.065 |
| 53504.463 | 148.78 | 213.5 | 0.951 | 0.096 |
| 53504.474 | 147.53 | 210.1 | 0.980 | 0.104 |
| 53504.484 | 146.38 | 206.8 | 0.947 | 0.088 |
| 53555.245 | 156.04 | 236.4 | 0.763 | 0.089 |
| 53555.254 | 155.63 | 233.9 | 0.963 | 0.058 |
| 53555.263 | 155.08 | 231.4 | 0.986 | 0.057 |
| 53555.272 | 154.39 | 229.0 | 0.975 | 0.063 |
| 53555.281 | 153.59 | 226.5 | 0.964 | 0.076 |
| 53555.290 | 152.70 | 223.9 | 0.949 | 0.074 |
| 53555.299 | 151.77 | 221.4 | 0.985 | 0.078 |
| 53555.307 | 150.80 | 218.8 | 0.995 | 0.083 |
| 53555.316 | 149.73 | 216.0 | 1.082 | 0.087 |
| 53555.326 | 148.61 | 213.1 | 1.004 | 0.120 |
| 53555.336 | 147.38 | 209.7 | 0.947 | 0.103 |
| 53868.359 | 107.64 | 99.7 | 0.889 | 0.103 |
| 53868.374 | 107.92 | 95.9 | 0.789 | 0.076 |
| 53868.389 | 107.71 | 92.2 | 0.816 | 0.056 |
| 53868.403 | 107.02 | 268.6 | 0.898 | 0.056 |
| 53868.421 | 105.54 | 264.1 | 0.975 | 0.074 |
| 53868.435 | 103.92 | 260.4 | 1.036 | 0.061 |
| 53868.449 | 101.92 | 256.7 | 0.964 | 0.065 |
| 53868.462 | 99.73 | 253.2 | 1.041 | 0.052 |
| 53868.475 | 97.29 | 249.5 | 1.013 | 0.046 |
| 53868.488 | 94.50 | 245.4 | 1.010 | 0.069 |
| 53954.177 | 106.40 | 266.4 | 0.996 | 0.100 |
| 53954.191 | 105.04 | 262.9 | 1.177 | 0.127 |
| 53954.206 | 103.16 | 259.0 | 1.017 | 0.078 |
| 53954.221 | 100.78 | 254.8 | 1.018 | 0.085 |
| 53954.235 | 98.35 | 251.0 | 1.041 | 0.134 |
| 53954.248 | 95.72 | 247.2 | 1.008 | 0.102 |
| 53954.261 | 92.89 | 243.1 | 0.926 | 0.091 |
| 53954.274 | 89.96 | 238.8 | 0.998 | 0.099 |
| 53954.288 | 86.73 | 234.0 | 0.966 | 0.091 |
| 53954.301 | 83.67 | 229.1 | 0.962 | 0.080 |
| 53958.259 | 329.81 | 168.4 | 0.903 | 0.055 |

Continued on Next Page...

Table. C.22 – Continued

| MJD | B (m) | PA (deg) | V_c | $\sigma(V_c)$ |
|-----------|----------|-------------|-------|---------------|
| 53958.275 | 329.38 | 164.9 | 0.880 | 0.045 |
| 53958.292 | 328.62 | 161.0 | 0.861 | 0.051 |
| 53959.168 | 329.99 | 189.3 | 1.097 | 0.123 |
| 53959.184 | 330.18 | 185.5 | 1.002 | 0.089 |
| 53959.200 | 330.26 | 181.8 | 0.966 | 0.069 |
| 53959.215 | 330.26 | 178.1 | 0.992 | 0.070 |
| 53959.231 | 330.18 | 174.5 | 0.941 | 0.078 |
| 53959.246 | 330.01 | 170.9 | 0.956 | 0.067 |
| 53959.261 | 329.70 | 167.4 | 0.809 | 0.064 |

C.20.2 Nightly Data Plots

The data from 2006/08/11 were not considered in the companion check because there were only three bracketed observations. The last calibrator data point in the 2006/08/12 dataset shows an unexpected rise in visibility that is probably due to some late-night seeing changes. The last object and calibrator data points were removed for the diameter calculation and companion check.

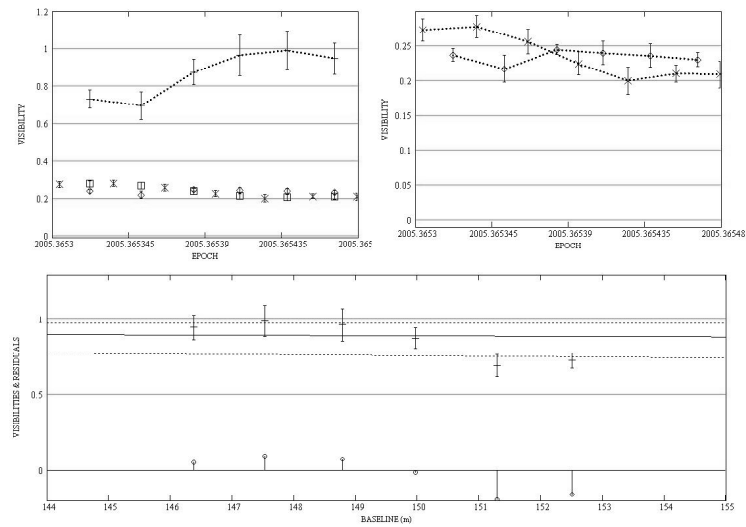


Figure. C.228: HD 145675: Intermediate baseline plots for 2005/05/14 data.

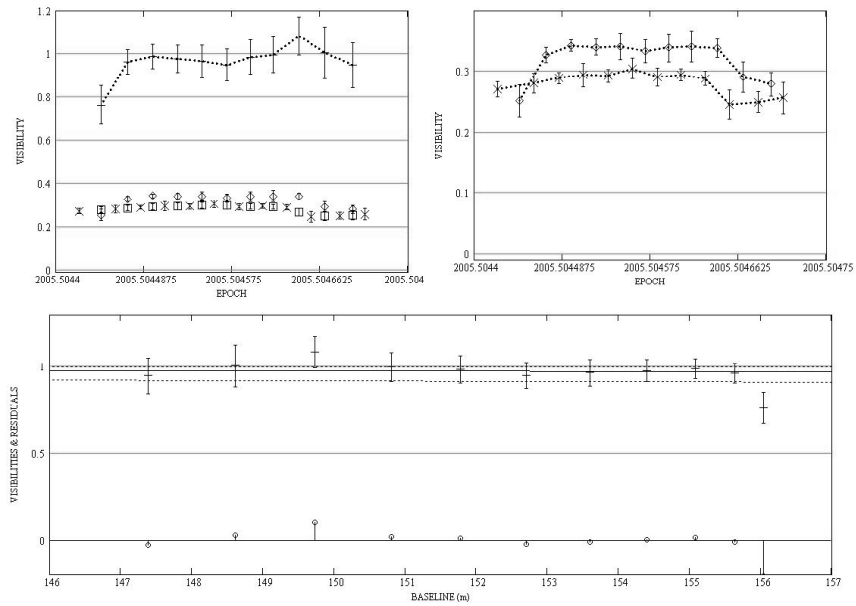


Figure. C.229: HD 145675: Intermediate baseline plots for 2005/07/04 data.

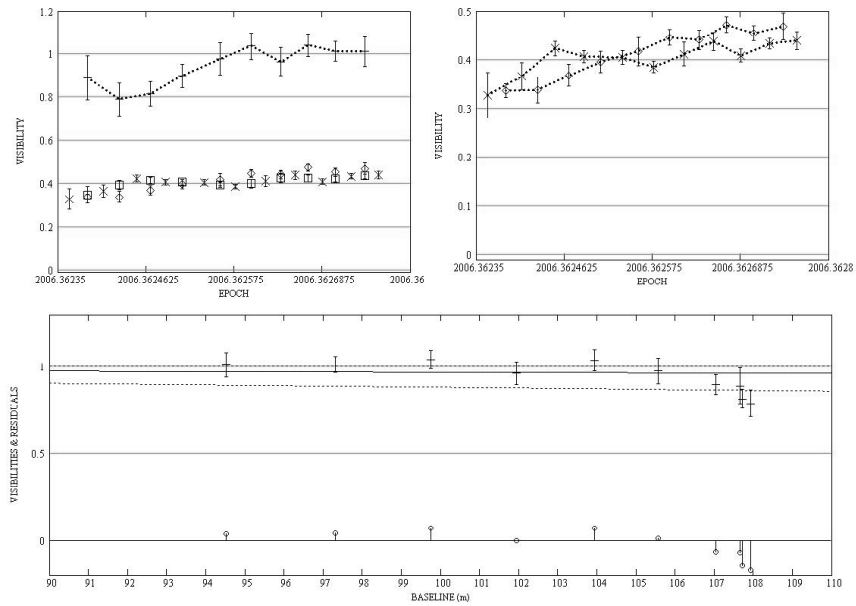


Figure. C.230: HD 145675: Intermediate baseline plots for 2006/05/13 data.

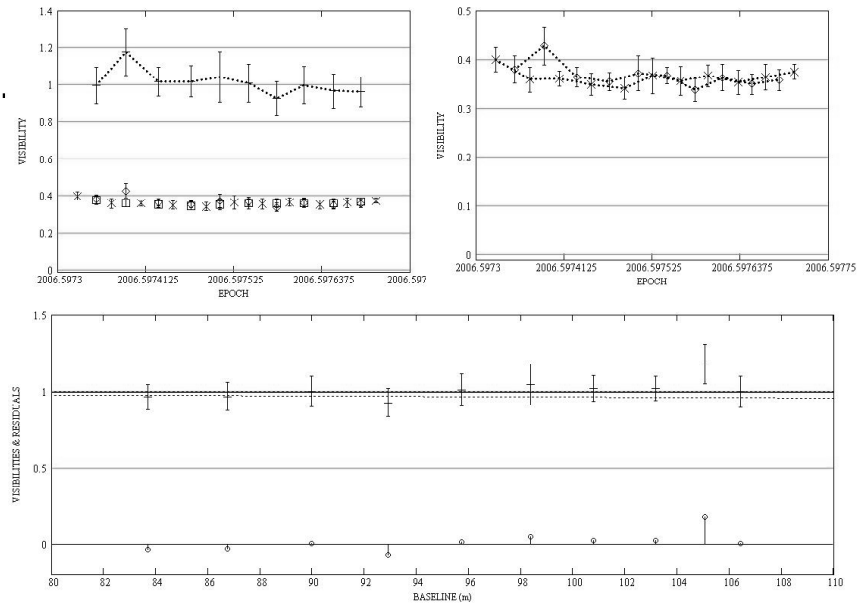


Figure. C.231: HD 145675: Intermediate baseline plots for 2006/08/07 data.

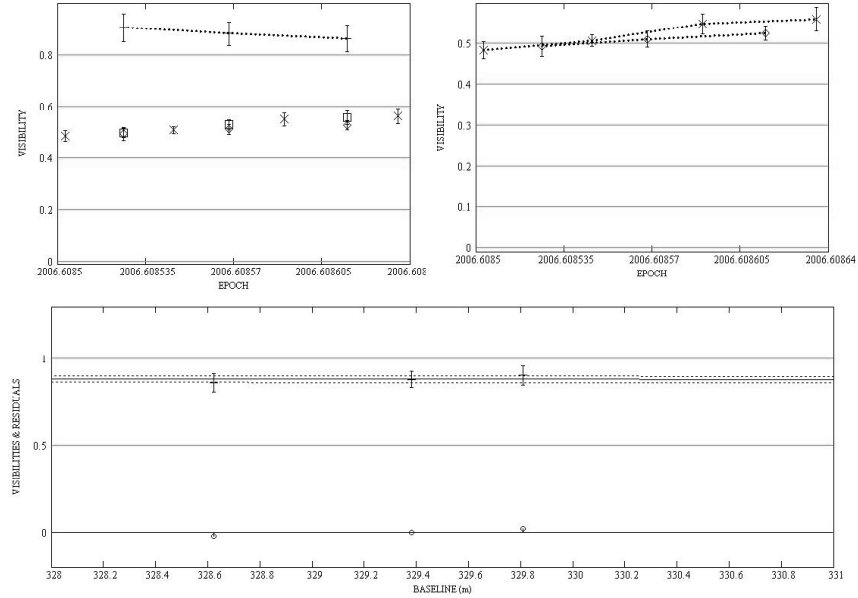


Figure. C.232: HD 145675: Long baseline plots for 2006/08/11 data.

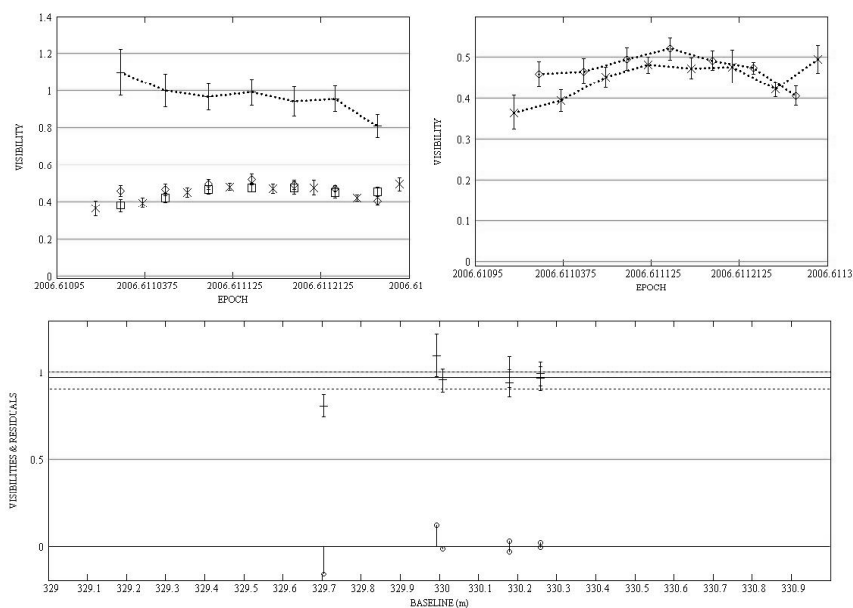


Figure. C.233: HD 145675: Long baseline plots for 2006/08/12 data.

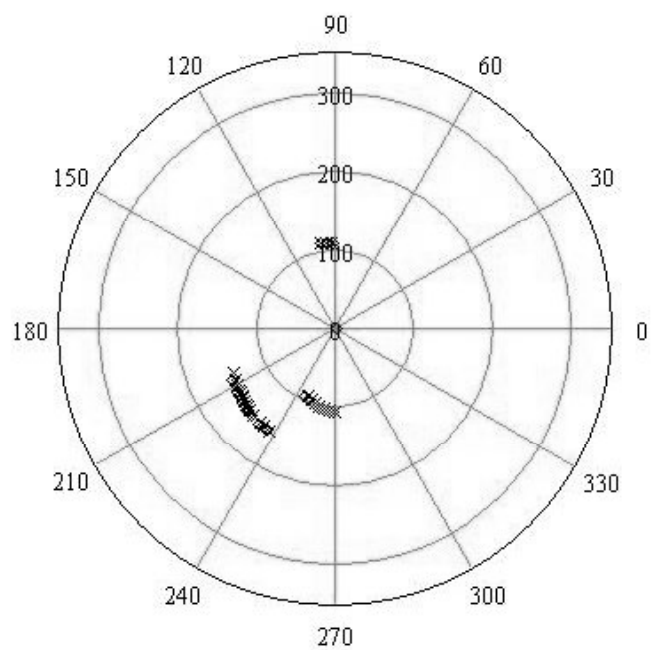


Figure. C.234: HD 145675: All data - Baseline vs. baseline position angle (using calibrator HD 144015).

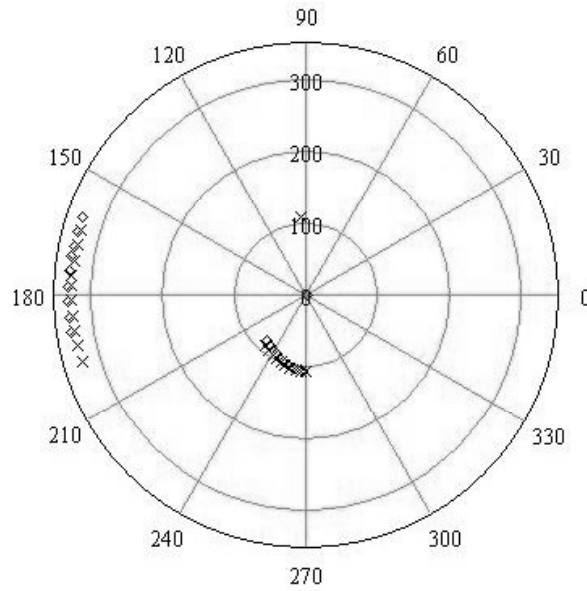


Figure. C.235: HD 145675: All data - Baseline vs. baseline position angle (using calibrator HD 151044).

C.20.3 Diameter Calculation

All S1-E1 data were used in the diameter measurement.

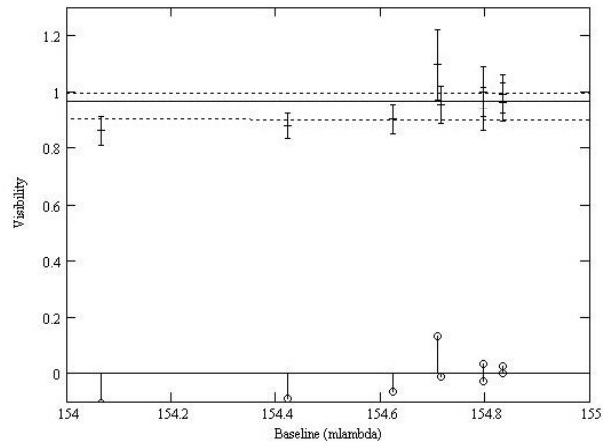


Figure. C.236: HD 145675: LD disk diameter fit: Visibility vs. baseline.

C.20.4 SFP Search

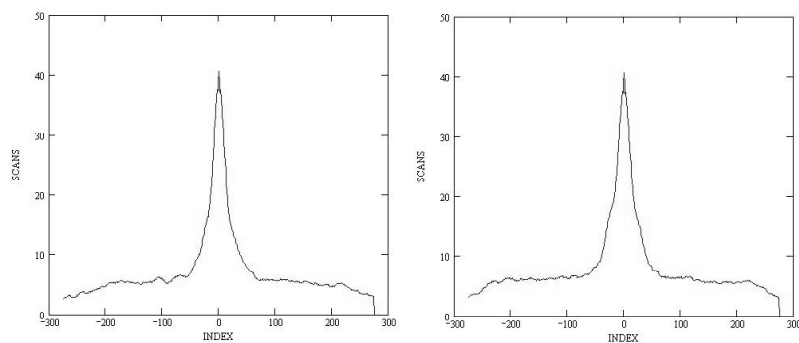


Figure. C.237: HD 145675: SFP inspection for 2005/05/14 data.

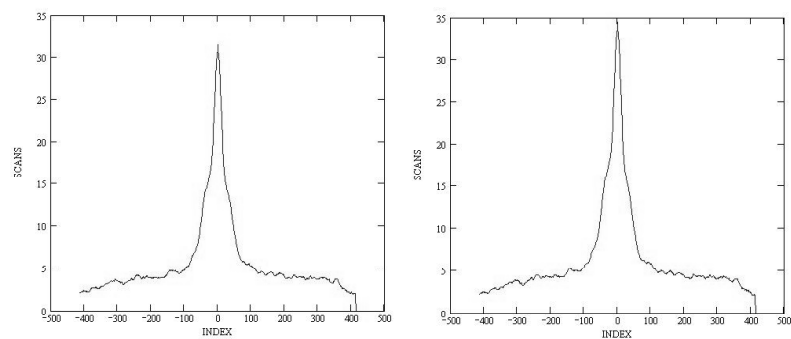


Figure. C.238: HD 145675: SFP inspection for 2005/07/04 data.

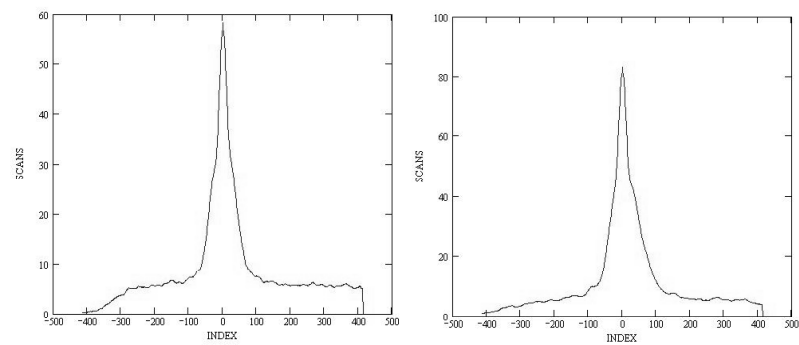


Figure. C.239: HD 145675: SFP inspection for 2006/05/13 data.

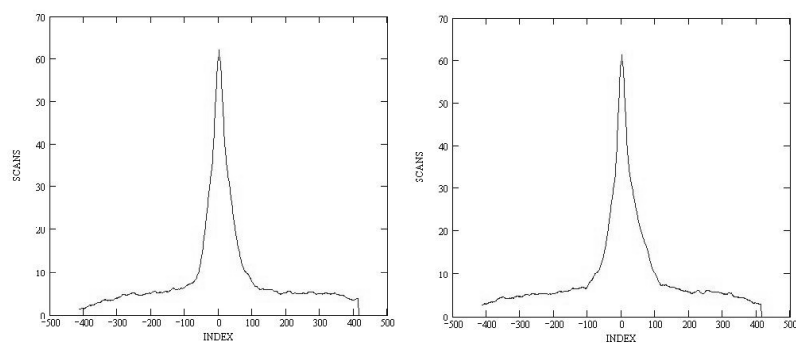


Figure. C.240: HD 145675: SFP inspection for 2006/08/07 data.

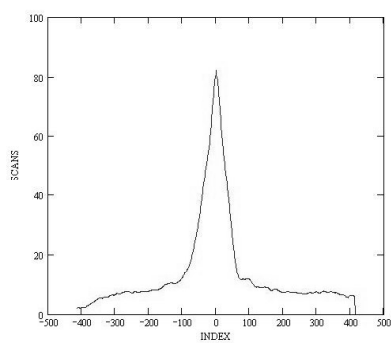


Figure. C.241: HD 145675: SFP inspection for 2006/08/11 data.

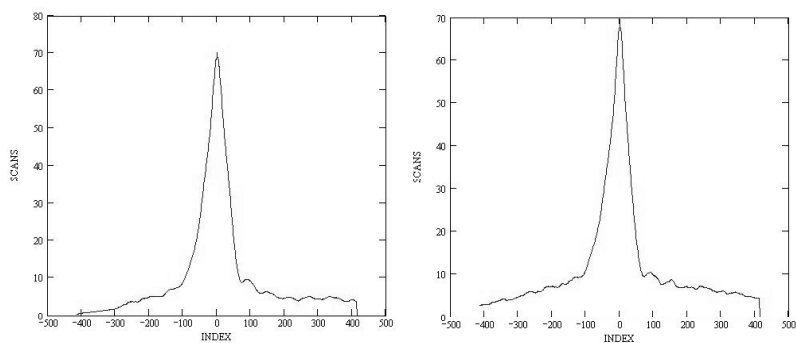


Figure. C.242: HD 145675: SFP inspection for 2006/08/12 data.

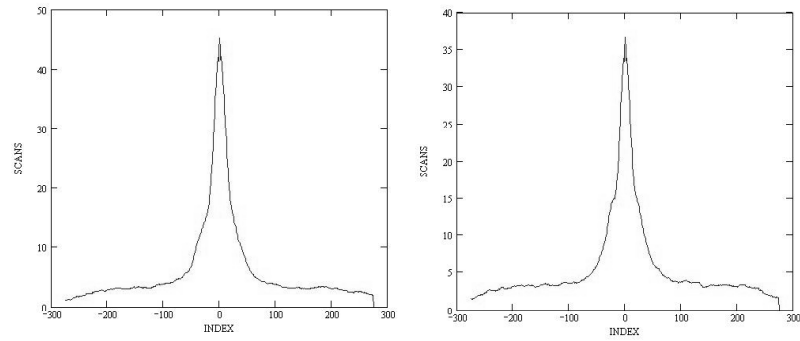


Figure. C.243: HD 144015: SFP inspection for 2005/05/14 data.

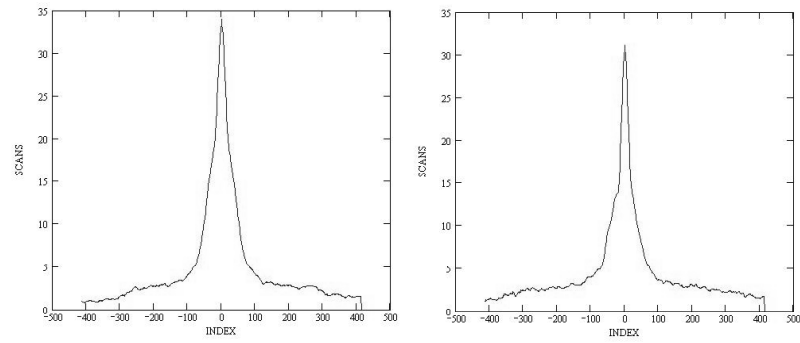


Figure. C.244: HD 144015: SFP inspection for 2005/07/04 data.

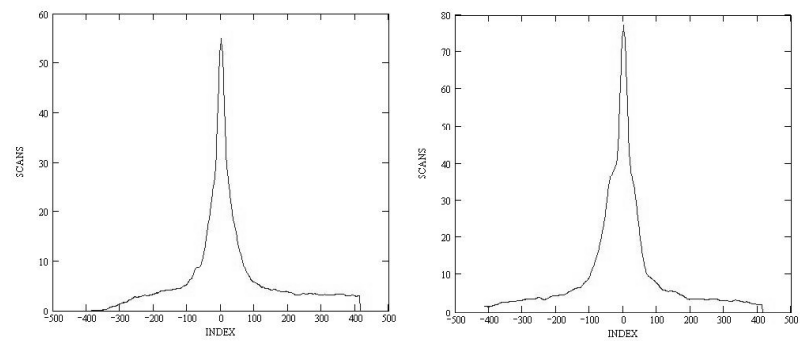


Figure. C.245: HD 144015: SFP inspection for 2006/05/13 data.

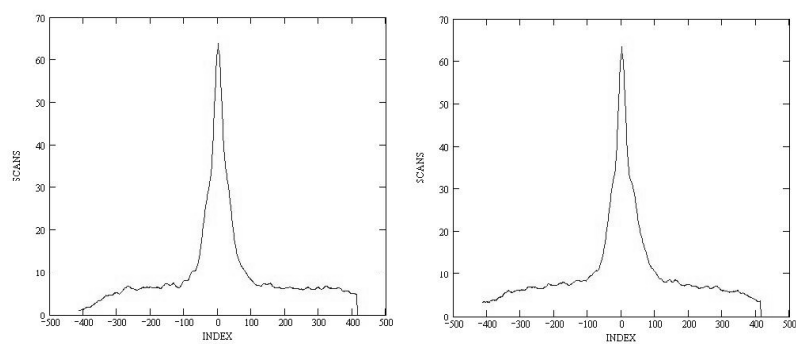


Figure. C.246: HD 151044: SFP inspection for 2006/08/07 data.

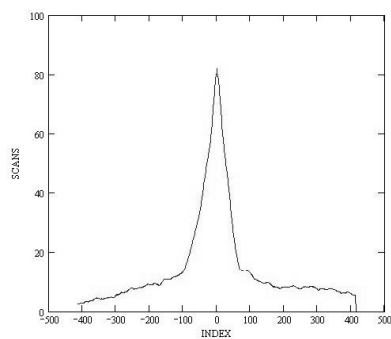


Figure. C.247: HD 151044: SFP inspection for 2006/08/11 data.

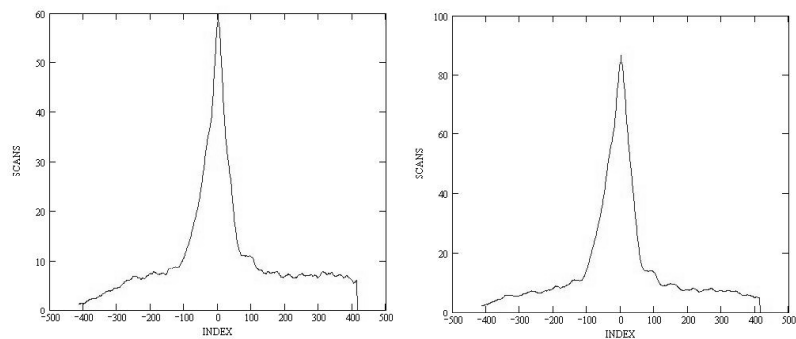


Figure. C.248: HD 151044: SFP inspection for 2006/08/12 data.

C.20.5 Notes

The tracking for the 2005/05/14, 2005/07/04, and 2006/05/13 datasets showed some very unusual characteristics. In all three nights, the object's and calibrator's visibilities changed enough to switch which one had the higher values, a behavior not often seen. I thought this intriguing enough to reobserve HD 145675 with a different calibrator and discovered that it was the first calibrator, HD 144015, and not the object that was behaving strangely. The tracking for the 2006/08/07 and 2006/08/12 data, obtained using HD 151044 as the calibrator, shows no such visibility flipping.

C.21 HD 168443

C.21.1 Calibrated Visibilities

Table. C.23: HD 168443: Calibrated Visibilities

| MJD | B (m) | PA (deg) | V_c | $\sigma(V_c)$ |
|-----------|----------|-------------|-------|---------------|
| 53592.201 | 105.62 | 92.4 | 0.990 | 0.120 |
| 53592.211 | 106.74 | 92.9 | 1.011 | 0.125 |
| 53592.223 | 107.67 | 93.6 | 1.235 | 0.104 |
| 53592.233 | 107.92 | 94.1 | 1.131 | 0.102 |
| 53592.245 | 107.70 | 94.7 | 1.081 | 0.092 |
| 53592.255 | 107.04 | 95.3 | 1.136 | 0.106 |
| 53592.278 | 104.11 | 96.6 | 1.114 | 0.124 |
| 53596.194 | 106.02 | 92.6 | 0.916 | 0.085 |
| 53596.203 | 107.04 | 93.1 | 1.001 | 0.122 |
| 53596.216 | 107.78 | 93.7 | 0.999 | 0.105 |
| 53596.228 | 107.89 | 94.3 | 1.036 | 0.090 |
| 53596.240 | 107.36 | 95.0 | 1.150 | 0.086 |
| 53596.255 | 105.95 | 95.9 | 1.140 | 0.092 |
| 53602.230 | 106.83 | 95.4 | 1.099 | 0.109 |
| 53602.246 | 104.82 | 96.3 | 1.082 | 0.129 |
| 53602.256 | 103.14 | 97.0 | 1.003 | 0.106 |
| 53602.265 | 101.08 | 97.6 | 1.055 | 0.099 |
| 53869.357 | 80.14 | 267.9 | 1.438 | 0.199 |
| 53869.372 | 86.52 | 268.8 | 1.351 | 0.152 |
| 53869.386 | 91.88 | 269.6 | 1.359 | 0.167 |
| 53869.400 | 96.61 | 90.4 | 1.794 | 0.240 |
| 53869.415 | 100.68 | 91.2 | 1.656 | 0.167 |
| 53869.430 | 103.70 | 91.9 | 1.715 | 0.210 |
| 53869.443 | 105.88 | 92.5 | 1.732 | 0.201 |
| 53869.458 | 107.30 | 93.3 | 1.472 | 0.148 |
| 53869.471 | 107.89 | 94.0 | 1.535 | 0.162 |

C.21.2 Nightly Data Plots

The first and last object and calibrator data points were given zero weight in the 2005/08/10 dataset due to gaps in time between the observations. The first two

data points for each of the object and calibrator were also given zero weight in the 2005/08/20 dataset because of the same reason. All data points are shown in Figures C.249 and C.251 but were not part of the diameter calculation or companion check.

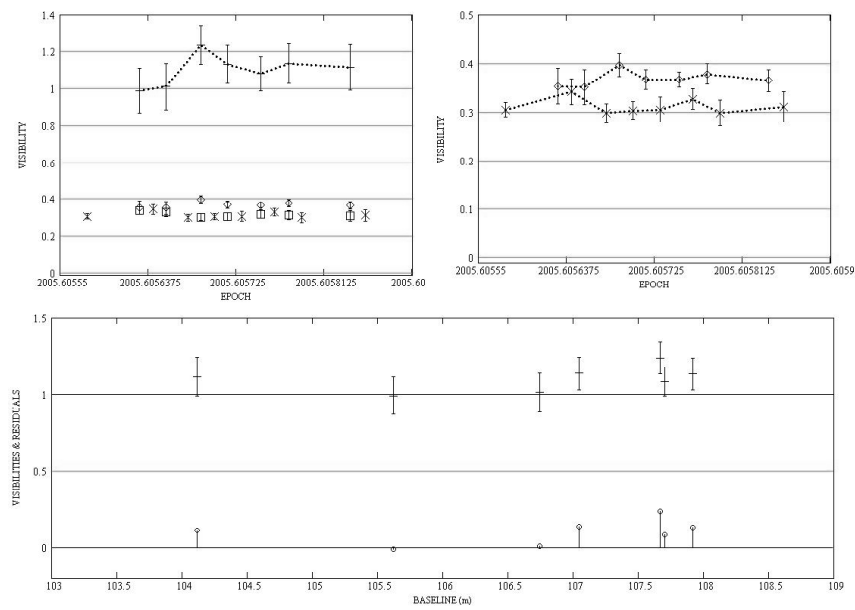


Figure. C.249: HD 168443: Intermediate baseline plots for 2005/08/10 data.

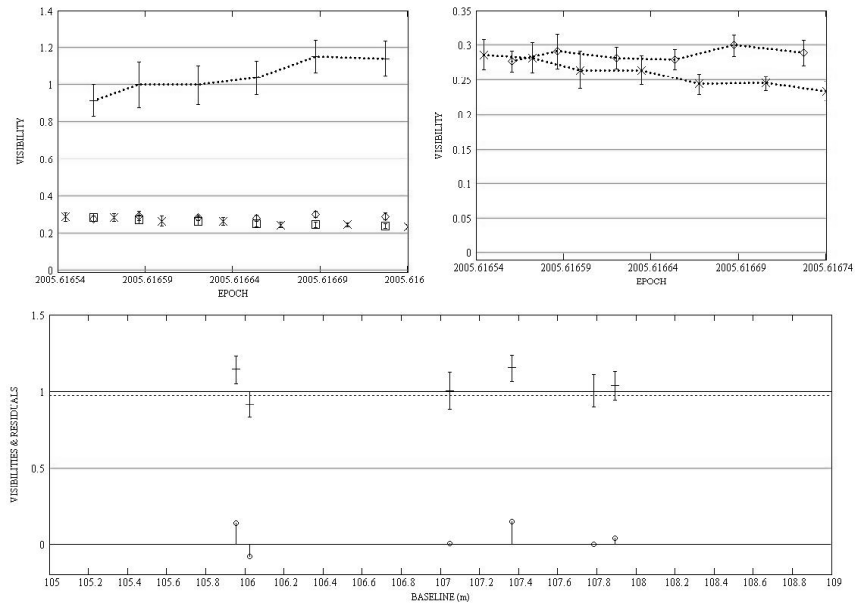


Figure. C.250: HD 168443: Intermediate baseline plots for 2005/08/14 data.

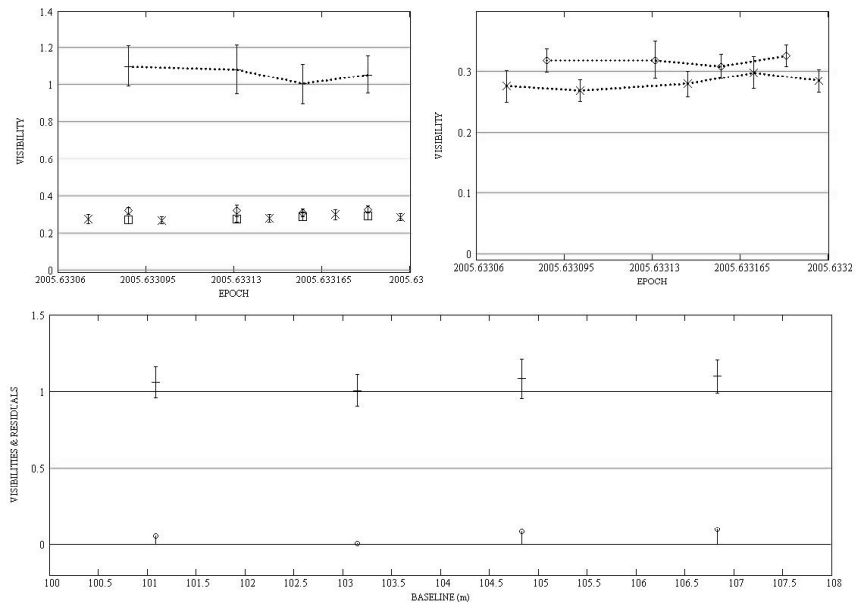


Figure. C.251: HD 168443: Intermediate baseline plots for 2005/08/20 data.

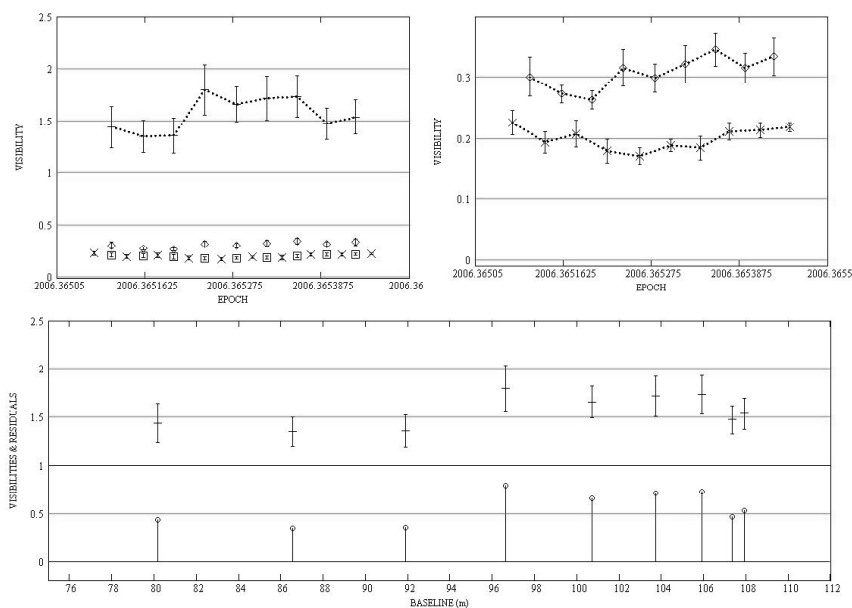


Figure. C.252: HD 168443: Intermediate baseline plots for 2006/05/14 data.

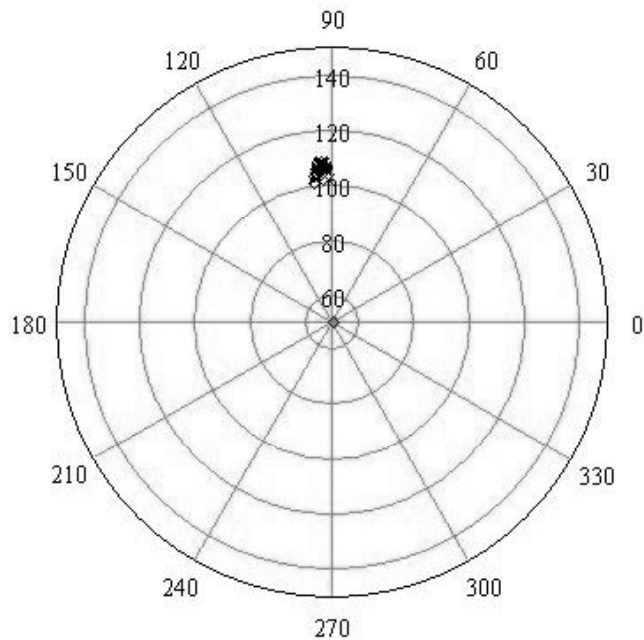


Figure. C.253: HD 168443: All data - Baseline vs. baseline position angle (using calibrator HD 169370).

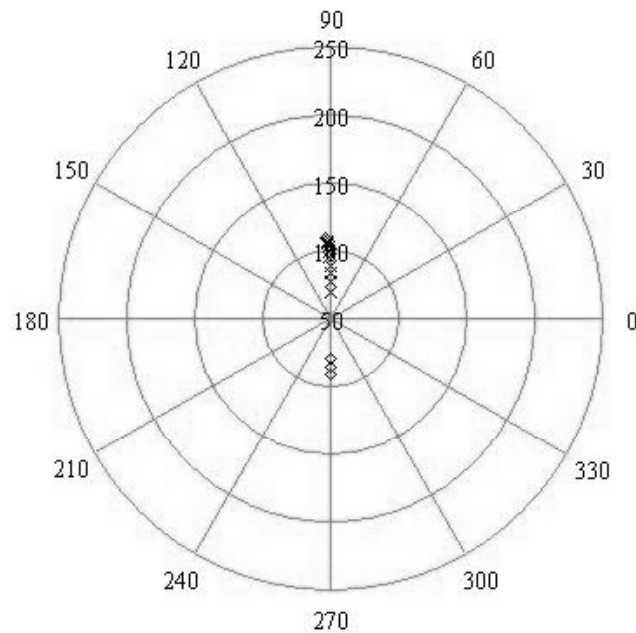


Figure. C.254: HD 168443: All data - Baseline vs. baseline position angle (using calibrator HD 173093).

C.21.3 Diameter Calculation

I attempted a diameter fit to the data that used HD 169370 and the result was 0.096 ± 0.273 mas - a nearly 300% error bar. This star is unresolved at the W1-W2 baselines used to observe it.

As can be seen in the previous plots, both calibrators were less than perfect. They produced calibrated visibilities greater than 1 and the diameter calculation failed to produced any reliable diameter measurements. A more reliable calibrator and more observations are required.

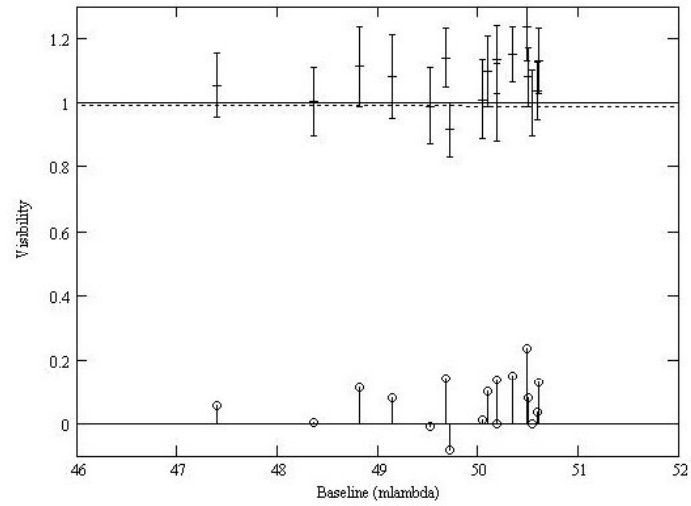


Figure. C.255: HD 168443: LD disk diameter fit: Visibility vs. baseline.

C.21.4 SFP Search

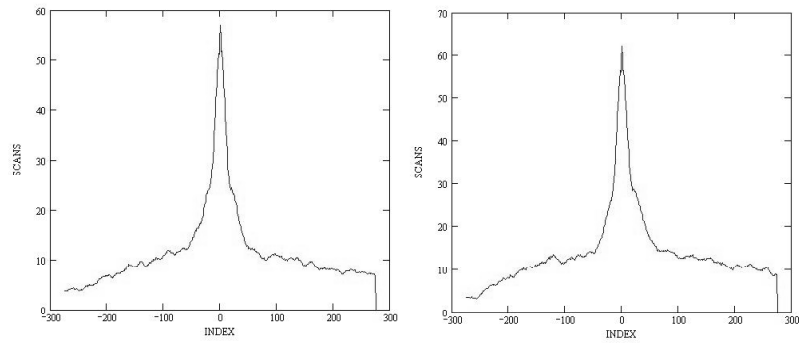


Figure. C.256: HD 168443: SFP inspection for 2005/08/10 data.

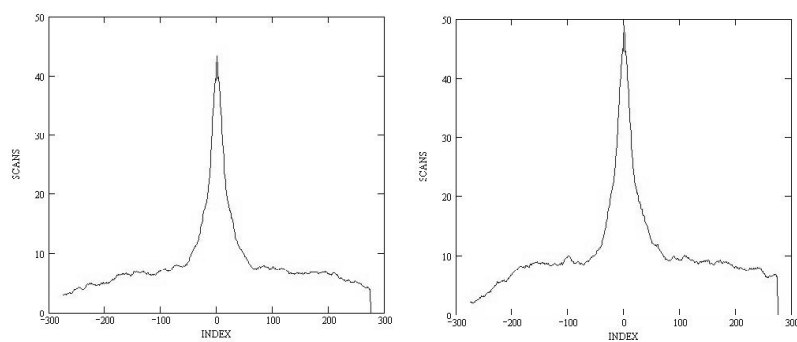


Figure. C.257: HD 168443: SFP inspection for 2005/08/14 data.

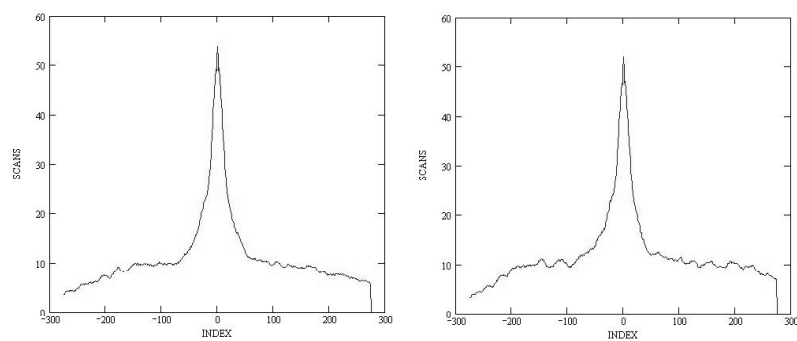


Figure. C.258: HD 168443: SFP inspection for 2005/08/20 data.

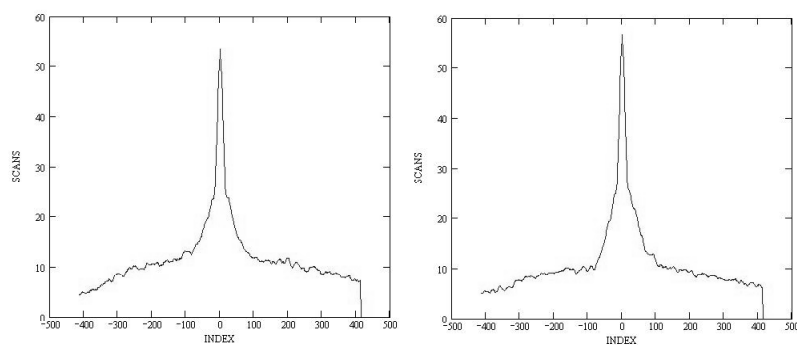


Figure. C.259: HD 168443: SFP inspection for 2006/05/14 data.

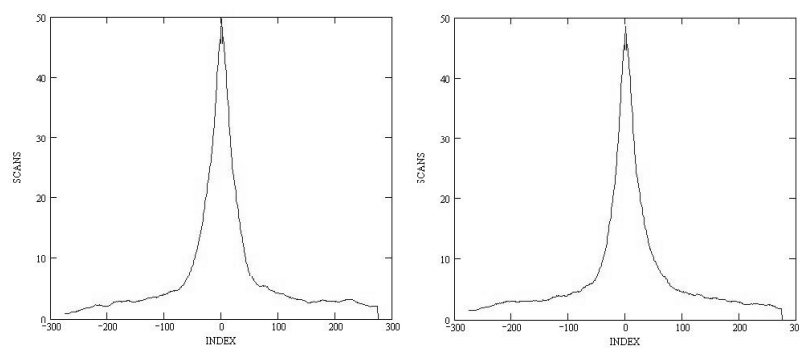


Figure. C.260: HD 169370: SFP inspection for 2005/08/10 data.

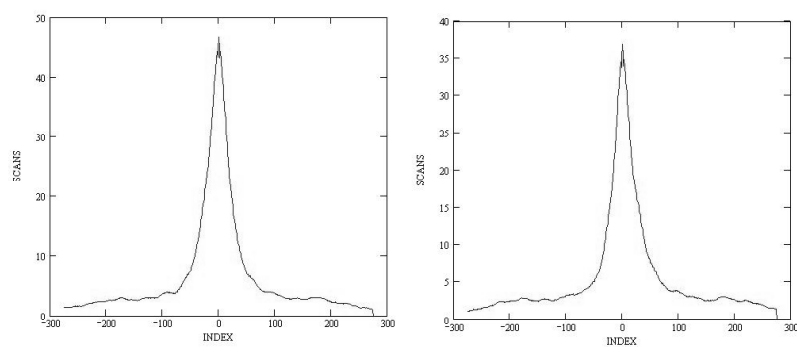


Figure. C.261: HD 169370: SFP inspection for 2005/08/14 data.

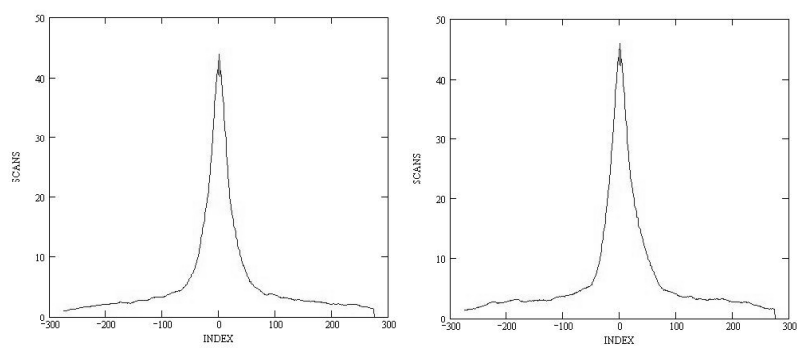


Figure. C.262: HD 169370: SFP inspection for 2005/08/20 data.

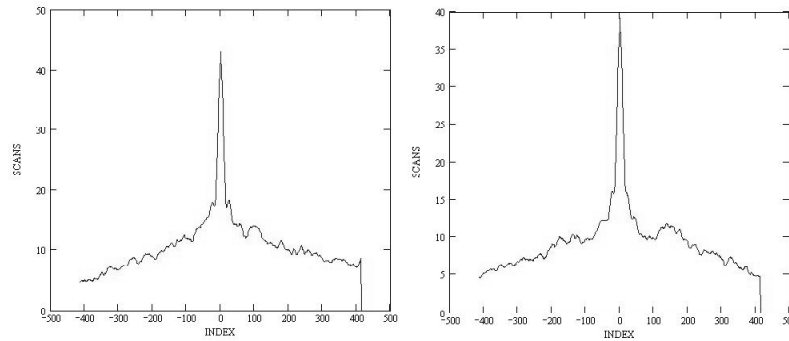


Figure. C.263: HD 173093: SFP inspection for 2006/05/14 data.

C.21.5 Notes

Due to the high calibrated visibilities that resulted from the bad calibrators, the σ_{res} produced from the failed diameter measurements were unnaturally high. In order to get a reliable σ_{res} , the angular diameter of the calibrator HD 169370 was altered until the resulting diameter calculation roughly matched the diameter estimated from HD 168443's SED fit. The corresponding σ_{res} was then compared to the ΔK_{max} for the binary systems. This process was repeated for each night of data, as the same altered angular diameter did not work for all three nights.

This procedure failed for the calibrator HD 173093; there was no angular size that could be assigned to the calibrator that would produce the diameter estimated from the SED fit for HD 168443.

I used the diameter estimated from HD 168443's SED fit in *Visibility Estimator*, as the diameter calculated from the data was unreliable.

C.22 HD 177830

C.22.1 Calibrated Visibilities

Table. C.24: HD 177830: Calibrated Visibilities

| MJD | B (m) | PA (deg) | V_c | $\sigma(V_c)$ |
|-----------|----------|-------------|-------|---------------|
| 53550.442 | 136.66 | 223.3 | 1.054 | 0.074 |
| 53550.462 | 130.63 | 217.0 | 1.085 | 0.062 |
| 53550.476 | 126.77 | 212.3 | 1.017 | 0.092 |
| 53550.489 | 123.22 | 207.4 | 1.030 | 0.061 |
| 53590.222 | 104.94 | 101.4 | 1.066 | 0.078 |
| 53590.237 | 106.63 | 99.0 | 1.017 | 0.060 |
| 53590.251 | 107.62 | 96.6 | 1.024 | 0.057 |
| 53590.266 | 107.91 | 94.2 | 0.811 | 0.072 |
| 53590.276 | 107.67 | 92.7 | 1.086 | 0.087 |
| 53895.335 | 330.37 | 215.0 | 0.875 | 0.080 |
| 53955.308 | 104.54 | 267.6 | 0.950 | 0.078 |
| 53955.323 | 102.03 | 265.2 | 1.012 | 0.074 |
| 53955.355 | 93.90 | 259.4 | 0.996 | 0.052 |
| 53955.369 | 89.58 | 256.6 | 0.965 | 0.061 |
| 53955.384 | 84.38 | 253.4 | 0.916 | 0.052 |
| 53955.397 | 79.41 | 250.2 | 0.919 | 0.072 |
| 53955.410 | 74.15 | 246.5 | 0.941 | 0.083 |
| 53960.191 | 330.06 | 209.5 | 0.898 | 0.074 |
| 53960.208 | 328.87 | 206.5 | 0.887 | 0.070 |
| 53960.223 | 327.38 | 203.5 | 0.951 | 0.086 |
| 53960.241 | 325.46 | 199.9 | 0.741 | 0.098 |
| 53960.259 | 323.36 | 195.8 | 0.707 | 0.097 |
| 53960.276 | 321.74 | 192.0 | 0.937 | 0.105 |

C.22.2 Nightly Data Plots

The first object and calibrator data points in the 2005/08/08 dataset were given zero weight, as there was a gap in time between the first object and second calibrator. Similarly, due to the gap in time between the second object and third calibrator observations in the 2006/08/08 data, the second object data points was given zero weight. This essentially broke the dataset into two bracketed sequences for the companion check.

Because the 2006/06/09 dataset only had one bracketed observation, it was not used in the companion check.

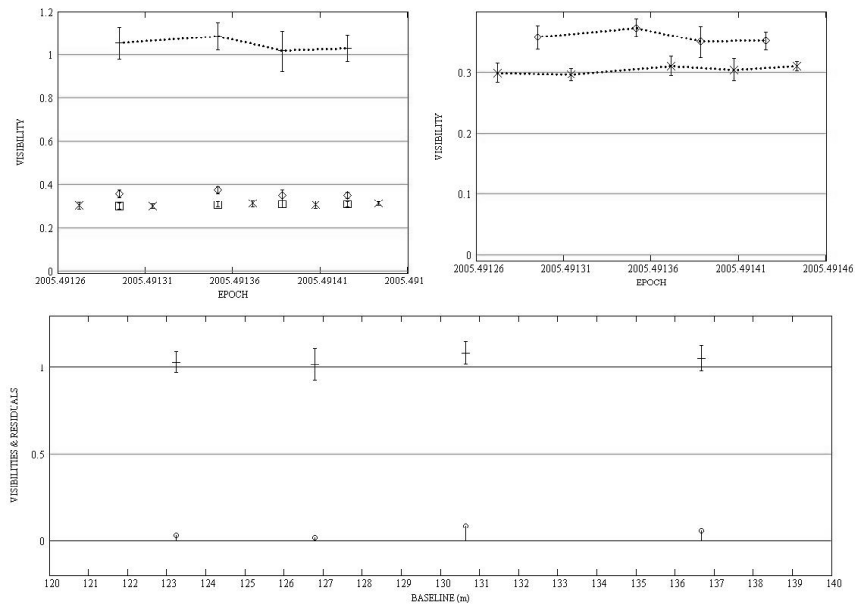


Figure. C.264: HD 177830: Intermediate baseline plots for 2005/06/29 data.

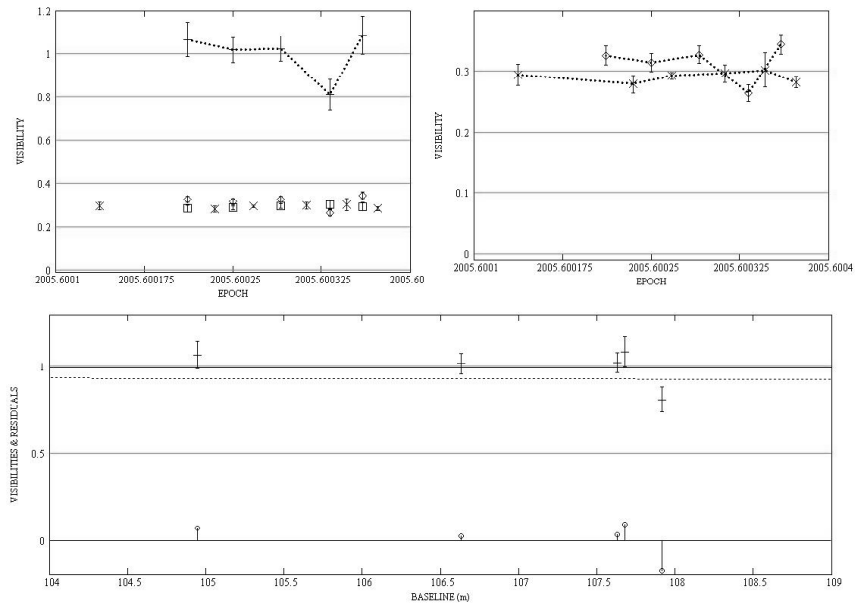


Figure. C.265: HD 177830: Intermediate baseline plots for 2005/08/08 data.

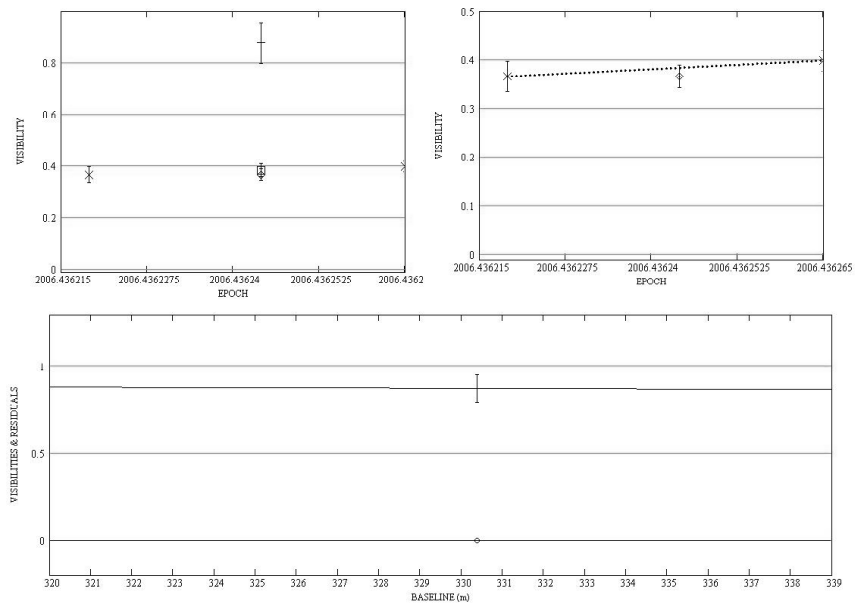


Figure. C.266: HD 177830: Long baseline plots for 2006/06/09 data.

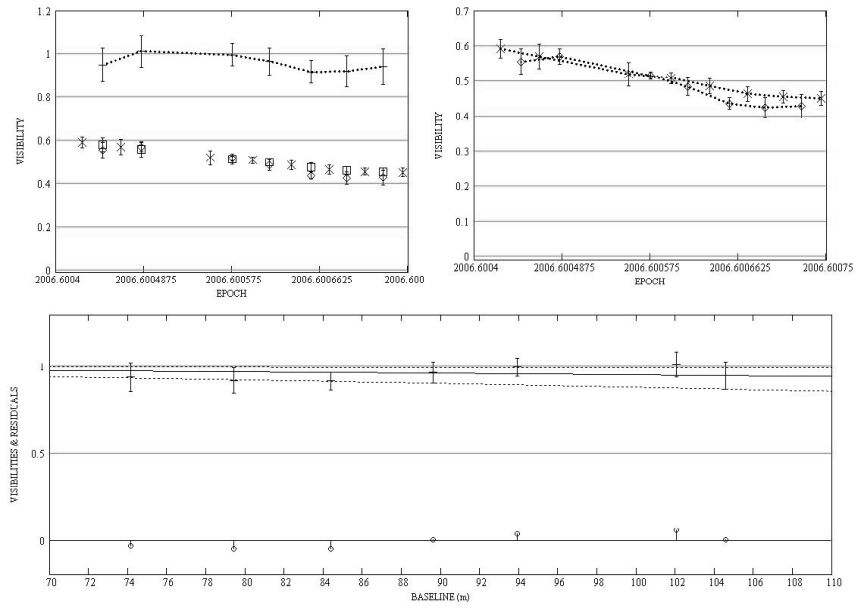


Figure. C.267: HD 177830: Intermediate baseline plots for 2006/08/08 data.

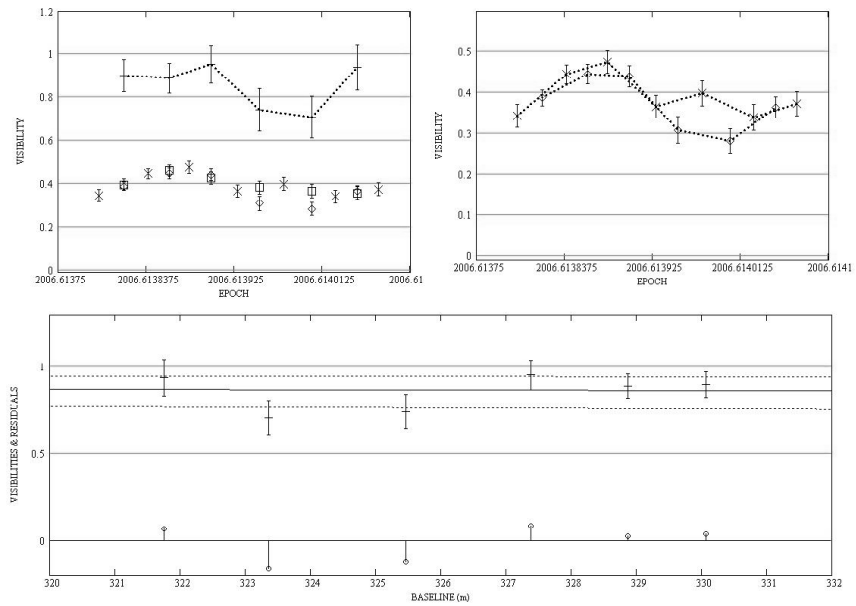


Figure. C.268: HD 177830: Long baseline plots for 2006/08/13 data.

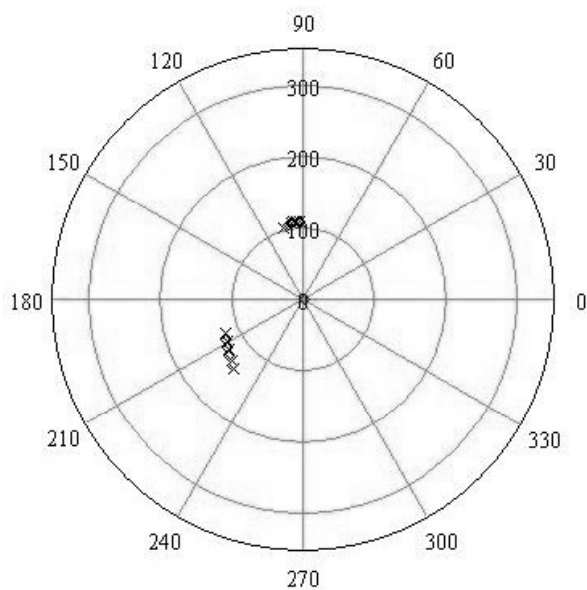


Figure. C.269: HD 177830: All data - Baseline vs. baseline position angle (using calibrator HD 17939).

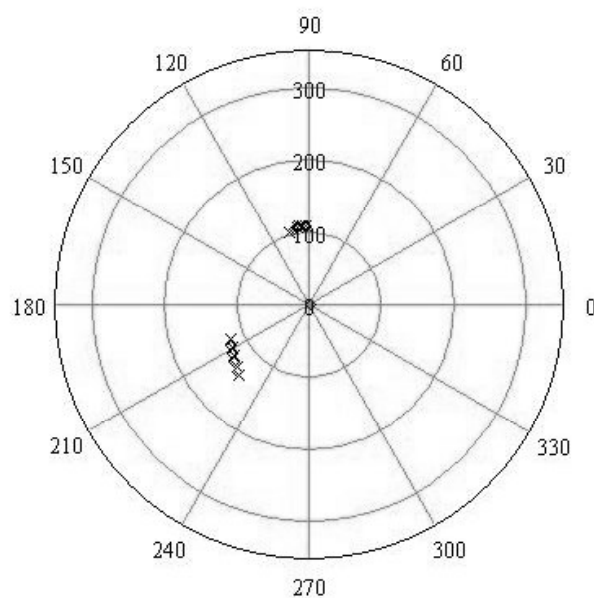


Figure. C.270: HD 177830: All data - Baseline vs. baseline position angle (using calibrator HD 176377).

C.22.3 Diameter Calculation

All the S1-E1 data were used in the diameter calculation.

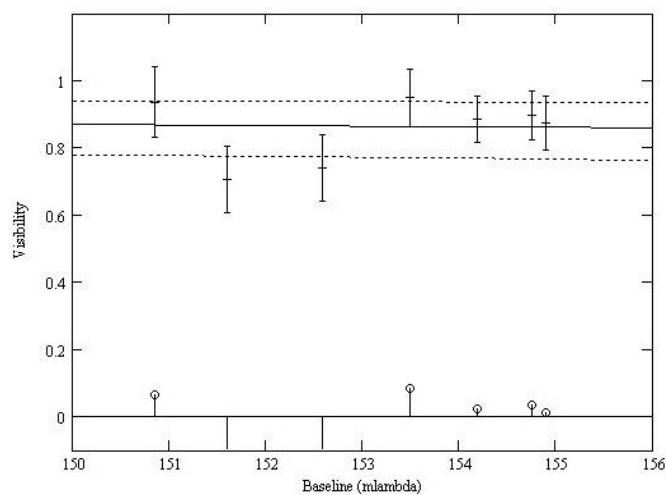


Figure. C.271: HD 177830: LD disk diameter fit: Visibility vs. baseline.

C.22.4 SFP Search

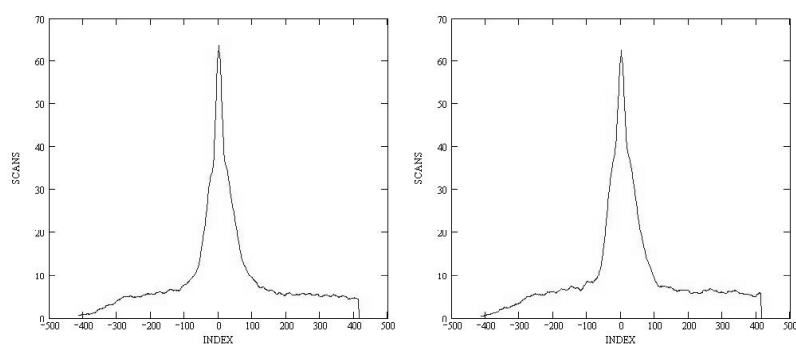


Figure. C.272: HD 177830: SFP inspection for 2005/06/29 data.

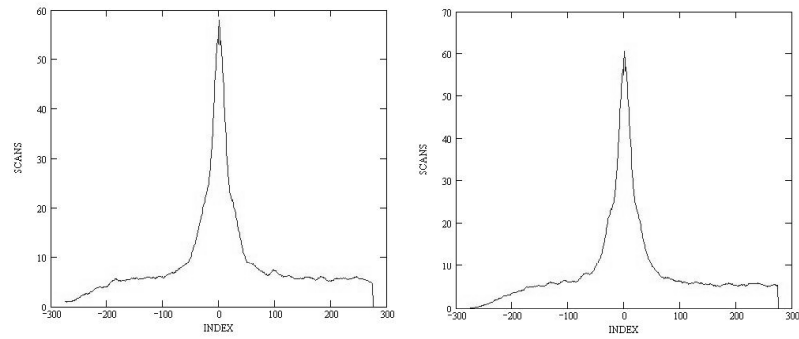


Figure. C.273: HD 177830: SFP inspection for 2005/08/08 data.

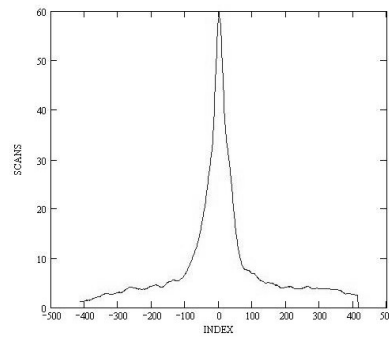


Figure. C.274: HD 177830: SFP inspection for 2006/06/09 data.

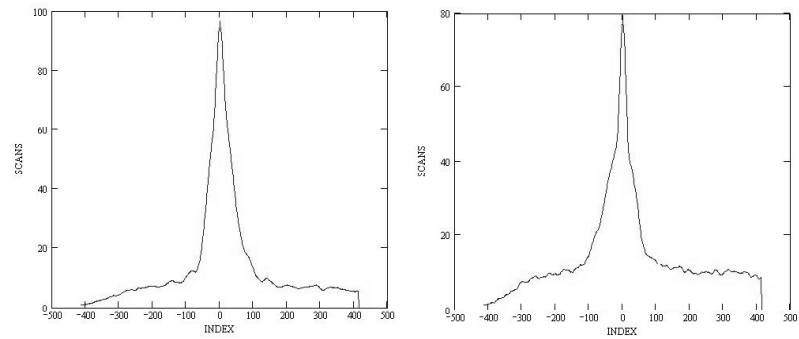


Figure. C.275: HD 177830: SFP inspection for 2006/08/08 data.

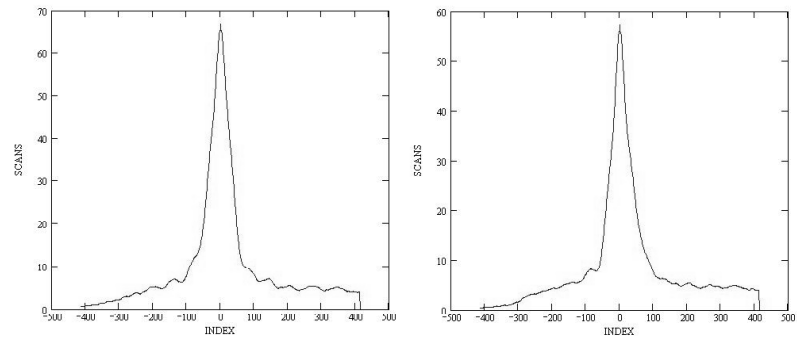


Figure. C.276: HD 177830: SFP inspection for 2006/08/13 data.

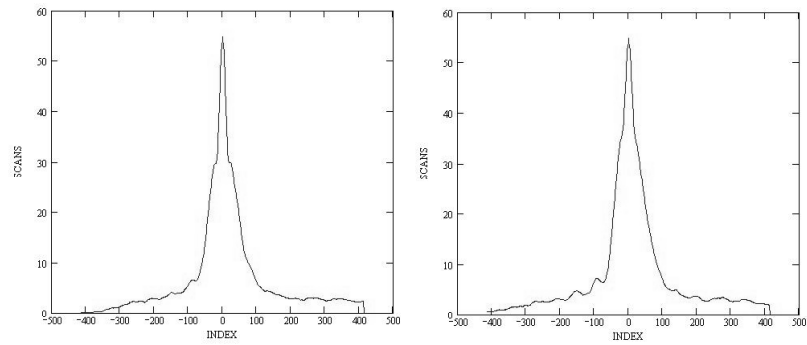


Figure. C.277: HD 176939: SFP inspection for 2005/06/29 data.

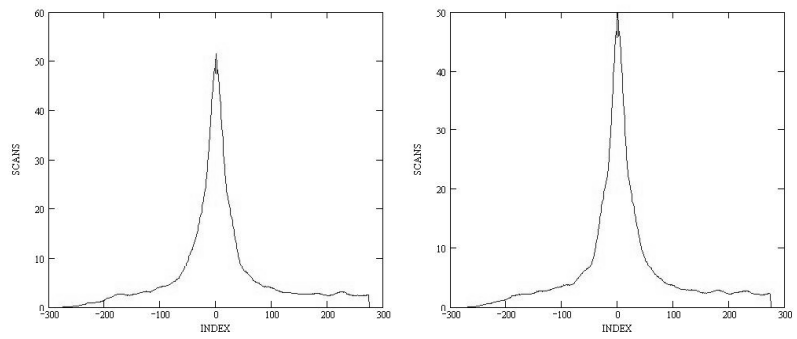


Figure. C.278: HD 176939: SFP inspection for 2005/08/08 data.

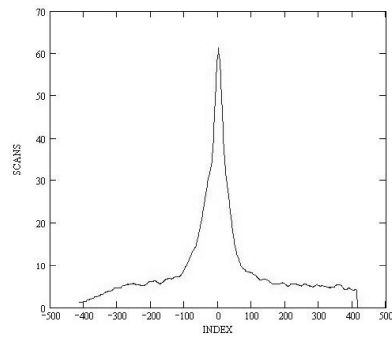


Figure. C.279: HD 176377: SFP inspection for 2006/06/09 data.

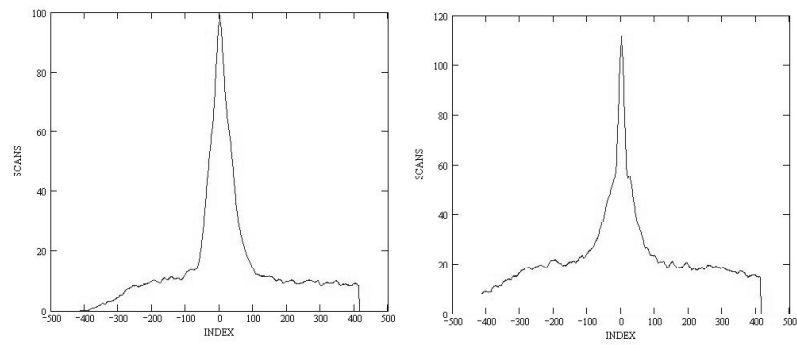


Figure. C.280: HD 176377: SFP inspection for 2006/08/08 data.

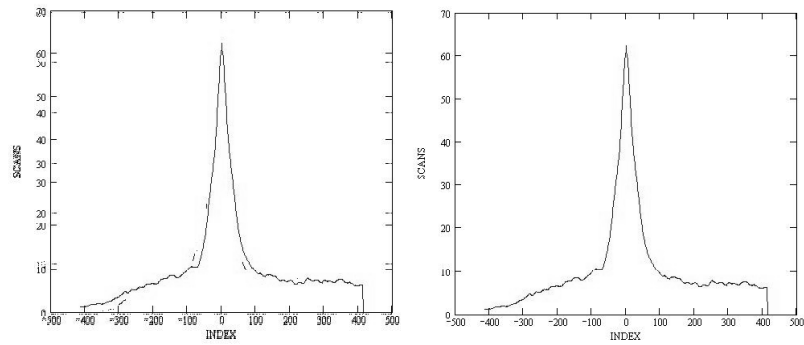


Figure. C.281: HD 176377: SFP inspection for 2006/08/13 data.

C.23 HD 186427

C.23.1 Calibrated Visibilities

Table. C.25: HD 186427: Calibrated Visibilities

| MJD | B (m) | PA (deg) | V_c | $\sigma(V_c)$ |
|-----------|----------|-------------|-------|---------------|
| 53551.378 | 155.75 | 242.0 | 0.955 | 0.143 |
| 53551.395 | 156.21 | 237.6 | 1.144 | 0.092 |
| 53551.409 | 156.25 | 234.0 | 1.086 | 0.086 |
| 53551.422 | 156.00 | 230.2 | 1.052 | 0.072 |
| 53551.435 | 155.54 | 226.5 | 1.022 | 0.066 |
| 53551.452 | 154.61 | 221.2 | 0.959 | 0.057 |
| 53551.467 | 153.64 | 216.6 | 0.968 | 0.045 |
| 53551.481 | 152.69 | 212.3 | 0.974 | 0.060 |
| 53586.243 | 105.98 | 110.3 | 1.046 | 0.102 |
| 53586.254 | 106.74 | 107.2 | 1.040 | 0.100 |
| 53586.265 | 107.32 | 104.0 | 0.938 | 0.090 |
| 53586.280 | 107.79 | 99.9 | 1.050 | 0.132 |
| 53586.289 | 107.92 | 97.3 | 1.017 | 0.132 |
| 53586.303 | 107.82 | 93.4 | 0.998 | 0.134 |
| 53586.315 | 107.47 | 90.1 | 1.034 | 0.085 |
| 53586.334 | 106.39 | 264.7 | 1.018 | 0.109 |
| 53586.352 | 104.88 | 259.7 | 1.054 | 0.061 |
| 53586.363 | 103.65 | 256.4 | 0.987 | 0.099 |
| 53960.308 | 325.22 | 190.2 | 0.841 | 0.129 |
| 53960.324 | 325.76 | 186.5 | 0.978 | 0.092 |
| 53960.337 | 326.01 | 183.3 | 0.984 | 0.112 |
| 53960.350 | 326.10 | 90.2 | 0.857 | 0.113 |
| 53960.363 | 326.03 | 177.0 | 0.898 | 0.090 |
| 53960.377 | 325.77 | 173.7 | 1.039 | 0.087 |

C.23.2 Nightly Data Plots

The first calibrator and object data points were given zero weight in the 2005/08/04 dataset, due to the gap in time between the first object and the second calibrator's visibility measurements.

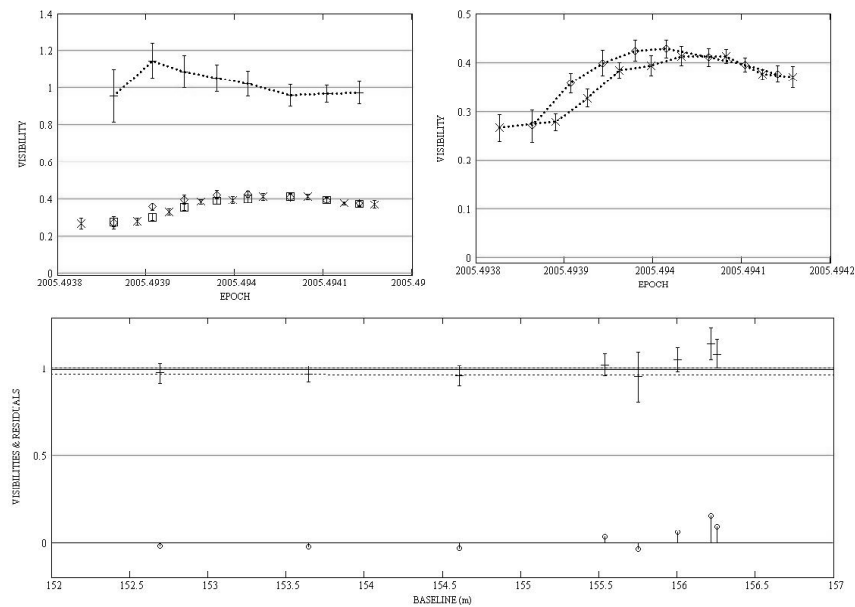


Figure. C.282: HD 186427: Intermediate baseline plots for 2005/06/30 data.

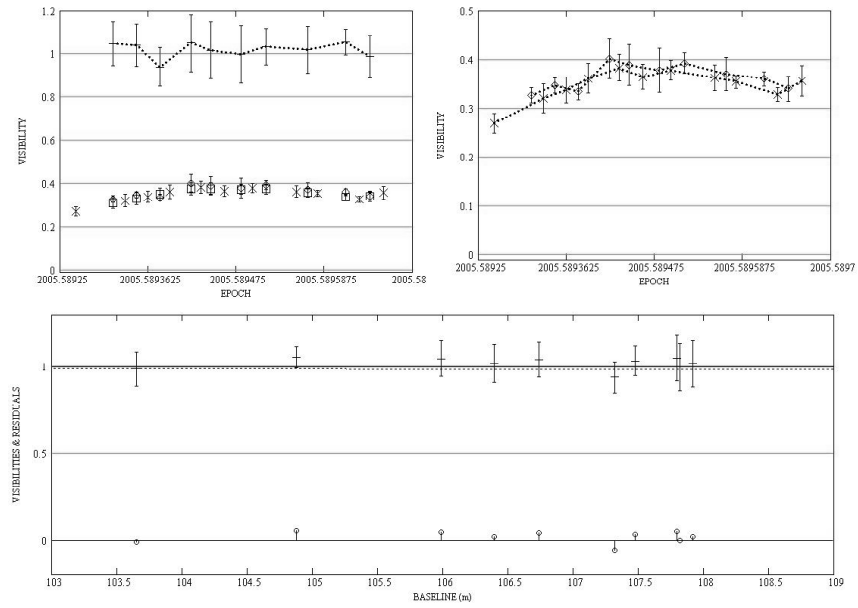


Figure. C.283: HD 186427: Intermediate baseline plots for 2005/08/04 data.

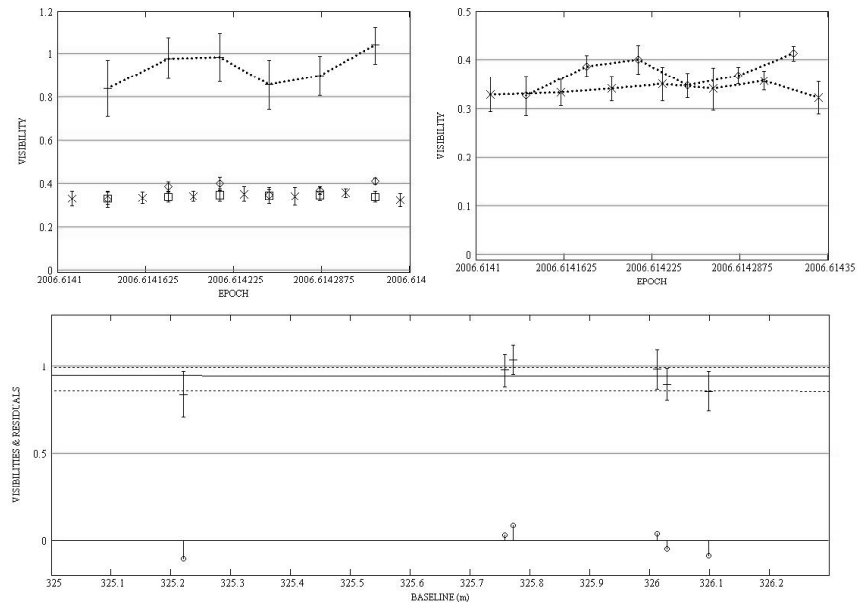


Figure. C.284: HD 186427: Long baseline plots for 2006/08/13 data.

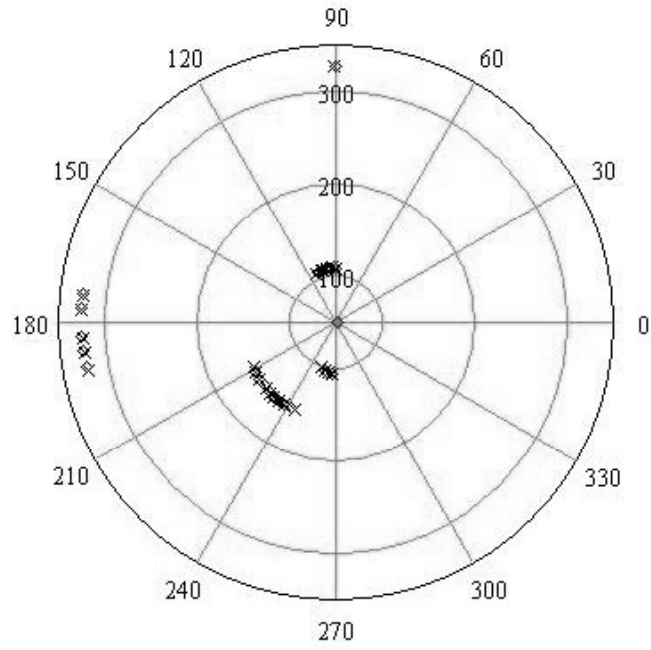


Figure. C.285: HD 186427: All data - Baseline vs. baseline position angle.

C.23.3 Diameter Calculation

All the S1-E1 data were used in the diameter calculation.

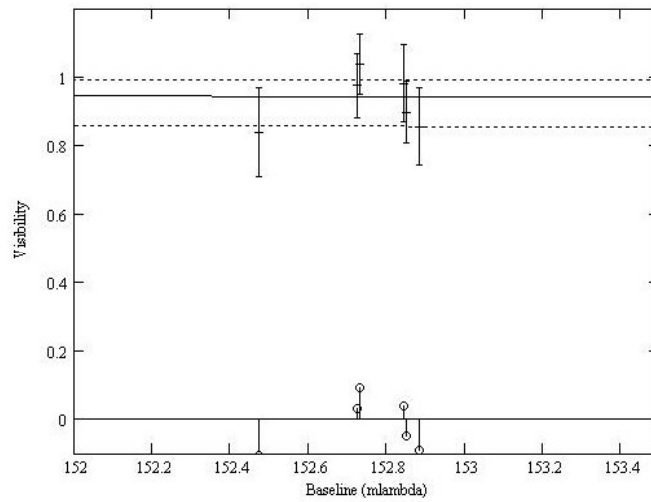


Figure. C.286: HD 186427: LD disk diameter fit: Visibility vs. baseline.

C.23.4 SFP Search

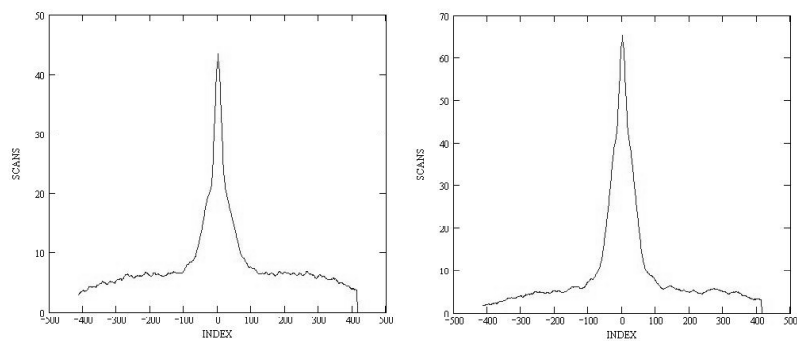


Figure. C.287: HD 186427: SFP inspection for 2005/06/30 data.

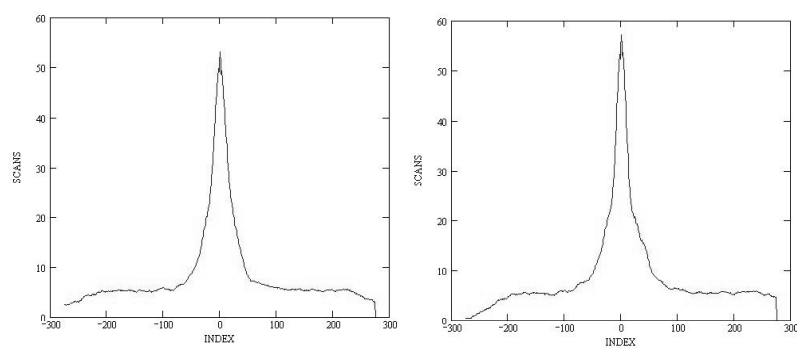


Figure. C.288: HD 186427: SFP inspection for 2005/08/04 data.

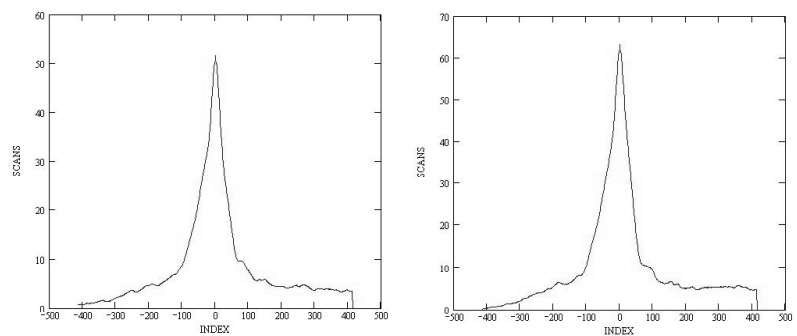


Figure. C.289: HD 186427: SFP inspection for 2006/08/13 data.

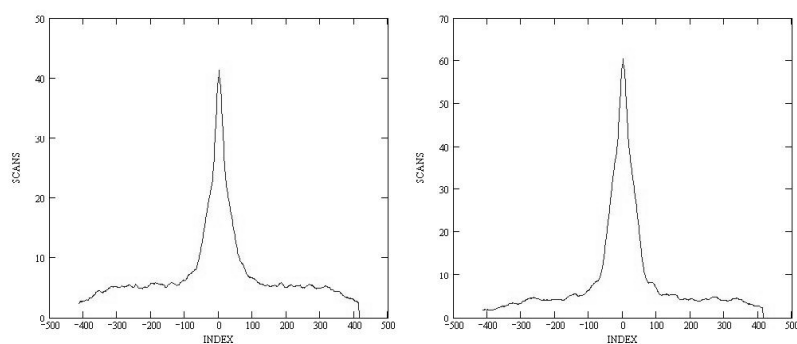


Figure. C.290: HD 184960: SFP inspection for 2005/06/30 data.

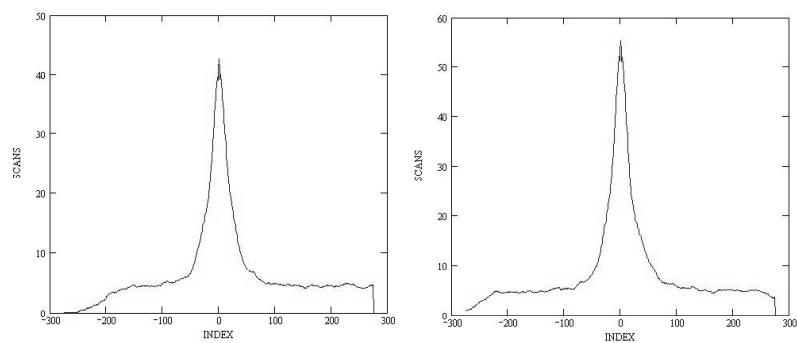


Figure. C.291: HD 184960: SFP inspection for 2005/08/04 data.

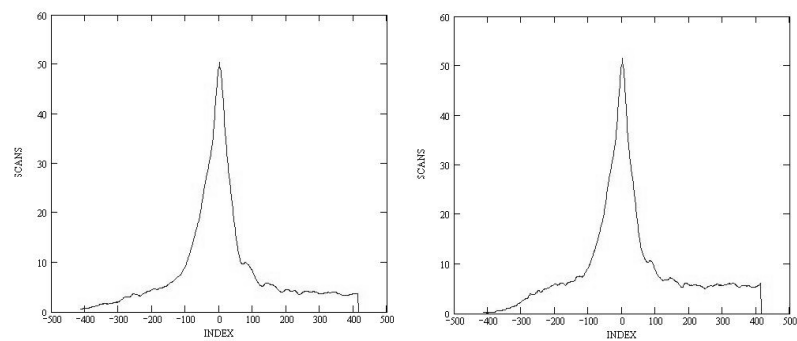


Figure. C.292: HD 184960: SFP inspection for 2006/08/13 data.

C.24 HD 190228

C.24.1 Calibrated Visibilities

Table. C.26: HD 190228: Calibrated Visibilities

| MJD | B (m) | PA (deg) | V_c | $\sigma(V_c)$ |
|-----------|----------|-------------|-------|---------------|
| 53552.420 | 151.88 | 236.5 | 0.834 | 0.074 |
| 53552.434 | 149.16 | 233.3 | 0.880 | 0.079 |
| 53552.448 | 146.23 | 230.1 | 0.911 | 0.080 |
| 53552.464 | 142.24 | 226.0 | 0.955 | 0.111 |
| 53552.477 | 138.71 | 222.2 | 1.045 | 0.118 |
| 53552.490 | 135.19 | 218.2 | 1.052 | 0.071 |
| 53601.190 | 97.18 | 110.5 | 0.941 | 0.119 |
| 53601.204 | 100.32 | 107.5 | 0.816 | 0.105 |
| 53601.218 | 103.01 | 104.7 | 0.917 | 0.120 |
| 53601.230 | 104.91 | 102.3 | 0.922 | 0.115 |
| 53601.243 | 106.43 | 100.0 | 0.895 | 0.101 |
| 53961.239 | 330.20 | 207.4 | 0.888 | 0.043 |
| 53961.253 | 329.42 | 204.8 | 0.884 | 0.061 |
| 53961.268 | 328.30 | 201.8 | 0.871 | 0.073 |
| 53961.282 | 327.09 | 198.8 | 0.922 | 0.106 |
| 53961.299 | 325.69 | 195.2 | 0.816 | 0.082 |
| 53961.313 | 324.58 | 191.9 | 0.860 | 0.084 |
| 53961.328 | 323.60 | 188.3 | 0.811 | 0.080 |
| 53961.346 | 322.86 | 184.1 | 0.935 | 0.108 |

C.24.2 Nightly Data Plots

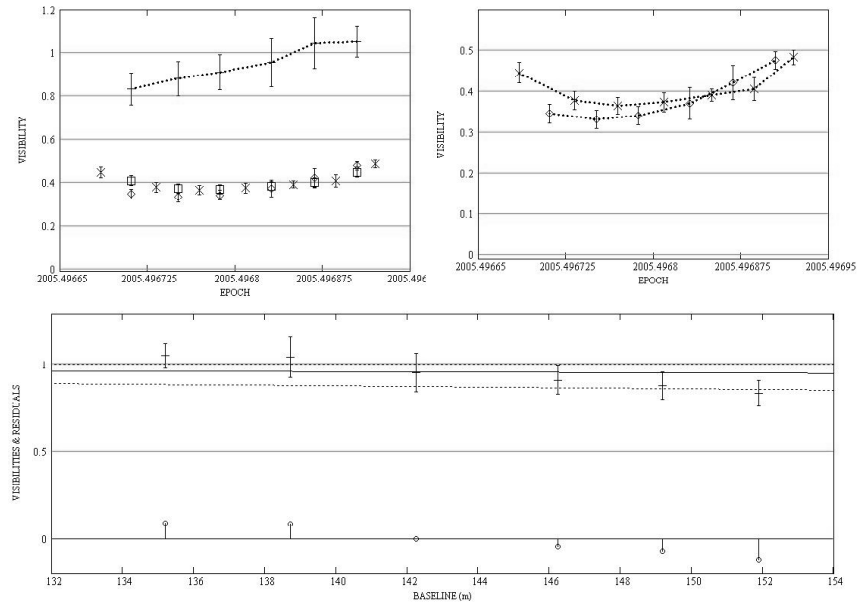


Figure. C.293: HD 190228: Intermediate baseline plots for 2005/07/01 data.

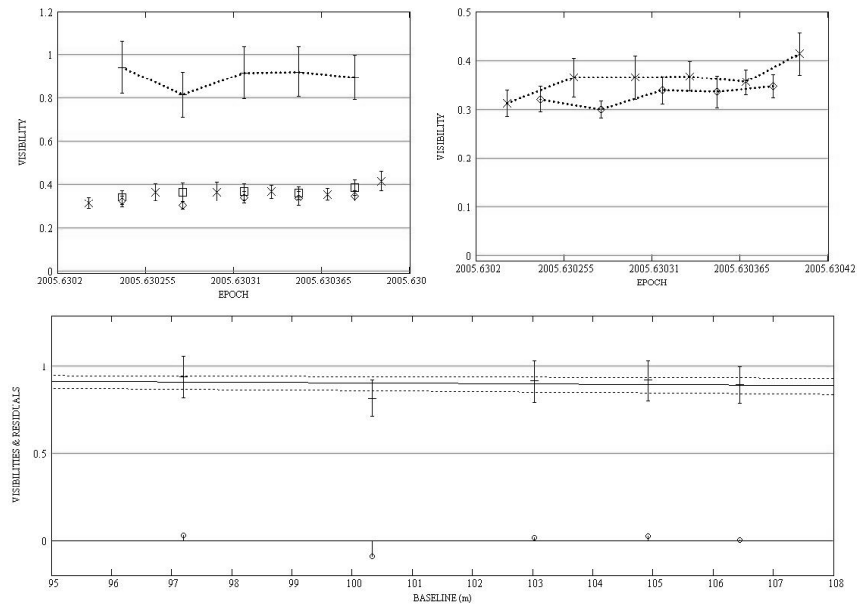


Figure. C.294: HD 190228: Intermediate baseline plots for 2005/08/19 data.

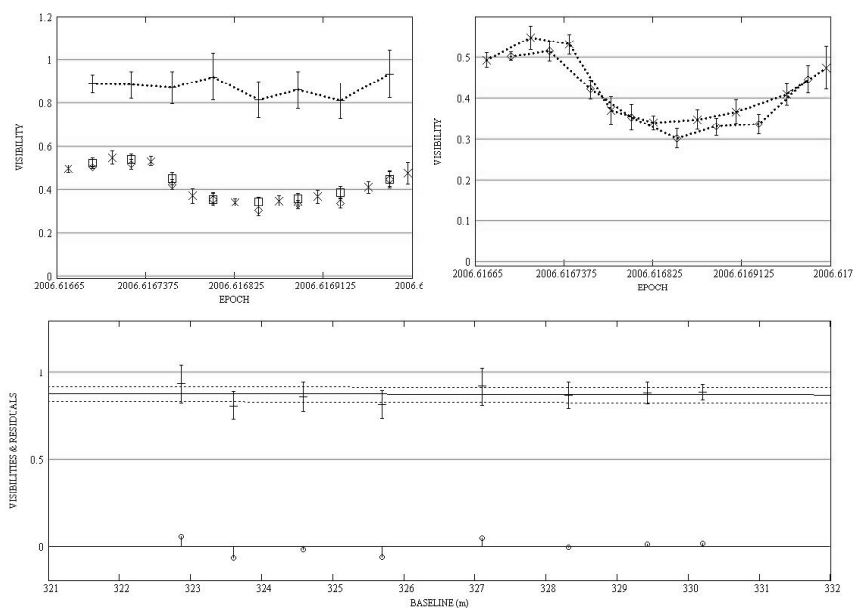


Figure. C.295: HD 190228: Long baseline plots for 2006/08/14 data.

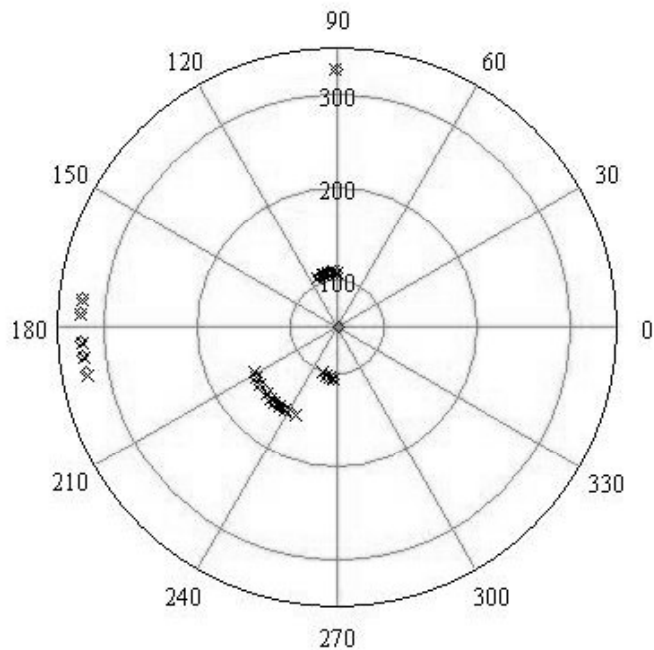


Figure. C.296: HD 190228: All data - Baseline vs. baseline position angle.

C.24.3 Diameter Calculation

All S1-E1 data were used in the diameter calculation.

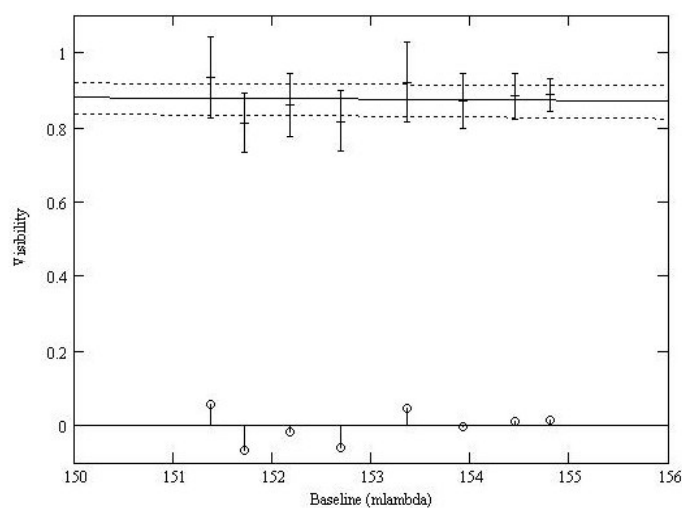


Figure. C.297: HD 190228: LD disk diameter fit: Visibility vs. baseline.

C.24.4 SFP Search

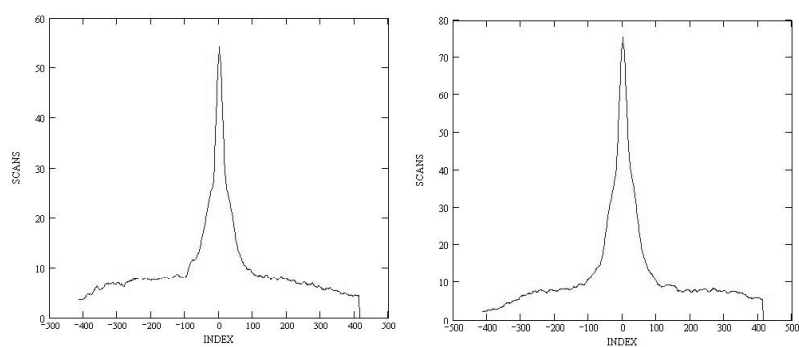


Figure. C.298: HD 190228: SFP inspection for 2005/07/01 data.

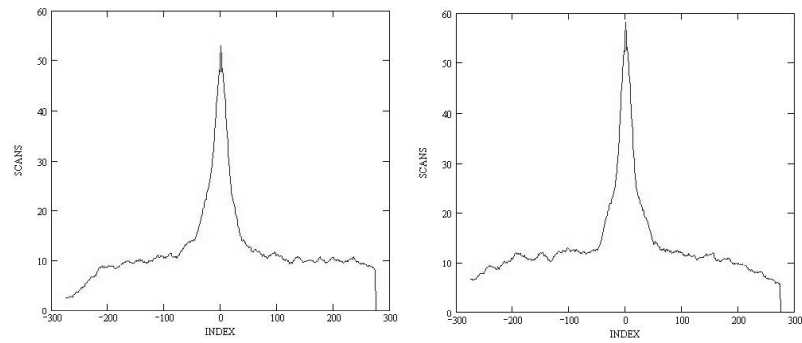


Figure. C.299: HD 190228: SFP inspection for 2005/08/19 data.

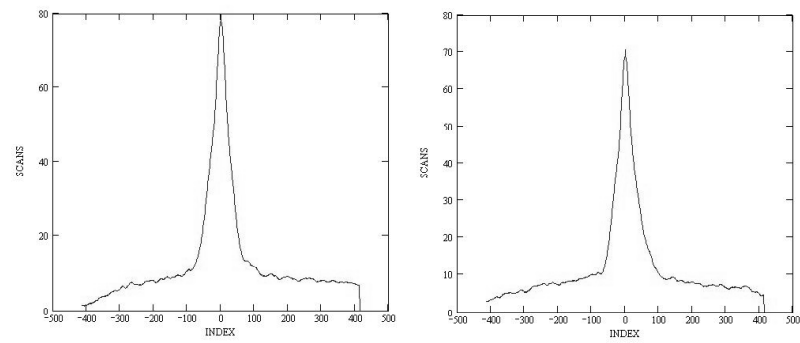


Figure. C.300: HD 190228: SFP inspection for 2006/08/14 data.

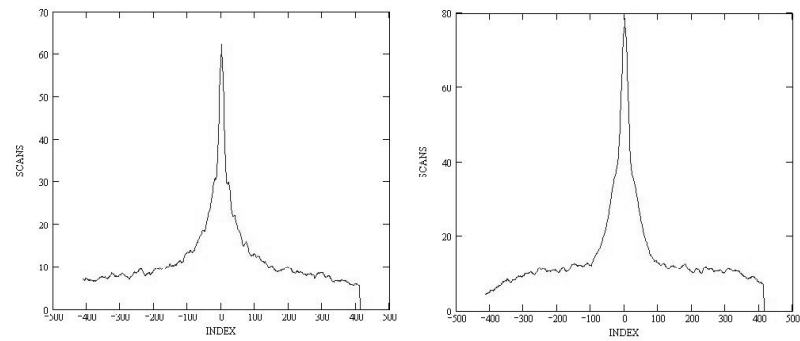


Figure. C.301: HD 190470: SFP inspection for 2005/07/01 data.

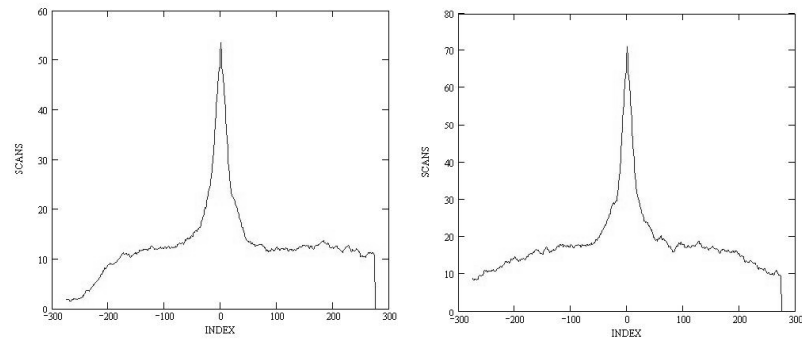


Figure. C.302: HD 190470: SFP inspection for 2005/08/19 data.

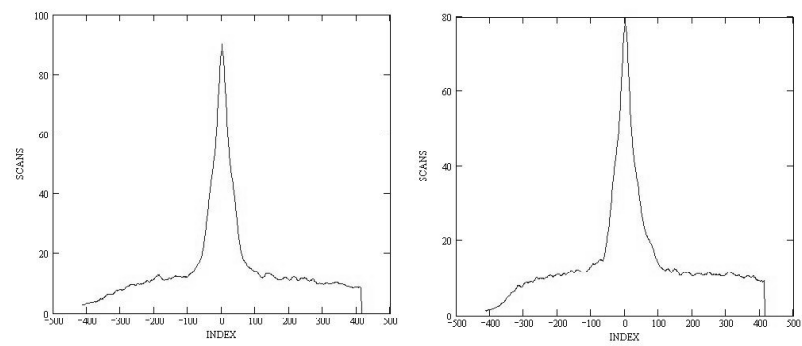


Figure. C.303: HD 190470: SFP inspection for 2006/08/14 data.

C.25 HD 190360

C.25.1 Calibrated Visibilities

Table. C.27: HD 190360: Calibrated Visibilities

| MJD | B (m) | PA (deg) | V_c | $\sigma(V_c)$ |
|-----------|----------|-------------|-------|---------------|
| 53593.229 | 101.16 | 107.5 | 1.005 | 0.124 |
| 53593.242 | 103.57 | 104.7 | 0.925 | 0.104 |
| 53593.255 | 105.35 | 102.3 | 0.902 | 0.069 |
| 53593.268 | 106.73 | 99.7 | 0.852 | 0.102 |
| 53593.291 | 107.89 | 95.5 | 0.936 | 0.105 |
| 53593.311 | 107.55 | 92.0 | 0.986 | 0.088 |
| 53593.328 | 106.25 | 268.9 | 0.891 | 0.081 |
| 53593.340 | 104.71 | 266.6 | 0.939 | 0.108 |
| 53593.352 | 102.84 | 264.5 | 0.989 | 0.081 |
| 53593.362 | 100.87 | 262.5 | 0.907 | 0.067 |
| 53895.487 | 326.62 | 193.4 | 0.760 | 0.049 |
| 53958.342 | 325.15 | 187.2 | 0.734 | 0.035 |
| 53958.357 | 324.67 | 183.6 | 0.747 | 0.035 |
| 53958.372 | 324.51 | 269.8 | 0.748 | 0.037 |
| 53958.388 | 324.72 | 176.0 | 0.793 | 0.056 |
| 53958.405 | 325.30 | 172.0 | 0.704 | 0.039 |
| 53958.421 | 326.15 | 168.2 | 0.663 | 0.052 |
| 53958.436 | 327.17 | 164.7 | 0.676 | 0.068 |
| 53958.451 | 328.17 | 161.6 | 0.642 | 0.060 |
| 53958.465 | 329.11 | 158.6 | 0.679 | 0.044 |

C.25.2 Nightly Data Plots

Because the 2006/06/09 dataset only had one bracketed observation, it was not used in the companion check.

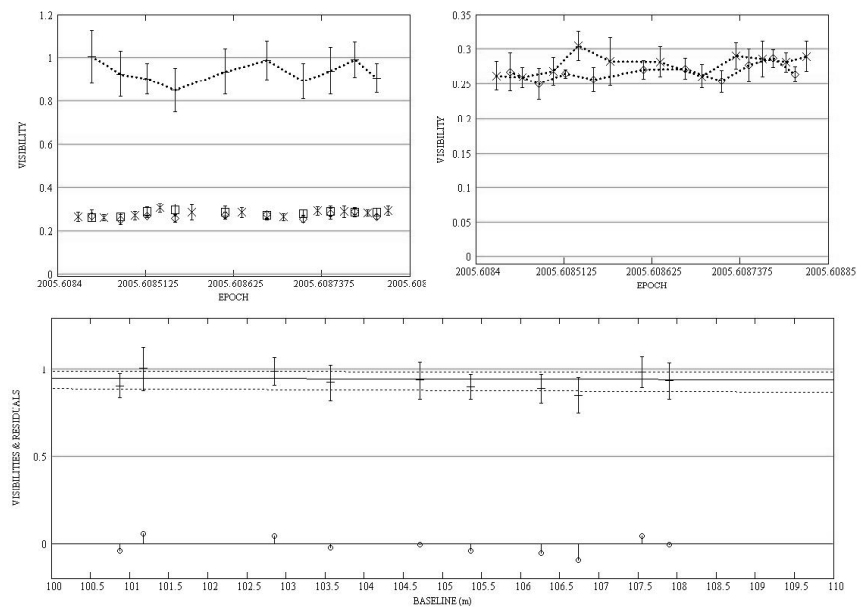


Figure. C.304: HD 190360: Intermediate baseline plots for 2005/08/11 data.

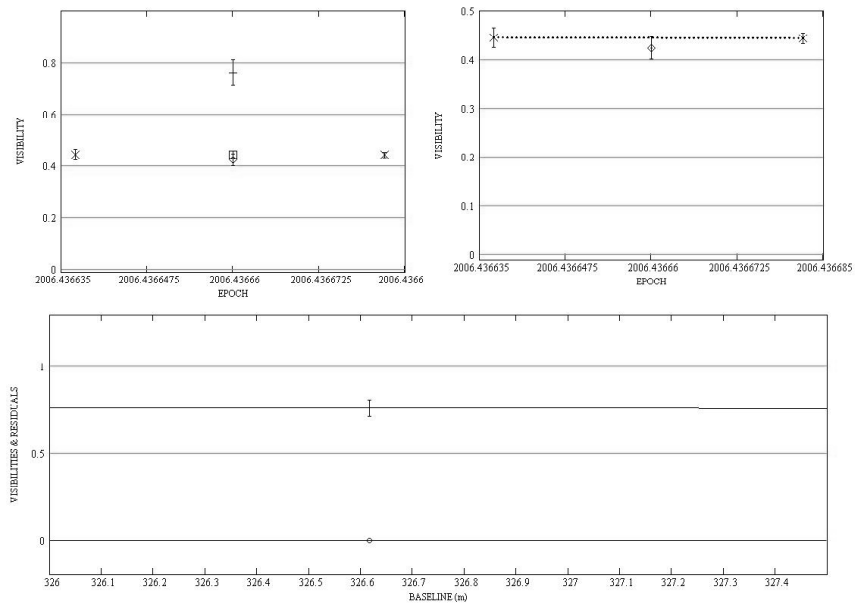


Figure. C.305: HD 190360: Long baseline plots for 2006/06/09 data.

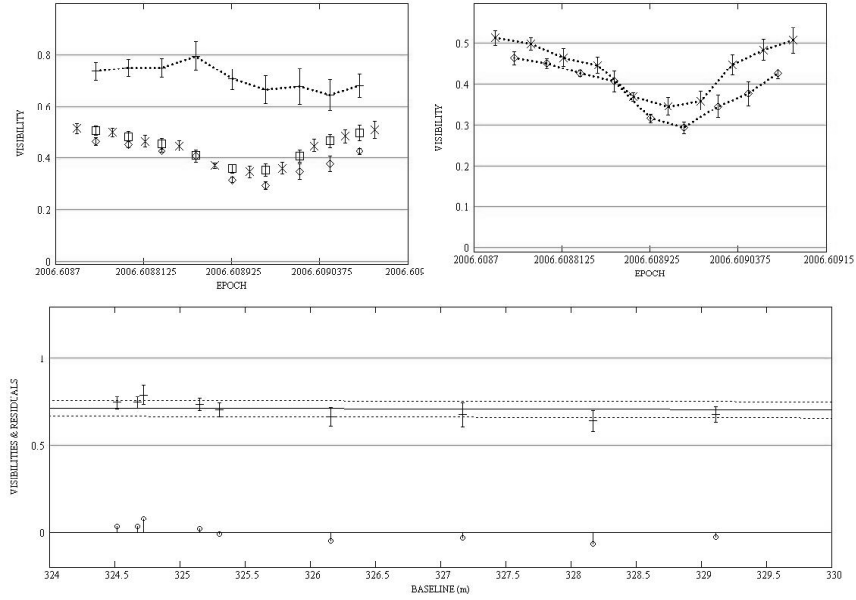


Figure. C.306: HD 190360: Long baseline plots for 2006/08/11 data.

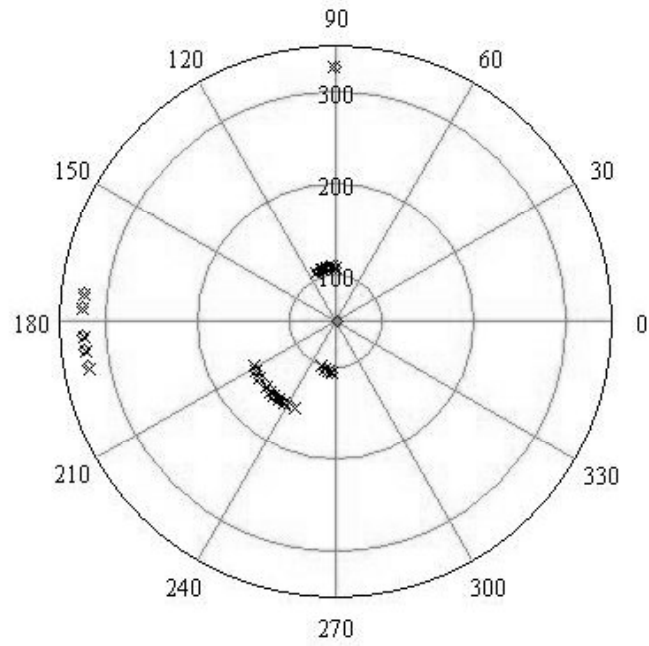


Figure. C.307: HD 190360: All data - Baseline vs. baseline position angle.

C.25.3 Diameter Calculation

All the S1-E1 data were used in the diameter measurement.

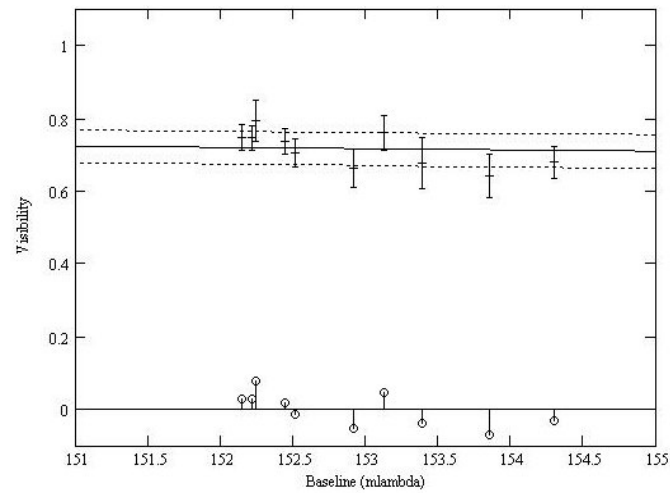


Figure. C.308: HD 190360: LD disk diameter fit: Visibility vs. baseline.

C.25.4 SFP Search

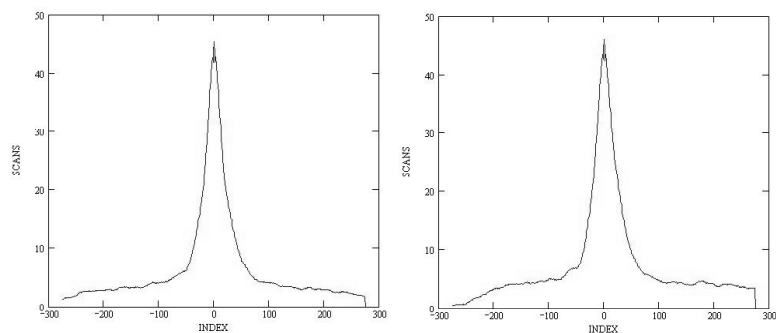


Figure. C.309: HD 190360: SFP inspection for 2005/08/11 data.

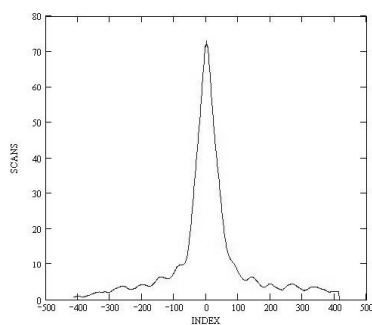


Figure. C.310: HD 190360: SFP inspection for 2006/06/09 data.

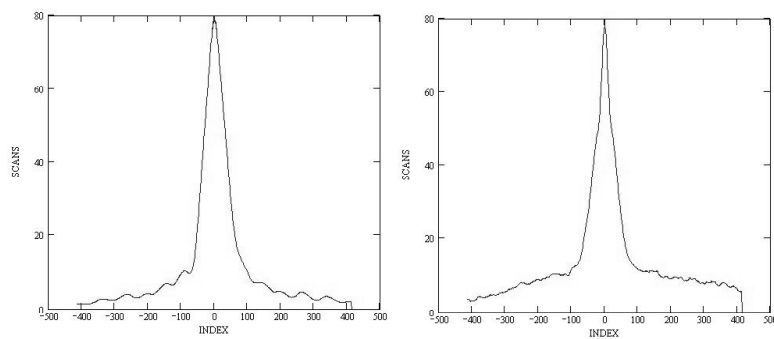


Figure. C.311: HD 190360: SFP inspection for 2006/08/11 data.

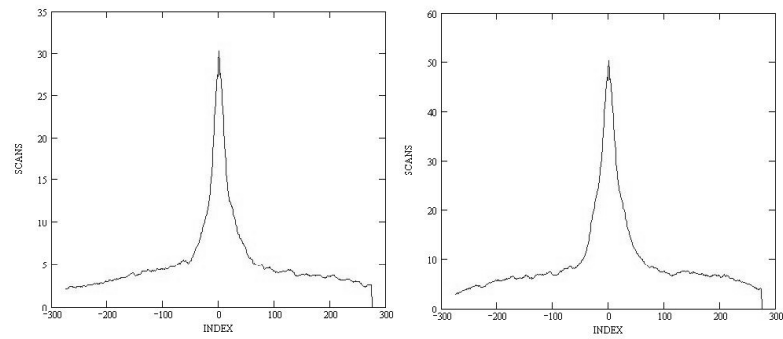


Figure. C.312: HD 189108: SFP inspection for 2005/08/11 data.

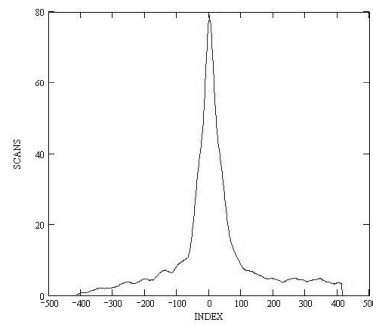


Figure. C.313: HD 189108: SFP inspection for 2006/06/09 data.

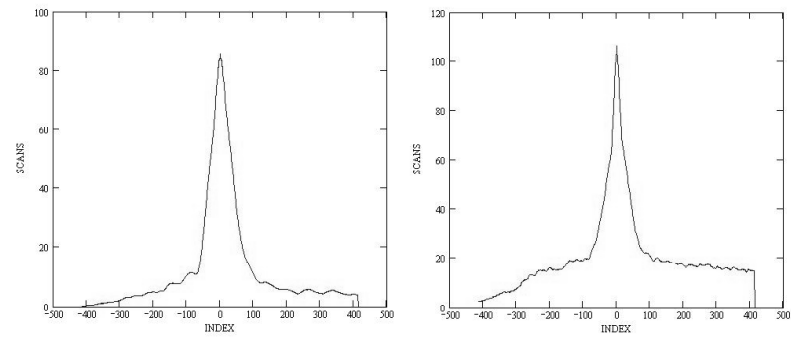


Figure. C.314: HD 189108: SFP inspection for 2006/08/11 data.

C.26 HD 192263

C.26.1 Calibrated Visibilities

HD 192263 was observed using the S1-E1 baseline on 2006/05/20. Unfortunately, there are only two bracketed observations and only one of them has good time sampling. Therefore I did not attempt a diameter measurement or the companion check.

Table. C.28: HD 192263: Calibrated Visibilities

| MJD | B (m) | PA (deg) | V_c | $\sigma(V_c)$ |
|-----------|----------|-------------|-------|---------------|
| 53875.442 | 312.49 | 216.5 | 1.010 | 0.117 |
| 53875.465 | 302.13 | 213.6 | 0.993 | 0.073 |

C.26.2 Nightly Data Plots

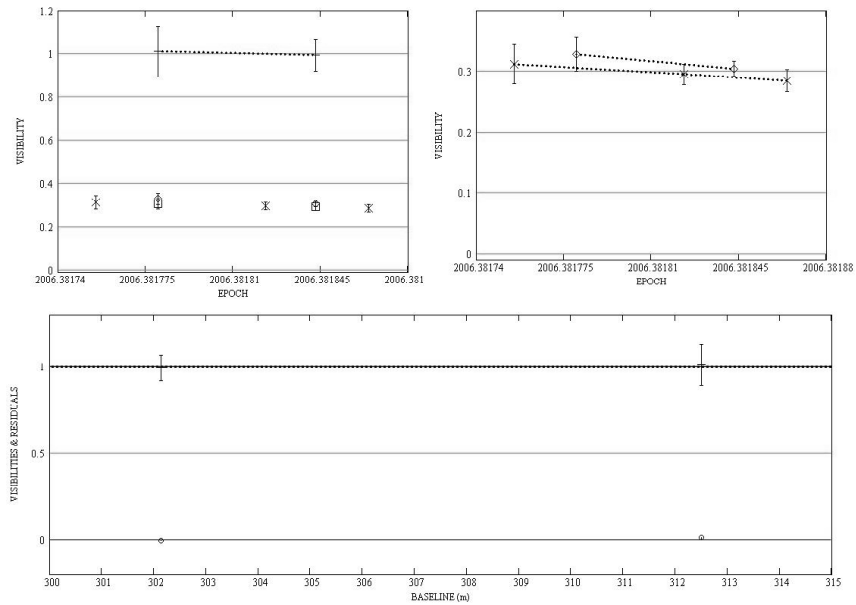


Figure. C.315: HD 192263: Long baseline plots for 2006/05/20 data.

C.26.3 SFP Search

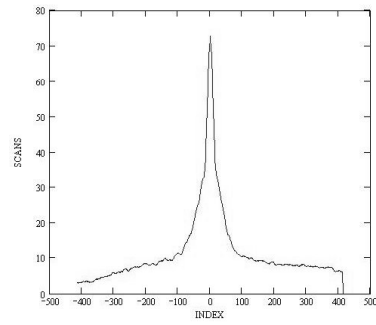


Figure. C.316: HD 192263: SFP inspection for 2006/05/20 data.

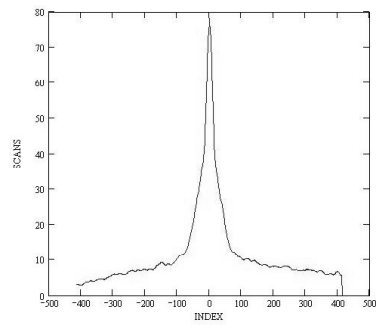


Figure. C.317: HD 188350: SFP inspection for 2006/05/20 data.

C.27 HD 195019

C.27.1 Calibrated Visibilities

Table. C.29: HD 195019: Calibrated Visibilities

| MJD | B (m) | PA (deg) | V_c | $\sigma(V_c)$ |
|-----------|----------|-------------|-------|---------------|
| 53593.401 | 94.18 | 264.0 | 1.005 | 0.087 |
| 53593.412 | 90.39 | 262.4 | 1.035 | 0.102 |
| 53593.422 | 86.71 | 260.9 | 0.928 | 0.095 |
| 53593.438 | 80.58 | 258.4 | 0.973 | 0.048 |
| 53593.448 | 76.03 | 256.4 | 0.916 | 0.066 |
| 53594.193 | 83.01 | 112.4 | 1.088 | 0.143 |
| 53594.204 | 86.89 | 110.1 | 1.026 | 0.100 |
| 53594.214 | 90.38 | 108.2 | 1.138 | 0.117 |
| 53594.224 | 93.66 | 106.3 | 1.026 | 0.086 |
| 53594.239 | 98.09 | 103.8 | 1.498 | 0.315 |
| 53594.251 | 100.90 | 102.1 | 1.325 | 0.252 |
| 53594.262 | 103.12 | 100.6 | 0.946 | 0.127 |
| 53594.273 | 104.93 | 99.2 | 1.111 | 0.086 |
| 53594.286 | 106.59 | 97.5 | 0.995 | 0.091 |
| 53594.297 | 107.47 | 96.1 | 1.030 | 0.098 |
| 53666.125 | 312.31 | 195.7 | 1.164 | 0.136 |
| 53666.138 | 310.16 | 192.6 | 1.023 | 0.095 |
| 53666.151 | 308.39 | 189.4 | 0.867 | 0.085 |
| 53666.165 | 307.07 | 186.0 | 0.937 | 0.108 |
| 53666.179 | 306.31 | 182.5 | 1.016 | 0.065 |
| 53666.193 | 306.19 | 178.8 | 0.983 | 0.081 |
| 53666.207 | 306.72 | 175.3 | 0.906 | 0.134 |
| 53666.228 | 308.61 | 170.1 | 0.988 | 0.262 |
| 53666.245 | 311.02 | 166.1 | 1.058 | 0.130 |
| 53666.260 | 313.73 | 162.5 | 0.879 | 0.079 |
| 53953.385 | 101.82 | 267.7 | 1.002 | 0.057 |
| 53953.399 | 98.60 | 266.1 | 0.949 | 0.058 |
| 53953.412 | 94.99 | 264.4 | 1.018 | 0.065 |
| 53953.424 | 90.87 | 262.6 | 1.070 | 0.081 |
| 53953.437 | 86.26 | 260.7 | 0.982 | 0.078 |
| 53953.450 | 80.85 | 258.5 | 0.847 | 0.089 |

C.27.2 Nightly Data Plots

There is an extreme outlier in the 2005/08/12 data when one of the calibrator's visibilities drops by almost half for one observation. The tracking for this observation was not as good as for the others in the dataset ($\sim 40\%$ of the scans were good versus the $\sim 60\%$ for the other observations) and there is no power spectrum. This point and the object visibilities immediately before and after it were given zero weight, which had the effect of breaking the dataset into two calibrated sections.

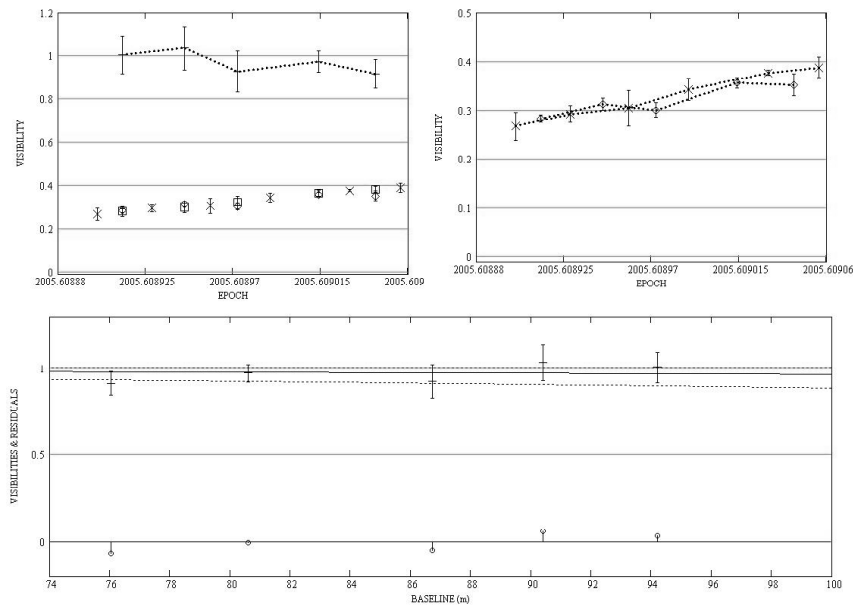


Figure. C.318: HD 195019: Intermediate baseline plots for 2005/08/11 data.

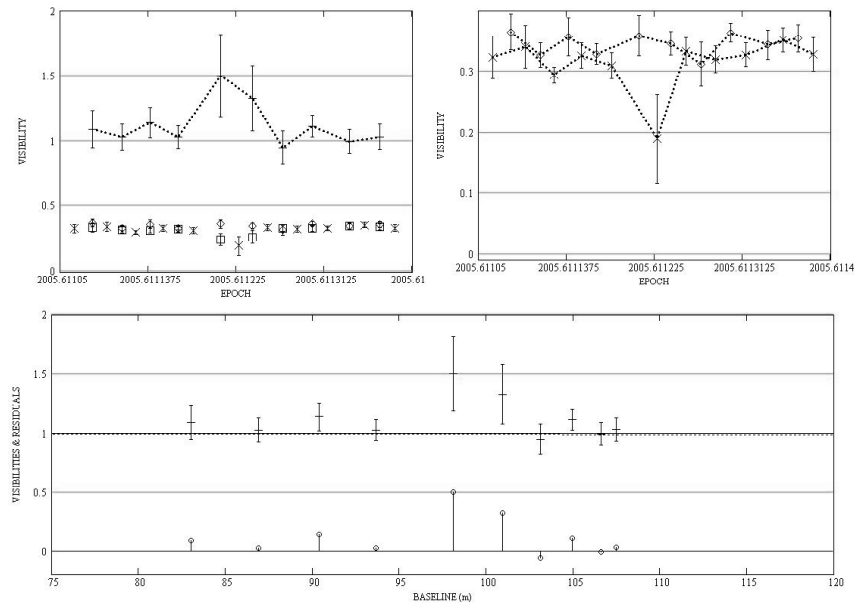


Figure. C.319: HD 195019: Intermediate baseline plots for 2005/08/12 data.

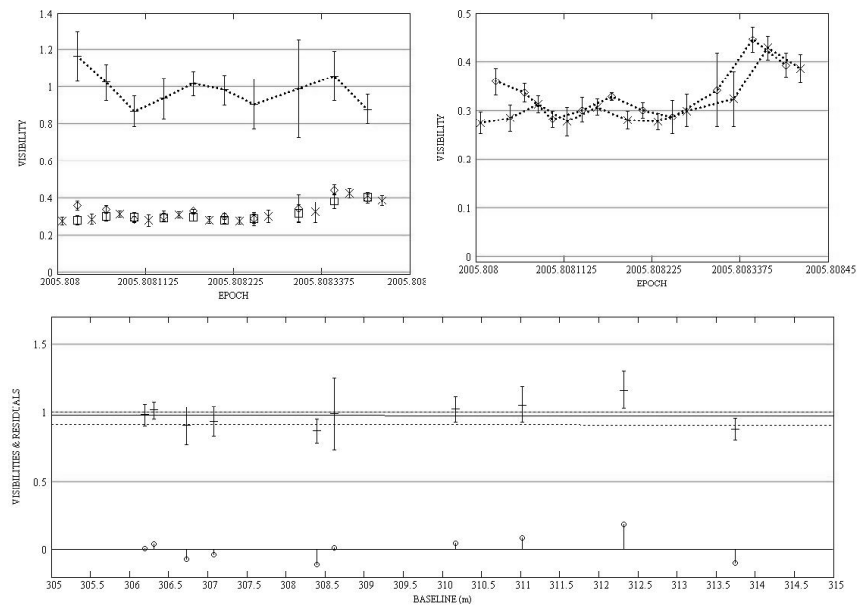


Figure. C.320: HD 195019: Long baseline plots for 2005/10/23 data.

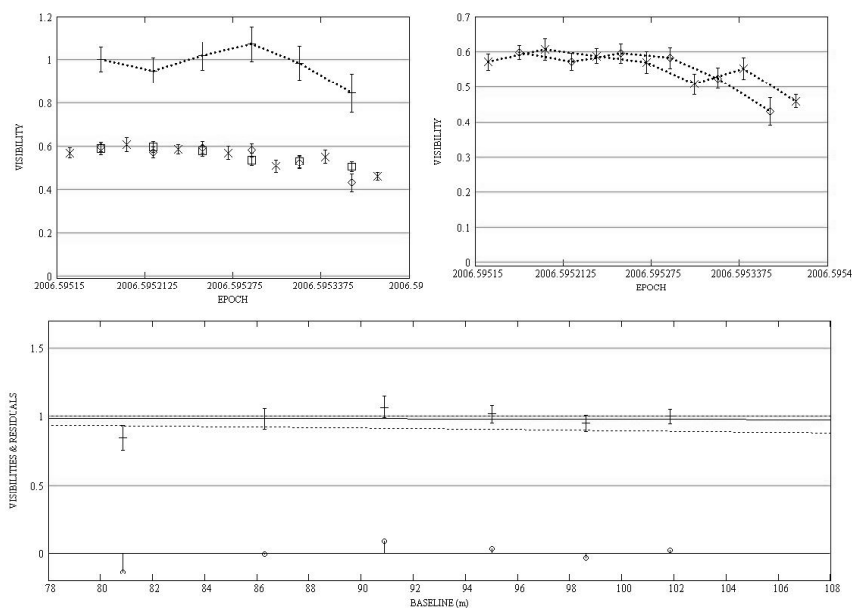


Figure. C.321: HD 195019: Intermediate baseline plots for 2006/08/06 data.

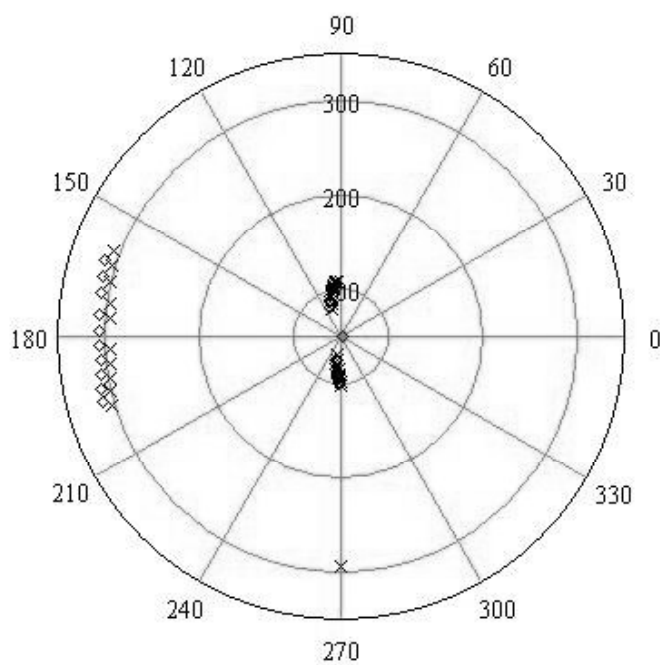


Figure. C.322: HD 195019: All data - Baseline vs. baseline position angle.

C.27.3 Diameter Calculation

All the S1-E1 data were used for the diameter calculation, but HD 195019 is basically unresolved even at this baseline. The diameter has a 90% error bar, which does not instill much confidence in this measurement.

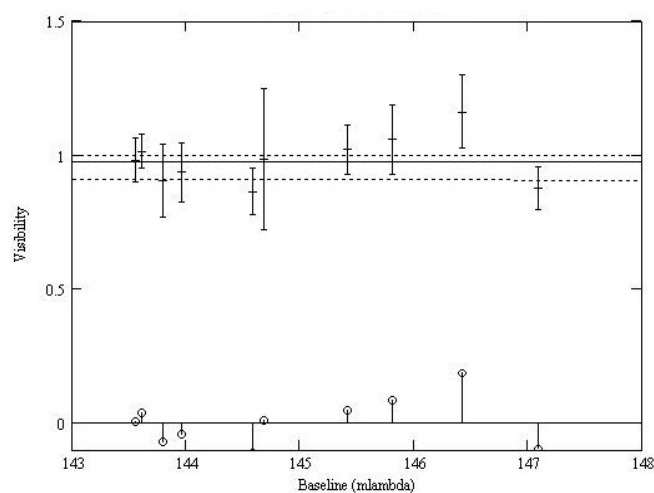


Figure. C.323: HD 195019: LD disk diameter fit: Visibility vs. baseline.

C.27.4 SFP Search

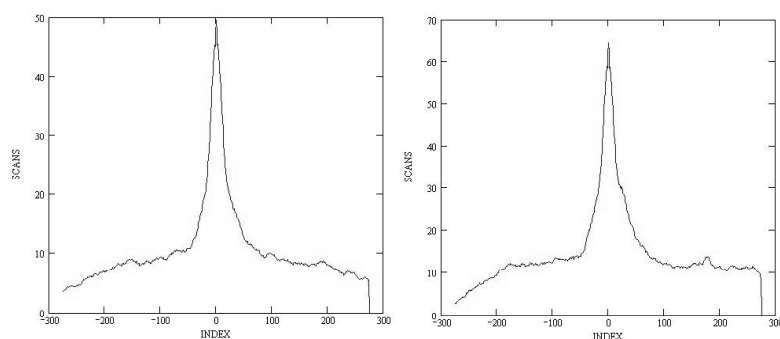


Figure. C.324: HD 195019: SFP inspection for 2005/08/11 data.

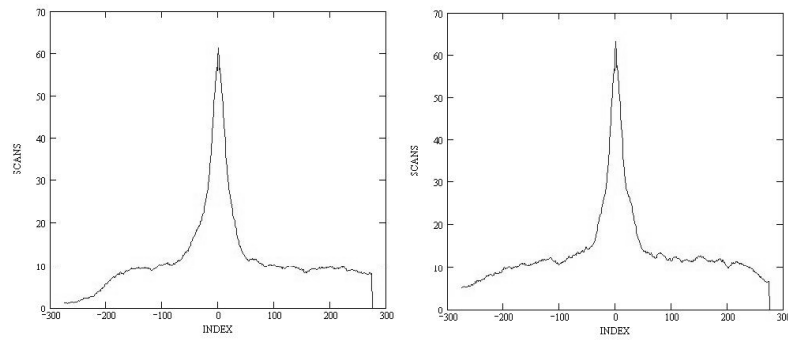


Figure. C.325: HD 195019: SFP inspection for 2005/08/12 data.

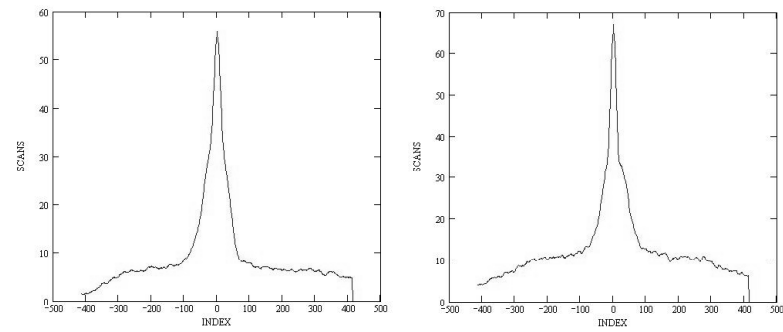


Figure. C.326: HD 195019: SFP inspection for 2005/10/23 data.

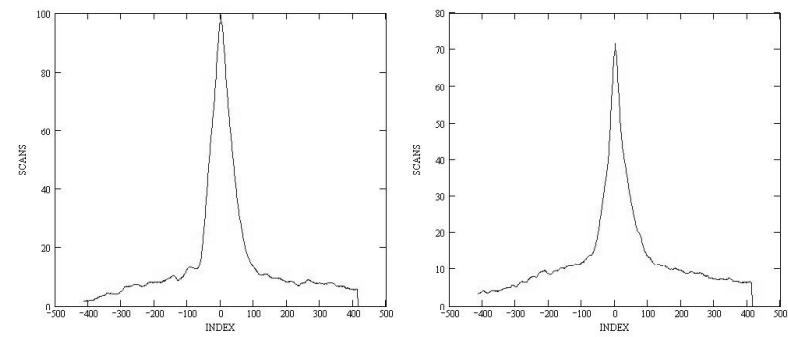


Figure. C.327: HD 195019: SFP inspection for 2006/08/06 data.

C.28 HD 196885

C.28.1 Calibrated Visibilities

Table. C.30: HD 196885: Calibrated Visibilities

| MJD | B (m) | PA (deg) | V_c | $\sigma(V_c)$ |
|-----------|----------|-------------|-------|---------------|
| 53670.153 | 289.70 | 188.8 | 0.912 | 0.085 |
| 53670.169 | 287.85 | 184.6 | 0.786 | 0.075 |
| 53670.183 | 287.18 | 180.7 | 0.851 | 0.072 |
| 53670.196 | 287.44 | 177.1 | 0.954 | 0.090 |
| 53672.173 | 121.94 | 230.9 | 1.017 | 0.086 |
| 53672.188 | 114.90 | 226.9 | 0.876 | 0.034 |
| 53672.201 | 108.68 | 222.7 | 0.957 | 0.093 |
| 53672.214 | 102.71 | 218.0 | 0.943 | 0.088 |
| 53672.227 | 96.98 | 212.4 | 0.922 | 0.062 |
| 53954.331 | 107.87 | 94.5 | 0.919 | 0.074 |
| 53954.344 | 107.74 | 93.5 | 0.903 | 0.062 |
| 53954.358 | 106.89 | 92.6 | 0.925 | 0.060 |
| 53954.373 | 105.01 | 91.6 | 0.906 | 0.043 |
| 53954.386 | 102.59 | 90.7 | 0.906 | 0.054 |
| 53954.400 | 99.35 | 269.7 | 1.034 | 0.074 |
| 53954.421 | 93.16 | 268.2 | 0.969 | 0.087 |
| 53954.434 | 88.37 | 267.1 | 0.933 | 0.072 |
| 53954.449 | 82.58 | 265.9 | 0.992 | 0.076 |
| 53954.462 | 76.36 | 264.5 | 0.941 | 0.096 |
| 53961.161 | 330.09 | 220.6 | 0.854 | 0.078 |
| 53961.175 | 330.66 | 219.7 | 0.903 | 0.078 |
| 53961.188 | 330.30 | 218.8 | 0.822 | 0.086 |
| 53961.201 | 329.05 | 217.5 | 0.930 | 0.064 |
| 53961.214 | 327.15 | 216.2 | 0.777 | 0.065 |

C.28.2 Nightly Data Plots

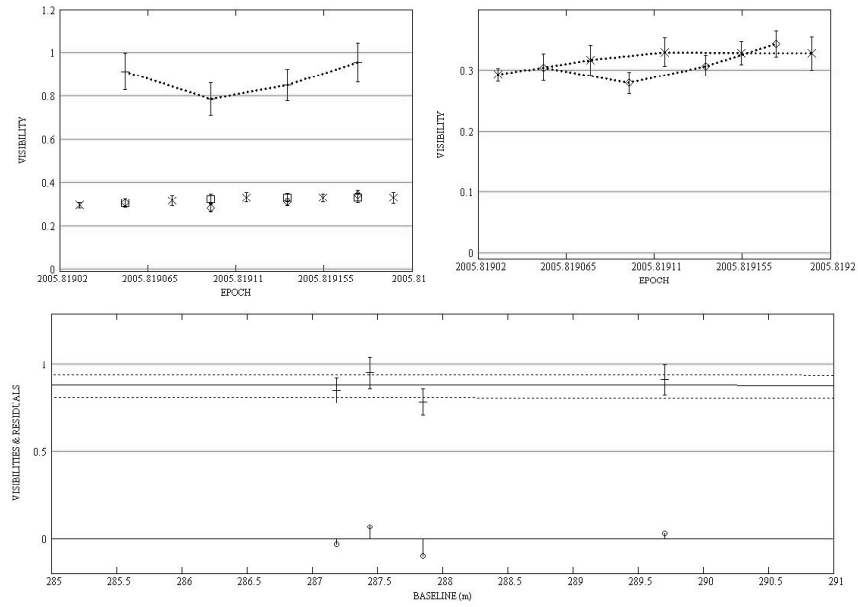


Figure. C.328: HD 196885: Long baseline plots for 2005/10/27 data.

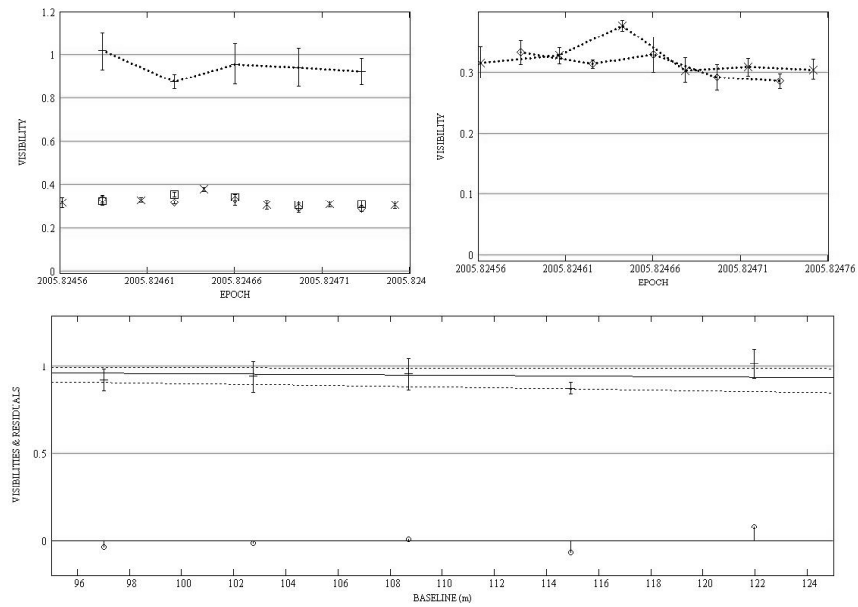


Figure. C.329: HD 196885: Intermediate baseline plots for 2005/10/29 data.

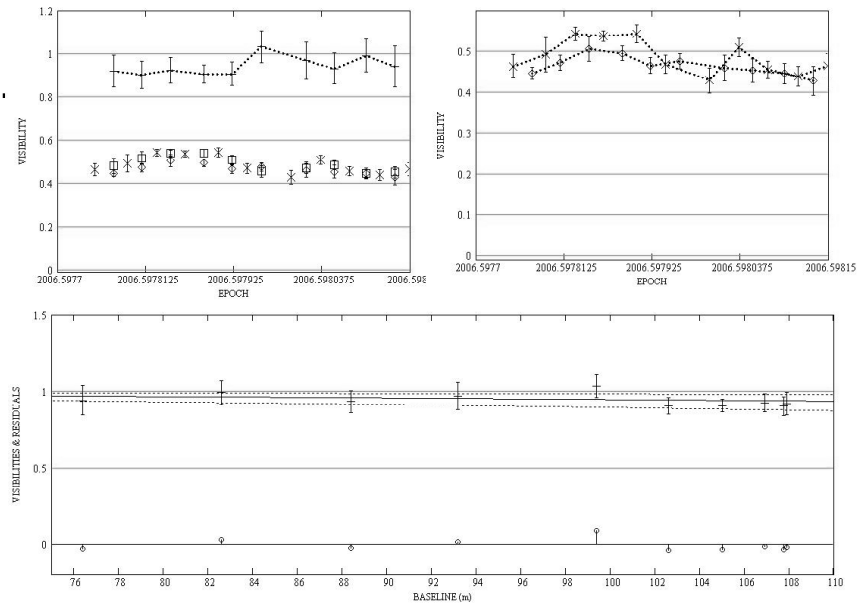


Figure. C.330: HD 196885: Intermediate baseline plots for 2006/08/07 data.

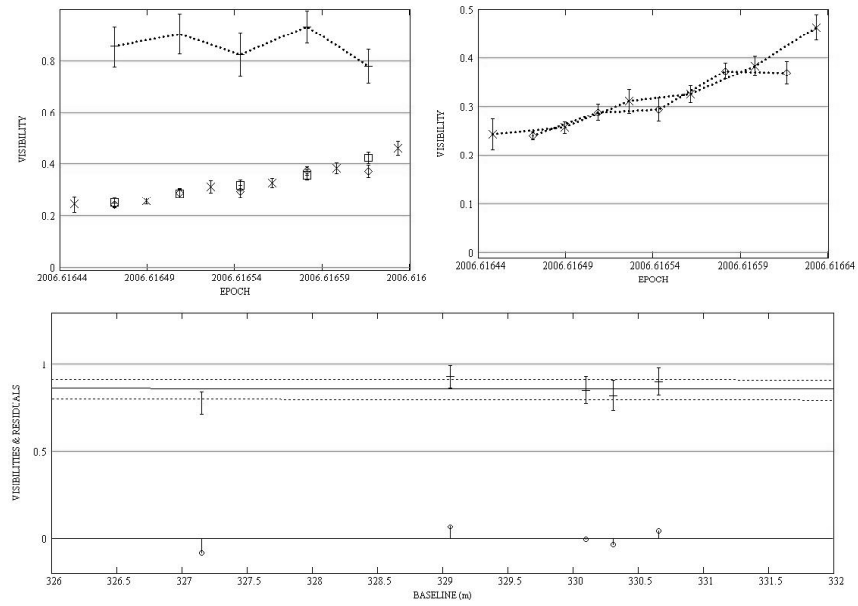


Figure. C.331: HD 196885: Long baseline plots for 2006/08/14 data.

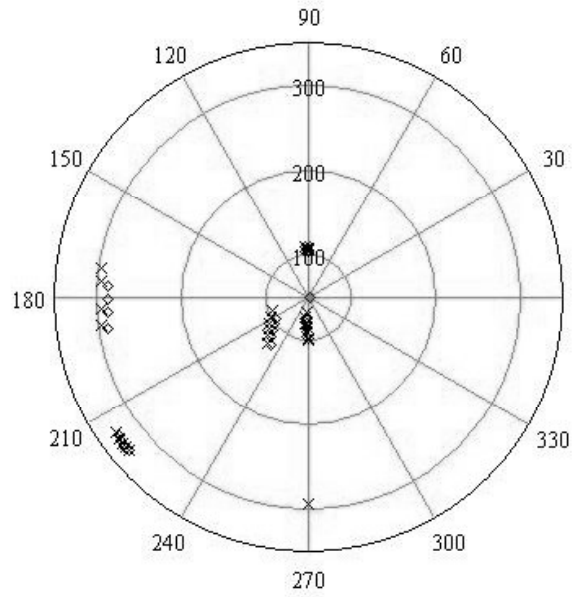


Figure. C.332: HD 196885: All data - Baseline vs. baseline position angle.

C.28.3 Diameter Calculation

All the S1-E1 data were used for the diameter calculation.

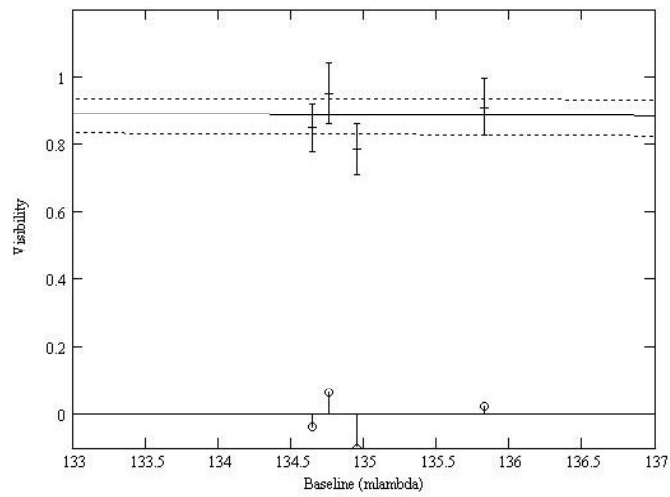


Figure. C.333: HD 196885: LD disk diameter fit: Visibility vs. baseline.

C.28.4 SFP Search

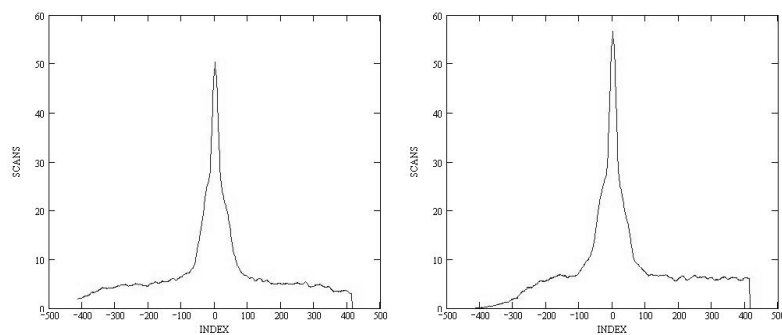


Figure. C.334: HD 196885: SFP inspection for 2005/10/27 data.

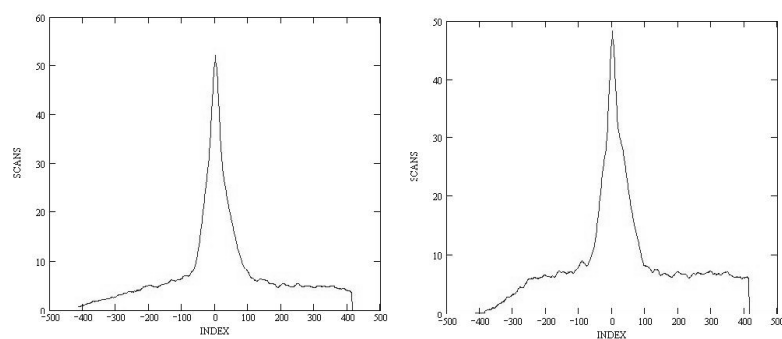


Figure. C.335: HD 196885: SFP inspection for 2005/10/29 data.

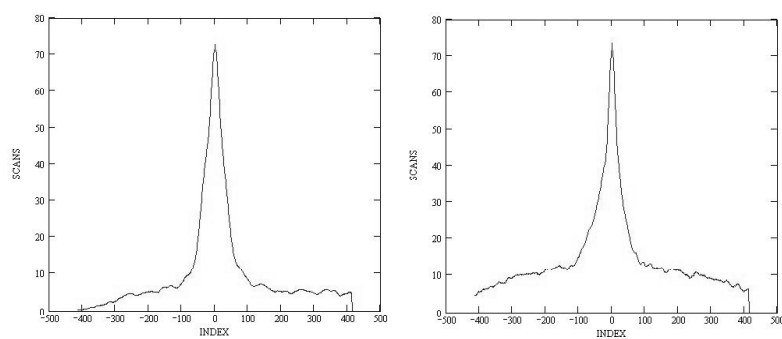


Figure. C.336: HD 196885: SFP inspection for 2006/08/07 data.

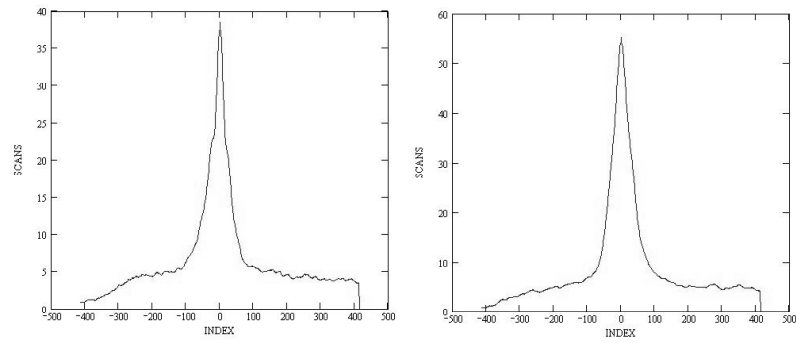


Figure. C.337: HD 196885: SFP inspection for 2006/08/14 data.

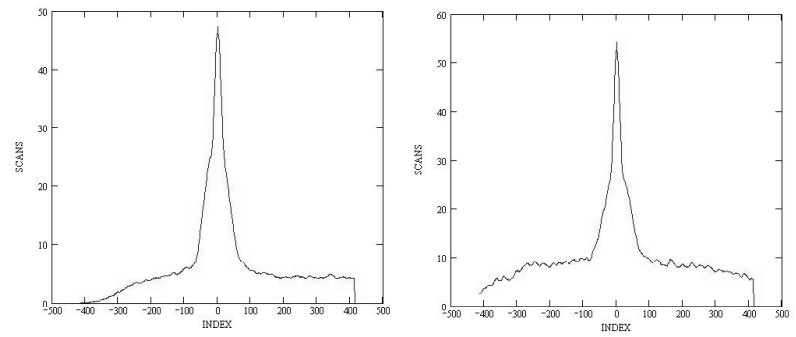


Figure. C.338: HD 194012: SFP inspection for 2005/10/27 data.

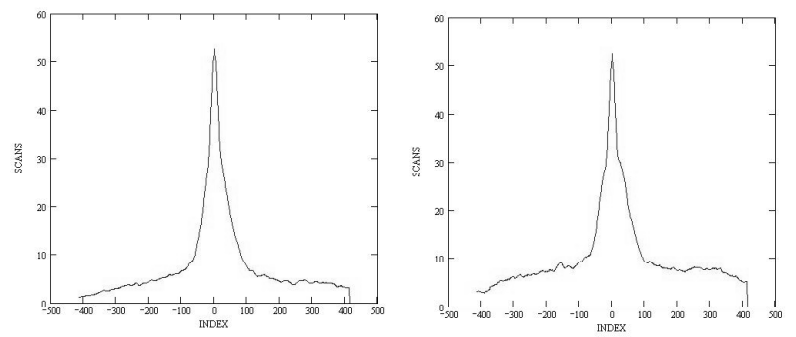


Figure. C.339: HD 194012: SFP inspection for 2005/10/29 data.

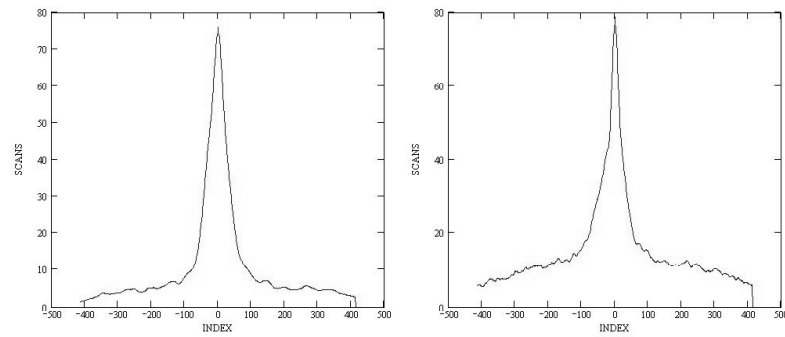


Figure. C.340: HD 194012: SFP inspection for 2006/08/07 data.

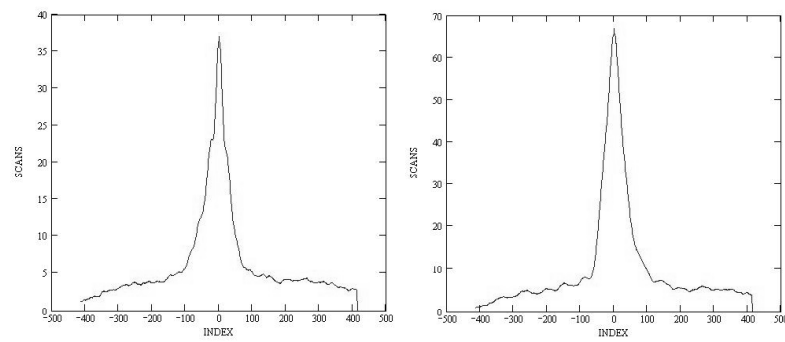


Figure. C.341: HD 194012: SFP inspection for 2006/08/14 data.

C.29 HD 217014

C.29.1 Calibrated Visibilities

Table. C.31: HD 217014: Calibrated Visibilities

| MJD | B (m) | PA (deg) | V_c | $\sigma(V_c)$ |
|-----------|----------|-------------|-------|---------------|
| 53585.442 | 107.91 | 94.1 | 0.620 | 0.051 |
| 53585.454 | 107.58 | 92.6 | 0.558 | 0.063 |
| 53585.469 | 106.33 | 90.7 | 0.465 | 0.046 |
| 53585.491 | 103.02 | 267.8 | 0.515 | 0.055 |
| 53594.332 | 95.58 | 106.6 | 0.915 | 0.089 |
| 53594.342 | 98.32 | 104.8 | 0.853 | 0.079 |
| 53594.352 | 100.76 | 103.1 | 0.848 | 0.047 |
| 53594.364 | 103.11 | 101.4 | 0.926 | 0.053 |
| 53594.379 | 105.54 | 99.2 | 0.990 | 0.123 |
| 53594.390 | 106.75 | 97.7 | 0.943 | 0.111 |
| 53594.401 | 107.53 | 96.3 | 0.943 | 0.091 |
| 53594.425 | 107.75 | 93.2 | 0.896 | 0.120 |
| 53594.437 | 107.01 | 91.6 | 0.944 | 0.079 |
| 53594.447 | 106.00 | 90.3 | 0.917 | 0.096 |
| 53594.460 | 104.16 | 268.6 | 0.941 | 0.098 |
| 53594.473 | 101.75 | 267.0 | 0.842 | 0.079 |
| 53594.487 | 98.34 | 265.0 | 0.860 | 0.062 |
| 53594.499 | 95.14 | 263.3 | 0.921 | 0.084 |
| 53959.290 | 329.68 | 218.7 | 0.678 | 0.070 |
| 53959.303 | 330.50 | 217.2 | 0.698 | 0.059 |
| 53959.316 | 330.63 | 215.6 | 0.640 | 0.061 |
| 53959.329 | 330.08 | 213.7 | 0.658 | 0.037 |
| 53959.343 | 328.87 | 211.6 | 0.700 | 0.049 |
| 53959.357 | 327.11 | 209.3 | 0.613 | 0.074 |
| 53959.372 | 324.94 | 206.7 | 0.714 | 0.056 |

C.29.2 Nightly Data Plots

The last object and calibrator data points in the 2005/08/03 dataset were given zero weight due to the long gap between the fourth calibrator and fourth object observations. As this leaves only three bracketed observations, this dataset was not used in the companion check.

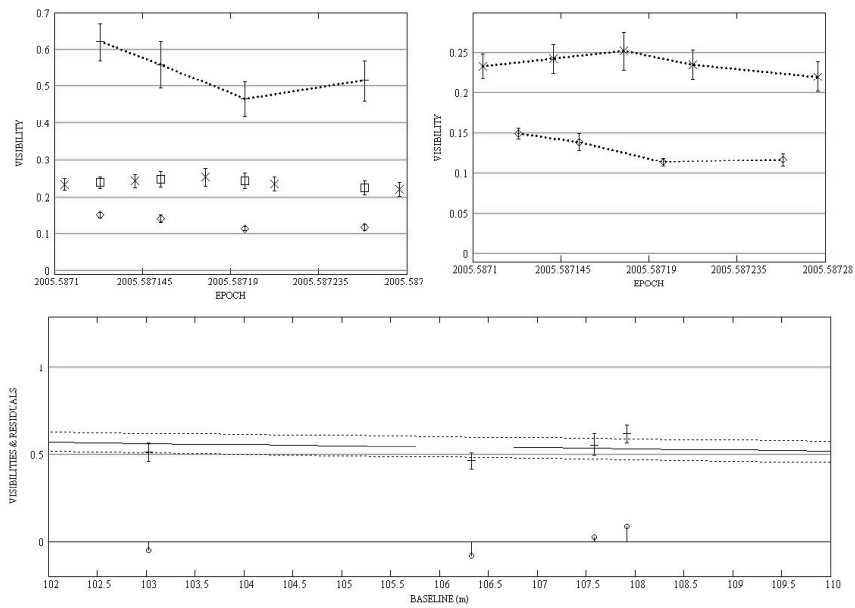


Figure. C.342: HD 217014: Intermediate baseline plots for 2005/08/03 data.

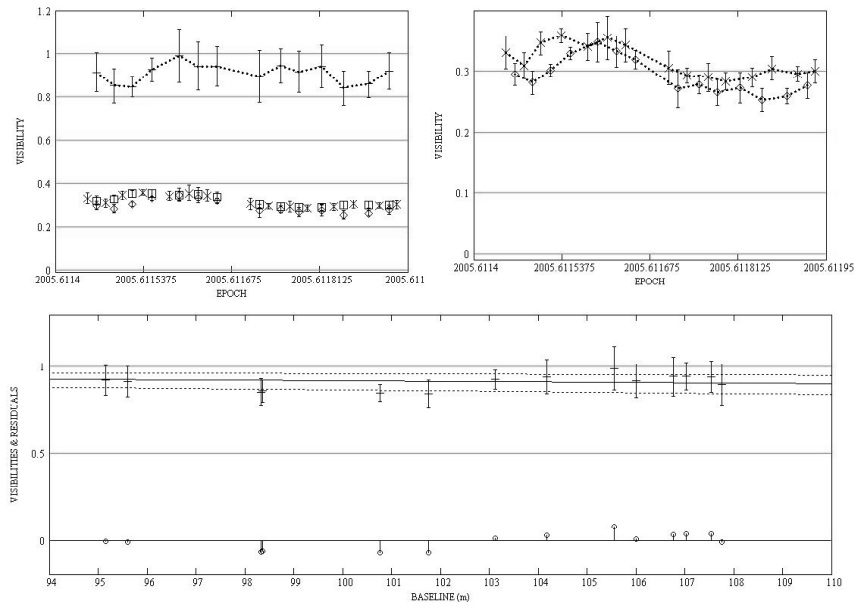


Figure. C.343: HD 217014: Intermediate baseline plots for 2005/08/12 data.

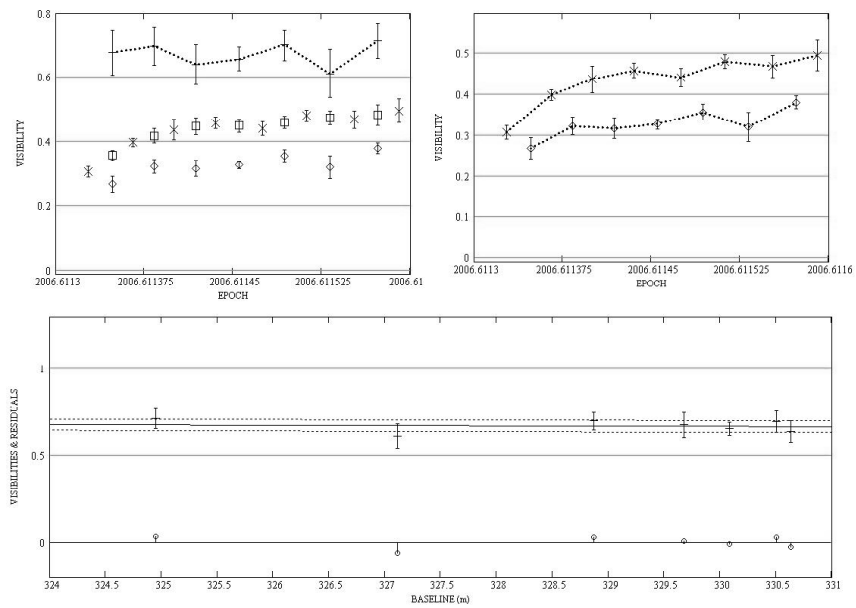


Figure. C.344: HD 217014: Long baseline plots for 2006/08/12 data.

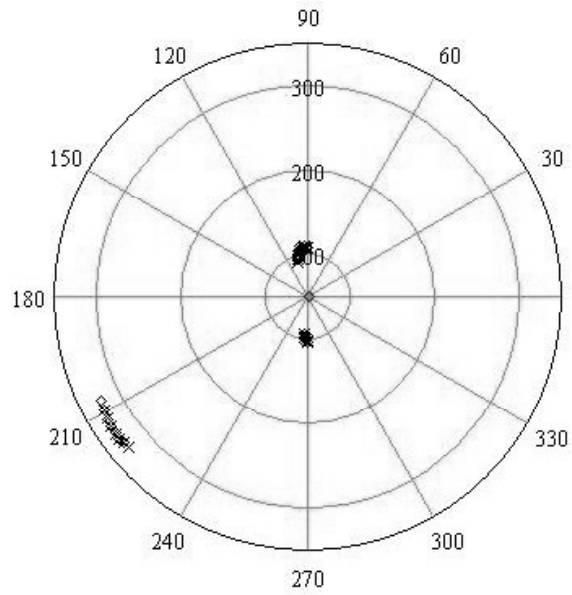


Figure. C.345: HD 217014: All data - Baseline vs. baseline position angle.

C.29.3 Diameter Calculation

The S1-E1 data from 2006/08/12 were used for the diameter calculation.

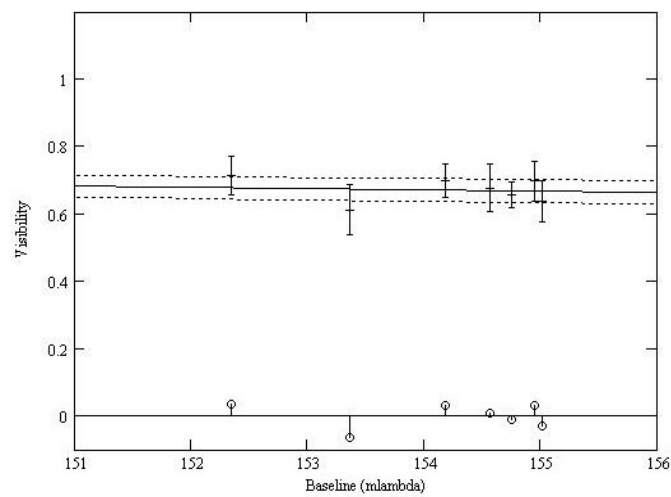


Figure. C.346: HD 217014: LD disk diameter fit: Visibility vs. baseline.

C.29.4 SFP Search

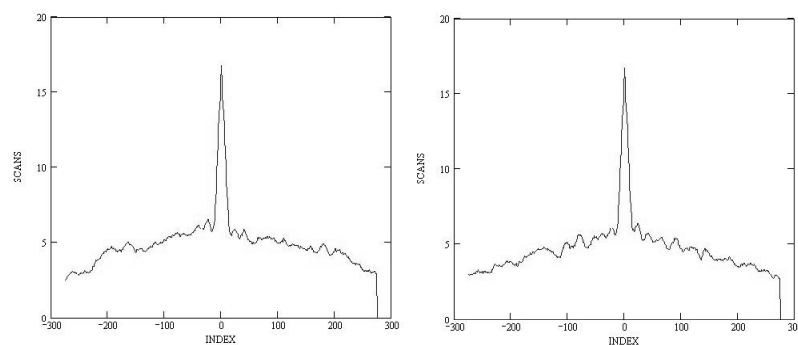


Figure. C.347: HD 217014: SFP inspection for 2005/08/03 data.

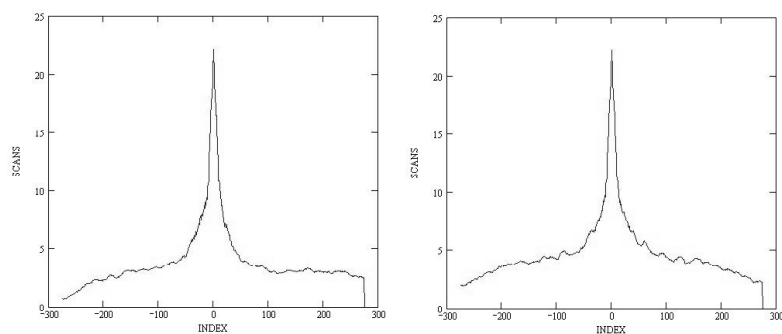


Figure. C.348: HD 217014: SFP inspection for 2005/08/12 data.

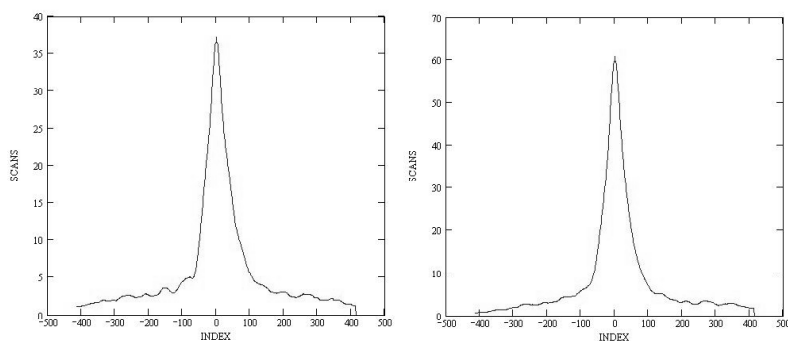


Figure. C.349: HD 217014: SFP inspection for 2006/08/12 data.

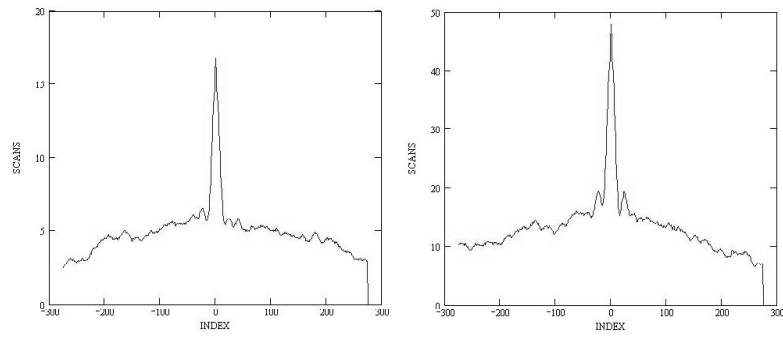


Figure. C.350: HD 218261: SFP inspection for 2005/08/03 data.

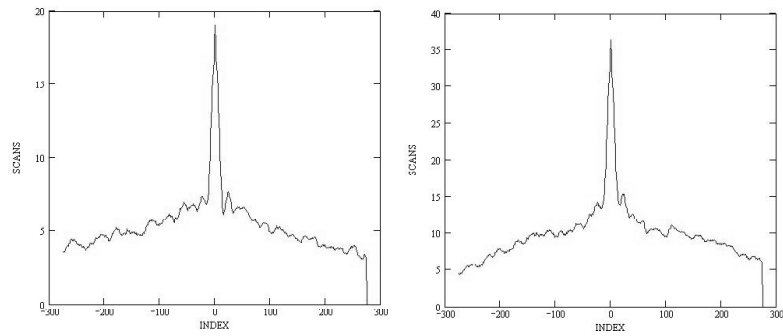


Figure. C.351: HD 218261: SFP inspection for 2005/08/12 data.

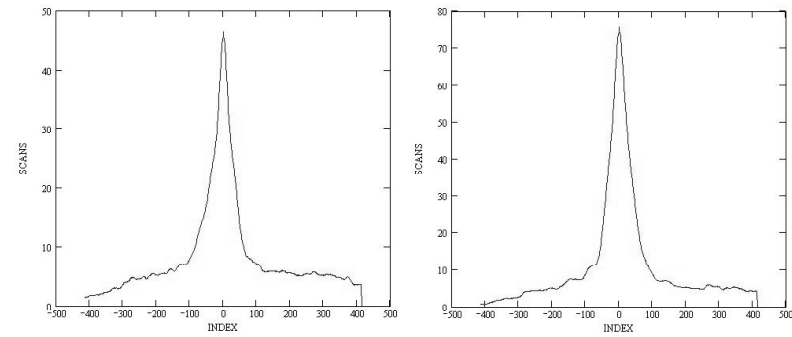


Figure. C.352: HD 218261: SFP inspection for 2006/08/12 data.

C.30 HD 217107

C.30.1 Calibrated Visibilities

Table. C.32: HD 217107: Calibrated Visibilities

| MJD | B (m) | PA (deg) | V_c | $\sigma(V_c)$ |
|-----------|----------|-------------|-------|---------------|
| 53717.150 | 278.09 | 128.3 | 0.885 | 0.098 |
| 53717.166 | 278.38 | 128.4 | 1.025 | 0.122 |
| 53717.181 | 277.11 | 128.8 | 0.888 | 0.086 |
| 54028.139 | 89.67 | 93.9 | 1.078 | 0.151 |
| 54028.151 | 94.14 | 93.8 | 1.139 | 0.141 |
| 54028.164 | 98.23 | 93.8 | 0.971 | 0.110 |
| 54028.176 | 101.29 | 93.8 | 1.034 | 0.119 |
| 54028.189 | 103.85 | 93.8 | 1.113 | 0.122 |
| 54028.200 | 105.66 | 93.8 | 1.013 | 0.127 |
| 54028.213 | 107.11 | 93.9 | 1.069 | 0.107 |
| 54028.225 | 107.81 | 94.0 | 1.070 | 0.118 |

C.30.2 Nightly Data Plots

Because there were only three bracketed data points in the 2005/12/13 dataset, it was not used in the companion check.

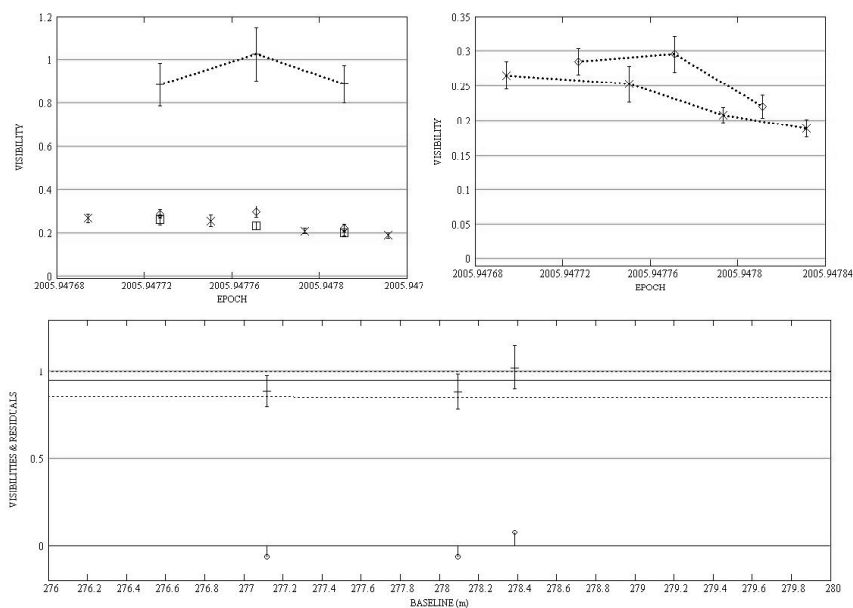


Figure. C.353: HD 217107: Intermediate baseline plots for 2005/12/13 data.

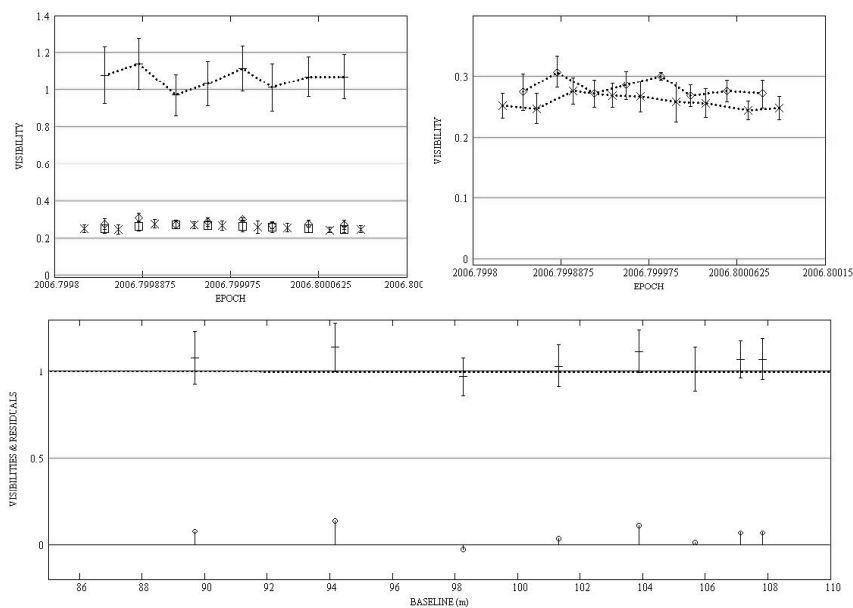


Figure. C.354: HD 217107: Intermediate baseline plots for 2006/10/20 data.

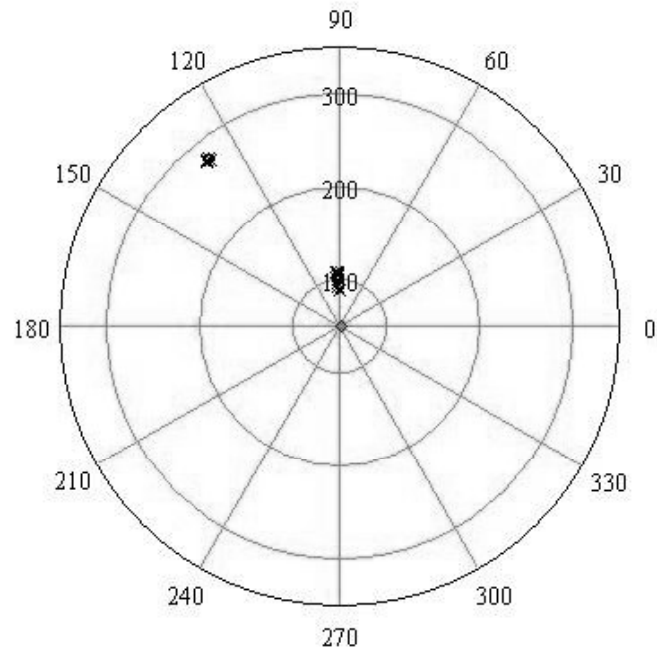


Figure. C.355: HD 217107: All data - Baseline vs. baseline position angle.

C.30.3 Diameter Calculation

No diameter calculation was performed for HD 217107. The W1-W2 data are extremely high on the visibility curve and the diameter calculation fails (0.021 ± 0.032 mas) and the W1-S1 data only have three data points and also fails (0.065 ± 0.050 mas). Therefore the diameter estimated from the SED fit was used for the companion check.

C.30.4 SFP Search

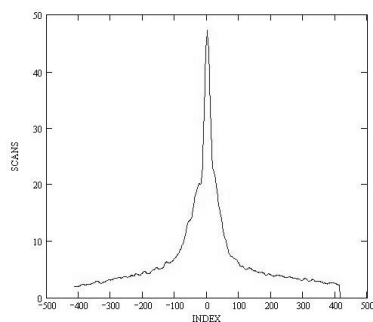


Figure. C.356: HD 217107: SFP inspection for 2005/12/13 data.

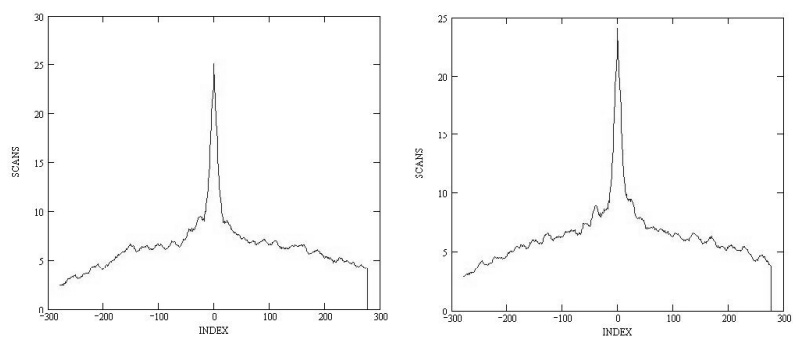


Figure. C.357: HD 217107: SFP inspection for 2006/10/20 data.

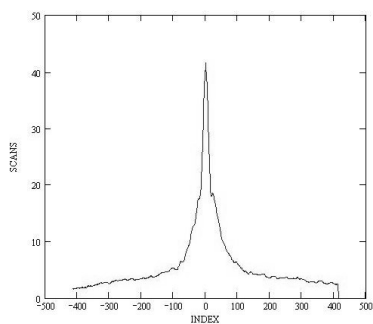


Figure. C.358: HD 216953: SFP inspection for 2005/12/13 data.

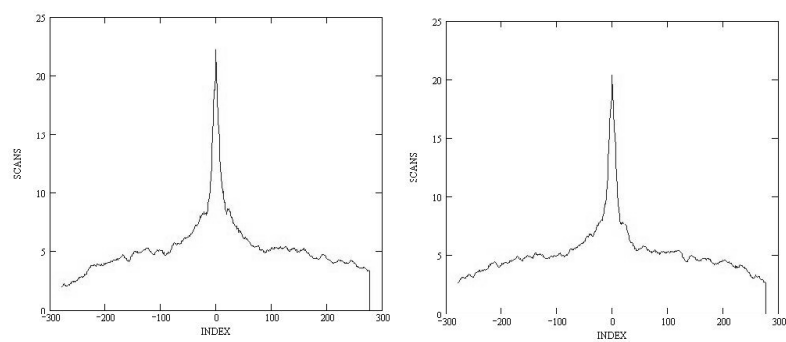


Figure. C.359: HD 216953: SFP inspection for 2006/10/20 data.